Cargo Delivery into Gram-negative Bacteria via Enterobactin Uptake Machinery

by

Tengfei Zheng
B. S. Chemistry
Peking University, 2007

SUBMITTED TO THE DEPARTMENT OF CHEMISTRY IN PARTIAL FULFILLMENT OF THE REQUIREMENTS FOR THE DEGREE OF

DOCTOR OF PHILOSOPHY IN BIOLOGICAL CHEMISTRY
AT THE
MASSACHUSETTS INSTITUTE OF TECHNOLOGY

June 2014

Signature of Author: Signature redacted
Department of Chemistry
May 5th 2014

Certified by: Signature redacted
Elizabeth M. Nolan
Pfizer-Laubach Career Development Assistant Professor
Thesis Advisor

Accepted by: Signature redacted
Robert W. Field
Chairman, Departmental Committee on Graduate Studies

This doctoral thesis has been examined by a committee of the Department of Chemistry as follows:

Signature redacted

JoAnne Stubbe
Novartis Professor of Chemistry and Professor of Biology
Committee Member

Signature redacted

Barbara Imperiali
Class of 1922 Professor of Biology and Professor of Chemistry
Committee Chairman

Signature redacted

Elizabeth M. Nolan
Pfizer-Laubach Career Development Assistant Professor of Chemistry
Thesis Advisor

Cargo Delivery into Gram-negative Bacteria via Enterobactin Uptake Machinery

By
Tengfei Zheng

Submitted to the Department of Chemistry on May 5, 2014 in partial fulfillment of the requirements for the Degree of Doctor of Philosophy in Biological Chemistry

Abstract

Chapter 1. Introduction to Iron Homeostasis and Siderophores

Iron is an essential nutrient for almost all living organisms. This Chapter presents an overview of iron homeostasis in human and bacteria, as well as the biology and chemistry of siderophores and siderophore conjugates. Siderophores are small-molecule iron chelators synthesized by bacteria for scavenging iron from the environment. Their iron-binding properties, structures, transport machineries and biosynthesis are discussed with a focus on enterobactin and salmochelins, which are the two siderophores studied in this thesis. The notion of conjugating functional molecules to siderophores has been actively studied for decades. The syntheses and applications of siderophore conjugates are summarized, with an emphasis on siderophore-antibiotic conjugates. New antimicrobial strategies targeting bacterial iron acquisition are also described. A summary of project goals and thesis organization is presented at the end of this Chapter.

Chapter 2. Siderophore-mediated Cargo Delivery to the Cytoplasm of *Escherichia coli* and *Pseudomonas aeruginosa*: Syntheses of Monofunctionalized Enterobactin Scaffolds and Evaluation of Enterobactin-cargo Conjugate Uptake

This Chapter describes the design and syntheses of monofunctionalized enterobactin (Ent, L- and D-isomers) scaffolds. A family of ten Ent-cargo conjugates is synthesized to probe the extent to which the Gram-negative ferric Ent uptake and processing machinery recognizes, transports, and utilizes derivatized

Ent scaffolds. The delivery of Ent-cargo conjugates is evaluated by a series of growth recovery assays. The results demonstrate that the *Escherichia coli* K12 and *Pseudomonas aeruginosa* PAO1 Ent transport machinery identifies and delivers select Ent-cargo conjugates to the cytoplasm, and *P. aeruginosa* PAO1 exhibits greater promiscuity than *E. coli* K12 for the uptake and utilization of the conjugates. This work affords a new native siderophore platform amendable for synthetic modification and cargo attachment. It also indicates that cargo size affects the delivery efficiency, which influences the conjugate design for Ent-mediated delivery strategies described in the following Chapters.

Chapter 3. Enterobactin-Mediated β-Lactam Delivery into Gram-negative Bacteria

The design, synthesis, and characterization of two enterobactin-antibiotic conjugates, where the β-lactam antibiotics ampicillin (Amp) and amoxicillin (Amx) are linked to a monofunctionalized enterobactin scaffold via a stable polyethyleneglycol linker are reported. Under conditions of iron limitation, these siderophore-modified antibiotics provide greatly enhanced antibacterial activity compared to the parent β-lactams against *Escherichia coli* strains that include several pathogens. The mechanism of the antimicrobial activity is probed and the results reveal that the improvement is due to Ent-mediated delivery. Strain-specific killing and faster time-kill kinetics are also observed for the conjugates. These studies demonstrate that the native enterobactin platform provides a means to effectively deliver antibacterial cargo across the outer membrane permeability barrier of Gram-negative pathogens that utilize enterobactin for iron acquisition.

Chapter 4. Stability Evaluation of Acyloxymethyl/Acyloxyethyl Ester Linker for the Design of Enterobactin-fluoroquinolone Conjugates

Fluoroquinolones are widely used antibiotics that target DNA gyrase. Prior studies with siderophore-fluoroquinolone conjugates suggest that a release step is required following cytosolic entry for the conjugates to exhibit antimicrobial activity. We design and synthesize enterobactin-fluoroquinolone conjugates harboring several acyloxymethyl/acyloxyethyl ester-based labile linkers and the stability of these likers and the conjugates are studied. These linkers exhibit relatively short half-lives and afford premature release of the antibiotics under our experimental conditions, which renders them not suitable for siderophore-based antibiotic delivery. This conclusion is also supported by the Ent-independent antimicrobial activity observed for the enterobactin-fluoroquinolone conjugates harboring the labile linkers.

Appendix 1. Chemoenzymatic Syntheses of Enterobactin-antibiotic Conjugates and Studies of Antimicrobial Activity

In this Appendix, cargo attachment to enterobactin by using chemoenzymatic reactions is described. This approach affords conjugates containing a 10-mer peptide as the linker between enterobactin and the cargo. A series of enterobactin conjugates harboring antimicrobial peptides and fluoroquinolone antibiotics are reported, and their antimicrobial activity against *E. coli* is evaluated. Unfortunately, none of these conjugates afford enhanced activity compared to the unmodified antimicrobial agents, which may result from impropriate cargo selection or linker design.

Appendix 2. NMR, HPLC and UV-Vis Characterizations of the Reported Compounds.

Thesis Supervisor: Professor Elizabeth M. Nolan

Title: Pfizer-Laubach Career Development Assistant Professor of Chemistry

To Yikai, Yueyang, Mom, Dad and Gram

Acknowledgement

The past five years has been a life-changing time for me. I have to admit that at the beginning of my Ph.D. journey, I was not sure where this degree would take me or even why I started it. But now I feel very grateful that I made a good choice, and I am really lucky to meet all the people who helped me, educated me and shared with me their enthusiasm, talent and diligence along the way. I would like to take this chance to thank all of them.

First I want to thank my advisor Liz, who shaped me from a college student to a mature researcher. As the first graduate student in the Nolan lab, I had a unique opportunity to learn from Liz about building a lab and starting projects from scratch. Liz spent lots of her precious time to educate me on experimental techniques, critical thinking, presentation skills and scientific writing, with patience as well as high standards, which equipped me to be a qualified scientist. Her rigorous attitude to science and persistent efforts towards success deeply influenced me, and will keep influencing me for the rest of my life.

I also want to thank Professor Barbara Imperiali and Professor JoAnne Stubbe for serving as my thesis committee members and the insightful scientific discussions we had during our meetings.

It is my pleasure to work with (literally) all the former and present Nolan lab members. I still vividly remember the first year when only Yoshi, Piotr and I were the 'permanent residents' in the big shining new lab, opening boxes. Yoshi and Piotr always helped me with their best efforts and encouraged me with their warm hearts, which supported me through the difficult project launching period. As the lab grew year by year, I met more and more great people. Megan and Haritha joined the lab the second year and both of them like singing and talking, which made the lab more fun and loud. Megan's optimistic attitude and Haritha's kindness and persistence impressed me. Phoom and Andy arrived later and accompanied me as synthetic folks. I appreciate Phoom's loyal interest in my research project from the beginning. I enjoy our collaboration now, and I am sure that he will make this project proceed well in the future. Andy gave me lots of good advice in organic synthesis and in life. I also want to thank Joshua for helpful scientific discussions. I appreciate the frank chatting with Toshiki and his efforts of trying to teach me how to party and dance. Jill shared her microbiology expertise as well as motherhood skills with me. The 'European group', Fabien, Julie and Simone, reminded me to enjoy life outside of lab.

I feel really lucky to have the opportunity to mentor Justin, a very talented MIT undergraduate. He worked with me for more than two years and made a great contribution to the first publication of my project. I will never forget his big smile no matter what happens and his hard work. Iulia, an undergraduate at University of Pennsylvania worked with me during summer 2013 and helped me prepare

many important synthetic intermediates. Other undergraduates, including Andrea, Shion, Lisa, Leann, I-ling and Hope brought the lab joy and fresh ideas.

The salmochelin work in my thesis was possible because of our collaboration with Professor Manuela Raffatellu at UC Irvine and her graduate student Martina Sassone-Corsi kindly helped us make all the mutant bacteria strains. We shared our research data and had great discussions about science. I want to thank Professor Steve Lippard to allow me using the IR and other experimental instruments in his lab. And many Lippard Lab members, including Justin, Semi, Mik, Victor and Yaorong helped me set up experiments and lent me chemicals. During the first few years I also bothered all our fifth floor neighbors, the Klibanov Lab, the Pentelutte Lab, the Stubbe Lab and the Imperiali Lab, for using instruments, borrowing reagents and asking suggestions, and they all helped me without any hesitation. I feel privileged to study in such a collaborative environment.

My classmates, especially Vinita and Jingnan, have been supporting me through the whole five years. We went through all the tests and exams together, helped each other with our best efforts, shared all the laughs and tears, and they become my lifelong friends. Marco helped me several times to prepare nice pictures of protein structures. Together with Michael, Ken, Yifeng, Jeff and Hongik, they all provided valuable suggestions when I prepared for my oral exams. Older students Stephanie, Jen and Michelle also gave me tips for surviving the Ph.D. I wish them all the best.

I want to acknowledge Professor John Dolhun for giving me the opportunity to teach the IAP undergraduate course 5.301 several times, where I met my undergraduate mentee Justin, as well as many other great freshmen who became my good friends afterwards. John and his wife's kindness and support for me and my family are greatly appreciated. I also want to thank Dr. Gang Liu for fixing our lab instruments and giving advice in my study and life.

Before coming to MIT, I studied a year in Professor Steve Bruner's lab in Boston College. Steve is a great advisor and he keeps supporting me even after I moved to MIT. I learned lots of basic biochemistry techniques in this one year period and all the Bruner lab members helped me unreservedly. I want to express my acknowledgement to all of them.

I would not be able to get where I am without my husband Yikai. His unconditional love makes every single day happy and fruitful. He is also a great scientist and I enjoyed the discussions about our research over dinners, during walking and when watching TV. I am grateful for the birth of our son Yueyang, who brightens our life and reminds us of the original human curiosity about the world, which is the driving force for the research we do. Lastly, I thank my grandma who brought me up, and my parents, for everything they have done for me, for making me who I am and for their understanding and support. I dedicate this thesis to them.

Table of Contents

Abstract..... 3

Dedication..... 6

Acknowledgements..... 7

Table of Contents..... 9

List of Tables..... 14

List of Schemes..... 15

List of Figures..... 17

Abbreviations..... 22

Chapter 1. Introduction to Iron Homeostasis and Siderophores..... 25

1.1 Iron Homeostasis in Humans and Bacteria..... 26

Iron Homeostasis in Humans: Acquisition, Transport, Storage and Regulation..... 26

Bacterial Iron Acquisition: Siderophores and Other Mechanisms of Iron Uptake..... 30

Iron Storage and Regulation in Bacteria..... 33

Battle for Iron between the Host and Microbes..... 35

1.2 Bacterial Siderophores..... 37

Siderophore-Iron Interaction: Selectivity, Affinity and Stability..... 37

Structures of Siderophores..... 40

Siderophore Tansportation: Systems Employed by Gram-positive and Gram-negative Organisms..... 43

Enterobactin and Salmochelins..... 46

1.3 Siderophore Conjugates and their Applications..... 52

Naturally Occurring Conjugates: Sideromycins..... 52

Synthetic Siderophore-Antimicrobial Conjugates..... 54

Siderophore-Based Iron Sensors..... 64

Siderophore Based Pathogen Detection..... 66

1.4 Other Antimicrobial Strategies Targeting Iron Assimilation..... 68
Chelation Therapy..... 68
Inhibiting Siderophore Biosynthesis..... 69
Disrupting Siderophore Export..... 73
1.5 Goals and Organization of the Thesis..... 74
References..... 75
Chapter 2. Siderophore-Mediated Cargo Delivery to the Cytoplasm of *Escherichia coli* and *Pseudomonas aeruginosa*: Syntheses of Monofunctionalized Enterobactin Scaffolds and Evaluation of Enterobactin-Cargo Conjugate Uptake..... 88
Introduction..... 89
Experimental Section..... 91
Reagents..... 91
General Synthetic Materials and Methods..... 97
General Liquid Chromatography and Mass Spectrometry Methods..... 92
Synthetic Procedures..... 92
General Microbiology Materials and Methods..... 110
Growth Recovery Assays..... 110
Fluorescence Titrations for Lipocalin 2 and Ent-Conjugates..... 111
Results and Discussion..... 111
Design of Monofunctionalized Ent Platform..... 111
Synthesis of Modified 2,3-Dihydroxybenzoic Acid..... 112
Syntheses of Monofunctionalized Ent Precursors..... 113
Design and Synthesis of Ent-Cargo Conjugates..... 115
Fe(III) Coordination of the Ent-Cargo Conjugates..... 119
Ent-cargo Conjugates Delivery to the *E. coli* Cytoplasm..... 119
Ent-cargo Conjugates Delivery to the *P. aeruginosa* Cytoplasm..... 125
Binding of Ent-cargo Conjugates to Lipocalin 2..... 129

Summary and Perspectives..... 133

Acknowledgements..... 136

References..... 136

Chapter 3. Enterobactin-Mediated β-Lactam Delivery into Gram-negative Bacteria..... 141

Introduction..... 142

Experimental Section..... 143

Reagents..... 143

General Synthetic Materials and Methods..... 144

Synthetic Procedures..... 145

General Microbiology Materials and Methods..... 149

General Procedure for Antimicrobial Activity Assays..... 150

Antimicrobial Assays with β-lactamase Inhibitors..... 151

Antimicrobial Assays in the Presence of Exogenous Ent..... 151

Killing Kinetic Assays..... 151

Mixed-Species Assays..... 151

Antimicrobial Activity Assays in the Presence of Lipocalin 2..... 152

Cytotoxicity Assays..... 152

Results and Discussion..... 152

Design and Syntheses of Enterobactin-β-lactam Conjugates..... 152

Antimicrobial Activity of Ent-Amp/Ent-Amx Against *E.coli* K12..... 155

Ent-Amp/Amx and L-Ent Compete for FepA Recognition..... 159

The Ent-Amp/Amx β-lactam Warhead is Essential for Antimicrobial Activity..... 161

Antimicrobial Activity of Ent-Amp/Ent-Amx against Clinically-relevant *E.coli*..... 162

Time-Kill Kinetics of Ent-Amp and Ent-Amx against *E.coli* K12 and CFT073..... 166

D-Ent-β-lactam Conjugates do not Further Improve Antimicrobial Activity..... 167

The Enhanced Antibacterial Activity of Ent-Amp/Amx is Specific to *E. coli*..... 168

Ent-β-lactam Conjugates Exhibit Selective Activity against *E. coli* in Mixed Bacterial Cultures..... 173

Ent Competes with Ent-β-lactam Conjugates for Lipocalin 2 Binding..... 173

Ent-Amp Exhibits Low Cytotoxicity to Mammallian Cells..... 174

Summary and Perspectives..... 175

Acknowledgements..... 176

References..... 176

Chapter 4. Stability Evaluation of Acyloxymethyl/Acyloxyethyl Ester Linker for the Design of Enterobactin-fluoroquinolone Conjugates..... 182

Introduction..... 183

Experimental Section..... 184

General Materials and Methods..... 184

General Spectroscopic Methods..... 185

Synthetic Procedures..... 185

Antimicrobial Activity Assays..... 194

Stability Studies of the Ciprofloxacin Conjugates..... 222

MceD Hydrolysis Assay with Ent-ciprofloxacin Conjugates..... 195

Results and Discussion..... 195

Design of Ent-Antibiotic Conjugates with Acyloxymethyl Ester Linker via Olefin Metathesis. 195

Synthesis of Modified Antibiotics with Acyloxymethyl Ester Linked Olefin Groups..... 196

Olefin Cross Metathesis Screening for the Synthesis of Ent-antibiotic Conjugates..... 197

Design and Synthesis of Ent-Antibiotic Conjugates with Acyloxymethyl Ester Linker via Aldehyde-Amine Reductive Amination..... 199

Antimicrobial Activity of Ent-ciprofloxacin Conjugate **22**..... 202

Stability Study of the Acyloxymethyl Ester Linker and Linker Modification..... 203

Stability Study of Ciprofloxacin-acyloxyethyl-benzoic Acid Conjugate with Amide Linkage.. 206

Synthesis and Stability of Ent-Ciprofloxacin Conjugates with Acyloxyethyl Linker via Acid-amine Coupling..... 208

Antimicrobial Activity of Ciprofloxacin-Ent Conjugates with Acyloxyethyl Linker..... 210

Summary and Perspectives..... 213

Acknowledgement..... 216

References..... 216

Appendix 1. Chemoenzymatic Syntheses of Enterobactin-antibiotic Conjugates and Studies of Antimicrobial Activity..... 218

Introduction..... 219

Experimental Section..... 219

General Materials and Methods..... 219

General Spectroscopic Methods..... 220

Antimicrobial Activity Assays..... 220

General Method for MceIJ-catalyzed Conjugate Assembly..... 221

Synthetic Procedures..... 222

Fluorescence Study of FL-C_{10}E492-MGE..... 224

FepA Cloning, Overexpression and Purification..... 224

Results and Discussion..... 225

General Strategy for the Design of Enterobactin-antibacterial Conjugates..... 225

Synthesis and Activity Study of Enterobactin-antimicrobial Peptides Conjugates..... 226

Synthesis and Activity Study of Enterobactin-Amino Terminal Cu and Ni Binging Motif (ATCUN) Conjugates..... 227

Synthesis and Activity Study of Enterobactin-small Molecule Antibiotic Conjugates..... 227

Fluorescence Study of FL-C_{10}E492-MGE (7) 235

Over-expression and Purification of FepA..... 236

Summary and Perspective..... 237

Acknowledgement..... 238

Reference..... 238

Appendix 4. NMR, HPLC, and UV-Vis Characterizations of Reported Compounds..... 240

List of Tables

Chapter 1

Table 1.2.1 Properties of select siderophores produced by bacteria and fungi..... 40

Chapter 2

Table 2.1 Characterization of Ent-cargo conjugates..... 118

Table 2.2 Bacterial strains used in this study..... 120

Chapter 3

Table 3.1 Bacterial strains employed in this study..... 155

Table 3.2 Iron content of the assay media..... 157

Table 3.3 MICs of the Ent-β-lactam conjugates..... 165

Chapter 4

Table 4.1 Half-lives of the ciprofloxacin derivatives..... 205

Table 4.2 MIC values of ciprofloxacin-Ent conjugate against *E. coli*..... 211

Appendix 1

Table A1.1 Characterizations of the Ent-antimicrobial conjugates..... 228

Table A1.2 Minimal inhibitory concentrations (MIC) of the Ent-antimicrobial conjugates determined without DP..... 233

Table A1.3 The MIC of the Ent-antimicrobial conjugates determined in the presence of DP... 234

List of Schemes

Chapter 2

Scheme 2.1 Synthesis of C5-modified DHB building block..... 113

Scheme 2.2 Synthetic scheme of monofunctionalized Ent platform by a tandem coupling strategy..... 114

Scheme 2.3 Synthetic scheme of one-pot synthesis of monofunctionalized Ent scaffolds..... 115

Scheme 2.4 Syntheses of PEG-derivatized cargos..... 116

Scheme 2.5 Syntheses of Ent-cargo conjugates 117

Scheme 2.6 Synthesis of enterobactin-ciprofloxacin conjugate 117

Scheme 2.7 Syntheses of enterobactin-cargo conjugates by Click chemistry..... 119

Scheme 2.8 Synthesis of Ent-cyclohexane 132

Chapter 3

Scheme 3.1 Syntheses of Ent-β-lactam conjugates 154

Scheme 3.2 Syntheses of hydrolyzed Ent-β-lactam conjugates 154

Chapter 4

Scheme 4.1 Syntheses of antibiotic-alkenes with acyloxymethyl ester linkages..... 196

Scheme 4.2 Proposed syntheses of Ent-antibiotics conjugates through olefin cross metathesis. 197

Scheme 4.3 Proposed synthesis of Ent-ciprofloxacin conjugate through olefin cross metathesis..... 199

Scheme 4.4 Synthesis of amine-modified ciprofloxacin with acyloxymethyl ester linkage..... 200

Scheme 4.5 Synthesis of Ent-ciprofloxacin conjugates via reductive amination..... 201

Scheme 4.6 Syntheses of ciprofloxacin-acyloxyethyl linker..... 206

Scheme 4.7 Syntheses of ciprofloxacin-acyloxyethyl-benzoic acids..... 207

Scheme 4.8 Syntheses of Ent-ciprofloxacin conjugates with acyloxyethyl linker via acid-amine coupling..... 209

Appendix 1

Scheme A1.1 Synthesis of penicillin-C_{10}E492..... 229

Scheme A1.2 Synthetic route for cipro/levofloxacin-C_{10}E492-MGE..... 230

List of Figures

Chapter 1

Figure 1.1.1	Fenton reaction catalyzed by iron and generates toxic hydroxyl radicals.....	26
Figure 1.1.2	Iron uptake by intestinal enterocytes.....	27
Figure 1.1.3	Transferrin receptor (TfR) mediated ferric transferrin uptake.....	28
Figure 1.1.4	Regulation of iron homeostasis by hepcidin.....	29
Figure 1.1.5	Heme uptake machinery of *S. aureus*.....	32
Figure 1.1.6	Trasnferrin (Tf) uptake machinery of *N. meningitidis*.....	33
Figure 1.1.7	Crystal structure of *E. coli* bacterioferritin and Dps.....	34
Figure 1.1.8	Fur regulation of iron acquisition genes.....	35
Figure 1.1.9	Crystal structure of Lcn2 with Fe-Ent modeled in the binding pocket.....	37
Figure 1.2.1	Structures of the commonly used iron-binding ligands in siderophores.....	38
Figure 1.2.2	Structures of [Fe(ferrioxamine B)], [Fe(ferrichrome)], [Fe(yersiniabactin)]$^{-}$, and $[V(enterobactin)]^{2-}$ determined by X-ray crystallographic analysis.....	39
Figure 1.2.3	Structures of selected siderophores.....	42
Figure 1.2.4	Model of the cell wall structures of Gram-positive and Gram-negative bacteria...	43
Figure 1.2.5	Crystal structure of *E. coli* enterobactin receptor FepA.....	44
Figure 1.2.6	Enterobactin (Ent) uptake system from *E. coli*.....	45
Figure 1.2.7	Biosynthesis of Ent by the EntABCDEF assembly line.....	47
Figure 1.2.8	Structure of representative salmochelins.....	49
Figure 1.2.9	Chemical synthesis of Ent.....	49
Figure 1.2.10	Representative synthetic analogs of Ent.....	50
Figure 1.2.11	Chemical synthesis of salmochelins.....	50
Figure 1.2.12	Salmochelin synthesis and uptake machinery.....	52

Figure 1.3.1	Structure of naturally occurring siderophore-antimicrobial conjugates albomycin, salmycin, ferrimycin A1 and MccE492m	53
Figure 1.3.2	Model of Gram-negative bacterial cell wall with nutrient passage pathway shown	55
Figure 1.3.3	Core structures of the β-lactam antibiotics used in siderophore conjugates synthesis	56
Figure 1.3.4	Structures of representative siderophore-β-lactam conjugates	58
Figure 1.3.5	Structures of representative siderophore-fluoroquinolone conjugates	60
Figure 1.3.6	Structures of representative siderophore-antibiotic conjguates	62
Figure 1.3.7	Structures of representative siderophore- fluorophore conjugates	64
Figure 1.3.8	Iron detection based on lanthanide displacement	66
Figure 1.3.9	Pathogen detection using siderophore-immobilization on glass chips	67
Figure 1.3.10	(A) Isolation of siderophore-binding proteins by using biotin-siderophore conjugates. (B) Structure of biotinylated petrobactin	68
Figure 1.4.1	Structures of synthetic iron chelators in clinical practice	69
Figure 1.4.2	Reaction mechanism of salicylate synthase	70
Figure 1.4.3	Inhibitors of salicylate synthase	70
Figure 1.4.4	Activation of salicylate catalyzed by adenylation enzymes	71
Figure 1.4.5	Inhibitors of salicylate adenylation enzymes	72
Figure 1.4.6	Inhibitors of *P. aeruginosa* enzyme PvdQ and non-NRPS enzyme SbnE and AsbA	73

Chapter 2

Figure 2.1	Siderophores and siderophore transport machinery relevant to this work	90
Figure 2.2	Enterobactin substituted at the C5 position	91
Figure 2.3	Structure of Microcin E492m	112
Figure 2.4	UV-spectra of represented apo/Fe-bound Ent and Ent-cargo conjugate	120

Figure 2.5 Growth recovery assay of *E. coli fes-*, *entA-*, and *fepA-* with Ent..... 121

Figure 2.6 Comparative effects of Ent-cargo conjugates on bacterial cell growth..... 122

Figure 2.7 Growth recovery assays of *E. coli entA-* with various concentrations of Ent and Ent-cargo conjugates..... 123

Figure 2.8 Growth recovery assays of *E. coli fes-*, *entA-* and *fepA-* with selected Ent-cargo conjugates..... 124

Figure 2.9 Competition assay of Ent-vancomycin conjugate and Ent..... 125

Figure 2.10 Growth recovery assay of *P. aeruginosa* (*pvd-*, *pch-*) with Ent, D-Ent and Ent-cargo conjugates..... 127

Figure 2.11 Growth recovery assay of *P. aeruginosa* PAO1 K407 (*pvd-*, *pFr-*) with Ent and selected Ent-cargo conjuate..... 128

Figure 2.12 Fluorescence spectra of Lcn2 titrated with $[Fe(MGE)]^{3-}$ in the absence or presence of ubiquitin..... 130

Figure 2.13 Fluorescence spectra of Lcn2 titrated with Fe(III) complexes of Ent, MGE, DGE and selected Ent-cargo conjugates..... 131

Figure 2.14 UV-Vis spectra and growth recovery assay of Ent-cyclohexane conjugate..... 133

Figure 2.15 Fluorescence spectra of Lcn2 titrated with Fe(III) complex of Ent-cyclohexane conjugate..... 133

Chapter 3

Figure 3.1 Structure of enterobactin , Ent-cargo conjugate for cargo delivery applications, and the two β-lactam antibiotic cargos..... 142

Figure 3.2 Antimicrobial activity assay of *E. coli* K12 with Ent-Amp and Ent-Amx..... 156

Figure 3.3 Ent uptake machinery of *E. coli* and possible fates of Ent-β-lactam conjugates.... 157

Figure 3.4 Antimicrobial activity assay of *E. coli* K12 and its mutants with Ent-Amp/Amx and Amp/Amx..... 158

Figure 3.5 Competition assays of Ent-β-lactam conjugates with Ent and Antimicrobial activity of apo or Fe(III) loaded Ent-β-lactam conjugates against wild type *E. coli* K12..... 159

Figure 3.6 Antimicrobial activity of the Ent-β-lactam conjugates against β-lactamase expressing strain..... 160

Figure 3.7 Antimicrobial activity of the Ent-Hydro-Amp/Amx against *E. coli* K12..... 161

Figure 3.8 Antimicrobial activity of the Ent-β-lactam conjugates against clinical isolated *E. coli* strains..... 163

Figure 3.9 Antimicrobial activity of the Ent- Hydro-Amp/Amx conjugates against *E. coli* CFT073..... 164

Figure 3.10 Killing kinetics of the Ent-β-lactam conjugates and the β-lactams against *E. coli* K12 and CFT073..... 166

Figure 3.11 Antimicrobial activity of D-Ent-Amp and D-Ent-Amx against *E. coli* CFT073 and 25922..... 167

Figure 3.12 Antimicrobial activity of the Ent-β-lactam conjugates against non-*E. coli* strains.. 169

Figure 3.13 Represented images of the mixed-culture assays..... 172

Figure 3.14 *E. coli* CFT073 growth with siderochalin and/or Ent-Amp..... 174

Figure 3.15 Cytotoxicity studies of Ent-Amp, Amp, Ent and DMSO against T84 cells..... 175

Chapter 4

Figure 4.1 Structure of a pyochelin-ciprofloxacin conjugate with labile linker and the general model of Ent-antibiotic conjugates with acyloxymethyl esters..... 184

Figure 4.2 Ruthenium-based olefin metathesis catalysts used for screening..... 197

Figure 4.3 HPLC trace of purified Ent-Ciprofloxacin conjugate..... 202

Figure 4.4 Antimicrobial activity of Ent-Ciprofloxacin conjugate and ciprofloxacin against *E. coli* K12, H1876, and *ent*-..... 203

Figure 4.5 HPLC traces of the ciprofloxacin conjugates with acyloxymethyl/ethyl linkers.... 204

Figure 4.6 Proposed degradation mechanism of Ent-Ciprofloxacin conjugate..... 205

Figure 4.7 HPLC traces of the ciprofloxacin-acyloxyethyl linker conjugates with amide or amine connection for stability study..... 208

Figure 4.8 HPLC traces of the Ent-ciprofloxacin conjugates..... 210

Figure 4.9 *E. coli ent-* growth in the presence of Fe-preloaded Ent-Ciprofloxacin conjugate and D-Ent..... 213

Figure 4.10 HPLC traces of Ent-Ciprofloxacin conjugate treated with or without MceD..... 213

Figure 4.11 Representative fitted degradation curves of ciprofloxacin conjugates..... 215

Appendix 1

Figure A1.1 General design of the Ent-antimicrobial conjugates..... 226

Figure A1.2 Analytical HPLC traces for ciprofloxacin-C_{10}E492-MGE and levofloxacin-C_{10}E492-MGE..... 230

Figure A1.3 Recovery assay for Ent and relative conjugates..... 231

Figure A1.4 Structure and fluorescent spectra of FL-C_{10}E492-MGE in the absence or present of Fe(III) compared to FL-C_{10}E492 and fluorescein..... 235

Figure A1.5 SDS-Page of purified illustrating the shift on the FepA band upon heating..... 236

Abbreviations

6-APA	6-aminopenicillic acid
Amp	ampicillin
AMP	adenosine monophosphate
Amx	amoxicillin
ANL	amino naphthalimide
Aq	aqueous
ATCC	American Type Culture Collection
ATCUN	amino terminal Cu and Ni binging motif
ATP	adenosine triphosphate
B. cereus	*Bacillus cereus*
Boc	*tert*-butyloxycarbonyl
BSA	bovine serum albumin
CFU	colony forming units
Cipro	ciprofloxacin
DCM	dichloromethane
DFO	desferrioxamine
DGE	diglucosylated enterabactin
DHB	2,3-Dihydroxybenzoic acid
DIPEA	*N*,*N*-diisopropylethylamine
DMAP	4-dimethylaminopyridine
DMF	dimethylformamide
DMSO	dimethyl sulfoxide
DP	2,2'-dipyridyl
DTT	dithiothreitol
E. coli	*Escherichia coli*
EDC	1-ethyl-3-(3-dimethylaminopropyl) carbodiimide
EDTA	ethylenediaminetetraacetic acid
ELISAs	enzyme-linked immunosorbent assays
Ent	enterobactin
ESI	electrospray ionization
FL	fluorescein
FT-ICR-MS	Fourier Transform Ion Cyclotron Resonance Mass Spectrometer
FT-IR	Fourier transform infrared spectroscopy
GDHB	5-glucosyl-2,3-dihydroxylbenzoic acid
HATU	1-[bis(dimethylamino)methylene]-1H-1,2,3-triazolo[4,5-b]pyridinium 3-oxid hexafluorophosphate
HEPES	4-(2-hydroxyethyl)-1-piperazineethanesulfonic acid
HO-1	heme oxygenase 1
HOAT	1-hydroxy-7-azabenzotriazole
HPLC	high-performance liquid chromatography

HRMS	high resolution mass spectrometry
IC_{50}	half maximal inhibitory concentration
IREs	iron response elements
IRP1	iron regulatory protein 1
IRP2	iron regulatory protein 2
LB	Luria Broth
LC-MS	liquid chromatography–mass spectrometry
Lcn2	lipocalin 2
Levo	levofloxacin
LMCT	ligand-to-metal charge transfer
M. tuberculosis	*Mycobacterium tuberculosis*
Mcc	microcin
MeCN	acetonitrile
MeOH	methanol
MGE	monoglucosylated enterabactin
MHB	Mueller Hinton Broth
MIC	minimum inhibitory concentration
MSI	Magainin-I
MTT	3-[4,5-dimethylthiazol-2-yl]-2,5 diphenyl tetrazolium bromide
NaAsc	sodium ascorbate
NADPH oxidase	nicotinamide adenine dinucleotide phosphate-oxidase
NBD	nitrobenz-2-oxa-1,3-diazole
NMR	nuclear magnetic resonance
NRPS	non-ribosomal peptide synthetases
P. aeruginosa	*Pseudomonas aeruginosa*
PB	poor broth
PBPs	penicillin binding proteins
PBS	phosphate-buffered saline
PC	potassium clavulanate
pch	pyochelin
PDMS	polydimethylsiloxane
PEG	polyethyleneglyco
PGI	Protegrin-I
Piv	pivalate
PMB	pentamethyl benzene
pvd	pyoverdine
PyAOP	(7-azabenzotriazol-1-yloxy)tripyrrolidinophosphonium hexafluorophosphate
PyBOP	benzotriazol-1-yl-oxytripyrrolidinophosphonium hexafluorophosphate
QDs	quantum dots
RT	room temprature
RT-PCR	reverse transcription polymerase chain reaction
S. aureus	*Staphylococcus aureus*

SB	sulbactam
SDS-PAGE	sodium dodecyl sulfate-polyacrylamide gel electrophoresis
S. Typhimurium	*Salmonella enterica* Typhimurium
TB	terrific broth
TBAF	tetra-*n*-butylammonium fluoride
TBS	*tert*-butyldimethylsilyl
TBSCl	*tert*-butyldimethylsilyl chloride
TBTA	tris[(1-benzyl-1H-1,2,3-triazol-4-yl)methyl]amine
TCEP	tris(2-carboxyethyl)phosphine
Tf	transferrin
TFA	trifluoroacetic acid
TfR	transferrin receptor
TGE	triglucosylated enterabactin
THF	tetrahydrofuran
TLC	thin-layer chromatography
TMS	trimethylsilyl
TMSCl	trimethylsilyl chloride
Tris	tris(hydroxymethyl)aminomethane
UDP-glucose	uridine diphosphate glucose

Chapter 1

Introduction to Iron Homeostasis and Siderophores

Part of the text and figures are published in *Metallomics,* **2012**, *24*, 866-880.

1.1 Iron Homeostasis in Humans and Bacteria

Iron is an essential metal for almost all living organisms. It is able to cycle between ferric (Fe^{3+}) and ferrous (Fe^{2+}) oxidation states readily and can therefore serve as a redox catalyst by donating or accepting electrons. Iron-containing proteins and enzymes fulfill many critical biological functions, including oxygen transport and storage (e.g., hemoglobin and myoglobin), metabolic processes like respiration (e.g., cytochromes), syntheses of key metabolites (e.g., ribonucleotide reductase and NADPH oxidase) and signaling (e.g., nitric oxide synthase).[1] Despite the vital nature of this element, "free" iron causes cellular toxicity by the Fe^{2+}-triggered Fenton reaction (Figure 1.1.1), which generates harmful reactive oxygen species including hydroxyl radicals that damage proteins, lipids and DNA. Therefore in biological organisms, iron is almost always associated with prosthetic groups (e.g., heme and Fe-S cluster) or coordinated by amino acid side chains of proteins. Moreover, the acquisition, storage and transport of iron are highly regulated in living organisms to maintain homeostasis and constrain its toxicity.

$$Fe^{3+} + {}^{\bullet}O_2^- \longrightarrow Fe^{2+} + O_2$$

$$Fe^{2+} + H_2O_2 \longrightarrow Fe^{3+} + OH^- + {}^{\bullet}OH$$

$$\text{Net reaction: } {}^{\bullet}O_2^- + H_2O_2 \longrightarrow O_2 + OH^- + {}^{\bullet}OH$$

Figure 1.1.1. Fenton reaction catalyzed by iron and generates toxic hydroxyl radicals.[2]

Iron Homeostasis in Humans: Acquisition, Transport, Storage and Regulation. Iron is one of the most abundant elements in the Earth's crust, although most living organisms face iron scarcity due to its low solubility in the ferric form under biological conditions (e.g., 10^{-18} M at neutral pH). In response, humans and other mammals evolved efficient mechanisms to conserve and internally recycle iron. Approximately 4-5 g of iron is in a healthy human adult body, most of which is in erythrocyte hemoglobin (~2-3 g), and only 1-2 mg of the total iron is lost daily.[3] Humans absorb iron in the heme-bound form more efficiently, which usually comes from meat, poultry and fish.[4] Plant-based foods contain iron complexed in insoluble forms, and these iron is poorly absorbed.[5] Iron uptake from the diet takes place in the proximal duodenum by the enterocytes (Figure 1.1.2). During digestion, iron can be partially released from heme or other protein complexes. This inorganic iron is reduced to ferrous ion by ferric reductases expressed in the brush-border side of the enterocytes, and subsequently transported by a divalent metal transporter DMT1 (also known as Nramp2) into the cytosol.[6] Heme- and ferritin- bound

iron are absorbed through other less understood mechanisms.[7] Heme iron is thought to be released by heme oxygenase 1 (HO-1), yielding ferrous iron.[1] Following absorption, ferrous iron is used in cellular processes, stored in ferritin, or exported through basolateral membrane by the iron exporter ferroportin (the only known human iron exporter in all cell types).[8] Copper-containing ferroxidases are also required for iron export,[9] most likely oxidizing Fe(II) to Fe(III) following export. Ferric iron is immediately bound by transferrin in the plasma for transport to other cells.

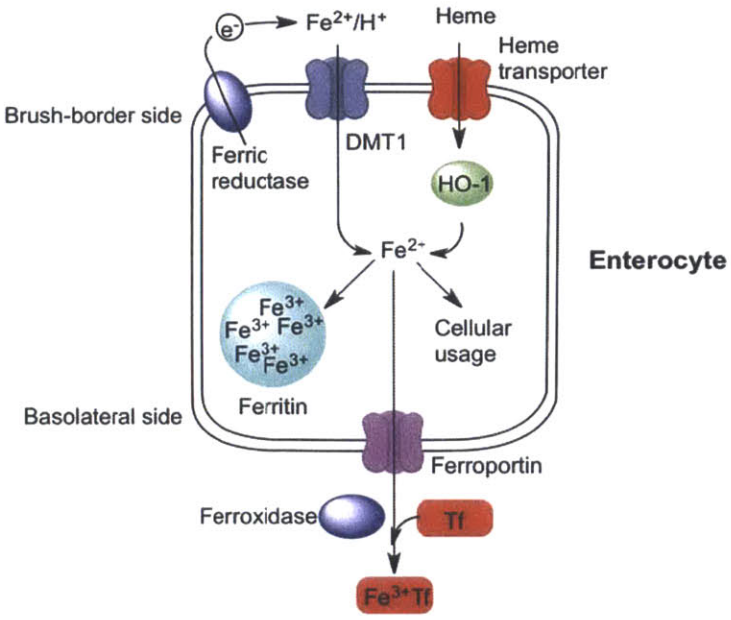

Figure 1.1.2. Iron uptake by intestinal enterocytes. Dietary ferric iron is reduced to ferrous iron prior to transport into the enterocyte by DMT1. Heme is imported by separate transporters, and heme oxygenase 1 (HO-1) degrades heme to releases iron. Ferrous iron can be used in cellular processes, stored in ferritin or exported to the plasma by ferroportin. Immediately following export, ferrous iron is oxidized by ferroxidase and bound to transferrin (Tf).

Transferrin (Tf) is a 79-kDa glycosylated protein and is the main iron carrier protein in the plasma. It can bind two ferric ions with a binding affinity of 10^{23} M^{-1} (K_a) at pH 7.4.[10] Upon reaching the target cell, Tf interacts with the transferrin receptor (TfR), and the complex is internalized by the cell via endocytosis (Figure 1.1.3). The acidic environment in the endosome causes the release of iron and the Tf-TfR complex is recycled to the cell surface. Ferrireductase STEAP3 in the endosome reduces the ferric iron unloaded from Tf to ferrous iron, which is exported to the cytosol by DMT1 for cellular use or

storage.[11] When plasma iron concentration exceeds the capacity of Tf, iron can also be complexed with acetate, citrate and albumin. The uptake mechanisms for those species are independent from the TfR. Besides inorganic iron, iron-containing heme and hemoglobin present in plasma are bound by hemopexin and haptoglobin, respectively, for delivery and recycling.[1]

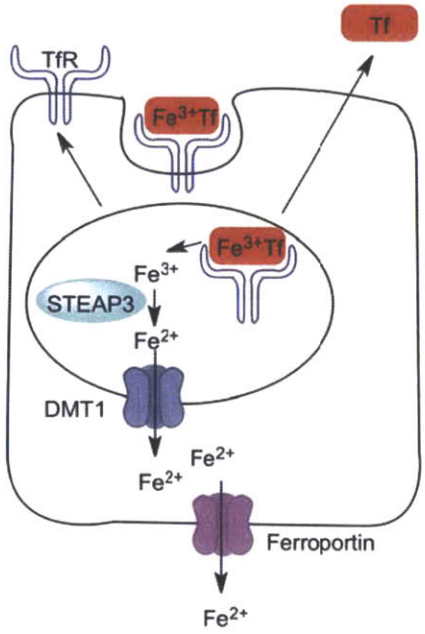

Figure 1.1.3. Transferrin receptor (TfR) mediated ferric transferrin uptake. The Fe-Tf/TfR complex is acquired by endocytosis. The acidic environment in endosome triggers the release of ferric iron from Tf, which is then reduced by STEP3 and exported to cytosol by DMT1. Tf and TfR are recycled.

Intracellular iron is used in heme and Fe-S cluster syntheses, which involve the mitochondria, or incorporated into metalloenzymes. Unused iron is stored in ferritin, which is a spherical heteropolymeric protein with a molecular weight of 450 kDa. Ferritin is composed by 24 units of heavy and light subunits, and it can store up to 4,500 iron atoms in its interior.[12] Ferrous ions released from the endosome are delivered to ferritin by chaperones (e.g., poly rC-binding protein 1),[13] oxidized by the ferroxidase domain of ferritin, and stored as a ferrihydrite or amorphous ferric phosphate core in the center cavity of ferritin. Release of iron from ferritin is not well understood. Proposed release mechanisms include gated pores, autophagy or lysosomal degradation of ferritin.[1]

Iron homeostasis in humans is tightly regulated at systemic and cellular levels. Systemically, the regulation is achieved by a hormone called hepcidin. Hepcidin is a cysteine-rich 25-aa peptide that is synthesized and secreted by hepatocytes and circulates in blood plasma.[14] Hepcidin acts by controlling

the membrane concentration of the iron exporter ferroportin post-translationally (Figure 1.1.4). Upon binding to ferroportin, hepcidin induces the endocytosis of the complex and ferroportin is degraded in lysosomes.[15] Because iron from dietary absorption, cellular storage, and recycling in macrophages needs to be exported by ferroportin, regulating ferroportin levels effectively controls the flux of iron into plasma and also the iron supply to all iron-consuming tissues. The transcription of the hepcidin gene in the liver is elevated with increased iron storage or plasma Fe-transferrin concentration, and upon inflammation. Elevated hepcidin levels decreases iron export via ferroportin and therefore decreases the iron concentration in plasma. In contrast, signals like accelerated erythropoiesis decrease hepcidin transcription, which allows more iron to be transported to the bone marrow (Figure 1.1.4).[1] On the cellular level, iron regulatory protein 1 and 2 (IRP1 and IRP2) control the cellular iron level post-transcriptionally. When cell is under iron depletion, IRPs exist in their apo-form, which bind to the iron response elements (IREs) in the mRNAs of proteins related to iron metabolism (e.g., ferritin and transferrin receptor) to enhance or prohibit protein translation.[16]

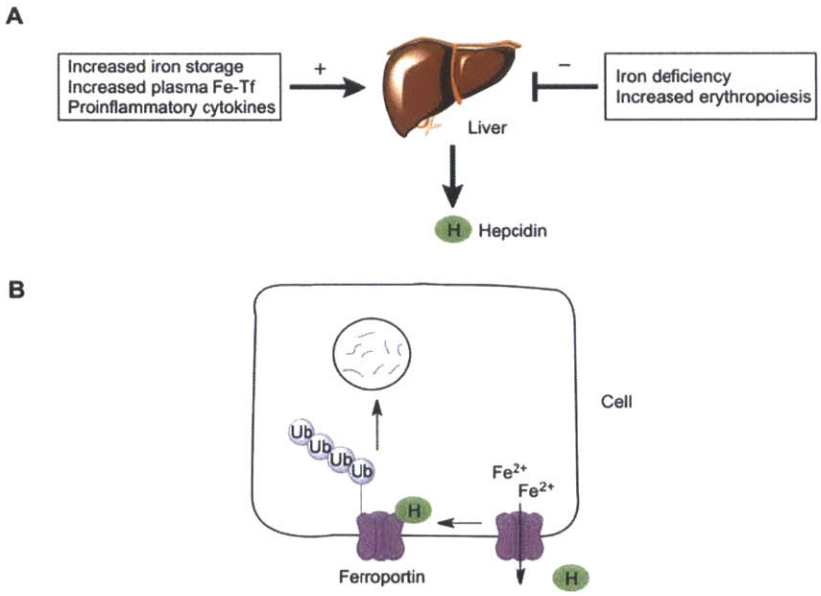

Figure 1.1.4. Regulation of iron homeostasis by hepcidin. A. Hepcidin production from hepatocytes is promoted with signals of increased iron storage, increased plasma Fe-Tf concentration or inflammatory cytokines like IL-6 and is inhibited with signals of iron deficiency or increased erythropoiesis. B. Hepcidin binds ferroportin and causes ubiquitination and degradation of ferroportin, which in turn decreases iron export.

Bacterial Iron Acquisition: Siderophores and Other Mechanisms of Iron Uptake. As for humans, iron is essential for most microorganisms and they face the challenge of limited iron availability in the environment. For pathogens, the iron scarcity is more pronounced because the host usually constrains the free iron levels tightly (e.g., 10^{-24} M in human serum)[17] and upon infection, enhanced iron-withholding is used as an innate immune response.[18] Therefore, microorganisms need highly efficient iron uptake systems.

The most well studied approach for bacterial iron uptake is through siderophore-mediated iron delivery. Siderophores are small-molecule ferric iron chelators (typically <1000 Da) produced by bacteria, fungi and plants under iron limited conditions. Siderophores coordinate iron with high binding constants (K_a) ranging from 10^{30} M^{-1} to 10^{49} M^{-1}, which allow them to solubilizing inorganic iron and outcompete with the host iron-binding proteins like transferrin.[19] Most siderophores are secreted into the environment, although some of them, like mycobactins from mycobacteria, are associated with the cell wall.[20] Ferric siderophores are recognized by specific receptors on bacterial cell membrane and internalized by dedicated proteins and enzymes. Within the bacterial cytosol, iron is released by either reduction of Fe(III) to Fe(II) or degradation of the siderophore. Different bacterial strains usually produce different siderophores, but many bacteria also have the receptors for xenosiderophores, which is an advantage when growing in the presence of other species. For example, human pathogen *Vibrio vulnificus* is able to use desferrioxamine B (**1**, Figure 1.2.3), a siderophore produced by *Streptomyces pilosus.* Therefore when treating iron overload diseases with deferoxamine, the patients face higher risk of *V. vulnificus* and other bacterial infections.[21] Because of their important role in iron assimilation, especially when bacteria colonize the hosts, many siderophores are considered as virulence factors.[22] The structures, iron-binding properties and transportation machineries of the siderophores are discussed in more detail in Section 1.2.

Besides siderophore-mediated ferric iron transport, ferrous iron uptake has also been described for bacteria. The first example of such systems was found in *E. coli*,[23] and later in many other species like *Salmonella*[24] and *Helicobacter pylori.*[25] Ferrous iron is more stable in anaerobic or acidic environments, and the genes encoding ferrous iron uptake machinery (e.g., *feoABC* and *efeUOB* in *E. coli)* are induced under such conditions.[26] In fact, mutation of the *feoB* gene in *E. coli* causes attenuated colonization in the mouse intestine, which may be due to its inability to uptake ferrous iron in the anaerobic mouse gut.[27] The mechanism of these ferrous iron uptake pathways are still under investigation. For example, within the *feoABC* system in *E. coli,* FeoB is a GTPase and thought to be the main energy-dependent transporter of Fe(II) in the cytosol membrane.[28] FeoA is a cytoplasmic protein that may interact with FeoB, although its function is not understood.[29] FeoC has been suggested to be a transcription regulator because of its helix-turn-helix structure.[30] Another type of inorganic iron

transporter is the metal transport protein dependent ABC system. These systems transport ferric iron directly, and are also used to transport other metals like Mn(II) and Zn(II). One example is the Sfu system of *Serratia marcescens*.[31] These ABC systems have been suggested to contribute to the virulence of some pathogenic bacteria.[32]

As most of the iron in the host is bound to heme or hemoproteins, bacterial pathogens have developed mechanisms to utilize heme directly. Heme uptake is achieved either by direct recognition of heme or heme-binding proteins by specific receptors or by hemophore-dependent systems.[33] A paradigm for the direct heme uptake system is the *S. aureus* iron-regulated surface determinate (Isd) system (Figure 1.1.5).[34] The Isd system contains cell surface receptors (IsdB and IsdH) that recognize hemoglobin and haptoglobin, cell wall shuttle proteins (IsdA and IsdC) that transfer heme to the cell membrane, ATP-binding cassette (ABC)-type transporters (IsdDEF) that internalize heme into the cytosol, and heme oxygenases IsdG and IsdI that degrade heme to iron and staphylobilin. Although *S. aureus* expresses other iron acquisition systems, including siderophore mediated machinery, heme was found to be the preferred iron source.[35] For hemophore-dependent systems, one example is the *Pseudomonas aeruginosa* Has system, in which a hemophore protein, HasAp, is secreted to the environment to steal heme from host hemoproteins. Next, it transfers the heme to the outer membrane receptor HasR, which is a TonB-dependent system, and an ABC type inner membrane transporter deliver the heme into the cytosol.[36] Gram-positive bacteria typically utilize the direct heme uptake machinery and Gram-negative bacteria employ the hemophore-mediated system as well.[37]

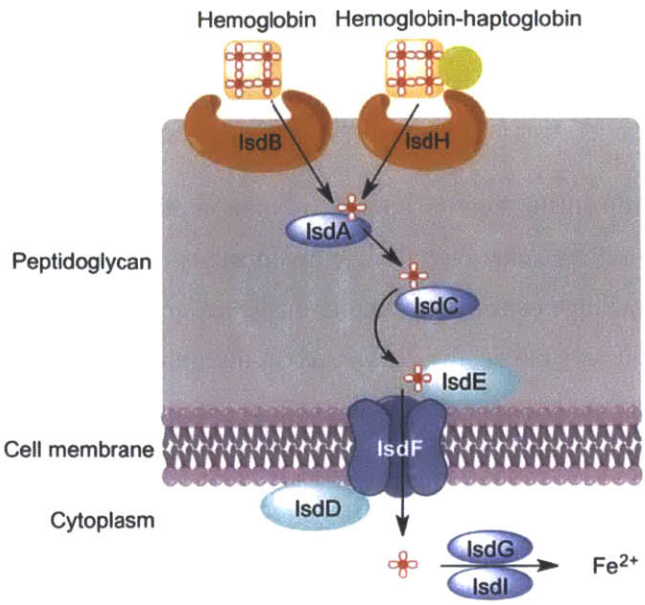

Figure 1.1.5. Heme uptake machinery of *S. aureus.* Heme is extracted from hemoglobin and transferred to the cell membrane by IsdA and IsdC. The ABC-type transporter IsdDEF delivers heme into cytoplasm where IsdG and IsdI degrade heme to release iron.

Transferrin (Tf) is the main iron-carrier protein in human plasma, and some pathogens have developed mechanisms to liberate iron from it by using specific transferrin receptors. *Neisseria meningitidis* encodes two transferrin receptors (TbpA and TbpB) which are located on the outer membrane. The receptors strip iron from Tf and release the apo Tf back to extracellular space. A periplasm ferric binding protein then transfers iron to the inner membrane where an ABC type transporter takes iron into the cytosol (Figure 1.1.6).[38] The structure of the TbpA-transferrin, TbpB transferrin and TbpA/TbpB/transferrin triple complex have been solved recently, revealing that an insertion of a helical element from TbpA into the transferrin iron-binding C loop induces iron release and transfer to the bacterial receptor.[39] The transferrin uptake machinery is important for the virulence of *Neisseria* spp.[40] Another iron-binding protein, lactoferrin, which is abundant in human neutrophils and plays important role in the innate immune system by lowering the iron concentration at the infection site,[41] has also been hijacked by bacteria. The lactoferrin uptake system is very similar to the Tf uptake system except that different receptors are used.[42]

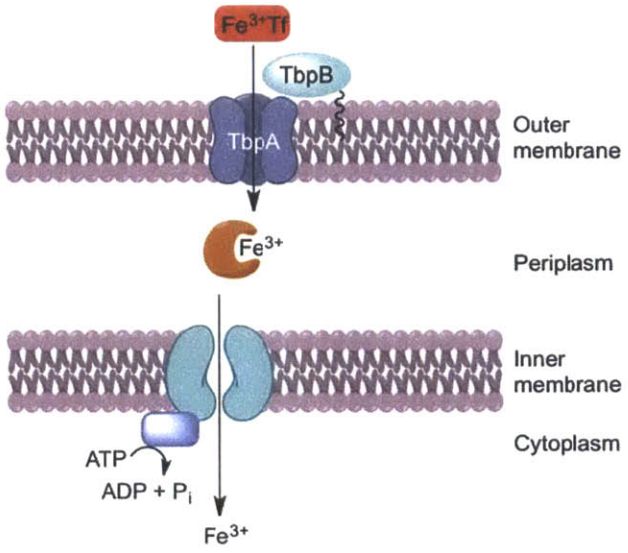

Figure 1.1.6. Transferrin (Tf) uptake machinery of *N. meningitidis*. Ferric iron is extracted from transferrin after binding to the outer membrane receptor. Periplasmic ferric binding protein then transfer Fe(III) to an ABC-type transporter on the inner membrane which delivers ferric iron into the cytoplasm.

Iron Storage and Regulation in Bacteria. Like humans, microorganisms also face the challenge of obtaining enough iron for normal biological activities and, at the same time, controlling the toxicity of iron by proper iron storage and regulation of iron uptake.

Three types of iron storage proteins are found in bacteria: ferritin, which is also found in eukaryotes, heme-containing bacterioferritin and a smaller Dps protein, which are specific for bacteria.[43] Ferritin and bacterioferritin have similar molecular assemblies. Both proteins are comprised of 24 subunits and form a spherical shape with a central cavity for iron storage (Figure 1.1.7).[44] What is unique about bacterioferritin is that it contains 12 heme molecules per 24-mer. The heme is proposed to facilitate reduction of the ferric iron core for releasing the metal.[45] Dps is a smaller protein (~250 kDa) comprised of 12 subunits (Figure 1.1.7). Its storage capacity is also lower (~500 iron atoms per 12-mer). Besides iron storage, Dps may have a more important role in protecting DNA from oxidative stress. Dps stands for DNA-binding proteins from starved cells. During iron storage, Dps uses H_2O_2 as the oxidant instead of O_2 at the ferroxidase centers, generating water rather than hydroxyl radical, which may contribute to its DNA protecting function.[46]

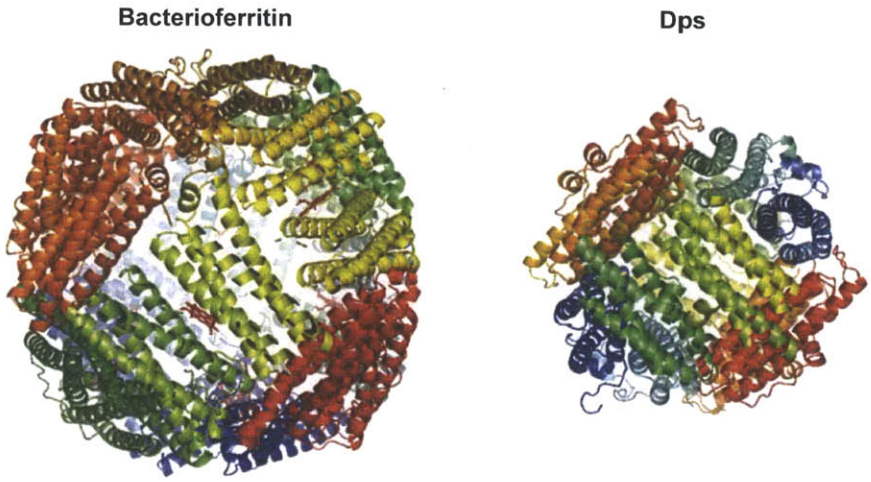

Figure 1.1.7. Crystal structure of *E. coli* bacterioferritin (left, heme is shown and labeled red) and Dps (right). (PDB 1BFR and 1DPS).

Iron regulation in bacteria is achieved mainly by iron-sensor proteins. In *E. coli*, the global regulator is the ferric-uptake regulator protein (Fur), and its homologs are found in many Gram-negative and some Gram-positive bacteria.[47] Fur controls more than 90 genes in *E. coli* on the transcriptional level, and functions primarily as a repressor. Fur exists as a homodimer, and each 17-kDa monomer can bind one regulatory ferrous iron. When the cellular iron concentration is high, Fur becomes iron-bound, which increases its affinity to its DNA binding site by ~1000-fold. Binding of the Fur protein blocks the RNA polymerases and thus inhibits the transcription of the downstream genes encoding iron uptake machineries and sideophore biosynthesis pathways (Figure 1.1.8).[48] Fur also regulates the expression of many genes indirectly. For example, Fe^{2+}-Fur represses a small regulatory RNA molecule RyhB, which is able to bind the mRNA sequence of iron-utilizing proteins and cause RNAase E-mediated degradation.[49] In this case, Fur acts as an indirect inducer. Examples of Fur acting as direct inducer are also reported.[50] Other divalent metal ions like Co(II), Mn(II) and Cu(II) can bind Fur competitively, although under physiological conditions the concentrations of these ions are much lower and reportedly do not affect the iron sensing of Fur.[51] It should be noted that the Fur regulation system is also important in oxidative stress response as it controls iron levels and affects many iron-containing enzymes that are involved in oxidative stress resistance.[2] Other iron-sensor proteins, e.g., IdeR in *Mycobacterium tuberculosis*,[52] operate in a similar mechanism as Fur, although they are genetically unrelated.

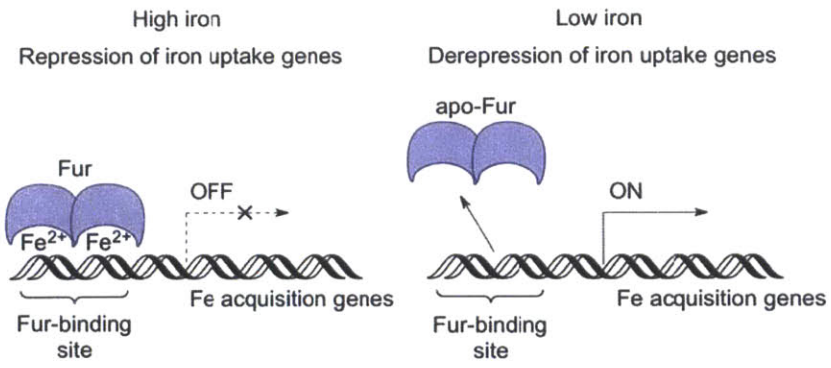

Figure 1.1.8. Fur regulation of iron acquisition genes. When cytosolic iron concentration is high, Fur becomes iron bound and it binds to the DNA, which prohibits the RNA polymerase binding and therefore turns of gene transcription. When cytosolic iron concentration is low, Fur is released from DNA and the downstream gene is expressed.

In some bacteria, quorum sensing was found to influence siderophore production as well as the regulation of iron-sensing proteins. Quorum sensing is a cell-density dependent signaling pathway that allows the bacterial cells to function in a coordinated manner in response to environmental change, and it can trigger biofilm formation and toxin production.[53] The siderophore pyochelin production in *P. aeruginosa* was decreased when the quorum sensing regulator *lasR* was mutated.[54] A similar affect has been reported for several other organisms including *V. harveyi*,[55] *V. alginolyticus*,[56] and *Actinobacillus actinomycetemcomitans.*[57] The detailed mechanism of how the quorum sensing pathway affects siderophore production remains to be elucidated.

Battle for Iron between the Host and Microbes. Iron is an essential nutrient for the host and microbes, and a battle for iron is always on-going at the host-pathogen interface. The human innate immune system has developed mechanisms to limit iron availability for invading microbes, which belongs to the defense mechanism often termed nutritional immunity.[58] At the same time, pathogens have evolved strategies to circumvent these iron-withholding mechanisms to acquire enough iron for their own physiological needs.

The two major components in the iron-related human immune response are lactoferrin and lipocalin 2 (Lcn2, also termed siderocalin or NGAL). Lactoferrin is an 80-kDa globular glycoprotein that belongs to the transferrin family. It was first identified in milk (therefore the name), and then in many other places like tears, saliva, nasal and genital secretions and the granules of neutrophils.[41] This protein can bind two ferric irons with a $K_d \sim 10^{-20}$ M,[59] which helps to create local iron deprivation and thereby

inhibits bacterial growth and also biofilm formation.[60] To overcome lactoferrin, bacteria employ lactoferrin receptors for removing iron from the protein directly as discussed earlier. In addition to chelating iron, lactoferrin has many other functions that include antiviral and anticancer activity, interaction with lipopolysaccharide, and activation of the immune system by acting like cytokines.[41]

Lcn2 was first identified in neutrophil granules, and it belongs to a functionally diverse protein family: lipocalins. These proteins generally bind small hydrophobic molecules and they share a conserved 8-stranded antiparallel β-barrel core structure (Figure 1.1.9). In 2002, Goetz and coworkers discovered that Lcn2 has bacteriostatic activity that results from its ability to scavenge enterobactin (Ent, **3**, Figure 1.2.3), a siderophore used by many Gram-negative bacteria.[61] Tryptophan fluorescence quenching assays revealed a K_d of ~0.4 nM for Fe-Ent binding to Lcn2, which indicates that Lcn2 is able to compete with the bacterial Ent receptor FepA (K_d = ~24 nM for Fe-Ent)[62] and prevent Ent-mediated iron uptake. Structural analysis of Lcn2 shows that it has three rigid binding pockets that fit the three catechol rings of Ent. The cation-π interactions from Lys125, Lys134 and Arg 81 are important for Ent recognition, as well as hydrogen bonding from Trp79 (Figure 1.1.9).[63] The chirality and macrolactone backbone of Ent does not affect the binding affinity significantly.[64] Lcn2 was observed to release iron in acidic endosomes, suggesting a possible destination and fate of the Lcn2-Ent complex.[65] Iron release is most likely due to acidic conditions in endosomes causing Ent degradation.[66] Besides Ent, Lcn2 was found to bind other siderophores like bacillibactin from *Bacillus anthracis* and some carboxymycobactins from *M. tuberulosis*.[67] In response, pathogenic bacteria utilize alternative siderophores to bypass Lcn2. One example is salmochelins, which are Ent analogs exhibiting sugar modifications on the catechols (**4**, Figure 1.2.3). The sugar modification creates significant steric clashes in the catechol binding pocket of Lcn2 and therefore decreases the binding affinity to K_d > 1 μM.[68] Bacteria carrying the genes for salmochelin synthesis (the *iroA* gene cluster), including pathogenic *E. coli, Klebsiella pneumoniae* and *Salmonella* spp., are shown to be insensitive to Lcn2 *in vitro* and exhibit increased virulence *in vivo* due to their ability to evade Lcn2.[68-69] *B. anthracis* utilizes another siderophore petrobactin (**8**, Figure 1.2.3), which also clashes with the Lcn2 pocket wall, and thus escaped capture of Lcn.[64] *E. coli* can also utilize aerobactin (**9**, Figure 1.2.3), which lacks the catechol groups, to avoid Lcn2 binding.[70] Although petrobactin and aerobactin are not captured by Lcn2, these siderophores bind iron with much lower affinity than bacillibactin and Ent.[71] Therefore, iron uptake via these alternative siderophores may be less efficient.

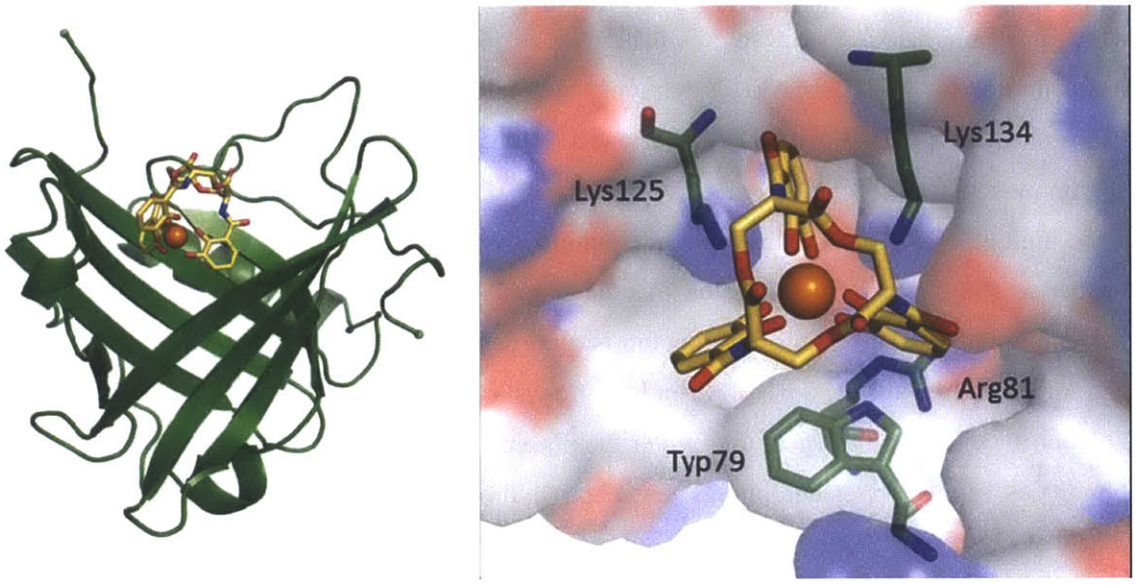

Figure 1.1.9. Crystal structure of Lcn2 with Fe-Ent modeled in the binding pocket. Left: overall fold of Lcn2. Right: binding pocket with the four key amino acid side chains shown (blue is positive charged region and red is negative charged region). (PDB 1L6M)

In summary, humans and microorganisms both evolved dedicated and complex systems to maintain the homeostasis of iron, the essential but also toxic nutrient. With the great efforts put in understanding host and microbe iron metabolism, new antimicrobial strategies that target bacterial iron assimilation are under intense investigation. However, there are still many important questions needed to be addressed like to what extent bacteria can alter its iron-uptake machineries in different conditions, and are there mammalian siderophores, and if so, what are their roles in human physiology.

1.2 Bacterial Siderophores

As mentioned in Section 1.1, siderophores are structurally diverse natural products that selectively bind ferric ion with high affinity. Since the first siderophore mycobactin P was isolated in 1949,[72] over 500 siderophores have been discovered, and approximately half of these molecules have been characterized structurally. Because of their impressive iron binding ability, their important roles in bacterial iron acquisition and relevance to virulence, significant efforts have been put into understanding the chemistry and biological processes of siderophores.

Siderophore-Iron Interaction: Selectivity, Affinity and Stability. All siderophores discovered to date possess higher affinity for ferric ion than ferrous ion. Besides the fact that iron exists as Fe^{3+} under aerobic conditions, another reason may be that it is harder to evolve a ligand that will differentiate Fe(II)

from many other biologically relevant divalent cations like Zn(II), Mn(II), Cu(II) and Ni(II). One possible competitor for Fe(III) is Al(III), which is also quite abundant in the environment. However, Al(III) has a much smaller radius (0.54 Å) than Fe(III) (0.65 Å),[73] and it is redox inert which means for many siderophores that release iron via redox process, Al(III) will not be unloaded.

The high Fe(III)-binding affinity of siderophores is mainly achieved by proper donor atoms and structural features that allow the formation of a octahedral coordination geometry with proper ligand-metal distance upon Fe(III) binding. Ferrous ion is a borderline Lewis acid preferring borderline donor atoms like nitrogen. In contrast, ferric ion is a hard Lewis acid and it prefers oxygen as the donor atoms and the higher the charge on oxygen, the tighter the binding will be. There are three main types of iron-binding moieties utilized by siderophores: catechol, hydroxamate and α-hydroxycarboxylate (Figure 1.2.1). Each of these moieties contains two oxygen atoms that can be deprotonated and bind Fe(III). Other iron-binding groups that contain nitrogen and sulfur as donor atoms are also found in siderophores, but these molecules have lower Fe(III) binding affinities. With few exceptions (i.e., pyochelin, **15**, Figure 1.2.3), most siderophores bind Fe(III) in a hexadentate mode with 1:1 stoichiometry and the six ligands provide an octahedral geometry which minimizes ligand repulsion. Such coordination favors the formation of the thermodynamically stable high-spin Fe(III) species. Crystal structures of four representative siderophores in their metal-bound forms are shown in Figure 1.2.2. The binding of other metal ions, including Al(III), Cr(III), Ga(III) and In(III), with catecholate ligands has been studied and Fe(III) exhibits the highest affinity.[74] The radius difference of metal ions was thought to be the main source of selectivity.

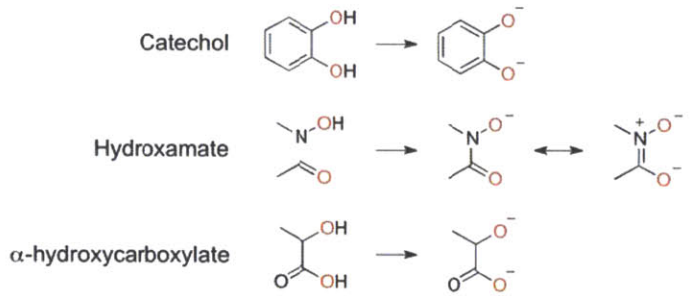

Figure 1.2.1. Structures of the commonly used iron-binding ligands in siderophores. The oxygen atoms involved in iron binding are labeled red.

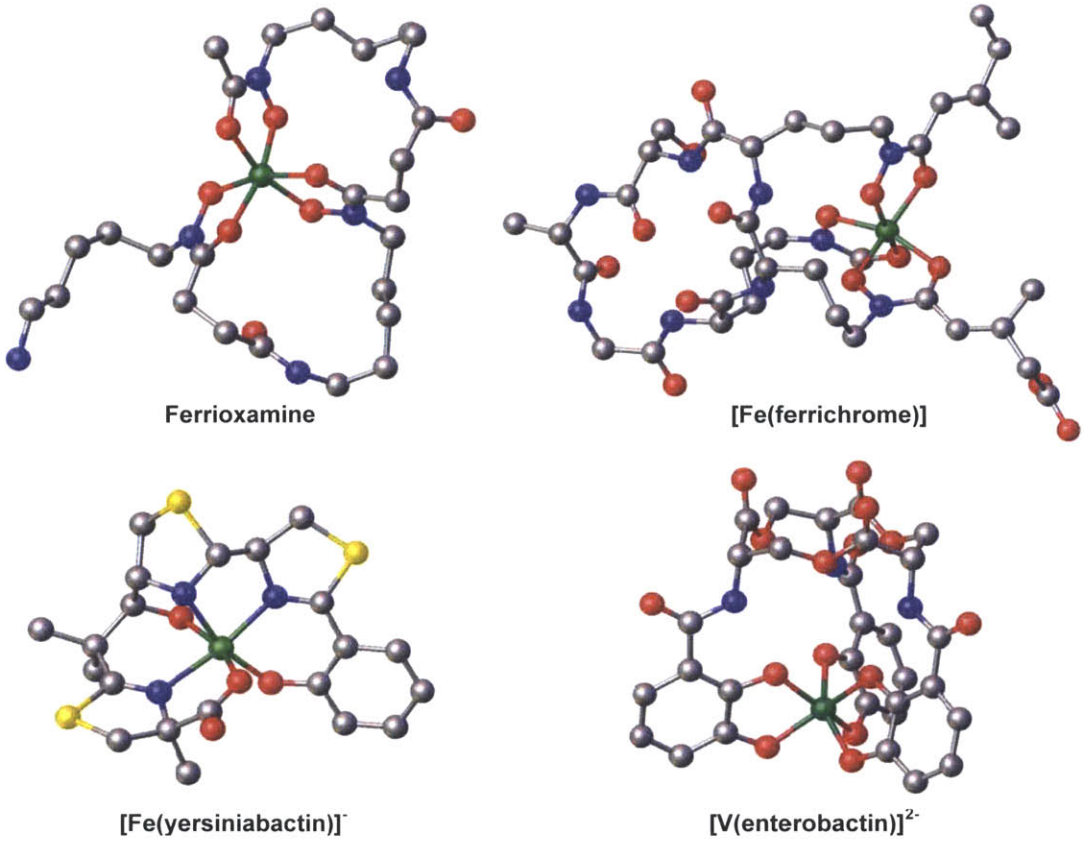

Figure 1.2.2. Structures of [Fe(ferrioxamine B)],[75] [Fe(ferrichrome)],[76] [Fe(yersiniabactin)]$^{-}$,[77] and [V(enterobactin)]$^{2-}$ [78] determined by X-ray crystallographic analysis. The oxygen atoms are depicted in red, the nitrogen atoms in blue, the sulfur atoms in yellow, and the carbon atoms in grey. The metal ions are labeled in green and the hydrogen atoms are omitted for clarity. This figure is published in *Metallomics,* **2012**, *24*, 866-880.

The stability of Fe(III)-siderophore complexes is contributed by both the enthalpy from donor-acceptor bond energies and the entropy changes associated with the complex formation. For example, hexadentate oxygen based siderophores generally exhibit high stability because i) the oxygen based ligands form stronger bonds with Fe(III) than nitrogen or sulfur ligands; ii) the hexadentate ligands have advantage in the entropy change from displacing coordinated water molecules comparing to lower denticity ligands. Moreover, some siderophores, like enterobactin (Ent, **3**, Figure 1.2.3), orient the iron-binding moieties to favorable positions (the chiral serine residues in Ent put the catechols to the same side of the macrolactone ring, Figure 1.2.2) before iron binding, which decreases the entropy loss of the siderophores upon iron binding. Table 1.2.1 summarizes the iron affinities and producer organisms of

select siderophores. Of note, the binding constants are pH dependent because most of the siderophores require deprotonation steps to form Fe(III) complexes. The p[Fe^{III}] values listed in Table 1.2.1 are defined as –log[$Fe^{3+}(H_2O)_6$] reported at a defined set of experimental conditions (usually at pH 7.4, total iron concentration of 1 μM and total ligand concentration of 10 μM), which can provide a more direct comparison between the affinities of different ligands. From the kinetic view, the dissociation rate of iron from hexadentate siderophores is very low at neutral pH, although acidic conditions can accelerate the process.[79] This slow release is beneficial for bacterial iron acquisition because the concentration of iron-bound siderophores may be very low in the environment and a long time may be needed for siderophores to reach their receptors. Tri- and bidentate siderophores exist and are more kinetically labile.[80] It is possible that these siderophores solubilize iron first and then transfer iron to hexadentate siderophores for cytosolic delivery. In terms of redox stability, siderophore coordination greatly reduces the redox potential of Fe(III). For example, the $[Fe(Ent)]^{3-}$ has a redox potential of -750 mV while the $[Fe(H_2O)_6]^{3+}$ value is +770 mV.[81]

Table 1.2.1 Properties of select siderophores produced by bacteria and fungi.

No	Siderophore	Producing Organism(s)[a]	logK_f (Fe^{III})[b]	p[Fe^{III}][c]	Ref[d]
1	Desferrioxamine B	*Nocardia* spp., *Streptomyces* spp.	30.6	26.6	82
2	Ferrichrome	*Aspergillus* spp., *Penicillium* spp., *Ustilago* spp.	29.1	25.2	83
3	Enterobactin	*Klebisella* spp., *Enterobacter* spp., *Erwinia* spp.	49	35.5	71b
7	Staphyloferrin B	*Staphylococcus hyicus*	n.d.[f]	n.d.[f]	
8	Petrobactin	*Marinobacter hydrocarbonoclasticus, Bacillus cereus, Bacillus anthracis*	43	23.1	71c
10	Parabactin	*Paracoccus denitrificans*	~48	n.d.[f]	84
11	Pyoverdine	*Pseudomonas* spp.	30.8	27	85
12	Mycobactin S	*Mycobacterium smegmatis*	26.6	n.d.[f]	86
13	Azotobactin *δ*	*Azotobacter vinelandii*	28.1	27.8	87
14	Yersiniabactin	*Yersinia enterocolitica, Yersinia pestis*	36.6	n.d.	88
15	Pyochelin	*Pseudomonas aeruginosa,*	5.4,		89
		Burkholderia cepacia	17.2[e]	16	90

[a] Select examples of producing organisms. [b] K_f is the apparent forming constant of Fe^{III} and the fully deprotonated ligand. [c] When $[Fe^{III}]_{total} = 10^{-6}$ M, $[L]_{total} = 10^{-5}$ M, at pH 7.4. [d] The references specify the source of the stability constant. [e] The first value was determined in methanol due to the low solubility of the siderophore. The second value was determined in 20% ethanol/water. [f] n.d. = not determined. This table is published in *Metallomics,* **2012**, *24*, 866-880.

Structures of Siderophores. The siderophores have very diverse structures, with bi- (**18**, Figure 1.2.3), tri- (**17**, Figure 1.2.3), tetra- (**15** and **16**, Figure 1.2.3) and hexadentate (**1-14**, Figure 1.2.3)

binding modes all observed. The bi- and hexadentate ligands usually form mononuclear complexes with Fe(III). With the tri- and tetrahexadente ligands, binuclear or even multinuclear complexes can be formed.[91] As mentioned previously, the hexadentate siderophores exhibit higher binding affinities and are most commonly observed. The backbone of siderophores can be linear (e.g. desferrioxamine B, **1**, Figure 1.2.3) or cyclic (e.g. ferrichrome, **2**, Figure 1.2.3). The amino acids components in the backbone can be a mixture of L- and D-enantiomers (e.g., achromobactin, **16**, Figure 1.2.3) which provides protection from lytic enzymes. Capping N- and C- termini and forming cyclic structures may also enhance the lifetime and avoid peptidase hydrolysis.[73] Some siderophores have fatty acyl chains attached (e.g., mycobactin S, **12**, Figure 1.2.3) and are expected to stay connected with the cell membrane. This feature may be beneficial for the bacteria that live in aqueous environments or have life cycles inside host cells.[92] Different organisms produce structurally diverse siderophores, and within one class of related organisms or even one species, many analogs of the same siderophore can be produced. For example, there are 62 variants of the *Pseudomas* siderophore pyoverdin reported.[73]

In Figure 1.2.3, selected structures representing the major groups of siderophores according to their coordinating ligands are shown. A well-known class of tris-hydroxamate siderophores are ferrioxamines (e.g. desferrioxamine B, **1**) produced by *Nocardia* spp. and *Streptomyces* spp. These siderophores are primarily assembled from alternating units of succinic acid and a monohydroxylated diamine. Another example of tris-hydroxamate siderophore is ferrichrome (**2**), which is produced by fungi. Tris-catecholate siderophores including enterobactin (**3**), salmochelins (**4**) and bacillibactin (**5**), produced by enterobacteria and *Bacilli* spp. They are assembled from 2,3-dihydroxybenzoic acid and L-serine, L-threonine and glycine with possible glucose modifications on the 2,3-dihydroxybenzoic acid moiety. Tris-α-hydroxycarboxylate siderophores include achromobactin (**6**) and staphyloferrin (**7**), produced by *Pectobacterium chrysanthemi* and *Staphylococcus* spp. These siderohpres are assembled by various carboxylic acids through the NRPS-independent (NIS) pathway. Besides these three classes, the vast majority of siderophores are comprised of a mixture of different types of bidentate donor ligands, as well as heterocycles as presented by compound **8-18** in Figure 1.2.3.

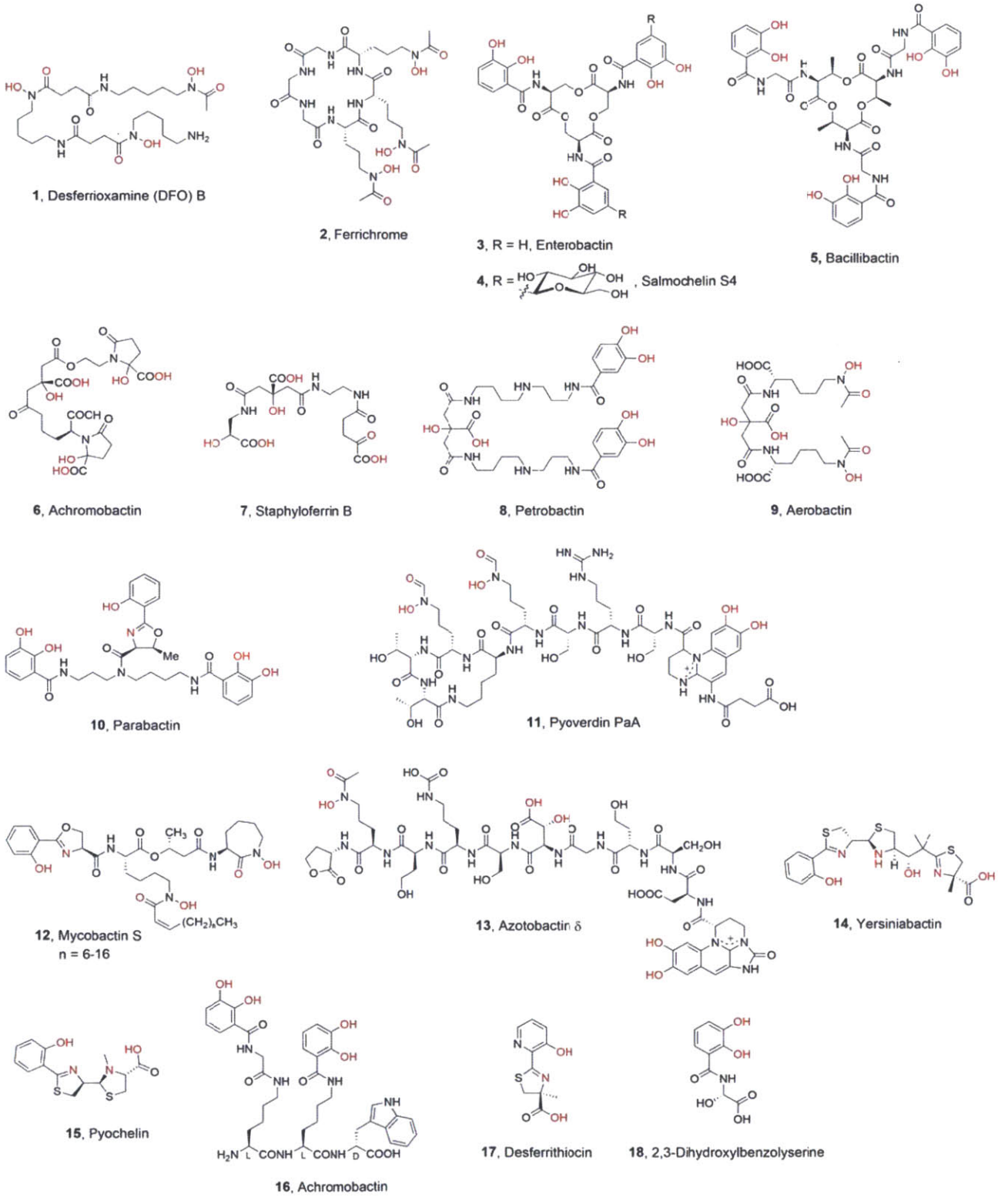

Figure 1.2.3. Structures of representative siderophores. The atoms involved in iron binding are labeled in red.

Siderophore Transportation: Systems Employed by Gram-positive and Gram-negative Organisms. Due to the different cell wall structures of Gram-positive and Gram-negative bacteria, the transportation mechanism of siderophores differs. The Gram-positive bacteria cell wall is comprised of a single layer phospholipid membrane encapsulated by a thick peptidoglycan cover. In contrast, Gram-negative bacteria have one outer and one inner phospholipid membrane, and the periplasmic space containing a thin peptidoglycan structure is in between (Figure 1.2.4). In both cases, the peptidoglycan confers mechanical stability for the cell.

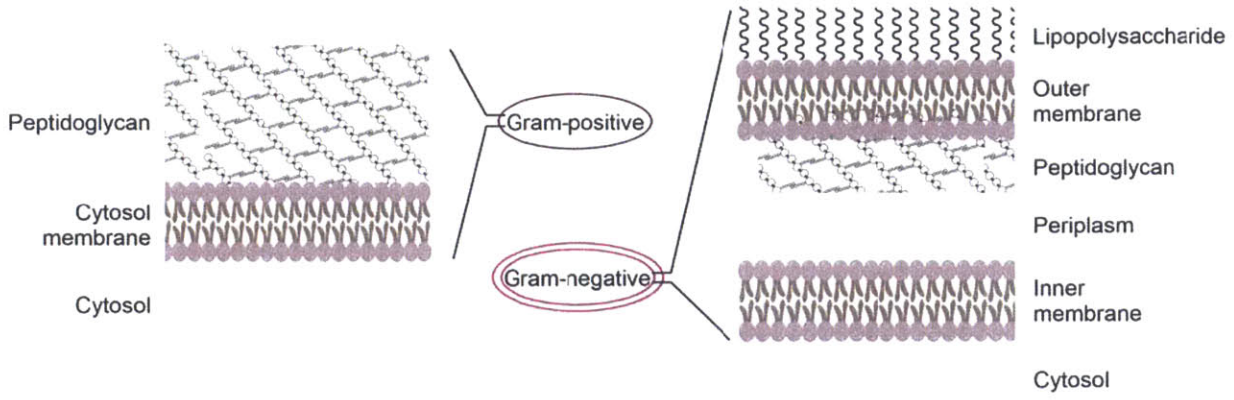

Figure 1.2.4. Model of the cell wall structures of Gram-positive and Gram-negative bacteria with phospholipid membranes and peptidoglycan shown.

The majority of siderophore transport studies have focused on Gram-negative bacteria. The uptake of siderophore-iron complex requires three steps: outer membrane receptor recognition, periplasmic transfer and inner membrane transport. Unlike smaller nutrients like sugars and amino acids that can diffuse through the outer membrane via channel proteins called porins, iron-bound siderophores have specialized receptor proteins to help cross the membrane. The affinities of the receptors to siderophore-iron complex are high, typically in the nM range, to allow efficient scavenge of the complexes from the environment. Many of these receptors have been structurally characterized and are found to share a transmembrane β-barrel structure consisting of 22 β-strands (e.g., Ent receptor FepA from *E. coli,* Figure 1.2.5).[93] The receptors also have an N-terminal globular domain composed of α-helixes and β-sheet that acts as a 'plug' of the barrel. It is hypothesized that the siderophore-iron complex binds to the extracellular loops of the receptor, which triggers a conformational change in the plug domain to allow the complex to pass through the transient channel.[94] This process also requires a periplamic protein complex TonB/ExbB/ExbD. TonB spans the periplasmic space and is found to interact with the N-terminal domain of the receptors and transmit the proton motive force from the inner

membrane as the energy source for this step.[93b, 95] The *tonB* gene is conserved in over 65 genera of Gram-negative bacteria and is involved in other active transportation systems.[96] A periplasmic binding protein (e.g., FepB for Ent in *E. coli*) then transfers the siderophore-iron complex to the inner membrane permeases. These periplasmic binding proteins exhibit greater ligand promiscuity and lower binding affinity compared to outer membrane receptors.[97] The inner membrane permeases are ABC-type transporters comprised of transmembrane channel proteins and ATPases tethered to the cytoplasmic side of the membrane. The active transport of iron-siderophore complexes through the inner membrane is energized by ATP hydrolysis by the ATPases.[98] The representative Ent uptake machinery for by *E. coli* is shown in Figure 1.2.6.

Figure 1.2.5. Crystal structure of *E. coli* enterobactin receptor FepA. The N-terminal plug domain is labeled with color and the β-barrel and extracellular loops are labeled grey. (PDB 1FEP)

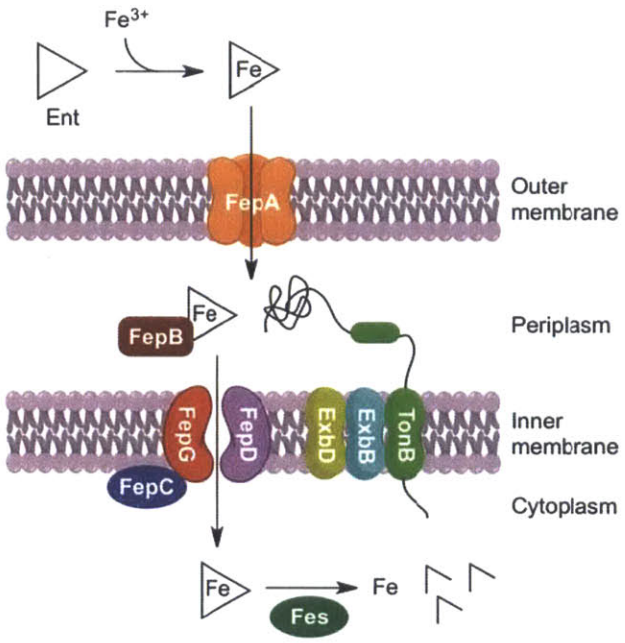

Figure 1.2.6. Enterobactin (Ent) uptake system from *E. coli.* The outer membrane receptor FepA recognizes ferric Ent and transports it into periplasm in a TonB-dependent manner. The periplasmic binding protein FepB delivers ferric Ent to inner membrane where the ABC-type permease complex FepCDG transport it into the cytosol. The esterase Fes hydrolyzes Ent backbone and iron is release from the complex.

Less is known about the siderophore uptake machinery in Gram-positive bacteria. Lipid-anchored extracellular proteins serve as the 'receptor' of siderophores, although they are homologous to the periplamic binding proteins in Gram-negative bacteria.[99] Higher binding affinities (K_d of 10-50 nM) were observed for these proteins compared to their Gram-negative homologues, which is reasonable because in Gram-positive bacteria these proteins serve as the first recognition step for siderophore transport. After binding to an iron-siderophore complex, they transfer the complex to the cytosol membrane where ABC-type permeases similar to those found in Gram-negatives deliver the complex into the cytosol.[96]

Within the cytosol, iron needs to be released from the siderophore in an efficient manner for cellular usage. The most often used strategy is through reduction of Fe(III) to Fe(II). As discussed previously, ferrous iron has much lower affinity to the siderophores and can therefore be removed. This mechanism also allows the recycling of apo-siderophores. Within the identified reductases involved in this process, only a few possess specificity to iron-siderophore complexes, suggesting that other established reductases can catalyze the reaction as well.[100] Extracellular and periplamic ferrisiderophore

reductases were also reported.[100] The reductases usually use the cofactors NADH and FMN,[101] although a Fe-S cluster dependent reductase was reported as well (FhuF in *E. coli*).[102] The tris-catecholate siderophores that bind Fe(III) with very high affinities, have redox potentials that are too low to allow for intracellular reduction. A separate iron release mechanism is used for these siderophores by reducing the denticity of the ligand. For example, esterase Fes in *E. coli* catalyzes hydrolysis of the Ent macrolactone backbone, which results in the change of a hexadentate ligand to bidentate ligands. The hydrolysis increases the redox potential from -750 mV to -350 mV,[81] and a siderophore-interacting protein YqjH is recently found to have reductase activity and may assist the release of iron by reduction following Fes hydrolysis.[103] Compared to the first mechanism, the hydrolysis-based iron release is more costly for the bacteria since it destroys siderophore scaffolds. However, hydrolyzed fragments of Ent were also found in the bacterial growth media and used as lower affinity siderophores for iron uptake (two receptors Cir and Fiu were identified to specifically recognize these fragments),[104] indicating possible recycling of these fragments.

Enterobactin and Salmochelins. The work described in this thesis focuses on conjugating enterobactin (Ent) and salmochelins with different types of cargos for versatile application. These two siderophores are high-affinity tris-catecholate siderophores that are widely used by Gram-negative Enterobacteriaceae including *E. coli, Salmonella* spp. and *Klebsiella* spp.. Ent is also used as xenosiderophores by other bacterial species (e.g., *Pseudomonas aeruginosa* and *Bacillus subtilis*).[105] Ent and salmochelins play important roles in bacterial virulence.[106] The *fep-ent* gene cluster encodes *fepABCDEG* and *entABCDEF* genes, which are responsible for the uptake and biosynthesis of Ent, respectively.[17] The *iroA* gene cluster encoding *iroBCDEN* genes is responsible for salmochelin biosynthesis and uptake, and is expressed in almost all pathogenic *Salmonella* serovars and many pathogenic *E. coli* and *Klebsiella* strains.[107] Both gene clusters are regulated by Fur. Their synthesis, secretion and uptake that are not covered in the previous sections are discussed in detail herein.

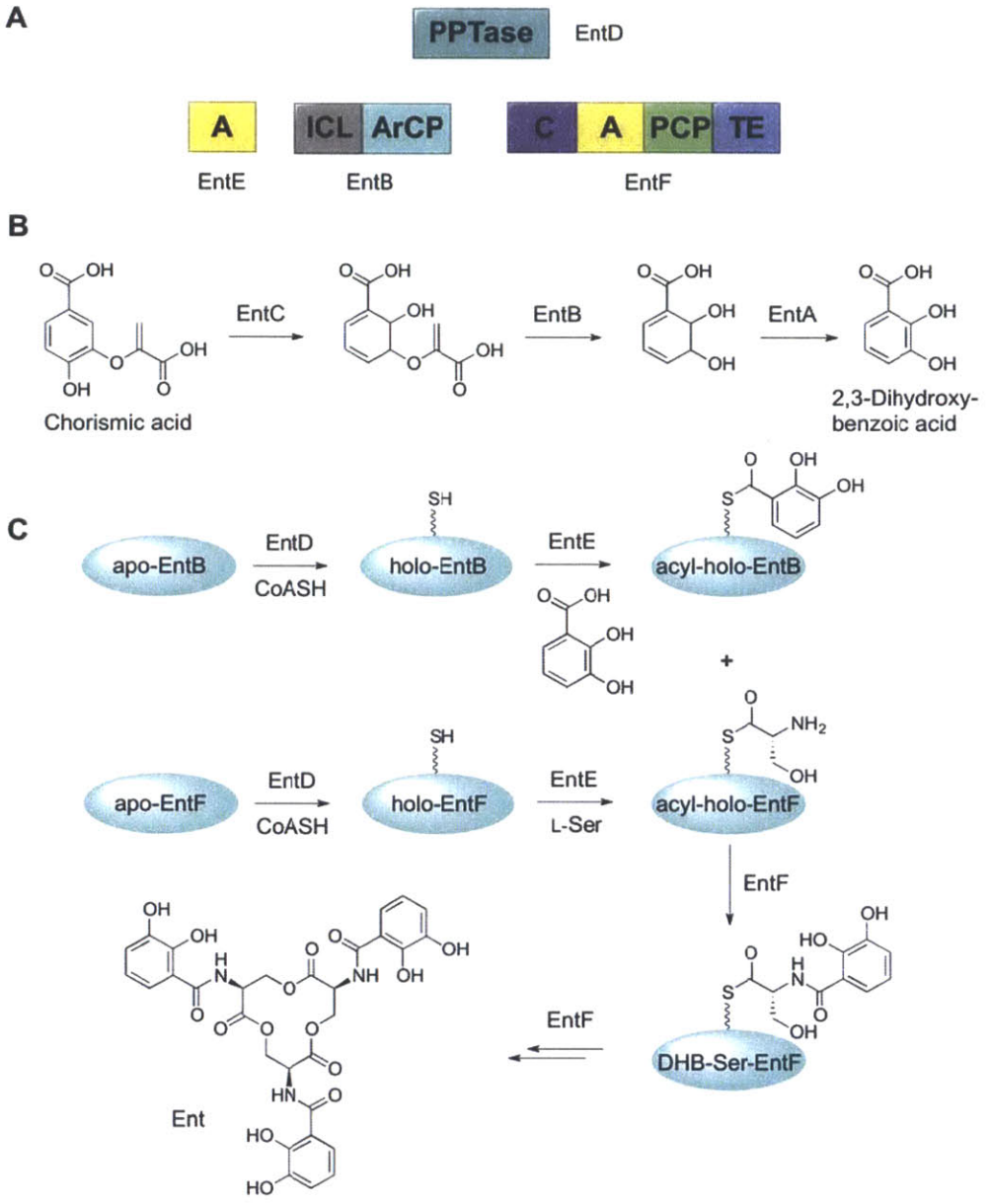

Figure 1.2.7. Biosynthesis of Ent by the EntABCDEF assembly line. A. Overview of the assembly line. Abbreviations: *PPTase*: phosphopantetheinyl transferase; *A*: adenylation domain; *ICL*: isochorismate lyase domain; *ArCP*: aryl carrier protein; *C*: condensation domain; *PCP*: peptidyl carrier protein; *TE*: thioesterase domain. B. 2,3-Dihydroxybenzoic acid (DHB) is synthesized by EntABC from chorismic acid. C. The construction of Ent is performed by EntBDEF. The aryl carrier domain of EntB and EntF is phosphopantetheinylated by EntD, and then acylated with activated DHB and serine by EntE. The formation of the amide bond is catalyzed by the condensation domain of EntF. EntF also catalyzes the cyclization and hydrolytic release of mature Ent.

Enterobactin and salmochelins are synthesized in bacteria by non-ribosomal peptide synthetases (NRPS). The aromatic amino acid precursor chorismic acid is used to build the 2,3-dihydroxybenzoic acid (DHB) through three steps catalyzed by Ent C, Ent B and Ent A (Figure 1.2.7). The construction of Ent from DHB and L-serine is achieved by adenylation enzyme EntE, phosphopantetheinyl transferase EntD, aryl carrier domain of EntB, and the multi-domain enzyme EntF (Figure 1.2.7). Salmochelins (Figure 1.2.8) are glucosylated Ent derivatives that result from post-assembly line tailoring, and the C-glycosyltransferase IroB is responsible for attaching the glucose moieties to Ent using UDP-glucose as a substrate.[108]

Significant amount of enterobactin can be isolated from the cultures of a mutant *E. coli* strain (~20 μmol per liter form *E. coli* AN311, which is deficient of Ent uptake),[109] and the chemical syntheses of enterobactin has also been reported. Corey and co-workers reported the first synthesis of Ent with low overall yield (~1%), in which the triserine backbone was constructed through sequential couplings of the monomers and involving multiple protection and deprotection steps.[110] Subsequently, Ramirez *et al.* reported an improved procedure with a single-step synthesis of the triserine lactone, which greatly shortened the synthesis and also allows other groups besides DHB to be installed on the lactone backbone (Figure 1.2.9).[111] Besides the native siderophore, many Ent analogues have been synthesized by changing the tri-serine backbone to e.g., alkyl ring (**19**),[112] tricyclic tripods (**20**),[113] 1,3,5 tri-substituted phenyl ring (**21**, TRIMCAM and **22**, MECAM),[114] tris(2-aminoethyl)amine (**23**, TRENCAM),[115] and a chiral macrocyclic peptide (**24**)[116] (Figure 1.2.10). These siderophore mimics all display lower iron binding affinity compared to Ent. The total synthesis of salmochelins was reported recently.[117] Benzyl-protected glucose was connected to the DHB building block via a diastereoselective Ni-catalyzed Negishi reaction, and this aryl *C*-glycoside subunit was subsequently coupled to the serine backbone to afford the salmochelins after global deprotection (Figure 1.2.11). To obtain salmochelin S4, a mixture of glucose-DHB and DHB subunits were used and statistical distribution of mono-, di- and tri-glucose modified products was obtained.

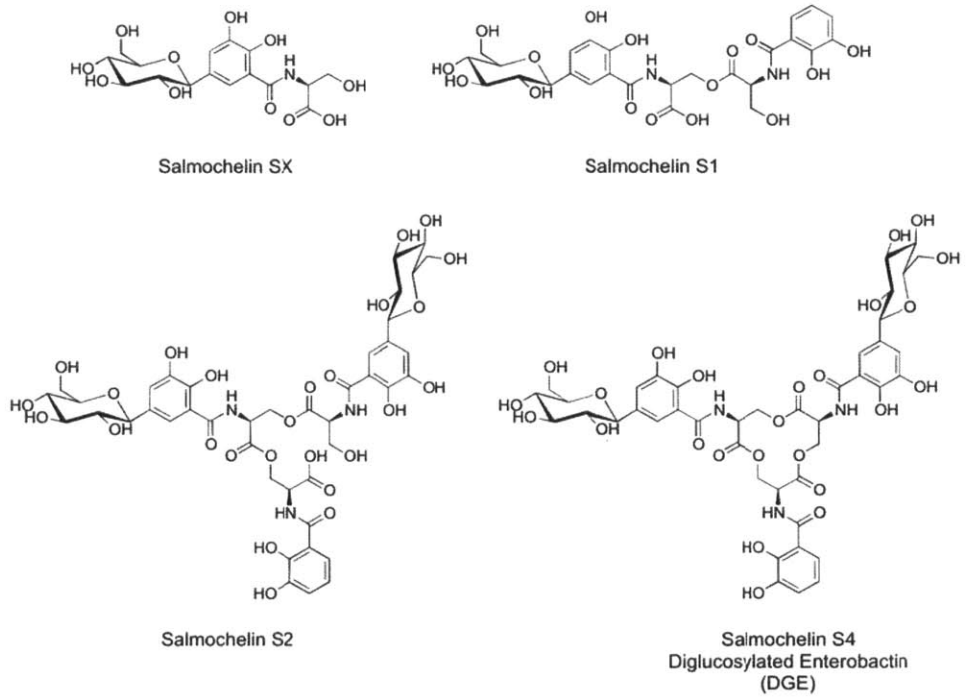

Figure 1.2.8. Structure of representative salmochelins.

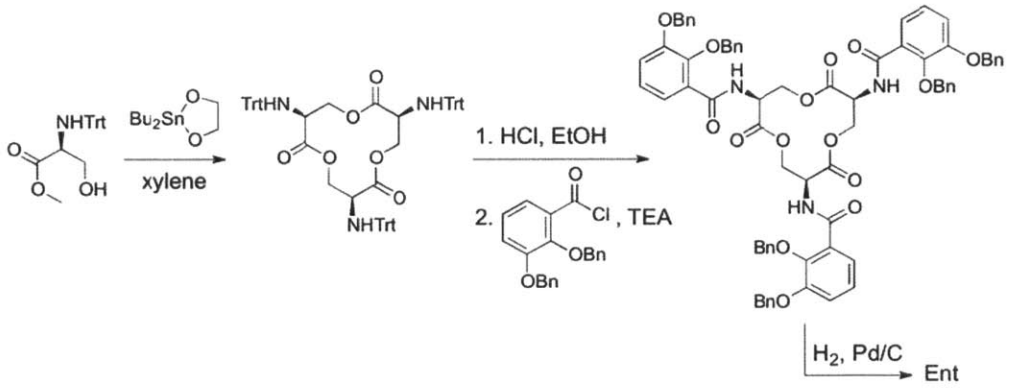

Figure 1.2.9. Chemical synthesis of Ent by Ramirez *et al.*[111]

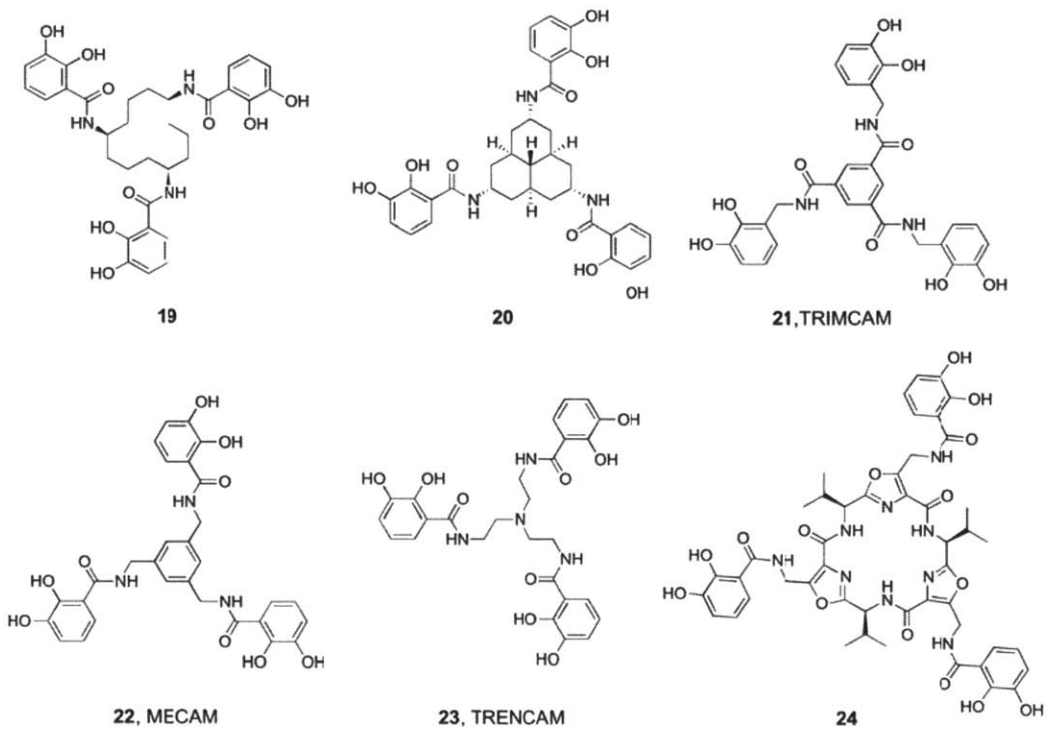

Figure 1.2.10. Representative synthetic analogs of Ent.

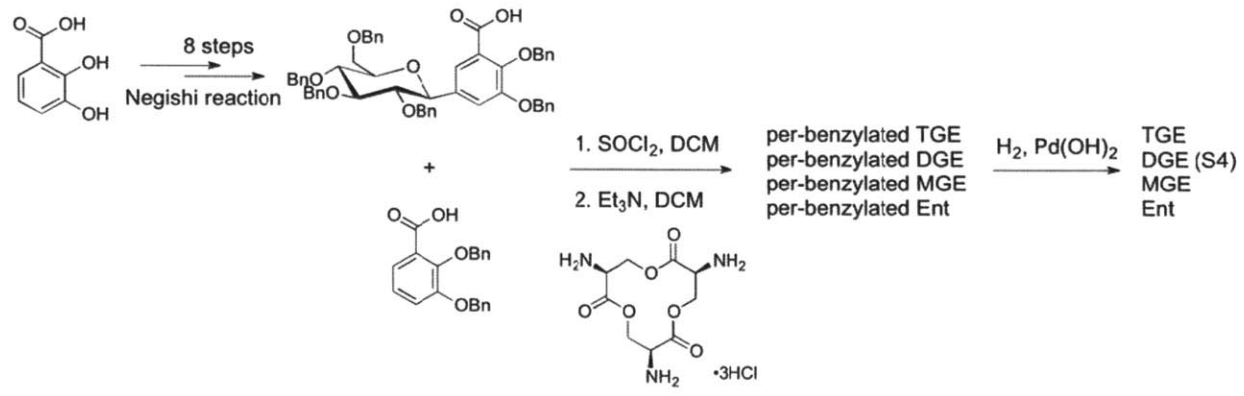

Figure 1.2.11. Chemical synthesis of salmochelins. DGE is salmochelin S4. MGE and TGE are mono- and tri-glucosylated Ent.[117]

The secretion of Ent across the inner membrane and into the periplasm is through an efflux pump EntS, and its expression is regulated by Fur. EntS contains 12 trans-membrane domains and belongs to the major facilitator superfamily.[118] The outer membrane channel protein TolC is reported to be required for Ent export, and therefore a two-step model is proposed for Ent secretion.[119] However, Ent

breakdown products were identified in the growth media of EntS or TolC deficient strains, which indicates that other secretion pathways exist for these smaller siderophores. For salmochelins, an ABC-type transporter IroC is reported to be the inner membrane exporter, and Ent is also a substrate of IroC.[106c]

As discussed previously, the uptake machinery for ferric enterobactin is comprised of outer membrane receptor FepA, periplasmic binding protein FepB, TonB/ExbB/ExbD complex, inner membrane ABC transporter FepD/FepG/FepC and cytoplasmic esterase Fes (Figure 1.2.6). The crystal structure of FepA is solved, and revealed that the extracellular loops of FepA extend 30-40 Å above the outer membrane and facilitate the recognition of ferric Ent. Several arginines located on the loops were hypothesized to interact with $[Fe(Ent)]^{3-}$ via electrostatic interactions. The total height of this 22-stranded antiparallel β barrel is about 70 Å with an elliptical cross-section of 40 Å x 30 Å.[93b] The dissociation constant (K_d) of FepA for ^{59}Fe-Ent was measured to be 24 nM and 0.2 nM by two different groups.[62, 120] Through testing synthetic Ent analogs that have opposite chirality, altered backbone or substituted triscatechol iron center, it was found that the coordinated catechol amide groups are essential for FepA recognition while the triserine backbone can be substituted with quite different scaffolds.[121] The structure of the periplasmic binding protein FepB has not been reported, although the binding affinity was reported to be 30 nM (K_d) and it selectively binds Ent, but not other catecholate siderophores like agrobactin.[122] Cytoplasmic esterase Fes belongs to the α/β hydrolase family and it prefers iron-bound Ent with a more than 100-fold lower K_m compared to apo-Ent.[123]

A model of the salmochelin biosynthesis and uptake system interplaying with the Ent system is shown in Figure 1.2.12. The uptake machinery of salmochelins overlaps with the Ent machinery. The outer membrane receptor IroN recognizes salmochelins and also transports Ent and its degradation products. Moreover, the inner membrane Ent transporter FepCDG transfers salmochelins.[124] No periplasmic salmochelin binding protein has been identified yet. The ABC-type transporter IroC was proposed to be the inner membrane permease for salmochelins,[125] although evidence for IroC functioning as the salmochelin exporter was also reported.[106c] Two esterases, IroD and IroE, hydrolyze salmochelins and Ent.[123] IroD is located in cytoplasm and, similar to Fes, it can cleave its substrates down to monomeric DHB-serine fragments. IroE is predicted to be located in the periplasm with an N-terminal transmembrane domain. The main product of IroE hydrolysis was found to be the linear trimer of the cyclic substrate. A later study reported that IroD preferred apo Ent and salmochilin substrates, while IroE catalyzed both iron-bound or apo substrate hydrolysis with equal efficiency.[125] Because linear backbone salmochelin S2 was found to be the major salmochelin fraction in the supernatant of salmochelin producers under iron-limited condition,[124] the IroD may have a more important role in the synthesis of salmochelins besides the hydrolytic release of iron. The uncatalyzed hydrolysis of the

trilactone backbone in aqueous solutions was observed (Chapter 4) and may also contribute to the isolation of linearized and fragmented salmochelin structures.

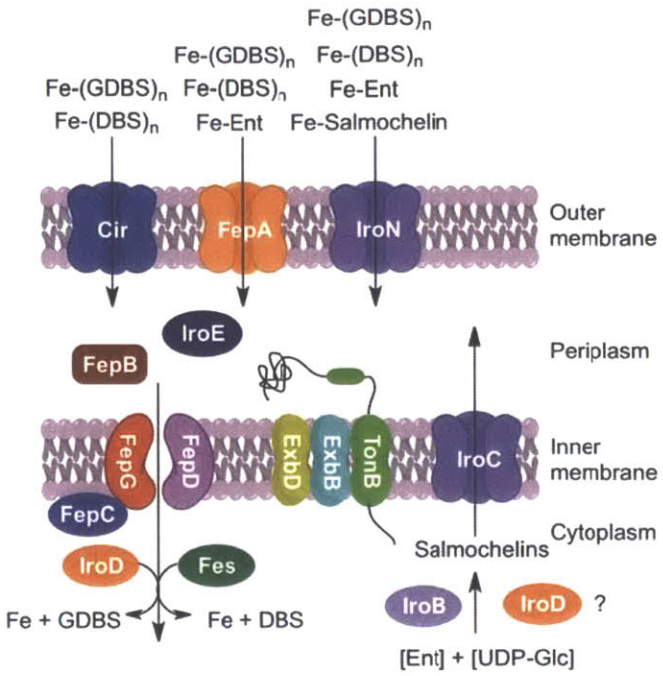

Figure 1.2.12. Salmochelin synthesis and uptake machinery. Glycotransferase IroB installs the glucose moieties onto Ent for salmochein synthesis. Esterase IroD may be involved in the synthesis to generate the linearized salmochelins. IroN is the main receptor for salmochelins, which also recognizes Ent and the degradation products of both siderophores. Ent receptor FepA and Cir can recognize degradation products of salmochelin as well. The inner membrane permease FepGDC for Ent is proposed to transport salmochelins. Periplasmic esterase IroE and cytoplasmic esterase IroD are involved in the release of iron. Glc = glucose; DBS = DHB-serine; GDBS = glucosylated DHB-serine.

1.3 Siderophore Conjugates and their Applications

The high iron-binding affinity, specific recognition and efficient uptake by bacteria make siderophores useful tools for antibiotic-delivery strategies, iron sensing, and pathogen detection. Siderophore conjugates reported for these applications are discussed herein.

Naturally Occurring Siderophore-antimicrobial Conjugates. As discussed above, bacteria have evolved dedicated machineries for iron uptake using siderophores. Besides *de novo* biosynthesis, they also express receptors to recognize xenosiderophores for more efficient iron acquisition. Taking advantage of this thievery process, some bacteria are able to biosynthesize and secret toxins ligated to

siderophores and use these conjugates to kill competitors that utilize the corresponding siderophores. Such naturally occurring conjugates include siderophore-small toxin conjugates termed sideromycins and siderophore-peptide conjugates that belong to the microcin family.

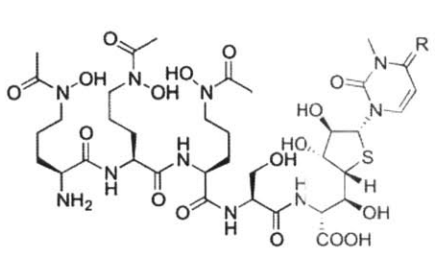

R = O, NH, $NCONH_2$
Albomycins

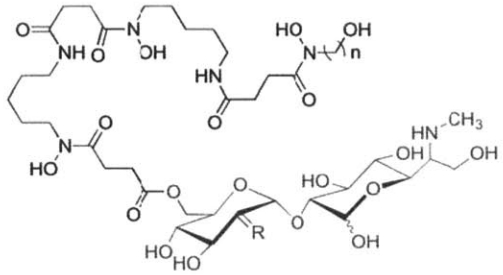

R = O, $(OH)_2$, or NOH; n = 4 or 5
Salmycins

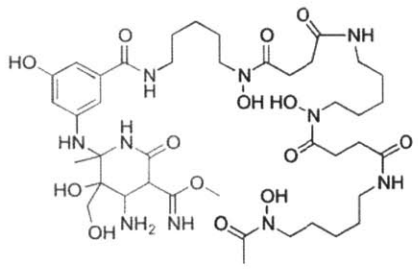

Ferrimycin A1

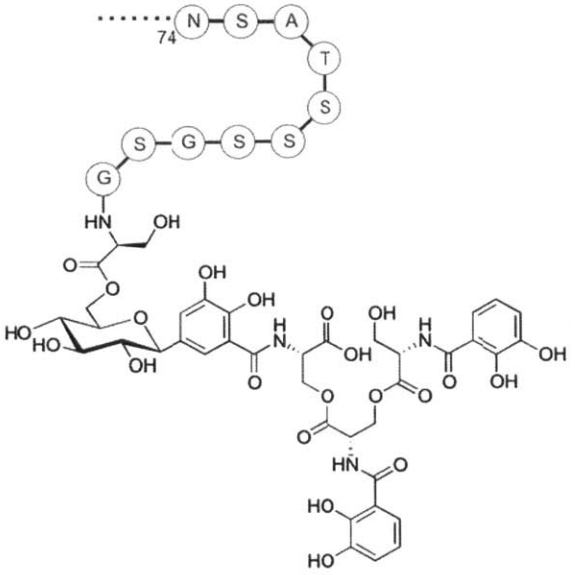

Microcin E492m (MccE492m)

Figure 1.3.1. Structure of naturally occurring siderophore-antimicrobial conjugates albomycin, salmycin, ferrimycin A1 and MccE492m. The antimicrobial components are labeled blue.

The discovery of sideromycins predated the discovery of siderophores, and siderophores were first thought to be antagonists of this class of antibiotics.[126] The most well-studied sideromycin is albomycin, (Figure 1.3.1) which is produced by *Actinomyces subtropicus*.[127] Albomycin is composed by a siderophore analog of ferrichrome and a thioribosyl pyrimidine antibiotic which is a seryl-tRNA synthesase inhibitor. The ferrichrome receptor FhuA, periplasmic carrier protein FhuD and inner

membrane transporter FhuBC were found to interact and deliver albomycin into the cytosol.[128] Following cytosol delivery, a serine peptidase N is required to cleave the conjugate and free the tRNA synthesase inhibitor.[129] Without the siderophore moiety, the inhibitor itself was 30,000-fold less effective against *E. coli* and *S. aureus* due to poor permeability.[130] Albomycin has been studied in animal models with quite promising results, although resistant mutants appeared with very high frequency as a result of either loss of the peptidase or decreased uptake efficiency.[131] Another sideromycin example is salmycin (Figure 1.3.1), produced by *S. violaceus*, and it acts almost exclusively on Gram-positive bacteria.[126] Salmycin is composed by a desferrioxamine B derivative and an aminodisaccharide that inhibits an unknown step in protein synthesis. This molecule exhibited a remarkable MIC value lower than that of ampicillin *in vitro,* although an *in vivo* experiment using a mouse model of *S. aureus* septicemia revealed limited efficacy and no further development towards clinical use was pursued.[126] Ferrimycin A1 is a less studied example in this class (Figure 1.3.1). It is produced by *Streptomyces griseoflavus,* and is comprised of desferrioxamine B and an iminoether group, and was recently suggested to be protein biosynthesis inhibitor.[132]

Besides sideomycins, which harbor small-molecule toxins, antimicrobial polypeptides attached to siderophores also exist. These conjugates belong to the microcin (Mcc) family, a class of antimicrobial peptides synthesized ribosomaly by enterobacteria.[133] Microcin E492m (MccE492m) is a paradigm for siderophore-peptide conjugates (Figure 1.3.1). First isolated from a *K. pneumoniae* strain, MccE492m is comprised of an 84-amino acid peptide and a linearized Ent, with a glucose moiety bridging these two functional units.[134] The peptide portion of this conjugate interacts with the inner membrane components of the mannose permease (ManY/ManZ) and presumably induces pore formation and inner membrane depolarization.[135] MccE492m is most active against Gram-negative enterobacteria which utilize Ent for iron uptake, with MIC values of 0.04-2.5 μM. Mutations of the Ent receptor FepA, Fiu and Cir abolished its activity.[134] Later on, three additional microcins, MccM, H47 and I47, were identified with or predicted to contain Ent component as in MccE492m.[136] It should be noted that many microcins that do not contain siderophore moieties utilize siderophore uptake machinery for cellular entry. For example, MccJ25, a lasso-peptide targeting RNA polymerase, hijacks the ferrichrome receptor FhuA for uptake.[137] The ability of siderophore receptors to transport these polypeptides with relatively large molecular size (5-10 kDa) suggests the promiscuity of the siderophore uptake machinery and the possibility to introduce modifications on siderophores while maintain their cell permeability.

Synthetic Siderophore-Antimicrobial Conjugates. Taking hints from natural sideromycins, researchers have been developing synthetic molecules conjoining siderophore or siderophore mimics with antibiotics for decades. Most of the synthetic conjugates were designed to target Gram-negative

bacteria. Bacterial infections caused by Gram-negatives are a big threat to public health. From an international study in intensive care units, 62% of hospital-acquired infections were caused by Gram-negative bacteria.[138] Gram-negative infections are generally harder to treat compared to Gram-positives due to permeability issue, and the siderophore-mediated delivery has a high potential to solve this problem. The high permeability barrier of Gram-negative bacteria is caused by the double-layer membrane structure, in which the outer membrane serves as a molecular sieve and only small nutrients and molecules with specific outer-membrane receptors can cross (Figure 1.3.2). Most antibiotics and small nutrients like sugars and nucleotides have to diffuse through protein channels called porins.[139] The porin channel has a constrained size and prefers hydrophilic molecules. The emergence of multi-drug resistant bacteria that express mutated porins or have decreased porin expression level makes the permeability problem more difficult to address.[140] The continuous and sometimes increased need for siderophore-mediated iron acquisition during infection makes the siderophore-antimicrobial conjugates a very promising solution. By hijacking the siderophore transport system, antibiotics will be delivered actively, and large or hydrophobic antibiotics may be delivered as well. Moreover, the delivery specificity to bacteria but not to host cells offers the possibility of recycling failed drug candidates with high toxicity or repurposing available drugs like anti-tumor reagents to be used as antibiotics. The delivery specificity can be further developed to select specific pathogens and leave the commensals intact based on the fact that different bacterial strains utilize different siderophores.

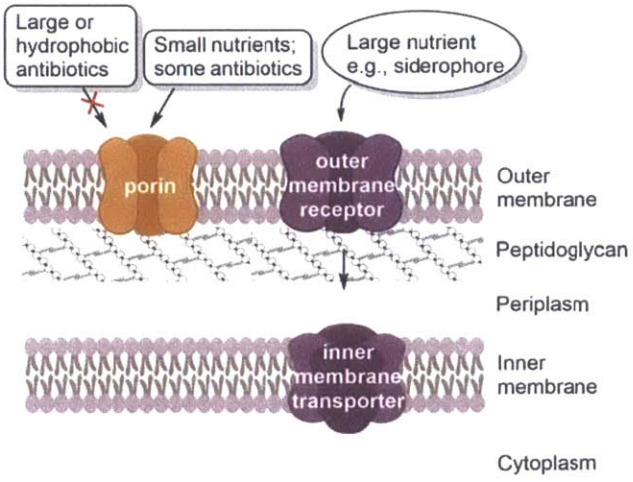

Figure 1.3.2. Model of Gram-negative bacterial cell wall with nutrient passage pathway shown.

The first examples of synthetic siderophore-antibiotic conjugates, reported in 1977 by a Japanese pharmaceutical company, were sulfonamide antibiotics linked to desferrioxamine B and ferricrocin.[141] These compounds exhibited very limited antimicrobial activities against *S. aureus*. In the 1980s, more reports were published from Japanese researchers addressing the attachment of siderophores to β-lactam antibiotics. Since the late 1980s, the Miller group at University of Notre Dame has been very active in this field and explored the syntheses and activities of many conjugates with various siderophores and antibiotics.[142] Other contributors to this field include the Braun group, the Budzikiewicz group and the Möllmann group in Germany, and the Mislin group in France. In industry, Pfizer, Bristol-Myers Squibb (BMS) and Basilea Pharmaceutica have described work with siderophore mimics conjugated with β-lactams.[143] Although many synthetic conjugates exhibit promising preliminary activity *in vitro*, there is only one compound, BAL-30072 from Basilea Pharmaceutica, that entered the clinical trials (Phase II) and the outcome is awaited.[143c] In the following text, major achievements in the development of siderophore-antibiotic conjugates are summarized by the class of antibiotics employed in the design.

Among the available antibiotics, β-lactams are the most widely used in the clinic and well-studied,[144] and they have also been the most investigated warheads for siderophore-antimicrobial conjugates. β-Lactam antibiotics covalently inhibit the transpeptidases, which are responsible for the synthesis of peptidoglycan during bacterial cell wall regeneration. Within the β-lactam family, penams, cephems, carbacephems and monobactams (Figure 1.3.3) have been applied to construct siderophore-antibiotics conjugates.

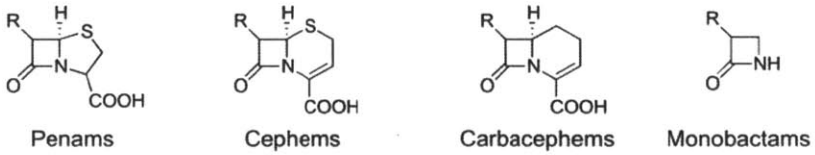

Figure 1.3.3. Core structures of the β-lactam antibiotics used in siderophore conjugates synthesis.

Aminopenicillins such as ampicillin and amoxicillin belong to the penam class, and a number of successful examples applying these antibiotics in siderophore conjugate synthesis were reported. The Möllmann group described several conjugates containing aminopenicillins, and catechol-based siderophore analogs were applied as the siderophore components (e.g., **25** and **26**, Figure 1.3.4).[145] The hydroxyl groups on the catechols were acetylated to form prodrugs to avoid potential methylation by a catechol *O*-methyltransferase presented in host liver, which will eliminate the iron binding property of

the catechols.[146] The conjugates exhibit much higher activity than their parent antibiotics against *P. aeruginosa, E. coli, K. pneumoniea* and *S. maltophilia* strains with minimal inhibitory concentrations (MICs) lower than 0.5 μg/mL. However, the conjugates are less effective than their parent antibiotics against Gram-positive *S. aureus.* More impressively, the conjugates remained active against efflux pump overexpressing strains, suggesting that siderophore conjugation helped the antibiotic to circumvent the efflux pathway. The increased activity was shown to be dependent on TonB and catecholate-siderophore receptor Cir and Fiu. The Budzikiewics group developed pyoverdin-ampicillin conjugates (**27** and **28**, Figure 1.3.4) to target *P. aeruginosa,* and low-micromolar MICs were observed against the corresponding pyoverdin producing strain, while ampicillin was not active at all.[147] Time-kill kinetic studies revealed that these conjugates delayed bacterial growth for 16 h and then mutant strains with impaired pyoverdin uptake systems started to proliferate. These mutant strains were expected to be less virulent under iron deficient conditions.[148] More recently, Miller group reported an Ent analog conjugated to ampicillin and amoxicillin (**29**, Figure 1.3.4) and the conjugates exhibit greatly enhanced activity against selected *P. aeruginosa* strains under iron-limited conditions, but no significant enhancement against *E. coli* or *K. pneumoniea* was observed.[149]

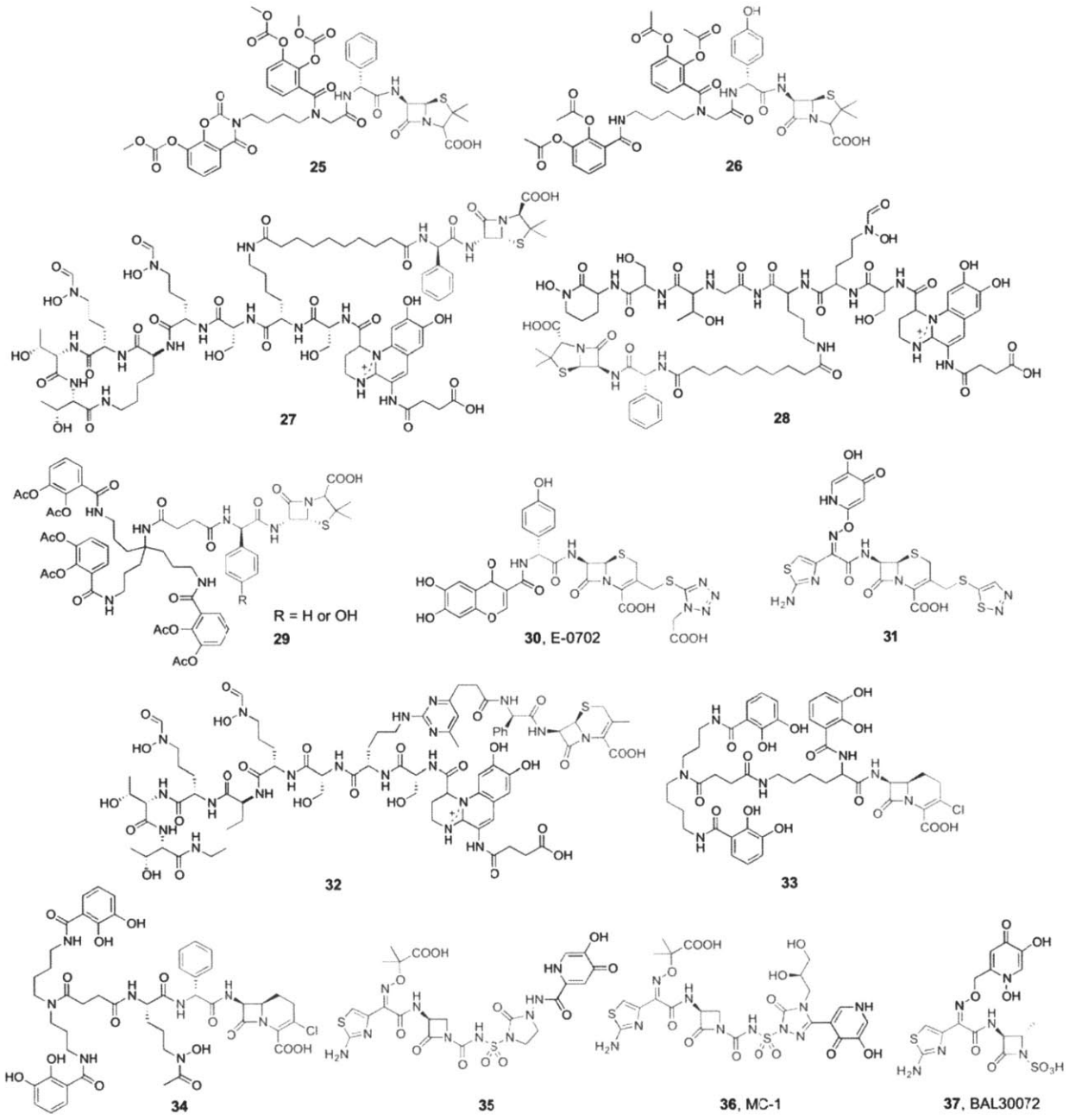

Figure 1.3.4. Structures of representative siderophore-β-lactam conjugates. The antimicrobial components are labeled blue.

Cephems have been conjugated with catechol-containing siderophores, hydroxypyridones and pyoverdines. Most of these molecules were studied in the late 1980s and through the 1990s. For example, E-0702 (**30**, Figure 1.3.4), a cephalosporin-catechol conjugate reported by Watanabe *et. al.*, exhibited enhanced activity against enteric bacteria and *P. aeruginosa*.[150] Spontaneous mutations in resistant

strains showed that E-0702 enters the bacteria via the *TonB*-dependent iron transport system.[151] Later Fiu and Cir were found to be the required outer membrane receptor in *E. coli*.[152] Hydroxypyridone (mimic of catechol) modified cephalosporins (e.g., **31**, Figure 1.3.4) showed very similar profiles as E-0702.[153] Pyoverdine-cephalexin conjugate with a pyrimidine linker (**32**, Figure 1.3.4) was reported to have no activity, and exhibited growth promotion against *P. aeriginosa*.[154] Miller's group investigated a number of carbacephem-catechol or hydroxamate conjugates in the 1990s (e.g., **33**, Figure 1.3.4).[148,155] Carbacephem-catechol/hydroxamate mixed ligand conjugates were also reported (e.g., **34**, Figure 1.3.4).[156] Compared to the penam-siderophore examples, most of these conjugates exhibit very limited activities, although siderophore receptor dependent uptake was observed.

Monobactam-siderophore conjugates have been investigated intensively. Most of these studies come from industrial research groups that focus on structure-activity relationships. The first example, reported by BMS, was a monocarbam (aztreonam) attached to a hydroxypyridone (**35**, Figure 1.3.4).[143b] Recently, Pfizer further developed this class of molecules and synthesized MC-1 (**36**, Figure 1.3.4),[143a] which exhibited moderate enhanced antibacterial activity against *P. aeruginosa*. However, MC-1 was not active against multidrug resistant species, and while the unmodified aztreonam was able to inhibit class C β-lactamases, MC-1 lost this activity. Resistance was acquired quite readily in *E. coli* by loss of TonB or the siderophore receptors.[157] Further optimization of MC-1 guided by a co-crystal structure of the molecule and the penicillin binding protein *Pae*PBP3 led to a new set of compounds with various linkers.[158] Moderate antimicrobial activity was observed for these conjugates against resistant *E. coli, P.aeruginosa* and *K. pneumoniae* strains and rat pharmacokinetic studies demonstrated low clearance and low plasma protein binding. *In vivo* efficacy studies for these compounds are awaited. Basilea Pharmaceutica developed another class of aztreonam-hydroxypyridone conjugates in which the positions of the hydroxypyridones were switched to the other side of the molecule to leave the sulfamate acid intact (e.g., **37**, BAL30072, Figure 1.3.4).[143c] BAL30072 exhibits potent activity against a broad spectrum of Gram-negative bacteria, is resistant to class B and C β-lactamases, and therefore is active against many multidrug-resistant species.[159] Unlike the previous examples, resistance against this molecule evolved relatively slowly and TonB or receptor mutations are rare. In *Burkholderia pseudomallei*, the activity of BAL30072 was suggested to be independent of siderophore uptake systems, whereas in *P. aeruginosa* altered siderophore preference was found in the resistant mutant.[160] It is possible that the siderophore moiety of BAL30072 has different functions against different bacterial species. This compound is currently in early clinical development.

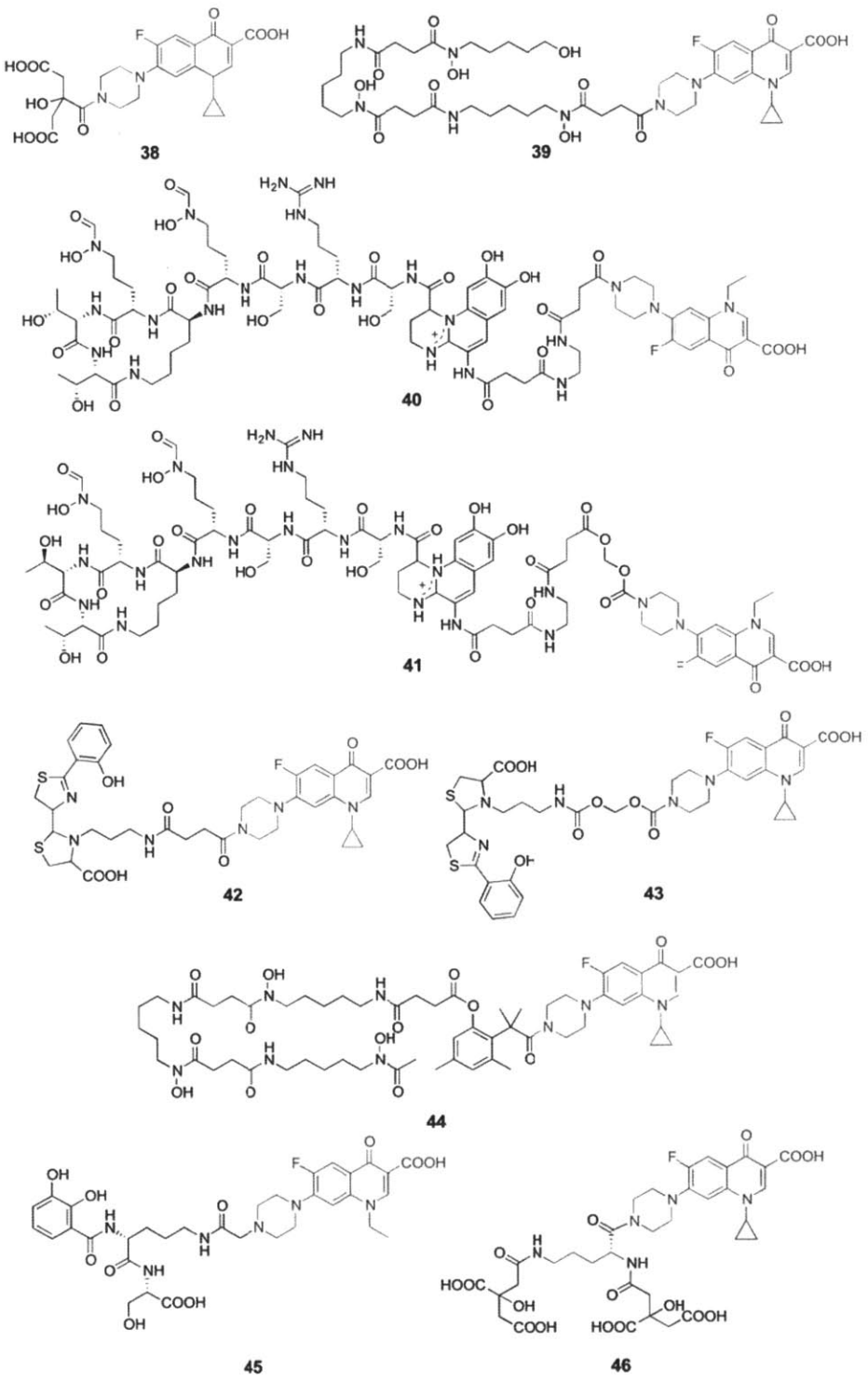

Figure 1.3.5. Structures of representative siderophore-fluoroquinolone conjugates. The antimicrobial components are labeled blue.

In addition to β-lactams, the fluoroquinolone antibiotics were investigated in a number of siderophore conjugate studies. These antibiotics target DNA gyrase and topoisomerase IV and cause DNA fragmentation in bacteria.[161] Siderophore moieties including citrate (**38**, Figure 1.3.5)[162], hydroxamate (**39** and **44** Figure 1.3.5)[163], pyoverdin (**40** and **41**, Figure 1.3.5)[164], pyochelin (**42** and **43**, Figure 1.3.5)[165], vanchrobactin (**45**, Figure 1.3.5)[166] and staphyloferrin A (**46**, Figure 1.3.5)[167] have been attached to fluoroquinolone antibiotics. Most of these conjugates exhibited decreased activity compared to the unmodified antibiotics, raising the concern about proper linker design. For example, Hennard *et al.* reported the synthesis of pyoverdin-norfloxacin conjugates with either a stable linker (**40**, Figure 1.3.5) or labile methylenedioxy linker (**41**, Figure 1.3.5).[164] Only the conjugates with the labile linker exhibited similar activity as norfloxacin and the conjugates with stable linker have decreased activity against *P. aeruginosa.* Transport assays employing ^{55}Fe-conjugate complexes suggested that all conjugates were delivered into the bacterial cell with similar efficiency as pyoverdin. However, the possibility of premature release of the antibiotic before delivery was not addressed in this work. *In vitro* inhibition assays with isolated DNA gyrase showed that the siderophore modification of the fluoroquinolone moieties render them up to 50-time less active compared to the parent antibiotic. Taken together, release of the antibiotic moiety upon uptake maybe highly desired for fluoroquinolones, for the purpose of not perturbing antibiotic-target interaction and preventing interference from the siderophore processing system. Recently the Miller group reported desferrioxamine-ciprofloxacin conjugates with potential esterase and phosphatase cleavable linker (e.g., **44**, Figure 1.3.5), but the results suggested that ciprofloxacin release in the cytosol was not achieved.[163]

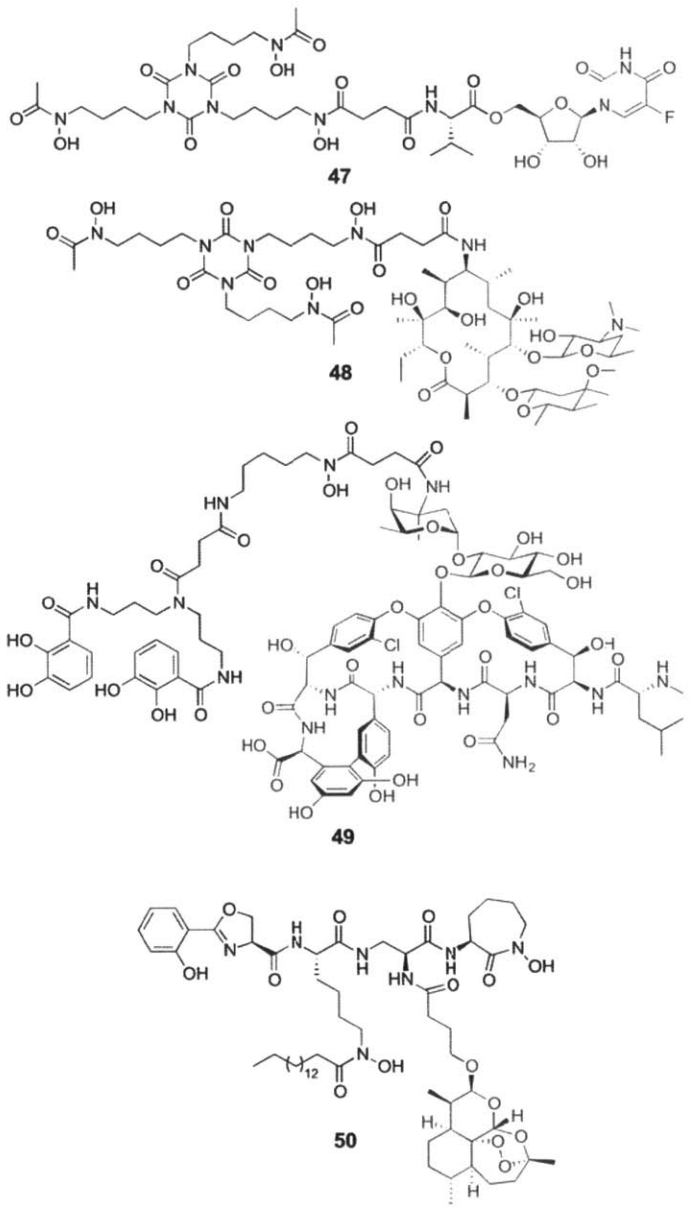

Figure 1.3.6. Structures of representative siderophore-antibiotic conjugates. The antimicrobial components are labeled blue.

Several other classes of antimicrobials including nucleosides (**47**, Figure 1.3.6),[168] macrolides (**48**, Figure 1.3.6) [168] and glycopeptides (**49**, Figure 1.3.6)[169] were investigated by the Miller group with very limited success. The antimicrobial peptide gallidermin was also explored with conjugation to pyochelin, desferrioxamin B and agrobactin by others.[170] Gallidermin belongs to the lantibiotic family and is active against Gram-positive bacteria by inhibiting peptidoglycan biosynthesis. Conjugating

siderophores used by Gram-negative bacteria might be able to help these peptides to penetrate the outer membrane and exhibit activity. Although these conjugates retained their activity against Gram-positives, they were not active against and even provided growth promotion for Gram-negative bacteria. On a separate note, in 2011, the Miller group developed a mycobactin-artemisinin conjugate (**50**, Figure 1.3.6) that was found to be a very potent inhibitor for *M. tuberculosis* growth.[171] Artemisinin is a natural product and in the presence of ferrous ion it can undergo reductive cleavage and generate toxic oxygen-based radicals which will eventually cause cell death.[172] Artemisinin itself is not active against *M. tuberculosis,* but after conjugating to mycobactin, the siderophore used by this species, it exhibited MIC values in the 0.078-1.25 μg/mL range against many *M. tuberculosis* strains including multidrug resistant isolates. The high potency is thought to be related to the reductive removal of iron from mycobactin following uptake, which presents ferrous iron in close proximity to artemisinin. *In vivo* studies of this anti-TB compound have not been reported.

Tremendous efforts have been put forth into developing siderophore-antimicrobial conjugates aiming to provide a new strategy for treating microbial infection. To date, very limited success has been achieved, and many lessons are learned: i) one important factor to consider when designing such conjugates is the redundancy of bacterial iron assimilation systems. The frequent resistance rate upon treating with the siderophore conjugates indicates that bacteria can alternate their iron acquisition methods easily *in vitro*, which presents a challenge for selecting proper siderophores in the design. With accumulated knowledge about siderophores' role during infection, this challenge may be addressed by selecting the ones that are required for bacterial virulence. On the other hand, the altered iron acquisition pattern of the resistance strain may impair bacterial virulence as reported,[148] and more information about the relative expression levels of different iron uptake systems during infection is desired. ii) Another possible aspect for improvement is applying native siderophores not siderophore analogs in the design. In general, the native siderophores exhibit higher iron binding affinities and more efficient recognition by the outer membrane receptors compared to their analogs. Therefore native siderophores have the ability to out-compete the analogs carrying the warhead during iron acquisition, causing insufficient uptake of the conjugates. Indeed the Pfizer group observed such competition when studying their hydropyridone-monobactam conjugate MB-1 against *P.aeruginosa* and pyoverdine production was found to be responsible for the attenuated MB-1 activity *in vivo.*[173] Very limited synthetic approaches for native siderophore modification are available, which poses a challenge for employing native siderophores in the design. iii) The linker between the siderophore and the antimicrobial moieties needs to be designed carefully based on the fact that many antimicrobial reagents studied are less or not active upon siderophore modification, or the siderophore processing machineries may constrain the conjugates

distribution in the cell and thereby prohibit the warheads to reach their target. In these cases an intracellularly cleavable but extracellularly stable linker is highly desirable.

Siderophore-Based Iron Sensors. In addition to delivering antimicrobial reagents, the exquisite specificity and high affinity of a siderophore for ferric ion or its receptor also provide the basis for using these molecules as sensors or probes. Many fluorescence based siderophore sensors that provide rapid, selective and sensitive responses to Fe(III) have been developed. These tools are useful for monitoring iron concentrations in environmental and clinical samples, and can also be applied in investigating iron uptake by siderophore-utilizing organisms and, more broadly, the roles of iron in biology with particular emphasis on the labile iron pool.[174] Iron is a paramagnetic metal ion and thus has a propensity to quench fluorophore emission. As a result, most of the sensors reported afford fluorescence quenching or "turn-off" following Fe(III) recognition.

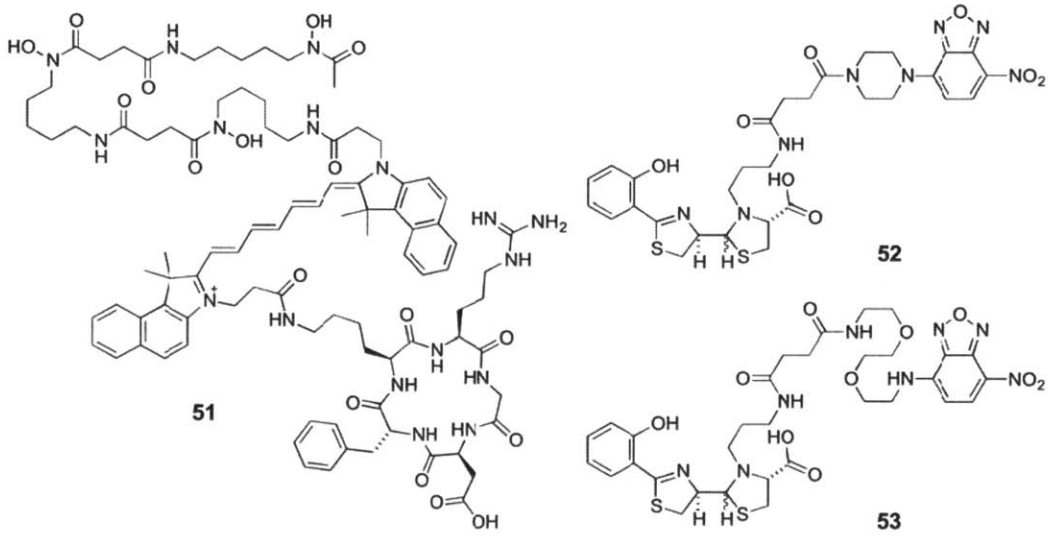

Figure 1.3.7. Structures of representative siderophore- fluorophore conjugates.

Naturally emissive siderophores exist and were applied in iron sensing in the 1990's. For example, pyoverdines (i.e. **11**, Figure 1.2.3) are well-studied fluorescent siderophores produced by all fluorescent pseudomonads including *P. aeruginosa* and *P. fluorescens*.[175] Pyoverdine exhibits high water solubility, forms a 1:1 complex with Fe(III), and exhibits maximum emission at ca. 450 nm in solution. It has been immobilized covalently to various solid phases and used in detecting aqueous samples in

flow cell settings.[176] Other natural siderophores utilized as iron sensors include azotobactin δ and parabactin (**13** and **10**, Figure 1.2.3).[177]

A complementary approach to siderophore-based optical detection of Fe(III) is to modify naturally-occurring siderophores with synthetic fluorophores, affording siderophore-fluorophore conjugates that provide changes in emission following Fe(III) coordination. This tactic requires that the siderophore has a functional group amenable to synthetic modification, and that fluorophore conjugation has negligible impact the iron-binding properties of the chelator. The desferrioxamine (DFO, **1**, Figure 1.2.3) and pyochelin (**15**, Figure 1.2.3) scaffolds have been utilized for the assembly of Fe(III) sensors. There are several applications involving DFO-fluorophore conjugates, and the most recent example is an integrin-targeted probe with a near-IR fluorescent moiety (cypate).[178] The conjugate (**51**, Figure 1.3.7) was designed for tumor imaging and treatment, and it was shown that compound **51** accumulated in the mitochondria, lysosomes and the cytosol. Further studies addressing intracellular iron chelation by the probe may afford insights about iron-related molecular-recognition processes. Two pyochelin-nitrobenz-2-oxa-1,3-diazole (NBD) sensors have been reported and were found to afford turn-on response upon iron binding (**52** and **53**, Figure 1.3.7).[179] In both molecules, the linkers are connected to pyochelin via the *N3*' position, which is involved in iron coordination. Five equivalents of Fe(III) were required for maximum turn-on with 2.9- and 3.2-fold emission enhancement observed for **52** and **53**, respectively. This turn-on behavior is in striking contrast to the fluorescence quenching observed for unmodified pyochelin following Fe(III) coordination,[180] and how the synthetic modifications at the N3" position influence the coordination behavior of pyochelin remains to be explored. Intracellular fluorescence from the NBD chromophore was observed and the pyochelin receptor FptA is required for the cytosol labeling of *P. aeruginosa.* These preliminary experiments indicate that **52** is suited for studying pyochelin uptake in *Pseudomonas* and other organisms.

Besides detecting iron by direct binding, a lanthanide displacement approach applying a desferrioxamin B-*N*-methylanthranyl conjugates (Figure 1.3.8) was also reported.[181] The *N*-methylanthranyl moiety serves as the antenna and thereby transfer energy to the coordinated Ln(III) ion, providing luminescence. Following excitation of **54** at 340 nm, Tb(III) emission was observed in organic solvents such as ethyl acetate and acetonitrile. Addition of Fe(III) to a solution of **54** in ethyl acetate resulted in luminescence quenching, attributed to displacement of Tb(III) from the chelate and formation of **56**. Because the Tb(III) emission was quenched in protic solvents, including methanol and methanol/water mixtures, which limits its utility, a β-diketonate derivative, **55**, was next prepared by using hexafluoroacetylacetone (Hfac) as a blocking ligand to prevent water molecules from binding to the Tb(III) center. This β-diketonate complex exhibited Tb(III) emission in water, which was quenched

following addition of Fe(III). A detection of 5 nM in water was reported; however, compound **55** was not tested in more complex or real-world samples.

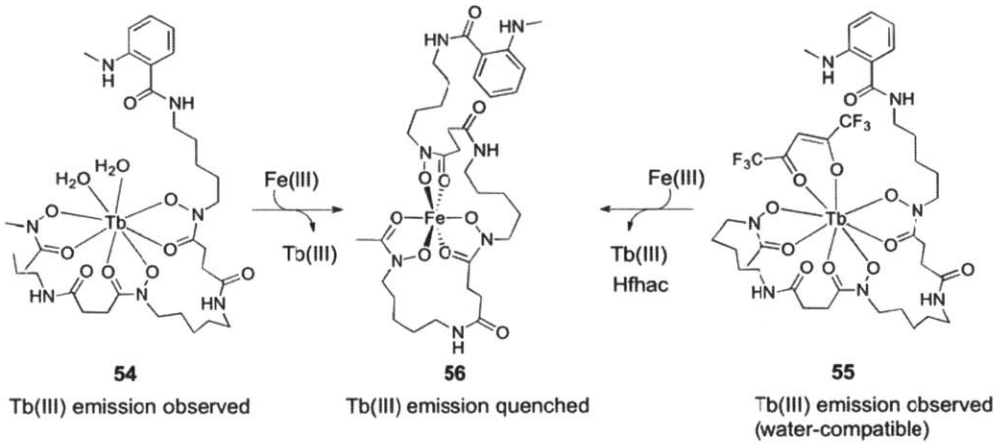

Figure 1.3.8. Iron detection based on lanthanide displacement. Molecules **54** and **55** exhibit terbium luminescence, which is quenched following Fe(III)-mediated Tb(III) displacement.

Siderophore Based Pathogen Detection. Quick and effective identification of bacterial species during infection is very important in clinical setting for diagnostics and proper treatment. The selectivity and high binding affinity of siderophores to their receptors is attractive for developing species-specific bacterial identification and capture technologies. Moreover, from the perspective of pathogen detection, targeting siderophore receptors is worthwhile because the expression of functional siderophore uptake pumps is essential for proliferation and virulence in the iron-limiting environment of the vertebrate host. The likelihood of pathogens mutating these receptors is low.

A recent proof-of-concept example of siderophore-based pathogen detection involved polydimethylsiloxane (PDMS) stamping and immobilization of pyoverdine onto gold-plated glass chips for the capture of the opportunistic human pathogen *P. aeruginosa* (Figure 1.3.9).[182] Pyoverdine was complexed with gallium and coupled to bovine serum albumin (BSA) by using carbodiimide chemistry. Subsequently, a PDMS stamp housing a pattern of repeating parallel ridges was treated with pyoverdine-BSA and employed to imprint a parallel pattern of pyoverdine-BSA onto gold-plate glass chips. Incubating the chips with *P. aeruginosa* cultures for only 15 min afforded maximum light scatting signal and the detection limitation was as low as 10^2-10^4 CFU/mL. *E. coli* or *Y. enterocolitica*, species that neither express FpvA nor utilize pyoverdine for iron acquisition, only exhibited negligible patterning, supporting the requirement of a pyoverdine receptor for detection. This method is further extended to the detection of *Y. enterocolitica* by immobilizing DFO to the chip.[183] As expected, rapid and sensitive

detection was achieved, although *V. cholerae* was also detected, pointing to a need for multiplexing and incorporating orthogonal siderophores on a given chip for rapid species-specific identification in mixed bacterial samples.

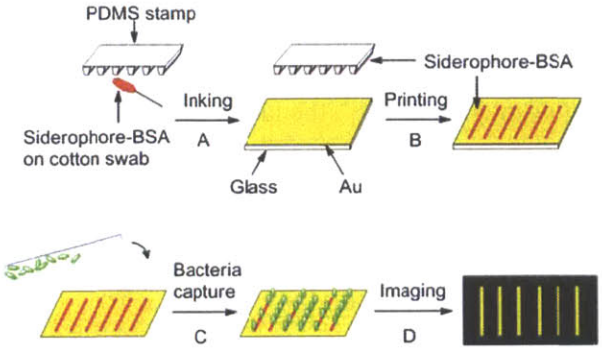

Figure 1.3.9. Pathogen detection using siderophore-immobilization on glass chips. (A) Application of the siderophore-BSA conjugate to a PDMS stamp. (B) Immobilization of siderophore-BSA onto a gold-plated glass chip. (C) Exposure of the chip to a bacterial culture. (D) Imaging of bacterial capture.

Siderophore-modified CdSe/ZnS quantum dots (QDs) were employed to capture *P. fluorescens* isolated from the Dong-Hu Lake in China.[184] In this work, QDs were coated with polyethyleneglycol-phosphoethanolamine (PEG-PD-QD) and ferrichrome was coupled to the terminal amino groups of PEG-PD-QD by using carbodiimide-based coupling chemistry. Incubation of the ferrichrome-QDs with cultures of *P. fluorescens* resulted in clustering and sedimentation observable by fluorescence microscopy and UV-visible spectroscopy. The clustering phenomenon was not observed when the ferrichrome-QDs were incubated with *B. subtilis* or with *P. fluorescens* cultures that were pre-incubated with ferrichrome.

The last proof-of-concept approach employs an immobilized siderophore designed to separate siderophore-binding proteins from cell extracts and is applicable to pathogen detection (Figure 1.3.10). Motivated to provide a simple and direct method for the discovery of siderophore-binding proteins in cell extracts, a biotinylated derivative of petrobactin (**57**, B-petrobactin) was synthesized. The ferric complex of B-petrobactin was incubated with streptavidin-agarose beads, which were used to prepare a petrobactin-affinity column. The column was able to detect one single protein from *B. subtilis* cell lysates, which is identified by SDS-PAGE and MS analysis as YclQ, an ABC transporter binding protein. Prior work has established that YclQ is the petrobactin-binding protein utilized by *B. subtilis,*[185] and this pull down assay suggested that it is the only petrobactin-binding protein expressed on the *B. subtilis* cell surface. Although this approach was intended for the discovery of siderophore-binding proteins, its applicability to pathogen capture is clear and warrants careful consideration. Incubating bacterial

samples with biotinylated siderophores and resin or magnetic beads bearing streptavidin affords a means to separate the bound and unbound cells. Moreover, the biotin/streptavidin interaction may be employed in other immobilization strategies. A biotinylated ferrichrome, prepared by chemical synthesis[186] and a biotinylated salmochelin, prepared by chemoenzymatic synthesis[187] have been reported in the chemical literature. Synthetic routes to other biotinylated siderophores, and biotin attachment strategies that do not compromise iron coordination or interaction with the target receptor, are required for this approach to be broadly applicable.

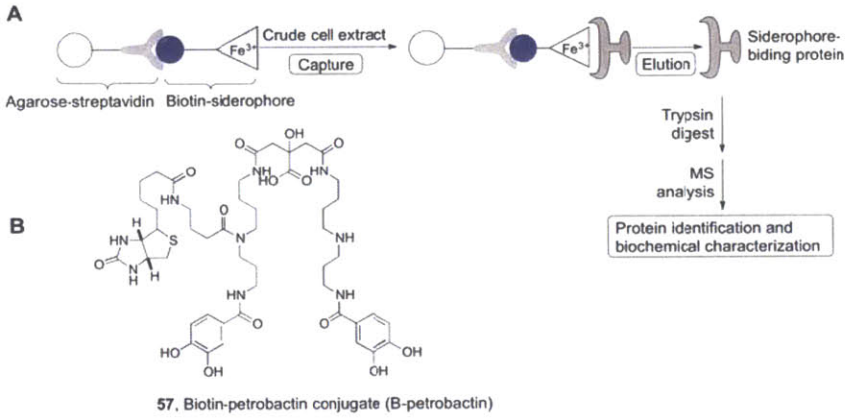

Figure 1.3.10. (A) Isolation of siderophore-binding proteins by using biotin-siderophore conjugates. (B) Structure of biotinylated petrobactin **57**.

1.4 Other Antimicrobial Strategies Targeting Iron Assimilation

Chelation Therapy. Besides hijacking iron uptake pathways by siderophore conjugates, other aspects of bacterial iron acquisition have been investigated for new antimicrobial strategies. The most straightforward approach to block bacterial iron uptake is by using iron chelators to directly compete with the bacterial siderophores. In humans, the iron-chelating proteins transferrin and lactoferrin are examples of this strategy.

Iron chelators used in treating iron-overload diseases have been evaluated for this purpose since they have been shown to be well tolerated in clinical trials. Deferoxamine B (DFO, **1**, Figure 1.2.3), which is a natural siderophore from *Streptomyces pilosus*, is the first iron chelator introduced to clinical practice.[188] The antimicrobial activity of DFO was evaluated against many human pathogens, although no promising MICs were observed *in vitro*.[189] Coadministrating DFO with antibiotics including cephalothin and gentamicin decreased the MICs of the antibiotics, probably due to the iron chelation

effect.[189] And since DFO is a siderophore, for the bacteria strain that can utilize DFO as xenosiderophore, growth enhancement was observed.

Because the risk of increasing susceptibility for bacterial infection using natural siderophores exists, more efforts have been made towards designing synthetic iron chelators. The clinical-approved chelator ciclopirox (Figure 1.4.1) was evaluated for its antibacterial and also antifungal activities *in vitro*, where antibacterial MICs ranging in 0.05-2 μg/mL and antifungal MICs ranging in 0.001-0.25 μg/mL were observed.[190] Due to its higher sensitivity against fungal pathogens, ciclopirox is used widely as a treatment for superficial fungal and yeast infections, and other mechanisms besides iron chelation have been proposed.[191] Similarly, deferiprone and deferasirox (Figure 1.4.1), two oral administrated drugs for chronic iron overload,[192] exhibit potent activity (MIC of ~3 μg/mL) against fungal pathogen *Rhizopus* spp., and mouse models proved their potency *in vivo*.[193] Although not many examples for antibacterial applications exist, such strategies are worthy of attention and further development. The lack of antibacterial activity may be due to lower iron binding affinity of the synthetic chelators compared to natural siderophores. Careful tuning of the iron chelator affinity is likely needed in the design so that it can capture iron before the siderophores do, but should not affect the host iron transport and acquisition.

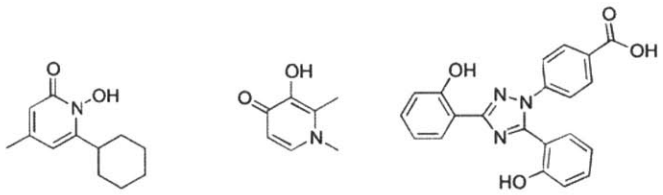

Figure 1.4.1. Structures of synthetic iron chelators in clinical practice.

Inhibiting Siderophore Biosynthesis. During infection, siderophores play an important role in bacterial iron acquisition, and many siderophores are shown to be required for virulence. Therefore, inhibiting the biosynthesis of siderophores is an attractive strategy for developing new antibiotics. Siderophore biosynthesis by nonribosomal peptide synthetases (NRPS) has been studied for decades, which provides a wealth of information for inhibitor design.[194] With the accumulated knowledge of catechol and salicyl containing siderophore biosynthesis, most of the efforts have focused on inhibiting the enzymes that are involved in synthesis or incorporation of the catechol and salicyl moieties in the assembly line. Another advantage for targeting these enzymes is that these two building blocks are not present in human metabolism, and therefore low toxicity is expected.

The salicylate synthases Irp9 in *Yersinia pestis* and MtbI in *M. tuberculosis* were investigated for inhibitor development. These two enzymes are responsible for the first committed step towards the syntheses of yersiniabactin (**8**, Figure 1.2.3) and mycobactin (**12**, Figure 1.2.3). They catalyze conversion of chorismate to salicylate in a two-step reaction (Figure 1.4.2). Benzoate analogs of chorismate like 2,3-dihydroxybenzoate ethers (**58**, Figure 1.4.3) were evaluated for their inhibitory activity against Irp9, which afforded inhibitors with K_i as low as 11 μM.[195] Similar molecules are tested with MtbI and subtle variation of the alkyl ether provides inhibitors with K_i in the 10 μM range (**59**, Figure 1.4.3).[196] In addition to rational design, a high throughput screening against MtbI was performed and a new series of compounds composed by benzimidazole-2-thiones were identified (**60**, Figure 1.4.3). This series was found to be noncompetitive reversible inhibitors with the best activity at IC_{50} of 7.6 μM.[197] Antimicrobial activity of these lead compounds in iron-limitation conditions has not been reported.

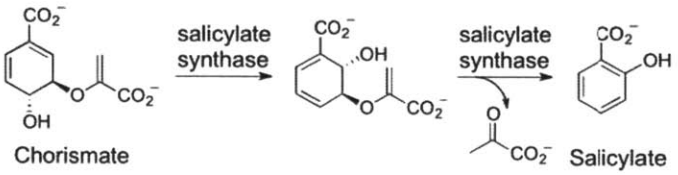

Figure 1.4.2. Reaction mechanism of salicylate synthase.

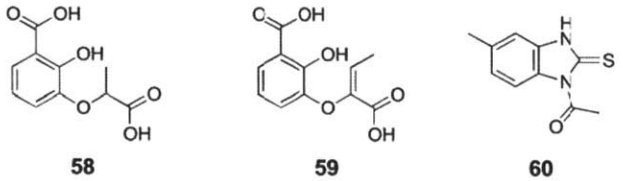

Figure 1.4.3. Inhibitors of salicylate synthase.

The adenylation enzymes that activate catechol and salicyl groups to be incorporated into the assembly line have attracted much attention as well. The adenylation reaction include two steps: first ATP is consumed to form the aryl adenylate; then the peptidyl carrier protein forms a thioester with the activated group and AMP is released (Figure 1.4.4). Nonhydrolyzable transition state mimics of the adenylation reaction were first studied and are found to be very potent inhibitors. For example, the

sulfamate analog of salicyl-AMP (**61**, Figure 1.4.5) exhibit apparent K_i of ~10 nM against the salicyl-adenylation enzymes of *P. aeruginosa* (PchD), *M. tuberculosis* (MtbA) and *Y. pestis* (YbtE). Inhibition of siderophore synthesis was observed, as well as inhibition of bacterial growth in iron-limited conditions (MIC ~10-100 μM) in *M. tuberculosis* and *Y. pestis*.[198] Preliminary pharmacokinetic studies in mouse demonstrated that this inhibitor has poor oral bioavailability.[199] Further optimizations afforded another sulfamate analog with modification on the base (**62**, Figure 1.4.5), which exhibited MIC of 49 nM against *M. tuberculosis,*[200] although no further development of this molecule is reported. Some conformationally constrained intermediate analogs were synthesized recently as an extension to this class (**63**, Figure 1.4.5). Although good enzymatic inhibition activities were observed, the MIC values of this extended class were not promising (>50 μM).[201] Besides transition state mimics, other types of inhibitors were found by screening. Computational studies using 3D-QSAR and shape-based virtual screening against MtbA were recently reported and provided novel structures that warrant experimental evaluation.[202] High-throughput screening was performed against the adenylation enzyme BasE, which initiates the acinetobactin biosynthesis in *A. baumannii*.[203] The most potent inhibitor found during the screen binds BasE in an unexpected way; its phenyl ring blocked the channel for the PCP to reach the AMP-activated intermediate (**64**, Figure 1.4.5).[203] Later on, the same group developed more inhibitors by modifying the hits from the screening and found an improved inhibitor with tight biding to BasE (K_d ~ 2 nM, **65**, Figure 1.4.5). The crystal structure of the inhibitor-bound BasE reveals that the inhibitor occupies all three substrate-binding sites; however, no antimicrobial activity of these BasE inhibitors against *A. baumannii* was observed in iron sufficient or deficient conditions.[204] Hypotheses to explain this lack of efficacy include the permeability issue due to loss of porins or efflux pump expression. Further investigation is needed to test the hypothesis.

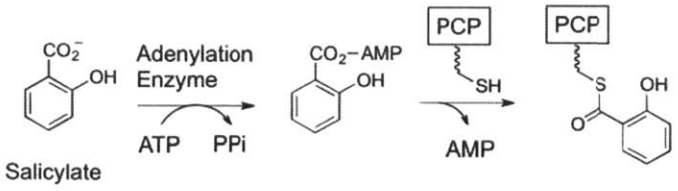

Figure 1.4.4. Activation of salicylate catalyzed by adenylation enzymes.

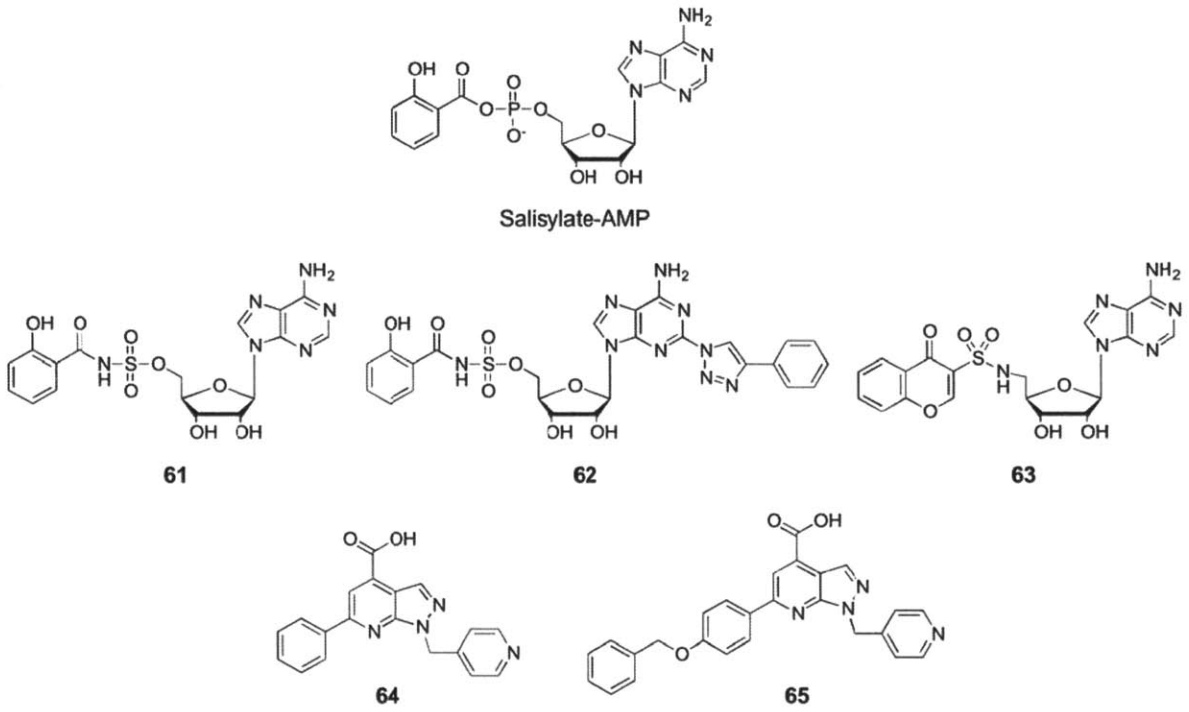

Figure 1.4.5. Inhibitors of salicylate adenylation enzymes.

Another siderophore biosynthesis enzyme investigated is PvdQ, the N-terminal nucleophile hydrolase involved in the maturation of *P. aeruginosa* siderophore pyoverdine. High-throughput screening of a bioactive molecule library afforded inhibitors with IC_{50} of 60-100 μM (**66**, Figure 1.4.6) and crystal structures of the most potent inhibitors bound to PvdQ are solved.[205] The inhibitors were found to bind deeply in the substrate binding pocket through hydrophobic interactions and not affect the catalytic residues. Therefore, the inhibition mechanism may involve disruption of the substrate positioning in the binding pocket. More recently, another class of inhibitors composed by alkylboronates from rational design were found to be very potent against PvdQ with $K_i \geq 190$ pM (**67**, Figure 1.4.6). These inhibitors were able to interact with the catalytic Ser residue in the active site to mimic the transition state. Although co-administration of an efflux pump inhibitor is required to observe growth inhibition of the bacteria in iron-limited conditions.[206]

Outside of the NRPS system, there are siderophores synthesized independently of these enzymes. Staphyloferrin B from *S. aureus* and petrobactin from *B. anthracis* (**7** and **8**, Figure 1.2.3) are two examples. High throughput screening using a library of marine microbial-derived natural product extracts against, SbnE and AsbA, two enzymes that are involved in the synthesis of staphyloferrin B and petrobactin, afforded a lead compound (**68**, Figure 1.4.6) with IC_{50} values of 4.8 μM against SbnE and

180 μM against AsbA. Moderate growth inhibition activity was also observed against *S. aureus*, *B. anthracis* and *E. coli* (MIC of 0.5-1 mM).[207] Although most of the works reported in this field are only proof-of-concept studies, siderophore biosynthesis pathways remain to be attractive targets for developing novel antimicrobial treatment.

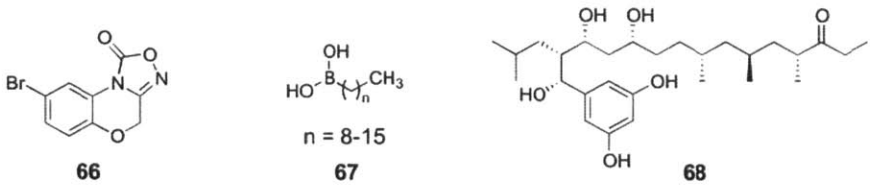

Figure 1.4.6. Inhibitors of *P. aeruginosa* enzyme PvdQ and non-NRPS enzyme SbnE and AsbA.

Disrupting Siderophore Export. For many of the siderophores that unload iron through reduction, the apo siderophores are recycled and secreted back to the outer cellular environment. It has been recently discovered that interfering this recycling process can result in self-poisoning of the producing bacteria.[208] In this study, the knock-out mutant of two membrane proteins MmrS4 and MmrS5 of *M. tuberculosis*, which were required for the export of mycobactin and carboxymycobactin, was found to be unable to recycle the siderophores. The mutant showed a strong virulence defect in a mouse model and was unable to grow when hemoglobin was the sole iron source. Addition of extra mycobactin and carboxymycobactin inhibited its growth at low micromolar concentration. Higher accumulation of carboxymycobactin inside of the bacteria was also observed. However, when siderophore biosynthesis was shut-down, the growth of the mutant was restored on a hemoglobin supplemented plate. Taken together, these results suggest that extra siderophores accumulated in the bacteria are toxic, probably by causing undesired iron deprivation. Another example is that when the Ent export protein TolC was knocked out, *E. coli* exhibited growth and morphological defects attributed to Ent accumulation in the periplasm.[209] In a separate study, Ent and salmochelin secretion deficient extraintestinal pathogenic *E. coli* strains (gene-knocked out of *entS* and *iroC*) were attenuated in a chicken infection model.[210] Intracellular accumulation of Ent and salmochelins were also observed by LC-MS analysis. Although no inhibitors have been reported for siderophore export, it is an interesting target for new antibiotic development because it will both limit siderophore mediated iron-uptake and also cause toxic siderophore accumulation unless siderophore biosynthesis is turned off.

1.5 Goals and Organization of the Thesis

The focus of this thesis is to evaluate whether native siderophore platforms provide new efficient approaches for delivering antibiotics and other functional molecules to Gram-negative bacteria. Since the wide clinic use of antibiotics in the 1950s, antibiotic resistance has been emerging at an alarming rate and new strategies to treat microbial infections are urgently needed. Siderophore mediated iron uptake machinery plays important role in virulence and pathogenicity, and is essential for the proliferation of bacteria, making it an attracting target for new antimicrobial development. Siderophore conjugates are able to hijack the siderophore uptake machinery and hold great potential for developing highly effective and microbe-selective antibiotics, as well as diagnostic tools and other applications.

One major challenge in siderophore-conjugate development is the very limited synthetic methods allowing site-specific modification on native siderophores. Enterobactin, the most well studied siderophore with the highest iron binding affinity among all characterized siderophores, has not been applied in the context of siderophore-conjugates, probably is due to lack of feasible synthetic approaches. In this thesis, we developed new synthetic routes to allow the native Ent scaffold to be employed in the siderophore-conjugate strategies. Different classes of cargo molecules were attached to Ent through these synthetic routes and the applications of these conjugates were evaluated.

In Chapter 2, a relatively short synthetic approach towards site-specific mono-, di- and tri-modification on native Ent structure is described. The resulting modified Ent scaffolds allow use of versatile functional groups for different applications. Next, the promiscuity of Ent uptake machinery towards Ent-cargo conjugates was evaluated in *E. coli* and *P. aeruginosa.* The ability of Ent receptor FepA to transport large protein like the 55-kD colicin B[211] and bacterial phages[212] make the assumption that FepA can accommodate large cargos appealing. However we found that the cargo sizes affect the delivery efficiency. This information is important for designing Ent-cargo conjugates that require cellular entry for fulfilling their function. It also raises a general concern for conjugate design using other siderophores, because their uptake machineries have similar features to that of Ent and may also present limitations to cargo size.

In Chapter 3, guided by the information obtained in Chapter 2, two β-lactam antibiotics, ampicillin and amoxicillin are attached to Ent, and the antimicrobial activity of conjugates are tested against a wide range of bacterial species with the expectation that Ent-mediated delivery will greatly enhance the activity of the antibiotics. These two widely used and well-studied antibiotics fall into the acceptable cargo size range, and a 100-1000 fold activity improvement was observed upon Ent modification against selected *E. coli* strains including human pathogens. The mechanism of the observed antimicrobial activity was probed by using mutant strains and conjugate analogs, which proves that the activity enhancement was due to Ent-mediated active delivery. Prior work employing ampicillin and

amoxicillin in Ent-analog-antibiotic conjugates synthesis only afforded moderate activity against *E coli.*[149] Our results indicate the selection of siderophores may have great influence on the spectrum of bacterial sensitivity.

In Chapter 4, fluoroquinolone antibiotics attached to Ent were reported with a focus on studying the linker design and stability. Different than β-lactams, fluoroquinolones target DNA gyrases locating in the bacterial cytoplasm, and it is suggested that a release step from the conjugate is required for their activity.[164] Ent-fluoroquinolone conjugates with a reported ester-based labile linker were synthesized, and the stability of the linker was evaluated under neutral pH, which revealed that such linker was not suitable for the siderophore conjugate application because it is very unstable and causes premature release of the antibiotics before cellular entry. Alternative labile linker scaffolds are needed for applying antibiotics targeting cytosolic enzymes in the siderophore conjugate strategy.

Lastly, chemoenzymatic approach for Ent-conjugate synthesis is reported in Appendix 1.

References

1. Ganz, T., Systemic iron homeostasis. *Physiol. Rev.* **2013,** *93* (4), 1721-1741.
2. Cornelis, P.; Wei, Q.; Andrews, S. C.; Vinckx, T., Iron homeostasis and management of oxidative stress response in bacteria. *Metallomics* **2011,** *3* (6), 540-549.
3. Green, R.; Charlton, R.; Seftel, H.; Bothwell, T.; Mayet, F.; Adams, B.; Finch, C.; Layrisse, M., Body iron excretion in man: a collaborative study. *Am. J. Med.* **1968,** *45* (3), 336-353.
4. Fairweather-Tait, S. J., Iron nutrition in the UK: getting the balance right. *Proc. Nutr. Soc.* **2004,** *63* (4), 519-528.
5. Zimmermann, M. B.; Hurrell, R. F., Nutritional iron deficiency. *Lancet* **2007,** *370* (9586), 511-520.
6. (a) Gunshin, H.; Mackenzie, B.; Berger, U. V.; Gunshin, Y.; Romero, M. F.; Boron, W. F.; Nussberger, S.; Gollan, J. L.; Hediger, M. A., Cloning and characterization of a mammalian proton-coupled metal-ion transporter. *Nature* **1997,** *388* (6641), 482-488; (b) Gunshin, H.; Starr, C. N.; Direnzo, C.; Fleming, M. D.; Jin, J.; Greer, E. L.; Sellers, V. M.; Galica, S. M.; Andrews, N. C., Cybrd1 (duodenal cytochrome b) is not necessary for dietary iron absorption in mice. *Blood* **2005,** *106* (8), 2879-2883.
7. Wyllie, J. C.; Kaufman, N., An electron microscopic study of heme uptake by rat duodenum. *Lab. Invest.* **1982,** *47* (5), 471-476.
8. Abboud, S.; Haile, D. J., A novel mammalian iron-regulated protein involved in intracellular iron metabolism. *J. Biol. Chem.* **2000,** *275* (26), 19906-19912.
9. Kosman, D. J., Redox cycling in iron uptake, efflux, and trafficking. *J. Biol. Chem.* **2010,** *285* (35), 26729-26735.
10. Aisen, P.; Leibman, A.; Zweier, J., Stoichiometric and site characteristics of the binding of iron to human transferrin. *J. Biol. Chem.* **1978,** *253* (6), 1930-1937.
11. Hentze, M. W.; Muckenthaler, M. U.; Andrews, N. C., Balancing acts: molecular control of mammalian iron metabolism. *Cell* **2004,** *117* (3), 285-297.
12. Andrews, S. C.; Arosio, P.; Bottke, W.; Briat, J. F.; Vondarl, M.; Harrison, P. M.; Laulhere, J. P.; Levi, S.; Lobreaux, S.; Yewdall, S. J., Structure, Function, and Evolution of Ferritins. *J. Inorg. Biochem.* **1992,** *47* (3-4), 161-174.

13. Shi, H. F.; Bencze, K. Z.; Stemmler, T. L.; Philpott, C. C., A cytosolic iron chaperone that delivers iron to ferritin. *Science* **2008,** *320* (5880), 1207-1210.
14. Ganz, T., Hepcidin and iron regulation, 10 years later. *Blood* **2011,** *117* (17), 4425-4433.
15. Nemeth, E.; Tuttle, M. S.; Powelson, J.; Vaughn, M. B.; Donovan, A.; Ward, D. M.; Ganz, T.; Kaplan, J., Hepcidin regulates cellular iron efflux by binding to ferroportin and inducing its internalization. *Science* **2004,** *306* (5704), 2090-2093.
16. Rouault, T. A., The role of iron regulatory proteins in mammalian iron homeostasis and disease. *Nat. Chem. Biol.* **2006,** *2* (8), 406-414.
17. Raymond, K. N.; Dertz, E. A.; Kim, S. S., Enterobactin: An archetype for microbial iron transport. *Proc. Natl. Acad. Sci. U. S. A.* **2003,** *100* (7), 3584-3588.
18. Cassat, J. E.; Skaar, E. P., Iron in infection and immunity. *Cell Host Microbe* **2013,** *13* (5), 509-519.
19. Hider, R. C.; Kong, X., Chemistry and biology of siderophores. *Nat. Prod. Rep.* **2010,** *27* (5), 637-657.
20. Rodriguez, G. M., Control of iron metabolism in Mycobacterium tuberculosis. *Trends Microbiol.* **2006,** *14* (7), 320-327.
21. Kim, C. M.; Park, Y. J.; Shin, S. H., A widespread deferoxamine-mediated iron-uptake system in Vibrio vulnificus. *J. Infect. Dis.* **2007,** *196* (10), 1537-1545.
22. (a) Lawlor, M. S.; O'Connor, C.; Miller, V. L., Yersiniabactin is a virulence factor for Klebsiella pneumoniae during pulmonary infection. *Infect. Immun.* **2007,** *75* (3), 1463-1472; (b) Taguchi, F.; Suzuki, T.; Inagaki, Y.; Toyoda, K.; Shiraishi, T.; Ichinose, Y., The Siderophore Pyoverdine of Pseudomonas syringae pv. tabaci 6605 Is an Intrinsic Virulence Factor in Host Tobacco Infection. *J. Bacteriol.* **2010,** *192* (1), 117-126; (c) Johnson, J. R., Virulence Factors in Escherichia-Coli Urinary-Tract Infection. *Clin. Microbiol. Rev.* **1991,** *4* (1), 80-128.
23. Hantke, K., Ferrous Iron Transport Mutants in Escherichia-Coli-K12. *FEMS Microbiol. Lett.* **1987,** *44* (1), 53-57.
24. Tsolis, R. M.; Baumler, A. J.; Heffron, F.; Stojiljkovic, I., Contribution of TonB- and Feo-mediated iron uptake to growth of Salmonella typhimurium in the mouse. *Infect. Immun.* **1996,** *64* (11), 4549-4556.
25. Velayudhan, J.; Hughes, N. J.; McColm, A. A.; Bagshaw, J.; Clayton, C. L.; Andrews, S. C.; Kelly, D. J., Iron acquisition and virulence in Helicobacter pylori: a major role for FeoB, a high-affinity ferrous iron transporter. *Mol. Microbiol.* **2000,** *37* (2), 274-286.
26. (a) Spiro, S.; Guest, J. R., Fnr and Its Role in Oxygen-Regulated Gene-Expression in Escherichia-Coli. *FEMS Microbiol. Lett.* **1990,** *75* (4), 399-428; (b) Cao, J.; Woodhall, M. R.; Alvarez, J.; Cartron, M. L.; Andrews, S. C., EfeUOB (YcdNOB) is a tripartite, acid-induced and CpxAR-regulated, low-pH Fe2+ transporter that is cryptic in Escherichia coli K-12 but functional in E. coli O157 : H7. *Mol. Microbiol.* **2007,** *65* (4), 857-875.
27. Stojiljkovic, I.; Cobeljic, M.; Hantke, K., Escherichia coli K-12 ferrous iron uptake mutants are impaired in their ability to colonize the mouse intestine. *FEMS Microbiol. Lett.* **1993,** *108* (1), 111-115.
28. Marlovits, T. C.; Haase, W.; Herrmann, C.; Aller, S. G.; Unger, V. M., The membrane protein FeoB contains an intramolecular G protein essential for Fe(II) uptake in bacteria. *Proc. Natl. Acad. Sci. U. S. A.* **2002,** *99* (25), 16243-16248.
29. Lau, C. K. Y.; Ishida, H.; Liu, Z. H.; Vogel, H. J., Solution Structure of Escherichia coli FeoA and Its Potential Role in Bacterial Ferrous Iron Transport. *J. Bacteriol.* **2013,** *195* (1), 46-55.
30. Cartron, M. L.; Maddocks, S.; Gillingham, P.; Craven, C. J.; Andrews, S. C., Feo - Transport of ferrous iron into bacteria. *BioMetals* **2006,** *19* (2), 143-157.
31. Zimmermann, L.; Angerer, A.; Braun, V., Mechanistically Novel Iron(Iii) Transport-System in Serratia-Marcescens. *J. Bacteriol.* **1989,** *171* (1), 238-243.
32. Koster, W., ABC transporter-mediated uptake of iron, siderophores, heme and vitamin B-12. *Res. Microbiol.* **2001,** *152* (3-4), 291-301.

33. Wandersman, C.; Stojiljkovic, I., Bacterial heme sources: the role of heme, hemoprotein receptors and hemophores. *Curr. Opin. Microbiol.* **2000,** *3* (2), 215-220.
34. Hammer, N. D.; Skaar, E. P., Molecular Mechanisms of Staphylococcus aureus Iron Acquisition. *Annu. Rev. Microbiol.* **2011,** *65*, 129-147.
35. Skaar, E. P.; Humayun, M.; Bae, T.; DeBord, K. L.; Schneewind, O., Iron-source preference of Staphylococcus aureus infections. *Science* **2004,** *305* (5690), 1626-1628.
36. Cornelis, P., Iron uptake and metabolism in pseudomonads. *Appl. Microbiol. Biot.* **2010,** *86* (6), 1637-1645.
37. Cassat, J. E.; Skaar, E. P., Iron in Infection and Immunity. *Cell Host Microbe* **2013,** *13* (5), 510-520.
38. Cornelissen, C. N.; Sparling, P. F., Iron Piracy - Acquisition of Transferrin-Bound Iron by Bacterial Pathogens. *Mol. Microbiol.* **1994,** *14* (5), 843-850.
39. Noinaj, N.; Easley, N. C.; Oke, M.; Mizuno, N.; Gumbart, J.; Boura, E.; Steere, A. N.; Zak, O.; Aisen, P.; Tajkhorshid, E.; Evans, R. W.; Gorringe, A. R.; Mason, A. B.; Steven, A. C.; Buchanan, S. K., Structural basis for iron piracy by pathogenic Neisseria. *Nature* **2012,** *483* (7387), 53-U92.
40. Cornelissen, C. N.; Kelley, M.; Hobbs, M. M.; Anderson, J. E.; Cannon, J. G.; Cohen, M. S.; Sparling, P. F., The transferrin receptor expressed by gonococcal strain FA1090 is required for the experimental infection of human male volunteers. *Mol. Microbiol.* **1998,** *27* (3), 611-616.
41. Vogel, H. J., Lactoferrin, a bird's eye view INTRODUCTION. *Biochem. Cell Biol.* **2012,** *90* (3), 233-244.
42. Wooldridge, K. G.; Williams, P. H., Iron uptake mechanisms of pathogenic bacteria. *FEMS Microbiol. Rev.* **1993,** *12* (4), 325-348.
43. Andrews, S. C., Iron storage in bacteria. *Adv. Microb. Physiol.* **1998,** *40*, 281-351.
44. Dautant, A.; Meyer, J. B.; Yariv, J.; Precigoux, G.; Sweet, R. M.; Kalb, A. J.; Frolow, F., Structure of a monoclinic crystal form of cytochrome b1 (bacterioferritin) from E-coli. *Acta Crystallogr. D* **1998,** *54*, 16-24.
45. Yasmin, S.; Andrews, S. C.; Moore, G. R.; Le Brun, N. E., A new role for heme, facilitating release of iron from the bacterioferritin iron biomineral. *J. Biol. Chem.* **2011,** *286* (5), 3473-3483.
46. Bellapadrona, G.; Ardini, M.; Ceci, P.; Stefanini, S.; Chiancone, E., Dps proteins prevent Fenton-mediated oxidative damage by trapping hydroxyl radicals within the protein shell. *Free Radic. Biol. Med.* **2010,** *48* (2), 292-297.
47. Hantke, K., Iron and metal regulation in bacteria. *Curr. Opin. Microbiol.* **2001,** *4* (2), 172-177.
48. Lee, J. W.; Helmann, J. D., Functional specialization within the Fur family of metalloregulators. *BioMetals* **2007,** *20* (3-4), 485-499.
49. Masse, E.; Vanderpool, C. K.; Gottesman, S., Effect of RyhB small RNA on global iron use in Escherichia coli. *J. Bacteriol.* **2005,** *187* (20), 6962-6971.
50. Dubrac, S.; Touati, D., Fur positive regulation of iron superoxide dismutase in Escherichia coli: Functional analysis of the sodB promoter. *J. Bacteriol.* **2000,** *182* (13), 3802-3808.
51. Bagg, A.; Neilands, J. B., Ferric Uptake Regulation Protein Acts as a Repressor, Employing Iron(Ii) as a Cofactor to Bind the Operator of an Iron Transport Operon in Escherichia-Coli. *Biochemistry* **1987,** *26* (17), 5471-5477.
52. Rodriguez, G. M.; Voskuil, M. I.; Gold, B.; Schoolnik, G. K.; Smith, I., ideR, an essential gene in Mycobacterium tuberculosis: Role of IdeR in iron-dependent gene expression, iron metabolism, and oxidative stress response. *Infect. Immun.* **2002,** *70* (7), 3371-3381.
53. Uroz, S.; Dessaux, Y.; Oger, P., Quorum Sensing and Quorum Quenching: The Yin and Yang of Bacterial Communication. *ChemBioChem* **2009,** *10* (2), 205-216.
54. Stintzi, A.; Evans, K.; Meyer, J. M.; Poole, K., Quorum-sensing and siderophore biosynthesis in Pseudomonas aeruginosa: lasR/lasI mutants exhibit reduced pyoverdine biosynthesis. *FEMS Microbiol. Lett.* **1998,** *166* (2), 341-345.
55. Lilley, B. N.; Bassler, B. L., Regulation of quorum sensing in Vibrio harveyi by LuxO and Sigma-54. *Mol. Microbiol.* **2000,** *36* (4), 940-954.

56. Wang, Q.; Liu, Q.; Ma, Y.; Rui, H.; Zhang, Y., LuxO controls extracellular protease, haemolytic activities and siderophore production in fish pathogen Vibrio alginolyticus. *J. Appl. Microbiol.* **2007,** *103* (5), 1525-1534.
57. Fong, K. P.; Gao, L.; Demuth, D. R., luxS and arcB control aerobic growth of Actinobacillus actinomycetemcomitans under iron limitation. *Infect. Immun.* **2003,** *71* (1), 298-308.
58. (a) Weinberg, E. D., Nutritional immunity. Host's attempt to withold iron from microbial invaders. *JAMA, J. Am. Med. Assoc.* **1975,** *231* (1), 39-41; (b) Hood, M. I.; Skaar, E. P., Nutritional immunity: transition metals at the pathogen-host interface. *Nat. Rev. Microbiol.* **2012,** *10* (8), 525-537.
59. Baker, H. M.; Baker, E. N., Lactoferrin and iron: structural and dynamic aspects of binding and release. *BioMetals* **2004,** *17* (3), 209-216.
60. Singh, P. K.; Parsek, M. R.; Greenberg, E. P.; Welsh, M. J., A component of innate immunity prevents bacterial biofilm development. *Nature* **2002,** *417* (6888), 552-555.
61. Goetz, D. H.; Holmes, M. A.; Borregaard, N.; Bluhm, M. E.; Raymond, K. N.; Strong, R. K., The neutrophil lipocalin NGAL is a bacteriostatic agent that interferes with siderophore-mediated iron acquisition. *Mol. Cell* **2002,** *10* (5), 1033-1043.
62. Payne, M. A.; Igo, J. D.; Cao, Z. H.; Foster, S. B.; Newton, S. M. C.; Klebba, P. E., Biphasic binding kinetics between FepA and its ligands. *J. Biol. Chem.* **1997,** *272* (35), 21950-21955.
63. Hoette, T. M.; Abergel, R. J.; Xu, J. D.; Strong, R. K.; Raymond, K. N., The Role of Electrostatics in Siderophore Recognition by the Immunoprotein Siderocalin. *J. Am. Chem. Soc.* **2008,** *130* (51), 17584-17592.
64. Abergel, R. J.; Wilson, M. K.; Arceneaux, J. E. L.; Hoette, T. M.; Strong, R. K.; Byers, B. R.; Raymond, K. N., Anthrax pathogen evades the mammalian immune system through stealth siderophore production. *Proc. Natl. Acad. Sci. U. S. A.* **2006,** *103* (49), 18499-18503.
65. Yang, J.; Goetz, D.; Li, J. Y.; Wang, W.; Mori, K.; Setlik, D.; Du, T.; Erdjument-Bromage, H.; Tempst, P.; Strong, R.; Barasch, J., An iron delivery pathway mediated by a lipocalin. *Mol. Cell* **2002,** *10* (5), 1045-1056.
66. Abergel, R. J.; Clifton, M. C.; Pizarro, J. C.; Warner, J. A.; Shuh, D. K.; Strong, R. K.; Raymond, K. N., The siderocalin/enterobactin interaction: a link between mammalian immunity and bacterial iron transport. *J. Am. Chem. Soc.* **2008,** *130* (34), 11524-11534.
67. Hoette, T. M.; Clifton, M. C.; Zawadzka, A. M.; Holmes, M. A.; Strong, R. K.; Raymond, K. N., Immune Interference in Mycobacterium tuberculosis Intracellular Iron Acquisition through Siderocalin Recognition of Carboxymycobactins. *ACS Chem. Biol.* **2011,** *6* (12), 1327-1331.
68. Fischbach, M. A.; Lin, H. N.; Zhou, L.; Yu, Y.; Abergel, R. J.; Liu, D. R.; Raymond, K. N.; Wanner, B. L.; Strong, R. K.; Walsh, C. T.; Aderem, A.; Smith, K. D., The pathogen-associated iroA gene cluster mediates bacterial evasion of lipocalin 2. *Proc. Natl. Acad. Sci. U. S. A.* **2006,** *103* (44), 16502-16507.
69. Raffatellu, M.; George, M. D.; Akiyama, Y.; Hornsby, M. J.; Nuccio, S. P.; Paixao, T. A.; Butler, B. P.; Chu, H. T.; Santos, R. L.; Berger, T.; Mak, T. W.; Tsolis, R. M.; Bevins, C. L.; Solnick, J. V.; Dandekar, S.; Baumler, A. J., Lipocalin-2 Resistance Confers an Advantage to Salmonella enterica Serotype Typhimurium for Growth and Survival in the Inflamed Intestine. *Cell Host Microbe* **2009,** *5* (5), 476-486.
70. Flo, T. H.; Smith, K. D.; Sato, S.; Rodriguez, D. J.; Holmes, M. A.; Strong, R. K.; Akira, S.; Aderem, A., Lipocalin 2 mediates an innate immune response to bacterial infection by sequestrating iron. *Nature* **2004,** *432* (7019), 917-921.
71. (a) Harris, W. R.; Carrano, C. J.; Raymond, K. N., Coordination Chemistry of Microbial Iron Transport Compounds .16. Isolation, Characterization, and Formation-Constants of Ferric Aerobactin. *J. Am. Chem. Soc.* **1979,** *101* (10), 2722-2727; (b) Loomis, L. D.; Raymond, K. N., Solution Equilibria of Enterobactin and Metal Enterobactin Complexes. *Inorg. Chem.* **1991,** *30* (5), 906-911; (c) Zhang, G. P.; Amin, S. A.; Kupper, F. C.; Holt, P. D.; Carrano, C. J.; Butler, A., Ferric Stability Constants of Representative Marine Siderophores: Marinobactins, Aquachelins, and Petrobactin. *Inorg. Chem.* **2009,** *48* (23), 11466-11473.

72. Francis, J.; Madinaveitia, J.; Macturk, H. M.; Snow, G. A., Isolation from Acid-Fast Bacteria of a Growth-Factor for Mycobacterium-Johnei and of a Precursor of Phthiocol. *Nature* **1949,** *163* (4140), 365-366.
73. Hider, R. C.; Kong, X. L., Chemistry and biology of siderophores. *Nat. Prod. Rep.* **2010,** *27* (5), 637-657.
74. (a) Hider, R. C.; Hall, A. D., Clinically useful chelators of tripositive elements. *Prog. Med. Chem.* **1991,** *28*, 41-173; (b) Avdeef, A.; Sofen, S. R.; Bregante, T. L.; Raymond, K. N., Coordination Chemistry of Microbial Iron Transport Compounds .9. Stability-Constants for Catechol Models of Enterobactin. *J. Am. Chem. Soc.* **1978,** *100* (17), 5362-5370; (c) Robert M. Smith, A. E. M., *Critical Stability Constants*. Plenum press: New York, 1977; Vol. 3.
75. Dhungana, S.; White, P. S.; Crumbliss, A. L., Crystal structure of ferrioxamine B: a comparative analysis and implications for molecular recognition. *J. Biol. Inorg. Chem.* **2001,** *6* (8), 810-818.
76. Vanderhelm, D.; Baker, J. R.; Engwilmot, D. L.; Hossain, M. B.; Loghry, R. A., Crystal-Structure of Ferrichrome and a Comparison with the Structure of Ferrichrome-A. *J. Am. Chem. Soc.* **1980,** *102* (12), 4224-4231.
77. Miller, M. C.; Parkin, S.; Fetherston, J. D.; Perry, R. D.; DeMoll, E., Crystal structure of ferric-yersiniabactin, a virulence factor of Yersinia pestis. *J. Inorg. Biochem.* **2006,** *100* (9), 1495-1500.
78. Karpishin, T. B.; Raymond, K. N., The 1st Structural Characterization of a Metal-Enterobactin Complex - [V(Enterobactin)]2-. *Angew. Chem. Int. Edit.* **1992,** *31* (4), 466-468.
79. Boukhalfa, H.; Crumbliss, A. L., Chemical aspects of siderophore mediated iron transport. *BioMetals* **2002,** *15* (4), 325-339.
80. Liu, Z. D.; Hider, R. C., Design of clinically useful iron(III)-selective chelators. *Med. Res. Rev.* **2002,** *22* (1), 26-64.
81. Dhungana, S.; Crumbliss, A. L., Coordination chemistry and redox processes in siderophore-mediated iron transport. *Geomicrobiol. J.* **2005,** *22* (3-4), 87-98.
82. Schwarzenbach, G.; Schwarzenbach, K., Hydroxamatkomplexe .1. Die Stabilitat Der Eisen(Iii)-Komplexe Einfacher Hydroxamsauren Und Des Ferrioxamins B. *Helv. Chim. Acta* **1963,** *46* (4), 1390-1401.
83. (a) Wong, G. B.; Kappel, M. J.; Raymond, K. N.; Matzanke, B.; Winkelmann, G., Coordination Chemistry of Microbial Iron Transport Compounds .24. Characterization of Coprogen and Ferricrocin, 2 Ferric Hydroxamate Siderophores. *J. Am. Chem. Soc.* **1983,** *105* (4), 810-815; (b) Anderegg, G.; Leplatte.F; Schwarzenbach, G., Hydroxamatkomplexe .3. Eisen(Iii)-Austausch Zwischen Sideraminen Und Komplexonen - Diskussion Der Bildungskonstanten Der Hydroxamatkomplexe. *Helv. Chim. Acta* **1963,** *46* (4), 1409-1422.
84. Bergeron, R. J.; Dionis, J. B.; Elliott, G. T.; Kline, S. J., Mechanism and Stereospecificity of the Parabactin-Mediated Iron-Transport System in Paracoccus-Denitrificans. *J. Biol. Chem.* **1985,** *260* (13), 7936-7944.
85. Albrechtgary, A. M.; Blanc, S.; Rochel, N.; Ocaktan, A. Z.; Abdallah, M. A., Bacterial Iron Transport - Coordination Properties of Pyoverdin Paa, a Peptidic Siderophore of Pseudomonas-Aeruginosa. *Inorg. Chem.* **1994,** *33* (26), 6391-6402.
86. Maccordick, H. J.; Schleiffer, J. J.; Duplatre, G., Radiochemical Studies of Iron-Binding and Stability in Ferrimycobactin-S. *Radiochim. Acta* **1985,** *38* (1), 43-47.
87. Palanche, T.; Blanc, S.; Hennard, C.; Abdallah, M. A.; Albrecht-Gary, A. M., Bacterial iron transport: coordination properties of azotobactin, the highly fluorescent siderophore of Azotobacter vinelandii. *Inorg. Chem.* **2004,** *43* (3), 1137-1152.
88. Perry, R. D.; Balbo, P. B.; Jones, H. A.; Fetherston, J. D.; DeMoll, E., Yersiniabactin from Yersinia pestis: biochemical characterization of the siderophore and its role in iron transport and regulation. *Microbiology* **1999,** *145 (Pt 5)*, 1181-1190.
89. Cox, C. D.; Graham, R., Isolation of an iron-binding compound from Pseudomonas aeruginosa. *J. Bacteriol.* **1979,** *137* (1), 357-364.

90. Brandel, J.; Humbert, N.; Elhabiri, M.; Schalk, I. J.; Mislin, G. L.; Albrecht-Gary, A. M., Pyochelin, a siderophore of Pseudomonas aeruginosa: physicochemical characterization of the iron(III), copper(II) and zinc(II) complexes. *Dalton Trans.* **2012,** *41* (9), 2820-2834.
91. Caudle, M. T.; Stevens, R. D.; Crumbliss, A. L., A Monomer-to-Dimer Shift in a Series of 1/1-Ferric Dihydroxamates Probed by Electrospray Mass-Spectrometry. *Inorg. Chem.* **1994,** *33* (26), 6111-6115.
92. Sandy, M.; Butler, A., Microbial Iron Acquisition: Marine and Terrestrial Siderophores. *Chem. Rev.* **2009,** *109* (10), 4580-4595.
93. (a) Ferguson, A. D.; Hofmann, E.; Coulton, J. W.; Diederichs, K.; Welte, W., Siderophore-mediated iron transport: crystal structure of FhuA with bound lipopolysaccharide. *Science* **1998,** *282* (5397), 2215-2220; (b) Buchanan, S. K.; Smith, B. S.; Venkatramani, L.; Xia, D.; Esser, L.; Palnitkar, M.; Chakraborty, R.; van der Helm, D.; Deisenhofer, J., Crystal structure of the outer membrane active transporter FepA from Escherichia coli. *Nat. Struct. Biol.* **1999,** *6* (1), 56-63; (c) Schalk, I. J.; Lamont, I. L.; Cobessi, D., Structure-function relationships in the bifunctional ferrisiderophore FpvA receptor from Pseudomonas aeruginosa. *BioMetals* **2009,** *22* (4), 671-678.
94. Chakraborty, R.; Lemke, E. A.; Cao, Z. H.; Klebba, P. E.; van der Helm, D., Identification and mutational studies of conserved amino acids in the outer membrane receptor protein, FepA, which affect transport but not binding of ferric-enterobactin in Escherichia coli. *BioMetals* **2003,** *16* (4), 507-518.
95. Pawelek, P. D.; Croteau, N.; Ng-Thow-Hing, C.; Khursigara, C. M.; Moiseeva, N.; Allaire, M.; Coulton, J. W., Structure of TonB in complex with FhuA, E-coli outer membrane receptor. *Science* **2006,** *312* (5778), 1399-1402.
96. Crosa, J. H.; Mey, A. R.; Payne, S. M., *Iron transport in bacteria.* ASM Press: Washington, D.C., 2004; p xix, 499 p.
97. (a) Clarke, T. E.; Ku, S. Y.; Dougan, D. R.; Vogel, H. J.; Tari, L. W., The structure of the ferric siderophore binding protein FhuD complexed with gallichrome. *Nat. Struct. Biol.* **2000,** *7* (4), 287-291; (b) Rohrbach, M. R.; Braun, V.; Koster, W., Ferrichrome Transport in Escherichia-Coli K-12 - Altered Substrate-Specificity of Mutated Periplasmic Fhud and Interaction of Fhud with the Integral Membrane-Protein Fhub. *J. Bacteriol.* **1995,** *177* (24), 7186-7193.
98. Karpowich, N.; Martsinkevich, O.; Millen, L.; Yuan, Y. R.; Dai, P. L.; MacVey, K.; Thomas, P. J.; Hunt, J. F., Crystal structures of the MJ1267 ATP binding cassette reveal an induced-fit effect at the ATPase active site of an ABC transporter. *Structure* **2001,** *9* (7), 571-586.
99. Sebulsky, M. T.; Heinrichs, D. E., Identification and characterization of fhuD1 and fhuD2, two genes involved in iron-hydroxamate uptake in Staphylococcus aureus. *J. Bacteriol.* **2001,** *183* (17), 4994-5000.
100. Halle, F.; Meyer, J. M., Iron release from ferrisiderophores. A multi-step mechanism involving a NADH/FMN oxidoreductase and a chemical reduction by FMNH2. *Eur. J. Biochem.* **1992,** *209* (2), 621-627.
101. Cowart, R. E., Reduction of iron by extracellular iron reductases: implications for microbial iron acquisition. *Arch. Biochem. Biophys.* **2002,** *400* (2), 273-281.
102. Matzanke, B. F.; Anemuller, S.; Schunemann, V.; Trautwein, A. X.; Hantke, K., FhuF, part of a siderophore-reductase system. *Biochemistry* **2004,** *43* (5), 1386-1392.
103. Miethke, M.; Hou, J.; Marahiel, M. A., The Siderophore-Interacting Protein YqjH Acts as a Ferric Reductase in Different Iron Assimilation Pathways of Escherichia coli. *Biochemistry* **2011,** *50* (50), 10951-10964.
104. Nikaido, H.; Rosenberg, E. Y., Cir and Fiu proteins in the outer membrane of Escherichia coli catalyze transport of monomeric catechols: study with beta-lactam antibiotics containing catechol and analogous groups. *J. Bacteriol.* **1990,** *172* (3), 1361-1367.
105. (a) Dertz, E. A.; Xu, J.; Stintzi, A.; Raymond, K. N., Bacillibactin-mediated iron transport in Bacillus subtilis. *J. Am. Chem. Soc.* **2006,** *128* (1), 22-23; (b) Poole, K.; Young, L.; Neshat, S., Enterobactin-mediated iron transport in Pseudomonas aeruginosa. *J. Bacteriol.* **1990,** *172* (12), 6991-6996.

106. (a) Williams, P. H.; Rabsch, W.; Methner, U.; Voigt, W.; Tschape, H.; Reissbrodt, R., Catecholate receptor proteins in Salmonella enterica: role in virulence and implications for vaccine development. *Vaccine* **2006,** *24* (18), 3840-3844; (b) Yancey, R. J.; Breeding, S. A.; Lankford, C. E., Enterochelin (enterobactin): virulence factor for Salmonella typhimurium. *Infect. Immun.* **1979,** *24* (1), 174-180; (c) Crouch, M. L. V.; Castor, M.; Karlinsey, J. E.; Kalhorn, T.; Fang, F. C., Biosynthesis and IroC-dependent export of the siderophore salmochelin are essential for virulence of Salmonella enterica serovar Typhimurium. *Mol. Microbiol.* **2008,** *67* (5), 971-983.
107. Muller, S. I.; Valdebenito, M.; Hantke, K., Salmochelin, the long-overlooked catecholate siderophore of Salmonella. *BioMetals* **2009,** *22* (4), 691-695.
108. Fischbach, M. A.; Lin, H. N.; Liu, D. R.; Walsh, C. T., In vitro characterization of IroB, a pathogen-associated C-glycosyltransferase. *Proc. Natl. Acad. Sci. U. S. A.* **2005,** *102* (3), 571-576.
109. Young, I. G.; Gibson, F., Isolation of enterochelin from Escherichia coli. *Methods Enzymol.* **1979,** *56*, 394-398.
110. Corey, E. J.; Bhattacharyya, S., Total Synthesis of Enterobactin, Macrocyclic Iron Transporting Agent of Bacteria. *Tetrahedron Lett.* **1977,** (45), 3919-3922.
111. Ramirez, R. J. A.; Karamanukyan, L.; Ortiz, S.; Gutierrez, C. G., A much improved synthesis of the siderophore enterobactin. *Tetrahedron Lett.* **1997,** *38* (5), 749-752.
112. Corey, E. J.; Hurt, S. D., Synthesis of Carbocyclic Analog of Enterobactin. *Tetrahedron Lett.* **1977,** (45), 3923-3924.
113. Tse, B.; Kishi, Y., Conformationally Rigid Tricyclic Tripods - Synthesis and Application to Preparation of Enterobactin Analogs. *J. Org. Chem.* **1994,** *59* (25), 7807-7814.
114. Ecker, D. J.; Loomis, L. D.; Cass, M. E.; Raymond, K. N., Coordination Chemistry of Microbial Iron Transport .39. Substituted Complexes of Enterobactin and Synthetic Analogs as Probes of the Ferric Enterobactin Receptor in Escherichia-Coli. *J. Am. Chem. Soc.* **1988,** *110* (8), 2457-2464.
115. Rodgers, S. J.; Lee, C. W.; Ng, C. Y.; Raymond, K. N., Ferric Ion Sequestering Agents .15. Synthesis, Solution Chemistry, and Electrochemistry of a New Cationic Analog of Enterobactin. *Inorg. Chem.* **1987,** *26* (10), 1622-1625.
116. Pinter, A.; Haberhauer, G., Synthesis and Investigation of a Chiral Enterobactin Analogue Based on a Macrocyclic Peptide Scaffold. *Chem. Eur. J.* **2008,** *14* (35), 11061-11068.
117. Yu, X. L.; Dai, Y. J.; Yang, T.; Gagne, M. R.; Gong, H. G., Facile synthesis of salmochelin S1, S2, MGE, DGE, and TGE. *Tetrahedron* **2011,** *67* (1), 144-151.
118. Furrer, J. L.; Sanders, D. N.; Hook-Barnard, I. G.; McIntosh, M. A., Export of the siderophore enterobactin in Escherichia coli: involvement of a 43 kDa membrane exporter. *Mol. Microbiol.* **2002,** *44* (5), 1225-1234.
119. Bleuel, C.; Grosse, C.; Taudte, N.; Scherer, J.; Wesenberg, D.; Krauss, G. J.; Nies, D. H.; Grass, G., TolC is involved in enterobactin efflux across the outer membrane of Escherichia coli. *J. Bacteriol.* **2005,** *187* (19), 6701-6707.
120. Newton, S. M. C.; Igo, J. D.; Scott, D. C.; Klebba, P. E., Effect of loop deletions on the binding and transport of ferric enterobactin by FepA. *Mol. Microbiol.* **1999,** *32* (6), 1153-1165.
121. (a) Ecker, D. J.; Matzanke, B. F.; Raymond, K. N., Coordination Chemistry of Microbial Iron Transport Compounds .35. Recognition and Transport of Ferric Enterobactin in Escherichia-Coli. *J. Bacteriol.* **1986,** *167* (2), 666-673; (b) Thulasiraman, P.; Newton, S. M.; Xu, J.; Raymond, K. N.; Mai, C.; Hall, A.; Montague, M. A.; Klebba, P. E., Selectivity of ferric enterobactin binding and cooperativity of transport in gram-negative bacteria. *J. Bacteriol.* **1998,** *180* (24), 6689-6696.
122. Sprencel, C.; Cao, Z.; Qi, Z.; Scott, D. C.; Montague, M. A.; Ivanoff, N.; Xu, J.; Raymond, K. M.; Newton, S. M.; Klebba, P. E., Binding of ferric enterobactin by the Escherichia coli periplasmic protein FepB. *J. Bacteriol.* **2000,** *182* (19), 5359-5364.
123. Lin, H.; Fischbach, M. A.; Liu, D. R.; Walsh, C. T., In vitro characterization of salmochelin and enterobactin trilactone hydrolases IroD, IroE, and Fes. *J. Am. Chem. Soc.* **2005,** *127* (31), 11075-11084.

124. Hantke, K.; Nicholson, G.; Rabsch, W.; Winkelmann, G., Salmochelins, siderophores of Salmonella enterica and uropathogenic Escherichia coli strains, are recognized by the outer membrane receptor IroN. *Proc. Natl. Acad. Sci. U. S. A.* **2003,** *100* (7), 3677-3682.
125. Zhu, M.; Valdebenito, M.; Winkelmann, G.; Hantke, K., Functions of the siderophore esterases IroD and IroE in iron-salmochelin utilization. *Microbiology* **2005,** *151* (Pt 7), 2363-2372.
126. Braun, V.; Pramanik, A.; Gwinner, T.; Koberle, M.; Bohn, E., Sideromycins: tools and antibiotics. *BioMetals* **2009,** *22* (1), 3-13.
127. Gause, G. F., Recent studies on albomycin, a new antibiotic. *Br. Med. J.* **1955,** *2* (4949), 1177-1179.
128. (a) Ferguson, A. D.; Braun, V.; Fiedler, H. P.; Coulton, J. W.; Diederichs, K.; Welte, W., Crystal structure of the antibiotic albomycin in complex with the outer membrane transporter FhuA. *Protein Sci.* **2000,** *9* (5), 956-963; (b) Rohrbach, M. R.; Braun, V.; Koster, W., Ferrichrome transport in Escherichia coli K-12: altered substrate specificity of mutated periplasmic FhuD and interaction of FhuD with the integral membrane protein FhuB. *J. Bacteriol.* **1995,** *177* (24), 7186-7193.
129. Braun, V.; Gunthner, K.; Hantke, K.; Zimmermann, L., Intracellular activation of albomycin in Escherichia coli and Salmonella typhimurium. *J. Bacteriol.* **1983,** *156* (1), 308-315.
130. Stefanska, A. L.; Fulston, M.; Houge-Frydrych, C. S.; Jones, J. J.; Warr, S. R., A potent seryl tRNA synthetase inhibitor SB-217452 isolated from a Streptomyces species. *J. Antibiot.* **2000,** *53* (12), 1346-1353.
131. Pramanik, A.; Stroeher, U. H.; Krejci, J.; Standish, A. J.; Bohn, E.; Paton, J. C.; Autenrieth, I. B.; Braun, V., Albomycin is an effective antibiotic, as exemplified with Yersinia enterocolitica and Streptococcus pneumoniae. *Int. J. Med. Microbiol.* **2007,** *297* (6), 459-469.
132. (a) Urban, A.; Eckermann, S.; Fast, B.; Metzger, S.; Gehling, M.; Ziegelbauer, K.; Rubsamen-Waigmann, H.; Freiberg, C., Novel whole-cell antibiotic biosensors for compound discovery. *Appl. Environ. Microbiol.* **2007,** *73* (20), 6436-6443; (b) Bickel, H.; Mertens, P.; Prelog, V.; Seibl, J.; Walser, A., Constitution of ferrimycin A1. *Antimicrob. Agents Chemother.* **1965,** *5*, 951-957.
133. Rebuffat, S., Microcins in action: amazing defence strategies of Enterobacteria. *Biochem. Soc. Trans.* **2012,** *40* (6), 1456-1462.
134. Thomas, X.; Destoumieux-Garzon, D.; Peduzzi, J.; Afonso, C.; Blond, A.; Birlirakis, N.; Goulard, C.; Dubost, L.; Thai, R.; Tabet, J. C.; Rebuffat, S., Siderophore peptide, a new type of post-translationally modified antibacterial peptide with potent activity. *J. Biol. Chem.* **2004,** *279* (27), 28233-28242.
135. Bieler, S.; Silva, F.; Soto, C.; Belin, D., Bactericidal activity of both secreted and nonsecreted microcin E492 requires the mannose permease. *J. Bacteriol.* **2006,** *188* (20), 7049-7061.
136. Vassiliadis, G.; Destoumieux-Garzon, D.; Lombard, C.; Rebuffat, S.; Peduzzi, J., Isolation and characterization of two members of the siderophore-microcin family, microcins M and H47. *Antimicrob. Agents Chemother.* **2010,** *54* (1), 288-297.
137. Destoumieux-Garzon, D.; Duquesne, S.; Peduzzi, J.; Goulard, C.; Desmadril, M.; Letellier, L.; Rebuffat, S.; Boulanger, P., The iron-siderophore transporter FhuA is the receptor for the antimicrobial peptide microcin J25: role of the microcin Val11-Pro16 beta-hairpin region in the recognition mechanism. *Biochem. J.* **2005,** *389* (Pt 3), 869-876.
138. Vincent, J. L.; Rello, J.; Marshall, J.; Silva, E.; Anzueto, A.; Martin, C. D.; Moreno, R.; Lipman, J.; Gomersall, C.; Sakr, Y.; Reinhart, K., International study of the prevalence and outcomes of infection in intensive care units. *JAMA, J. Am. Med. Assoc.* **2009,** *302* (21), 2323-9.
139. Schirmer, T., General and specific porins from bacterial outer membranes. *J. Struct. Biol.* **1998,** *121* (2), 101-109.
140. Fernandez, L.; Hancock, R. E., Adaptive and mutational resistance: role of porins and efflux pumps in drug resistance. *Clin. Microbiol. Rev.* **2012,** *25* (4), 661-681.
141. (a) Miller, M. J., Syntheses and Therapeutic Potential of Hydroxamic Acid Based Siderophores and Analogs. *Chem. Rev.* **1989,** *89* (7), 1563-1579; (b) Zahner, H.; Diddens, H.; Keller-Schierlein, W.;

Nageli, H. U., Some experiments with semisynthetic sideromycins. *Jpn. J. Antibiot.* **1977,** *30 Suppl*, 201-206.
142. Miller, M. J.; Zhu, H.; Xu, Y.; Wu, C.; Walz, A. J.; Vergne, A.; Roosenberg, J. M.; Moraski, G.; Minnick, A. A.; McKee-Dolence, J.; Hu, J.; Fennell, K.; Kurt Dolence, E.; Dong, L.; Franzblau, S.; Malouin, F.; Mollmann, U., Utilization of microbial iron assimilation processes for the development of new antibiotics and inspiration for the design of new anticancer agents. *BioMetals* **2009,** *22* (1), 61-75.
143. (a) Han, S.; Zaniewski, R. P.; Marr, E. S.; Lacey, B. M.; Tomaras, A. P.; Evdokimov, A.; Miller, J. R.; Shanmugasundaram, V., Structural basis for effectiveness of siderophore-conjugated monocarbams against clinically relevant strains of Pseudomonas aeruginosa. *Proc. Natl. Acad. Sci. U. S. A.* **2010,** *107* (51), 22002-22007; (b) Sykes, R. B.; Koster, W. H.; Bonner, D. P., The new monobactams: chemistry and biology. *J. Clin. Pharmacol.* **1988,** *28* (2), 113-119; (c) Page, M. G.; Dantier, C.; Desarbre, E., In vitro properties of BAL30072, a novel siderophore sulfactam with activity against multiresistant gram-negative bacilli. *Antimicrob. Agents Chemother.* **2010,** *54* (6), 2291-2302.
144. Kong, K. F.; Schneper, L.; Mathee, K., Beta-lactam antibiotics: from antibiosis to resistance and bacteriology. *APMIS* **2010,** *118* (1), 1-36.
145. (a) Heinisch, L.; Wittmann, S.; Stoiber, T.; Berg, A.; Ankel-Fuchs, D.; Mollmann, U., Highly antibacterial active aminoacyl penicillin conjugates with acylated bis-catecholate siderophores based on secondary diamino acids and related compounds. *J. Med. Chem.* **2002,** *45* (14), 3032-3040; (b) Heinisch, L.; Wittmann, S.; Stoiber, T.; Scherlitz-Hofmann, I.; Ankel-Fuchs, D.; Mollmann, U., Synthesis and biological activity of tris- and tetrakiscatecholate siderophores based on poly-aza alkanoic acids or alkylbenzoic acids and their conjugates with beta-lactam antibiotics. *Arzneim. Forsch.* **2003,** *53* (3), 188-195; (c) Wittmann, S.; Schnabelrauch, M.; Scherlitz-Hofmann, I.; Mollmann, U.; Ankel-Fuchs, D.; Heinisch, L., New synthetic siderophores and their beta-lactam conjugates based on diamino acids and dipeptides. *Bioorg. Med. Chem.* **2002,** *10* (6), 1659-1670.
146. Ohi, N.; Aoki, B.; Kuroki, T.; Matsumoto, M.; Kojima, K.; Nehashi, T., Semisynthetic beta-lactam antibiotics. III. Effect on antibacterial activity and comt-susceptibility of chlorine-introduction into the catechol nucleus of 6-[(R)-2-[3-(3,4-dihydroxybenzoyl)-3-(3-hydroxypropyl)-1-ureido]-2-phenylacetamido]penicillanic acid. *J. Antibiot.* **1987,** *40* (1), 22-28.
147. Kinzel, O.; Tappe, R.; Gerus, I.; Budzikiewicz, H., The synthesis and antibacterial activity of two pyoverdin-ampicillin conjugates, entering Pseudomonas aeruginosa via the pyoverdin-mediated iron uptake pathway. *J. Antibiot.* **1998,** *51* (5), 499-507.
148. Brochu, A.; Brochu, N.; Nicas, T. I.; Parr, T. R.; Minnick, A. A.; Dolence, E. K.; Mckee, J. A.; Miller, M. J.; Lavoie, M. C.; Malouin, F., Modes of Action and Inhibitory Activities of New Siderophore Beta-Lactam Conjugates That Use Specific Iron Uptake Pathways for Entry into Bacteria. *Antimicrob. Agents Chemother.* **1992,** *36* (10), 2166-2175.
149. Ji, C.; Miller, P. A.; Miller, M. J., Iron transport-mediated drug delivery: practical syntheses and in vitro antibacterial studies of tris-catecholate siderophore-aminopenicillin conjugates reveals selectively potent antipseudomonal activity. *J. Am. Chem. Soc.* **2012,** *134* (24), 9898-9901.
150. Katsu, K.; Kitoh, K.; Inoue, M.; Mitsuhashi, S., In vitro antibacterial activity of E-0702, a new semisynthetic cephalosporin. *Antimicrob. Agents Chemother.* **1982,** *22* (2), 181-185.
151. Watanabe, N. A.; Nagasu, T.; Katsu, K.; Kitoh, K., E-0702, a New Cephalosporin, Is Incorporated into Escherichia-Coli-Cells Via the Tonb-Dependent Iron Transport-System. *Antimicrob. Agents Chemother.* **1987,** *31* (4), 497-504.
152. Curtis, N. A. C.; Eisenstadt, R. L.; East, S. J.; Cornford, R. J.; Walker, L. A.; White, A. J., Iron-Regulated Outer-Membrane Proteins of Escherichia-Coli-K-12 and Mechanism of Action of Catechol-Substituted Cephalosporins. *Antimicrob. Agents Chemother.* **1988,** *32* (12), 1879-1886.
153. Maejima, T.; Inoue, M.; Mitsuhashi, S., In vitro antibacterial activity of KP-736, a new cephem antibiotic. *Antimicrob. Agents Chemother.* **1991,** *35* (1), 104-110.
154. Kinzel, O.; Budzikiewicz, H., Synthesis and biological evaluation of a pyoverdin-beta-lactam conjugate: a new type of arginine-specific cross-linking in aqueous solution. *J. Pept. Res.* **1999,** *53* (6), 618-625.

155. Mckee, J. A.; Miller, M. J., Synthesis, Siderophore, and Antimicrobial Evaluation of a Spermidine-Based Tricatecholate Siderophore and Carbacephalosporin Conjugate. *Bioorg. Med. Chem. Lett.* **1991,** *1* (10), 513-518.
156. (a) Ghosh, A.; Ghosh, M.; Niu, C.; Malouin, F.; Moellmann, U.; Miller, M. J., Iron transport-mediated drug delivery using mixed-ligand siderophore-beta-lactam conjugates. *Chem. Biol.* **1996,** *3* (12), 1011-1019; (b) Wencewicz, T. A.; Miller, M. J., Biscatecholate-Monohydroxamate Mixed Ligand Siderophore-Carbacephalosporin Conjugates are Selective Sideromycin Antibiotics that Target Acinetobacter baumannii. *J. Med. Chem.* **2013,** *56* (10), 4044-4052.
157. McPherson, C. J.; Aschenbrenner, L. M.; Lacey, B. M.; Fahnoe, K. C.; Lemmon, M. M.; Finegan, S. M.; Tadakamalla, B.; O'Donnell, J. P.; Mueller, J. P.; Tomaras, A. P., Clinically Relevant Gram-Negative Resistance Mechanisms Have No Effect on the Efficacy of MC-1, a Novel Siderophore-Conjugated Monocarbam. *Antimicrob. Agents Chemother.* **2012,** *56* (12), 6334-6342.
158. Brown, M. F.; Mitton-Fry, M. J.; Arcari, J. T.; Barham, R.; Casavant, J.; Gerstenberger, B. S.; Han, S.; Hardink, J. R.; Harris, T. M.; Hoang, T.; Huband, M. D.; Lall, M. S.; Lemmon, M. M.; Li, C.; Lin, J.; McCurdy, S. P.; McElroy, E.; McPherson, C.; Marr, E. S.; Mueller, J. P.; Mullins, L.; Nikitenko, A. A.; Noe, M. C.; Penzien, J.; Plummer, M. S.; Schuff, B. P.; Shanmugasundaram, V.; Starr, J. T.; Sun, J.; Tomaras, A.; Young, J. A.; Zaniewski, R. P., Pyridone-Conjugated Monobactam Antibiotics with Gram-Negative Activity. *J. Med. Chem.* **2013,** *56* (13), 5541-5552.
159. Higgins, P. G.; Stefanik, D.; Page, M. G. P.; Hackel, M.; Seifert, H., In vitro activity of the siderophore monosulfactam BAL30072 against meropenem-non-susceptible Acinetobacter baumannii. *J. Antimicrob. Chemother.* **2012,** *67* (5), 1167-1169.
160. (a) Mima, T.; Kvitko, B. H.; Rholl, D. A.; Page, M. G. P.; Desarbre, E.; Schweizer, H. P., In vitro activity of BAL30072 against Burkholderia pseudomallei. *Int. J. Antimicrob. Ag.* **2011,** *38* (2), 157-159; (b) Page, M. G., Siderophore conjugates. *Ann. N.Y. Acad. Sci.* **2013,** *1277*, 115-126.
161. Aldred, K. J.; Kerns, R. J.; Osheroff, N., Mechanism of quinolone action and resistance. *Biochemistry* **2014,** *53* (10), 1565-1574.
162. Md-Saleh, S. R.; Chilvers, E. C.; Kerr, K. G.; Milner, S. J.; Snelling, A. M.; Weber, J. P.; Thomas, G. H.; Duhme-Klair, A. K.; Routledge, A., Synthesis of citrate-ciprofloxacin conjugates. *Bioorg. Med. Chem. Lett.* **2009,** *19* (5), 1496-1498.
163. Ji, C.; Miller, M. J., Chemical syntheses and in vitro antibacterial activity of two desferrioxamine B-ciprofloxacin conjugates with potential esterase and phosphatase triggered drug release linkers. *Bioorg. Med. Chem.* **2012,** *20* (12), 3828-3836.
164. Hennard, C.; Truong, Q. C.; Desnottes, J. F.; Paris, J. M.; Moreau, N. J.; Abdallah, M. A., Synthesis and activities of pyoverdin-quinolone adducts: a prospective approach to a specific Therapy against Pseudomonas aeruginosa. *J. Med. Chem.* **2001,** *44* (13), 2139-2151.
165. Rivault, F.; Liebert, C.; Burger, A.; Hoegy, F.; Abdallah, M. A.; Schalk, I. J.; Mislin, G. L., Synthesis of pyochelin-norfloxacin conjugates. *Bioorg. Med. Chem. Lett.* **2007,** *17* (3), 640-644.
166. Souto, A.; Montaos, M. A.; Balado, M.; Osorio, C. R.; Rodriguez, J.; Lemos, M. L.; Jimenez, C., Synthesis and antibacterial activity of conjugates between norfloxacin and analogues of the siderophore vanchrobactin. *Bioorg. Med. Chem.* **2013,** *21* (1), 295-302.
167. Milner, S. J.; Seve, A.; Snelling, A. M.; Thomas, G. H.; Kerr, K. G.; Routledge, A.; Duhme-Klair, A. K., Staphyloferrin A as siderophore-component in fluoroquinolone-based Trojan horse antibiotics. *Org. Biomol. Chem.* **2013,** *11* (21), 3461-3468.
168. Ghosh, M.; Miller, M. J., Design, synthesis, and biological evaluation of isocyanurate-based antifungal and macrolide antibiotic conjugates: iron transport-mediated drug delivery. *Bioorg. Med. Chem.* **1995,** *3* (11), 1519-1525.
169. Ghosh, M.; Miller, M. J., Synthesis and in vitro antibacterial activity of spermidine-based mixed catechol- and hydroxamate-containing siderophore-vancomycin conjugates. *Bioorg. Med. Chem.* **1996,** *4* (1), 43-48.
170. Yoganathan, S.; Sit, C. S.; Vederas, J. C., Chemical synthesis and biological evaluation of gallidermin-siderophore conjugates. *Org. Biomol. Chem.* **2011,** *9* (7), 2133-2141.

171. Miller, M. J.; Walz, A. J.; Zhu, H.; Wu, C.; Moraski, G.; Mollmann, U.; Tristani, E. M.; Crumbliss, A. L.; Ferdig, M. T.; Checkley, L.; Edwards, R. L.; Boshoff, H. I., Design, synthesis, and study of a mycobactin-artemisinin conjugate that has selective and potent activity against tuberculosis and malaria. *J. Am. Chem. Soc.* **2011,** *133* (7), 2076-2079.
172. Chaturvedi, D.; Goswami, A.; Saikia, P. P.; Barua, N. C.; Rao, P. G., Artemisinin and its derivatives: a novel class of anti-malarial and anti-cancer agents. *Chem. Soc. Rev.* **2010,** *39* (2), 435-454.
173. Tomaras, A. P.; Crandon, J. L.; McPherson, C. J.; Banevicius, M. A.; Finegan, S. M.; Irvine, R. L.; Brown, M. F.; O'Donnell, J. P.; Nicolau, D. P., Adaptation-Based Resistance to Siderophore-Conjugated Antibacterial Agents by Pseudomonas aeruginosa. *Antimicrob. Agents Chemother.* **2013,** *57* (9), 4197-4207.
174. Esposito, B. P.; Epsztejn, S.; Breuer, W.; Cabantchik, Z. I., A review of fluorescence methods for assessing labile iron in cells and biological fluids. *Anal. Biochem.* **2002,** *304* (1), 1-18.
175. Mossialos, D.; Amoutzias, G. D., Siderophores in fluorescent pseudomonads: new tricks from an old dog. *Future Microbiol.* **2007,** *2* (4), 387-395.
176. (a) Barrero, J. M.; Morino-Bondi, M. C.; Perez-Conde, M. C.; Camara, C., A biosensor for ferric ion. *Talanta* **1993,** *40* (11), 1619-1623; (b) Pulido-Tofino, P.; Moreno, J. M.; Perez-Conde, M. C., A flow-through fluorescent sensor to determine Fe(III) and total inorganic iron. *Talanta* **2000,** *51* (3), 537-545.
177. (a) Palanche, T.; Marmolle, F.; Abdallah, M. A.; Shanzer, A.; Albrecht-Gary, A. M., Fluorescent siderophore-based chemosensors: iron(III) quantitative determinations. *J. Biol. Inorg. Chem.* **1999,** *4* (2), 188-198; (b) Chung Chun Lam, C. K.; Jickells, T. D.; Richardson, D. J.; Russell, D. A., Fluorescence-based siderophore biosensor for the determination of bioavailable iron in oceanic waters. *Anal. Chem.* **2006,** *78* (14), 5040-5045.
178. Ye, Y.; Bloch, S.; Xu, B.; Achilefu, S., Novel near-infrared fluorescent integrin-targeted DFO analogue. *Bioconjugate Chem.* **2008,** *19* (1), 225-234.
179. Noel, S.; Guillon, L.; Schalk, I. J.; Mislin, G. L., Synthesis of fluorescent probes based on the pyochelin siderophore scaffold. *Org. Lett.* **2011,** *13* (5), 844-847.
180. Namiranian, S.; Richardson, D. J.; Russell, D. A.; Sodeau, J. R., Excited state properties of the siderophore pyochelin and its complex with zinc ions. *Photochem. Photobiol.* **1997,** *65* (5), 777-782.
181. Orcutt, K. M.; Jones, W. S.; McDonald, A.; Schrock, D.; Wallace, K. J., A Lanthanide-Based Chemosensor for Bioavailable Fe3+ Using a Fluorescent Siderophore: An Assay Displacement Approach. *Sensors-Basel* **2010,** *10* (2), 1326-1337.
182. Doorneweerd, D. D.; Henne, W. A.; Reifenberger, R. G.; Low, P. S., Selective Capture and Identification of Pathogenic Bacteria Using an Immobilized Siderophore. *Langmuir* **2010,** *26* (19), 15424-15429.
183. Kim, Y.; Lyvers, D. P.; Wei, A.; Reifenberger, R. G.; Low, P. S., Label-free detection of a bacterial pathogen using an immobilized siderophore, deferoxamine. *Lab Chip* **2012,** *12* (5), 971-976.
184. Wu, S. M.; Zhang, Z. L.; Wang, X. D.; Zhang, M. X.; Peng, J.; Xie, Z. X.; Pang, D. W., Quantum Dot-Ferrichrome Bioprobes for Recognition of Pseudomonas fluorescens. *J. Phys. Chem. C* **2009,** *113* (21), 9169-9174.
185. Zawadzka, A. M.; Kim, Y.; Maltseva, N.; Nichiporuk, R.; Fan, Y.; Joachimiak, A.; Raymond, K. N., Characterization of a Bacillus subtilis transporter for petrobactin, an anthrax stealth siderophore. *Proc. Natl. Acad. Sci. U. S. A.* **2009,** *106* (51), 21854-21859.
186. Lin, Y. M.; Miller, M. J., Practical synthesis of hydroxamate-derived siderophore components by an indirect oxidation method and syntheses of a DIG-siderophore conjugate and a biotin-siderophore conjugate. *J. Org. Chem.* **1999,** *64* (20), 7451-7458.
187. Nolan, E. M.; Walsh, C. T., Investigations of the MceIJ-catalyzed posttranslational modification of the microcin E492 C-terminus: Linkage of ribosomal and nonribosomal peptides to form "Trojan Horse" antibiotics. *Biochemistry* **2008,** *47* (35), 9289-9299.
188. Bannerman, R. M.; Callender, S. T.; Williams, D. L., Effect of Desferrioxamine and D.T.P.A. in Iron Overload. *Br. Med. J.* **1962,** *2* (5319), 1573-1577.

189. Hartzen, S. H.; Frimodt-Moller, N.; Thomsen, V. F., The antibacterial activity of a siderophore. 2. The influence of deferoxamine alone and combined with ascorbic acid on the activity of antibiotics against Staphylococcus aureus. *APMIS* **1991,** *99* (10), 879-886.
190. Kokjohn, K.; Bradley, M.; Griffiths, B.; Ghannoum, M., Evaluation of in vitro activity of ciclopirox olamine, butenafine HCl and econazole nitrate against dermatophytes, yeasts and bacteria. *Int. J. Dermatol.* **2003,** *42 Suppl 1*, 11-17.
191. Gupta, A. K.; Plott, T., Ciclopirox: a broad-spectrum antifungal with antibacterial and anti-inflammatory properties. *Int. J. Dermatol.* **2004,** *43 Suppl 1*, 3-8.
192. Neufeld, E. J., Oral chelators deferasirox and defefiprone for transfusional iron overload in thalassen a major: new data, new questions. *Blood* **2006,** *107* (9), 3436-3441.
193. (a) Ibrahim, A. S.; Edwards, J. E., Jr.; Fu, Y.; Spellberg, B., Deferiprone iron chelation as a novel therapy for experimental mucormycosis. *J. Antimicrob. Chemother.* **2006,** *58* (5), 1070-1073; (b) Ibrahim, A. S.; Gebermariam, T.; Fu, Y.; Lin, L.; Husseiny, M. I.; French, S. W.; Schwartz, J.; Skory, C. D.; Edwards, J. E., Jr.; Spellberg, B. J., The iron chelator deferasirox protects mice from mucormycosis through iron starvation. *J. Clin. Invest.* **2007,** *117* (9), 2649-2657.
194. Strieker, M.; Tanovic, A.; Marahiel, M. A., Nonribosomal peptide synthetases: structures and dynamics. *Curr. Opin. Struct. Biol.* **2010,** *20* (2), 234-240.
195. Payne, R. J.; Kerbarh, O.; Miguel, R. N.; Abell, A. D.; Abell, C., Inhibition studies on salicylate synthase. *Org. Biomol. Chem.* **2005,** *3* (10), 1825-1827.
196. Manos-Turvey, A.; Bulloch, E. M. M.; Rutledge, P. J.; Baker, E. N.; Lott, J. S.; Payne, R. J., Inhibition Studies of Mycobacterium tuberculosis Salicylate Synthase (Mbtl). *ChemMedChem* **2010,** *5* (7), 1067-1079.
197. Vasan, M.; Neres, J.; Williams, J.; Wilson, D. J.; Teitelbaum, A. M.; Remmel, R. P.; Aldrich, C. C., Inhibitors of the Salicylate Synthase (Mbtl) from Mycobacterium tuberculosis Discovered by High-Throughput Screening. *ChemMedChem* **2010,** *5* (12), 2079-2087.
198. Ferreras, J. A.; Ryu, J. S.; Di Lello, F.; Tan, D. S.; Quadri, L. E., Small-molecule inhibition of siderophore biosynthesis in Mycobacterium tuberculosis and Yersinia pestis. *Nat. Chem. Biol.* **2005,** *1* (1), 29-32.
199. Lun, S.; Guo, H.; Adamson, J.; Cisar, J. S.; Davis, T. D.; Chavadi, S. S.; Warren, J. D.; Quadri, L. E.; Tan, D. S.; Bishai, W. R., Pharmacokinetic and in vivo efficacy studies of the mycobactin biosynthesis inhibitor salicyl-AMS in mice. *Antimicrob. Agents Chemother.* **2013,** *57* (10), 5138-5140.
200. Gupte, A.; Boshoff, H. I.; Wilson, D. J.; Neres, J.; Labello, N. P.; Somu, R. V.; Xing, C.; Barry, C. E.; Aldrich, C. C., Inhibition of siderophore biosynthesis by 2-triazole substituted analogues of 5'-O-[N-(salicyl)sulfamoyl]adenosine: antibacterial nucleosides effective against Mycobacterium tuberculosis. *J. Med. Chem.* **2008,** *51* (23), 7495-7507.
201. Engelhart, C. A.; Aldrich, C. C., Synthesis of chromone, quinolone, and benzoxazinone sulfonamide nucleosides as conformationally constrained inhibitors of adenylating enzymes required for siderophore biosynthesis. *J. Org. Chem.* **2013,** *78* (15), 7470-7481.
202. Maganti, L.; Ghoshal, N., 3D-QSAR studies and shape based virtual screening for identification of novel hits to inhibit MbtA in Mycobacterium tuberculosis. *J. Biomol. Struct. Dyn.* **2014**.
203. Drake, E. J.; Duckworth, B. P.; Neres, J.; Aldrich, C. C.; Gulick, A. M., Biochemical and structural characterization of bisubstrate inhibitors of BasE, the self-standing nonribosomal peptide synthetase adenylate-forming enzyme of acinetobactin synthesis. *Biochemistry* **2010,** *49* (43), 9292-9305.
204. Neres, J.; Engelhart, C. A.; Drake, E. J.; Wilson, D. J.; Fu, P.; Boshoff, H. I.; Barry, C. E., 3rd; Gulick, A. M.; Aldrich, C. C., Non-nucleoside inhibitors of BasE, an adenylating enzyme in the siderophore biosynthetic pathway of the opportunistic pathogen Acinetobacter baumannii. *J. Med. Chem.* **2013,** *56* (6), 2385-2405.
205. Drake, E. J.; Gulick, A. M., Structural characterization and high-throughput screening of inhibitors of PvdQ, an NTN hydrolase involved in pyoverdine synthesis. *ACS Chem. Biol.* **2011,** *6* (11), 1277-1286.

206. Clevenger, K. D.; Wu, R.; Er, J. A.; Liu, D.; Fast, W., Rational design of a transition state analogue with picomolar affinity for Pseudomonas aeruginosa PvdQ, a siderophore biosynthetic enzyme. *ACS Chem. Biol.* **2013,** *8* (10), 2192-2200.
207. Tripathi, A.; Schofield, M. M.; Chlipala, G. E.; Schultz, P. J.; Yim, I.; Newmister, S. A.; Nusca, T. D.; Scaglione, J. B.; Hanna, P. C.; Tamayo-Castillo, G.; Sherman, D. H., Baulamycins A and B, broad-spectrum antibiotics identified as inhibitors of siderophore biosynthesis in Staphylococcus aureus and Bacillus anthracis. *J. Am. Chem. Soc.* **2014,** *136* (4), 1579-1586.
208. Jones, C. M.; Wells, R. M.; Madduri, A. V.; Renfrow, M. B.; Ratledge, C.; Moody, D. B.; Niederweis, M., Self-poisoning of Mycobacterium tuberculosis by interrupting siderophore recycling. *Proc. Natl. Acad. Sci. U. S. A.* **2014,** *111* (5), 1945-1950.
209. Vega, D. E.; Young, K. D., Accumulation of periplasmic enterobactin impairs the growth and morphology of Escherichia coli tolC mutants. *Mol. Microbiol.* **2014,** *91* (3), 508-521.
210. Caza, M.; Lepine, F.; Dozois, C. M., Secretion, but not overall synthesis, of catecholate siderophores contributes to virulence of extraintestinal pathogenic Escherichia coli. *Mol. Microbiol.* **2011,** *80* (1), 266-282.
211. Devanathan, S.; Postle, K., Studies on colicin B translocation: FepA is gated by TonB. *Mol. Microbiol.* **2007,** *65* (2), 441-453.
212. Rabsch, W.; Ma, L.; Wiley, G.; Najar, F. Z.; Kaserer, W.; Schuerch, D. W.; Klebba, J. E.; Roe, B. A.; Gomez, J. A. L.; Schallmey, M.; Newton, S. M. C.; Klebba, P. E., FepA- and TonB-dependent bacteriophage H8: Receptor binding and genomic sequence. *J. Bacteriol.* **2007,** *189* (15), 5658-5674.

Chapter 2

Siderophore-Mediated Cargo Delivery to the Cytoplasm of *Escherichia coli* and *Pseudomonas aeruginosa*: Syntheses of Monofunctionalized Enterobactin Scaffolds and Evaluation of Enterobactin-Cargo Conjugate Uptake

Most work in this Chapter is published in *J. Am. Chem. Soc.*, **2012**, 134, 18388-18400.

Introduction

Siderophores are low-molecular-weight high-affinity Fe(III) chelators that are biosynthesized and exported by bacteria, fungi, and plants during periods of nutrient limitation for acquiring this essential metal ion from the extracellular milieu.[1] Enterobactin (Ent, **1**, Figure 2.1A) is a canonical siderophore biosynthesized by Gram-negative species of *Enterobacteriaceae* that include *Escherichia coli*, *Salmonella*, and *Klebsiella*.[2] Decades of exploration pertaining to enterobactin biosynthesis and coordination chemistry, in addition to investigations of the proteins involved in its cellular transport and processing, provide a detailed molecular and physiological understanding of how this chelator contributes to bacterial iron homeostasis and colonization.[2] Enterobactin coordinates Fe(III) by its three catecholate groups with $K_a \sim 10^{49}$ M^{-1}.[3] In *E. coli*, the outer membrane transporter FepA (and to a lesser extent Cir and Fiu) recognizes and binds ferric enterobactin with sub-nanomolar affinity,[4] and provides periplasmic entry where the siderophore forms a complex with the periplasmic binding protein FepB.[5] Subsequently, $[Fe(Ent)]^{3-}$ is transported into the cytosol, which requires the action of ExbBD, TonB, and FepCDG, the latter of which constitute the inner-membrane ATP-binding cassette (ABC) transporter system (Figure 2.1B).[6] Fes, the cytosolic enterobactin esterase, catalyzes the hydrolysis of the $[Fe(Ent)]^{3-}$ macrolactone (Figure 2.1B),[7] and the ferric reductase YgjH may subsequently assist in Fe(III) release such that the metal ion can be used metabolically.[8] Several pathogenic Gram-negative species harbor gene clusters (e.g., *iroA*, MccE492) responsible for post-assembly line modifications of the enterobactin scaffold to provide the salmochelins.[7, 9] Salmochelins are a family of glucosylated enterobactin derivatives where the sugar moieties are attached to the C5 position of one or more catecholate rings (e.g., MGE **2** and DGE **3**, Figure 2.1A).[10]

Gram-negative bacteria have an outer membrane that serves as a permeability barrier and prevents cellular entry of many molecules, including antibiotics (e.g., vancomycin). Siderophore uptake machinery provides one route to overcome this permeability barrier,[11] and enterobactin and its transporter FepA have been identified as a desirable siderophore/receptor pair for cargo delivery to Gram-negative bacterial species.[9c, 11f] FepA-mediated uptake of the ribosomal peptide antibiotics colicin B[12] and MccE492m,[13] in addition to bacteriophage,[14] indicates that this receptor has the capacity to transport large molecules. Moreover, the catecholate siderophore transporters of *E. coli* (e.g., Fiu, Cir) recognize synthetic catechol-modified β-lactam antibiotics;[15] these serendipitous observations motivated early "Trojan horse" delivery strategies. Indeed, small-molecule antibiotics appended to siderophore-inspired di- and tricatecholate platforms have been evaluated for antibacterial activity with mixed results.[16] Recently, amoxicillin and ampicillin, β-lactam antibiotics that act in the periplasm and target bacterial cell wall biosynthesis, were covalently linked to a tripodal catecholate platform and remarkably afforded ca. 10^2- to 10^3-fold enhanced activity against *Pseudomonas aeruginosa* PAO1 compared to the free drug.[16c]

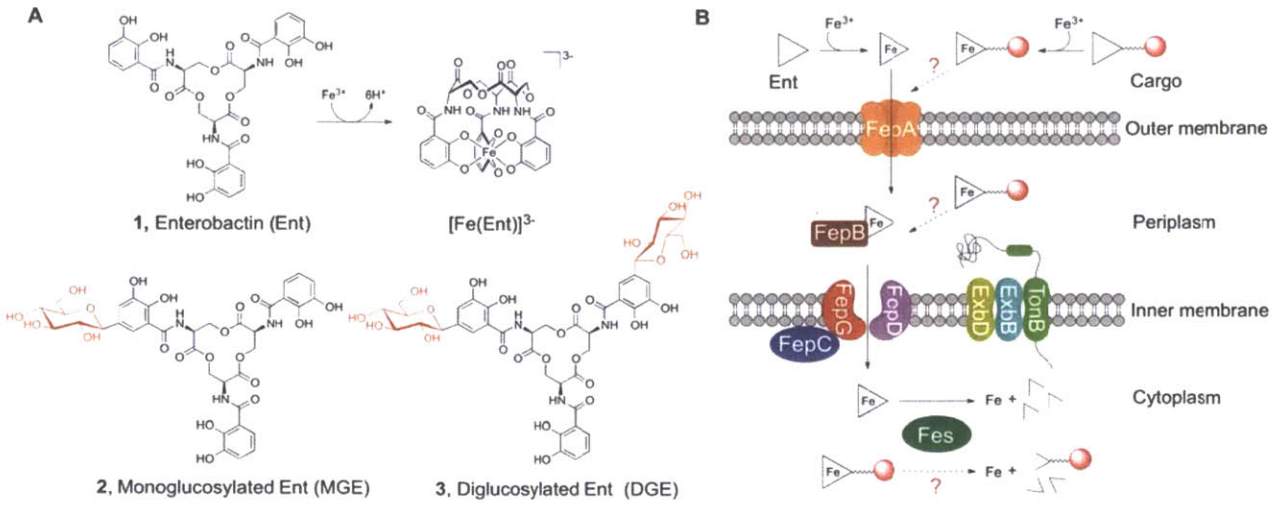

Figure 2.1. Siderophores and siderophore transport machinery relevant to this work. (A) Structures of enterobactin **1** and the salmochelins MGE **2** and DGE **3**. (B) Cartoon depiction of the enterobactin transport and processing machinery in *E. coli*.

The ability of FepABCDG and the TonB-ExbB-ExbD system of *E. coli*, as well as the enterobactin transport machinery of other bacterial species, to recognize and provide cytosolic transport of unnatural cargo appended to the native ligand remains unexplored. Enterobactin exhibits C_3 symmetry and houses no unique functional group for site-specific synthetic modification. Total syntheses of enterobactin,[17] hydrolytically stable enterobactin analogs,[18] and salmochelins[19] have been reported. To the best of our knowledge, no enterobactin scaffold housing a site-specific synthetic handle has been presented. Such scaffolds are a pre-requisite for employing enterobactin in a variety of paradigms that include cargo delivery, iron and siderophore detection, and bacterial capture.

In this Chapter, we expand the current toolkit of site-specifically modifiable siderophore scaffolds to include triscatecholate enterobactin. Inspired by the salmochelins, we have derivatized enterobactin at the C5 position of the catecholate, which provides a point for site-specific modification without compromising the Fe(III)-binding groups or the macrolactone (Figure 2.2). A family of ten enterobactin-cargo conjugates that are based on a monofunctionalized enterobactin scaffold was synthesized. We further demonstrated that depending on the cargo size, several synthetic enterobactin-cargo conjugates are actively transported to the cytoplasm of the Gram-negative bacterial species *E. coli* and *P. aeruginosa* by the enterobactin uptake machinery.

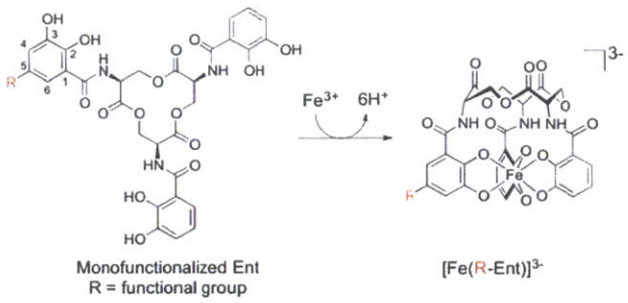

Figure 2.2. Enterobactin substituted at the C5 position.

Experimental Section

Reagents. Dimethylformamide (DMF) and dichloromethane (CH_2Cl_2) were dried over 4 Å molecular sieves or by using a VAC solvent purification system (Vacuum Atmospheres). Anhydrous dimethyl sulfoxide (DMSO) was purchased from Sigma-Aldrich and used as received. The triserine lactone **4** and its D-isomer **5** were synthesized according to a literature procedure.[17d] 2,3-Bis(benzyloxy)benzoic acid **6**,[20] vancomycin-alkyne **7**,[21] and *tert*-butyl (2-oxo-2-(prop-2-yn-1-ylamino)ethyl)carbamate **8**,[21] were synthesized according to literature procedures. L-Ent **1** and its D-isomer **9** were synthesized as reported elsewhere.[17d, e] Monoglucosylated Ent (MGE) and diglucosylated Ent (DGE) were synthesized according to literature procedures.[22] *Tert*-butyl (2-(2-(2-(2-aminoethoxy)ethoxy)-ethoxy)ethyl)carbamate **10** was purchased from BOC Sciences (Shirley, NY), 11-azido-3,6,9-trioxaundecan-1-amine **11** was purchased from Fluka, 6-((*tert*-butyoxycarbonyl)amino) hexanoic acid **12** was purchased from Advanced Chem Tech, and Fmoc-PEG-CO_2H **13** was purchased from Chem-Impex International, Inc. Methyl-5-allyl-3-methoxysalicylate **19** was obtained from Sigma-Aldrich. All other chemicals were purchased from Sigma-Aldrich, Alfa Aesar, or TCI in the highest available purity and used as received.

General Synthetic Materials and Methods. EMD TLC silica gel 60 F_{254} plates were used for analytical thin-layer chromatography. EMD PLC silica gel 60 F_{254} plates of 1-mm thickness were used for preparative TLC. Zeoprep 60HYD silica gel (40-63 μm) obtained from Zeochem was used for flash chromatography. ^1H, ^{19}F, and ^{13}C NMR spectra were collected on a Varian 300 or 500 MHz spectrophotometer, which were operated at ambient probe temperature (283 K) and housed in the Department of Chemistry Instrumentation Facility. The ^1H and ^{13}C NMR spectra were referenced to internal standards and ^{19}F spectra were referenced to an external CF_3Cl standard. An Avatar FTIR instrument was used to acquire IR spectra. Optical absorption spectra were recorded on an Agilent 8453

diode array spectrophotometer (1-cm quartz cuvettes, Starna). ^{1}H and ^{13}C NMR spectra are provided in Appendix 2.

General Liquid Chromatography and Mass Spectrometry Methods. HPLC-grade acetonitrile (MeCN) and trifluoroacetic acid (TFA) were purchased from EMD. LC-MS grade MeCN containing 0.1% formic acid and water containing 0.1% formic acid were obtained from J. T. Baker. Semi-preparative and analytical high-performance liquid chromatography (HPLC) were performed by using an Agilent 1200 series HPLC system outfitted with an Agilent Zorbax reverse-phase C18 column (5-μm pore size, 9.4 x 250 mm) at a flow rate of 4 mL/min and a Clipeus reverse-phase C18 column (5-μm pore size, 4.6 x 250 mm; Higgins Analytical, Inc.) at a flow rate of 1 mL/min, respectively. The multi-wavelength detector was set to read the absorption at 220, 280, and 316 (catecholate absorption) nm. For all HPLC runs, solvent A was 0.1% TFA/H_2O and solvent B was 0.1% TFA/MeCN. Each semi-preparative or analytical run began with a five-minute equilibration at the %B used at the start of the gradient followed by a gradient of increasing %B. The HPLC solvents were prepared with HPLC-grade MeCN and TFA, and Milli-Q water (18.2 $m\Omega cm^{-1}$), and filtered through a 0.2-μm filter before use. For analytical HPLC to evaluate conjugate purity, the entire portion of each HPLC-purified compound was dissolved in a mixture of 1:1:1 1,4-dioxane/methanol/water and an aliquot was taken for HPLC analysis, and the solution was subsequently lyophilized. Conjugate **42** was an exception, and this molecule was dissolved in DMSO prior to analytical HPLC. Analytical HPLC traces of the purified compounds were generated using the gradient of 0% B for 5 min followed by 0-100% B over 30 min, 1 mL/min. Most high-resolution mass spectrometry was performed by using an Agilent LC-MS system comprised of an Agilent 1260 series LC system outfitted with an Agilent Poroshell 120 EC-C18 column (2.7-μm pore size) and an Agilent 6230 TOF system housing an Agilent Jetstream ESI source. For all LC-MS analyses, solvent A was 0.1% formic acid / H_2O and solvent B was 0.1% formic acid / MeCN. The samples were run using a gradient of 5-95% B over five min with a flow rate of 0.4 mL/min. In some instances, high-resolution mass spectrometry was performed by staff at the MIT Department of Chemistry Instrumentation Facility, which houses a Bruker Daltonics APEXIV 4.7 Tesla Fourier Transform Ion Cyclotron Resonance Mass Spectrometer (FT-ICR-MS) with a direct analysis in real time (DART) ionization source.

***N*-(2-(2-(2-(2-Aminoethoxy)ethoxy)ethoxy)ethyl)cyclohexanecarboxamide (14).** Cyclohexanecarboxylic acid (64 mg, 0.50 mmol) and **7** (192 mg, 0.599 mmol) were combined in 5 mL of dry CH_2Cl_2, and 1-ethyl-3-(3-dimethylaminopropyl) carbodiimide (EDC, 143 mg, 0.751 mmol), 4-dimethylaminopyridine (DMAP, 30 mg, 0.25 mmol), and *N*,*N*-Diisopropylethylamine (DIPEA, 435 μL, 2.52 mmol) were added. The reaction was stirred for 4 h at rt, and the organic phase was washed with 50

mM HCl (3 x 20 mL) and brine (1 x 20 mL). The organic phase was dried over Na_2SO_4 and concentrated. Flash chromatography on silica gel with a solvent gradient (CH_2Cl_2 to 10% MeOH/CH_2Cl_2) afforded the Boc-protected product as colorless oil (190 mg, 94%). TLC R_f = 0.65 (10% MeOH/CH_2Cl_2). ^{1}H NMR ($CDCl_3$, 300 MHz), δ 1.13-1.37 (14H, m), 1.58-1.60 (1H, m), 1.68-1.78 (4H, m), 1.97-2.05 (1H, m), 3.23-3.24 (2H, m), 3.34-3.40 (2H, m), 3.45-3.50 (4H, m), 3.53-3.59 (8H, m), 5.09 (1H, bs), 6.11 (1H, bs). ^{13}C NMR ($CDCl_3$, 125 MHz), δ 25.5, 28.2, 29.4, 38.7, 40.1, 45.2, 69.7, 69.9, 70.0, 70.2, 78.9, 155.8, 176.0. FT-IR (NaCl disk, cm^{-1}), 3443 (m), 3325 (s), 3074 (w), 2976 (s), 2930 (s), 2858 (s), 1698 (s), 1652 (s), 1535 (s), 1451 (s), 1391 (m), 1366 (s), 1351 (m), 1329 (w), 1273 (s), 1253 (s), 1217 (w), 1173 (s), 1126 (s), 1041 (w), 969 (w), 945 (w), 895 (w), 865 (w), 780 (w), 756 (m). HRMS (ESI): $[M+Na]^+$ *m*/z calcd., 425.2622; found, 425.2654.

A portion of this Boc-protected product (118 mg, 0.278 mmol) was dissolved in 2.5 mL of 40% TFA/CH_2Cl_2 and the light red solution was stirred at rt for 2.5 h. The reaction was concentrated to give **14** as light-yellow oil in quantitative yield. TLC R_f = 0.2 (10% MeOH/CH_2Cl_2). ^{1}H NMR ($CDCl_3$, 500 MHz), δ 1.13-1.37 (5H, m), 1.62-1.64 (1H, m), 1.71-1.77 (4H, m), 2.10-2.15 (1H, m), 3.16 (2H, bs), 3.36 (2H, bs), 3.48-3.65 (10H, m), 3.76 (2H, bs), 6.93 (1H, bs), 7.88 (2H, bs). ^{13}C NMR ($CDCl_3$, 125 MHz), δ 25.4, 25.5, 29.4, 39.1, 39.7, 45.1, 66.6, 69.6, 69.8, 69.9, 145.8. FT-IR (NaCl disk, cm^{-1}), 3307 (m), 3084 (m), 2932 (s), 2855 (m), 1680 (s), 1644 (s), 1542 (m), 1453 (w), 1433 (w), 1351 (w), 1321 (w), 1308 (w), 1273 (w), 1203 (s), 1178 (s), 1137 (s), 932 (w), 897 (w), 836 (w), 799 (w), 722 (w), 706 (w). HRMS (ESI): $[M+Na]^+$ *m/z* calcd., 325.2098; found, 325.2119.

***N*-(2-(2-(2-(2-Aminoethoxy)ethoxy)ethoxy)ethyl)-2-naphthamide (15).** Compound **15** was synthesized as described for **14** except that 2-naphthoic acid (86 mg, 0.50 mmol) was used instead of cyclohexanecarboxylic acid. The Boc-protected product was obtained as light yellow oil (178 mg, 80%). TLC R_f = 0.7 (10% MeOH/CH_2Cl_2). ^{1}H NMR ($CDCl_3$, 500 MHz), δ 1.36 (9H, s), 3.11-3.12 (2H, m), 3.28 (2H, t, J = 5.2 Hz), 3.34-3.35 (2H, m), 3.45 (2H, t, J = 4.5 Hz), 3.54-3.60 (4H, m), 3.65 (4H, bs), 4.99 (1H, bs), 6.82 (1H, bs), 7.37 (1H, dd, J = 7.8, 7.8 Hz), 7.43-7.49 (2H, m), 7.55 (1H, d, J = 7.0 Hz), 7.79-7.83 (2H, m), 8.26 (1H, d, J = 8.0 Hz). ^{13}C NMR ($CDCl_3$, 125 MHz), δ 28.2, 39.5, 39.9, 69.5, 69.7, 70.0, 70.1, 70.2, 78.9, 124.5, 124.9, 125.2, 126.1, 126.7, 128.0, 129.9, 130.2, 133.4, 134.3, 155.7, 169.4. FT-IR (NaCl disk, cm^{-1}), 3438 (w), 3326 (m), 3050 (w), 2975 (m), 2933 (m), 2870 (m), 1708 (s), 1648 (s), 1592 (w), 1580 (w), 1530 (s), 1455 (w), 1391 (w), 1366 (m), 1351 (w), 1303 (m), 1254 (m), 1172 (s), 1124 (s), 1041 (w), 970 (w), 866 (w), 807 (w), 785 (m), 756 (w), 655 (w). HRMS (ESI): $[M+Na]^+$ *m/z* calcd., 469.2309; found, 469.2335.

Compound **15** was obtained as light orange oil (quantitative yield from 91.6 mg, 0.205 mmol of the Boc-protected precursor). TLC R_f = 0.15 (10% MeOH/CH_2Cl_2). ^{1}H NMR ($CDCl_3$, 300 MHz), δ 3.06

(2H, bs), 3.56-3.66 (14H, m), 7.15 (1H, bs), 7.40-7.56 (6H, m), 7.85-7.94 (2H, m), 8.08-8.11 (1H, m). ^{13}C NMR ($CDCl_3$, 125 MHz), δ 39.3, 39.6, 66.4, 69.6, 69.6, 69.7, 69.9, 124.7, 125.0, 125.1, 126.3, 127.0, 128.3, 129.8, 130.6, 133.5, 133.7, 170.7. FT-IR (NaCl disk, cm^{-1}), 3270 (w), 3075 (m), 2918 (m), 2872 (m), 1680 (s), 1638 (s), 1592 (w), 1539 (m), 1480 (w), 1455 (w), 1429 (w), 1350 (w), 1307 (w), 1259 (w), 1203 (s), 1174 (s), 1135 (s), 945 (w), 880 (w), 834 (w), 798 (m), 785 (m), 721 (w), 706 (w). HRMS (ESI): $[M+Na]^+$ *m/z* calcd., 369.1785; found, 369.1806.

***N*-(2-(2-(2-Aminoethoxy)ethoxy)ethoxy)ethyl)-4-benzylbenzamide (16).** Compound **16** was synthesized as described for **14** except that 4-benzylbenzoic acid (106 mg, 0.50 mmol) was used instead of cyclohexanecarboxylic acid. The Boc-protected product was obtained as light yellow oil (220 mg, 90%). TLC R_f = 0.7 (10% MeOH/CH_2Cl_2). ^{1}H NMR ($CDCl_3$, 500 MHz), δ 1.48 (9H, s), 3.32 (2H, s), 3.51-3.54 (1H, m), 3.61-3.71(11H, m), 4.07 (2H, s), 5.10 (1H, s), 6.82 (1H, s), 7.21-7.34 (6H, m), 7.78-7.81 (2H, m). ^{13}C NMR ($CDCl_3$, 125 MHz), δ 28.3, 39.6, 40.2, 41.7, 69.8, 70.1, 70.1, 70.2, 70.4, 70.4, 79.1, 94.0, 126.2, 127.2, 128.5, 128.8, 128.9, 132.4, 140.3, 144.7, 145.8, 145.8, 155.9, 167.3. FT-IR (NaCl disk, cm^{-1}), 3346 (s), 3092 (w), 3071 (w), 3027 (m), 2977 (s), 2929 (s), 2863 (s), 2708 (w), 2498 (w), 1956 (w), 1693 (s), 1649 (s), 1543 (s), 1505 (s), 1454 (s),1392 (m), 1366 (s), 1301 (s),1251 (s), 1251 (s), 1201 (s), 1165 (s), 1131 (s), 1030 (m), 943 (w), 863 (m), 831 (m), 801 (m), 753 (s), 720 (m), 700 (s). HRMS (ESI): $[M+Na]^+$ *m/z* calcd., 509.2622; found, 509.2628.

Compound **16** was obtained as brown oil (quantitative yield from 220 mg of the Boc-protected precursor). TLC R_f = 0.4 (10% MeOH/CH_2Cl_2). ^{1}H NMR ($CDCl_3$, 500 MHz), δ 3.12 (2H, s), 3.55-3.62 (12H, m), 3.63-3.71 (2H, m), 4.00 (2H, s), 7.15-7.30 (8H, m), 7.68-7.73 (5H, m), 8.49 (3H, m). ^{13}C NMR ($CDCl_3$, 125 MHz), δ 39.2, 39.5, 41.6, 67.1, 66.8, 69.6, 70.09, 126.2, 127.4, 128.5, 128.7, 128.9, 131.5, 140.3, 145.1. FT-IR (NaCl disk, cm^{-1}), 3426 (m), 3027 (m), 2918 (m), 1948 (w), 1683 (m), 1632 (m), 1548 (m), 1505 (m), 1454 (m), 1420 (m), 1351 (m), 1309 (m), 1203 (m), 1134 (m), 1022 (w), 940 (w), 862 (w), 836 (w), 801 (m), 743 (m), 722 (m), 700 (m). HRMS (ESI): $[M+Na]^+$ *m/z* calcd., 409.2098; found, 409.2093.

***N*-(2-(2-(2-Aminoethoxy)ethoxy)ethoxy)ethyl)-11-oxo-2,3,5,6,7,11-hexahydro-1H-pyrano-[2,3-f]pyrido[3,2,1-ij]quinoline-10-carboxamide (17).** Coumarin 343 (142 mg, 0.50 mmol), EDC (143 mg, 0.751 mmol), DMAP (30 mg, 0.25 mmol), and DIPEA (435 μL, 2.52 mmol) were mixed in 15 mL of CH_2Cl_2. A portion (280 μL, 1.50 mmol) of 2,2'-((oxybis(ethane-2,1-diyl))bis(oxy))-diethanamine was added and the reaction mixture was stirred overnight at rt. The solvent was removed under reduced pressure and **17** was purified by preparative TLC (15% MeOH/CH_2Cl_2 with 1% TEA) and obtained as orange oil (86 mg, 38%). TLC R_f = 0.8 (10% MeOH/CH_2Cl_2). ^{1}H NMR ($CDCl_3$, 300 MHz), δ 1.95 (4H,

bs), 2.75 (2H, t, J = 6.0 Hz), 2.85 (2H, t, J = 6.3 Hz), 3.22 (2H, bs), 3.29-3.34 (4H, m), 3.56-3.70 (14H, m), 3.89 (2H, bs), 7.03 (1H, s), 7.65 (2H, bs), 8.55 (1H, s), 9.10 (1H, s). ^{13}C NMR ($CDCl_3$, 125 MHz), δ 19.8, 19.9, 20.8, 27.2, 39.3, 39.9, 49.6, 50.0, 66.5, 69.8, 69.9, 70.0, 105.3, 107.8, 108.0, 119.6, 127.0, 148.1, 148.2, 152.4, 162.8, 164.1. FT-IR (NaCl disk, cm^{-1}), 3412 (s), 2976 (m), 2919 (m), 2742 (m), 2673 (m), 2535 (m), 2497 (m), 1694 (s), 1616 (s), 1583 (s), 1521 (s), 1485 (s), 1445 (s), 1367 (s), 1398 (m), 1367 (s), 1310 (s), 1243 (m), 1212 (s), 1175 (s), 1098 (s), 1037 (m), 962 (w), 932 (w), 895 (w), 851 (w), 832 (w), 793 (m), 751 (m), 664 (w). HRMS (ESI): $[M+H]^+$ *m/z* calcd., 460.2442; found, 460.2435.

7-(4-(3-(2-(2-(2-Aminoethoxy)ethoxy)ethoxy)propanoyl)piperazin-1-yl)-1-cyclopropyl-6-fluoro-4-oxo-1,4-dihydroquinoline-3-carboxylic acid (18). Ciprofloxacin (115 mg, 0.50 mmol) and DIPEA (0.5 mL, 2.8 mmol) were mixed in 5 mL of CH_2Cl_2, and TMSCl (135 mL, 1.45 mmol) was added to give a clear yellow solution. Fmoc-PEG-CO_2H **13** (333 mg, 1.50 mmol), EDC (144 mg, 1.50 mmol), DMAP (30 mg, 0.050 mmol), and DIPEA (0.35 mL, 2 mmol) were dissolved in 2 mL of dry CH_2Cl_2, and the two solutions were combined and stirred at rt overnight. The resulting solution was washed with water (1x10 mL), 0.1 M HCl (2x20 mL), and brine (1x20 mL), dried over Na_2SO_4, and purified by flash chromatography on silica gel (3% isopropanol/CH_2Cl_2) to give the product as yellow solid (206 mg, 54%). TLC R_f = 0.6 (10% MeOH/CH_2Cl_2); mp = 83 °C (decomp). ^{1}H NMR ($CDCl_3$, 300 MHz), δ 1.11-1.16 (2H, m), 1.30-1.34 (2H, m), 2.64 (2H, t, J = 6.6 Hz), 3.23-3.69 (19H, m), 3.78-3.83 (4H, m), 4.17 (1H, t, J = 6.9 Hz), 4.35 (2H, d, J = 6.9 Hz), 5.64-5.66 (1H, m), 7.26-7.31 (3H, m), 7.34-7.39 (2H, m), 7.57-7.59 (2H, m), 7.70-7.73 (2H, m), 7.90-7.94 (1H, m), 8.66 (1H, s), 14.9 (1H, s). ^{13}C NMR ($CDCl_3$, 125 MHz), δ 7.7, 33.0, 35.0, 40.5, 40.7, 44.9, 46.8, 49.5, 66.1, 66.8, 69.7, 69.8, 70.0, 70.0, 104.7, 170.2, 111.3, 111.6, 119.0, 119.1, 119.5, 124.7, 126.7, 127.3, 138.5, 140.7, 143.5, 144.8, 145.0, 146.9, 151.3, 154.6, 156.2, 166.4, 169.3, 176.2, 176.3. ^{19}F NMR ($CDCl_3$, 282 MHz), δ -121.2. FT-IR (KBr pellet, cm^{-1}), 3309 (m), 3049 (w), 3010 (w), 2924 (m), 2868 (m), 1719 (s), 1627 (s), 1508 (m), 1465 (s), 1390 (w), 1337 (w), 1295 (w), 1260 (m), 1148 (w), 1112 (w), 1024 (w), 949 (w), 884 (w), 833 (w), 807 (w), 745 (m). HRMS (ESI): $[M+Na]^+$ *m/z* calcd., 779.3063; found, 779.3052.

A portion of this product (182 mg, 0.240 mmol) was dissolved in CH_2Cl_2 (2 mL) and diethylamine (2 mL, 19.3 mmol) was added. The solution was stirred for 2 h and concentrated under reduced pressure, and this procedure was repeated. A portion of the crude yellow product was dissolved in 3:7 H_2O/DMSO and purified by semi-preparative HPLC (0% B for 5 min followed by 20%-70% B over 20 min, 4 mL/min). Compound **18** eluted at 11 min and a yellow powder was obtained after lyophilization (38 mg). TLC R_f = 0.15 (10% MeOH/CH_2Cl_2). ^{1}H NMR ($CDCl_3$, 500 MHz), δ 1.15 (2H, bs), 1.41 (2H, bs), 2.70 (2H, bs), 3.19 (2H, bs), 3.30-3.37 (4H, m), 3.62-3.82 (17 H, m), 7.37 (1H, bs), 7.83-7.85 (1H, m), 8.16 (3H, bs), 8.65 (1H, s). ^{13}C NMR ($CDCl_3$, 125 MHz), δ 8.1, 33.1, 35.5, 40.0, 41.3,

45.2, 49.0, 49.6, 66.4, 67.1, 69.9, 70.1, 70.2, 105.4, 107.7, 111.9, 112.1, 119.8, 119.8, 139.0, 145.2, 145.3, 147.4, 152.4, 152.4, 167.0, 170.4, 176.8. ^{19}F NMR ($CDCl_3$, 282 MHz) δ -121.4, -75.6. FT-IR (KBr pellet, cm^{-1}), 2918 (m), 2876 (m), 1718 (m), 1692 (s), 1628 (s), 1506 (m), 1470 (m), 1385 (w), 1340 (w), 1295 (w), 1251 (w), 1201 (m), 1178 (w), 1125 (m), 1025 (w), 947 (w), 886 (w), 831 (w), 799 (w), 776 (w), 748 (w), 720 (w). HRMS (ESI): $[M+H]^+$ *m/z* calcd., 535.2563; found, 535.2578.

Methyl-5-allyl-2,3-dihydroxybenzoate (20). Methyl-5-allyl-3-methoxysalicylate (**19**, 2.22 g, 10.0 mmol) and anhydrous DIPEA (1.94 g, 15.0 mmol) were dissolved in 125 mL of dry CH_2Cl_2 and stirred at rt for five min. The solution was cooled to −78 °C in an acetone/dry ice bath, and boron tribromide (BBr_3, 1M solution in CH_2Cl_2, 30 mL, 30 mmol) was added slowly over ca. 10 min via a syringe to afford a yellow solution. The reaction was stirred at 78 °C for 1 h, warmed to 30 °C over the course of 1 h, and subsequently warmed to rt and stirred for another 4.5 h. Water (200 mL) was added slowly to quench the reaction, and the organic phase was washed with saturated aqueous potassium bicarbonate (K_2CO_3, 3100 mL). The organic phase was dried over sodium sulfate (Na_2SO_4), and the solvent was removed under reduced pressure to afford brown oil. Flash chromatography on silica gel with a solvent gradient (100% hexanes to 20% EtOAc/hexanes) gave the product as a white solid (1.09 g, 53%). TLC R_f = 0.5 (silica, CH_2Cl_2); mp = 55-56 °C. ^{1}H NMR ($CDCl_3$, 500 MHz), δ 3.29 (2H, d, J = 7.0 Hz), 3.95 (3H, s), 5.05-5.10 (2H, m), 5.80 (1H, s), 5.91 (1H, m), 6.97 (1H, s), 7.18 (1H, s), 10.76 (1H, s). ^{13}C NMR ($CDCl_3$, 125 MHz), δ 39.4, 52.3, 111.9, 116.0, 119.8, 120.4, 131.1, 137.0, 144.8, 147.2, 170.7. FT-IR (KBr pellet, cm^{-1}), 3467 (s), 3177 (m), 3079 (m), 3005 (m), 2978 (m), 2955 (m), 2905 (m), 2854 (w), 1678 (s), 1640 (w), 1622 (m), 1485 (s), 1442 (s), 1411 (w), 1370 (m), 1319 (s), 1282 (s), 1235 (m), 1195 (s), 1168 (s), 1130 (m), 916 (m), 867 (w), 791 (s), 772 (w), 681 (m), 630 (w). HRMS (DART): $[M+Na]^+$ *m/z* calcd., 231.0628; found, 231.0637.

5-Allyl-2,3-bis(benzyloxy)benzoic acid (21). Alkene **20** (2.18 g, 10.5 mmol), benzyl bromide (10.8 g, 60.3 mmol), and K_2CO_3 (24.5 g, 17.8 mmol) were combined in 200 mL of acetone at rt. The reaction was refluxed under N_2 for 16 h, which provided a yellow solution with white solids, and the mixture was cooled to rt and filtered. The filtrate was concentrated under reduced pressure to afford yellow oil. The oil was dissolved in a 375-mL mixture of 4:1 MeOH / 5 M NaOH (aq). The resulting solution was refluxed for 3.5 h and concentrated under reduced pressure to afford white-yellow oil. Water (300 mL) was added to the oil, and the aqueous phase was washed with hexanes (4 x 100 mL). The pH of the aqueous phase was adjusted to ca. 1 by addition of 12 M HCl and the product precipitated as a white solid. A 100-mL portion of CH_2Cl_2 was added, and the resulting mixture was partitioned. The aqueous phase was extracted with additional CH_2Cl_2 (2 x 100 mL) and the combined organic layers were dried

over Na_2SO_4 and concentrated under reduced pressure to yield **21** as a white solid (3.9 g, 99%). TLC R_f = 0.55 (silica, 100% CH_2Cl_2); mp = 135-136 °C. ^{1}H NMR ($CDCl_3$, 300 MHz), δ 3.38 (2H, d, J = 6.6 Hz), 5.06-5.14 (2H, m), 5.17 (2H, s), 5.22 (2H, s), 5.92 (1H, m), 7.09 (1H, d, J = 2.1 Hz), 7.31-7.50 (10H, m), 7.58 (1H, m).^{13}C NMR ($CDCl_3$, 125 MHz), δ 39.6, 71.4, 76.9, 116.7, 119.3, 122.6, 123.9, 127.8, 128.4, 128.7, 128.7, 129.1, 129.2, 134.8, 135.8, 136.2, 137.2, 145.5, 151.2, 165.6. FT-IR (KBr pellet, cm^{-1}), 3062 (m), 3032 (m), 2976 (m), 2937 (m), 2912 (m), 2889 (m), 1692 (s), 1639 (w), 1603 (w), 1578 (w), 1482 (m), 1453 (w), 1414 (w), 1378 (w), 1331 (m), 1268 (m), 1219 (w), 1146 (w), 1049 (m), 1028 (w), 968 (w), 914 (w), 858 (w), 791 (w), 758 (w), 697 (m). HRMS (DART): [M-H]$^-$ *m/z* calcd., 373.1445; found, 373.1439.

(*E*)-2,3-Bis(benzyloxy)-5-(prop-1-en-1-yl)benzoic acid (22). A 30-mL portion of methanol (MeOH) was degassed with N_2 for 4 h at rt and **21** (750 mg, 2.00 mmol) was subsequently added. The mixture was stirred at rt until **21** dissolved and $PdCl_2$ (58 mg, 0.32 mmol) was added to give a cloudy brown solution. The reaction was stirred at rt for 24 h and filtered. The filtrate was concentrated and purified by column chromatography using silica gel (1:4:5 EtOAc/hexanes/CH_2Cl_2) to yield **22** as a light yellow solid (666 mg, 89%). TLC R_f = 0.4 (40% EtOAc/hexanes); mp = 140-142 °C. ^{1}H NMR ($CDCl_3$, 300 MHz), δ 1.88-1.90 (3H, m), 5.19 (2H, s), 5.23 (2H, s), 6.25 (1H, dq, J = 15.9, 6.0 Hz), 6.32-6.38 (1H, m), 7.22 (1H, d, J = 2.1 Hz), 7.32-7.51 (10H, m), 7.69 (1H, d, J = 2.1 Hz). ^{13}C NMR ($CDCl_3$, 125 MHz), δ 18.3, 71.4, 77.0, 115.8, 121.6, 122.7, 127.4, 127.7, 128.4, 128.7, 129.1, 129.2, 129.3, 134.7, 135.0, 135.9, 145.7, 151.3, 165.5. FT-IR (KBr pellet, cm^{-1}), 3084 (w), 3063 (m), 3031 (m), 2955 (m), 2941 (m), 2876 (m), 2846 (m), 1692 (s), 1599 (m), 1574 (m), 1498 (m), 1483 (m), 1454 (m), 1414 (m), 1377 (m), 1336 (m), 1272 (m), 1256 (m), 1218 (m), 1153 (m), 1081 (w), 1051 (s), 1028 (w), 958 (s), 940 (m), 914 (w), 887 (w), 859 (m), 843 (w), 782 (m), 757 (s), 744 (m), 727 (m), 695 (s), 650 (w). HRMS (DART): [M-H]$^-$ *m/z* calcd., 373.1445; found, 373.1457.

Tertbutyl-((3S,7S,11S)-7,11-bis(2,3-bis(benzyloxy)benzamido)-2,6,10-trioxo-1,5,9-trioxacyclododecan-3-yl)carbamate (23). A portion (370 mg, 1.00 mmol) of **4** and DIPEA (1.42 g, 11.0 mmol) were dissolved in 5.0 mL of dry DMSO and stirred for 10 min at rt to give a colorless solution. PyBOP (1.04 g, 2.00 mmol) and **6** (463 mg, 1.41 mmol) were dissolved in 12.0 mL of dry DMSO and the solution was added to the solution containing **4** and DIPEA drop-wise over 20 min with stirring. The reaction was stirred at rt for 3 h and di-*tert*-butyldicarbonate (434 mg, 2.00 mmol) was added. After another 4 h of stirring at rt, the orange-red solution was mixed with 100 of mL CH_2Cl_2 and 100 mL of water. The organic phase was washed with brine (3 x 100 mL), dried over Na_2SO_4, and concentrated to afford an orange-brown oil. Flash chromatography on silica with a solvent gradient (100% hexanes to 55%

EtOAc/hexanes) yielded the product as a white oil (150 mg, 15%). TLC R_f = 0.3 (40% EtOAc/hexanes). ^{1}H NMR ($CDCl_3$, 300 MHz), δ 1.42 (9H, s), 4.02-4.21 (4H, m), 4.29-4.39 (2H, m), 4.60 (1H, bm), 4.80-4.94 (2H, m), 5.05-5.23 (8H, m), 7.07-7.47 (22H, m), 7.62-7.66 (2H, m), 8.51 (1H, d, J = 7.2 Hz), 8.59 (1H, d, J = 7.5 Hz). HRMS (DART): $[M+H]^+$ *m/z* calcd., 994.3757; found, 994.3721.

***N,N'*-((3S,7S,11S)-11-(5-allyl-2,3-Bis(benzyloxy)benzamido)-2,6,10-trioxo-1,5,9-trioxacyclo-dodecane-3,7-diyl)bis(2,3-bis(benzyloxy)benzamide) (24).** A portion (200 mg, 0.200 mmol) of **23** was dissolved in 13.5 mL of dry CH_2Cl_2 and the solution was cooled on ice. TFA (1.5 mL) was added to the solution drop-wise and the reaction was stirred on ice for 5 h. The reaction was washed by using a saturated aqueous solution of $NaHCO_3$ (3 x 10 mL), dried over Na_2SO_4, and concentrated to afford a light yellow solid, which was dissolved in 10 mL of dry CH_2Cl_2. DIPEA (258 mg, 2.00 mmol), PyBOP (208 mg, 0.400 mmol) and **6** (149 mg, 0.400 mmol) were added and the reaction was stirred overnight at rt. After concentrating under reduced pressure, the crude product was purified by flash chromatography on silica gel (5% to 50% EtOAc/hexanes) followed by preparative TLC on silica gel (20% EtOAc/CH_2Cl_2) to yield **24** as a white solid (26 mg, 10%). TLC R_f = 0.45 (50% EtOAc/hexanes). ^{1}H NMR ($CDCl_3$, 300 MHz), δ 3.36 (2H, d, J = 6.6 Hz), 3.99-4.05 (3H, m), 4.09-4.18 (3H, m), 4.88-4.95 (3H, m), 4.99-5.17 (12H, m), 5.92 (1H, m), 6.98-7.51 (33H, m), 7.65-7.68 (2H, m), 8.47-8.51 (3H, m). (10.11.10) HRMS (DART): $[M+H]^+$ *m/z* calcd., 1250.4645; found, 1250.4653.

***N,N'*-((3S,7S,11S)-11-(2,3-Bis(benzyloxy)-5-((E)-prop-1-en-1-yl)benzamido)-2,6,10-trioxo-1,5,9-trioxacyclododecane-3,7-diyl)bis(2,3-bis(benzyloxy)benzamide) (25).** Trilactone **4** (740 mg, 2.00 mmol) and DIPEA (2.58 g, 20.0 mmol) were mixed in dry DMSO (8 mL) and stirred for 10 min at rt to give a clear solution. PyAOP (3.13 g, 6.07 mmol), **22** (748 mg, 2.00 mmol) and **6** (1.00 g, 2.99 mmol) were dissolved in dry DMSO (10 mL) and added to the solution containing **4**, and the reaction turned yellow and became orange after stirring for 2 h at rt. The orange solution was mixed with EtOAc (50 mL) and water (50 mL) and partitioned. The organic phase was washed with brine (350 mL), dried over Na_2SO_4, and concentrated to afford a yellow oil. Flash chromatography on silica gel with a solvent gradient (10% EtOAc/hexanes to 55% EtOAc/hexanes) yielded the product as a white foam (931 mg, 37%). TLC R_f = 0.3 (50% EtOAc/hexanes); mp = 100-102 °C (decomp). ^{1}H NMR ($CDCl_3$, 300 MHz), δ 1.88-1.91 (3H, m), 4.01-4.11 (3H, m), 4.16-4.22 (3H, m), 4.91-4.98 (3H, m), 5.03-5.19 (12H, m), 6.17-6.40 (2H, m), 7.10-7.47 (32H, m), 7.66-7.71 (3H, m), 8.51-8.53 (3H, m). ^{13}C NMR ($CDCl_3$, 125 MHz), δ 18.2, 40.6, 51.2, 63.9, 70.9, 76.0, 76.1, 114.2, 117.3, 120.4, 122.8, 124.1, 125.7, 126.1, 126.3, 127.4, 127.5, 127.9, 128.0, 128.2, 128.4, 128.4, 128.4, 128.7, 128.7, 129.6, 134.1, 135.8, 135.8, 136.0, 136.0, 145.5, 146.7, 151.4, 151.4, 164.7, 168.8, 168.8. FT-IR (NaCl disk, cm^{-1}), 3356 (m), 3065 (w), 3031 (w),

2954 (w), 2927 (w), 2876 (w), 1752 (s), 1660 (s), 1597 (w), 1576 (m), 1514 (s), 1455 (m), 1424 (w), 1376 (w), 1346 (m), 1312 (m), 1266 (s), 1205 (s), 1133 (w), 1082 (w), 1054 (w), 1029 (w), 962 (w), 914 (w), 852 (w), 806 (w), 754 (s), 698 (s), 668 (w). HRMS (DART): $[M+H]^+$ *m/z* calcd., 1250.4645; found, 1250.4653.

***N,N'*-((3S,7S,11S)-11-(2,3-Bis(benzyloxy)-5-formylbenzamido)-2,6,10-trioxo-1,5,9-trioxacyclododecane-3,7-diyl)bis(2,3-bis(benzyloxy)benzamide) (26).** A portion of compound **25** (285 mg, 0.228 mmol) was dissolved in 1,4-dioxane (9 mL) at rt, and water (3 mL) was added to give a colorless solution. Osmium tetraoxide (OsO_4, 68μL of 2.5% wt solution in 2-methyl-2 propanol, 6.7 μmol) was added and the reaction was stirred for 0.5 h at rt, which afforded a light brown solution. Sodium periodate ($NaIO_4$, 76.5 mg, 0.570 mmol) was then added and the reaction was stirred for another 2 h at rt. The suspension was partitioned in water (20 mL) and EtOAc (50 mL). The organic phase was washed with 0.1 M sodium thiosulfate ($Na_2S_2O_3$, 320 mL) and brine (220 mL), and dried over Na_2SO_4. Flash chromatography on silica gel with a solvent gradient (20% EtOAc/hexanes to 65% EtOAc/hexanes) yielded the product as white solid (165 mg, 58%). TLC R_f = 0.6 (70% EtOAc/hexanes); mp = 74 °C (decomp). ^{1}H NMR ($CDCl_3$, 300 MHz), δ 4.03-4.11 (3H, m), 4.18-4.26 (3H, m), 4.90-4.96 (3H, m), 5.05-5.28 (12H, m), 7.09-7.44 (31H, m), 7.65-7.67 (2H, m), 8.14-8.15 (1H, m), 8.46-8.52 (3H, m), 9.86 (1H, s). ^{13}C NMR ($CDCl_3$, 125 MHz), δ 51.4, 51.4, 51.7, 64.1, 64.2, 71.0, 71.2, 76.2, 76.2, 76.5, 113.1, 117.3, 117.4, 122.9, 123.0, 124.2, 126.2, 126.3, 126.5, 127.5, 127.6, 127.8, 128.1, 128.3, 128.4, 128.4, 128.5,128.5, 128.5, 128.6, 128.8, 128.9, 132.1, 135.2, 135.3, 135.9, 135.9, 136.0, 146.7, 146.8, 151.5, 151.5, 151.7, 152.2, 163.7, 164.9, 164.9, 168.7, 168.9, 169.1, 190.6. FT-IR (KBr pellet, cm^{-1}), 3359 (m), 3062 (w), 3031 (w), 2957 (w), 2881 (w), 1752 (s), 1697 (m), 1660 (s), 1601 (w), 1577 (m), 1516 (s), 1454 (m), 1376 (m), 1345 (m), 1312 (m), 1266 (s), 1205 (s), 1135 (w), 1081 (w), 1053 (w), 1027 (w), 956 (w), 915 (w), 851 (w), 754 (s), 698 (s), 668 (w). HRMS (DART): $[M+H]^+$ *m/z* calcd., 1238.4287; found, 1238.4279.

3,4-Bis(benzyloxy)-5-(((3S,7S,11S)-7,11-bis(2,3-bis(benzyloxy)benzamido)-2,6,10-trioxo-1,5,9-trioxacyclododecan-3-yl)carbamoyl)benzoic acid (27). A portion of **26** (112 mg, 90.3 μmol) was dissolved in 1,4-dioxane (3 mL) at rt. Sulfamic acid (NH_3SO_3, 15.8 mg, 0.162 mmol) was dissolved in water (0.75 mL) and added to the dioxane solution. Sodium chlorite ($NaClO_2$, 14.7 mg, 0.163 mmol) was dissolved in 0.2 mL of water and the resulting solution was added to the reaction over the course of 10 min, and the reaction turned yellow. After stirring for 0.5 h at rt, the reaction was partitioned in water (10 mL) and EtOAc (20 mL), the aqueous phase was extracted with EtOAc (210 mL), and the combined organic phases were dried over Na_2SO_4. Flash chromatography on silica gel with a solvent gradient

(CH_2Cl_2 to 10% MeOH/CH_2Cl_2) yielded the product as white solid (87 mg, 76%). TLC R_f = 0.5 (10% MeOH/ CH_2Cl_2); mp = 128-129 °C (decomp). ^{1}H NMR ($CDCl_3$, 500 MHz), δ 4.05-4.08 (3H, m), 4.22-4.25 (3H, m), 4.93-4.98 (3H, m), 5.06-5.25 (12H, m), 7.06-7.47 (31H, m), 7.67-7.69 (2H, m), 7.86 (1H, s), 8.44-8.47 (2H, m), 8.54-8.57 (2H, m). ^{13}C NMR ($CDCl_3$, 125 MHz), δ 51.4, 51.5, 51.6, 64.1, 71.1, 71.2, 76.2, 76.4, 117.5, 117.6, 123.0, 124.2, 125.4, 125.6, 126.2, 127.5, 127.6, 127.8, 128.1, 128.3, 128.4, 128.4, 128.5, 128.6, 128.7, 128.8, 128.9, 135.4, 135.6, 135.9, 136.1, 146.8, 150.7, 151.4, 151.5, 164.1, 165.0, 168.8, 168.9, 169.0, 169.3. FT-IR (KBr pellet, cm^{-1}), 3654 (w), 3628 (w), 3359 (m), 3088 (w), 3064 (w), 3032 (w), 2946 (w), 2933 (w), 2874 (w), 1761 (s), 1660 (m), 1599 (w), 1576 (m), 1519 (m), 1490 (m), 1454 (m), 1427 (w), 1374 (m), 1345 (m), 1267 (m), 1203 (m), 1134 (w), 1081 (w), 1048 (w), 1028 (w), 954 (w), 912 (w), 849 (w), 807 (w), 754 (s), 734 (s), 697 (s). HRMS (DART): $[M+H]^+$ *m/z* calcd., 1254.4230; found, 1254.4204.

***N,N'*-((3*R*,7*R*,11*R*)-11-(2,3-Bis(benzyloxy)-5-((*E*)-prop-1-en-1-yl)benzamido)-2,6,10-trioxo-1,5,9-trioxacyclododecane-3,7-diyl)bis(2,3-bis(benzyloxy)benzamide) (28).** Compound **5** (0.441 g, 1.19 mmol) was dissolved in 8 mL of DMSO and DIPEA (2.28 mL, 13.1 mmol) was added. In a separate flask, compounds **6** (0.591 g, 1.78 mmol), **22** (0.669 g, 1.78 mmol), and PyAOP (2.48 g, 4.76 mmol) were combined in 15 mL of DMSO. This mixture was added drop wise to the solution of **5**, and the resulting solution was stirred for 2 h at rt during which time it turned dark red-brown. The reaction was diluted with 50 mL of EtOAc and 25 mL of water. The layers were partitioned, and the organic phase was washed with saturated brine (2 x 25 mL). The organic phase was dried over Na_2SO_4 and concentrated under reduced pressure, which yielded red-orange oil. Flash chromatography on silica gel with a solvent gradient (10% EtOAc/hexanes to 50% EtOAc/hexanes) afforded **28** as a white-yellow solid (207 mg, 15%). TLC R_f = 0.4 (50% EtOAc/Hexanes). ^{1}H NMR ($CDCl_3$, 500 MHz), δ 1.88-1.89 (3H, m) 4.01-4.04 (3H, m) 4.14-4.16 (3H, m) 4.91-4.92 (3H, m) 5.02-5.27 (12H, m) 6.18-6.22 (1H, m) 6.35-6.40 (1H, m) 7.12-7.68 (36H, m) 8.48-8.49 (3H, d, J = 7.5 Hz). ^{13}C NMR ($CDCl_3$, 500 MHz) δ 18.4, 51.4, 51.4, 64.1, 71.2, 76.3, 76.4, 76.7, 117.6, 120.7, 123.2, 124.3, 126.0, 126.4, 126.5, 127.6, 127.7, 127.8, 128.2, 128.4, 128.6, 128.6, 128.8, 128.8, 128.9, 128.9, 129.3, 129.8, 134.3, 136.0, 136.3, 147.0, 151.6, 164.9, 169.1. FT-IR (KBr pellet, cm^{-1}), 3356 (m), 3058 (w), 3032 (w), 2929 (w), 2881 (w), 1750 (s), 1660 (s), 1597 (w), 1576 (m), 1514 (s), 1455 (m), 1375 (w), 1346 (w), 1312 (w), 1266 (s), 1204 (s), 1133 (w), 1082 (w), 1053 (w), 1027 (w), 962 (w), 914 (w), 851 (w), 802 (w), 754 (s), 698 (m). HRMS (ESI): $[M+Na]^+$ *m/z* calcd., 1272.4464; found, 1272.4434.

***N,N'*-((3*R*,7*R*,11*R*)-11-(2,3-Bis(benzyloxy)-5-formylbenzamido)-2,6,10-trioxo-1,5,9-trioxa-cyclododecane-3,7-diyl)bis(2,3-bis(benzyloxy)benzamide) (29)**. Compound **28** (159 mg, 0.127 mmol)

was dissolved in 6 mL of 1,4-dioxane. Water (2 mL) was slowly added drop wise to the solution. With each drop of water, a white cloudy precipitate appeared and then disappeared. OsO_4 (39 μL of a 2.5 wt % solution in 2-methyl-2-propanol, 3.8 μmol) was then added to the solution, and the reaction was stirred for 0.5 h, which yielded a brown solution. $NaIO_4$ (67 mg, 0.42 mmol) was added to the reaction, which was stirred for 2 h and a white precipitate formed. The reaction was diluted with EtOAc (25 mL) and water (10 mL). The organic phase was washed with 0.1 M NaS_2O_3 (3 x 20 mL) and brine (1 x 20 mL). The organic phase gained a yellow tint with the addition of NaS_2O_3. The organic phase was dried over Na_2SO_4 and concentrated *in vacuo*. Flash chromatography on silica gel using a solvent gradient (20% EtOAc/hexanes to 70% EtOAc/hexanes) yielded the product as a white foam (101 mg, 64%). TLC R_f = 0.7 (10% MeOH/CH_2Cl_2). ^{1}H NMR ($CDCl_3$, 500 MHz), δ 4.00-4.08 (3H, m), 4.15-4.22 (3H, m), 4.88-4.93 (3H, m), 5.03-5.26 (12H, m), 7.08-7.43 (31H, m) 7.65-7.65 (2H, m), 8.14 (1H, s), 8.41-8.47 (3H, m), 9.88 (1H, s). ^{13}C NMR ($CDCl_3$, 125 MHz), δ 51.4, 51.5, 51.5, 51.7, 64.1, 64.3, 71.2, 71.3, 76.3, 76.6, 113.2, 117.5, 117.5, 123.1, 123.2, 124.3, 126.3, 126.3, 126.6, 127.6, 127.6, 127.8, 128.2, 128.2, 128.4, 128.4, 128.5, 128.6, 128.6, 128.7, 128.9, 128.9, 129.0, 132.2, 135.3, 135.4, 136.0, 136.0, 136.2, 146.8, 146.9, 151.6, 151.8, 152.3, 163.8, 165.0, 165.0, 168.8, 169.0, 169.2, 190.7. FT-IR (NaCl disk, cm^{-1}), 3358 (m), 3062 (w), 3031 (w), 2957 (w), 2928 (w), 2876 (w), 1751 (s), 1697 (m), 1660 (s), 1577 (m), 1517 (s), 1455 (m), 1375 (w), 1346 (w), 1303 (w), 1266 (s), 1206 (m), 1134 (w), 1082 (w), 1054 (w), 1022 (w), 957 (w), 914 (w), 851 (w), 806 (w), 754 (s), 698 (m). HRMS (ESI): $[M+Na]^+$ *m/z* calcd., 1260.4101; found, 1260.4094.

3,4-Bis(benzyloxy)-5-(((3*R*,7*R*,11*R*)-7,11-bis(2,3-bis(benzyloxy)benzamido)-2,6,10-trioxo-1,5,9-trioxacyclododecan-3-yl)carbamoyl)benzoic acid (30). Aldehyde **29** (0.092 g, 0.074 mmol) was dissolved in 2 mL of 1,4-dioxane. In a separate flask, NH_3SO_3 (12.8 mg, 0.132 mmol) was dissolved in 0.5 mL of H_2O. The sulfamic acid solution was added to the 1,4-dioxane solution. The reaction turned cloudy shortly after the addition of NH_3SO_3. $NaClO_2$ (12 mg, 0.13 mmol) was dissolved in 0.4 mL of H_2O and added drop wise over ten minutes to the dioxane solution. The reaction was stirred for 30 min and diluted with 10 mL of H_2O and 10 mL of EtOAc. The aqueous phase was back extracted with EtOAc (2 x 10 mL), and the combined organic phases were dried over Na_2SO_4 and concentrated under reduced pressure. Flash chromatography on silica gel with a solvent gradient (CH_2Cl_2 to 10% MeOH/CH_2Cl_2) yielded a white solid (83 mg, 89%). TLC R_f = 0.6 (10% MeOH/CH_2Cl_2). ^{1}H NMR ($CDCl_3$, 500 MHz), δ 4.08-4.11 (3H, m), 4.25-4.28 (3H, m), 4.96-5.00 (3H, m), 5.08-5.29 (12H, m), 7.14-7.51 (30H, m), 7.70-7.72 (2H, m), 7.89 (1H, s), 8.45-8.48 (2H, m), 8.53-8.59 (2H, m). ^{13}C NMR ($CDCl_3$, 125 MHz), δ 29.1, 51.5, 53.6, 64.2, 71.1, 71.3, 76.3, 76.5, 117.5, 123.1, 124.3, 126.3, 127.6, 127.6, 127.9, 128.2, 128.4, 128.5, 128.6, 128.7, 128.8, 128.9, 129.0, 135.5, 135.6, 136.0, 136.2, 145.9, 146.9, 150.8, 151.4, 151.6,

164.1, 165.1, 168.9, 169.0, 169.1. FT-IR (KBr pellet, cm^{-1}), 3356 (m), 3088 (w), 3064 (w), 3032 (w), 2957 (w), 2924 (w), 2872 (w), 1753 (s), 1718 (m), 1662 (s), 1599 (w), 1577 (s), 1517 (s), 1454 (s), 1427 (w), 1375 (m), 1346 (m), 1267 (s), 1205 (s), 1133 (w), 1112 (w), 1082 (m), 1052 (m), 1029 (m), 957 (m), 914 (m), 851 (w), 808 (w), 755 (s), 736 (s), 699 (s).

***Tert*-butyl(1-(3-(((3S,7S,11S)-7,11-bis(2,3-dihydroxybenzamido)-2,6,10-trioxo-1,5,9-trioxacyclododecan-3-yl)carbamoyl)-4,5-dihydroxyphenyl)-1-oxo-5,8,11-trioxa-2-azatridecan-13-yl)carbamate (31).** Compound **27** (50 mg, 40 μmol), PyAOP (34 mg, 60 μmol) and DIPEA (15.2 μL, 160 μmol) were mixed in 2 mL of dry CH_2Cl_2 at rt. A portion of **7** (15 mg, 48 μmol) was then added and the resulting yellow solution was stirred for 4 h at rt. The crude reaction was washed with 0.01 N HCl (2 x 10 mL), dried over Na_2SO_4, and concentrated. The benzyl-protected product was purified by preparative TLC (10% MeOH/CH_2Cl_2) and obtained as a white viscous solid (46 mg, 75%). TLC R_f = 0.7 (10% MeOH/CH_2Cl_2). ^{1}H NMR ($CDCl_3$, 500 MHz), δ 1.42 (9H, s), 3.27-3.28 (2H, m), 3.50-3.52 (2H, m), 3.59-3.66 (12H, m), 4.02-4.07 (3H, m), 4.15-4.18 (3H, m), 4.90-4.94 (3H, m), 5.03-5.20 (12H, m), 7.10-7.45 (36H, m), 7.65-7.67 (2H, m), 7.85-7.85 (1H, m), 7.99 (1H, bs), 8.49-8.54 (3H, m). ^{13}C NMR ($CDCl_3$, 125 MHz), δ 28.3, 39.9, 40.2, 51.3, 51.4, 63.9, 64.1, 69.7, 70.0, 70.2, 70.3, 70.4, 71.1, 71.2, 76.2, 76.3, 79.0, 116.7, 117.5, 120.3, 123.0, 124.2, 125.4, 126.1, 126.2, 127.6, 127.6, 127.8, 128.2, 128.3, 128.4, 128.4, 128.4, 128.5, 128.6, 128.6, 128.7, 128.8, 128.8, 129.0, 130.2, 135.4, 135.7, 135.9, 135.9, 136.1, 146.8, 146.9, 149.0, 151.5, 151.8, 155.9, 164.2, 164.8, 164.9, 165.8, 168.9, 169.0, 169.1. FT-IR (NaCl disk, cm^{-1}), 3356 (m), 3064 (w), 3033 (w), 2931 (m), 2872 (m), 1752 (s), 1710 (m), 1661 (s), 1577 (m), 1516 (s), 1455 (s), 1367 (m), 1346 (m), 1266 (s), 1205 (s), 1130 (m), 1083 (m), 1047 (m), 958 (w), 915 (w), 851 (w), 808 (w), 755 (m), 699 (m). HRMS (ESI): $[M+Na]^+$ *m/z* calcd., 1550.5942; found, 1550.5977.

This benzyl-protected product was dissolved in 2 mL of 1:1 EtOAc/EtOH, the reaction flask was purged with N_2, and 45 mg Pd/C (10% wt) was added. The reaction was stirred under H_2 (1 atm) for 6 h at rt, and the Pd/C was removed by centrifugation (13,000 rpm, 10 min). The clear supernatant was decanted, concentrated, and re-dissolved in a 4:2:1 mixture of 1,4-dioxane/H_2O/MeOH, and purified by semi-preparative HPLC (20% B for 5 min followed by 20-70% B over 15 min, 4 mL/min). The product eluted at 15.8 min and was lyophilized to give **31** as white solid (15 mg, 50%). The analytical HPLC trace of the purified product is reported in Appendix 2. HRMS (ESI): $[M+Na]^+$ *m/z* calcd., 1010.3125; found, 1010.3173.

***N*^{3}-((3S,7S,11S)-7,11-Bis(2,3-dihydroxybenzamido)-2,6,10-trioxo-1,5,9-trioxacyclododecan-3-yl)-*N*^{1}-(1-cyclohexyl-1-oxo-5,8,11-trioxa-2-azatridecan-13-yl)-4,5-dihydroxyisophtha-lamide (32).** Compound **32** was synthesized as described for **31** except that **14** (13.6 mg, 45.0 μmol) was used instead

of **7**. After purification by preparative TLC (10% MeOH/CH_2Cl_2), the benzyl-protected precursor of **32** was obtained as a white viscous solid (37 mg, 60%). TLC R_f = 0.6 (10% MeOH/CH_2Cl_2). ^{1}H NMR ($CDCl_3$, 500 MHz), δ 1.17-1.21 (3H, m), 1.37-1.43 (2H, m), 1.62-1.63 (1H, m), 1.72-1.74 (2H, m), 1.78-1.81 (2H, m), 2.00-2.06 (1H, m), 3.39-3.42 (2H, m), 3.51-3.53 (2H, m), 3.59-3.61 (2H, m), 3.64-3.65 (10H, m), 4.01-4.06 (3H, m), 4.13-4.17 (3H, m), 4.88-4.93 (3H, m), 5.04-5.21 (12H, m), 6.23-6.25 (1H, m), 7.09-7.45 (35H, m), 7.64-7.66 (2H, m), 7.86 (1H, d, J = 2.0 Hz), 8.02 (1H, d, J = 2.0 Hz), 8.49-8.54 (3H, m). ^{13}C NMR ($CDCl_3$, 125 MHz), δ 25.6, 29.5, 38.8, 40.0, 45.3, 51.3, 51.4, 63.9, 64.1, 69.8, 69.8, 70.0, 70.3, 70.4, 70.4, 71.2, 71.2, 76.2, 76.3, 116.8, 117.5, 120.4, 123.0, 124.3, 125.4, 126.1, 126.2, 127.6, 127.6, 127.9, 128.2, 128.3, 128.4, 128.4, 128.5, 128.5, 128.6, 128.6, 128.8, 128.8, 128.9, 129.0, 130.1, 135.4, 135.7, 135.9, 136.0, 136.1, 146.8, 146.9, 149.1, 151.6, 151.8, 164.3, 164.9, 164.9, 165.8, 168.9, 169.0, 169.1, 176.2. FT-IR (NaCl disk, cm^{-1}), 3353 (m), 3065 (w), 3032 (w), 3010 (w), 2930 (m), 2855 (m), 1752 (s), 1660 (s), 1593 (w), 1577 (m), 1518 (s), 1454 (m), 1424 (w), 1374 (w), 1346 (m), 1301 (m), 1265 (s), 1206 (s), 1130 (m), 1083 (m), 1050 (m), 1022 (w), 957 (w), 915 (w), 850 (w), 809 (w), 755 (s), 699 (m), 659 (w). HRMS (ESI): $[M+Na]^+$ *m/z* calcd., 1560.6150; found, 1560.6269. Following benzyl deprotection, compound **32** was purified by semi-preparative HPLC (20% B for 5 min followed by 20-70% B over 15 min, 4 mL/min). The product eluted at 15.1 min and was obtained as white solid (20 mg, 58%). The analytical HPLC trace of the purified product is reported in Appendix 2. HRMS (ESI): $[M+Na]^+$ *m/z* calcd., 1020.3333; found, 1020.3346.

***N*^{3}-((3R,7R,11R)-7,11-Bis(2,3-dihydroxybenzamido)-2,6,10-trioxo-1,5,9-trioxacyclododecan-3-yl)-*N*^{1}-(1-cyclohexyl-1-oxo-5,8,11-trioxa-2-azatridecan-13-yl)-4,5-dihydroxyisophthalamide (33).** Compound **33** was synthesized as described for **32** except that **30** (36 mg, 29 μmol) was used instead of **27**. After purification by preparative TLC (10% MeOH/CH_2Cl_2), the benzyl-protected precursor of **33** was obtained as a white oily solid (29 mg, 65%).TLC R_f = 0.6 (10% MeOH/CH_2Cl_2). ^{1}H NMR ($CDCl_3$, 500 MHz), δ 1.17-1.25 (3H, m), 1.38-1.44 (2H, m), 1.63 (1H, m), 1.72-1.81 (4H, m), 2.01-2.06 (1H, m), 3.40-3.41 (2H, m), 3.39-3.42 (2H, m), 3.51-3.53 (2H, m), 3.58-3.65 (12H, m), 4.01-4.06 (3H, m), 4.13-4.16 (3H, m), 4.87-4.95 (3H, m), 5.03-5.21 (12H, m), 6.22-6.23 (1H, m), 7.09-7.45 (35H, m), 7.65-7.66 (2H, m), 7.86 (1H, s), 8.02 (1H, s), 8.49-8.54 (3H, m). ^{13}C NMR ($CDCl_3$, 125 MHz), δ 25.6, 29.5, 38.8, 40.0, 45.3, 51.3, 51.4, 63.9, 64.1, 69.8, 69.8, 70.0, 70.3, 70.4, 70.4, 71.2, 71.2, 76.2, 76.3, 116.8, 117.5, 120.4, 123.0, 124.3, 125.4, 126.1, 126.2, 127.6, 127.6, 127.9, 128.2, 128.3, 128.4, 128.4, 128.5, 128.5, 128.6, 128.6, 128.8, 128.8, 128.9, 129.0, 130.1, 135.4, 135.7, 135.9, 136.0, 136.1, 146.8, 146.9, 149.1, 151.6, 151.8, 164.3, 164.9, 164.9, 165.8, 168.9, 169.0, 169.1, 176.2. FT-IR (NaCl disk, cm^{-1}), 3354 (m), 3062 (w), 3032 (w), 3006 (w), 2929 (m), 2855 (m), 1752 (s), 1660 (s), 1577 (m), 1518 (s), 1454 (m), 1374 (w), 1346 (w), 1303 (w), 1265 (m), 1206 (m), 1130 (w), 1083 (w), 1061 (w), 1031 (w), 957 (w), 915 (w), 850

(w), 811 (w), 755 (s), 698 (m). HRMS (ESI): $[M+Na]^+$ *m/z* calcd., 1560.6150; found, 1560.6141. Following benzyl deprotection, compound **33** was purified by semi-preparative HPLC (20% B for 5 min followed by 20-70% B over 15 min, 4 mL/min). The product eluted at 14.8 min and was obtained as white solid (5.1 mg, 27% yield). The analytical HPLC trace of the purified product is reported in Appendix 2. HRMS (ESI): $[M+Na]^+$ *m/z* calcd., 1020.3333; found, 1020.3328.

***N*^{3}-((3S,7S,11S)-7,11-Bis(2,3-dihydroxybenzamido)-2,6,10-trioxo-1,5,9-trioxacyclododecan-3-yl)-4,5-dihydroxy-*N*^{1}-(1-(naphthalen-2-yl)-1-oxo-5,8,11-trioxa-2-azatridecan-13-yl)isophthalamide (34).** Compound **34** was synthesized as described for **31** except that **15** (20 mg, 44 μmol) was used instead of **7**. After purification by preparative TLC (5% $MeOH/CH_2Cl_2$), the benzyl-protected precursor of **34** was obtained as a white-yellow oily solid (37 mg, 59%). TLC R_f = 0.6 (10% $MeOH/CH_2Cl_2$). ^1H NMR ($CDCl_3$, 500 MHz), δ 3.44-3.74 (16H, m), 3.94-4.08 (4H, m), 4.12-4.16 (2H, m), 4.78-4.82 (1H, m), 4.87-4.92 (2H, m), 5.02-5.17 (12H, m), 7.01-7.52 (39H, m), 7.58-7.59 (1H, m), 7.64-7.66 (2H, m), 7.79-7.84 (3H, m), 7.94-7.94 (1H, m), 8.29-8.31 (1H, m), 8.47-8.50 (3H, m). ^{13}C NMR ($CDCl_3$, 125 MHz), δ 39.6, 39.9, 51.4, 51.4, 63.9, 64.1, 69.6, 69.7, 70.2, 70.4, 71.1, 71.2, 71.2, 76.2, 76.3, 76.3, 116.7, 117.5, 120.3, 123.1, 124.3, 124.6, 125.0, 125.2, 125.4, 126.1, 126.2, 126.2, 126.9, 127.6, 127.6, 127.9, 128.1, 128.2, 128.4, 128.4, 128.5, 128.6, 128.6, 128.8, 128.9, 128.9, 129.0, 130.0, 130.1, 130.3, 133.5, 134.5, 135.4, 135.7, 135.9, 136.0, 136.2, 146.9, 146.9, 149.0, 151.6, 151.7, 164.2, 164.9, 164.9, 165.7, 168.9, 169.0, 169.1, 169.6. FT-IR (NaCl disk, cm^{-1}), 3353 (m), 3067 (w), 3028 (w), 2997 (w), 2924 (m), 2859 (m), 1751 (s), 1659 (s), 1577 (m), 1519 (s), 1455 (m), 1372 (w), 1346 (w), 1295 (m), 1205 (m), 1122 (w), 1083 (w), 1053 (w), 1027 (w), 958 (w), 914 (w), 845 (w), 806 (w), 785 (w), 754 (m), 698 (m). HRMS (ESI): $[M+Na]^+$ *m/z* calcd., 1604.5837; found, 1604.5964. Following benzyl deprotection, compound **34** was purified by semi-preparative HPLC (20% B for 5 min followed by 30-55% B over 10 min, 4mL/min) and eluted at 12.7 min. The isolated product was lyophilized and obtained as a white solid (4.4 mg, 18%). The analytical HPLC trace of the purified product is provided in Appendix 2. HRMS (ESI): $[M+Na]^+$ *m/z* calcd.,1064.3020; found,1064.3084. Mass spectrometric analysis of the crude reaction indicated M+4 in addition to the desired product **34** and suggested partial reduction of the naphthalene cargo under the deprotection conditions. From analysis of HPLC peak areas, the ratio between **34** and the partial reduction product is ca. 4:1.

***N*^{1}-(1-(3-Benzylphenyl)-1-oxo-5,8,11-trioxa-2-azatridecan-13-yl)-*N*^{3}-((3S,7S,11S)-7,11-bis-(2,3-dihydroxybenzamido)-2,6,10-trioxo-1,5,9-trioxacyclododecan-3-yl)-4,5-dihydroxyisophthalamide (35).** Compound **35** was synthesized as described for **31** except that **16** (24 mg, 62 μmol) was used instead of **7**. Partial purification by preparative TLC (10% $MeOH/CH_2Cl_2$) afforded the benzyl-protected

precursor of **35** as a white-yellow solid with a grease contamination (43 mg, 67%).TLC R_f = 0.6 (10% MeOH/CH_2Cl_2). ^{1}H NMR ($CDCl_3$, 500 MHz), δ 3.57-3.61 (12H, m), 3.94-3.95 (2H, d, J = 6.0 Hz) 3.97-4.05 (3H, m), 4.07-4.15 (3H, m), 4.85-4.90 (3H, m), 5.01-5.17 (12H, m), 7.01-7.40 (30H, m) 7.62-7.70 (3H, m), 7.82 (1H, d, J = 2.0 Hz), 7.99-8.00 (1H, d, J = 2.0 Hz), 8.47-8.51 (3H, m). FT-IR (NaCl disk, cm^{-1}), 3356 (m), 3071 (w), 3031 (w), 2924 (m), 2868 (m), 1751 (s), 1660 (s), 1576 (m), 1519 (s), 1454 (m), 1374 (w), 1346 (m), 1301 (m), 1265 (s), 1205 (m), 1130 (w), 1083 (w), 1057 (w), 1022 (w), 957 (w), 915 (w), 851 (w), 806 (w), 754 (s), 698 (m). HRMS (ESI): $[M+Na]^+$ *m/z* calcd., 1644.6150; found, 1644.6105. A portion (32.5 mg, 20.0 μmol) of this material was carried on without further purification or characterization. Following benzyl deprotection, compound **35** was purified by semi-preparative HPLC (20% B for 5 min followed by 20-70% B over 15 min, 4 mL/min). The product eluted at 15.8 min and was obtained as white solid (13.5 mg, 62%). The analytical HPLC trace of the purified product is provided in Appendix 2. HRMS (ESI): $[M+Na]^+$ *m/z* calcd., 1104.3333; found, 1104.3305.

***N*^{3}-((3S,7S,11S)-7,11-Bis(2,3-dihydroxybenzamido)-2,6,10-trioxo-1,5,9-trioxacyclododecan-3-yl)-4,5-dihydroxy-*N*^{1}-(1-oxo-1-(11-oxo-2,3,5,6,7,11-hexahydro-1*H*-pyrano[2,3-*f*]pyrido[3,2,1*ij*]quinolin-10-yl)-5,8,11-trioxa-2-azatridecan-13-yl)isophthalamide (36).** Compound **36** was synthesized as described for **31** except that **17** (18 mg, 39 μmol) was used instead of **7**. After purification by preparative TLC (10% MeOH/CH_2Cl_2) the benzyl-protected precursor of **36** was obtained as an orange oily solid (18 mg, 26%). TLC R_f = 0.7 (10% MeOH/CH_2Cl_2). ^{1}H NMR ($CDCl_3$, 500 MHz), δ 1.93-1.95 (4H, m), 2.71-2.83 (4H, m), 3.26-3.32 (4H, m), 3.56-3.69 (16H, m), 3.99-4.18 (6H, m), 4.88-4.94 (3H, m), 5.01-5.18 (12H, m), 6.94 (1H, s), 7.06-7.43 (35H, m), 7.62-7.66 (2H, m), 7.80-7.80 (1H, m), 7.97-7.97 (1H, m), 8.47-8.53 (4H, m), 9.02-9.03 (1H, m). ^{13}C NMR ($CDCl_3$, 125 MHz), δ 19.9, 20.0, 21.0, 27.3, 39.4, 40.1, 49.7, 50.2, 51.5, 64.1, 69.9, 71.1, 71.2, 76.3, 105.4, 108.1, 115.9, 117.5, 119.8, 123.0, 124.3, 125.7, 126.3, 127.2, 127.6, 127.6, 127.8, 128.1, 128.2, 128.5, 128.5, 128.6, 128.9, 128.9, 129.0, 130.0, 135.7, 136.0, 136.2, 146.9, 148.2, 148.3, 149.0, 151.6, 151.7, 152.6, 162.9, 164.4, 165.0, 165.0, 168.9, 169.1. FT-IR (NaCl disk, cm^{-1}), 3350 (m), 3088 (w), 3065 (w), 3033 (w), 2931 (m), 2868 (m), 1752 (s), 1660 (s), 1616 (m), 1577 (s), 1518 (s), 1455 (s), 1369 (m), 1348 (m), 1309 (s), 1266 (s), 1211 (s), 1152 (w), 1129 (m), 1083 (m), 1053 (w), 1027 (w), 958 (w), 912 (m), 844 (s), 794 (w), 734 (s), 699 (m). HRMS (ESI): $[M+Na]^+$ *m/z* calcd., 1717.6313; found, 1717.6287. Following benzyl deprotection, compound **36** was purified by semi-preparative HPLC (20% B for 5 min followed by 20-70% B over 15 min, 4 mL/min). The product eluted at 17.1 min and was obtained as an orange solid (4.5 mg, 48%). The analytical HPLC trace of the purified product is provided in Appendix 2. HRMS (ESI): $[M+Na]^+$ *m/z* calcd., 1177.3496; found, 1177.3540.

7-(4-(1-(3-(((3S,7S,11S)-7,11-Bis(2,3-dihydroxybenzamido)-2,6,10-trioxo-1,5,9-trioxacyclododecan-3-yl)carbamoyl)-4,5-dihydroxyphenyl)-1-oxo-5,8,11-trioxa-2-azatetradecan-14-oyl)piperazin-1-yl)-1-cyclopropyl-6-fluoro-4-oxo-1,4-dihydroquinoline-3-carboxylic acid (37). Compound **37** was synthesized as described for **31** except that **18** (26 mg, 48 μmol) was used instead of 7, and TMSCl (10 μL, 79 μmol) and DIPEA (15 μL, 160 μmol) was mixed with **18** before addition to the solution containing **27**. After purification by preparative TLC (10% MeOH/CH_2Cl_2), the benzyl-protected precursor of **37** was obtained as a yellow oily solid (46 mg, 65%). TLC R_f = 0.65 (10% MeOH/CH_2Cl_2). ^{1}H NMR ($CDCl_3$, 500 MHz), δ 1.13 (2H, bs), 1.33 (2H, bs), 2.64 (2H, bs), 3.23-3.30 (4H, m), 3.51 (1H, bs), 3.63 (14H, bs), 3.79 (4H, bs), 3.99-4.04 (3H, m), 4.11-4.14 (3H, m), 4.86-4.91 (3H, m), 5.01-5.19 (12H, m), 7.06-7.43 (39H, m), 7.59-7.61 (2H, m), 7.83 (1H, s), 7.97-7.99 (2H, m), 8.45-8.49 (3H, m), 8.69 (1H, s). ^{13}C NMR ($CDCl_3$, 125 MHz), δ 8.2, 33.4, 35.4, 40.0, 41.1, 45.3, 49.3, 50.0, 51.3, 51.4, 51.4, 63.9, 64.1, 67.1, 69.7, 70.2, 70.3, 70.4, 70.5, 71.2, 71.3, 76.2, 76.3, 105.2, 108.0, 112.3, 112.4, 116.7, 117.5, 120.0, 120.0, 120.5, 123.0, 124.3, 125.6, 126.1, 126.1, 127.6, 127.6, 127.8, 128.2, 128.3, 128.4, 128.4, 128.5, 128.6, 128.6, 128.8, 128.8, 128.8, 129.0, 130.2, 135.5, 135.7, 135.9, 136.0, 136.1, 138.9, 145.2, 145.3, 146.8, 146.8, 147.4, 149.0, 151.6, 151.6, 151.8, 152.4, 154.4, 164.2, 164.9, 164.9, 165.8, 166.9, 168.9, 169.0, 169.1, 169.7, 176.9. ^{19}F NMR ($CDCl_3$, 282 MHz), δ -121.3. FT-IR (NaCl disk, cm^{-1}), 3369 (m), 3075 (w), 3036 (m), 3015 (m), 2950 (m), 2907 (m), 2855 (m), 1750 (s), 1662 (s), 1627 (s), 1577 (m), 1512 (s), 1464 (s), 1375 (m), 1339 (m), 1302 (m), 1263 (s), 1208 (s), 1121 (m), 1082 (m), 1053 (m), 1027 (m), 962 (m), 910 (w), 884 (w), 867 (w), 849 (w), 806 (w), 754 (s), 699 (m), 664 (w). HRMS (ESI): $[M+Na]^+$ *m/z* calcd., 1792.6434; found, 1792.6337. Following benzyl deprotection, compound **37** was purified by semi-preparative HPLC (20% B for 5 min followed by 20-70% B over 10 min, 4mL/min) and eluted at 15.2 min. The isolated product was lyophilized and obtained as a white solid (2.5 mg, 9%). The HPLC trace of the purified product is provided in Appendix 2. HRMS (ESI): $[M+Na]^+$ *m/z* calcd., 1252.3617; found, 1252.3633.

7-(4-(6-Aminohexanoyl)piperazin-1-yl)-1-cyclopropyl-6-fluoro-4-oxo-1,4-dihydro-quinoline-3-carboxylic acid (38). Ciprofloxacin (**39**, 331 mg, 1.00 mmol) and DIPEA (1.0 mL, 5.7 mmol) were mixed in 6 mL of dry CH_2Cl_2, and TMSCl (370 μL , 2.91 mmol) was added to give a clear yellow solution. 6-((*Tert*-butoxycarbonyl)amino)hexanoic acid (**12**, 346 mg, 1.50 mmol), PyAOP (834 mg, 1.60 mmol), and DIPEA (700 μL, 4.02 mmol) were dissolved in 4 mL of dry CH_2Cl_2, and the two solutions were combined and stirred overnight at rt. The reaction was quenched with MeOH (10 mL), and the resulting solution was concentrated to dryness, and the crude product was redissolved in 40 mL of EtOAc. The organic phase was washed with 10 mM HCl (2 x 40 mL) and saturated aqueous $NaHCO_3$ (2 x 40 mL), dried over Na_2SO_4, and purified by flash chromatography on silica gel (3% MeOH/CH_2Cl_2) to give **40** as

yellow solid (243 mg, 45%). TLC R_f = 0.7 (5% MeOH/CH_2Cl_2). ^{1}H NMR ($CDCl_3$, 300 MHz), δ 1.14-1.20 (2H, m), 1.32-1.53 (13H, m), 1.59-1.69 (2H, m), 2.36 (2H, t, J = 6.0 Hz), 3.08 (2H, dt, J = 6.3, 6.3 Hz), 3.26-3.56 (4H, m), 3.51-3.59 (1H, m), 3.69-3.82 (4H, m), 4.68 (1H, bs), 7.32 (1H, d, J = 7.2 Hz), 7.82 (1H, d, J = 12.9 Hz), 8.60 (1H, s), 14.9 (1H, bs). ^{13}C NMR ($CDCl_3$, 125 MHz), δ 8.1, 24.7, 26.4, 28.3, 29.8, 32.9, 35.3, 40.2, 41.0, 45.1, 49.3, 49.9, 78.9, 105.0, 107.7, 111.9, 112.1, 119.6, 119.7, 138.8, 145.2, 145.3, 147.3, 152.4, 154.4, 155.9, 166.6, 171.4, 176.7. ^{19}F NMR ($CDCl_3$, 282 MHz), δ -121.1. FT-IR (NaCl disk, cm^{-1}), 3345 (m), 3019 (m), 2967 (m), 2931 (m), 2863 (m), 1707 (s), 1628 (s), 1509 (s), 1467 (s), 1389 (m), 1365 (w), 1338 (m), 1301 (w), 1260 (s), 1170 (m), 1109 (w), 1026 (m), 988 (w), 940 (w), 888 (w), 834 (w), 807 (w), 751 (m), 711 (w), 665 (w). HRMS (ESI): $[M+H]^+$ *m/z* calcd., 545.2775; found, 545.2768.

The TFA salt of **38** (202 mg, 98%) was obtained as a yellow solid from **40** (201 mg, 0.369 mmol) by stirring **40** in 40% TFA/CH_2Cl_2 at rt for 3 h and removing the solvent. TLC R_f = 0.1 (10% MeOH/CH_2Cl_2). ^{1}H NMR (CD_3OD, 300 MHz), δ 1.41-1.52 (4H, m), 1.65-1.77 (4H, m), 2.52 (2H, t, J = 7.2 Hz), 2.96 (2H, t, J = 7.2 Hz), 3.34-3.43 (4H, m), 3.82 (5H, m), 7.57 (1H, d, J = 7.5 Hz), 7.85 (1H, d, J = 13.2 Hz), 8.76 (1H, s). ^{13}C NMR ($CDCl_3$, 125 MHz), δ 7.8, 23.8, 25.4, 26.5, 26.6, 32.2, 35.4, 39.0, 39.1, 41.0, 45.0, 48.1, 48.3, 48.5, 48.6, 48.8, 49.0, 49.1, 49.5, 105.0, 107.0, 111.6, 111.8, 119.3, 119.4, 138.8, 145.1, 145.2, 147.4, 152.3, 154.3, 167.3, 171.8, 176.5. ^{19}F NMR ($CDCl_3$, 282 MHz), δ -76.0, -120.9. FT-IR (NaCl disk, cm^{-1}), 2954 (m), 2922 (m), 2859 (m), 1718 (m), 1682 (s), 1616 (s), 1469 (s), 1385 (w), 1333 (w), 1255 (w), 1199 (m), 1165 (m), 1139 (m), 1022 (w), 828 (w), 799 (w), 720 (w). HRMS (ESI): $[M+H]^+$ *m/z* calcd., 445.2251; found, 445.2255.

7-(4-(6-(3-(((3S,7S,11S)-7,11-Bis(2,3-dihydroxybenzamido)-2,6,10-trioxo-1,5,9-trioxacyclododecan-3-yl)carbamoyl)-4,5-dihydroxybenzamido)hexanoyl)piperazin-1-yl)-1-cyclo-propyl-6-fluoro-4-oxo-1,4-dihydroquinoline-3-carboxylic acid (42). Compound **42** was synthesized as described for **37** except that DMSO (1.5 mL) was used as the solvent and compound **38** (19.4 mg, 34.8 μmol) was used instead of **18**. After preparative TLC purification (10% MeOH/CH_2Cl_2), **41** was obtained as white viscous solid (17 mg, 74%). TLC R_f = 0.6 (10% MeOH/CH_2Cl_2). ^{1}H NMR ($CDCl_3$, 300 MHz), δ 1.17-1.83 (10H, m), 2.40 (2H, bs), 3.29-3.44 (6H, m), 3.70-3.86 (5H, m), 4.02-4.17 (6H, m), 4.86-4.93 (3H, m), 5.04-5.21 (12H, m), 7.07-7.42 (33H, m), 7.60-7.64 (2H, m), 7.85-8.05 (3H, m), 8.47-8.50 (3H, m), 8.74 (1H, bs), 15.0 (1H, bs). ^{13}C NMR ($CDCl_3$, 125 MHz), δ 8.1, 12.3, 17.2, 18.6, 24.4, 26.3, 26.4, 26.5, 29.0, 32.8, 34.7, 39.7, 41.2, 45.3, 46.2, 46.3, 51.4, 51.5, 51.5, 52.0, 54.8, 63.9, 64.1, 64.2, 71.1, 71.2, 71.2, 76.2, 76.3, 76.3, 105.2, 109.5, 113.0, 113.2, 116.6, 117.5, 120.1, 123.0, 124.3, 125.5, 126.1, 127.6, 127.8, 128.2, 128.3, 128.4, 128.4, 128.5, 128.6, 128.6, 128.6, 128.8, 128.9, 128.9, 129.0, 130.3, 135.5, 135.8, 135.9, 136.0, 136.1, 138.1, 145.4, 146.8, 148.4, 149.0, 151.6, 151.8, 152.3, 164.4, 164.9, 165.0, 165.8, 166.1, 168.8,

169.0, 169.1, 171.5. FT-IR (NaCl disk, cm^{-1}), 3354 (m), 3065 (w), 3028 (m), 3009 (m), 2933 (m), 2859 (w), 1751 (s), 1658 (s), 1619 (s), 1577 (m), 1499 (s), 1455 (s), 1374 (m), 1346 (s), 1308 (s), 1262 (s), 1208 (s), 1128 (w), 1083 (m), 1028 (m), 979 (w), 957 (w), 914 (w), 851 (w), 806 (w), 754 (s), 699 (s), 665 (m). HRMS (ESI): $[M+H]^+$ *m/z* calcd., 1680.6303; found, 1680.6352. Following benzyl deprotection, compound **42** was purified by semi-preparative HPLC (20% B for 5 min followed by 20-70% B over 15 min, 4mL/min) and eluted at 16.1 min. The isolated product was lyophilized and obtained as a white-yellow solid (6.7mg, 59%). The HPLC trace of the purified product is provided in Appendix 2. HRMS (ESI): $[M+H]^+$ *m/z* calcd., 1140.3486; found, 1140.3482.

N_1-(2-(2-(2-(2-Azidoethoxy)ethoxy)ethoxy)ethyl)-4,5-bis(benzyloxy)-N_3-((3S,7S,11S)-7,11-bis(2,3-bis(benzyloxy)benzamido)-2,6,10-trioxo-1,5,9-trioxacyclododecan-3-yl)isophthala-mide (43). 11-Azido-3,6,9-trioxaundecan-1-amine (**11**, 8.2 μL, 42 μmol) and **27** (40 mg, 32 μmol) were dissolved in 1 mL of dry CH_2Cl_2. PyAOP (33.2 mg, 63.8 μmol) and DIPEA (22.2 μL, 128 μmol) were added to give a light yellow solution. The reaction was stirred for 4 h at rt and concentrated, and the crude product was purified by preparative TLC (50% EtOAc/CH_2Cl_2) to afford **43** as a light yellow oil (31 mg, 68%). TLC R_f = 0.3 (50% EtOAc/CH_2Cl_2). ^{1}H NMR ($CDCl_3$, 300 MHz), δ 3.34 (2H, t, J = 5.1 Hz), 3.61-3.69 (14H, m), 3.97-4.18 (6H, m), 4.88-4.94 (3H, m), 5.02-5.22 (12H, m), 7.08-7.46 (34H, m), 7.64-7.67 (2H, m), 7.85 (1H, d, J = 1.8 Hz), 7.99 (1H, d, J = 2.1 Hz), 8.48-8.52 (3H, m). ^{13}C NMR ($CDCl_3$, 125 MHz), δ 40.0, 50.6, 51.4, 64.0, 64.1, 69.7, 69.9, 70.3, 70.6, 71.2, 71.2, 76.3, 116.7, 117.5, 120.4, 123.1, 124.3, 125.5, 126.2, 126.2, 127.6, 127.6, 127.9, 128.3, 128.4, 128.4, 128.5, 128.6, 128.7, 128.8, 128.9, 129.0, 130.2, 135.5, 135.8, 136.0, 136.0, 136.2, 146.9, 146.9, 149.1, 151.6, 151.8, 164.2, 164.9, 164.9, 165.9, 168.9, 169.1, 169.1. FT-IR (NaCl disk, cm^{-1}), 3409 (s), 3002 (w), 2963 (m), 2918 (m), 2855 (m), 1748 (m), 1660 (s), 1576 (w), 1541 (w), 1437 (m), 1403 (m), 1342 (w), 1313 (m), 1260 (m), 1204 (w), 1025 (s), 953 (m), 845 (w), 798 (w), 703 (w). HRMS (ESI): $[M+Na]^+$ *m/z* calcd., 1476.5323; found, 1476.5345.

Vancomycin-PEG-Ent (44). A DMSO solution of **43** (19 mg/mL, 1.3 mM, 250 μL), an aqueous solution of **8** (20 mg/mL, 1.3 mM, 250 μL), a DMF solution of benzoic acid (49 mg/mL, 450 mM, 50 μL), and an aqueous solution of $CuSO_4$ (10 mg/mL, 45 mM, 50 μL) were mixed together, and an additional 400 μL of DMSO was added to yield a clear light blue solution. An aqueous solution of sodium ascorbate (NaAsc, 18 mg/mL, 90 mM, 50 μL) was subsequently added. The reaction become colorless to yellow and was stirred at rt for 15 min, at which time another 50 μL of aqueous NaAsc was added. After stirring for 15 min, the crude reaction was frozen and lyophilized to give brown oil. The oil was dissolved in a 2:1:1 ratio of dioxane/MeOH/H_2O and purified by semi-preparative HPLC (50% B for 5 min followed by 50-100% B over 11 min, 4 mL/min). The benzyl-protected precursor of **44** eluted at 13 min and was

obtained as white solid after lyophilization (3.5 mg, 36%). HRMS (ESI): $[M+2Na]^{2+}/2$ *m/z* calcd., 1520.5030; found, 1520.5171.

A portion of this precursor (14 mg, 4.7 μmol; obtained from four 250-μL scale Click reactions) was dissolved in 30% H_2O/MeOH, the flask was purged with N_2, and 16 mg Pd/C (10% wt) was added. The reaction was stirred under H_2 (1 atm) for 24 h at rt, and the Pd/C was removed by centrifugation (13,000 rpm, 10 min). The supernatant was concentrated by lyophilization and the resulting residue was dissolved in a 2:1:1 mixture of dioxane/MeOH/H_2O. HPLC purification (20% B for 5 min followed by 20-46% B over 8 min, 4 mL/min) gave **44** as white solid (6.3 mg, 55%). The HPLC trace of the purified product is reported in Appendix 2. HRMS (ESI): $[M+2H]^{2+}/2$ *m/z* calcd., 1228.37960; found, 1228.37961.

***tert*-Butyl(2-(((1-(1-(3-(((3S,7S,11S)-7,11-bis(2,3-dihydroxybenzamido)-2,6,10-trioxo-1,5,9-trioxacyclododecan-3-yl)carbamoyl)-4,5-dihydroxyphenyl)-1-oxo-5,8,11-trioxa-2-azatridecan-13-yl)-1H-1,2,3-triazol-4-yl)methyl)amino)-2-oxoethyl)carbamate (45).** Compound **45** was synthesized as described for **44** except that a DMSO solution of **7** (2.8 mg/mL, 13 mM, 25 μL) was used instead of **8**. HPLC purification gave 3.3 mg of the benzyl-protected precursor of **45** as a white solid (58%). HRMS (ESI): $[M+H]^+$ *m/z* calcd., 1688.6489; found, 1688.6421. Compound **45** (3.3 mg, 33%) was obtained from the precursor (13.3 mg, 7.88 μmol; obtained from four 25-μL scale Click reactions) following the same procedure as synthesizing **44**. HPLC purification (0% B for 5 min followed by 0-45% B over 8 min, 4 mL/min) afforded **45** as a white solid with a retention time of 12.8 min. The HPLC trace of the purified product is reported in Appendix 2. HRMS (ESI): $[M+H]^+$ *m/z* calcd., 1126.3853; found, 1126.3832.

***N*^{3}-((3S,7S,11S)-7,11-Bis(2,3-dihydroxybenzamido)-2,6,10-trioxo-1,5,9-trioxacyclododecan-3-yl)-*N*^{1}-cyclohexyl-4,5-dihydroxyisophthalamide (46).** Compound **46** was synthesized as described for **31** except that compound **27** (60.0 mg, 47.8 μM) and cyclohexanamine (8.2 μL, 72 μmol) instead of **7** were used in the reaction. After purification by preparative TLC (5% MeOH/CH_2Cl_2), the benzyl-protected precursor of **46** was obtained as a white viscous solid (36.6 mg, 57%). TLC R_f = 0.7 (10% MeOH/CH_2Cl_2). ^{1}H NMR ($CDCl_3$, 300 MHz), δ 1.10-1.42 (4H, m), 1.64-1.78 (4H, m), 1.98-2.01 (2H, m), 3.92-3.96 (1H, m), 4.01-4.09 (3H, m), 4.14-4.21 (3H, m), 4.88-4.93 (3H, m), 5.02-5.22 (12H, m), 6.18 (1H, d, J = 7.8 Hz), 7.08-7.44 (35H, m), 7.64-7.67 (2H, m), 7.86 (2H, m), 8.48-8.54 (3H, m). HRMS (ESI): $[M+Na]^+$ *m/z* calcd., 1357.4992; found, 1357.4990. Following Pd/C catalyzed hydrogenation, compound **46** was purified by semi-preparative HPLC (20% B for 5 min followed by 20-70% B over 15 min, 4 mL/min). The product eluted at 15.8 min and was obtained as white solid (12 mg, 55%). The analytical HPLC trace of the purified product is reported in Appendix 2. HRMS (ESI): $[M+Na]^+$ *m/z* calcd., 817.2175; found, 817.2135.

General Microbiology Materials and Methods. *E. coli* 33475 (*ent-*) was purchased from American Type Culture Collection (ATCC). *E. coli* K-12 JW0576 (*fes-*) was obtained from the Keio Collection (Japan). *P. aeruginosa* K648 (*pvd-/pch-*) and K407 (p*vd-/pFr-*) were gifts from Professor Keith Poole (Department of Biomedical and Molecular Sciences, Queen's University, Canada). Freezer stocks of all *E. coli* strains were prepared in 25% glycerol/Luria Broth (LB) medium. Freezer stocks of all *P. aeruginosa* strains were prepared in 7.5% DMSO/LB base medium supplemented with 2.5 g/L NaCl. LB (tryptone 10 g/L, yeast extract 5 g/L, NaCl 10 g/L), LB base (pancreatic digest of casein 10 g/L, yeast extract 5 g/L, NaCl 0.5 g/L), Mueller Hinton Broth (MHB, beef extract powder 2.0 g/L, acid digest of casein 17.5 g/L, soluble starch 1.5 g/L), and agar were purchased from BD. All growth media and Milli-Q water used for bacterial cultures or for preparing solutions of the enterobactin-cargo conjugates were sterilized by using an autoclave. The iron chelator 2,2'-dipyridyl (DP) was purchased from Sigma-Aldrich. A DP stock solution (200 mM) was prepared in DMSO and used in the bacteria growth assays. All enterobactin-cargo conjugates, L-Ent and D-Ent were stored as DMSO stock solutions at -20 °C. With the exception of the coumarin 343 conjugate, the stock solution concentrations were determined by using the reported extinction coefficient for enterobactin (316 nm, 9,500 $M^{-1}cm^{-1}$)[23] with the assumption that the cargo had no effect on catecholate absorption. Working dilutions of the Ent conjugates, L-Ent, and D-Ent were prepared in 20% DMSO/H_2O. For all growth recovery assays, the cultures contained 2% v/v DMSO. Sterile polypropylene culture tubes and sterile polystyrene 96-well plates used for culturing were manufactured by VWR and Corning Incorporated, respectively. OD_{600} values were recorded on an Agilent 8453 diode array spectrophotometer or by using a BioTek Synergy HT plate reader.

Growth Recovery Assays. Overnight cultures were prepared by inoculating 5 mL of LB (*E. coli*) or LB base supplemented with 2.5 g/L NaCl (*P. aeruginosa*) with the appropriate freezer stocks and the cultures were incubated at 37 °C in a tabletop incubator shaker set at 150 rpm. The overnight culture was diluted 1:100 into 5 mL of fresh media with or without 200 μM 2,2'-dipyridyl (DP) and incubated at 37 °C with shaking at 150 rpm until the optical density at 600 nm (OD_{600}) reached 0.6. The cultures were diluted to an OD_{600} value of 0.001 in 50% reduced MHB medium (10.5 g/L) with or without 200 μM (*E. coli*) or 600 μM DP (*P. aeruginosa*). A 90-μL aliquot of the diluted culture was mixed with a 10-μL aliquot of a 10x solution of the siderophore or siderophore-cargo conjugate in a 96-well plate, which was wrapped in parafilm and incubated at 30°C with shaking at 150 rpm for 19 h. Bacterial growth was assayed by measuring OD_{600} using a BioTek Synergy HT plate reader. Each well condition was prepared in duplicate and three independent replicates of each assay were conducted on different days. The resulting mean OD_{600} are reported and the error bars are the standard deviation of the mean obtained from the three independent replicates.

Fluorescence Titrations for Lipocalin 2 and Ent-Conjugates. The titration was performed according to a reported procedure.[24] Recombinant human lipocalin 2 (or Lcn2, from mouse myeloma cell line, NS0-derived, Gln21-Gly198, with a C-terminal His_{10} tag) was purchased from R&D Systems (Minneapolis, MN). Ubiquitin (from bovine erythrocytes) was purchased from Sigma. Lcn2 was diluted in the assay buffer containing NaCl (150 mM), DMSO (5%), TCEP (5 mM) and Tris at pH 7.5 (50 mM) to final concentration of 0.88 μM and kept on ice. Ent-conjuagtes (100 mM) were incubated with one equiv. of $FeCl_3$ in the assay buffer for 1 h at room temperature, which afforded a wine-color solution. This solution was further diluted to 5 μM in the assay buffer. Ubiquitin was dissolved in the assay buffer to afford a 16 mg/mL solution.

At the beginning of the titration, Lcn2 and ubiquitin were added to the assay buffer to afford a final concentration of 88 nM and 32 μg/mL, respectively. The total volume of the solution was 1 mL and was equilibrated in the fluoremeter for 18 min before the emission spectrum was collected. Then an aliquot (2 μL) of the ferric Ent-conjugate solution (5 μM) was added at a time (0.1 equiv.). After each addition the solution was mixed by inverting the cuvette, equilibrated for 2 min and the emission spectrum was collected from 300 nm to 450 nm with integration time of 1 s (λ_{ex} = 281 nm). In total 18 data points were recorded and the fluorescence intensities at 340 nm versus the concentration of Ent-conjugate added were plotted and the resulting titration curves were fit to a one-site binding model using the DynaFit software to obtain the approximate binding affinity. The fluoremeter slit widths were set to 3 nm for all measurements.

Results and Discussion

Design of Monofunctionalized Ent Platform. As probably the most well studied siderophore, Ent has not been studied in the context of siderophore conjugates. One challenge for applying Ent in such strategies is that, excluding the catechol hydroxyl moieties required for iron chelation, Ent presents no functional group amenable to modification. Therefore, the first step towards Ent-mediated cargo delivery is to synthesize a modified Ent or Ent precursor that can be easily attached to other molecules without affecting iron binding or recognition by the Ent receptor. The structures of MGE and DGE (Figure 2.1A) indicate that the C5 position of one catechol ring, which is remote from the iron-binding hydroxyl groups and the macrolactone ring, is a promising modification site (Figure 2.2). Glucosylation at this position does not compromise Fe(III) binding or subsequent esterase hydrolysis of the macrolactone.[7, 25] Moreover, the naturally occurring antimicrobial peptide-Ent conjugate MccE492m also has the modification at the C5 position (Figure 2.3).[26] Therefore, we decided to synthesize 2,3-dihydroxy-benzoic acid with a functional group at C5, which enables the access to mono-, di- and tri-functionalized Ent platforms. Inspired by the structure of MccE492m, we focused on the monofunctionalized form in this work.

Moreover, we reasoned that monofunctionalized platforms would maximize transport efficiency based on the fact that DGE seems to be less efficiently (if at all) transported into the *E. coli* strain used in this study comparing to MGE (*vide supra*).

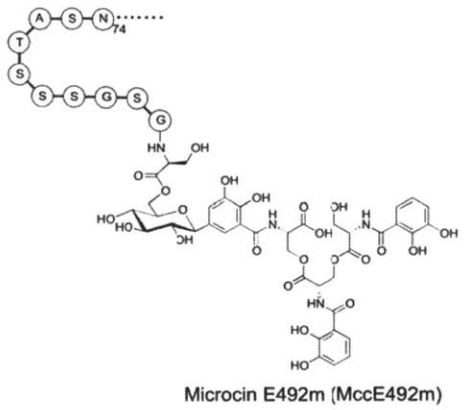

Figure 2.3. Structure of Microcin E492m.

Synthesis of Modified 2,3-Dihydroxybenzoic Acid. To obtain 2,3-dihydroxybenzoic acid modified at the C5 position, we started with a commercially available starting material **19** (Scheme 2.1). Demethylation of **19** was performed in the presence of BBr_3 at -78 °C. Following a reported demethylation procedure,[27] a byproduct resulting from HBr addition to the double bond was observed by LCMS, which also revealed that the crude reaction contained both mono-demethylated and double-demethylated products. The double-demethylated product was minor and difficult to separate by flash chromatography because of tailing on the column, therefore we focused on obtaining the mono-demethylated product **20**. To suppress the formation of brominated byproduct, DIPEA was added to the reaction prior to the addition of BBr_3 to deprotonate the phenols. The best yield (53%) of **20** was obtained when 1.5 equiv. of DIPEA and 3 equiv. of BBr_3 were employed. Benzyl protection and subsequent methyl ester hydrolysis of **20** followed literature procedures[20] using benzyl bromide and sodium hydroxide afforded the C5 modified DHB building block **21** in 99% yield as a white powder. Isomerization of terminal olefin **21** to **22** was performed because the internal olefin afforded much higher yield in later oxidative transformations to the aldehyde or carboxylic acid. Palladium-catalyzed isomerization of the alkene was achieved by using $PdCl_2$ in degassed methanol and **22** was obtained in 89% yield as a light yellow solid.

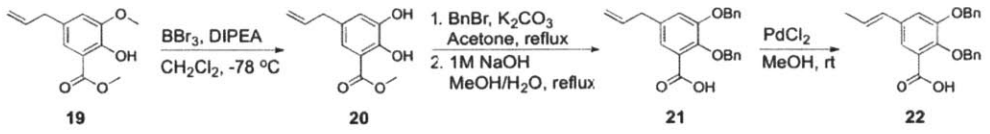

Scheme 2.1. Synthesis of C5-modified DHB building block **22**.

Syntheses of Monofunctionalized Ent Precursors. To achieve the monofunctionalized Ent scaffold, two synthetic routes were explored. First, a tandem coupling approach was evaluated (Scheme 2.2). We aimed to first couple two unmodified DHB to the trilactone backbone and couple one C5-modified DHB in the subsequent step. In the first step, benzyl-protected DHB **6** was coupled to trilactone **4** using a controlled ratio, and any remaining free amine groups on **4** were capped by addition of di-*tert*-butyl dicarbonate (Boc_2O) to simplify purification. The highest yield of **23** was obtained when 1.5 equiv. of **6** was used, and the rate of addition (over 5 min to 1 h) of **4** did not affect the yield significantly. A statistic mixture of **23**, mono-DHB-di-Boc, tri-DHB, and tri-Boc derivatives was obtained, which was separated by flash chromatography. According to the isolated yield, ~15% of the trilactone was converted to **23** and ~10% was converted to the mono-DHB-di-Boc analogue. Compound **23** was treated with 10% TFA at 4 °C to remove the Boc group and coupled with **21** without purification to yield **24**. However, the reaction was messy and low yielding, most likely due to hydrolysis of the trilactone ring following TFA treatment. HPLC analysis of Benzyl-protected Ent subjected to the same condition confirmed this hypothesis (data not shown). Further optimization showed that using 1.25 M HCl in methanol at rt to remove the Boc group minimizes by-product formation resulting from Ent hydrolysis. Based on the statistical distribution of mono-, di- and tri-DHB derivatives found during the synthesis of compound **23**, we reasoned that the Boc protection would not improve the yield of di-DHB trilactone derivative, therefore this step may not be necessary, which led us to develop the second synthetic route.

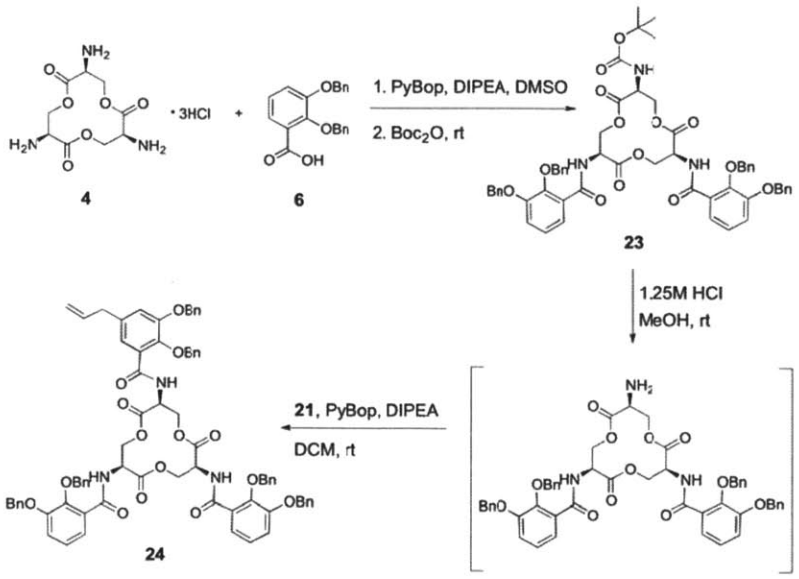

Scheme 2.2. Synthetic scheme of monofunctionalized Ent platform by a tandem coupling strategy.

The second route involves a one-pot coupling of C5-modified DHB **22**, DHB **6** and the trilactone **4** to generate the desired product (Scheme 2.3). We reasoned that this route should afford higher yield because it avoids the Boc protection and deprotection steps. A similar mixture of all possible products was formed that can be separated by careful silica gel chromatography, affording gram quantities of **24**. Further optimization revealed that the addition of 1.5 equiv. **6** and 1 equiv. **22** relative to the tri-lactone afforded the highest yield of **25** (37%). The multi-step synthesis could only provide an overall yield of 15%.

Starting from the alkene group on **25**, further transformations can afford versatile functional groups. For example, in the current study, **25** was oxidized to aldehyde **26** by OsO_4 and $NaIO_4$ in mixed 1,4-dioxane/water with 58% yield. Further oxidation with $NaClO_2$ afforded carboxylic acid **27** in 76% yield (Scheme 2.3). These monofunctionalized Ent scaffolds can be obtained in gram quantities and are stable when stored as dry solids at 4 °C. It is noteworthy that other transformations can be done on Ent derivatives **25-27** for other applications.

The one-pot coupling and oxidations were also performed using triserine lactone **5** to afford the D-enantiomers alkene **28**, aldehyde **29**, and acid **30** (Scheme 2.3). The D-enantiomer of Ent is transported into *E. coli* by FepA, but it is not a substrate for the enterbactin esterase Fes.[28] We therefore reasoned that conjugates based on D-Ent would provide useful controls for conjugate uptake studies, and that this enantiomer may also be advantageous in antibacterial drug delivery applications because it provides an iron-starvation effect (see Chapter 3).

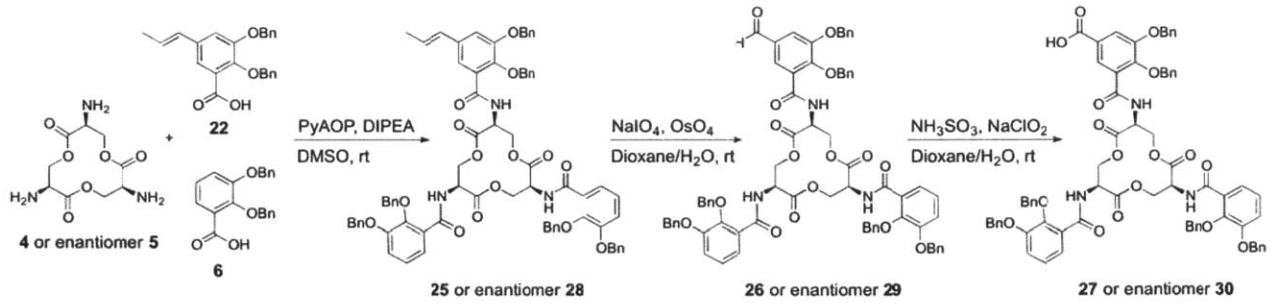

Scheme 2.3. Synthetic scheme of one-pot synthesis of monofunctionalized Ent scaffolds.

Design and Synthesis of Ent-Cargo Conjugates. With the monofunctionalized Ent scaffolds **25-30** in hand, we first aimed to construct a series of Ent-cargo conjugates with variable cargo sizes and structures. These compounds were utilized to probe the promiscuity of the bacterial Ent uptake machinery. Compound **27** was selected as a starting point and two strategies for appending cargo to **27** were evaluated. In one thrust, an amide coupling was used to link cargo to the Ent acid; in the other approach, Cu(I) catalyzed azide-alkyne cycloaddition (or 'Click' chemistry) was used. A global benzyl deprotection unmasked the Ent catecholates as the last step in both strategies and afford the final Ent-cargo conjugates.

Before installation of the cargos, a proper linker needs to be chosen such that the functions of the Ent scaffold are minimally perturbed. We selected PEG_3 as a stable and water-compatible linker which provides ca. 14-Å separation between Ent and the cargo. When coupling a PEG_3 linker with two primary-amine termini to the Ent scaffold, degradation of the Ent backbone was observed. Therefore we chose compound **10**, which is a commercially available PEG_3 linker with mono-Boc protection. This linker was first coupled to the cargos followed by Boc deprotection to reveal the second amine (Scheme 2.4), affording the PEG-derivatized cargos. In order to probe the consequences of variable linker composition and hydrophilicity, a C_5 alkyl chain was evaluated in one Ent-cargo conjugate (Scheme 2.6).

For the cargos, we selected a variety of commercially available molecules housing carboxylic acids for attachment to the linker. The selected cargos include Boc, cyclohexane, naphthalene, phenylmethylbenzene, ciprofloxacin, and coumarin 343. Besides variations in size and shape, this selection contains cargo expected to be non-toxic (e.g., Boc, cyclohexane) in addition to an antibiotic (ciprofloxacin) and a fluorophore (coumarin 343). These Ent-cargo conjugates were prepared by coupling the PEG-derivatized cargo **10**, **14-18** to **27** using PyAOP as the coupling reagent. The resulting benzyl-protected conjugates were purified by preparative TLC and obtained in yields ranging from 26% (Bn-**36**) to 75% (Bn-**31**). Benzyl deprotection reactions were performed by hydrogenation over Pd/C and the resulting enterobactin-cargo conjugates were purified by reverse-phase semi-preparative HPLC.

Conjugates **31-37** were obtained in milligram quantities and high purity judging by analytical HPLC (Appendix 2) and LC/MS analysis (Table 2.1). Conjugate **33** houses D-Ent and was prepared to probe the role of Fes-mediated hydrolysis in the bacterial growth recovery assays (*vide infra*). The conjugate **42** containing C_5 alkyl chain linker was obtained by reacting ciprofloxacin with 6-Boc-aminohexanoic acid **12** followed by Boc deprotection, coupling of the resulting free amine to **27**, and benzyl deprotection (Scheme 2.5). The carboxylic acid of ciprofloxacin was protected *in situ* with trimethylsilyl chloride (TMSCl) to prevent self-coupling in the syntheses of both **37** and **42**. In this general approach of attaching a carboxylic acid cargo, the linkers were first coupled to the cargo rather than to the Ent scaffold because the Ent macrolactone decomposed in the presence of primary amines or under highly acidic conditions required to remove Boc protecting groups.

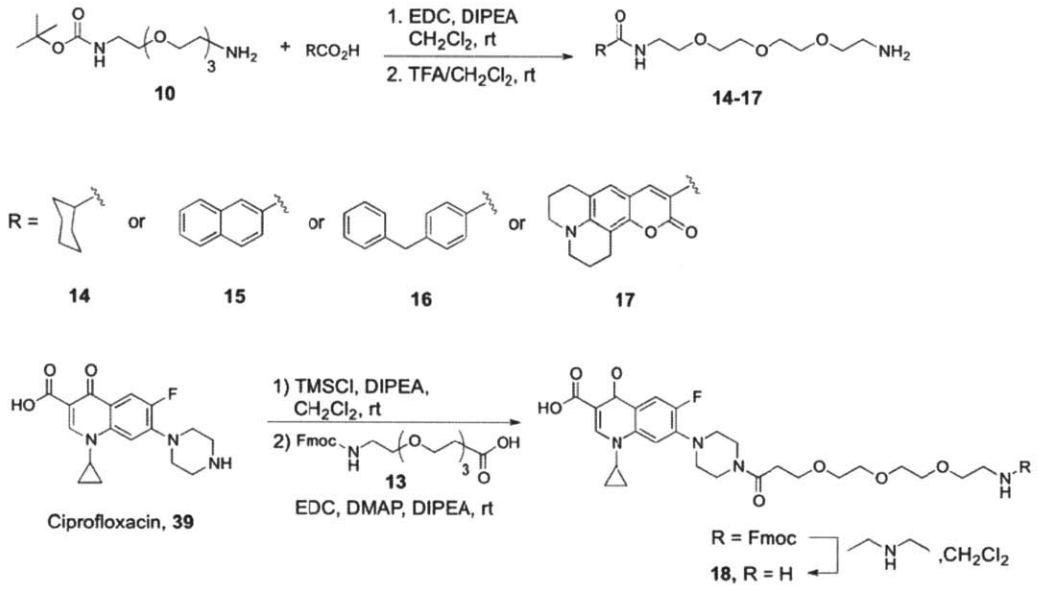

Scheme 2.4. Syntheses of PEG-derivatized cargos **14-18**.

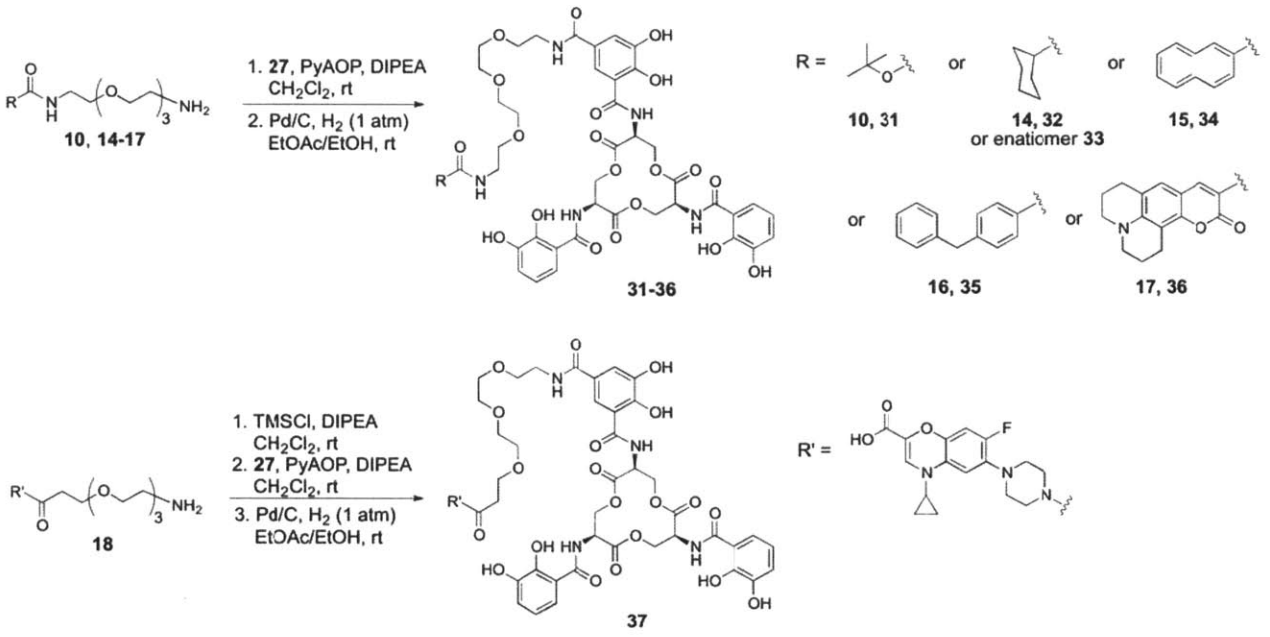

Scheme 2.5. Syntheses of Ent-cargo conjugates **31-37**.

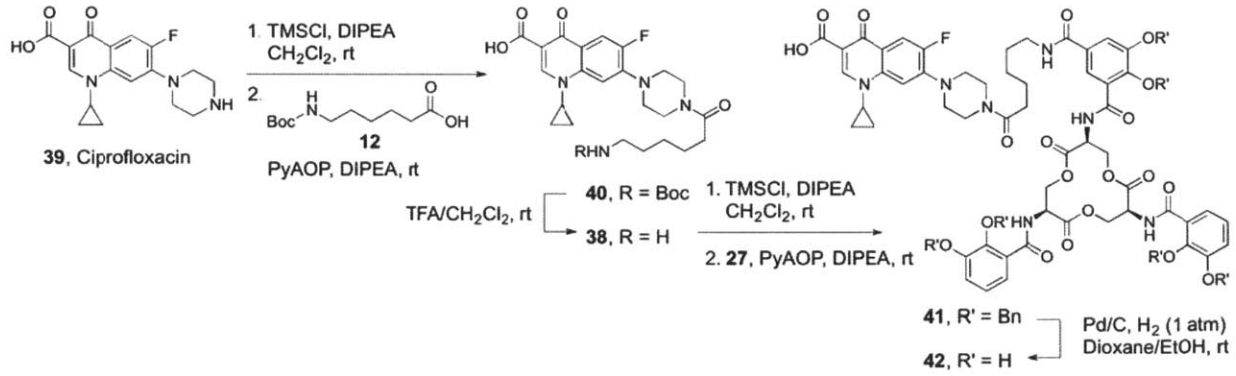

Scheme 2.6. Synthesis of enterobactin-ciprofloxacin conjugate **42**.

Using the second approach involving the "click" reaction, we present the synthesis of **44**, an Ent-vancomycin conjugate (Scheme 2.7). Vancomycin is a nonribosomal peptide antibiotic active against Gram-positive organisms that inhibits cell wall biosynthesis by binding to the D-Ala-D-Ala of lipid II and blocking peptidoglycan cross-linking.[29] The reason to use "click" reaction for the conjugate assembly is to avoid complications with the various functional groups exhibited by vancomycin. This antibiotic exhibits poor activity against Gram-negative bacteria because it is too large to cross the outer membrane.

Moreover, it is important to test if the Ent uptake machinery will accept a large cargo like vancomycin. If it is the case, then siderophore modification may greatly increase the activity of vancomycin against Gram-negative bacteria. Modification of the vancomycin C-terminal carboxylic acid with a PEG chain did not perturb its antibacterial activity;[30] therefore, we selected this site as a point of attachment. The azide-functionalized PEG linker **11** was first coupled to **27** to generate Ent-azide **43** in 68% yield. Copper(I)-catalyzed azide-alkyne cycloaddition of **43** with alkyne **8**[21] subsequently afforded Ent-vancomycin **44** in 55% yield after hydrogenation and purification. This synthetic approach was extended to **45**, a small analog of **44** that houses a *tert*-butyl cargo, and the strategy is also applicable to other alkyne-substituted cargos that are compatible with the benzyl deprotection condition.

Table 2.1 Characterization of Ent-cargo conjugates.

No.	Cargo	HPLC retention time (min)[a]	*m/z* obs.	*m/z* cald.[b]
31	Boc	25.3	1010.3173	1010.3125
32	Cyclohexyl	24.6	1020.3346	1020.3333
33	Cyclohexyl (D-Ent)	24.6	1020.3328	1020.3333
34	Napthyl	25.3	1064.3086	1064.3020
35	Phenylmethylbenzyl	25.2	1104.3305	1104.3333
36	Coumarin 343	27.2	1177.3570	1177.3496
37	Ciprofloxacin (PEG)	24.9	1252.3633	1252.3617
42	Ciprofloxacin (alkyl)	26.7	1140.3482	1140.3486 [d]
44	Vancomycin (triazole)	20.4	1228.3796	1228.3796 [c]
45	Boc-glycine (triazole)	23.8	1126.3775	1126.3832 [d]
46	Cyclohexyl (no linker)	25.6	817.2175	817.2135

[a]HPLC gradient used for all compounds is 0% B for 5 min followed by 0-100% B over 30 min, 1 mL/min. [b]All *m/z* valuescorrespond to $[M+Na]^+$ unless specified otherwise.[c]The *m/z* value corresponds to $[M+2Na]^{2+}$. [d]The *m/z* value corresponds to $[M+H]^+$.

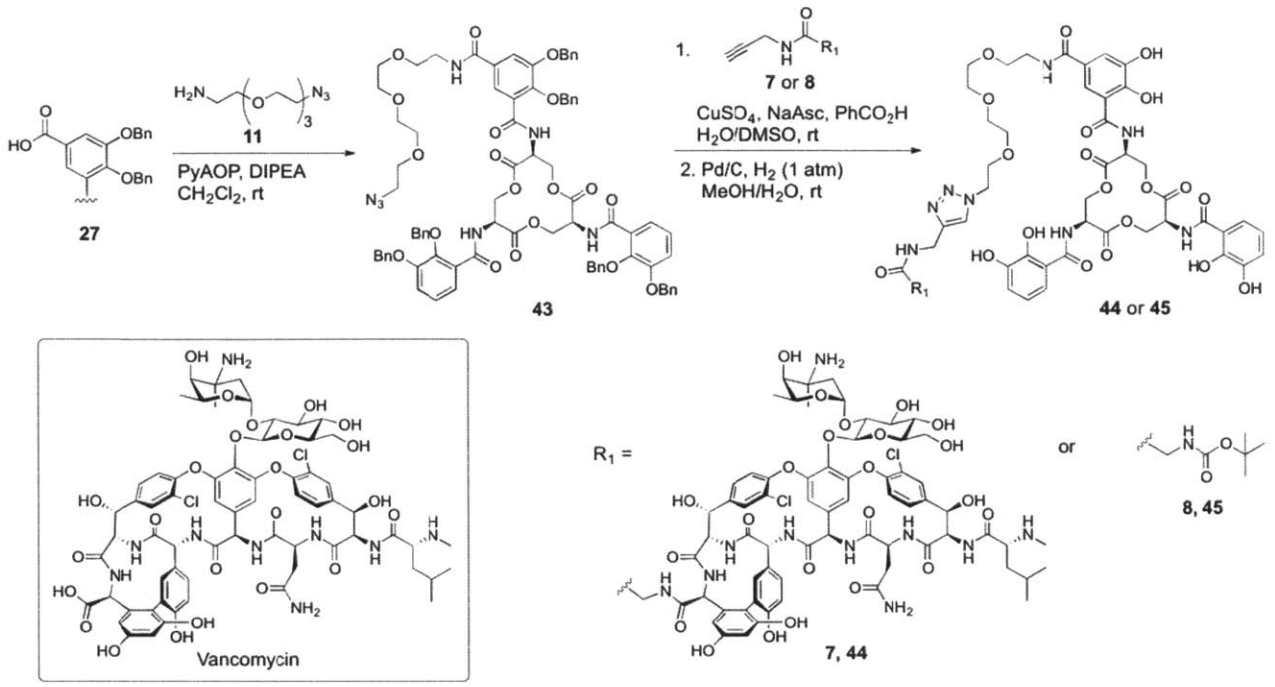

Scheme 2.7. Syntheses of enterobactin-cargo conjugates by Click chemistry.

Fe(III) Coordination of the Ent-Cargo Conjugates. Before evaluating the delivery of the Ent-cargo conjugates into Gram-negative bacteria, it is important to ascertain the cargo attachment does not impair the Fe(III) coordination by the Ent moiety. The optical absorption spectrum of each enterobactin-cargo conjugate exhibited catecholate absorption at ca. 316 nm (MeOH, rt). With the exception of **36**, which afforded a yellow solution because of the coumarin moiety, methanolic solutions of each conjugate turned from colorless to wine-colored following the addition of ca. one equiv. of aqueous Fe(III), and the expected ligand-to-metal charge transfer (LMCT) bands were observed, indicating Fe(III) coordination to the enterobactin catecholates (Figure 2.4 and Appendix 2).[23] The binding affinity of Fe(III) and the conjugates were not determined.

Ent-cargo Conjugates Delivery to the *E. coli* Cytoplasm. To probe Ent-cargo conjugate delivery into bacterial cells, a growth recovery assay was designed. Three nonpathogenic *E. coli* strains which are defective in Ent biosynthesis, Ent transport or ferric Ent utilization (Table 2.2) were used in this assay. *E. coli* ATCC 33475 (*entA*-) cannot biosynthesize Ent, but retains the capacity to import and metabolize the siderophore.[31] *E. coli* H1187 (*fepA-)* lacks the outer membrane Ent receptor. *E. coli* K-12 JW0576 (*fes*-) can accumulate ferric Ent, but cannot release the iron because it is deficient in the Ent esterase Fes. As a result of these defects in iron metabolism, all three strains grow poorly under

conditions of iron limitation.[31] The iron chelator DP was used to generate iron-deficient conditions and promote expression of siderophore transport machinery in the growth recovery assays. For *E. coli entA-* grown in the presence of DP, if the growth media is supplemented with Ent or Ent-cargo conjugate that can be transported to the bacterial cytosol and releases iron, a recovery of bacterial growth should be observed. The extent of recovery can qualitatively indicate the delivery efficiency of the conjugates to the cytoplasm. For the *fepA-* and *fes-* strain, we expect no growth recovery because they cannot transport or utilize ferric Ent.

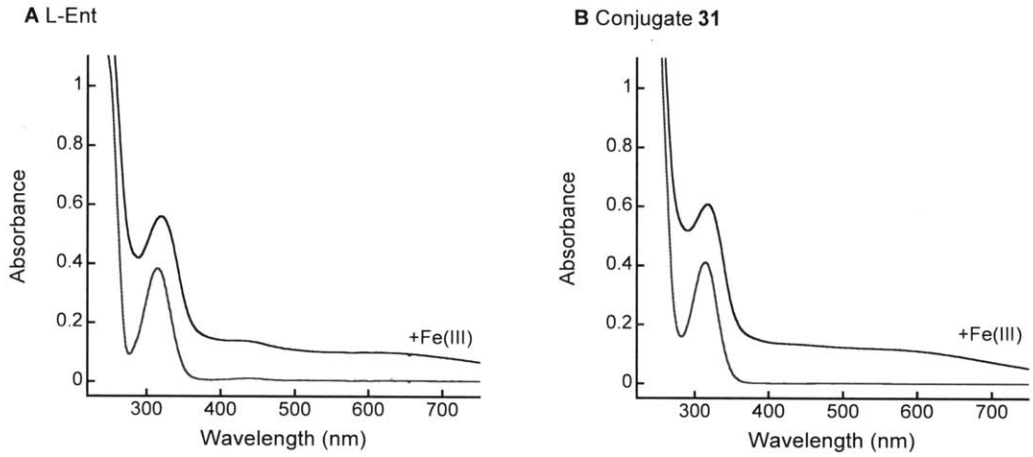

Figure 2.4. UV-spectra of represented apo/Fe-bound Ent (A) and Ent-cargo conjugate **31** (B)

Table 2.2. Bacterial strains used in this study.

Bacterial strain	Description	Source
E. coli ATCC 33475	*ent-*	ATCC
E. coli JW0576	*fes-*	Kieo Collection
P. aeruginosa K648	*pvd-, pch-*	Professor Keith Poole (Queen's University, Canada)
P. aeruginosa K407	*pvd-, pFr-*	Professor Keith Poole (Queen's University Canada)

We first validated the assay using unmodified Ent. In 96-well plates, *E. coli entA-* grew to OD_{600} = ~ 0.35 in 50% MHB medium (30 °C, t = 19 h), and this value decreased to <0.05 when 200 μM DP was added to the media. Low-micromolar concentrations of Ent restored growth, as expected,[31] and the cultures reached OD_{600} ~ 0.2 in the presence of 10 μM Ent (Figure 2.5A). No growth restoration was observed when *E. coli fepA-* or *E. coli fes-* were cultured with Ent (Figure 2.5B), which supports the notion that the growth recovery of *E. coli entA-* results from FepA-mediated cytoplasmic transport and

Fes-catalyzed hydrolysis of the enterobactin moiety to release iron. Moreover, the D-enantiomer of Ent, D-Ent **9**, is not a substrate for Fes and does not provide growth recovery (Figure 2.5C).[28] Therefore we concluded that these assays are suitable for evaluating Ent-cargo conjugate delivery. We also tested the growth recovery effect of monoglucosylated Ent (MGE, **2**) and diglucosylated Ent (DGE, **3**) on *E. coli entA-* (Figure 2.5D), which revealed that MGE afforded growth recovery but to a less extend compared to Ent. In contrast, DGE did not provide any growth recovery under iron limited conditions and exhibited growth inhibition under iron sufficient conditions, most likely due to iron sequestration by DGE. These data indicate that a monofunctionalized Ent may be better tolerated by the Ent uptake machinery than difunctionalized scaffolds, which influenced our decision to proceed with monofunctionaliation of Ent.

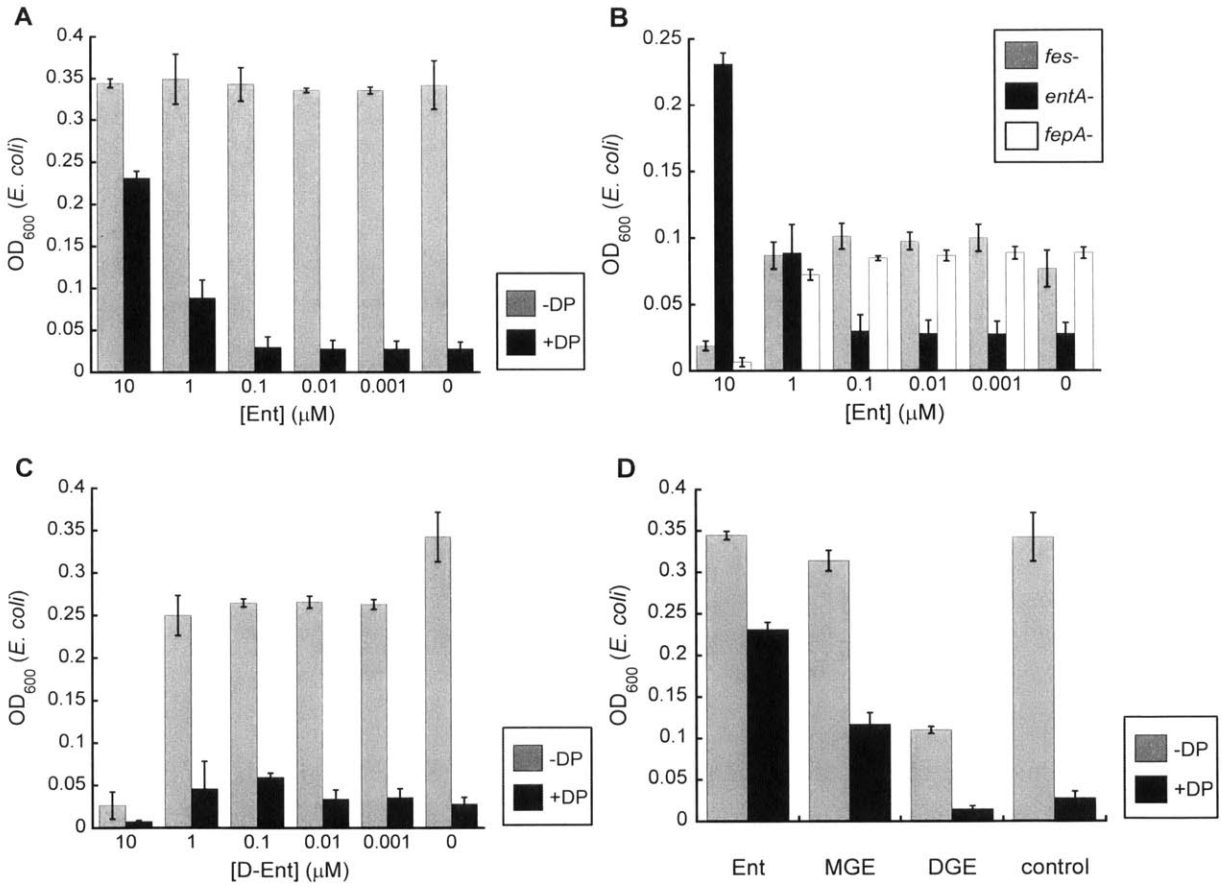

Figure 2.5 (A) Growth recovery assay of *E. coli entA-* with Ent in the absence and presence of 200 μM DP. (B) Growth recovery assay of *E. coli fes-, entA-* and *fepA-* with Ent in the presence of 200 μM DP. (C) Growth recovery assay of *E. coli entA-* with D-Ent. (D) Growth recovery assay of *E. coli entA-* with Ent, MGE and DGE at 10 μM concentration. Error bars are the standard deviation of the mean for at least three independent repetitions.

With validation of the growth recovery assays, we tested whether the Ent-cargo conjugates deliver iron to the *E. coli* cytoplasm. Like Ent, low-micromolar concentrations of **31-35** and **45** exhibiting Boc (**31, 45**), cyclohexyl (**32**), napthyl (**34**), and phenylmethylbenzyl (**35**) cargos afforded growth recovery to similar levels as Ent (Figures 2.6 and 2.7). No growth restoration was observed when *E. coli fepA-* or *E. coli fes-* were cultured with **31** or **32** (Figure 2.8). Moreover, no growth promotion occurred when *E. coli entA-* was treated with conjugate **33**, the D-enantiomer of **32** (Figures 2.6 and 2.7). Taken together, these results demonstrate that the Ent transport machinery has the capacity to recognize and transport cargo-derivatized Ent scaffolds to the *E. coli* cytoplasm, and that these molecules are substrates for the cytoplasmic esterase Fes.

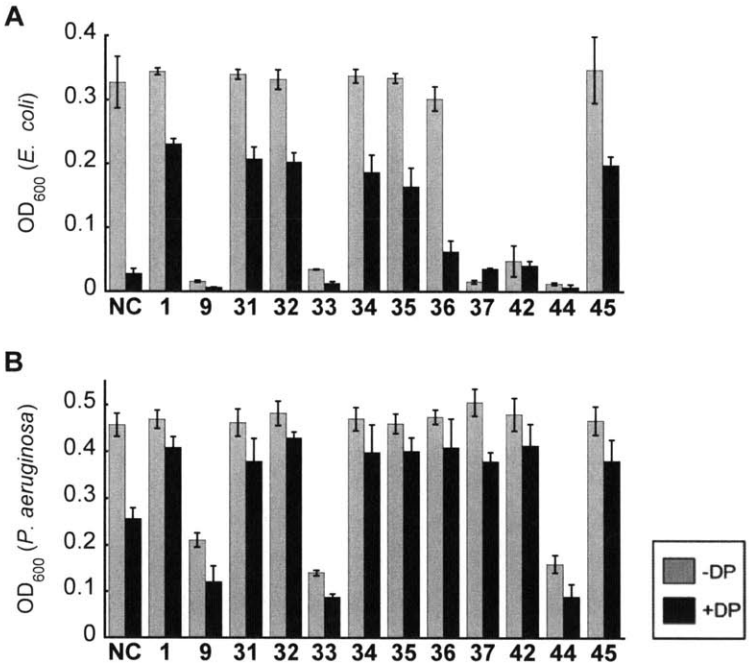

Figure 2.6. Comparative effects of Ent-cargo conjugates on bacterial cell growth. *E. coli* (A) and *P. aeruginaosa* (B) were cultured in the presence of 10 μM of the tested compounds. NC refers to a no-conjugate control. Error bars are the standard deviation of the mean for at least three independent repetitions.

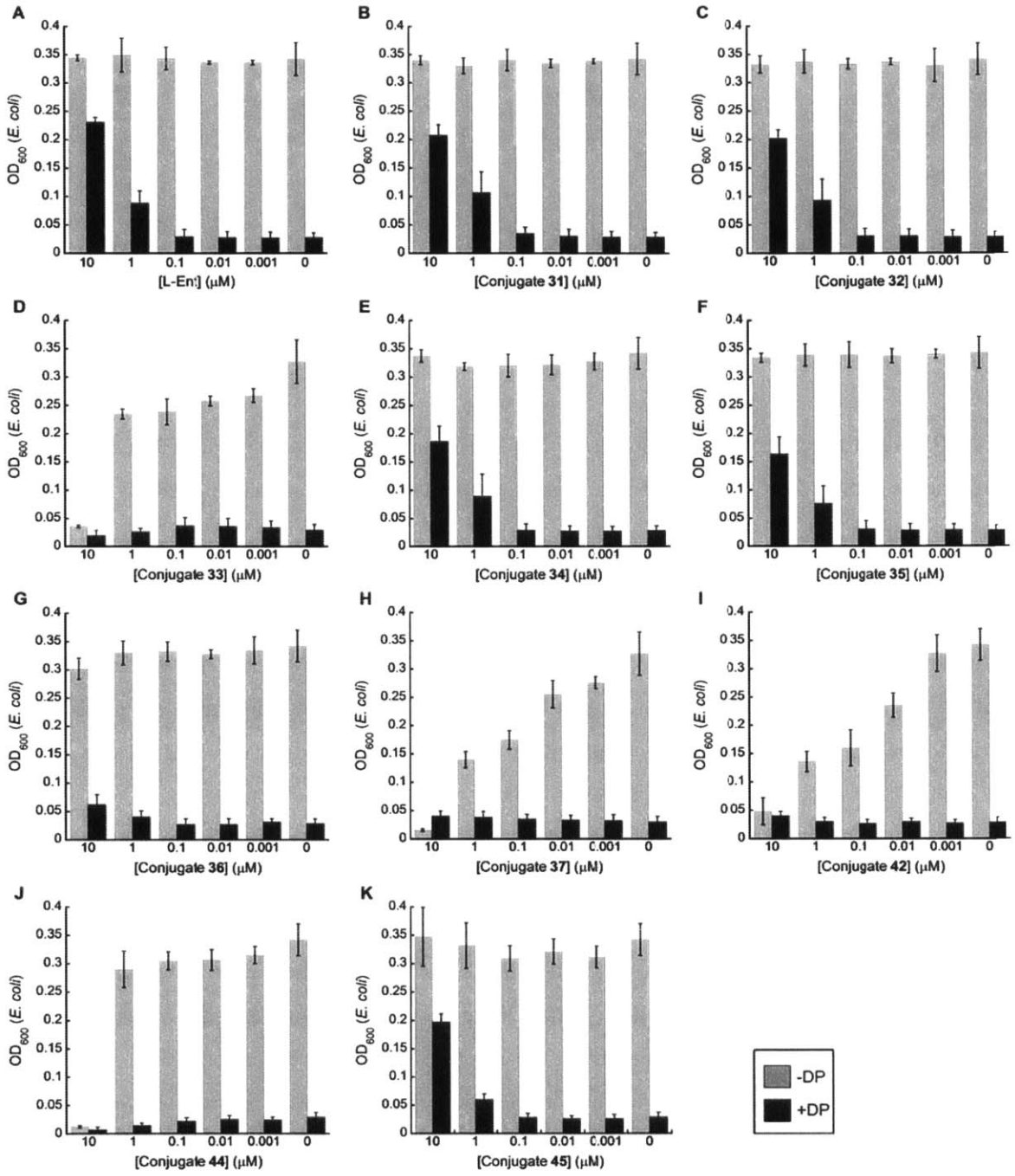

Figure 2.7. Growth recovery assays of *E. coli entA*- with various concentrations of Ent, compound **31-37**, **42**, **44** and **45** in the absence and presence of 200-μM DP. Error bars are the standard deviation of the mean for at least three independent repetitions.

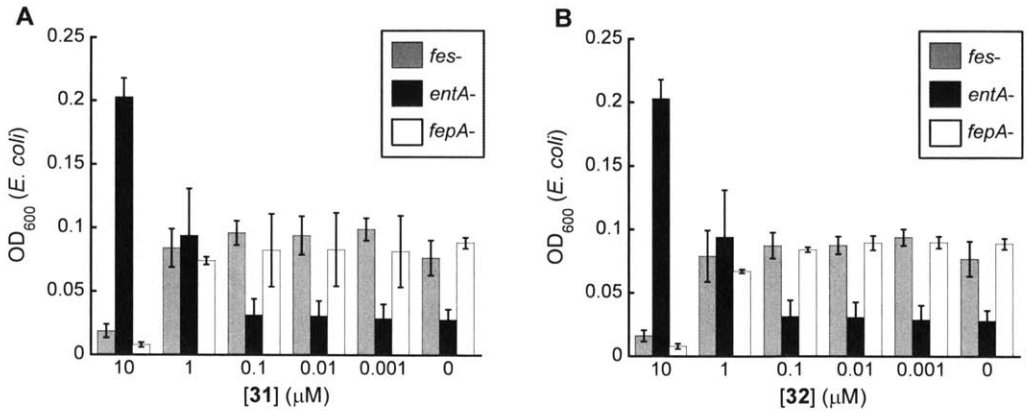

Figure 2.8. Growth recovery assays of *E. coli fes-*, *entA-* and *fepA-* with compound **31** (A) and **32** (B) in the presence of 200 μM of DP. Error bars are the standard deviation of the mean for at least three independent repetitions.

For larger cargos like coumarin in conjugate **36**, much less growth recovery was observed under iron limitation condition, and no toxicity was observed when grown in iron sufficient condition, indicating that *E. coli entA-* may not readily import **36** (Figure 2.6). Similarly, no growth recovery occurred following treatment of *E. coli* with either ciprofloxacin **37** or **42** (Figure 2.6). However, in the absence of DP, these conjugates afforded a concentration-dependent inhibition of *E. coli* growth. Likewise, 10 μM Ent-vancomycin **44** inhibited the growth of *E. coli* (± DP, Figure 2.6). This behavior contrasts that of unmodified vancomycin, which is inactive against *E. coli* over the concentration range employed in this study (data not shown). Two possible origins for inhibitory activity of the ciprofloxacin and vancomycin conjugates are (i) Ent-antibiotic uptake and resulting antibacterial action or (ii) a lack of active transport into *E. coli*, resulting in extracellular iron chelation and hence nutrient deprivation. Taking all observations into account, including those for *P. aeruginosa* described below, we contend that the latter option is the most probable explanation. Based on this hypothesis, we probed whether such large cargo-Ent conjugates would occupy and block the Ent uptake machinery by performing a competition assay where varying concentrations of Ent were added at the same time or one hour after the addition of a fixed concentration of Ent-vancomycin **44** to *E. coli entA-*. The growth inhibition diminished with an Ent:**44** ratio of 1:1 or greater (Figure 2.9), with or without pre-incubating the bacteria with **44**. Moreover, in the presence of DP, a grow recovery effect was observed as the concentration of Ent increased (Figure 2.9B). These data indicate that the Ent uptake machinery was not blocked by Ent-vancomycin and remained functional in the presence of Ent.

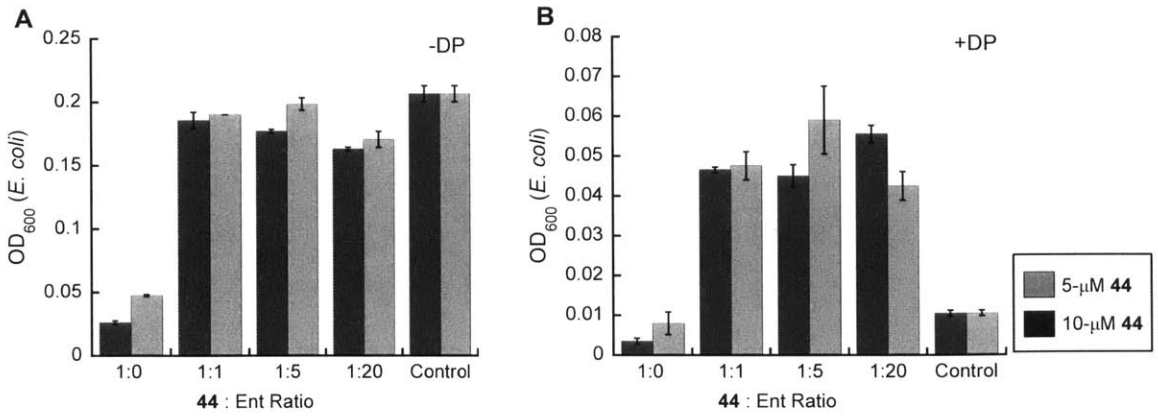

Figure 2.9. Competition assay of Ent-vancomycin conjugate **44** and Ent in the absence (A) or presence (B) of 200 μM DP. Compound **44** (5 or 10 μM) was incubated with the bacterial culture for 1 h, and various concentrations of Ent were added. Similar results were obtained without pre-incubating **44** with the bacteria. Error bars are the standard deviation of the mean for at least three independent repetitions.

The data presented above suggested that the Ent uptake machinery is able to transport cargo attached to Ent; however, it has a size limitation. The growth recovery observed when Ent was co-administrated with compound **44** suggests that **44** exhibits inhibitory effect solely because of extra-cellular iron-chelation, therefore most likely FepA is excluding large cargos to be transported. However, other components in the Ent transportation machinery, e.g., FepCDG, may also discriminate between different cargos. Further experiment to determine the contribution of these proteins to this size cut-off effect will provide more insights about the promiscuity of the whole Ent uptake system and help the design of Ent-cargo conjugates with higher uptake efficiency.

Ent-cargo Conjugates Delivery to the *P. aeruginosa* Cytoplasm. Many Gram-negative bacteria utilize Ent for iron uptake, even if they do not biosynthesize this molecule. Because in physiologically relevant environments a mixture of different bacterial species is often found where they share nutrients and encounter the same pool of chemicals, it is important to learn how these microorganisms respond to Ent-cargo conjugates. For this purpose, we chose *P. aeruginosa* PAO1, a Gram-negative opportunistic human pathogen which synthesizes and exports two siderophores, pyoverdine (pvd) and pyochelin (pch), and employs multiple additional mechanisms for iron acquisition.[32] *P. aeruginosa* utilizes Ent as a xenosiderophore, and the genes *pfeA*[33] and *pirA*[34] encode outer membrane enterobactin transporters. Similar to the *E. coli* experiments, we focused on using *P. aeruginosa* strains deficient in siderophore production or utilization in growth recovery assays. *P. aeruginosa* K648 (*pvd*-, *pch*-) is deficient in both

pyoverdine and pyochelin biosynthesis, and shows attenuated growth in iron-deficient conditions, whereas *P. aeruginosa* K407 (*pvd-*, *pFr-*) is deficient in pyoverdine biosythesis and lacks the Ent transporter PfeA (Table 2.2).[33a]

Under the same condition used for earlier *E. coli* studies, *P. aeruginosa* K648 (*pvd-*, *pch-*) grew to OD_{600} ~ 0.45 (30 °C, t = 19 h) and this value diminished to ca. 0.25 in the presence of 600 μM of DP. Supplementation of the iron-limiting growth medium with low-micromolar concentrations of L-Ent resulted in the restoration of *P. aeruginosa* growth to OD_{600} ~ 0.40 (Figure 2.10 A). Comparable growth recovery was observed for cultures treated with eight of the nine conjugates based on L-Ent (Figure 2.6B and Figure 2.10). Vancomycin **44**, which exhibits the largest cargo, afforded a growth inhibitory effect (±DP) as observed for *E. coli entA-*. In contrast to its L-Ent analog **32**, conjugate **33** based on D-Ent was growth inhibitory as was D-Ent (Figure 2.6B and Figure 2.10D). This result demonstrates that *P. aeruginosa* also requires the L-isomer for iron utilization. Lastly, no growth enhancement of *P. aeruginosa* K407 (*pFr-*) was observed in the presence of L-Ent or conjugate **32** (600 μM DP); instead, these siderophores caused growth inhibition at micromolar concentrations (Figure 2.11). These results demonstrate that PfeA is necessary for conjugate-mediated growth recovery, supporting its role as a transporter for the Ent-cargo conjugates. In total, these assays demonstrate that the Ent transport machinery of *P. aeruginosa*, and PfeA in particular, recognizes and delivers various cargo-modified Ent scaffolds to the cytoplasm.

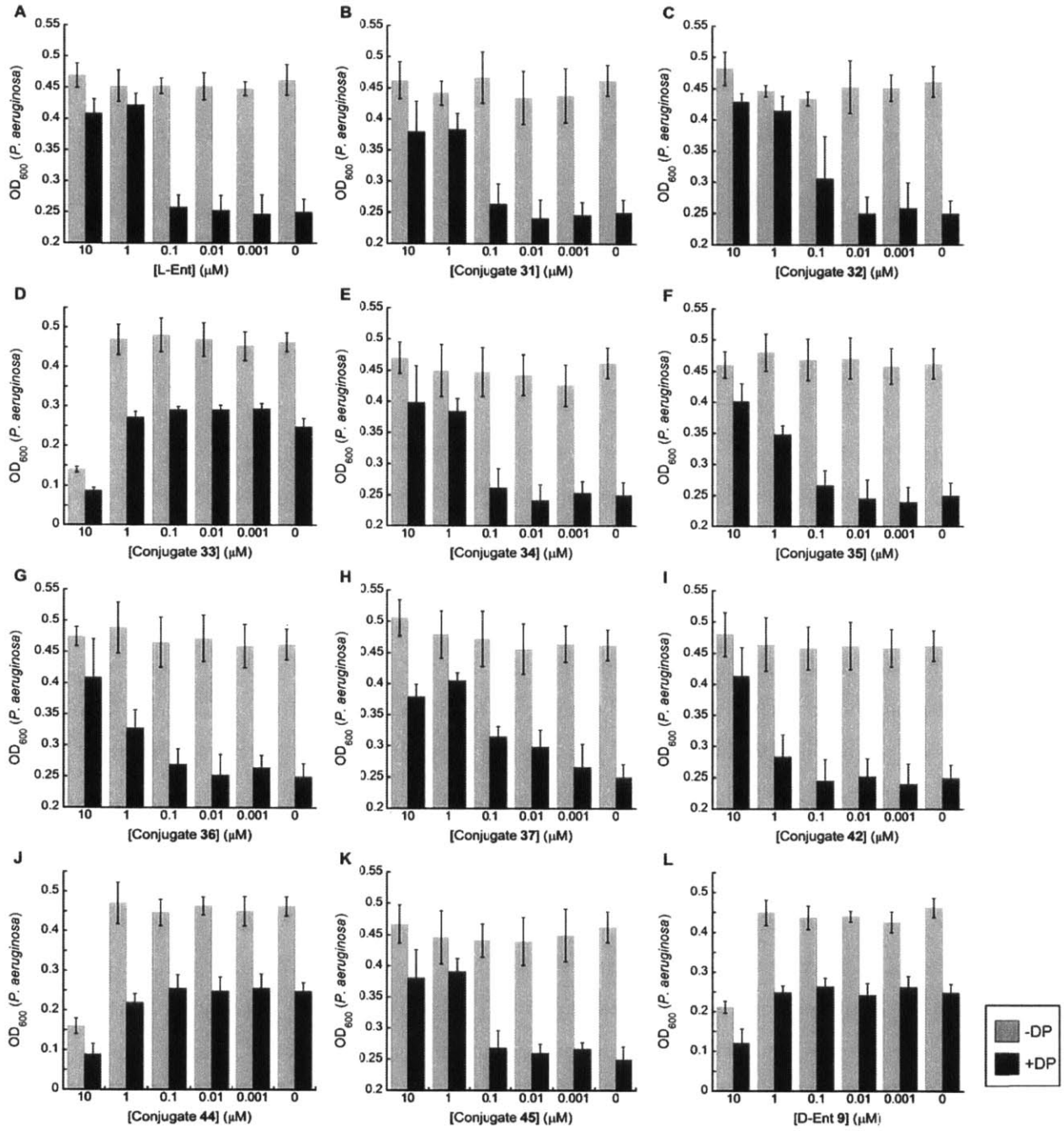

Figure 2.10. Growth recovery assay of *P. aeruginosa* (*pvd-, pch-*) with Ent (**1**), D-Ent (**9**), compound **31-37**, **42**, **44** and **45**. The DP concentration was 600 μM to achieve significant growth inhibition. Error bars are the standard deviation of the mean for at least three independent repetitions.

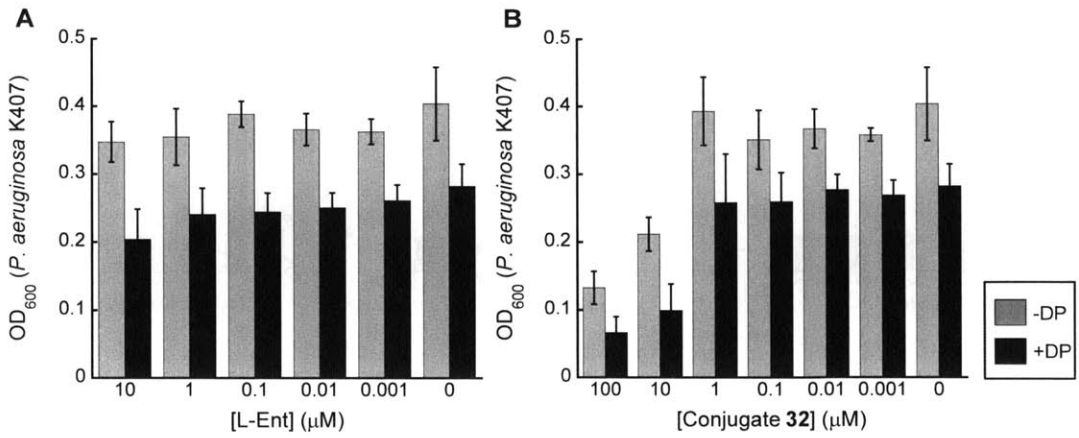

Figure 2.11. Growth recovery assay of *P. aeruginosa* PAO1 K407 (*pvd-*, *pFr-*) with Ent (A) and conjugate **32** (B). The DP concentration was 600 μM. Error bars are the standard deviation of the mean for at least three independent repetitions.

Ciprofloxacin is a fluoroquinolone antibiotic that acts in the cytoplasm and inhibits DNA gyrase.[35] The fact that ciprofloxacin conjugates **37** and **42** each restored *P. aeruginosa* growth demonstrated that the cargo was successfully delivered to the cytoplasm of this microbe with negligible impact of the variable linker composition, and that conjugation of ciprofloxacin to Ent attenuated its antibacterial activity. This observation is in general agreement with reports of pyoverdine-fluoroquinoline[36] and pyochelin-fluoroquinoline[37] conjugates where the antibiotic was covalently attached to the siderophore and point to the need for appropriate linker design for fluoroquinolone delivery and release after cellular entry.[38] These pyoverdine/pyochelin-antibiotic conjugates afforded no antipseudomonal activity or diminished activity relative to the unmodified drug, and the pyoverdine-fluoroquinolone antibiotic exhibited decreased *E. coli* gyrase inhibitory activity *in vitro*.[36] Further exploration for optimizing the linker to achieve an Ent-ciprofloxacin conjugate with antimicrobial activity is discussed in Chapter 4.

A comparison of the Ent-cargo growth recovery profiles for *E. coli* and *P. aeruginosa* (Figure 2.6) reveals that these particular microbes have different capacities for internalizing Ent-cargo conjugates, and that cargo size is an important factor. Vancomycin has a rigid dome-like structure and a molecular weight of ca. 1.4 KDa, and the assays presented above suggest that this molecule is too big for Ent-mediated transport into *E. coli* or *P. aeruginosa* (Figure 2.7J and Figure 2.10J). In contrast, small and malleable cargos such as a Boc protecting group and cyclohexane afforded growth recovery comparable to that of L-Ent for both strains. A comparison of OD_{600} values for bacterial cultures treated with such conjugates (e.g., **31**, **32**, **33**, **36**) shows that growth recovery to levels comparable to that of L-Ent occurs at a conjugate

concentration of 1 μM for *P. aeruginosa* whereas 10 μM is required for *E. coli* (Figure 2.7BCDG and Figure 2.10BCDG). *P. aeruginosa* responds to lower Ent concentrations than *E. coli*, which indicates a higher uptake efficiency. Coumarin 343 is an example of a cargo that exhibits no signs of toxicity over the concentration range tested and affords markedly different results on microbial growth promotion for these two species. A comparison of the ciprofloxacin conjugate **37** and **42** data for *E. coli* and *P. aeruginosa* also suggests differential uptake. For both the ciprofloxacin and coumarin cargo, the growth recovery assays indicate that the Ent transport machinery of *P. aeruginosa* imports these cargos whereas the *E. coli* system does not do so readily. Although no significant growth recovery was observed for *E. coli*, the Ent-coumarin conjugate **36** is not growth inhibitory under iron sufficient conditions, which suggests less efficient transport. In fact, this compound was sent to Professor Kevin Young at University of Arkansas recently and they observed TonB-dependent accumulation of fluorescent signal in *E. coli*, supporting our hypothesis that this molecule is taken up by the bacteria via the Ent transportation system.[39] These observations suggest that species-selective targeting may be possible with strategic cargo choice even when a siderophore is utilized by multiple microbial species.

Binding of Ent-cargo Conjugates to Lipocalin 2. One potential application of Ent-cargo conjugates is the delivery of antibiotics (see Chapter 3). If used to treat a bacterial infection, the conjugate will be exposed to mammalian physiological environment where lipocalin 2 (Lcn2, also known as siderocalin or NGAL) is present. During infection, Lcn2 binds Ent to interfere with bacterial iron acquisition and thus inhibit bacterial growth.[24, 40] At the same time, some bacteria synthesize modified Ent derivatives (salmochelins), which cannot be recognized by Lcn2, to evade this immune response.[41] It is important to determine whether the Ent-cargo conjugates interact with Lcn2 in order to gain some insights about the potential fate of these conjugates if administrated to the host.

An *in vitro* binding assay for Lcn2 and its ligands has been reported,[24,42] and recombinant human Lcn2 may be purchased from R&D Systems. The reported binding assay measures the intrinsic tryptophan fluorescence quenching upon ligand binding. In this assay, besides Lcn2, its ligand and a buffer system, TCEP and ubiquitin were also included in the experimental solutions. During the assay optimization, it was found that TCEP (5 mM) was necessary to minimize self-quenching of the protein. Ubiquitin (32 μg/mL) was required to reproduce the reported weak binding behavior of monoglucosylated Ent (MGE) (Figure 2.12A and B).[41] Without Ubiquitin, MGE causes fluorescent quenching similar to that of Ent (Figure 2.12A and Figure 2.13A). However, the function of ubiquitin in this assay is not clear from the available literature. It should be noted that the buffer pH affect the fluorescence property of Lcn2. The relatively high concentration of TCEP was found to be able to lower the pH of the final solution to ~5.5 and without pH adjustment a blue shift of the emission spectrum with decreased fluorescence intensity

was observed. Therefore pH adjustment should be performed after adding TCEP to the buffer solution to maintain the desired pH value.

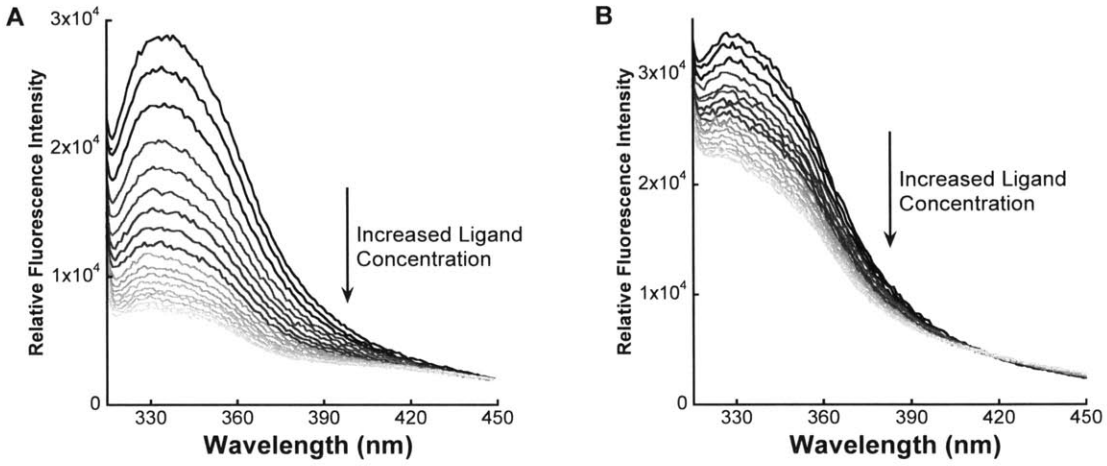

Figure 2.12. Fluorescence spectra of Lcn2 (88 nM) titrated with 0-180 nM of $[Fe(MGE)]^{3-}$ in the absence (A) or presence (B) of ubiquitin. The assay buffer contains NaCl (150 mM), DMSO (5%), TCEP (5 mM) and Tris at pH 7.5 (50 mM). λ_{ex} = 281 nm; slit widths = 3 nm; integration time = 1 s.

Two conjugates, **32** (Figure 2.13B) and **35** (Figure 2.13C), were tested in this assay together with Ent, MGE and DGE (structures shown in Figure 2.13E). From the growth recovery assays, compound **32** was internalized by the Ent transportation machinery with similar efficiency as Ent, and the uptake of **35** was less effective (Figures 2.6A and 2.7CF). The Lcn2 binding titrations show that the ferric complexes of **32** and **35** both bind to Lcn2 with affinities higher than MGE and DGE but lower than Ent, and **35** binds Lcn2 more tightly than **32** (Figure 2.13D). Preliminary analysis using a one-site binding model by DynaFit gave K_d values as following: Ent, 2.4 nM (reported K_d is 0.43 nM[41]); **32**, 29 nM; **35**, 9.9 nM; MGE, 84 nM; and DGE, 15 μM. These experiments need to be repeated and optimized for accurate binding affinity determination, although these preliminary data suggested it is highly possible that the Ent-cargo conjugates with PEG linker will be captured by Lcn2 and this protein may have different promiscuity than the bacterial proteins involved in the Ent uptake machinery.

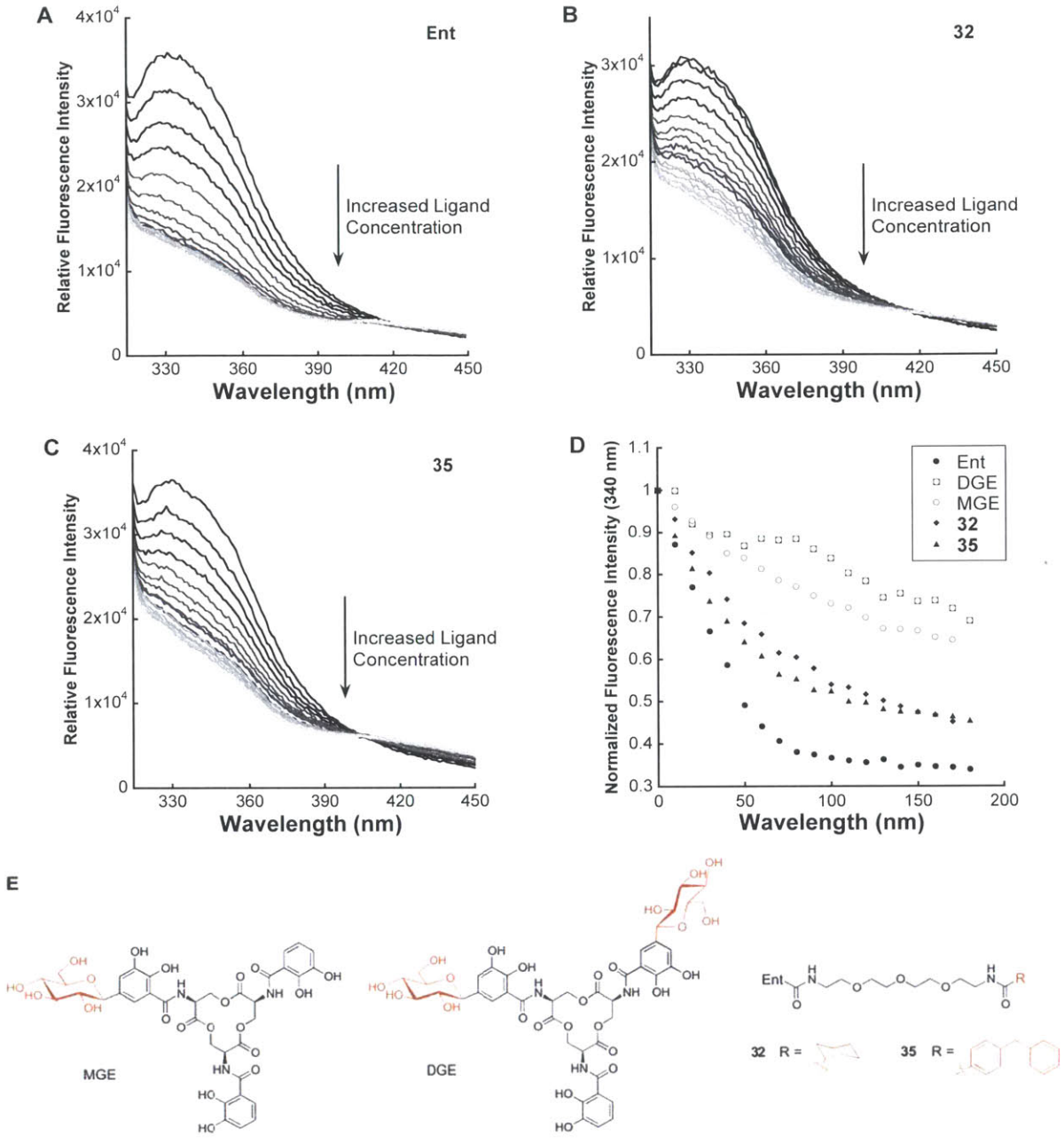

Figure 2.13. Fluorescence spectra of Lcn2 titrated with Fe(III) complexes of Ent (A), **32** (B) and **35** (C). Summarized titration curves (D) and the structures of the tested compounds (E) are also shown. The titration buffer contains NaCl (150 mM), DMSO (5%), TCEP (5 mM), ubiquitin (32 μg/mL) and Tris at pH 7.5 (50 mM). λ_{ex} = 281 nm; slit widths = 3 nm; integration time = 1 s.

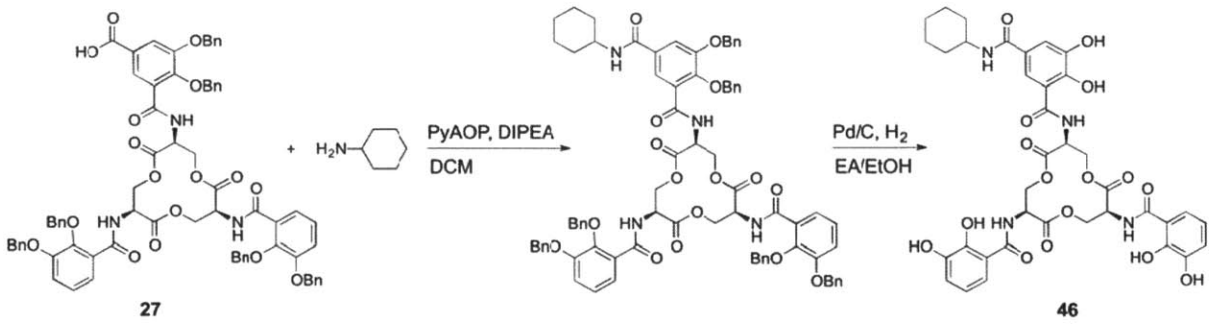

Scheme 2.8. Synthesis of Ent-cyclohexane **46**.

To deliver antimicrobial compounds into Gram-negative bacteria and better to treat infection, it would be ideal to have the Ent-cargo conjugates that cannot interact with Lcn2. Inspired by the structure of MGE and DGE, one possible linker modification is to install a cyclohexane moiety at the C5 position on the catechol to mimic the glucose structure. Following this notion, compound **46** was synthesized from benzyl-Ent-COOH **27** and aminocyclohexane through acid-amine coupling followed by Pd/C catalyzed hydrogenation (Scheme 2.8). Optimal absorption spectroscopy of **46** in the presence and absence of 1 equiv. of $FeCl_3$ afforded spectra similar to those of Ent, showing the modification did not affect the iron-binding property (Figure 2.14A). In growth recovery assays, **46** also gave a similar level of *E. coli* growth promotion as Ent, indicating successful cellular entry (Figure 2.14B). Fluorescence titration suggested that this molecule binds Lcn2 with similar affinity as Ent (Figure 2.15, K_d is ~4.2 nM calculated by DynaFit). Therefore, addition of the cyclohexyl moiety did not significantly affect the interaction between Lcn2 and Ent conjugate. The decreased binding affinity of MGE and DGE may not only come from steric hindrance of the glucose. The charge effect or hydrophilic properties of the glucose moiety may play a more important role. Possible further modifications to prevent conjugate binding to Lcn2 is to synthesize conjugates based on MGE or DGE, which may still be transported by bacterial strains that utilize MGE and DGE and at the same time circumvent Lcn2 capture.

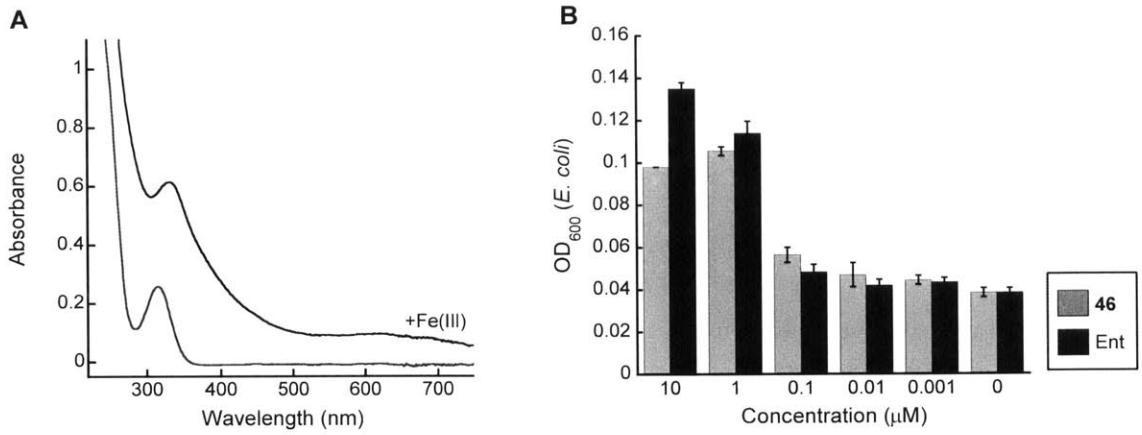

Figure 2.14. (A) UV-spectra of Ent-cyclohexane conjugate **46** in the absence or presence of Fe(III). (B) Growth recovery assay of compound **46** (grey bars) and Ent (black bars) in the presence of DP.

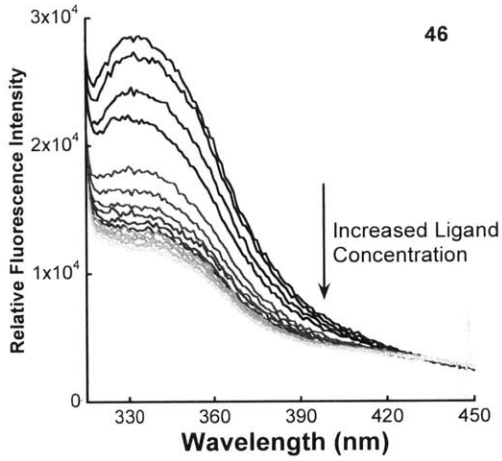

Figure 2.15 Fluorescence spectra of Lcn2 titrated with Fe(III) complex of **46**. The titration buffer contains NaCl (150 mM), DMSO (5%), TCEP (5 mM), ubiquitin (32 μg/mL) and Tris at pH 7.5 (50 mM). λ_{ex} = 281 nm; slit widths = 3 nm; integration time = 1 s.

Summary and Perspectives

We have designed and prepared a family of monofunctionalized enterobactin derivatives, and utilized these scaffolds for the preparation of enterobactin-cargo conjugates bearing cargos of varying size and complexity. Growth recovery assays employing *E. coli* and *P. aeruginosa* revealed that the enterobactin uptake machineries of these Gram-negative species recognize and transport enterobactin-cargo conjugates to the Gram-negative cytoplasm. These studies are significant in several respects. First,

the notion of using siderophores for antibiotic delivery across the Gram-negative outer membrane, which serves as a permeability barrier, has achieved long-term interest.[11a-c, 11f] Such "Trojan horse" antibiotics are largely inspired by the sideromycins,[11e, 11i] a family of siderophore-antibiotic conjugates produced by the soil bacterium *Streptomyces*, and by early observations that catechol-modified β-lactams were recognized by the iron-uptake machinery of Gram-negative microbes.[15] Significant efforts have been made to prepare and characterize synthetic siderophore-antibiotic conjugates with the goal of targeting drug-resistant Gram-negative pathogens.[11f, g] Timely examples of siderophore-antibiotic conjugates with antimicrobial activity include a mycobactin-artemisinin conjugate that kills *Mycobacterium tuberculosis* and *Plasmodium falciparum*,[43] and amoxicillin/ampicillin-appended tripodal triscatecholates that exhibit potent antipseudomonal activity relative to the parent β-lactam antibiotics.[16c] One bottleneck with this general approach, and using siderophores in other applications, is that few synthetically tractable and modifiable native siderophores are available. DFO B and pyoverdine, which are readily obtained commercially (DFO B) or from bacterial cultures (pyoverdines), provide free amino groups useful for conjugation and are most commonly derivatized for application-based work.[44] Syntheses of modified pyochelin,[45] petrobactin,[46] and mycobactin[43, 47] platforms that house functional groups amenable to site-specific elaboration have been reported, and these scaffolds are important contributions to the toolkit of siderophores that can be modified without compromising Fe(III) coordination in addition to recognition by siderophore-binding proteins. The syntheses described in this work provide enterobactin with a functional handle for exploring new chemical space, and will allow strategic use of this canonical siderophore in a multitude of chemical biology and biotechnology initiatives.

Unanswered questions regarding the antibacterial activity and fate of reported synthetic siderophore-antibiotic conjugates exist. Whether a given conjugate is actively transported into the bacterial cell is oftentimes unclear. Because FepA recognizes relatively large biomolecules including MccE492m (84-aa) and colicin B (324-aa), it is tempting to predict that FepA may accommodate almost any cargo appended to an enterobactin or catecholate platform. The results presented in this work challenge this notion and indicate that cargo size is an important and species-specific parameter. Our assays indicate that *P. aeruginosa* PAO1 has a greater capacity to import enterobactin-cargo conjugates than *E. coli* ATCC 33475. It will be interesting to determine the cargo scope of other *E. coli* strains and bacterial species that utilize enterobactin for iron acquisition, and understand the molecular and physiological basis for such variations. Colicins are largely α-helical[12] and MccE492m shares some sequence homology with colicins.[48] It is likely that some enterobactin receptors have decreased propensity to transport synthetic small molecules or natural products with less structural malleability (i.e. vancomycin) than an α-helical peptide.

The mechanisms of iron release from siderophores, which vary tremendously for the myriad of siderophores produced by different bacterial species, are another important consideration in siderophore-cargo conjugate design. Guided by studies of chiral recognition in enterobactin transport, which demonstrated that D-Ent is transported into *B. subtilis* but cannot be hydrolyzed by Fes,[28] we designed the monofunctionalized D-Ent scaffolds to probe cytosolic delivery. This design feature prevents esterase-catalyzed iron release from enterobactin-based conjugates in the cytoplasm and may have practical utility. From the standpoint of drug delivery, a tug-of-war may result from utilizing an iron-supplying siderophore that confers a growth advantage for delivering a toxic payload to a bacterial cell, and preventing iron release may be beneficial. In other applications, siderophore-fluorophore conjugates are of interest for bacterial detection and diagnostics, and Fe(III) binding to and release from the siderophore will likely influence the photophysical properties of such molecules.

The mammalian protein lipocalin 2 (Lcn2) generated from the innate immune system specifically binds Ent and inhibit bacteria growth by iron depletion.[49] For the purpose of drug delivery, the interaction of Ent-conjugates with Lcn2 should be minimized. It is reported that glucose adducts of Ent (salmochelins, including MGE and DGE) binds lipocalin 2 with $> 10^3$-fold weaker affinity than Ent, and structural analyses revealed significant steric clashes after modeling in a single glucose in the catechol-binding pockets of Lcn2.[41] Moreover, synthetic analogs of Ent with methyl or *tert*-butyl groups at the C5 position on all three catechol moieties do not bind Lcn2.[42] Based on these observations, it is unexpected to find several Ent-cargo conjugates synthesized in the current work still bind Lcn2, including compound **46** in which a cyclohexane group is appended to the C5 position through an amide bond. The flexible PEG linker in these conjugates may help to guide the cargo group away from the binding pocket, although this model does not explain the binding of **46**. The binding pocket of Lcn2 is hydrophobic, which may contribute to the relatively high binding affinity of **46** compared to MGE. Other factors besides steric constraints may contribute to the weak binding of salmochelins. To preclude binding to Lcn2, one possible modification is to introduce glucose moieties to the Ent-cargo conjugates and applying these salmochelin scaffolds for antibiotic delivery.

In summary, these investigations reveal that the enterobactin transport machineries of *E. coli* (e.g., FepABCDG and TonB-ExbB-ExbD) and *P. aeruginosa* will deliver enterobactin-modified cargo to the Gram-negative cytoplasm. Moreover, the preparative work affords a new siderophore platform amenable to synthetic elaboration and an entry route for employing the native enterobactin scaffold in a multitude of application-based initiatives that include intracellular cargo delivery, iron sensing, siderophore labeling, protein and pathogen detection, and therapeutic development.

Acknowledgements

The Searle Scholars Program (Kinship Foundation), the Department of Chemistry and the Undergraduate Research Opportunities Program (UROP) at MIT, and the Amgen Scholars Program (J.L.B) are gratefully acknowledged for financial support. We thank MIT undergraduate student Justin Bullock for participating in the project and synthesizing intermediates used in this work. We thank Professor Keith Poole for providing the *Pseudomonas aeruginosa* strains employed in this work, and Professor Stephen J. Lippard for use an IR spectrophotometer and a melting point apparatus. *E. coli* K-12 JW0576 was obtained from the Keio Collection.[50]

References

1. (a) Hider, R. C.; Kong, X., Chemistry and biology of siderophores. *Nat. Prod. Rep.* 2010, *27* (5), 637-657; (b) Miethke, M.; Marahiel, M. A., Siderophore-based iron acquisition and pathogen control. *Microbiol. Mol. Biol. Rev.* **2007**, *71* (3), 413-451.
2. Raymond, K. N.; Dertz, E. A.; Kim, S. S., Enterobactin: an archetype for microbial iron transport. *Proc. Natl. Acad. Sci. U. S. A.* **2003**, *100* (7), 3584-3588.
3. Loomis, L. D.; Raymond, K. N., Solution Equilibria of Enterobactin and Metal Enterobactin Complexes. *Inorg. Chem.* **1991**, *30* (5), 906-911.
4. (a) Buchanan, S. K.; Smith, B. S.; Venkatramani, L.; Xia, D.; Esser, L.; Palnitkar, M.; Chakraborty, R.; van der Helm, D.; Deisenhofer, J., Crystal structure of the outer membrane active transporter FepA from Escherichia coli. *Nat. Struct. Biol.* **1999**, *6* (1), 56-63; (b) Newton, S. M. C.; Igo, J. D.; Scott, D. C.; Klebba, P. E., Effect of loop deletions on the binding and transport of ferric enterobactin by FepA. *Mol. Microbiol.* **1999**, *32* (6), 1153-1165.
5. Stephens, D. L.; Choe, M. D.; Earhart, C. F., Escherichia-Coli Periplasmic Protein Fepb Binds Ferrienterobactin. *Microbiology U. K.* **1995**, *141*, 1647-1654.
6. (a) Chenault, S. S.; Earhart, C. F., Organization of Genes Encoding Membrane-Proteins of the Escherichia-Coli Ferrienterobactin Permease. *Mol. Microbiol.* **1991**, *5* (6), 1405-1413; (b) Shea, C. M.; Mcintosh, M. A., Nucleotide-Sequence and Genetic Organization of the Ferric Enterobactin Transport-System - Homology to Other Periplasmic Binding Protein-Dependent Systems in Escherichia-Coli. *Mol. Microbiol.* **1991**, *5* (6), 1415-1428; (c) Chakraborty, R.; Storey, E.; van der Helm, D., Molecular mechanism of ferricsiderophore passage through the outer membrane receptor proteins of Escherichia coli. *BioMetals* **2007**, *20* (3-4), 263-274; (d) Krewulak, K. D.; Vogel, H. J., Structural biology of bacterial iron uptake. *Biochim. Biophys. Acta. Biomembr.* **2008**, *1778* (9), 1781-1804; (e) Chu, B. C.; Garcia-Herrero, A.; Johanson, T. H.; Krewulak, K. D.; Lau, C. K.; Peacock, R. S.; Slavinskaya, Z.; Vogel, H. J., Siderophore uptake in bacteria and the battle for iron with the host; a bird's eye view. *BioMetals* **2010**, *23* (4), 601-611.
7. Lin, H.; Fischbach, M. A.; Liu, D. R.; Walsh, C. T., In vitro characterization of salmochelin and enterobactin trilactone hydrolases IroD, IroE, and Fes. *J. Am. Chem. Soc.* **2005**, *127* (31), 11075-11084.
8. Miethke, M.; Hou, J.; Marahiel, M. A., The Siderophore-Interacting Protein YqjH Acts as a Ferric Reductase in Different Iron Assimilation Pathways of Escherichia coli. *Biochemistry* **2011**, *50* (50), 10951-10964.
9. (a) Baumler, A. J.; Norris, T. L.; Lasco, T.; Voigt, W.; Reissbrodt, R.; Rabsch, W.; Heffron, F., IroN, a novel outer membrane siderophore receptor characteristic of Salmonella enterica. *J. Bacteriol.* **1998**, *180* (6), 1446-1453; (b) Lagos, R.; Baeza, M.; Corsini, G.; Hetz, C.; Strahsburger, E.; Castillo, J. A.; Vergara, C.; Monasterio, O., Structure, organization and characterization of the gene cluster involved in

the production of microcin E492, a channel-forming bacteriocin. *Mo. Microbiol.* **2001**, *42* (1), 229-243; (c) Nolan, E. M.; Fischbach, M. A.; Koglin, A.; Walsh, C. T., Biosynthetic tailoring of microcin e492m: Post-translational modification affords an antibacterial siderophore-peptide conjugate. *J. Am. Chem. Soc.* **2007**, *129* (46), 14336-14347; (d) Fischbach, M. A.; Lin, H. N.; Liu, D. R.; Walsh, C. T., In vitro characterization of IroB, a pathogen-associated C-glycosyltransferase. *Proc. Natl. Acad. Sci. U. S. A.* **2005**, *102* (3), 571-576.

10. Muller, S.; Valdebenito, M.; Hantke, K., Salmochelin, the long-overlooked catecholate siderophore of Salmonella. *BioMetals* **2009**, *22* (4), 691-695.

11. (a) Miller, M. J., Syntheses and Therapeutic Potential of Hydroxamic Acid Based Siderophores and Analogs. *Chem. Rev.* **1989**, *89* (7), 1563-1579; (b) Roosenberg, J. M., II; Lin, Y.-M.; Lu, Y.; Miller, M. J., Studies and syntheses of siderophores, microbial iron chelators, and analogs as potential drug delivery agents. *Curr. Med. Chem.* **2000**, *7* (2), 159-197; (c) Budzikiewicz, H., Siderophore-antibiotic conjugates used as trojan horses against Pseudomonas aeruginosa. *Curr. Top. Med. Chem.* **2001**, *1* (1), 73-82; (d) Mollmann, U.; Heinisch, L.; Bauernfeind, A.; Kohler, T.; Ankel-Fuchs, D., Siderophores as drug delivery agents: application of the "Trojan Horse" strategy. *BioMetals* **2009**, *22* (4), 615-624; (e) Braun, V., Active transport of siderophore-mimicking antibacterials across the outer membrane. *Drug Resist. Update* **1999**, *2* (6), 363-369; (f) Ji, C.; Juarez-Hernandez, R. E.; Miller, M. J., Exploiting bacterial iron acquisition: siderophore conjugates. *Future Med. Chem.* **2012**, *4* (3), 297-313; (g) Miller, M. J.; Zhu, H.; Xu, Y.; Wu, C.; Walz, A. J.; Vergne, A.; Roosenberg, J. M.; Moraski, G.; Minnick, A. A.; McKee-Dolence, J.; Hu, J.; Fennell, K.; Kurt Dolence, E.; Dong, L.; Franzblau, S.; Malouin, F.; Mollmann, U., Utilization of microbial iron assimilation processes for the development of new antibiotics and inspiration for the design of new anticancer agents. *BioMetals* **2009**, *22* (1), 61-75; (h) Ballouche, M.; Cornelis, P.; Baysse, C., Iron metabolism: a promising target for antibacterial strategies. *Recent Pat. Anti-infect. Drug Discovery* **2009**, *4* (3), 190-205; (i) Braun, V.; Pramanik, A.; Gwinner, T.; Koberle, M.; Bohn, E., Sideromycins: tools and antibiotics. *BioMetals* **2009**, *22* (1), 3-13.

12. Cao, Z.; Klebba, P. E., Mechanisms of colicin binding and transport through outer membrane porins. *Biochimie* **2002**, *84* (5-6), 399-412.

13. Lagos, R.; Tello, M.; Mercado, G.; Garcia, V.; Monasterio, O., Antibacterial and Antitumorigenic Properties of Microcin E492, a Pore-Forming Bacteriocin. *Curr. Pharm. Biotechnol.* **2009**, *10* (1), 74-85.

14. Rabsch, W.; Ma, L.; Wiley, G.; Najar, F. Z.; Kaserer, W.; Schuerch, D. W.; Klebba, J. E.; Roe, B. A.; Gomez, J. A. L.; Schallmey, M.; Newton, S. M. C.; Klebba, P. E., FepA- and TonB-dependent bacteriophage H8: Receptor binding and genomic sequence. *J. Bacteriol.* **2007**, *189* (15), 5658-5674.

15. (a) Katsu, K.; Kitoh, K.; Inoue, M.; Mitsuhashi, S., Invitro Antibacterial Activity of E-0702, a New Semi-Synthetic Cephalosporin. *Antimicrob. Agents Chemother.* **1982**, *22* (2), 181-185; (b) Watanabe, N.-A.; Nagasu, T.; Katsu, K.; Kitoh, K., E-0702, a New Cephalosporin, Is Incorporated into Escherichia-Coli-Cells Via the Tonb-Dependent Iron Transport-System. *Antimicrob. Agents Chemother.* **1987**, *31* (4), 497-504; (c) Nakagawa, S.; Sanada, M.; Matsuda, K.; Hazumi, N.; Tanaka, N., Biological-Activity of Bo-1236, a New Antipseudomonal Cephalosporin. *Antimicrob. Agents Chemother.* **1987**, *31* (7), 1100-1105; (d) Hashizume, T.; Sanada, M.; Nakagawa, S.; Tanaka, N., Comparison of Transport Pathways of Catechol-Substituted Cephalosporins, Bo-1236 and Bo-1341, through the Outer-Membrane of Escherichia-Coli. *J. Antibiot.* **1990**, *43* (12), 1617-1620.

16. (a) Mollmann, U.; Ghosh, A.; Dolence, E. K.; Dolence, J. A.; Ghosh, M.; Miller, M. J.; Reissbrodt, R., Selective growth promotion and growth inhibition of Gram-negative and Gram-positive bacteria by synthetic siderophore-beta-lactam conjugates. *BioMetals* **1998**, *11* (1), 1-12; (b) Mckee, J. A.; Sharma, S. K.; Miller, M. J., Iron Transport Mediated Drug Delivery Systems - Synthesis and Antibacterial Activity of Spermidine-Based and Lysine-Based Siderophore-Beta-Lactam Conjugates. *Bioconjugate Chem.* **1991**, *2* (4), 281-291; (c) Ji, C.; Miller, P. A.; Miller, M. J., Iron Transport-Mediated Drug Delivery: Practical Syntheses and In Vitro Antibacterial Studies of Tris-Catecholate Siderophore-Aminopenicillin Conjugates Reveals Selectively Potent Antipseudomonal Activity. *J. Am. Chem. Soc.* **2012**, *134* (24), 9898-9901; (d) Diarra, M. S.; Lavoie, M. C.; Jacques, M.; Darwish, I.; Dolence, E. K.; Dolence, J. A.; Ghosh, A.; Ghosh, M.; Miller, M. J.; Malouin, F., Species selectivity of new siderophore-

drug conjugates that use specific iron uptake for entry into bacteria. *Antimicrob. Agents Chemother.* **1996**, *40* (11), 2610-2617; (e) Ghosh, A.; Ghosh, M.; Niu, C.; Malouin, F.; Moellmann, U.; Miller, M. J., Iron transport-mediated drug delivery using mixed-ligand siderophore-beta-lactam conjugates. *Chem. Biol.* **1996**, *3* (12), 1011-1019.

17. (a) Corey, E. J.; Bhattacharyya, S., Total synthesis of enterobactin, a macrocyclic iron transporting agent of bacteria. *Tetrahedron Lett.* **1977**, *45*, 3919-3922; (b) Rastetter, W. H.; Erickson, T. J.; Venuti, M. C., Synthesis of iron chelators. Enterobactin, enantioenterobactin, and a chiral analogue. *J. Org. Chem.* **1981**, *46*, 3579-3590; (c) Shanzer, A.; Libman, J., Total synthesis of enterobactin via an organotin template. *J. Chem. Soc., Chem. Commun.* **1983**, *15*, 846-847; (d) Ramirez, R. J. A.; Karamanukyan, L.; Ortiz, S.; Gutierrez, C. G., A Much Improved Synthesis of the Siderophore Enterobactin. *Tetrahedron Lett.* **1997**, *38*, 749-752; (e) Marinez, E. R.; Salmassian, E. K.; Lau, T. T.; Gutierrez, C. G., Enterobactin and Enantioenterobactin. *J. Org. Chem.* **1996**, *61*, 3548-3550.

18. (a) Rodgers, S. J.; Lee, C.-W.; Ng, C. Y.; Raymond, K. N., Ferric Ion Sequestering Agents .15. Synthesis, Solution Chemistry, and Electrochemistry of a New Cationic Analog of Enterobactin. *Inorg. Chem.* **1987**, *26* (10), 1622-1625; (b) Tor, Y.; Libman, J.; Shanzer, A.; Felder, C. E.; Lifson, S., Chiral Siderophore Analogs - Enterobactin. *J. Am. Chem. Soc.* **1992**, *114* (17), 6661-6671; (c) Ecker, D. J.; Loomis, L. D.; Cass, M. E.; Raymond, K. N., Coordination Chemistry of Microbial Iron Transport .39. Substituted Complexes of Enterobactin and Synthetic Analogs as Probes of the Ferric Enterobactin Receptor in Escherichia-Coli. *J. Am. Chem. Soc.* **1988**, *110* (8), 2457-2464; (d) Stack, T. D. P.; Hou, Z. G.; Raymond, K. N., Rational Reduction of the Conformational Space of a Siderophore Analog through Nonbonded Interactions - the Role of Entropy in Enterobactin. *J. Am. Chem. Soc.* **1993**, *115* (14), 6466-6467.

19. Yu, X.; Dai, Y.; Yang, T.; Gagne, M. R.; Gong, H., Facile synthesis of salmochelin S1, S2, MGE, DGE, and TGE. *Tetrahedron* **2011**, *67*, 144-151.

20. Gardner, R. A.; Kinkade, R.; Wang, C. J.; Phanstiel, O. I., Total synthesis of petrobactin and its homologues as potential growth stimuli for Marinobacter hydrocarbonoclasticus, an oil-degrading bacteria. *J. Org. Chem.* **2007**, *72* (8), 3158-3158.

21. Arnusch, C. J.; Bonvin, A. M. J. J.; Verel, A. M.; Jansen, W. T. M.; Liskamp, R. M. J.; de Kruijff, B.; Pieters, R. J.; Breukink, E., The Vancomycin-Nisin(1-12) Hybrid Restores Activity against Vancomycin Resistant Enterococci. *Biochemistry* **2008**, *47* (48), 12661-12663.

22. (a) Fischbach, M. A.; Lin, H. N.; Liu, D. R.; Walsh, C. T., In vitro characterization of IroB, a pathogen-associated C-glycosyltransferase. *Proc. Natl. Acad. Sci. U. S. A.* **2005**, *102* (3), 571-576; (b) Nolan, E. M.; Fischbach, M. A.; Koglin, A.; Walsh, C. T., Biosynthetic tailoring of microcin e492m: Post-translational modification affords an antibacterial siderophore-peptide conjugate. *J. Am. Chem. Soc.* **2007**, *129* (46), 14336-14347.

23. Scarrow, R. C.; Ecker, D. J.; Ng, C.; Liu, S.; Raymond, K. N., Iron(IiI) Coordination Chemistry of Linear Dihydroxyserine Compounds Derived from Enterobactin. *Inorg. Chem.* **1991**, *30* (5), 900-906.

24. Goetz, D. H.; Holmes, M. A.; Borregaard, N.; Bluhm, M. E.; Raymond, K. N.; Strong, R. K., The neutrophil lipocalin NGAL is a bacteriostatic agent that interferes with siderophore-mediated iron acquisition. *Mol. Cell* **2002**, *10* (5), 1033-1043.

25. Luo, M. K.; Lin, H.; Fischbach, M. A.; Liu, D. R.; Walsh, C. T.; Groves, J. T., Enzymatic tailoring of enterobactin alters membrane partitioning and iron acquisition. *ACS Chem. Biol.* **2006**, *1* (1), 29-32.

26. Thomas, X.; Destoumieux-Garzon, D.; Peduzzi, J.; Afonso, C.; Blond, A.; Birlirakis, N.; Goulard, C.; Dubost, L.; Thai, R.; Tabet, J. C.; Rebuffat, S., Siderophore peptide, a new type of post-translationally modified antibacterial peptide with potent activity. *J. Biol. Chem.* **2004**, *279* (27), 28233-28242.

27. Alonso, F.; Riente, P.; Yus, M., Wittig-Type Olefination of Alcohols Promoted by Nickel Nanoparticles: Synthesis of Polymethoxylated and Polyhydroxylated Stilbenes. *Eur. J. Org. Chem.* **2009**, (34), 6034-6042.

28. Abergel, R. J.; Zawadzka, A. M.; Hoette, T. M.; Raymond, K. N., Enzymatic Hydrolysis of Trilactone Siderophores: Where Chiral Recognition Occurs in Enterobactin and Bacillibactin Iron Transport. *J. Am. Chem. Soc.* **2009**, *131* (35), 12682-12692.
29. Hubbard, B. K.; Walsh, C. T., Vancomycin assembly: Nature's way. *Angew. Chem. Int. Ed.* **2003**, *42* (7), 730-765.
30. Lawson, M. C.; Shoemaker, R.; Hoth, K. B.; Bowman, C. N.; Anseth, K. S., Polymerizable Vancomycin Derivatives for Bactericidal Biomaterial Surface Modification: Structure-Function Evaluation. *Biomacromolecules* **2009**, *10* (8), 2221-2234.
31. Wayne, R.; Frick, K.; Neilands, J. B., Siderophore protection against colicins M, B, V, and Ia in Escherichia coli. *J. Bacteriol.* **1976**, *126*, 7-12.
32. (a) Mossialos, D.; Amoutzias, G. D., Siderophores in fluorescent pseudomonads: new tricks from an old dog. *Future Microbiol.* **2007**, *2* (4), 387-395; (b) Cornelis, P., Iron uptake and metabolism in pseudomonads. *App. Microbiol. Biotechnol.* **2010**, *86* (6), 1637-1645.
33. (a) Poole, K.; Young, L.; Neshat, S., Enterobactin-Mediated Iron Transport in Pseudomonas aerugionsa. *J. Bacteriol.* **1990**, *172*, 6991-6996; (b) Dean, C. R.; Neshat, S.; Poole, K., PfeR, an Enterobactin-Responsive Activator of Ferric Enterobactin Receptor Gene Expression in Pseudomonas aerugionsa. *J. Bacteriol.* **1996**, *178*, 5361-5369.
34. Ghysels, B.; Ochsner, U.; Mollman, U.; Heinisch, L.; Vasil, M.; Cornelis, P.; Matthijs, S., The Pseudomonas aeruginosa pirA gene encodes a second receptor for ferrienterobactin and synthetic catecholate analogues. *FEMS Microbiol. Lett.* **2005**, *246* (2), 167-174.
35. Collin, F.; Karkare, S.; Maxwell, A., Exploiting bacterial DNA gyrase as a drug target: current state and perspectives. *App. Microbiol. Biotechnol.* **2011**, *92* (3), 479-497.
36. Hennard, C.; Truong, Q. C.; Desnottes, J.-F.; Paris, J. M.; Moreau, N. J.; Abdallah, M. A., Synthesis and activities of pyoverdin-quinolone adducts: A prospective approach to a specific therapy against Pseudomonas aeruginosa. *J. Med. Chem.* **2001**, *44* (13), 2139-2151.
37. (a) Rivault, F.; Liebert, C.; Burger, A.; Hoegy, F.; Abdallah, M. A.; Schalk, I. J.; Mislin, G. L. A., Synthesis of pyochelin-norfloxacin conjugates. *Bioorg. Med. Chem. Lett.* **2007**, *17* (3), 640-644; (b) Noel, S.; Gasser, V.; Pesset, B.; Hoegy, F.; Rognan, D.; Schalk, I. J.; Mislin, G. L. A., Synthesis and biological properties of conjugates between fluoroquinolones and a N3 "-functionalized pyochelin. *Org. Biomol. Chem.* **2011**, *9* (24), 8288-8300.
38. Ji, C.; Miller, M. J., Chemical syntheses and in vitro antibacterial activity of two desferrioxamine B-ciprofloxacin conjugates with potential esterase and phosphatase triggered drug release linkers. *Bioorg. Med. Chem.* **2012**, *20* (12), 3828-3836.
39. Vega, D. E.; Young, K. D., Accumulation of periplasmic enterobactin impairs the growth and morphology of Escherichia coli tolC mutants. *Mol. Microbiol.* **2014,** *91* (3), 508-521.
40. Clifton, M. C.; Corrent, C.; Strong, R. K., Siderocalins: siderophore-binding proteins of the innate immune system. *BioMetals* **2009**, *22* (4), 557-564.
41. Fischbach, M. A.; Lin, H.; Zhou, L.; Yu, Y.; Abergel, R. J.; Liu, D. R.; Raymond, K. N.; Wanner, B. L.; Strong, R. K.; Walsh, C. T.; Aderem, A.; Smith, K. D., The pathogen-associated iroA gene cluster mediates bacterial evasion of lipocalin 2. *Proc. Natl. Acad. Sci. U. S. A.* **2006**, *103* (44), 16502-16507.
42. Abergel, R. J.; Moore, E. G.; Strong, R. K.; Raymond, K. N., Microbial evasion of the immune system: structural modifications of enterobactin impair siderocalin recognition. *J. Am. Chem. Soc.* **2006**, *128* (34), 10998-10999.
43. Miller, M. J.; Walz, A. J.; Zhu, H.; Wu, C.; Moraski, G.; Mollmann, U.; Tristani, E. M.; Crumbliss, A. L.; Ferdig, M. T.; Checkley, L.; Edwards, R. L.; Boshoff, H. I., Design, synthesis, and study of a mycobactin-artemisinin conjugate that has selective and potent activity against tuberculosis and malaria. *J. Am. Chem. Soc.* **2011**, *133* (7), 2076-2079.
44. Zheng, T.; Nolan, E. M., Siderophore-based detection of Fe(III) and microbial pathogens. *Metallomics* **2012**, 24, 866-880
45. Noel, S.; Guillon, L.; Schalk, I. J.; Mislin, G. L. A., Synthesis of Fluorescent Probes Based on the Pyochelin Siderophore Scaffold. *Org. Lett.* **2011**, *13* (5), 844-847.

46. Bugdahn, N.; Peuckert, F.; Albrecht, A. G.; Miethke, M.; Marahiel, M. A.; Oberthur, M., Direct Identification of a Siderophore Import Protein Using Synthetic Petrobactin Ligands. *Angew. Chem. Int. Ed.* **2010**, *49* (52), 10210-10213.
47. Xu, Y.; Miller, M. J., Total syntheses of mycobactin analogues as potent antimycobacterial agents using a minimal protecting group strategy. *J. Org. Chem.* **1998**, *63* (13), 4314-4322.
48. Pons, A. M.; Zorn, N.; Vignon, D.; Delalande, F.; Van Dorsselaer, A.; Cottenceau, G., Microcin E492 is an unmodified peptide related in structure to colicin V. *Antimicrob. Agents Chemother.* **2002**, *46* (1), 229-230.
49. Flo, T. H.; Smith, K. D.; Sato, S.; Rodriguez, D. J.; Holmes, M. A.; Strong, R. K.; Akira, S.; Aderem, A., Lipocalin 2 mediates an innate immune response to bacterial infection by sequestrating iron. *Nature* **2004**, *432* (7019), 917-921.
50. Baba, T.; Ara, T.; Hasegawa, M.; Takai, Y.; Okumura, Y.; Baba, M.; Datsenko, K. A.; Tomita, M.; Wanner, B. L.; Mori, H., Construction of Escherichia coli K-12 in-frame single-gene knockout mutants: the Keio Collection. *Mol. Sys. Biol.* **2006**, 1-11.

Chapter 3

Enterobactin-Mediated β-Lactam Delivery into Gram-negative Bacteria

Introduction

Building upon the synthetic routes developed for monofunctionalized enterobactin (Ent) scaffolds and the cargo size tolerance evaluation for the Ent uptake machinery described in Chapter 2, we aim to incorporate cargos with defined functions into the Ent-cargo conjugates to explore possible applications (Figure 3.1). With the increasing demand for new antimicrobial treatments, it is very attempting to test whether the Ent-mediated delivery of existing antibiotics will result in enhanced antimicrobial activity. Decreases in the retention of antibiotics within the bacterial cells caused by either decreased membrane permeability or expression of efflux pumps greatly contribute to the frequently observed antibiotic resistance.[1] Siderophore mediated delivery employs specific uptake machineries including membrane receptors, periplasmic binding proteins and permeases, therefore has the potential of bypassing these resistance mechanisms. Siderophores play very important role in pathogenesis, and the possibility for the bacteria to evolve resistance towards siderophore-mediated delivery and at the same time maintain virulence is very low.

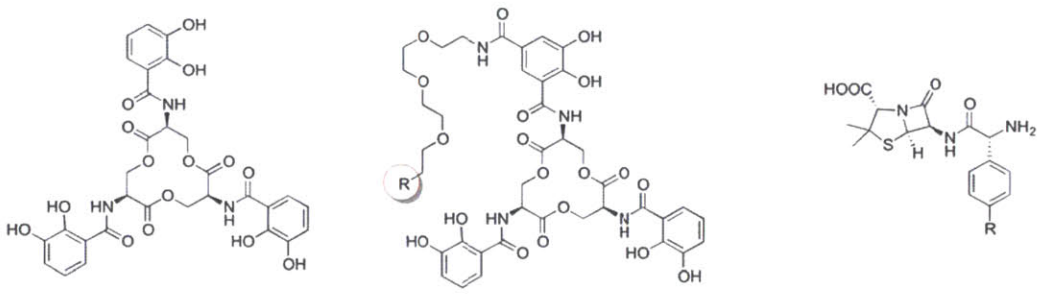

Figure 3.1. Structure of enterobactin , Ent-cargo conjugate for cargo delivery applications, and the two β-lactam antibiotic cargos (ampicillin and amoxicillin) studied in this Chapter.

A wealth of literature discussing synthetic siderophore-antibiotic conjugates exists;[2] however, Ent has not been studied in this context, likely due to the synthetic challenge of modifying this molecule without affecting its extraordinary iron binding affinity. There are several advantages of applying Ent in this strategy. The uptake machinery for Ent is well characterized, which will facilitate investigations of antimicrobial activity mechanisms for the Ent-antibiotic conjugates. Ent is widely produced by many pathogenic *Escherichia coli, Salmonella* and *Klebsiella* species and was found to be required for virulence in some infection models.[3] Other bacteria like *Pseudomonas aeruginosa* that do not synthesize Ent also utilize Ent as a xenosiderophore for iron uptake,[4] which suggests another possible target for Ent-mediated antibiotic delivery. However, it should be noted that lipocalin 2 (Lcn2), a host protein produced

by the innate immune system to scavenge Ent and prevent bacterial iron acquisition, makes Ent less effective during infection.[5]

Several classes of antibiotics have been employed in siderophore conjugate studies, from which the β-lactams are most investigated (see Chapter 1). The β-lactam antibiotics target transpeptidases (or penicillin binding proteins or PBPs), which are responsible for the synthesis of peptidoglycan during bacterial cell wall construction. Covalent modification by β-lactams causes inactivation of the PBPs and cell wall decomposition, which eventually results in cell death. Extensive studies of the mechanism of β-lactam action, including the targets, the drug-target interaction and resistant mechanism are available.[6] The most often observed β-lactam resistance either comes from the expression of β-lactamases, which hydrolyze the β-lactam core structure and inactivate the antibiotic, or alteration of PBPs to decrease the binding affinity of the antibiotics. However, reduced membrane permeability also accounts for resistance,[7] which can be overcome by Ent-mediated delivery. The molecular weights of these antibiotics are ca. 300-400 Da, which falls into the range of proper cargo sizes for Ent-mediated delivery based on our previous results (Chapter 2)., Two compounds within this antibiotic class, ampicillin (Amp) and amoxicillin (Amx), were selected for our current study. Both of these β-lactams belong to the semisynthetic aminopenicillin family, and harbor a primary amine group (Figure 3.1). Modifications of Amp and Amx on the amine group for different applications have been reported, including conjugation to siderophores, and the results suggested that manipulation at this site does not affect their interaction with the target PBPs.[8] Therefore, the primary amine groups can be used as a synthetic handle for conjugation to Ent.

In this Chapter, the synthesis of Ent-Amp and Ent-Amx conjugates were achieved through copper(I) catalyzed azide-alkyne cycloaddition. The D-enantiomer of Ent was also incorporated in the conjugate synthesis to probe whether the Ent enantiomer will afford periplasmic delivery. The antimicrobial activity of these conjugates was evaluated against a range of bacterial species, including Gram-negative *E. coli, P. aeruginosa, K. pneumoniae* and Gram-positive *B. cereus* and *S. aureus.* The mechanism of the antimicrobial activity was investigated by testing the conjugates against mutant *E. coli* strains that either lack the components of Ent uptake machinery or express β-lactamases. A time-kill kinetic study was also performed to probe if the conjugates result in faster cell death due to Ent-mediated active delivery. Strain selectivity of the conjugates was investigated. Lastly, the possibility of Lcn2 binding to the conjugates and cytotoxicity to human cells were studied.

Experimental Section

Synthetic Reagents. Dimethylformamide (DMF) and dichloromethane (CH_2Cl_2) were obtained from a VAC solvent purification system (Vacuum Atmospheres). Anhydrous dimethyl sulfoxide (DMSO)

was purchased from Sigma-Aldrich and used as received. HPLC-grade acetonitrile (MeCN) was purchased from EMD. L-Ent **1** was synthesized according to a previously reported procedure.[9] The D-enantiomer of benzyl-protected Ent-CO_2H **2** and the benzyl-protected Ent-PEG_3-N_3 **3** were reported in Chapter 2. 11-Azido-3,6,9-trioxaundecan-1-amine was purchased from Fluka. All other chemicals and solvents were purchased from Sigma-Aldrich or Alfa Aesar in the highest available purity and used as received.

General Synthetic Materials and Methods. EMD TLC silica gel 60 F_{254} plates were used for analytical thin-layer chromatography. ^1H and ^{13}C NMR spectra were collected on a Varian 300 or 500 MHz spectrophotometer operating at ambient probe temperature (293 K) housed in the Department of Chemistry Instrumentation Facility. The ^1H and ^{13}C NMR spectra were referenced to internal standards. ^1H and ^{13}C NMR spectra are provided in Appendix 2. An Avatar FTIR instrument was used to acquire IR spectra. Optical absorption spectra were recorded on an Agilent 8453 diode array or Beckman Coulter DU800 spectrophotometer (1-cm quartz cuvettes, Starna). Semi-preparative and analytical high-performance liquid chromatography (HPLC) were performed by using an Agilent 1200 series HPLC system outfitted with an Agilent Zorbax reverse-phase C18 column (5-μm pore size, 9.4 x 250 mm) at a flow rate of 4 mL/min and a Clipeus reverse-phase C18 column (5-μm pore size, 4.6 x 250 mm; Higgins Analytical, Inc.) at a flow rate of 1 mL/min, respectively. The multi-wavelength detector was set to read the absorbance at 220, 280, and 316 (catecholate absorption) nm. Preparative HPLC was performed by using an Agilent PrepStar system outfitted with a Phenomenex Luna reverse-phase C18 column (10-μm pore size, 21.2 x 250 mm) at a flow rate of 10 mL/min. Absorbance at 220 and 280 nm was monitored for preparative HPLC. For all HPLC, solvent A was 0.1% TFA/H_2O (or 0.05% TFA/H_2O for the Ent-Amx/Amp conjugates) and solvent B was 0.1% TFA/MeCN (or 0.05% TFA/MeCN for the Ent-Amx/Amp conjugates). Each HPLC method began with a five-minute equilibration at the %B used at the start of the gradient followed by a gradient of increasing %B. The HPLC solvents were prepared with HPLC-grade MeCN and TFA, and Milli-Q water (18.2 $m\Omega cm^{-1}$), and filtered through a 0.2-μm filter before use. For analytical HPLC performed to evaluate conjugate purity, the entire portion of each HPLC-purified compound was dissolved in a mixture of 1:1 MeCN/H_2O and an aliquot was taken for HPLC analysis, and the remaining solution was subsequently frozen and lyophilized to dryness. Analytical HPLC traces of the purified compounds were generated using the gradient of 0% B for 5 min followed by 0-100% B over 30 min, 1 mL/min. High-resolution mass spectrometry was performed by using an Agilent LC-MS system comprised of an Agilent 1260 series LC system outfitted with an Agilent Poroshell 120 EC-C18 column (2.7-μm pore size) and an Agilent 6230 TOF system housing an Agilent Jetstream ESI source. For all LC-MS analyses, solvent A was 0.1% formic acid/H_2O and solvent B was 0.1% formic

acid/MeCN. The samples were analyzed using a solvent gradient of 5-95% B over 5 min with a flow rate of 0.4 mL/min.

***N1*-(2-(2-(2-(2-Azidoethoxy)ethoxy)ethoxy)ethyl)-*N3*-((3S,7S,11S)-7,11-bis(2,3-dihydroxy-benzamido)-2,6,10-trioxo-1,5,9-trioxacyclododecan-3-yl)-4,5-dihydroxy-isophthal-amide (4).** Benzyl-protected Ent-azide **3** (80 mg, 55 μmol) and pentamethyl benzene (PMB, 147 mg, 0.99 mmol) were dissolved in 5 mL of anhydrous CH_2Cl_2 to give a light yellow solution. This solution was cooled to -78 °C in an acetone/dry ice bath under N_2, and BCl_3 (660 μL of 1 M solution in CH_2Cl_2, 660 μmol) was added slowly along the flask wall. After stirring for 1.5 h, DIPEA (300 μL, 1.73 mmol) was added to the flask, followed by addition of MeOH (2 mL) to quench the reaction. The reaction was then warmed to room temperature and the solvents were removed under reduced pressure. The resulting white solid was dissolved in 5:3 MeOH/1,4-dioxane and purified by preparative HPLC (33% B for 5 min and 33-60% B over 20 min, 10 mL/min). The product eluted at 17 min and was lyophilized to yield compound **4** as white solid (13.9 mg, 28%). ^{1}H NMR (DMSO-d_6, 500 MHz), δ 3.35-3.57 (16H, m), 4.38-4.41 (3H, m), 4.63-4.69 (3H, m), 4.89-4.96 (3H, m), 6.74 (2H, dd, J = 7.5, 8.0 Hz), 6.97 (2H, d, J = 7.5 Hz), 7.35 (2H, d, J = 8.0 Hz), 7.46 (1H, s), 7.94 (1H, s), 8.33-8.35 (1H, m), 9.12 (2H, d, J = 6.0 Hz), 9.29 (1H, d, J = 6.0 Hz), 9.44 (2H, bs), 9.76 (1H, bs), 11.6 (2H, bs), 11.9 (1H, bs). ^{13}C NMR ($CDCl_3$, 125 MHz), δ 50.1, 51.5, 63.6, 69.1, 69.4, 69.8, 69.8, 69.9, 69.9, 115.3, 115.4, 115.4, 117.7, 118.5, 118.7, 119.4, 125.2, 145.9, 146.3, 148.7, 148.7, 150.8, 166.0, 168.4, 169.1, 169.6, 169.7. IR (KBr disk, cm^{-1}), 3389, 2954, 2928, 2868, 2111, 1754, 1645, 1589, 1535, 1460, 1384, 1329, 1266, 1176, 1132, 1074, 992, 846. HRMS (ESI): $[M+Na]^+$ *m/z* calcd., 932.2506; found, 932.2520.

***N1*-(2-(2-(2-(2-Azidoethoxy)ethoxy)ethoxy)ethyl)-4,5-bis(benzyloxy)-*N3*-((3R,7R, 11R)-7,11-bis(2,3-bis(benzyloxy)benzamido)-2,6,10-trioxo-1,5,9-trioxacyclo-dodecan-3-yl) iso-phthalamide (5).** 11-Azido-3,6,9-trioxaundecan-1-amine (36.4 μL, 0.186 mmol) and D-Bn_6Ent-COOH (**2**, 177 mg, 0.142 mmol) were dissolved in 5 mL of dry CH_2Cl_2. PyAOP (147 mg, 283 μmol) and DIPEA (98.5 μL, 0.568 mmol) were added to give a light yellow solution. The reaction was stirred for 4 h at rt and concentrated, and the crude product was purified by preparative TLC (50% EtOAc/CH_2Cl_2) to afford **5** as a white foam (159 mg, 77%). TLC R_f = 0.6 (10% MeOH/CH_2Cl_2). ^{1}H NMR (DMSO-d_6, 500 MHz), δ 3.33 (2H, J = 5.2 Hz), 3.62-3.69 (14H, m), 4.02-4.06 (3H, m), 4.15-4.18 (3H, m), 4.91-4.94 (3H, m), 5.04-5.21 (12H, m), 6.96 (1H, s), 7.11-7.45 (36H, m), 7.65-7.67 (2H, m), 7.85-7.85 (1H, m), 7.97-7.97 (1H, m), 8.50-8.54 (3H, m). ^{13}C NMR ($CDCl_3$, 125 MHz), δ 39.9, 50.5, 51.3, 51.4, 63.9, 64.1, 69.6, 69.8, 70.2, 70.5, 70.5, 71.1, 71.2, 76.2, 76.3, 116.7, 117.5, 120.3, 123.0, 124.2, 125.4, 126.1, 126.2, 1276, 127.6, 127.8, 128.1, 128.3, 128.4, 128.4, 128.4, 128.5, 128.5, 128.6, 128.7, 128.8, 128.8, 129.0, 130.2, 135.4, 135.7, 135.9, 135.9,

136.1, 146.8, 146.8, 149.0, 151.5, 151.8, 164.1, 164.8, 164.9, 165.8, 168.9 169.0, 169.0. IR (neat, cm^{-1}), 3357, 3062, 3032, 2958, 2923, 2859, 2104, 1751, 1551, 1576, 1515, 1455, 1375, 1345, 1299, 1264, 1204, 1126, 1082, 1040, 1018, 957, 915, 854, 811. HRMS (ESI): $[M+H]^+$ *m/z* calcd., 1476.5323; found, 1476.5318.

***N*1-(2-(2-(2-(2-Azidoethoxy)ethoxy)ethoxy)ethyl)-*N*3-((3R,7R,11R)-7,11-bis(2,3-dihydroxybenzamido)-2,6,10-trioxo-1,5,9-trioxacyclododecan-3-yl)-4,5-dihydroxyiso-phthal-amide (6).** Compound **6** was synthesized from **5** (153 mg, 105 μmol) following the same procedure as for compound **4**. The crude reaction was purified by preparative HPLC (33% B for 5 min and 33-60% B over 20 min, 10 mL/min). The product eluted at 17.0 min and was lyophilized to yield compound **6** as white solid (31 mg, 33%). The analytical HPLC trace of the purified product is reported in Appendix 2. ^{1}H NMR ($CDCl_3$, 500 MHz), δ 3.34-3.56 (16H, m), 4.39-4.41 (3H, m), 4.61-4.66 (3H, m), 4.88-4.94 (3H, m), 6.74 (2H, dd, J = 7.8, 7.8 Hz), 6.96 (2H, d, J = 7.8 Hz), 7.33 (2H, d, J = 7.8 Hz), 7.44 (1H, s), 7.91 (1H, s), 8.31-8.33 (1H, m), 9.12-9.13 (2H, m), 9.27-9.28 (1H, m), 9.50 (2H, bs), 9.84 (1H, bs), 11.6 (2H, bs), 11.9 (1H, bs). ^{13}C NMR ($CDCl_3$, 125 MHz), δ 50.1, 51.5, 63.6, 69.1, 69.4, 69.8, 69.8, 69.9, 69.9, 115.3, 115.4, 115.4, 117.7, 118.5, 118.7, 119.4, 125.2, 145.9, 146.3, 148.7, 148.7, 150.8, 166.0, 168.4, 169.1, 169.6, 169.7. IR (KBr disk, cm^{-1}), 3390, 2958, 2925, 2863, 2110, 1754, 1645, 1589, 1535, 1460, 1384, 1342, 1262, 1176, 1117, 1074, 841, 800. HRMS (ESI): $[M+Na]^+$ *m/z* calcd., 936.2506; found, 936.2512.

(2S,5R,6R)-6-((R)-2-(Hex-5-ynamido)-2-phenylacetamido)-3,3-dimethyl-7-oxo-4-thia-1-aza-bicyclo[3.2.0]heptane-2-carboxylic acid (7). 5-Hexynoic acid (113 μL, 1.00 mmol) and thionyl chloride (1.00 mL, 13.8 mmol) were combined and refluxed for 1 h. The reaction was cooled to room temperature and concentrated under reduced pressure, and the resulting crude acetyl chloride was dissolved in acetone (0.5 mL) and carried on to the next step without purification. Ampicillin sodium salt (186 mg, 0.500 mmol) was dissolved in a solution of $NaHCO_3$ (210 mg, 2.5 mmol) in 4:1 water/acetone (2.5 mL) and cooled on ice, to which the acetyl chloride was added slowly with stirring. The reaction was subsequently warmed to room temperature and stirred for 1 h. Water (3 mL) was added to the reaction and the aqueous phase was washed with EtOAc (2 x 10 mL), acidified to pH 2 by addition of HCl, and extracted with EtOAc (20 mL). The resulting organic phase was washed with cold water (2 x 5 mL), dried over Na_2SO_4, and concentrated under reduced pressure. The crude reaction was triturated with hexanes, which afforded a yellow solid (180 mg, 77%). This solid was used in the following steps without further purification. TLC R_f = 0.1 (10% MeOH/CH_2Cl_2). ^{1}H NMR (DMSO-d_6, 500 MHz), δ 1.41 (3H, s), 1.55 (3H, s), 1.64-1.69 (2H, m), 2.13-2.16 (2H, m), 2.29-2.32 (2H, m), 2.77-2.78 (1H, m), 4.20 (1H, s), 5.39 (1H, d, J = 4.0 Hz), 5.52 (1H, dd, J = 4.0, 8.0 Hz), 5.70 (1H, d, J = 8.0 Hz), 7.25-7.43 (5H, m), 8.57 (1H, d, J = 8.0 Hz),

9.11 (1H, d, J = 8.0 Hz). ^{13}C NMR (DMSO-d_6, 125 MHz), δ 17.4, 24.4, 26.6, 30.4, 33.8, 55.5, 58.1, 63.7, 67.3, 70.3, 71.5, 84.2, 127.2, 127.6, 128.2, 138.2, 169.0, 170.2, 171.5, 173.5. IR (KBr disk, cm^{-1}), 3297, 3058, 3023, 2970, 2937, 2863, 2626, 2526, 2120, 1780, 1688, 1518,1455, 1437, 1390, 1373, 1324, 1295, 1208, 1139, 1027, 1001, 843. HRMS (ESI): $[M+H]^+$ m/z calcd., 444.1588; found, 444.1585.

(2S,5R,6R)-6-((R)-2-(Hex-5-ynamido)-2-(4-hydroxyphenyl)acetamido)-3,3-dimethyl-7-oxo-4-thia-1-azabicyclo[3.2.0]heptane-2-carboxylic acid (8). Compound **8** was synthesized as described for compound **7** except that amoxicillin (760 mg, 2.08 mmol) was used instead of ampicillin sodium salt. Compound **8** was obtained as light yellow solid (533 mg, 56%) after trituration and employed without further purification. TLC R_f = 0.1 (10% MeOH/CH_2Cl_2). ^{1}H NMR (DMSO-d_6, 500 MHz), δ 1.42 (3H, s), 1.56 (3H, s), 1.63-1.68 (2H, m), 2.12-2.15 (2H, m), 2.25-2.29 (2H, m), 2.76-2.78 (1H, m), 4.19 (1H, s), 5.39 (1H, d, J = 4.0 Hz), 5.51-5.54 (2H, m), 6.69 (2H, d, J = 8.5 Hz), 7.19 (2H, d, J = 8.5 Hz), 8.41 (1H, d, J = 8.0 Hz), 8.93 (1H, d, J = 8.0 Hz), 9.40 (1H, bs). ^{13}C NMR (DMSO-d_6, 125 MHz), δ 17.6, 24.5, 26.8, 30.4, 34.0, 55.4, 58.2, 63.9, 71.6, 71.7, 84.4, 115.1, 128.4, 128.7, 128.8, 157.0, 169.2, 170.9, 171.7, 173.8. IR (KBr disk, cm^{-1}), 3356, 3294, 3045, 2970, 2928, 1770, 1738, 1650, 1615, 1515, 1457, 1373, 1208, 1009, 945, 839, 815. HRMS (ESI): $[M+Na]^+$ m/z calcd., 460.1537; found, 460.1534.

(4S)-2-(((R)-2-(hex-5-ynamido)-2-phenylacetamido)methyl)-5,5-dimethylthiazolidine-4-carboxylic acid (9). Compound **7** (60 mg, 0.13 mmol) was dissolved in 1:1 H_2O/MeCN (5 mL) and TFA was added to a final concentration of 1%. The solution was incubated at 37 °C for 24 h and purified by preparative HPLC (20-50% B over 25 min, 10mL/min), which afforded a white powder (12 mg, 25%). The white powder is a diastereomeric mixture of products and no further separation was performed. ^{1}H NMR (DMSO-d_6, 500 MHz), δ (mixture of two diastereomers) 1.22-1.23 (3H, pair of s), 1.54-1.58 (3H, pair of s), 1.62-1.68 (2H, m), 2.12-2.14 (2H, m), 2.28-2.30 (2H, m), 2.77 (1H, s), 3.18-3.24 (0.5H, m), 3.30-3.36 (0.5H, m), 3.44-3.49 (0.5H, m), 3.55-3.60 (0.5H, m), 3.92 (0.5H, s), 4.01 (0.5H, s), 4.67 (0.5H, dd, J = 6.7, 6.5 Hz), 4.78 (0.5H, dd, J = 5.2, 5.2 Hz), 5.45-5.48 (1H, m), 7.27-7.40 (5H, m), 8.50-8.61 (2H, m). ^{13}C NMR (DMSO-d_6, 125 MHz), δ (mixture of two diastereomers) 18.1, 25.0, 27.6, 28.1, 28.4, 29.5, 34.4, 42.2, 56.8, 56.8, 72.1, 72.2, 84.8, 127.9, 128.2, 128.9, 139.2, 139.4, 171.2, 171.4, 172.0. IR (KBr disk, cm^{-1}), 3297, 3071, 3041, 2967, 2938, 2535, 2124, 1734, 1653, 1527, 1456, 1427, 1375, 1299, 1199, 1137, 1070, 1027, 836. HRMS (ESI): $[M+Na]^+$ m/z calcd., 440.1614; found, 440.1626.

(4S)-2-(((R)-2-(hex-5-ynamido)-2-(4-hydroxyphenyl)acetamido)methyl)-5,5-dime-thylthiazolidine-4-carboxylic acid (10). Compound **10** was synthesized as described for compound **9** except that compound **8** was used instead of **7** (60 mg, 0.13 mmol). The product was purified by

preparative HPLC (20-50% B over 25 min, 10mL/min), and obtained as white powder (14.5 mg, 24%). ^{1}H NMR (DMSO-d_6, 500 MHz), δ (mixture of two diastereomers) 1.26 (3H, s), 1.55-1.59 (3H, pair of s), 1.61-1.67 (2H, m), 2.12-2.14 (2H, m), 2.24-2.27 (2H, m), 2.77 (1H, s), 3.20-3.26 (0.5H, m), 3.34-3.39 (0.5H, m), 3.42-3.47 (0.5H, m), 3.56-3.60 (0.5H, m), 4.03 (0.5H, s), 4.12 (0.5H, s), 4.68 (0.5H, dd, J = 6.5, 6.5 Hz), 4.79 (0.5H, dd, J = 5.5, 5.5 Hz), 5.28-5.31 (1H, m), 6.69 (2H, d, J = 8.5 Hz), 7.17 (2H, d, J = 8.5 Hz), 8.36-8.50 (3H, m). ^{13}C NMR (DMSO-d_6, 125 MHz), δ (mixture of two diastereomers) 17.5, 24.3, 26.9, 27.5, 27.7, 28.8, 33.8, 41.4, 55.7, 55.8, 71.4, 71.6, 84.2, 114.8, 115.0, 128.5, 128.7, 128.8, 156.9, 158.3, 158.6, 171.2, 171.3. IR (KBr disk, cm^{-1}), 3301, 3071, 3028, 2973, 2928, 2548, 2111, 1737, 1662, 1606, 1593, 1515, 1435, 1377, 1197, 1139, 837. HRMS (ESI): $[M+Na]^+$ *m/z* calcd., 456.1564; found, 456.1569.

Ent-Amp (11). Ampicillin-alkyne **7** (120 µL of an 80-mM solution in DMSO, 9.6 µmol) and Ent-PEG$_3$-N$_3$ (**4**, 250 µL of a 13-mM solution in 1,4-dioxane, 3.25 µmol) were combined and 400 µL of DMSO was added. $CuSO_4$ (100 µL of a 90-mM solution in water, 9.0 µmol) and tris[(1-benzyl-1*H*-1,2,3-triazol-4-yl)methyl]amine (TBTA, 200 µL of a 50-mM solution in DMSO, 10 µmol) were combined and 100 µL of DMSO was added to give a blue-green solution, to which NaAsc (400 µL of a 90-mM solution in water, 36.0 µmol) was added. This solution became light yellow and was immediately added to the alkyne/azide solution. The reaction was shaken on a bench-top rotator for 2 h at room temperature and purified by semi-preparative HPLC (20% B for 5 min and 20%-50% B over 11 min, 4 mL/min; 0.005% TFA was used in the solvent system to prevent decomposition of the β-lactam). The HPLC fractions containing **11** were collected manually and flash frozen in liquid N_2 immediately after collection to prevent β-lactam decomposition. The product was obtained as white powder (3.3 mg, 76%). The analytical HPLC trace of the purified product is reported in Appendix 2. ^{1}H NMR (DMSO-d_6, 500 MHz), δ 1.40 (3H, s), 1.54 (3H, s), 1.78-1.81 (2H, m), 2.27 (2H, t, J = 6.8 Hz), 2.58 (2H, t, J = 6.5 Hz), 3.48 (12H, m), 3.76 (2H, s), 4.19 (1H, s), 4.38-4.44 (5H, m), 4.64-4.66 (3H, m), 4.91-4.92 (3H, m), 5.39 (1H, d, J = 3.5 Hz), 5.51-5.52 (1H, m), 5.72 (1H, d, J = 7.5 Hz), 6.74 (2H, dd, J = 7.8, 7.8 Hz), 6.96 (2H, d, J = 7.5 Hz), 7.26-7.35 (5H, m), 7.42-7.45 (3H, m), 7.81 (1H, s), 7.92 (1H, s), 8.33 (1H, s), 8.55 (1H, d, J = 7.5 Hz), 9.12 (3H, d, J = 7.0 Hz), 9.29 (1H, d, J = 6.5 Hz), 9.42 (2H, bs), 9.74 (1H, s), 11.6 (2H, s), 11.9 (1H, bs), 13.35 (1H, bs). HRMS (ESI): $[M+Na]^+$ *m/z* calcd., 1379.4021; found, 1379.4046.

Ent-Amx (12). Compound **12** was synthesized as describe for **11** except that compound **8** was used instead of compound **7**. The product was obtained as white powder (2.9 mg, 66%). The analytical HPLC trace of the purified product is reported in Appendix 2. ^{1}H NMR (DMSO-d_6, 500 MHz), δ 1.40 (3H, s), 1.54 (3H, s), 1.78-1.80 (2H, m), 2.23 (2H, t, J = 6.5 Hz), 2.57 (2H, t, J = 6.5 Hz), 3.47 (12H, m),

3.76 (2H, bs), 4.18 (1H, s), 4.39-4.43 (5H, m), 4.63-4.65 (3H, m), 4.90 (3H, bs), 5.38 (1H, s), 5.52-5.56 (2H, m), 6.68 (2H, d, J = 8.5 Hz), 6.73 (2H, dd, J = 7.8, 7.8 Hz), 6.96 (2H, d, J = 7.5), 7.19 (2H, d, J = 8.5 Hz), 7.33 (2H, d, J = 7.5 Hz), 7.44 (1H, s), 7.80 (1H, s), 7.92 (1H, s), 8.33-8.39 (2H, m), 8.94 (1H, d, J = 8.0 Hz), 9.11-9.12 (2H, m), 9.29 (1H, bs), 9.38-9.43 (3H, m), 9.75 (1H, s), 11.6 (2H, bs), 11.9 (1H, bs). HRMS (ESI): $[M+Na]^+$ *m/z* calcd., 1395.3970; found, 1395.3982.

D-Ent-Amp (13). Compound **13** was synthesized as described for **11** except that compound **6** was used instead of compound **4**. The product was obtained as white powder (1.6 mg, 36%). The analytical HPLC trace of the purified product is reported in Appendix 2. HRMS (ESI): $[M+Na]^+$ *m/z* calcd., 1379.4021; found, 1379.4022.

D-Ent-Amx (14). Compound **14** was synthesized as described for **12** except that compound **6** was used instead of compound **4**. The product was obtained as white powder (2.9 mg, 66%). The analytical HPLC trace of the purified product is reported in Appendix 2. HRMS (ESI): $[M+Na]^+$ *m/z* calcd., 1395.3970; found, 1395.3995.

Ent-Hydro-Amp (15). Compound **15** was synthesized as described for **11** except that compound **9** was used instead of compound **7**. The product was obtained as white powder (1.8 mg, 21%). The analytical HPLC trace of the purified product is reported in Appendix 2. HRMS (ESI): $[M+H]^+$ *m/z* calcd., 1331.4409; found, 1331.4389.

Ent-Hydro-Amx (16). Compound **16** was synthesized as described for **12** except that compound **10** was used instead of compound **8**. The product was obtained as white powder (1.5 mg, 17%). The analytical HPLC trace of the purified product is reported in Appendix 2. HRMS (ESI): $[M+Na]^+$ *m/z* calcd., 1369.4177; found, 1369.4191.

General Microbiology Materials and Methods. Information pertaining to all bacterial strains used in this study is listed in Table 3.1. Freezer stocks of all *Escherichia coli*, *Klebsiella pneumoniae*, *Bacillus cereus* and *Staphylococcus aureus* strains were prepared from single colonies in 25% glycerol/Luria Broth (LB) medium. Freezer stocks of *Pseudomonas aeruginosa* strains were prepared from single colonies in 7.5% DMSO/LB base medium supplemented with 2.5 g/L NaCl. Luria Broth (tryptone 10 g/L, yeast extract 5 g/L, NaCl 10 g/L), Luria Broth base (pancreatic digest of casein 10 g/L, yeast extract 5 g/L, NaCl 0.5 g/L), M9 minimal media (Na_2HPO_4 6.8 g/L, KH_2PO_4 3 g/L, NaCl 0.5 g/L, NH_4Cl 1 g/L, 0.4% glucose, 2 mM $MgSO_4$, 0.1 mM $CaCl_2$) and agar were purchased from BD. Mueller

Hinton Broth (MHB, beef extract powder 2.0 g/L, acid digest of casein 17.5 g/L, soluble starch 1.5 g/L) was purchased from Fluka. MHB purchased from Bacto afforded similar bacterial growth for *E. coli* K-12 and CFT073 cultured in both the absence and presence of 2,2'-dipyridyl and thus was not used in the current study. CHROM-UTI plates were purchased from Hardy Diagnostics (Santa Maria, CA). Recombinant human lipocalin-2 was purchased from R&D System (Minneapolis, MN). The iron chelator 2,2'-dipyridyl (DP) was purchased from Sigma-Aldrich. All growth media and Milli-Q water used for bacterial cultures or for preparing solutions of the enterobactin-antibiotic conjugates were sterilized by using an autoclave. A DP stock solution (200 mM) was prepared in DMSO and used in the bacteria growth assays requiring iron-dependent conditions. All enterobactin-antibiotic conjugates and Ent were stored as DMSO stock solutions at -20 °C. The stock solution concentrations were determined by using the reported extinction coefficient for enterobactin in MeOH (316 nm, 9,500 $M^{-1}cm^{-1}$).[10] Working dilutions of the Ent conjugates and Ent were prepared in 10% DMSO/H_2O. For all assays, the final cultures contained 1% v/v DMSO. Sterile polypropylene culture tubes and sterile polystyrene 96-well plates used for culturing were purchased from VWR and Corning Incorporated, respectively. The optical density at 600 nm (OD_{600}) values were recorded on a Beckman Coulter DU800 spectrophotometer or by using a BioTek Synergy HT plate reader.

General Procedure for Antimicrobial Activity Assays. Overnight cultures of the bacterial strains were prepared by inoculating 5 mL of LB with the appropriate freezer stock and the cultures were incubated at 37 °C in a tabletop incubator shaker set at 150 rpm. The overnight culture grew to saturation in 16-19 h and was diluted 1:100 into 5 mL of fresh LB media containing 200 μM DP and incubated at 37 °C with shaking at 150 rpm until OD_{600} reached 0.6. The cultures were subsequently diluted to an OD_{600} value of 0.001 in 50% reduced MHB medium (10.5 g/L) with or without 200 μM DP. A 90-μL aliquot of the diluted culture was combined with a 10-μL aliquot of a 10x solution of the antibiotic or Ent-antibiotic conjugate in a 96-well plate, which was wrapped in parafilm and incubated at 30 °C with shaking at 150 rpm for 19 h in a tabletop incubator housing a beaker of water to maintain the humidity in the incubator. Bacterial growth was determined by measuring OD_{600} using a BioTek Synergy HT plate reader at the endpoint. Each well condition was prepared in duplicate and at least three independent replicates using two different synthetic batches of each conjugate were conducted on different days. A 10-fold dilution series were employed to determine the minimal inhibitory concentration (MIC) values. The resulting mean OD_{600} are reported and the error bars are the standard error of the mean obtained from the independent replicates.

Antimicrobial Assays with β-lactamase Inhibitors. These assays were performed with *E. coli* ATCC 35218 and *K. pneumoniae* ATCC 13883 following the general procedure except that sulbactam (SB) or potassium clavulanate (PC) were mixed with ampcillin or amoxicillin and Ent-Amp or Ent-Amx, respectively. The molar ratios of the mixtures are: sulbactam/Amp or Ent-Amp, 1.5:1; potassium clavulanate/Amx or Ent-Amx, 0.9:1. These ratios were taken from the recipe of commercial drug combinations.[11] Sulbactam and potassium clavulanate were stored as DMSO solutions at -20 °C.

Antimicrobial Assays in the Presence of Exogenous Ent. These assays were performed with *E. coli* K-12 and CFT073 following the general procedure except that varying concentrations (1-100 μM) of synthetic L-Ent were mixed with Ent-Amp/Amx.

Killing Kinetic Assays. A 5 mL-overnight culture of *E. coli* K-12 or CFT073 grown in LB was diluted 1:100 into 5 mL of fresh LB media with 200 μM DP and incubated at 37 °C with shaking at 150 rpm until OD_{600} reached ~0.3. The culture was centrifuged (3000 rpm x 10 min, rt) and the resulting pellet was resuspended 50% MHB and centrifuged two times. The resulting pellet was resuspended in 50% MHB with or without DP and the OD_{600} was adjusted to 0.3. A 90-μL aliquot of the resulting culture was mixed with a 10-μL aliquot of a 10x solution of the β-lactam or Ent-β-lactam conjugate in a 96-well plate, which was wrapped in parafilm and incubated at 37 °C with shaking at 150 rpm. The OD_{600} values were recorded by using a plate reader at t = 0, 1, 2, 3 h. In a parallel experiment, a 10-μL aliquot of the culture was taken at t = 0, 1, 2, 3 h and serially diluted by using sterile phosphate-buffered saline (PBS) and plated on LB-Agar to obtain colony forming units (CFU/mL). Each well condition was repeated at least three times independently on different days. The resulting mean OD_{600} or CFU/mL is reported and the error bars are the standard error of the mean.

Mixed-Species Assays. A 5-mL overnight culture of tested bacterial strain grown in LB was diluted 1:100 into 5 mL of fresh LB media with 200 μM DP and incubated at 37 °C with shaking at 150 rpm until OD_{600} reached 0.6. The cultures were diluted to 10^6 CFU/mL in 50% MHB separately or in a 1:1 mixture (10^6 CFU/mL for each strain), with or without 200 μM DP. These cultures were serially diluted by using sterile PBS and aliquots were plated on a CHROM-UTI plate as the 'starter culture plate' to confirm the CFU of the starter culture. A 90-μL aliquot of these cultures was combined with a 10-μL aliquot of a 10-μM solution of the antibiotic or Ent-antibiotic conjugate in a 96-well plate, which was wrapped in parafilm and incubated at 30 °C with shaking at 150 rpm for 19 h. Bacterial growth was assayed both by measuring OD_{600} using the plate reader and by plating on CHROM-UTI plates after serial dilution as the 'assay plate'. Each well condition was repeated at least three times independently on

different days. The resulting mean OD_{600} is reported and the error bars are the standard error of the mean. Images of representative plates are presented.

Antimicrobial Activity Assays in the Presence of Lipocalin 2. This assay is based on a published protocol[12] and was conducted with *E. coli* CFT073. Overnight cultures of *E. coli* CFT073 were grown in M9 minimal medium. Each overnight culture was serially diluted into M9 minimal medium to provide 10^3-10^4 CFU/mL. Lipocalin 2 was diluted in PBS from a concentration of ~110 μM to 10 μM upon arrival, aliquoted, and stored at -20 °C until use. A 90-μL aliquot of the diluted culture was added to well of a 96-well plate that contained varying concentrations of lipocalin 2, Ent-Amp, and Ent, and the final volume was adjusted to 100 μL with sterile PBS. The 96-well plate was incubated at 37 °C for 24 h in a tabletop incubator set at 150 rpm and bacterial growth was determined by measuring OD_{600} using a plate reader. Each well condition was repeated at least three times independently on different days and with different batches of lipocalin 2. The resulting mean OD_{600} is reported and the error bars are the standard error of the mean.

Cytotoxicity Assays. The human colon epithelial T84 cell line was purchased from ATCC and grown in DMEM/F12 medium with 1% penicillin and streptomycin (v/v, purchased from ATCC). The cells were grown to 70-80% confluency and passed and plated in a 96-well flat-bottom plate ~16 h before treatment. Each well contained 90 μL of the cell culture at a density of 10^5/mL. Stock solutions (10x) of Ent, Ent-Amp and Amp were prepared in sterile-filtered 10% DMSO/water and 10 μL of each solution was added to the appropriate well. The plate was incubated at 37 °C and under 5% CO_2 for 24 h at which time 20 μL of 3-[4,5-dimethylthiazol-2-yl]-2,5 diphenyl tetrazolium bromide (MTT, 5 mg/mL in sterile PBS) was added to each well. The plate was incubated at 37 °C and under 5% CO_2 for 4 h and the supernatant was removed from each well. DMSO (100 μL) was added to each well and the absorbance at 550 nm was recorded by using a plate reader. Blank readings were recorded on wells that only contained the growth medium. The assay was repeated in triplicate on different days and the mean and standard errors are reported. The effect of DMSO on cell growth was also evaluated by performing the same assay with varying DMSO concentrations and 1% DMSO had no effect on cell viability over the course of this assay.

Results and Discussion

Design and Syntheses of Enterobactin-β-lactam Conjugates. As described in Chapter 2, we developed synthetic approaches to obtain monofunctionalized enterobactin (Ent) scaffolds and Ent-cargo conjugates, and cellular uptake of the conjugates with proper cargo sizes were observed. To expand the

application of this Ent-mediated delivery strategy, we selected to incorporate the small antibiotics ampicillin (Amp) and amoxicillin (Amx) into the Ent scaffold and hypothesized that Ent-mediated active delivery of the antibiotics would result in improved antimicrobial activity.

During the initial attempts to synthesize Ent-Amp/Amx, we found that the previously developed synthetic route for the Ent-cargo conjugates presented in Chapter 2 was not suitable for these targets. The thioether present in Amp and Amx poisoned the Pd catalyst in the final step for benzyl group removal, and the two molecules themselves were not stable under hydrogenation conditions. We observed similar sulfur-related catalyst poisoning during the synthesis of Ent-biotin conjugates (data not shown). Therefore, we selected to remove the benzyl groups before attaching the β-lactams to Ent. This modification raised a new challenge for the acid-amine coupling step designed in the original synthetic routes because the unmasked catechols were found to interfere with the coupling reaction and form byproducts. Inspired by the Ent-vancomycin conjugate synthesis presented in Chapter 2, we replaced acid-amine coupling by Cu(I) catalyzed azide-alkyne cycloaddition ('click chemistry'). The triazole structure formed in this cycloaddition reaction does not affect uptake of the conjugate by the bacteria as demonstrated in Chapter 2. A PEG_3 linker was included in the design to separate the β-lactams and Ent for minimizing possible intramolecular interference of their own functions.

In our previous work, an Ent intermediate featured an azide PEG linker (**3**) was already reported (Scheme 3.1). The benzyl group was removed from compound **3** using BCl_3 at -78 °C rather than hydrogenation over Pd/C because the latter condition is not compatible with the azide group.[13] The resulting product was purified by reverse-phase preparative HPLC and obtained in 28% yield. For the β-lactam moiety, an alkyne group was installed by thionyl chloride coupling of 5-hexynoic acid to the primary amines of Amp and Amx, which afford compound **7** and **8** (Scheme 3.1). The final step for the conjugate synthesis was through 'click chemistry'. Initial attempts following the procedure used for the synthesis of Ent-vancomycin failed, probably due to copper catalyzed decomposition of the β-lactams.[14] Including the copper ligand tris[(1-benzyl-1H-1,2,3-triazol-4-yl)methyl]amine (TBTA) in the reaction mixture greatly improved the yield (Scheme 3.1).[15] The final Ent-Amx and Ent-Amp conjugates were purified by semi-preparative HPLC and obtained as white powders in yields of 66% and 76%, respectively. The synthesis was repeated to afford different batches of these conjugates, all of which were tested in the following antimicrobial assays to assure the results are independent of any given batch. It should be noted that the β-lactam moiety in the conjugates is prone to hydrolysis even when stored at -20 °C as a DMSO stock solution. After a month, ca. 10% of the conjugates were degraded to hydrolyzed derivatives judging by peak area in the analytical HPLC traces. Further decarboxylation of the hydrolyzed derivatives was also observed in LC-MS analysis. Such degradation behavior is well documented for β-lactams in physiologically relevant conditions.[16]

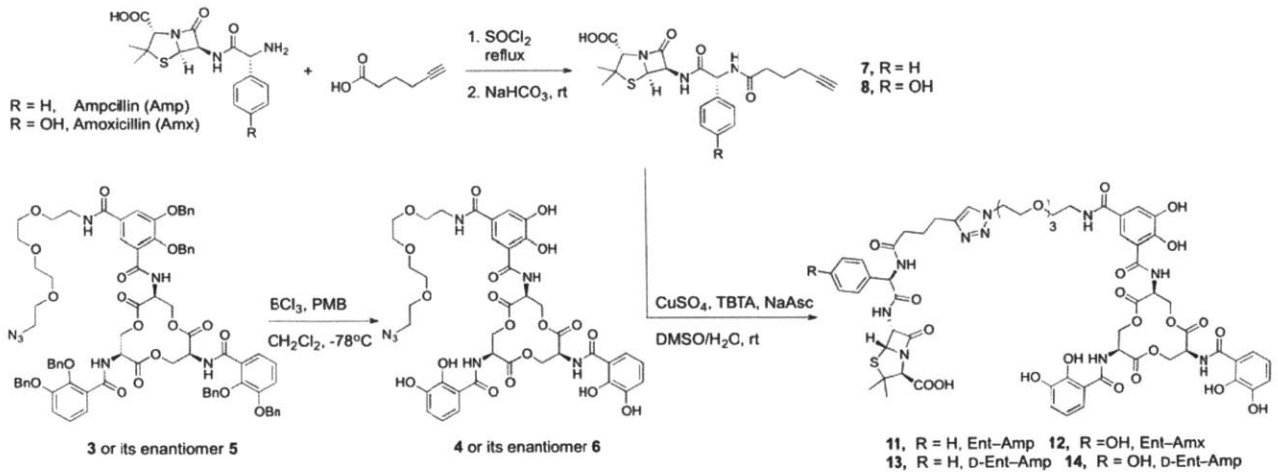

Scheme 3.1. Syntheses of Ent-β-lactam conjugates **11-14**.

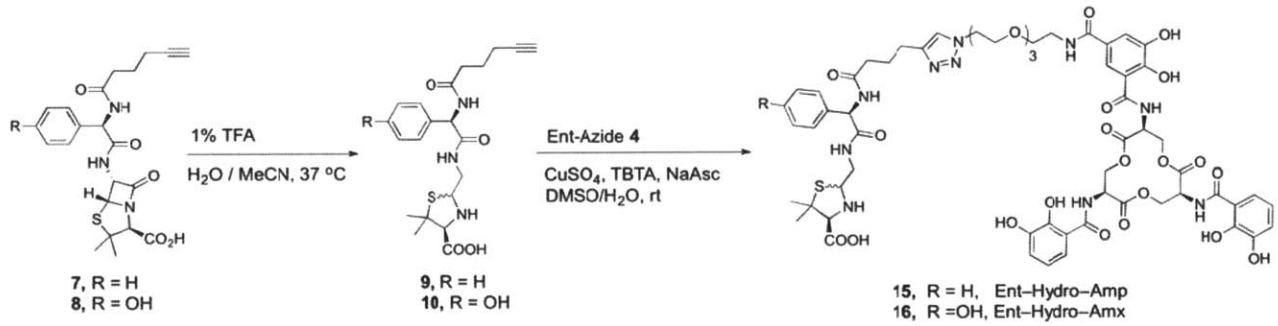

Scheme 3.2. Syntheses of hydrolyzed Ent-β-lactam conjugates **15** and **16.**

The β-lactam conjugates with D-Ent were also synthesized following the same route (Scheme 3.1). D-isomer of Ent binds Fe(III) similarly as its L-isomer and can be transported into bacterial cytosol, but it is not a substrate for the Fes esterase and cannot be used by the bacteria for iron uptake.[17] Therefore D-Ent can inhibit bacterial growth by iron-starvation (see Chapter 2). With D-Ent-β-lactam conjugates we aim to test if the enantiomer will affect the delivery of the conjugates. Moreover, two Ent-β-lactam analogs **15** and **16** featuring products of Amp and Amx degradation **9** and **10** were synthesized. These two compounds have similar structure as the Ent-β-lactam conjugates, and they should not exhibit antimicrobial activity as the β-lactam structure is perturbed. Hydrolysis of **7** and **8** in acidic conditions under elevated temperature afforded **9** and **10** as diastereomeric mixtures (Scheme 3.2). The formation of these derivatives followed reported degradation pathways for penicillin and no further degradation was observed during the course of their synthesis and purification.[16a] Compound **9** and **10** were then

conjugated to Ent via click chemistry following the same conditions for compound **11-14**. Conjugates **15** and **16** were obtained as white powder in 21% and 17% yield, respectively (Scheme 3.2). The lower yield resulted from further degradation of the β-lactam analogs under the click conditions as evidenced by HPLC traces, the reason for which is unclear. The purified **15** and **16** remained stable during the course of the experiments.

Table 3.1. Bacterial strains employed in this study.

Strain	Source	Comments
E. coli K-12	ATCC	
E. coli fepA-, fepB- feC-, fes-	Keio Collection	Single gene knock-out of E. coli K-12
E. coli 25922	ATCC	FDA strain Seattle 1946 Clinical isolate
E. coli CFT073	ATCC	Clinical isolate, uropathogenic Salmochelin production
E. coli UTI89	L. Cegelski (Stanford Univ.)	Clinical isolate, uropathogenic Salmochelin production
E. coli H9049	C. T. Walsh (HMS)	Clinical isolate
E. coli 43895	ATCC	Serotype O157:H7 Clinical isolate from raw hamburger meat implicated in hemorrhagic colitis outbreak
E. coli 35401	ATCC	Serotype O78:H11 Clinical isolate
E. coli 35218	ATCC	β-lactamase-producing strain Isolated from canine
P. aeruginosa PAO1	K. Poole (Queen's Univ.)	Renamed as K1184, wild type
K. pneumoniae 13883	ATCC	Chromosomally-encoded β-lactamase
S. aureus 25923	ATCC	Seattle 1945 Clinical isolate, standard laboratory test strain
B. cereus 14579	ATCC	

Antimicrobial Activity of Ent-Amp/Ent-Amx Against *E.coli* K12. First, we chose to test the activity of the Ent-β-lactam conjugates against *E. coli* K12. *E. coli,* like other Gram-negative bacteria, generally exhibits relatively low sensitivity to β-lactams due to the outer membrane permeability barrier.[18] At the same time, they utilize Ent as the major siderophore for iron uptake. Therefore, we expect an increase of activity from the Ent-β-lactam conjugates compared to the unmodified β-lactams under iron

limited conditions. The experimental data agreed with our hypothesis. About 100-fold decrease in MIC value was observed for Ent-Amp (**11**) and Ent-Amx (**12**) compared to the parent antibiotics when the bacteria were grown in the presence of 200 μM of 2,2'-dipyridyl (Figure 3.2B). 2,2'-Dipyridyl (DP) is an iron chelator commonly used to generate iron-deficient conditions and promote expression of siderophore transport machinery.[19] When the antimicrobial assay was performed without DP, less activity improvement was observed (Figure 3.2A), which indicates that the enhanced activity of Ent-Amx and Ent-Amp is related to the iron uptake mechanism.

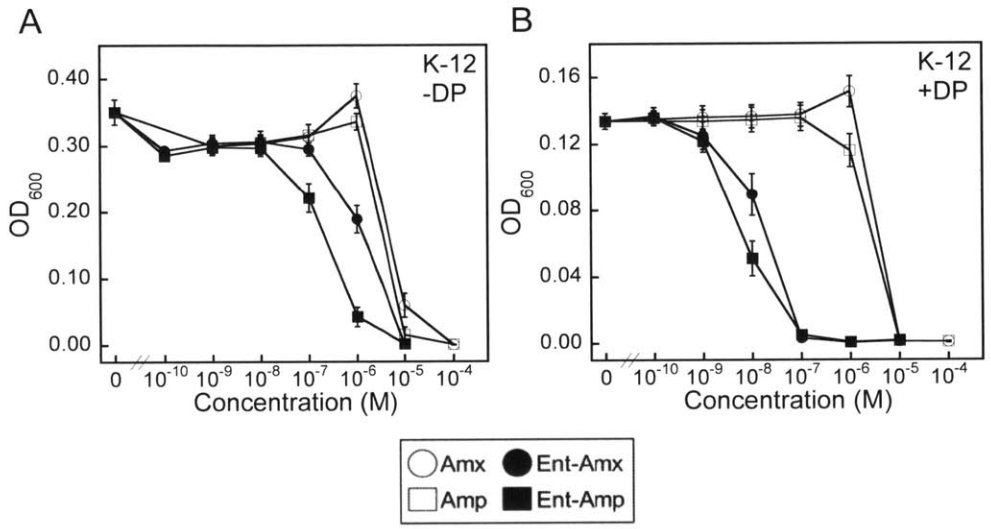

Figure 3.2. Antimicrobial activity assay of *E. coli* K12 with Ent-Amp (**11**, solid square), Ent-Amx (**12**, solid circle), Amp (hollow square) and Amx (hollow circle). The bacterial growth is represented by OD_{600} values. Error bars are the standard error of the mean for at least three independent repetitions.

To further probe the mechanism of activity enhancement observed for the conjugates, a series of single gene knock-out mutants of *E. coli* K12 were tested under the same conditions. The knock-out genes include the outer membrane receptor of Ent (*fepA*), the inner membrane transporter component (*fepC*), and the cytosol esterase of Ent (*fes*) (Figure 3.3). These three mutants lose the ability to utilize Ent for iron acquisition, but the transport is halted at different stages. In the case of the *fepA*- strain, the activity of Ent-Amx and Ent-Amp decreased to MIC of 10 μM, whereas the unmodified antibiotic exhibited the same activity as compared to wild-type (Figure 3.4A and B). This result is expected because, without FepA, the conjugates should not be able to cross the outer membrane. The growth inhibition at 10-μM concentration is most likely due to an iron starvation effect. A similar MIC was observed when this strain was treated with D-Ent and other Ent conjugates with large cargos as described in Chapter 2. ICP-OES of

the 50% MHB revealed a total iron concentration of ca. 4 μM (Table 3.2), which can be compared to 10 μM of a high-affinity extracellular iron chelator. These data confirmed that FepA is required for the enhanced antimicrobial activity observed for Ent-Amp/Amx.

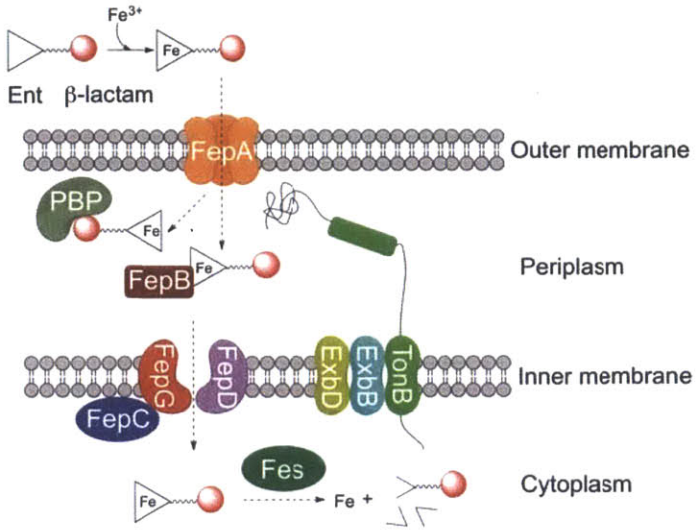

Figure 3.3. Ent uptake machinery of *E. coli* and possible fates of Ent-β-lactam conjugates.

Table 3.2. Iron content of the assay media.[a]

Media	Fe concentration (ppm)	Fe concentration (μM)
Luria Broth (LB)	0.339	6.05
	0.342	6.11
50% Mueller Hinton Broth (MHB, Fluka)	0.265	4.73
	0.173	3.09
M9 Minimal Media	n.d.[b]	n.d.[b]
	n.d.[b]	n.d.[b]

[a] ICP-OES (University of Illinois Urbana-Champaign) was used to determine the total iron content of the growth media. Two independently prepared batches of media were autoclaved as described in the main text and sent to analysis without any dilution, and both values are reported. Samples were stored at room temperature and shipped at ambient temperature. [b] The iron content is below the detection limit (n.d. = not determined).

In contrast, for the *fepC*- and *fes*- strains, the conjugates exhibited similar activity as against the wild type, which indicates that the activity enhancement benefits from increased outer membrane permeability and the downstream processing steps of Ent do not affect the activity of Ent-Amp/Amx significantly (Figure 3.4 C and D). This observation is reasonable because the PBPs are located in the periplasm in Gram-negative bacteria; as long as the conjugates cross the outer membrane through FepA,

the PBPs can interact with the β-lactam moieties on the conjugates. The lack of further enhanced activity from the *fepC*- and *fes*- strains compared to wild type also indicates that the Ent uptake machinery (i.e., FepB) was not able to compete with the PBPs for Ent-Amp/Amx. A more direct answer to this question may be achieved from testing a *fepB*- mutant, which lacks the periplasm binding protein of Ent. However, the *fepB*- mutant from the Keio collection exhibited a severe growth defect under iron-deficient conditions and we observed contradictory results from different experimental trials with either enhanced or decreased activity observed using this strain comparing to wild type. Therefore, no conclusion is drawn at this time.

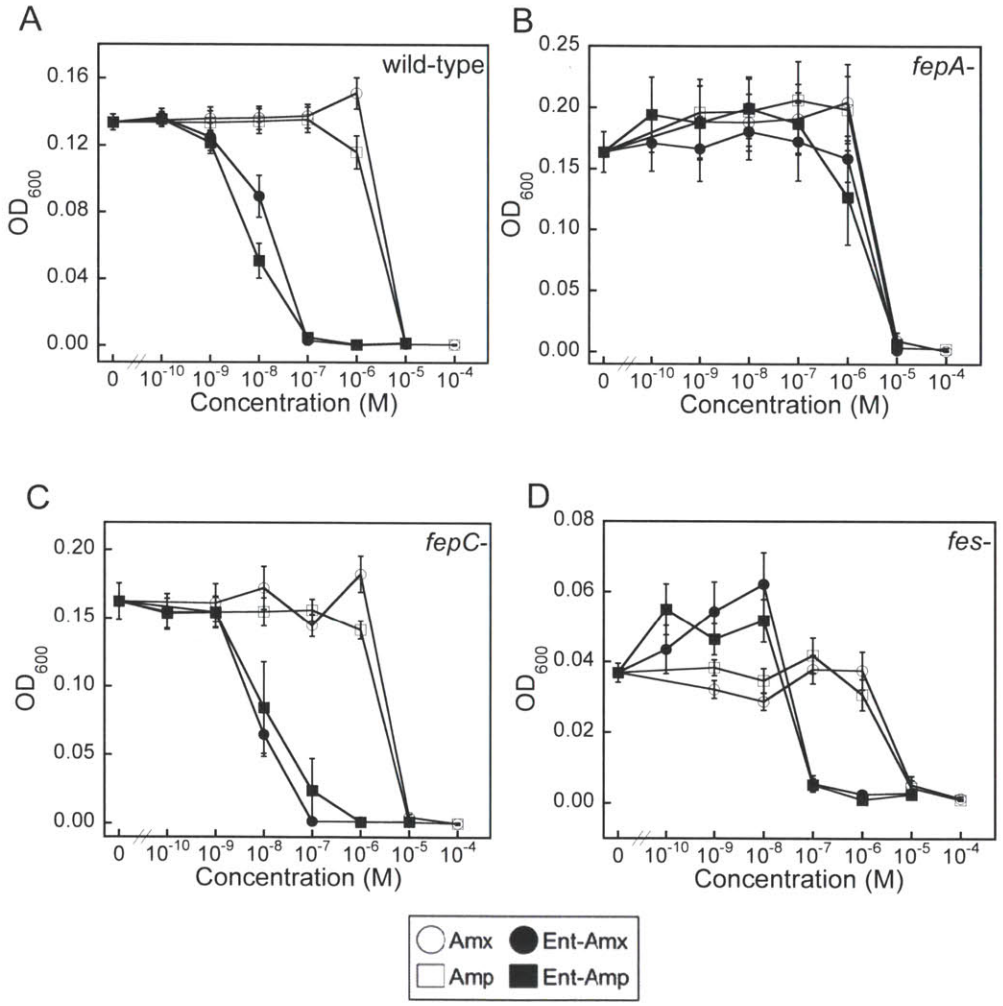

Figure 3.4. Antimicrobial activity assay of *E. coli* K12 and its mutants with Ent-Amp (solid square), Ent-Amx (solid circle), Amp (hollow square) and Amx (hollow circle). The bacterial growth is represented by OD_{600} values (data presented here are all obtained in the presence of 200 μM DP in the growth medium). Error bars are the standard error of the mean for at least three independent repetitions.

Ent-Amp/Amx and L-Ent Compete for FepA Recognition. In addition to employing mutant strains to prove the increased activity observed for the conjugates were due to Ent-mediated delivery, we designed and conducted a competition assay where a fixed concentration of the conjugates (1 μM) were added to *E. coli* K12 together with various amount of Ent. Bacterial growth was recovered when an excess amount of exogenous Ent was added to the media (Figure 3.5A), indicating an competition between the conjugates and Ent in the uptake process.

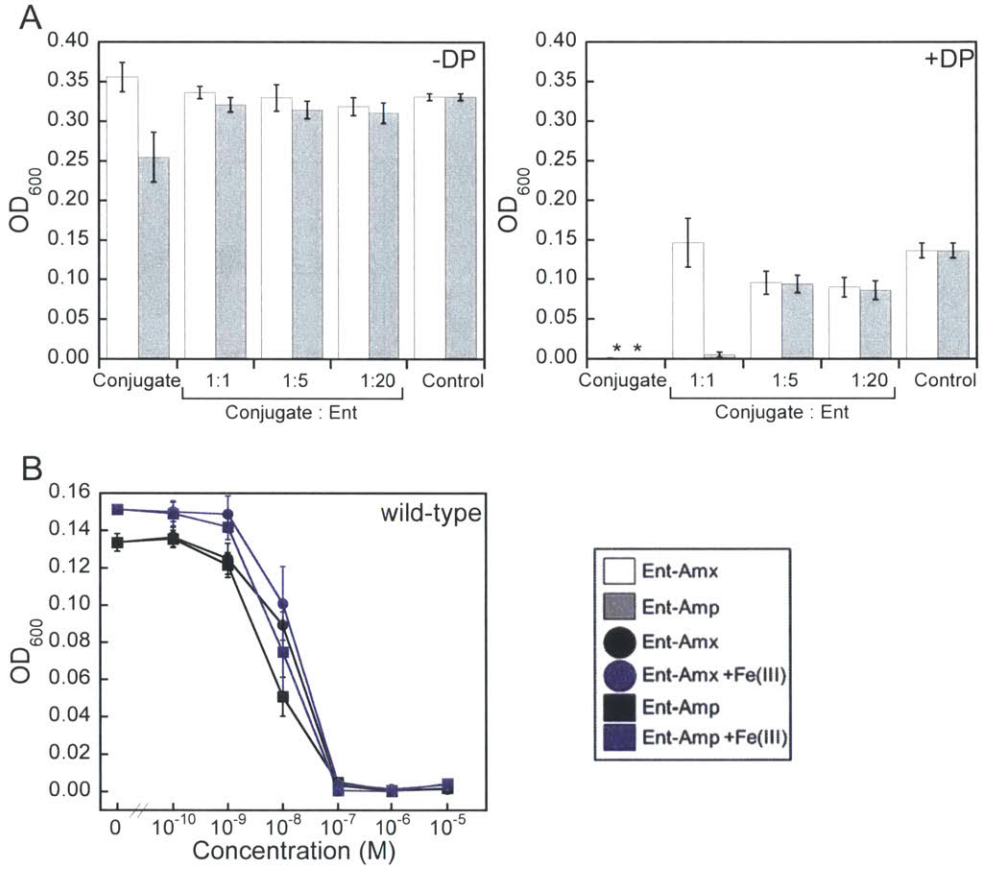

Figure 3.5. A. Competition assays of Ent-β-lactam conjugates (1 μM) and Ent (various concentrations as labeled) against *E. coli* K12. B. Antimicrobial activity of apo or Fe(III) loaded Ent-β-lactam conjugates against wild type *E. coli* K12. Error bars are the standard error of the mean for at least three independent repetitions. The "**" indicates $OD_{600} < 0.01$.

Under iron-limited conditions, the Ent-Amp conjugate requires higher Ent concentration to recover the bacteria growth (5 equiv.) comparing to Ent-Amx (1 equiv.), which may result from a more efficient delivery. Only ~75% growth recovery was observed when ≥5 equiv. of Ent was included in the

assay for both Ent-Amp and Ent-Amx. The Fe concentration in the assay media was evaluated to be ca. 4 μM (Table 3.2) and the total concentration of Ent was 5 μM and 20 μM for the 1:5 and 1:20 condition, respectively. The excess amount of Ent compared to total Fe may result in slight growth inhibition because it may prevent bacteria from accessing other forms of iron in the growth media. We also observed that pre-incubating the conjugates with 1 equiv. $FeCl_3$ gave similar antimicrobial activity as the apo conjugates (Figure 3.5B), which ruled out the possibility that the activity observed is due to nonsufficient uptake and iron starvation. These data suggest that Ent-Amp and Ent-Amx share the same uptake pathway as Ent.

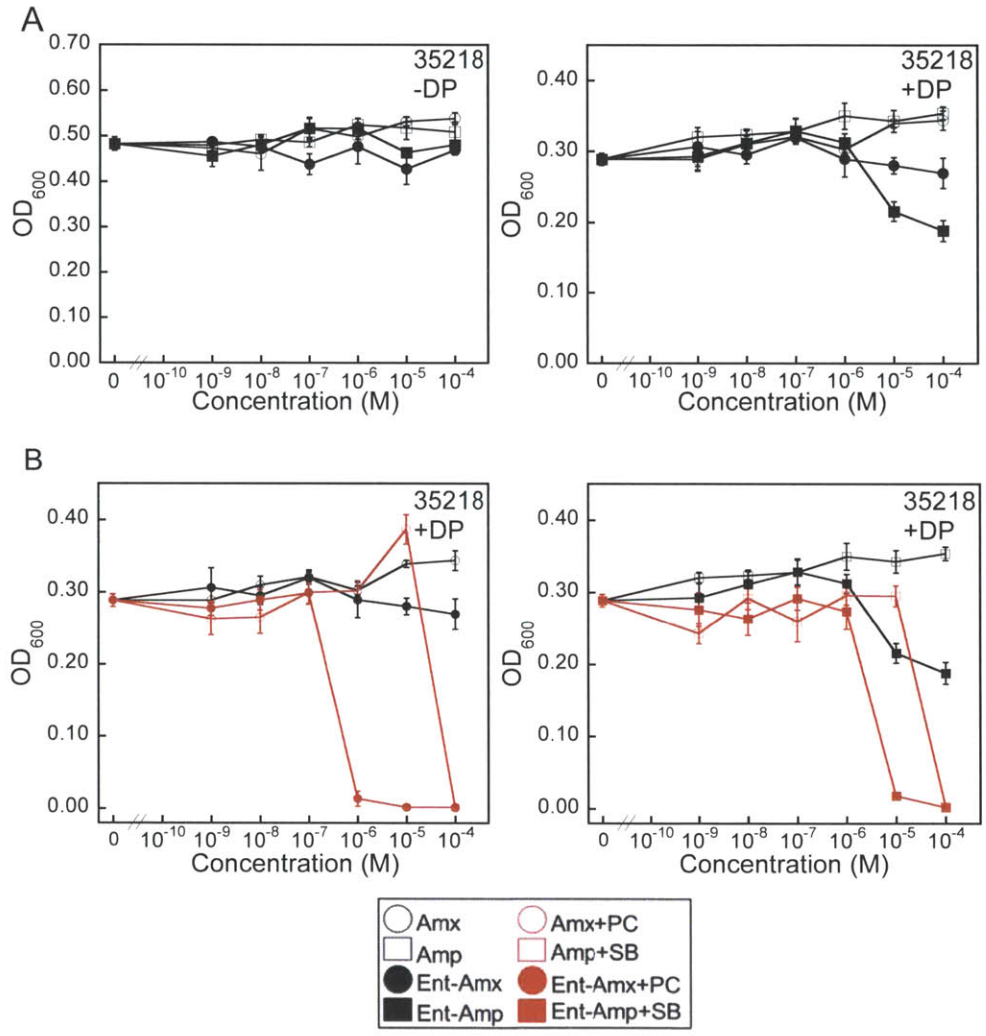

Figure 3.6. Antimicrobial activity of the Ent-β-lactam conjugates against β-lactamase expressing strain *E. coli* 35218 with (B) or without (A) β-lactamase inhibitors. Error bars are the standard error of the mean for at least three independent repetitions.

The Ent-Amp/Amx β-lactam Warhead is Essential for Antimicrobial Activity. With support for Ent-mediated delivery of Ent-Amp/Amx to the *E. coli* periplasm, we sought to confirm the essentiality of the β-lactam warheads in antibacterial action. We performed two experiments to demonstrate that the killing effect from the conjugates results from the activity of the β-lactam warhead. *E. coli* 35218 is a class A serine β-lactamase expressing strain available from ATCC.[11] When tested against this strain, both the conjugates and the β-lactams lost their activity in both iron sufficient and iron deficient conditions (Figure 3.6A). Slight growth inhibition was observed at 10 μM under conditions of iron limitation, which may be attributed to iron chelation. When β-lactamase inhibitors (sulbactam, SB or potassium clavulate, PC) were included in the assay, the activities of the conjugates as well as the unmodified antibiotics were regained, and the conjugates exhibited greater antibacterial activity than the parent antibiotics (Figure 3.6B.) It should be noted that SB itself exhibited a MIC value of 100 μM against this strain (data not shown), and the possibility of a synergistic effect from the inhibitors and conjugates cannot be ruled out completely. When the Ent-β-lactam analogs **15** and **16** which contain a hydrolyzed β-lactam analog were tested against *E. coli* K12, no antimicrobial activity could be observed (Figure 3.7). These data supported the conclusion that the β-lactam moieties are required for the antimicrobial activity observed from the conjugates and their interaction with PBPs was not affected by the Ent attachment.

All the results described above strongly suggest that the enhanced activity of the Ent-β-lactams is due to increased delivery of the β-lactams via Ent uptake machinery and inhibition of the PBPs by the β-lactam moieties. Both β-lactams and Ent retain their original function in the conjugates.

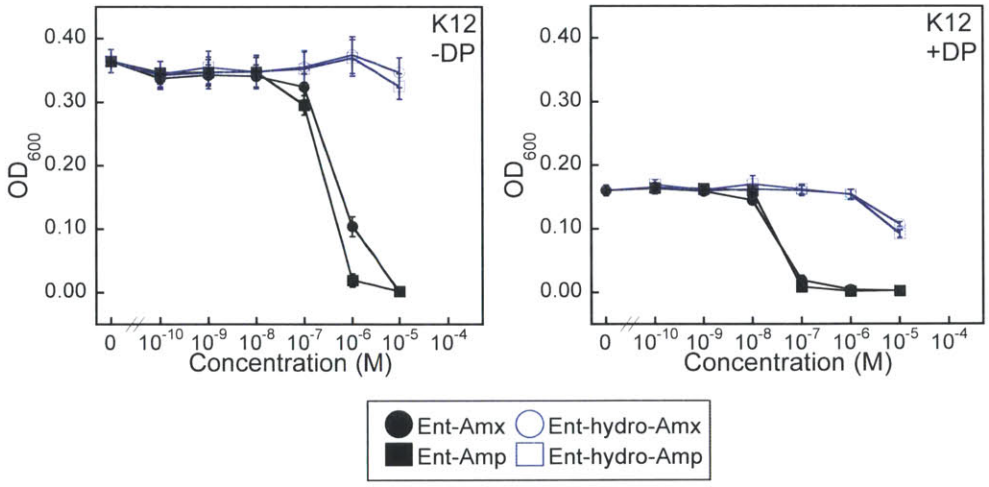

Figure 3.7. Antimicrobial activity of the Ent-Hydro-Amp/Amx (**15** and **16**) against *E. coli* K12. Error bars are the standard error of the mean for at least three independent repetitions.

Antimicrobial Activity of Ent-Amp/Ent-Amx against Clinically-relevant *E.coli* Strains. Following the activity improvement found for *E. coli* K12, we tested the conjugates against several other *E. coli* strains to see if such improvement is a general behavior against *E. coli*. We selected six clinical isolates, including urinary tract pathogenic strains CFT073 and UTI89, non-pathogenic clinical isolate strain H9049, diarrhea causing enterohemorrhagic (EHEC) strain 43895 (O157:H7) and enterotoxigenic (ETEC) strain 35401(O78:H11), and a standard antibiotic activity testing strain ATCC 25922 (Table 3.1). Among these *E. coli* strains, the genome of *E. coli* K12, CFT073, 43895 and UTI89 are available and a BLAST search revealed that besides the Ent uptake machinery, the genome of *E. coli* CFT073 and UTI89 contains the *iroA* gene cluster for salmochelin (C-glucosylated Ent derivatives) biosynthesis and uptake. *E. coli* 25922 was reported to be sensitive to lipocalin 2,[20] which indicates that its major iron acquisition pathway is through Ent and it does not produce salmochelin. The urinary tract pathogen *E. coli* CFT073 has more than one receptor for importing iron-bound Ent and its linear degradation products, including FepA and Iha.[21]

For these six *E. coli* strains, the β-lactams exhibit the same minimum inhibition concentrations (MICs), which are 10 μM, in both iron sufficient and deficient conditions. Each of the six strains responds differently to the conjugates, but with a general trend that all are more sensitive to the conjugates under iron limited conditions compared to iron sufficient conditions (10 to 100-fold decrease of MICs, Figure 3.8 and Table 3.3). This difference agrees with the Ent-mediated delivery mechanism. Ent-Amp/Amx are 100-fold more potent against *E. coli* 25922, UTI89, and H9049 than Amp/Amx under iron deficient conditions (Figure 3.8 A, B and D). Although the MIC values for *E. coli* 35401 and 43895 are only ca. 10-fold higher than Amp/Amx in this assay (Figure 3.8 E and F), a significant reduction in growth is observed at 100 nM Ent-Amp/Amx whereas this concentration of Amp/Amx affords no growth inhibition.

The lowest MICs of Ent-Amp/Amx were found for uropathogenic *E. coli* CFT073, which is more sensitive to the conjugates than to the β-lactams in both iron sufficient and deficient conditions (0.1 μM without DP, 0.01 μM with DP, Figure 3.9 A and 3.8 C). Moreover, when the Ent-hydro-Amp and Ent-hydro-Amx were tested against this strain under iron deficient condition, growth promotion was observed (Figure 3.9B). Compared to the results obtained for the hydrolyzed conjugates with *E. coli* K12 (Figure 3.7), which is slight growth inhibition at the highest concentration tested, the growth promotion implies a more efficient uptake of at least the hydrolyzed conjugates by this strain. This may explain why *E. coli* CFT073 is more sensitive than other strains. *E. coli* CFT073 expresses multiple outer membrane siderophore receptors including the salmochelin receptor IroN, which is able to transport Ent as well, and Iha, an outer membrane Ent receptor distinct from FepA. It is possible that these extra receptors also transport the conjugates and contribute to the distinct sensitivity.

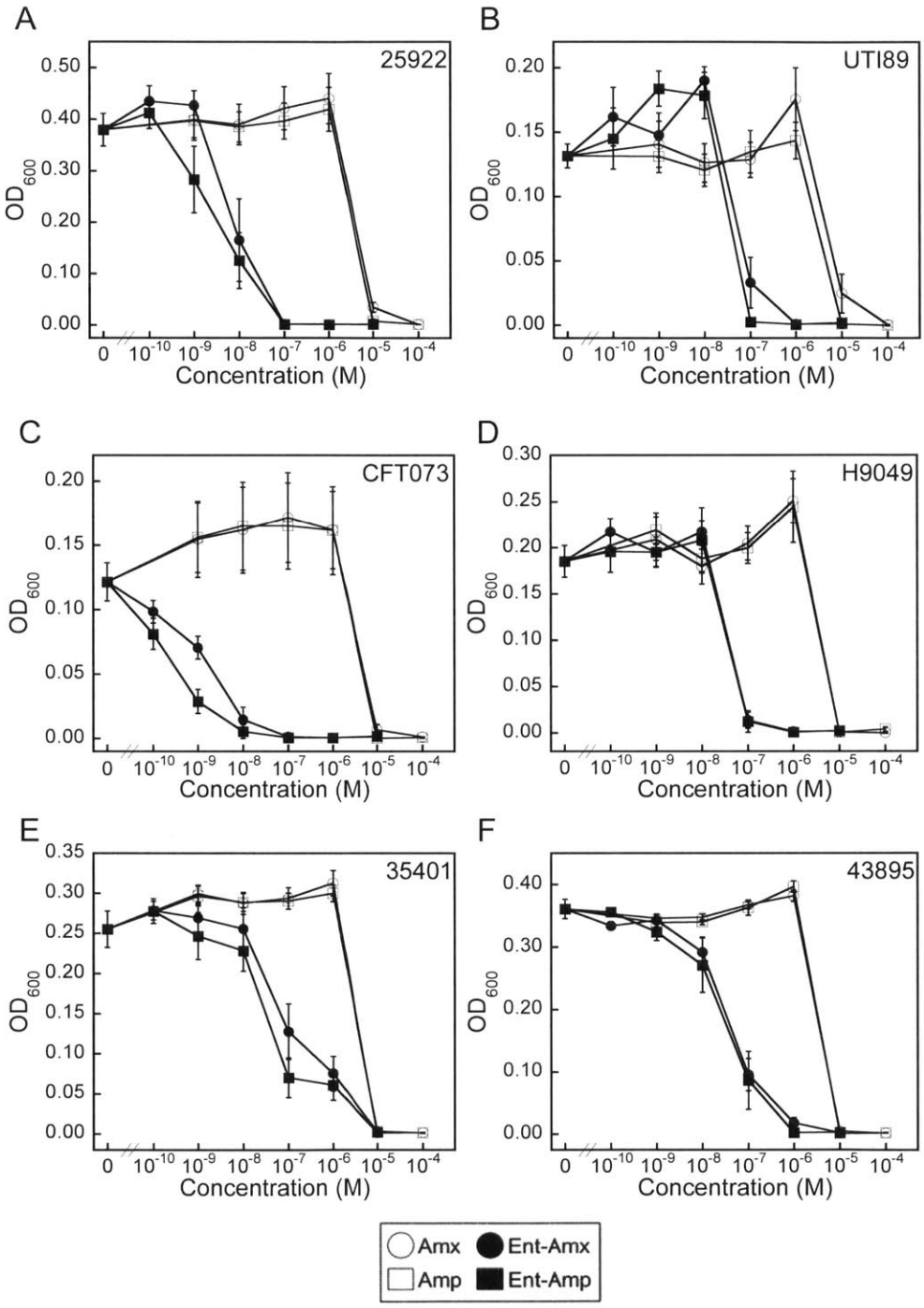

Figure 3.8. Antimicrobial activity of the Ent-β-lactam conjugates against clinical isolated *E. coli* strains in the presence of 200 μM DP. Error bars are the standard error of the mean for at least three independent repetitions.

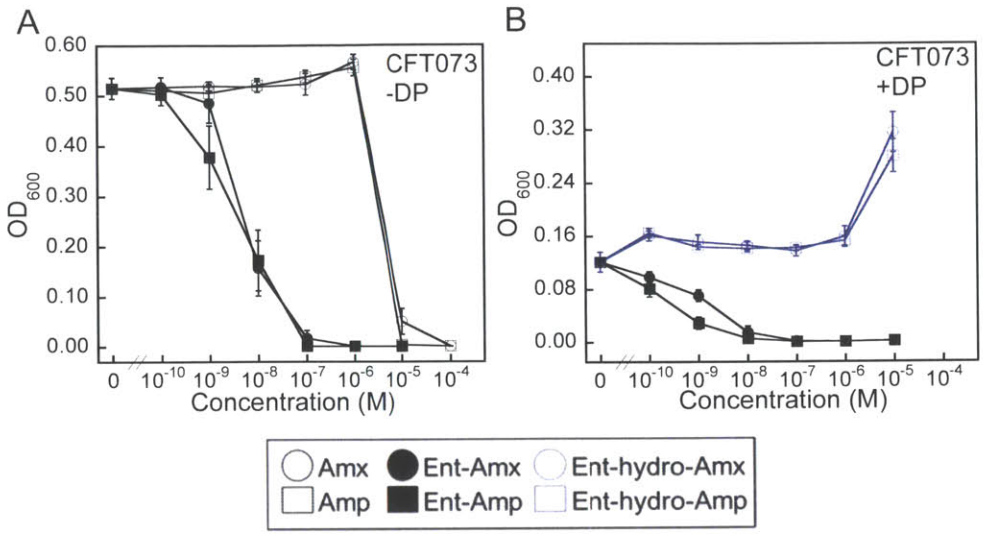

Figure 3.9. A. Antimicrobial activity of the Ent-β-lactam conjugates against *E. coli* CFT073 without DP. B. Antimicrobial activity of the Ent-β-lactam conjugates and their analogs against *E. coli* CFT073 with DP. Error bars are the standard error of the mean for at least three independent repetitions.

Table 3.3 MICs of the Ent-β-lactam conjugates. Values are reported in μM.

Strain Name	Ent-Amp		Ent-Amx		Amp		Amx		Ent-hydro-Amp		Ent-hydro-Amx		D-Ent Amp		D-Ent-Amx	
	-[a]	+[b]	-	+	-	+	-	+	-	+	-	+	-	+	-	+
E. coli K12	10	0.1	10	0.1	10	10	10	10	>10	>10	>10	>10	10	1	10	1
E. coli fepA-	10	10	10	10	10	10	10	10								
E. coli fepC-	10	1	1	0.1	10	10	10	10								
E. coli fes-	10	0.1	10	0.1	10	10	10	10								
E. coli 25922	10	0.1	10	0.1	10	10	10	10					10	1	10	1
E. coli CFT073	0.1	0.01	0.1	0.01	10	10	10	10	>10	>10	>10	>10	1	0.1	1	0.1
E. coli UTI89	10	1	1	0.1	10	10	10	10								
E. coli H9049	10	0.01	10	0.01	10	10	10	10								
E. coli 43895	10	1	10	1	10	10	10	10					10	1	10	1
E. coli 35401	10	10	10	10	10	10	10	10					10	1	10	10
E. coli 35218	>100	>100	>100	>100	>100	>100	>100	>100								
P. aeruginosa PAO1	10	10	10	10	>100	>100	>100	>100								
K.pneumoniae 13883	>10	>10	>10	10	>100	>100	>100	>100								
S. Typhimurium IR715	0.1	0.1	0.1	0.1	10	10	10	10								
S. aureus 25923	10	10	10	10	1	1	1	1								
B. cereus 14579	>10	>10	10	10	100	100	100	100								

[a]. Growth conditions without 200 μM of DP. [b]. Growth conditions with 200 μM of DP.

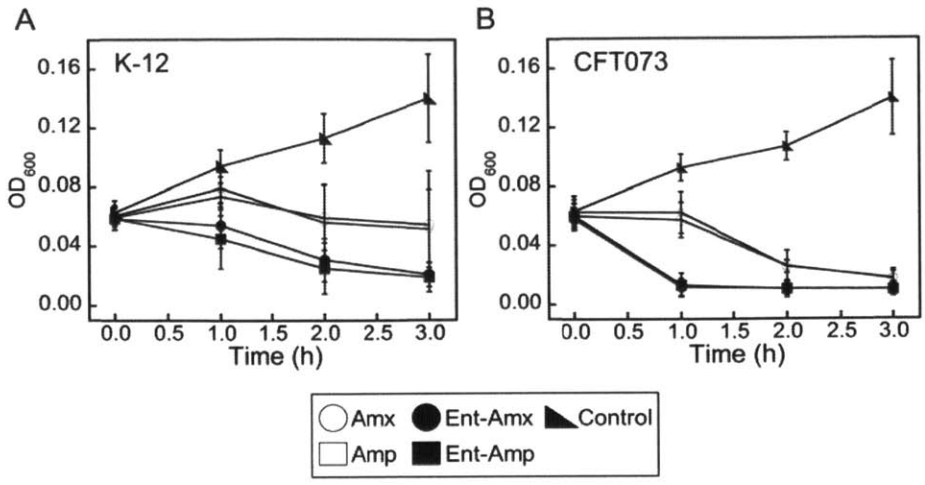

Figure 3.10. A. Killing kinetics of the Ent-β-lactam conjugates and the β-lactams against *E. coli* K12. All compounds were tested at 50 μM concentration. B. Killing kinetics of the Ent-β-lactam conjugates and the β-lactams against *E. coli* CFT073. Ent-β-lactam conjugates were tested at 5 μM concentration and the β-lactams were tested at 50 μM concentration. A 200-μM DP was added to all assays present in this figure. Error bars are the standard error of the mean for at least three independent repetitions.

Time-Kill Kinetics of Ent-Amp and Ent-Amx against *E.coli* K12 and CFT073. All small-molecule antibiotics enter Gram-negative bacteria through outer membrane channel proteins called porins by passive diffusion.[22] Ent-mediated antibiotic delivery changes this outer membrane entering process from passive diffusion to active transport, which may not only increase the amount, but also the speed of the antibiotic influx. Therefore we performed a time-kill kinetics study to compare the time needed for the conjugates and the β-lactams to cause bacterial death. Following reported procedures,[23] exponential phase bacterial cultures were treated with the conjugates or the β-lactams and grown at 37 °C. At different time points, the OD_{600} values were recorded and the colony forming units (CFU/mL) were measured by plating the culture on agar plates after serial dilutions. Higher concentrations of the conjugates and the β-lactams than their MICs were used because a more dense culture (~10^8 CFU/mL) was treated in such assays. Two *E. coli* strains, K12 and CFT073, were evaluated. Under the same concentration (50 μM), the conjugates cause bacterial population decrease faster in both OD_{600} and CFU measurement for *E. coli* K12 (Figure 3.10 A). For *E. coli* CFT073, the results were more remarkable. The OD_{600} value was almost reduced to the baseline value at t =1 h for 5 μM Ent-Amp/Amx, corresponding to a two-fold log reduction in CFU/mL. In contrast, the change in OD_{600} and CFU/mL for *E. coli* CFT073 treated with 50 μM unmodified Amp/Amx exhibits negligible change over this time period. (Figure 3.10 B). This is in

accordance with the enhanced antibacterial activity observed for CFT073 relative to the other *E. coli* strains considered in this work. Taken together, these data suggest that besides lowering the MIC values, the Ent mediated delivery strategy also help the β-lactams to reach their target more rapidly.

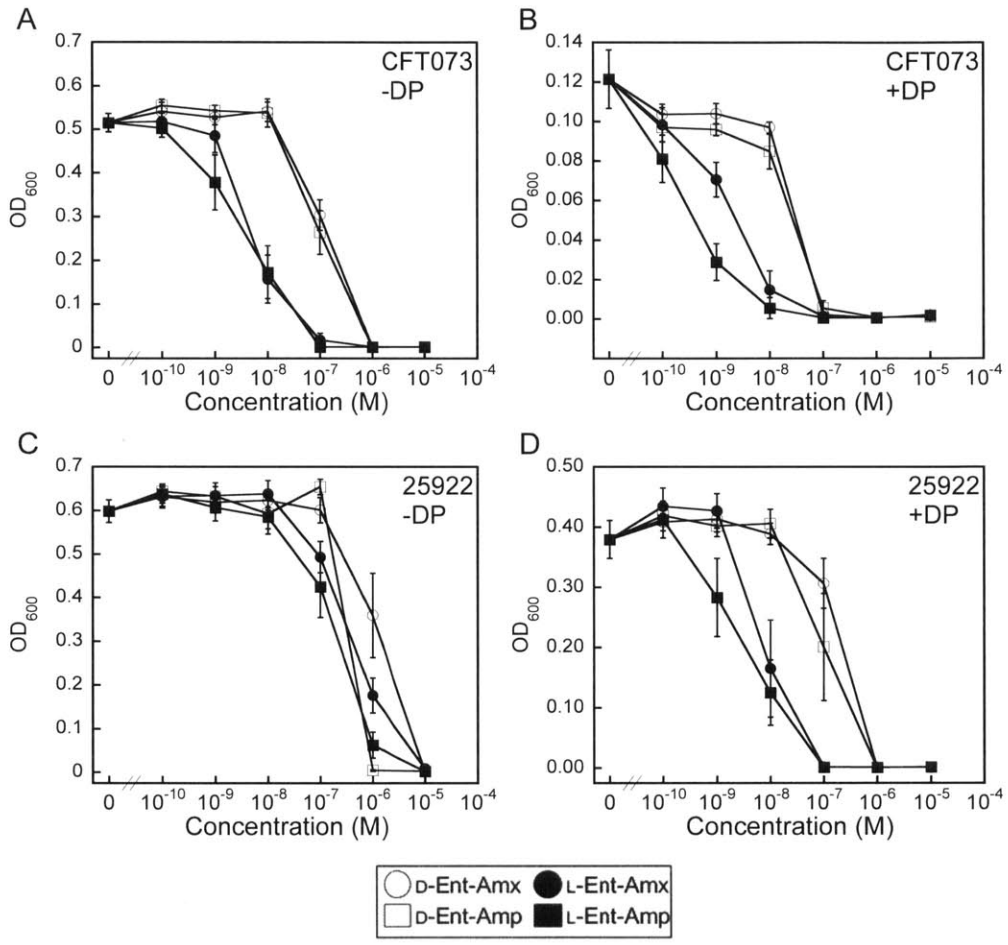

Figure 3.11. Antimicrobial activity of D-Ent-Amp and D-Ent-Amx against *E. coli* CFT073 and 25922. Data for L-Ent-Amp and L-Ent-Amx are plotted for comparison. Error bars are the standard error of the mean for at least three independent repetitions.

D-Ent-β-lactam Conjugates do not Further Improve Antimicrobial Activity. The enantiomer of Ent, D-Ent, binds Fe(III) with similar affinity and was suggested to be recognized by all the components of Ent transport machinery except for the cytosol esterase Fes.[17] Therefore when D-Ent is added to the growth medium, it exhibited growth inhibitory effect due to iron starvation (Chapter 2). We conjugated Amp and Amx to D-Ent via the same synthetic route for Ent-Amp and Ent-Amx to afford compound **13** (D-Ent-Amp) and **14** (D-Ent-Amx), and these two compound were tested against several *E.*

coli strains to see if the D-enantiomer of Ent affects the delivery of the antibiotics. The experiments were carried out the same way as with Ent-Amp/Amx, and the results showed a ~10 fold decrease of activity (Figure 3.11 A-D and Table 3.3). These conjugates still exhibit higher activity in the presence of DP comparing to no DP condition, which indicates they were delivered through the Ent-uptake machinery. It is reported that D-Ent binds to the outer membrane receptor FepA with similar affinity of L-Ent;[24] however, its overall uptake efficiency maybe lower than L-Ent. The same literature also reported lack of transport of D-Ent-Fe into *E. coli* BN1071.[24] Therefore, the activity decrease comparing to the L-conjugates may due to a less effective transport, which can be studied in the future by treating the bacteria with radioactive Fe-conjugate.

The Enhanced Antibacterial Activity of Ent-Amp/Amx is Specific to *E. coli*. In addition to *E. coli*, many other bacteria species utilize Ent for iron uptake. We therefore selected several other strains that are known to express the Ent receptor to determine whether Ent-Amp/Amx exhibit broad-range or species-selective activity. These selected bacterial strains include Gram-negative *Pseudomonas aeruginosa* PAO1, *Klebsiella pneumoniae* 13883, *Salmonella* Typhimurium IR715, and Gram-positive *Bacillus cereus* 14579, and *Staphylococcus aureus* 25923 (Table 3.1). *P. aeruginosa* is a Gram-negative bacteria that utilizes enterobactin as a xenosiderophore and expresses two Ent receptors PfeA and PirA.[4, 25] *K. pneumoniae* is a Gram-negative species that biosynthesizes and utilizes enterobactin for iron acquisition.[26] *S. aureus* and *B. cereus* are both Gram-positive bacterial species and their ability to utilize ferric enterobactin as an iron source is reported.[27] In contrast to Gram-negative bacteria, where the PBPs are located in the periplasm, the targets of β-lactam antibiotics are in the extracellular peptidoglycan of Gram-positive organisms.

When tested with Ent-Amp and Ent-Amx, these bacterial strains were generally less sensitive compared to *E. coli* (Figure 3.12 and Table 3.3). The MIC of the conjugates against *P. aeruginosa* PAO1was 10 μM with or without DP present in the growth media, which is higher than the values observed for *E. coli*, but still lower than the unmodified β-lactams (> 100 μM, Figure 3.12 A). However, the activity improvement compared to the β-lactams may not result from the Ent-mediated delivery because of the lack of correlation with iron supply. From our previous study in Chapter 2, an iron starvation effect resulting from no delivery usually affords a MIC of 10 μM. It should be noted that Miller *et al.* reported two Ent analog-Amp/Amx conjugates exhibiting selective high activity against *P. aeruginosa* but not *E. coli*.[8b] The two conjugates reported in this paper featured different structures than our conjugates with a modified Ent backbone and a different attachment site for the β-lactams. As reported in Chapter 2, the Ent uptake machinery in *P. aeruginosa* and *E. coli* have different response or tolerance for cargo sizes and shapes, which may explain why different strain sensitivity was observed.

Moreover, various *P. aeruginosa* strains exhibit different phenotypes, and highly variable activity of triscatecholate-β-lactam conjugates against multiple *P. aeruginosa* strains has been observed.[8b] Therefore, it is possible that the lack of sensitivity is only specific to the particular strain utilized in our current study. Another possibility is quick induction or selection of resistant strains during the course of antimicrobial assays. Budzikiewicz *et al.* reported pyoverdin-ampicillin conjugates that were able to delay the growth of *P. aeruginosa* 27853 for approximately 16 h and the bacterial culture started to grow again with mutation in pyoverdin uptake machinery identified.[28] Because we only took an end point reading after 19 h incubation time in our antimicrobial assays, it is possible that some growth delay effect was missed. A kinetic growth curve study with Ent-Amx/Amp will be helpful to evaluate this hypothesis.

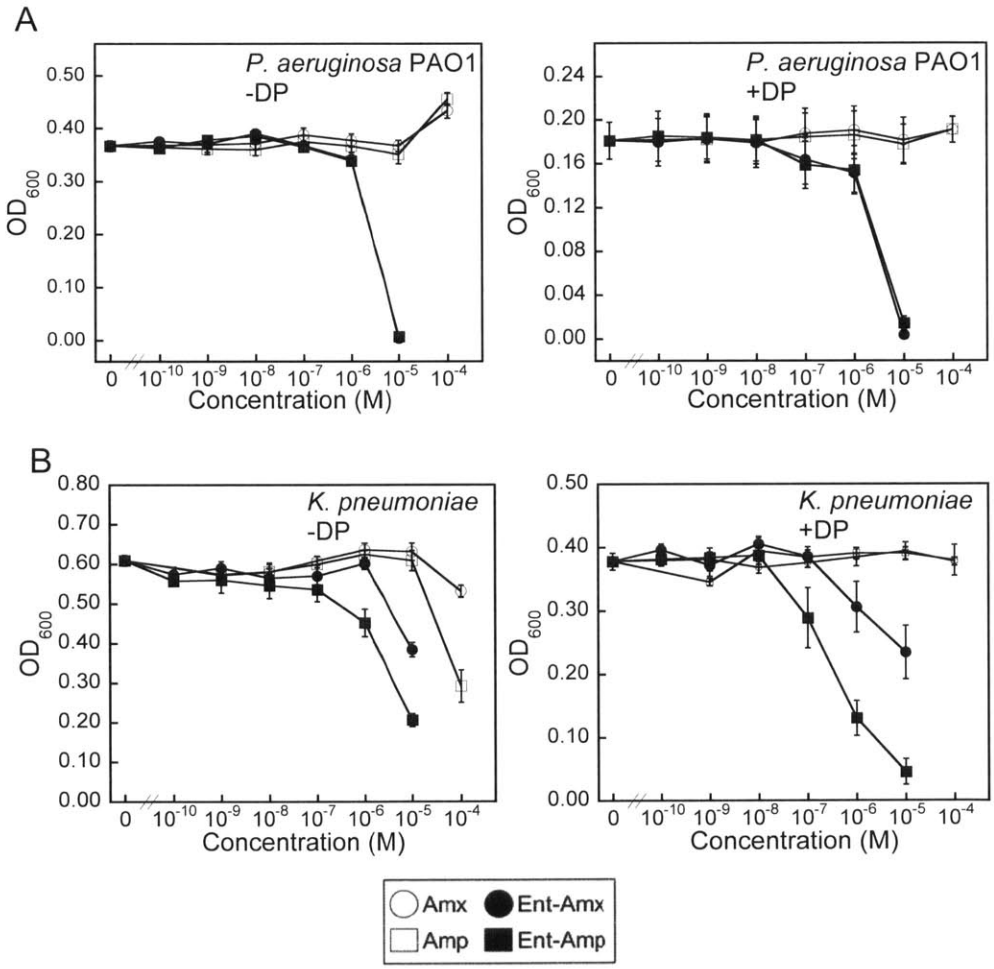

Figure 3.12. Antimicrobial activity of the Ent-β-lactam conjugates against non-*E. coli* strains. Error bars are the standard error of the mean for at least three independent repetitions. To be continued on the next page.

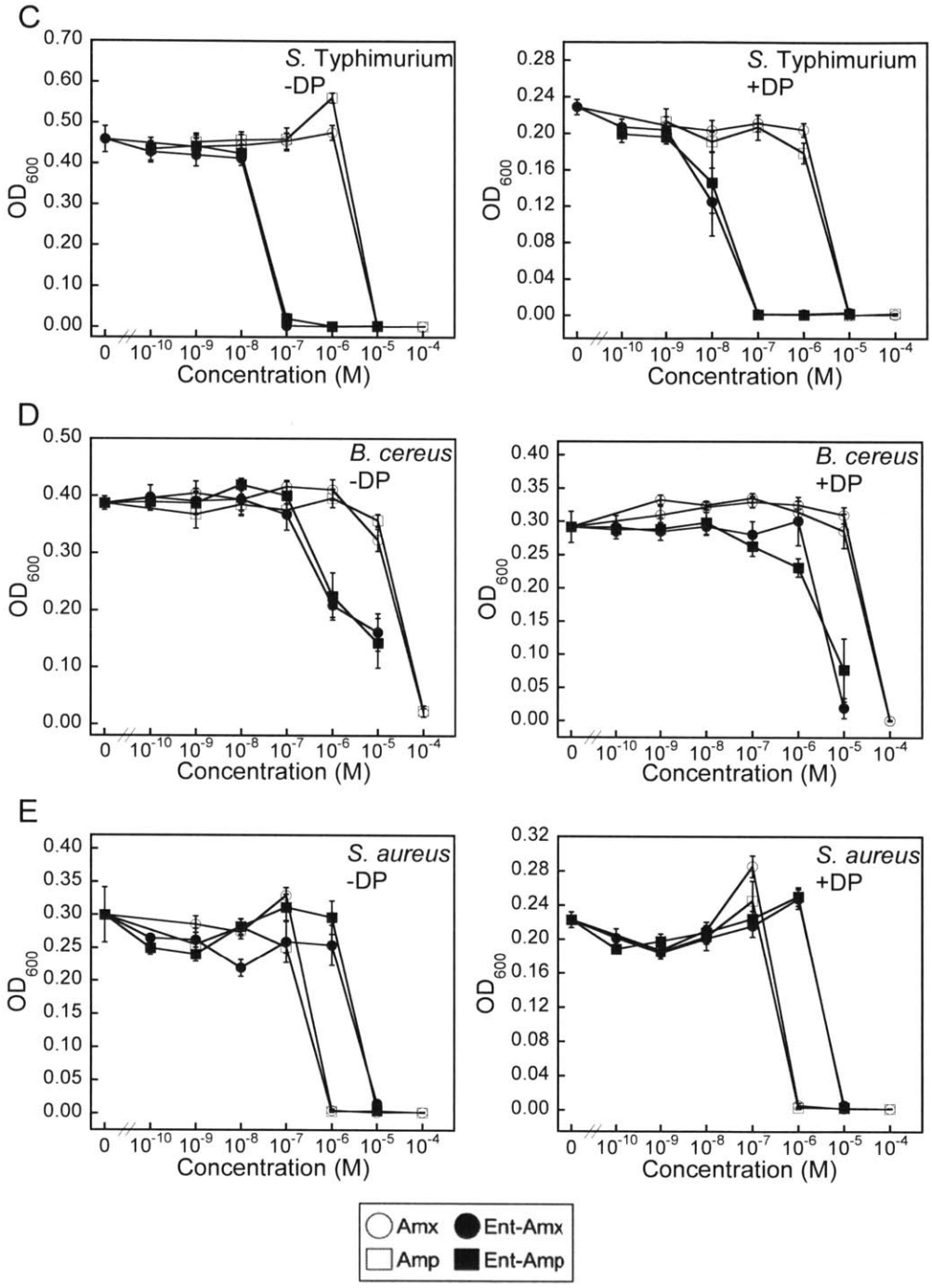

Figure 3.12-continued. Antimicrobial activity of the Ent-β-lactam conjugates against non-*E. coli* strains. Error bars are the standard error of the mean for at least three independent repetitions.

The *K. pneumoniae* strain was not sensitive to Amp or Amx, and the conjugates at high concentration (10 μM) only provided slight growth inhibition (Figure 3.12 B). However, the lack of activity for this strain likely results from β-lactamase expression, not insufficient delivery. *K. pneumoniae* 13883 chromosomally encodes Class A β-lactamase (SHV-1).[29] Indeed, when β-lactamase inhibitors were included in the assays, *K. pneumoniae* exhibited greater sensitivity to Amp/Amx (with MIC of 100 μM) and Ent-Amp/Amx (with MIC of 10 μM); however, we observed some growth inhibitory activity of the β-lactamase inhibitor sulbactam (100 μM) alone and the possibility of a synergistic effect from the inhibitors and conjugates cannot be ruled out completely. The lack of activity of Ent-Amp/Amx against *K. pneumoniae* ATCC 13883 is reminiscent of results published by Miller and co-workers of Amp/Amx-substituted triscatecholate ligands.[8b] In that study, the MIC of the siderophore-antibiotic conjugates were determined to be >100 μM against the *K. pneumoniae* ATCC8303X68 strain. The low sensitivity was hypothesized to result from resistance strains evolved during the course of antimicrobial assays. *S.* Typhimurium IR715 behaves similarly as *E. coli* CFT073 in the way that even without DP, it is quite sensitive to the conjugates (with MIC of 0.1 μM, Figure 3.12 C). These two strains both are able to synthesize and utilize salmochelins, therefore express the IroN receptor, although whether this common feature contribute to their unique response under iron sufficient conditions was not clear.

The two Gram-positive bacteria tested both exhibited MICs of approximately 10 μM with Ent-Amp/Amx, in iron sufficient or deficient conditions (Figure 3.12 D and E). For *B. cereus* this value is a 10-fold decrease compared to the β-lactams, but the lack of response to DP may indicate other mechanisms rather than Ent-mediated delivery. Surprisingly, for *S. aureus*, the conjugates exhibit a 10-fold lower activity than the β-lactams. *S. aureus* is generally more sensitive to β-lactams than many other bacterial species.[6a] It should be noted that Gram-positive bacteria have dense cell wall structures and the target of the β-lactams (PBPs) are located within the peptidoglycan layer which is outside of the bacteria membrane. Two possible explanations for the conjugates to be less active than their parent antibiotics are: i) the increased molecular size slows down their diffusion within the cell wall and lowers the chance of hitting the PBPs; ii) the Ent uptake machinery transports the conjugates into the cytosol which is away from the targeted PBPs. Without further studies we cannot draw any conclusions, although the lack of response to DP may indicate the first hypothesis is more likely.

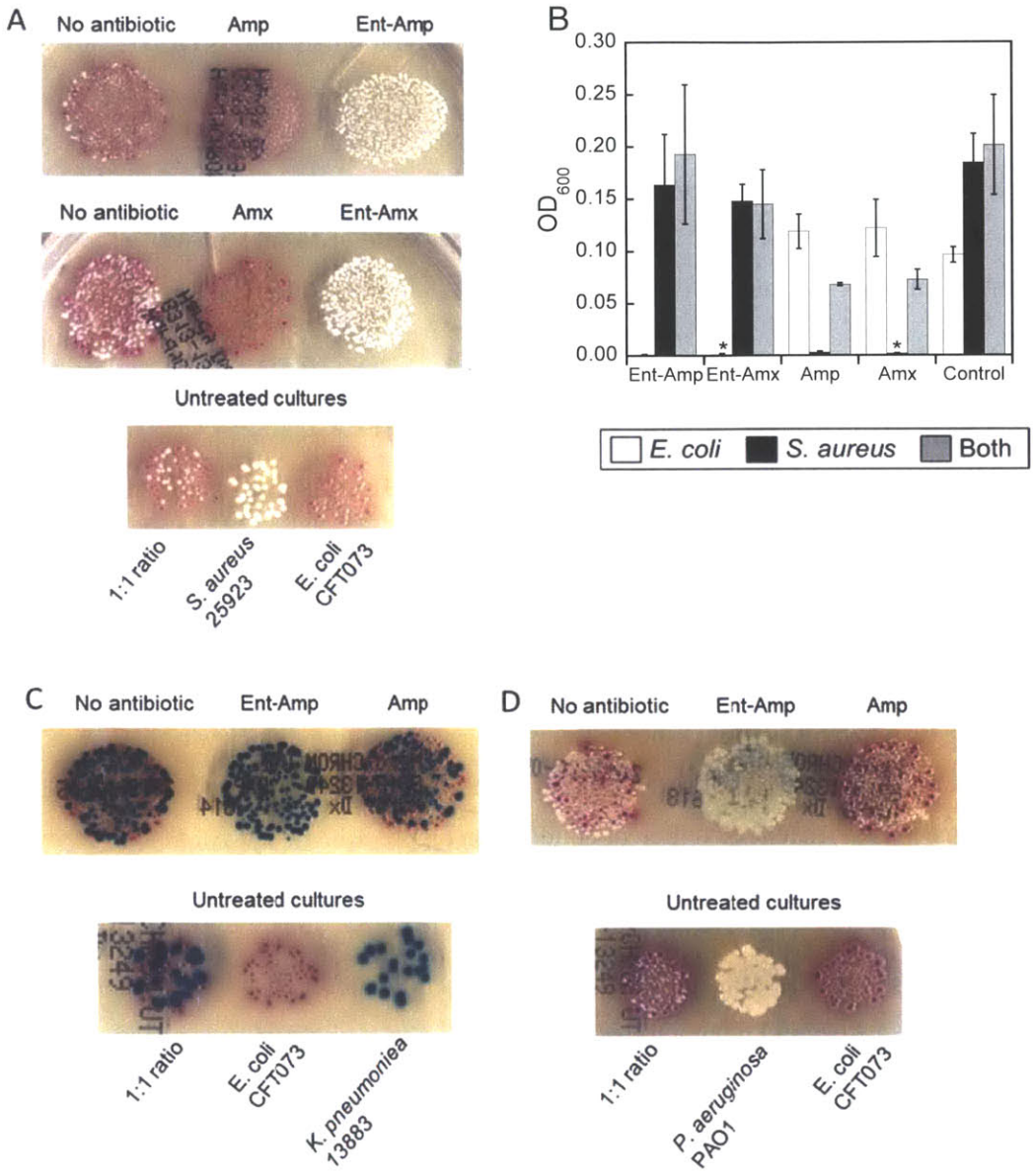

Figure 3.13. A. Representative images of the colonies from mixed cultures of *E. coli* CFT073/*S. aureus* 25923 treated with Ent-β-lactam conjugates (1 μM) or β-lactams (1 μM) in the presence of 200 μM DP (similar results were obtained without DP with more colonies). B. Bacterial growth monitored by OD_{600} in the mixed culture assay of *E. coli* CFT073/*S. aureus* 25923 in the presence of 200 μM DP (similar results were obtained without DP with higher OD values). The "*" indicates $OD_{600} < 0.01$. Error bars are the standard error of the mean for at least three independent repetitions. C and D. Represented pictures of the colonies from mixed cultures of *E. coli* CFT073/*K. pneumoniae*13883 or *E. coli* CFT073/*P. aeruginosa* PAO1 treated with Ent-Amp (1 μM) or Amp (1 μM) in the absence of DP (similar results were obtained with DP with less colonies). All experiments were repeated three times.

Ent-β-lactam Conjugates Exhibit Selective Activity against *E. coli* in Mixed Bacterial Cultures. Inspired by the different responses from different bacterial species when treated with the Ent-β-lactam conjugates, we hypothesized that when treating a mixed culture comprised of different species, we should be able to selectively inhibit the growth of a sensitive strain without affecting the growth of other species. Such selective targeting is important because when treating bacterial infection, there is often a mixed bacterial population and ideally the antibiotic should only kill the pathogens and leave the commensals intact. We selected *E. coli* CFT073 to pair with *S. aureus* 25923, or *K. pneumoniae* 13883, or *P. aeruginosa* PAO1 as model systems based on their responses after treating with the conjugates. In these mixed-culture assays, we combined the two species in about 1:1 ratio based on CFU values, treated with the conjugates or the β-lactams, grew the culture overnight at 30 °C, recorded the OD_{600} values and plated the culture on a CHROM-UTI plate. This plate contains a mixture of chromophores and different bacteria give colonies with different colors, which allows us to differentiate the species in the assay culture easily.[30] Single species controls were ran in parallel with the mixed culture. In accord with our hypothesis, selective killing was observed in these experiments. For example, in the *E. coli* CFT073/*S. aureus* 25923 pair, at 1 μM concentration, the conjugate treated culture had only white *S. aureus* colonies, the β-lactam treated culture had only pink *E. coli* colonies, and the control culture had a mixed pick and white colonies (Figure 3.13 A). The same results were observed from OD_{600} values (Figure 3.13 B). For the other two pairs, the conjugates kill only the *E. coli* CFT073 as well (Figure 3.13 C and 3.13 D). Based on these observations, it is very promising that with careful design the Ent-mediated delivery strategy can achieve highly selective activity against targeted bacteria.

Ent Competes with Ent-β-lactam Conjugates for Lipocalin 2 Binding. Lipocalin 2 (Lcn2, also known as siderocalin or NGAL) is a protein produced by mammalian immune system during bacterial infection. It binds Ent to interfere with bacterial iron uptake and thus inhibits bacterial growth.[31] In Chapter 2, it was found that several Ent-cargo conjugates also bind Lcn2, albeit to less degrees than Ent, and it is possible that the Ent-β-lactam conjugates behave similarly. We tested this hypothesis by performing an antimicrobial assay with Lcn2 in the growth medium. We chose the *E. coli* CFT073 strain to minimize Lcn2 usage. Because this strain requires a lower concentration of the conjugates to inhibit bacterial growth, most likely a lower concentration of Lcn2 is needed to block the activity. M9 minimal medium was used following a reported condition for assessing the antimicrobial activity of Lcn2.[12] Although under this condition, Lcn2 failed to inhibit the growth of *E. coli* CFT073 up to a 1-μM concentration, it was able to recover the growth of the bacteria at 0.5 and 1 μM concentration when 0.1 μM of Ent-Amp was present (Figure 3.14A). When the same amount of bovine serum albumin (BSA) was added instead of Lcn2, the Ent-Amp remained active. This observation suggests that Ent-Amp

specifically binds to Lcn2 and the binding attenuated the activity of Ent-Amp. However, Ent was found to be able to compete with Ent-Amp. At fixed concentrations of Ent-Amp (0.1 μM) and Lcn2 (0.5 μM), increased amount of Ent (0 - 0.5 μM) was able to recover the activity of Ent-Amp (Figure 3.14B). When a 1:1 ratio of Lcn2 and either Ent-Amp (Figure 3.13A) or Ent (Figure 3.14B) were included in the assay, no growth was observed, indicating Lcn2 may bind Ent better than Ent-Amp. Therefore, when treating bacterial infection, because of the presence of Ent secreted by the bacteria, the conjugates still may be able to escape Lcn2 and reach the bacterial cells.

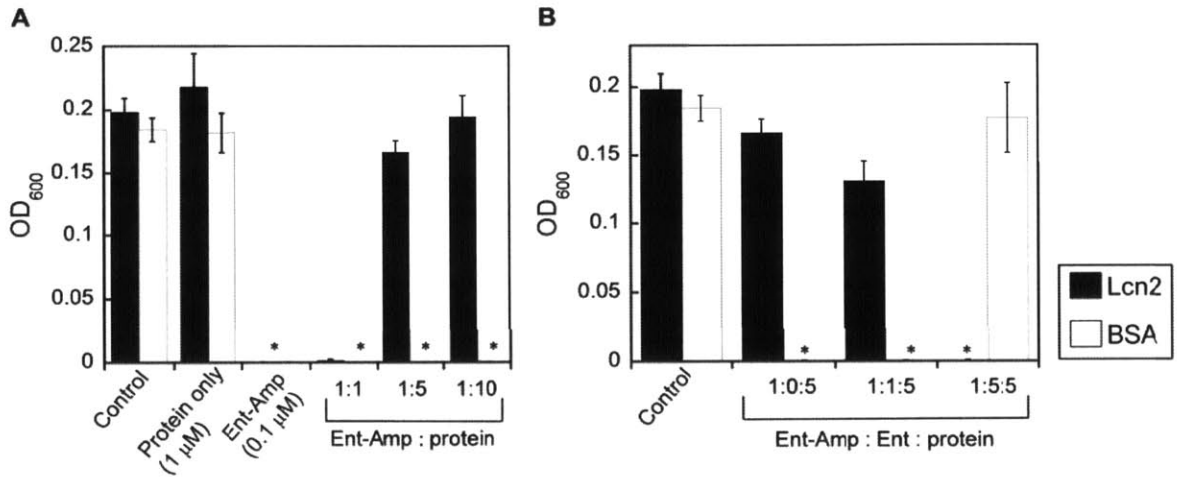

Figure 3.14 A. *E. coli* CFT073 growth in M9 minimal media with siderochalin and/or Ent-Amp. B. *E. coli* CFT073 growth in M9 minimal media with siderochalin, Ent, and Ent-Amp. BSA with the same concentration as siderochalin was tested as a control. Error bars are the standard error of the mean for at least three independent repetitions. The "*" indicates $OD_{600} < 0.01$.

Ent-Amp Exhibits Low Cytotoxicity to Mammallian Cells. One advantage of applying Ent-mediated delivery strategy to treat bacterial infection is that Ent should be able to direct the antibiotics or other cargo compounds specifically to bacteria and leave the host cells intact. Therefore, we evaluated the cytotoxicity of Ent-Amp against a colon epithelial cell line (T84). We choose this cell line because the Ent-β-lactam conjugates were most sensitive against *E. coli* and colon is the most common environment for these bacteria to live. The survival of mammalian cells was evaluated by MTT (3-[4,5-dimethylthiazol-2-yl]-2,5 diphenyl tetrazolium bromide) assay after 24 h treatment with Ent-Amp, Amp or Ent. To assess whether Ent will chelate iron in the growth medium and result in any iron-starvation effect, these compounds were also preincubated with one equiv. of Fe (III) and tested in parallel. Up to a 10 μM concentration, Ent-Amp did not exhibit any obvious cytotoxicity, neither did Amp (with or

without Fe) (Figure 3.15A and B). Apo Ent with a 10 μM concentration seems to decrease the percent survival of T84 cells by approximately 30%, but with pre-loaded Fe no effect was observed (Figure 3.15C). The effect of DMSO was also evaluated, and no growth inhibition was observed at 1% of DMSO in the media (Figure 3.15D). Therefore, the Ent-β-lactam conjugates were not toxic to the mammalian cells at the highest concentration used in the current study.

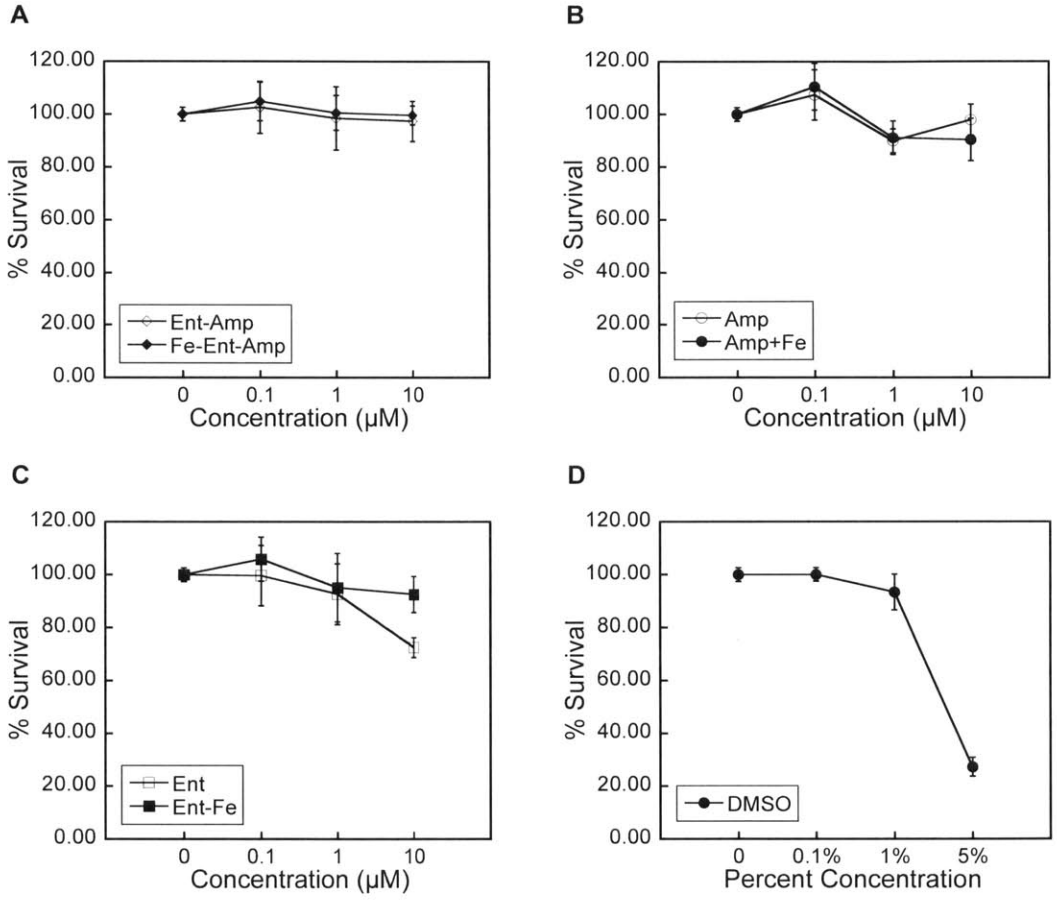

Figure 3.15. Cytotoxicity studies of Ent-Amp (A), Amp (B), Ent (C) and DMSO (D) against T84 cells. Percent cell survival quantified by MTT assay after a 24 h treatment. Error bars are the standard error of the mean for at least three independent repetitions.

Summary and Perspectives

In this chapter, we described the synthesis of two enterobactin-antibiotic conjugates, Ent-Amp and Ent-Amx, as well as their analogs featuring D-enantiomer of Ent or hydrolyzed β-lactam moieties. The synthetic route employing copper catalyzed azide-alkyne cycloaddition is robust and reliable, and can be applied to incorporate other cargos into the Ent scaffolds as well as to append Ent to surfaces, other

materials, or biomolecules harboring alkyne groups. This synthesis also provides possibilities for elaborating β-lactams in a variety of applications. Indeed, very few examples employing copper(I)-catalyzed click chemistry with fused β-lactams are reported in the literature,[8a, 32] and it is likely that this paucity stems from the fact that β-lactams are incompatible with standard conditions for copper-catalyzed click chemistry.[14] The conditions defined in this work employing TBTA allow for copper-catalyzed triazole formation and preserve the penam core structure.

Microbiological studies with the Ent-Amp/Amx conjugates revealed potent and unique antimicrobial properties. The conjugates were significantly more active against various *E. coli* strains, including human pathogens, under iron-deficient conditions compared to the unmodified antibiotics. We also demonstrated that the activity enhancement requires the presence of Ent receptor FepA as well as an intact β-lactam warhead, which suggests that the improved activity is due to Ent-mediated antibiotic delivery. However, it is possible that the cell killing mechanism is more complex. Capture of Ent-Amp/Amx by PBPs presumably results in accumulation of ferric enterobactin in the periplasm. The fact that knock-out mutants of inner membrane Ent permease FepC and cytosol Ent esterase Fes exhibited similar response upon conjugates treatment as the wild-type strain indicates the conjugates do not enter the cytosolic space. A recent study of an *E. coli* TolC mutant indicated that enterobactin accumulation in the periplasm affords growth defects and abnormal cellular morphologies.[33] Although the origins of this effect are unclear, this study suggests the possibility of dual action for our conjugates.

Another interesting observation from the current work is that Ent-Amp/Amx exhibit quite different activities against different bacterial strains. Within the *E. coli* groups, the uropathogen CFT073 was the most sensitive strain, with a MIC value as low as 10 nM under iron-deficient conditions, and significant growth inhibition was observed at 1 nM concentration. Although CFT073 and the other uropathogen UTI89 both harbor the salmochelin synthesis and uptake gene cluster *iroA,* UIT89 was less sensitive. Other *E. coli* strains each has slightly different response upon conjugate treatment. The redundant Ent transport machineries as seen in CFT073, different capacities for transporting modified Ent and different expression levels of Ent uptake machineries in different species may contribute to such diverse responses. Outside of the *E. coli* group, other bacteria tested in the current work were all less sensitive to the conjugates. For example, the *P. aeruginosa* PAO1 only exhibited a MIC of 10 μM which is also independent of DP presence. In contrast, catecholate-based siderophore analogs have been reported for conjugation with ampicillin and amoxicillin by the Möllmann group and Miller group, and these conjugates exhibit greatly improved antimicrobial activity against selected *P. aeruginosa* strains in response of iron-deficiency, although in these studies *E. coli* 25922 appeared to be less sensitive than *P. aeruginosa.*[8b,34] The origin of such different strain selectivity was not clear. Incorporating native siderophore (Ent) as shown in our study rather than siderophore analogs may affect the conjugate uptake

by different species. And the *P. aeruginosa* strains used in each study were different which makes it difficult to draw direct comparisons. One common observation we notice is that *S. aureus* was less sensitive against the conjugates reported by the Möllmann group compared to unmodified antibiotics,[32] and older work involving catecholate-piperacillin/cephalosporin conjugates reported similar results.[35] Together with our data, *S. aureus* may not be a good target to be treated with catechol-based siderophore-β-lactam conjugates.

Ent-Amp and Ent-Amx were shown to be able to kill *E. coli* CFT073 selectively in the presence of other bacterial species including *S. aureus* 25923, *P. aeruginosa* PAO1 and *K. pneumoniea* 13883. The strain selective properties of Ent-Amp and Ent-Amx may be an advantage for new antimicrobial therapeutic development. The vast microbe population colonized in human body greatly affects our physiology, metabolism, nutrition and immune function.[36] Traditional administration of therapeutic doses of antibiotics cause disturbance of the normal microbiota.[37] New antibiotics that can specifically target the pathogenic subpopulation will be beneficial.

Another remarkable property of the conjugates is that they cause faster bacterial population decrease than the unmodified antibiotics. We hypothesize that this improvement is due to active transport through the Ent uptake machinery, and the quick influx of significant amount of antibiotics may allow less time for the bacteria to turn on the resistance response.

Although the Ent-β-lactam conjugates exhibited great antimicrobial properties in our *in vitro* experiments, several limitations still exist. It is known that human neutrophil and epithelial cells express lipocalin 2 in response to inflammatory signals, which is bacteriostatic due to its Ent-binding property.[12] Our studies demonstrated that excess Lcn2 attenuated the antimicrobial activity of Ent-Amp, and Ent competitively recovers its activity. This data suggests possible capture of the Ent-β-lactam conjugates by Lcn2 if the molecules are tested in infection models *in vivo,* which will affect their efficacy. One solution to this issue is to modify the Ent moiety with glucose, because it is reported that the glucosylated Ent derivatives (salmochelins) can escape Lcn2 binding.[38] Another unaddressed point is the possibility of resistance upon treatment with the conjugates caused by mutation in iron uptake machineries *in vitro*, which is observed with many siderophore- or siderophore-analog-β-lactam conjugates.[28, 39] Growth curve study with extended incubation time to monitor regrowth of the affected strains is one way to gain insights into this issue. With the resistance caused by β-lactamase expressing, other β-lactam antibiotics, e.g. monobactams like aztreonam, that are stable to β-lactamases can be incorporated into the conjugate design. Pfizer and Basilea Pharmaceutic have reported conjugates employing monobactams and activities against multi-drug-resistant strains were observed.[40] Therefore, we reason that by changing the antibiotic warhead in the Ent conjugates more improved antimicrobial activity may be achieved.

Acknowledgements

The Pacific Southwest Regional Center of Excellent for Biodefense and Emerging Infectious Disease, the Searle Scholars Program (Kinship Foundation), and the Department of Chemistry at MIT are gratefully acknowledged for financial support. We thank Prof. Manuela Raffatellu, Dr. Simone Moser, and Dr. Andrew Wommack for insightful discussions; Prof. Keith Poole for providing *Pseudomonas aeruginosa* PAO1; Prof. Lynette Cegelski for providing *E. coli* UTI89; Prof. Christopher T. Walsh for providing *E. coli* H9049; and Prof. Stephen J. Lippard for use an IR spectrophotometer. We thank Justin Bullock, Phoom Chairatana, and Iulia Tapescu for providing synthetic precursors to the modified enterobactin platforms. Single gene knock-out strains of *E. coli* K-12 were obtained from the Keio Collection.[41]

References

1. (a) Delcour, A. H., Outer membrane permeability and antibiotic resistance. *BBA-Proteins Proteom.* **2009,** *1794* (5), 808-816; (b) Li, X. Z.; Nikaido, H., Efflux-Mediated Drug Resistance in Bacteria An Update. *Drugs* **2009,** *69* (12), 1555-1623; (c) Pages, J. M.; James, C. E.; Winterhalter, M., The porin and the permeating antibiotic: a selective diffusion barrier in Gram-negative bacteria. *Nat. Rev. Microbiol.* **2008,** *6* (12), 893-903.

2. Ji, C.; Juarez-Hernandez, R. E.; Miller, M. J., Exploiting bacterial iron acquisition: siderophore conjugates. *Future Med. Chem.* **2012,** *4* (3), 297-313.

3. (a) Yancey, R. J.; Breeding, S. A.; Lankford, C. E., Enterochelin (enterobactin): virulence factor for Salmonella typhimurium. *Infect. Immun.* **1979,** *24* (1), 174-180; (b) Nagy, T. A.; Moreland, S. M.; Andrews-Polymenis, H.; Detweiler, C. S., The Ferric Enterobactin Transporter Fep Is Required for Persistent Salmonella enterica Serovar Typhimurium Infection. *Infect. Immun.* **2013,** *81* (11), 4063-4070.

4. Poole, K.; Young, L.; Neshat, S., Enterobactin-mediated iron transport in Pseudomonas aeruginosa. *J. Bacteriol.* **1990,** *172* (12), 6991-6996.

5. Abergel, R. J.; Clifton, M. C.; Pizarro, J. C.; Warner, J. A.; Shuh, D. K.; Strong, R. K.; Raymond, K. N., The siderocalin/enterobactin interaction: a link between mammalian immunity and bacterial iron transport. *J. Am. Chem. Soc.* **2008,** *130* (34), 11524-11534.

6. (a) Kong, K. F.; Schneper, L.; Mathee, K., Beta-lactam antibiotics: from antibiosis to resistance and bacteriology. *APMIS* **2010,** *118* (1), 1-36; (b) Sauvage, E.; Kerff, F.; Terrak, M.; Ayala, J. A.; Charlier, P., The penicillin-binding proteins: structure and role in peptidoglycan biosynthesis. *FEMS Microbiol. Rev.* **2008,** *32* (3), 556-556.

7. Harder, K. J.; Nikaido, H.; Matsuhashi, M., Mutants of Escherichia-Coli That Are Resistant to Certain Beta-Lactam Compounds Lack the Ompf Porin. *Antimicrob. Agents Chemother.* **1981,** *20* (4), 549-552.

8. (a) Staub, I.; Sieber, S. A., beta-lactams as selective chemical probes for the in vivo labeling of bacterial enzymes involved in cell wall biosynthesis, antibiotic resistance, and virulence. *J Am Chem Soc* **2008,** *130* (40), 13400-13409; (b) Ji, C.; Miller, P. A.; Miller, M. J., Iron transport-mediated drug delivery: practical syntheses and in vitro antibacterial studies of tris-catecholate siderophore-aminopenicillin conjugates reveals selectively potent antipseudomonal activity. *J Am Chem Soc* **2012,** *134* (24), 9898-9901.

9. Ramirez, R. J. A.; Karamanukyan, L.; Ortiz, S.; Gutierrez, C. G., A much improved synthesis of the siderophore enterobactin. *Tetrahedron Lett* **1997,** *38* (5), 749-752.

10. Scarrow, R. C.; Ecker, D. J.; Ng, C.; Liu, S.; Raymond, K. N., Iron(Iii) Coordination Chemistry of Linear Dihydroxyserine Compounds Derived from Enterobactin. *Inorg Chem* **1991,** *30* (5), 900-906.
11. Butler, D. L.; Jakielaszek, C. J.; Miller, L. A.; Poupard, J. A., Escherichia coli ATCC 35218 as a quality control isolate for susceptibility testing of Haemophilus influenzae with haemophilus test medium. *Antimicrob. Agents Chemother.* **1999,** *43* (2), 283-286.
12. Goetz, D. H.; Holmes, M. A.; Borregaard, N.; Bluhm, M. E.; Raymond, K. N.; Strong, R. K., The neutrophil lipocalin NGAL is a bacteriostatic agent that interferes with siderophore-mediated iron acquisition. *Mol. Cell* **2002,** *10* (5), 1033-1043.
13. Corey, E. J.; Link, J. O., A General, Catalytic, and Enantioselective Synthesis of Alpha-Amino-Acids. *J. Am. Chem. Soc.* **1992,** *114* (5), 1906-1908.
14. Fernandez-Gonzalez, A.; Badia, R.; Diaz-Garcia, M. E., Insights into the reaction of beta-lactam antibiotics with copper(II) ions in aqueous and micellar media: Kinetic and spectrometric studies. *Anal. Biochem.* **2005,** *341* (1), 113-121.
15. Chan, T. R.; Hilgraf, R.; Sharpless, K. B.; Fokin, V. V., Polytriazoles as copper(I)-stabilizing ligands in catalysis. *Org. Lett.* **2004,** *6* (17), 2853-2855.
16. (a) RobinsonFuentes, V. A.; Jefferies, T. M.; Branch, S. K., Degradation pathways of ampicillin in alkaline solutions. *J. Pharm. Pharmacol.* **1997,** *49* (9), 843-851; (b) Suwanrumpha, S.; Freas, R. B., Identification of Metabolites of Ampicillin Using Liquid-Chromatography Thermospray Mass-Spectrometry and Fast Atom Bombardment Tandem Mass-Spectrometry. *Biomed. Environ. Mass.* **1989,** *18* (11), 983-994.
17. Abergel, R. J.; Zawadzka, A. M.; Hoette, T. M.; Raymond, K. N., Enzymatic Hydrolysis of Trilactone Siderophores: Where Chiral Recognition Occurs in Enterobactin and Bacillibactin Iron Transport. *J. Am. Chem. Soc.* **2009,** *131* (35), 12682-12692.
18. Nikaido, H., Role of permeability barriers in resistance to beta-lactam antibiotics. *Pharmacol. Ther.* **1985,** *27* (2), 197-231.
19. Hantke, K., Regulation of Ferric Iron Transport in Escherichia-Coli-K12 - Isolation of a Constitutive Mutant. *Mol. Gen. Genet.* **1981,** *182* (2), 288-292.
20. Berger, T.; Togawa, A.; Duncan, G. S.; Elia, A. J.; You-Ten, A.; Wakeham, A.; Fong, H. E.; Cheung, C. C.; Mak, T. W., Lipocalin 2-deficient mice exhibit increased sensitivity to Escherichia coli infection but not to ischemia-reperfusion injury. *Proc. Nat. Acad. Sci. U. S. A.* **2006,** *103* (6), 1834-1839.
21. (a) Garcia, E. C.; Brumbaugh, A. R.; Mobley, H. L., Redundancy and specificity of Escherichia coli iron acquisition systems during urinary tract infection. *Infect. Immun.* **2011,** *79* (3), 1225-1235; (b) Leveille, S.; Caza, M.; Johnson, J. R.; Clabots, C.; Sabri, M.; Dozois, C. M., Iha from an Escherichia coli urinary tract infection outbreak clonal group A strain is expressed in vivo in the mouse urinary tract and functions as a catecholate siderophore receptor. *Infect. Immun.* **2006,** *74* (6), 3427-3436.
22. Schirmer, T., General and specific porins from bacterial outer membranes. *J. Struct. Biol.* **1998,** *121* (2), 101-109.
23. Kohanski, M. A.; Dwyer, D. J.; Hayete, B.; Lawrence, C. A.; Collins, J. J., A common mechanism of cellular death induced by bactericidal antibiotics. *Cell* **2007,** *130* (5), 797-810.
24. Thulasiraman, P.; Newton, S. M.; Xu, J.; Raymond, K. N.; Mai, C.; Hall, A.; Montague, M. A.; Klebba, P. E., Selectivity of ferric enterobactin binding and cooperativity of transport in gram-negative bacteria. *J. Bacteriol.* **1998,** *180* (24), 6689-6696.
25. (a) Dean, C. R.; Neshat, S.; Poole, K., PfeR, an enterobactin-responsive activator of ferric enterobactin receptor gene expression in Pseudomonas aeruginosa. *J. Bacteriol.* **1996,** *178* (18), 5361-5369; (b) Ghysels, B.; Ochsner, U.; Mollman, U.; Heinisch, L.; Vasil, M.; Cornelis, P.; Matthijs, S., The Pseudomonas aeruginosa pirA gene encodes a second receptor for ferrienterobactin and synthetic catecholate analogues. *FEMS Microbiol. Lett.* **2005,** *246* (2), 167-174.
26. Perry, R. D.; Sanclemente, C. L., Siderophore Synthesis in Klebsiella-Pneumoniae and Shigella-Sonnei during Iron-Deficiency. *J. Bacteriol.* **1979,** *140* (3), 1129-1132.
27. (a) Sebulsky, M. T.; Heinrichs, D. E., Identification and characterization of fhuD1 and fhuD2, two genes involved in iron-hydroxamate uptake in Staphylococcus aureus. *J. Bacteriol.* **2001,** *183* (17),

4994-5000; (b) Zawadzka, A. M.; Abergel, R. J.; Nichiporuk, R.; Andersen, U. N.; Raymond, K. N., Siderophore-mediated iron acquisition systems in Bacillus cereus: Identification of receptors for anthrax virulence-associated petrobactin. *Biochemistry* **2009,** *48* (16), 3645-3657.
28. Kinzel, O.; Tappe, R.; Gerus, I.; Budzikiewicz, H., The synthesis and antibacterial activity of two pyoverdin-ampicillin conjugates, entering Pseudomonas aeruginosa via the pyoverdin-mediated iron uptake pathway. *J. Antibiot.* **1998,** *51* (5), 499-507.
29. Hæggman, S. Evolution of Beta-Lactam resistance in Klebsiella pneumoniae. Karolinska Institute, Stockholm, Sweden, 2010.
30. Merlino, J.; Siarakas, S.; Robertson, G. J.; Funnell, G. R.; Gotlieb, T.; Bradbury, R., Evaluation of CHROMagar orientation for differentiation and presumptive identification of gram-negative bacilli and Enterococcus species. *J. Clin. Microbiol.* **1996,** *34* (7), 1788-1793.
31. (a) Clifton, M. C.; Corrent, C.; Strong, R. K., Siderocalins: siderophore-binding proteins of the innate immune system. *BioMetals* **2009,** *22* (4), 557-64; (b) Goetz, D. H.; Holmes, M. A.; Borregaard, N.; Bluhm, M. E.; Raymond, K. N.; Strong, R. K., The neutrophil lipocalin NGAL is a bacteriostatic agent that interferes with siderophore-mediated iron acquisition. *Mol. Cell* **2002,** *10* (5), 1033-1043.
32. Pearson, H. A.; Urban, M. W., Simple click reactions on polymer surfaces leading to antimicrobial behavior. *J. Mater. Chem. B* **2014,** *2* (15), 2084-2087.
33. Vega, D. E.; Young, K. D., Accumulation of periplasmic enterobactin impairs the growth and morphology of Escherichia coli tolC mutants. *Mol. Microbiol.* **2014,** *91* (3), 508-521.
34. (a) Heinisch, L.; Wittmann, S.; Stoiber, T.; Berg, A.; Ankel-Fuchs, D.; Mollmann, U., Highly antibacterial active aminoacyl penicillin conjugates with acylated bis-catecholate siderophores based on secondary diamino acids and related compounds. *J. Med. Chem.* **2002,** *45* (14), 3032-3040; (b) Wittmann, S.; Schnabelrauch, M.; Scherlitz-Hofmann, I.; Mollmann, U.; Ankel-Fuchs, D.; Heinisch, L., New synthetic siderophores and their beta-lactam conjugates based on diamino acids and dipeptides. *Bioorg. Med. Chem.* **2002,** *10* (6), 1659-1670.
35. (a) Basker, M. J.; Frydrych, C. H.; Harrington, F. P.; Milner, P. H., Antibacterial Activity of Catecholic Piperacillin Analogs. *J. Antibiot.* **1989,** *42* (8), 1328-1330; (b) Nakagawa, S.; Sanada, M.; Matsuda, K.; Hashizume, T.; Asahi, Y.; Ushijima, R.; Ohtake, N.; Tanaka, N., In vitro and in vivo antibacterial activities of BO-1341, a new antipseudomonal cephalosporin. *Antimicrob. Agents Chemother.* **1989,** *33* (9), 1423-1427.
36. Sekirov, I.; Russell, S. L.; Antunes, L. C. M.; Finlay, B. B., Gut Microbiota in Health and Disease. *Physiol. Rev.* **2010,** *90* (3), 859-904.
37. Rafii, F.; Sutherland, J. B.; Cerniglia, C. E., Effects of treatment with antimicrobial agents on the human colonic microflora. *Ther. Clin. Risk. Manag.* **2008,** *4* (6), 1343-1358.
38. Fischbach, M. A.; Lin, H. N.; Zhou, L.; Yu, Y.; Abergel, R. J.; Liu, D. R.; Raymond, K. N.; Wanner, B. L.; Strong, R. K.; Walsh, C. T.; Aderem, A.; Smith, K. D., The pathogen-associated iroA gene cluster mediates bacterial evasion of lipocalin 2. *Proc. Nat. Acad. Sci. U. S. A.* **2006,** *103* (44), 16502-16507.
39. Ghosh, A.; Ghosh, M.; Niu, C.; Malouin, F.; Moellmann, U.; Miller, M. J., Iron transport-mediated drug delivery using mixed-ligand siderophore-beta-lactam conjugates. *Chem. Biol.* **1996,** *3* (12), 1011-1019.
40. (a) Han, S.; Zaniewski, R. P.; Marr, E. S.; Lacey, B. M.; Tomaras, A. P.; Evdokimov, A.; Miller, J. R.; Shanmugasundaram, V., Structural basis for effectiveness of siderophore-conjugated monocarbams against clinically relevant strains of Pseudomonas aeruginosa. *Proc. Nat. Acad. Sci. U. S. A.* **2010,** *107* (51), 22002-22007; (b) Flanagan, M. E.; Brickner, S. J.; Lall, M.; Casavant, J.; Deschenes, L.; Finegan, S. M.; George, D. M.; Granskog, K.; Hardink, J. R.; Huband, M. D.; Hoang, T.; Lamb, L.; Marra, A.; Mitton-Fry, M.; Mueller, J. P.; Mullins, L. M.; Noe, M. C.; O'Donnell, J. P.; Pattavina, D.; Penzien, J. B.; Schuff, B. P.; Sun, J. M.; Whipple, D. A.; Young, J.; Gootz, T. D., Preparation, Gram-Negative Antibacterial Activity, and Hydrolytic Stability of Novel Siderophore-Conjugated Monocarbam Diols. *ACS Med. Chem. Lett.* **2011,** *2* (5), 385-390.

41. Baba, T.; Ara, T.; Hasegawa, M.; Takai, Y.; Okumura, Y.; Baba, M.; Datsenko, K. A.; Tomita, M.; Wanner, B. L.; Mori, H., Construction of Escherichia coli K-12 in-frame, single-gene knockout mutants: the Keio collection. *Mol. Syst. Biol.* **2006,** *2*, 1-11.

Chapter 4

Stability Evaluation of Acyloxymethyl/Acyloxyethyl Ester Linker for the Design of Enterobactin-fluoroquinolone Conjugates

Introduction

With the success of synthetically modifying Ent and applying the scaffold for cargo delivery into Gram-negative bacterial cytosol described in Chapter 2 and the greatly enhanced activity from Ent-β-lactam conjugates described in Chapter 3, we aimed to load the Ent scaffold with antibiotic cargos that have cytosolic targets. We hypothesized that Ent-mediated delivery would increase the activity of these antibiotics as well.

Fluoroquinolones are a class of widely used antibiotics that target DNA topoisomerase IV and gyrases, both of which are located in the cytoplasm.[1] These bacterial enzymes are responsible for modulating the topological state of the DNA double strands by generating transient DNA breaks and ligating them back after switching the two strands.[2] Fluoroquinolone antibiotics noncovalently bind to the active site of the enzyme-DNA complex, stabilize the transient DNA breaks and prevent the ligation step occurring, which eventually causes DNA fragmentation and cell death.[3] Resistance to fluoroquinolones mainly comes from mutations of the target enzymes that lower the binding affinity of these drugs.[4] Down regulation of porin expression levels and increased expression of efflux pumps also contribute to resistance.[4] Conjugation of fluoroquinolones to Ent may help overcome resistance caused by the insufficient drug uptake and retention.

Siderophore-fluoroquinolone conjugates have been reported by several groups using different types of siderophores, including desferrioxamine B,[5] pyoverdine,[6] pyochelin[7] and staphyloferrin A.[8] From these studies, as well as the observations in Chapter 2, siderophore-fluoroquinolone conjugates with a stable linker (e.g., PEG_3 or polymethylene as in the Ent-ciprofloxacin conjugate **37** and **42** in Chapter 2) exhibit decreased or no antimicrobial activity compared to the unmodified antibiotics. However, *in vitro* assays with purified DNA gyrase and DNA templates demonstrated that some of the conjugates still retain some inhibitory activity against DNA gyrase.[8] Successful cytosolic delivery was observed for the Ent-ciprofloxacin conjugates by *P. aeruginosa* in Chapter 2, although no antimicrobial activity was observed. Taken together, these data suggest that a release step following cell entry may be required to apply fluoroquinolones in a siderophore-mediated delivery strategy. Meanwhile, the conjugates need to be stable before cellular entry to prevent premature release of the antibiotics which will compromise the siderophore-mediated delivery strategy. Therefore, we aim to design Ent-fluoroquinolone conjugates with labile linkers to enable the release of antibiotic from the conjugates only in the cytoplasmic space.

Inspired by the pyochlin-norfloxacin conjugate reported by Rivault *et al.*(Figure 4.1),[7] in which an acyloxymethyl ester linker was used and the modified conjugates exhibited activities that were equal to or exceeded the free drug by two to four folds, we selected this linker as a start point. Acyloxymethyl esters (Figure 4.1) are widely used in pro-drug synthesis to improve the gastrointestinal absorption of drugs containing ionizable polar groups like carboxylic acids.[9] This labile linker was also used to modify

electron paramagnetic resonance (EPR) imaging agents to allow the imaging agents to cross the brain-blood barrier.[10] These studies suggested that the acyloxymethyl esters were hydrolyzed by intracellular esterases, which releases the original molecules. We pursued three synthetic routes to obtain Ent-antibiotic conjugates containing this ester linker: olefin metathesis, reductive amination, and acid-amine coupling reactions (These works were performed before the optimized routes were developed as presented in Chapter 2 and 3, and they provided important intermediates and information for the optimized routes). Antimicrobial activity of these conjugates was evaluated, and more importantly, the linker stability in aqueous solution was studied. To achieve Ent-mediated delivery, the linker should remain intact prior to cellular entry. Our stability studies demonstrated that the conjugates featuring the acyloxymethyl/ethyl ester linkers decompose quickly in aqueous solution; thus, the antimicrobial activity observed likely results from the released antibiotics rather than the Ent-mediated delivery. This result suggests that these linkers are not suitable for the design of siderophore-antibiotic conjugates.

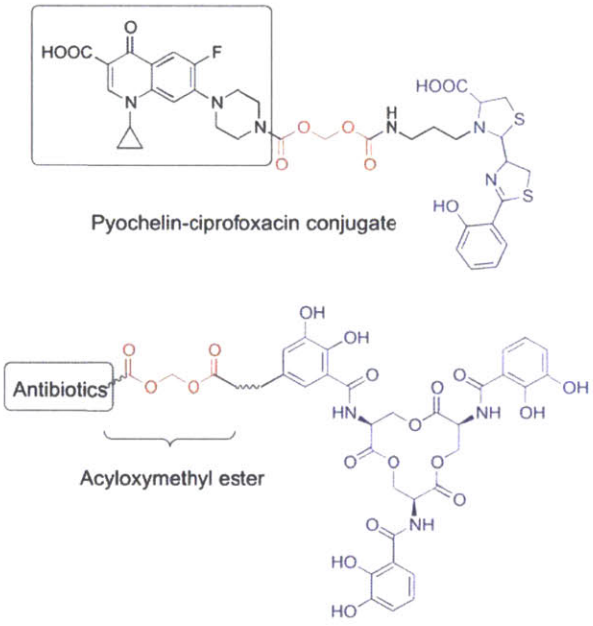

Figure 4.1. Structure of a pyochelin-ciprofloxacin conjugate with labile linker[7] and the general model of Ent-antibiotic conjugates with acyloxymethyl esters. The antibiotic moiety is highlighted with a black box, the siderophore moiety is labeled blue and the acyloxymethyl ester is labeled red.

Experimental Section

General Materials and Methods. Dimethylformamide (DMF) and dichloromethane (CH_2Cl_2) were dried over 4 Å molecular sieves. Anhydrous dimethyl sulfoxide (DMSO) was purchased from

Sigma-Aldrich and used as received. EMD TLC silica gel 60 F_{254} plates were used for analytical thin-layer chromatography. EMD PLC sillica gel 60 F_{254} plates of 1-mm thickness were used for preparative TLC. Zeoprep 60HYD silica gel (40-63 μm) from Zeochem was used for flash chromatography. The syntheses of compounds **8**, **9**, **10**, **11**, **20, 34, 39** and **40** were described in Chapter 2. Other chemicals were purchased from Sigma-Aldrich, Alfa Aesar or TCI and used as received. Semi-preparative and analytical high-performance liquid chromatography (HPLC) were performed by using an Agilent 1200 series HPLC system outfitted with an Agilent Zorbax reverse-phase C18 column (5-μm pore size, 9.4 x 250 mm) at a flow rate of 4 mL/min or a Clipeus reverse-phase C18 column (5-μm pore size, 4.6 x 250 mm) from Higgins Analytical, Inc. at a flow rate of 1 mL/min, respectively. Solvents used in all HPLC experiments are: solvent A, 0.1%TFA/H_2O; solvent B, 0.1%TFA/MeCN. Absorbance at 220, 280 and 316 nm was monitored. NMR spectra were collected on a Varian 300 or 500 MHz spectrophotometer operating at ambient probe temperature (298 K) in the Department of Chemistry Instrumentation Facility. The ^1H NMR spectra were referenced to internal standards and ^{19}F spectra were referenced to an external CF_3Cl standard. ^1H and ^{13}C NMR spectra are provided in Appendix 2. Most of the high-resolution mass spectrometry was performed by using an Agilent LC-MS system comprised of an Agilent 1260 series LC system outfitted with an Agilent Poroshell 120 EC-C18 column (2.7-μm pore size) and Agilent 6230 TOF system outfitted with an Agilent Jetstream ESI source. Solvents used for LC-MS are A, 0.1% formic acid/H_2O and B, 0.1% Fomic acid/MeCN. All samples were run using a gradient of 5-95% B over 5 min at 0.4 mL/min. In some instances, high-resolution mass spectrometry was performed by staff at the MIT Department of Chemistry Instrumentation Facility, which houses a Bruker Daltonics APEXIV 4.7 Tesla Fourier Transform Ion Cyclotron Resonance Mass Spectrometer (FT-ICR-MS) with a direct analysis in real time (DART) ionization source.

General Spectroscopic Methods. Millipore water (18.2 $M\Omega.cm^{-1}$) was used for all aqueous solutions. Buffers are prepared by using minimum 99.5% (titration) 4-(2-hydroxyethyl)-1-piperazineethanesulfonic acid (HEPES) from Sigma-Aldrich. A Mettler ToleDo In lab Routine Pro glass electrode, calibrated prior to each use, was used to adjust solution pH. Optical absorption spectra and optical density measurements were obtained by using an Agilent 8453 UV-visible diode array spectrophotometer operating at room temperature. An Agilent ultra-micro quartz cuvette (50 μL) or VWR semi-micro two sided disposable plastic cuvettes (1 mL) with 1-cm path lengths were employed for UV-visible measurements.

Chloromethyl pent-4-enoate (1). 4-Pentenoic acid (500 mg, 5.00 mmol) was dissolved in 25 mL of aqueous $NaHCO_3$ (2.0 g, 24 mmol) and tetrabutylammonium hydrogen sulfate (170 mg, 0.500 mmol).

The colorless solution was stirred at rt for 10 min and bubbles formed. Chloromethyl chlorosulfate (1.45 g, 8.80 mmol) was then added drop-wise with stirring and 25 mL of CH_2Cl_2 was subsequently added to the reaction, which was stirred vigorously at rt overnight. The organic phase was separated and washed with brine (3 × 25 mL), dried over Na_2SO_4, and passed through a 10 g silica plug. A portion of the solvent was removed by distillation under atmospheric pressure to give a colorless product solution in CH_2Cl_2 (469 mg, 63%; the yield was calculated from the ratio of CH_2Cl_2 and the product based on ^1H NMR integration). TLC R_f = 0.8 (silica, CH_2Cl_2). ^1H NMR ($CDCl_3$, 300 MHz), δ 2.42 (2H, m), 2.49 (2H, m), 5.01-5.12 (2H, m), 5.71 (2H, s), 5.82 (1H, m). HRMS (DART): $[M+H]^+$ *m/z* calcd., 149.0364; found, 149.0375.

Chloromethyl hex-5-enoate (2). As described for **1**, except that hex-5-enoic acid (114 mg, 1.00 mmol) was used as the starting material. The product was obtained as a CH_2Cl_2 solution (83 mg, 51%; the yield was calculated from the ratio of CH_2Cl_2 and the product based on ^1H NMR integration). TLC R_f = 0.8 (silica, CH_2Cl_2). ^1H NMR ($CDCl_3$, 300 MHz), δ 1.76 (2H, m), 2.10 (2H, m), 2.39 (2H, t, J = 7.5 Hz), 4.93-5.03 (2H, m), 5.70 (2H, s), 5.76 (1H, m).

Chloromethyl hept-6-enoate (3). As described for **1**, except that hept-6-enoic acid (128 mg, 1.00 mmol) was used as starting material. The product was obtained as a CH_2Cl_2 solution (119 mg, 68%; the yield was calculated from the ratio of CH_2Cl_2 and the product based on ^1H NMR integration). TLC R_f = 0.8 (silica, CH_2Cl_2). ^1H NMR ($CDCl_3$, 300 MHz), δ 1.43 (2H, m), 1.66 (2H, m), 2.06 (2H, m), 2.38 (2H, t, J = 7.2 Hz), 4.92-5.03 (2H, m), 5.69 (2H, s), 5.77 (1H, m).

(Pent-4-enoyloxy)methyl-9-fluoro-3-methyl-10-(4-methylpiperazin-1-yl)-7-oxo-3,7-dihyro-2H-[1,4]oxazino[2,3,4-ij]quinoline-6-carboxylate (4). Levofloxacin (180 mg, 0.500 mmol) was dissolved in 5 mL of dry DMF to give a light yellow solution. A portion (160 mg, 1.16 mmol) of K_2CO_3 was added to the solution and the mixture was stirred at 50 °C for 5 h to afford a gel-like mixture. A portion (81 mg, 0.55 mmol) of **1** was dissolved in 1 mL of dry DMF and added to the reaction together with a few crystals of KI. The reaction was stirred overnight at 50 °C. Water (10 mL) and CH_2Cl_2 (30 mL) were added to the reaction, and the organic phase was washed with brine (3 x 15 mL). The organic phase was dried over Na_2SO_4 and concentrated under reduced pressure to yield a light yellow solid. Flash chromatography on silica gel with a solvent gradient (100% CH_2Cl_2 to 10% MeOH/CH_2Cl_2) afforded the product as a white solid (94.4 mg, 40%). TLC R_f = 0.4 (silica, 10% MeOH/CH_2Cl_2). ^1H NMR ($CDCl_3$, 500 MHz) δ 1.50 (3H, d, J = 6.5 Hz), 2.36 (3H, s), 2.38 (2H, m), 2.49 (2H, t, J = 7.5 Hz), 2.55 (4H, bm),

3.34 (4H, bm), 4.36 (2H, m), 4.49 (1H, m), 4.97-5.06 (2H, m), 5.80 (1H, m), 5.92 (2H, m), 7.37 (1H, d, J = 12.5 Hz), 8.18 (1H, s). HRMS (DART): $[M+H]^+$ *m/z* calcd., 474.2035; found, 474.2017.

(Hex-5-enoyloxy)methyl-9-fluoro-3-methyl-10-(4-methylpiperazin-1-yl)-7-oxo-3,7-dihydro-2H-[1,4]oxazino[2,3,4-ij]quinoline-6-carboxylate (5). As described for **4**, except that compound **2** (83 mg, 0.51 mmol) was used instead of compound **1** and EtOAc was used to extract the product instead of CH_2Cl_2. The product was obtained as an impure white solid and no further purification was performed. TLC R_f = 0.45 (silica, 10% MeOH/CH_2Cl_2). ^{1}H NMR ($CDCl_3$, 300 MHz), δ 1.50 (3H, d, J = 6.6 Hz), 1.73 (2H, m), 2.08 (2H, m), 2.40 (3H, s), 2.40 (2H, t, J = 7.5 Hz), 2.65 (4H, bm), 3.37 (4H, bm), 4.35 (2H, m), 4.49 (1H, m), 4.93-5.06 (2H, m), 5.74 (1H, m), 5.93 (2H, m), 7.38 (1H, d, J = 12.3 Hz), 8.17 (1H, s). HRMS (DART): $[M+H]^+$ *m/z* calcd., 488.2191, found: 488.2202.

(Hept-6-enoyloxy)methyl-9-fluoro-3-methyl-10-(4-methylpiperazin-1-yl)-7-oxo-3,7-dihydro-2H-[1,4]oxazino[2,3,4-ij]quinoline-6-carboxylate (6). As described for **4** except that compound **3** (119 mg, 0.672 mmol) was used instead of compound **1**, and EtOAc was used to extract the product instead of CH_2Cl_2. The product was obtained as an impure white solid and no further purification was performed. TLC R_f = 0.45 (silica, 10% MeOH/CH_2Cl_2). ^{1}H NMR ($CDCl_3$, 300 MHz), δ 1.42 (2H, m), 1.51 (3H, d, J = 6.6 Hz), 1.65 (2H, m), 2.04 (2H, m), 2.41 (3H, s), 2.41 (2H, t, J = 7.5 Hz), 2.61 (4H, bm), 3.38 (4H, bm), 4.37 (2H, m), 4.47 (1H, m), 4.90-5.02 (2H, m), 5.76 (1H, m), 5.94 (2H, m), 7.45 (1H, d, J = 12.6 Hz), 8.20 (1H, s). HRMS (DART): $[M+H]^+$ *m/z* calcd., 502.2348; found, 502.2342.

(1R,7S)-(Pent-4-enoyloxy)methyl-3,3-dimethyl-6-oxo-7-(2-phenylacetamido)-2-thiabicyclo [3.2.0]heptane-4-carboxylate (7). Penicillin G potassium salt (373 mg, 1.00 mmol) and **1** (327 mg, 2.00 mmol) were combined in 10 mL of dry DMF with a few crystals of KI. The mixture was stirred at 40 °C overnight to afford an orange solution with some white solids. Water (20 mL) and CH_2Cl_2 (50 mL) were added to the reaction, and the organic phase was washed with brine (3 x 30 mL) and dried over Na_2SO_4. The solvent was removed under reduced pressure to give an orange oil. Flash chromatography on silica gel with a solvent gradient (5% to 50% EtOAc/hexanes) afforded the product as a white solid (139 mg, 31%). TLC R_f = 0.5 (silica, 40% EtOAc/hexanes). ^{1}H NMR ($CDCl_3$, 300 MHz), δ 1.43 (3H, s), 1.44 (3H, s), 2.38 (2H, m), 2.47 (2H, m), 3.64 (2H, s), 4.38 (2H, s), 5.00-5.10 (2H, m), 5.49 (1H, d, J = 4.2 Hz), 5.66 (1H, dd, J = 4.2, 9.3 Hz), 5.73-5.86 (3H, m), 6.04 (1H, d, J = 9.3 Hz), 7.25-7.40 (5H, m). HRMS (DART): $[M+H]^+$ *m/z* calcd., 447.1632; found, 447.1624.

8-(3,4-Bis(benzyloxy)-5-(((3S,7S,11S)-7,11-bis(2,3-bis(benzyloxy)benzamido)-2,6,10-trioxo-1,5,9-trioxacyclododecan-3-yl)carbamoyl)phenyl)oct-6-enoic acid (12). A portion of **8** (14 mg, 11 μmol) and hept-6-enoic acid (6.4 mg, 50 μmol) were dissolved in dry CH_2Cl_2 (10 mL). Hoveyda-Grubbs second generation catalyst (2.5 mg, 4 μmol) and 1,4-benzoquinone (0.22 mg, 2 μmol) were added. The reaction flask was then purged with N_2 three times, and the solution was stirred at 35 °C overnight. The solvent was removed and the crude reaction was purified by preparative TLC (8% MeOH/CH_2Cl_2) to yield **8** as a white solid (9.6 mg, 64%). TLC R_f = 0.6 (10% MeOH/CH_2Cl_2). ^{1}H NMR ($CDCl_3$, 300 MHz) δ 8.49-8.46 (3H, m), 7.66-7.64 (1H, m), 7.41-6.96 (37H, m), 5.51-5.49 (2H, m), 5.16-4.91 (15H, m), 4.14-4.13 (3H, m), 4.04-4.01 (3H, m), 3.29-3.28 (2H, m), 2.32 (2H, m), 2.05-2.03 (2H, m), 1.64-1.61 (2H, m), 1.42-1.40 (2H, m). HRMS (ESI): $[M+H]^+$ *m/z* calcd., 1350.5175; found, 1350.5131.

7-(4-((Chloromethoxy)carbonyl)piperazin-1-yl)-1-cyclopropyl-6-fluoro-4-oxo-1,4-dihydro-quinoline-3-carboxylic acid (13). Ciprofloxacin (331mg, 1.00 mmol), trimethylsilyl chloride (TMSCl, 350 μL, 2.76 mmol) and DIPEA (1.7 mL, 10 mmol) were combined in 20 mL of dry CH_2Cl_2 to give a light yellow solution. The solution was stirred at rt for 20 min, and chloromethyl chloroformate (108 μL, 1.20 mmol) was subsequently added slowly to afford a dark orange solution. The reaction was stirred overnight at rt, water (10 mL) was added, and the mixture was stirred vigorously for another 1 h. The mixture was extracted with CH_2Cl_2 (3 x 20 mL), and the combined organic phase was washed with 0.02M HCl (4 x 50 mL). After drying over Na_2SO_4, the organic phase was concentrated to give **13** as an orange solid (284 mg, 67%). TLC R_f = 0.75 (10% MeOH/CH_2Cl_2). ^{1}H NMR ($CDCl_3$, 300 MHz), δ 1.20-1.23 (2H, m), 1.37-1.42 (2H, m), 3.33-3.35 (4H, m), 3.53 (1H, m), 3.78-3.90 (4H, m), 5.83 (2H, s), 7.39 (1H, d, J = 6.9 Hz), 8.06 (1H, d, J = 12.9 Hz), 8.78 (1H, s). ^{19}F NMR ($CDCl_3$, 300 MHz), δ -121.36- -121.29 (m). HRMS (DART): $[M+H]^+$ *m/z* calcd., 424.1070; found, 424.1057.

3-(((4-(3-Carboxy-1-cyclopropyl-6-fluoro-4-oxo-1,4-dihydroquinolin-7-yl)piperazine-1-carbonyl)oxy)methoxy)-3-oxopropan-1-aminium-2,2,2-trifluoroacetate (14). TMSCl (65 μL, 0.51 mmol), DIPEA (118 μL, 0.674 mmol) and **13** (57 mg, 0.14 mmol) were combined in 3 mL of dry DMF and stirred for 5 min at rt to give a light yellow solution. *N*-Boc-β-alanine (56 mg, 0.30 mmol) and DIPEA (118 μL, 0.674 mmol) were combined in 2 mL of dry DMF to give a colorless solution. The two solutions were mixed together and stirred overnight at 75 °C. EtOAc (15 mL) and water (15 mL) were added to the reaction, and the organic phase was washed with H_2O (2 x 15 mL). The aqueous phase was back extracted once by using 10 mL of EtOAc, and the combined organic layers were dried over Na_2SO_4 and concentrated. The crude product was purified by preparative TLC (10% MeOH/CH_2Cl_2) to yield Boc protected precursor of **14** as a light yellow solid (45 mg, 57%). TLC R_f = 0.7 (10% MeOH/CH_2Cl_2). ^{1}H

NMR ($CDCl_3$, 300 MHz), δ 1.18-1.21 (2H, m), 1.37-1.39 (2H, m), 1.43 (9H, s), 2.61 (2H, t, J = 6.9 Hz), 3.28-3.38 (4H, m), 3.41 (2H, t, J = 6.9 Hz), 3.71-3.80 (4H, m), 5.00 (1H, s), 5.83 (2H, s), 7.37 (1H, d, J = 7.2 Hz), 8.03 (1H, d, J = 13.5 Hz), 8.76 (1H, s). ^{19}F NMR ($CDCl_3$, 300 MHz), δ -121.27 (d, J = 12.6 Hz).

A portion (45 mg, 0.078 mmol) of this product was dissolved in 1.2 mL CH_2Cl_2, and TFA (0.8 mL) was added drop-wise to give a yellow solution. The reaction was stirred for 3 h at rt, and concentrated under reduced pressure to afford **14** as a light yellow solid (29 mg, 79%). TLC R_f = 0.2 (10% MeOH/CH_2Cl_2). ^{1}H NMR (DMSO, 300 MHz), δ 1.17-1.19 (2H, m), 1.29-1.32 (2H, m), 2.72 (2H, t, J = 6.9 Hz), 3.03 (2H, t, J = 6.9 Hz), 3.32-3.35 (4H, m), 3.61-3.64 (4H, m), 3.80 (1H, m), 5.75 (2H, s), 7.58 (1H, m), 7.84 (3H, m), 7.92 (1H, d, J = 13.5 Hz), 8.65 (1H, s). ^{19}F NMR (DMSO, 300 MHz), δ -121.41 (1F, m), -73.16 (3F, s). HRMS (DART): $[M+H]^+$ *m/z* calcd., 477.1780; found, 477.1762.

2-(((4-(3-Carboxy-1-cyclopropyl-6-fluoro-4-oxo-1,4-dihydroquinolin-7-yl)piperazine-1-carbonyl)oxy)methoxy)-*N*-methyl-2-oxoethanaminium 2,2,2-trifluoroacetate (19). Trityl-protected *N*-methylglycine was synthesized from *N*-methylglycine (Alfa Aesar) by using a literature procedure.[11] Trimethylsilyl chloride (TMSCl, 100 μL, 0.785 mmol), DIPEA (236 μL, 1.34 mmol) and **13** (114 mg, 0.270 mmol) were combined in 3 mL of dry DMF and stirred for 5 min at rt to give a light yellow solution. *N*-Trityl-methylglycine (223 mg, 0.675 mmol) and DIPEA (236 μL, 1.34 mmol) were combined in 2 mL of dry DMF to give a colorless solution. The two solutions were mixed together and stirred overnight at 75 °C. EtOAc (15 mL) and water (15 mL) were added to the dark orange solution, and the organic phase was washed with brine (2 x 15mL). The aqueous phase was back-extracted once by using 10 mL of EtOAc, and the combined organic layers were dried over Na_2SO_4 and concentrated. The crude reaction product was purified by two silica flash columns (50% hexanes/EtOAc and 10% MeOH/CH_2Cl_2) to yield **18** as a light yellow solid (119 mg, 62%). TLC R_f= 0.7 (10% MeOH/CH_2Cl_2). ^{1}H NMR ($CDCl_3$, 300 MHz) δ 14.9 (1H, bs), 8.77 (1H, s), 8.06 (1H, d, J = 12.6 Hz), 7.54-7.12 (15H, m), 5.88 (1H, s), 3.75 (4H, bs), 3.46 (1H, bs), 3.30 (4H, bs), 3.09 (2H, s), 2.14 (3H, s), 1.34-1.26 (4H, m).

Compound **19** was obtained from **18** according to a reported procedure.[12] A portion of **18** (59.0 mg, 82.0 μmol) was dissolved in 2 mL of CH_2Cl_2 and 2% TFA and 1% H_2O was added to give an orange solution. The reaction was stirred for 1.5 h at rt and concentrated. Water was removed by lyophilization, and the crude product was redissolved in 1 mL of acetone. Compound **19** precipitated as a yellow solid following addition of 20 mL of diethyl ether. (35.7 mg, 74%). TLC R_f = 0.1 (10% MeOH/CH_2Cl_2). ^{1}H NMR ($CDCl_3$, 300 MHz) δ 8.68 (1H, s), 7.91 (1H, d, J = 12.9 Hz), 7.35 (1H, bs), 5.78 (1H, s), 3.91-3.82 (7H, m), 3.63 (4H, bs), 2.64 (3H, s), 1.31 (2H, s), 1.10 (2H, s). ^{19}F NMR ($CDCl_3$, 282 MHz), δ -75.9, -121.1. HRMS (ESI): $[M+H]^+$ *m/z* calcd., 477.1786; found, 477.1775.

7-(4-(((2-((3-(((3S,7S,11S)-7,11-Bis(2,3-dihydroxybenzamido)-2,6,10-trioxo-1,5,9-trioxacyclododecan-3-yl)carbamoyl)-4,5-dihydroxybenzyl)(methyl)amino)acetoxy)methoxy)carbonyl)piperazin-1-yl)-1-cyclopropyl-6-fluoro-4-oxo-1,4-dihydroquinoline-3-carboxylic acid (22). In 0.7 mL of DMSO, **19** (11.8 mg, 20.0 μmol) and **20** (12.4 mg, 10.0 μmol) were dissolved. Then, $NaBH_3CN$ (2.8 mg, 40 μmol) was added to afford a yellow solution. The reaction was stirred at rt overnight, and partitioned in 30 mL of EtOAc and 15 mL of brine. The organic phase was washed by brine (2 x 15 mL), dried over Na_2SO_4 and concentrated. The product was purified by preparative TLC (10% MeOH/CH_2Cl_2) to yield **21** as a light yellow solid (8.6 mg, 51%). TLC R_f = 0.6 (10% MeOH/CH_2Cl_2). ^{1}H NMR ($CDCl_3$, 300 MHz) δ 14.9 (1H, bs), 8.75 (1H, s), 8.49-8.44 (3H, m), 8.04 (1H, d, J = 12.6 Hz), 7.66-7.63 (1H, m), 7.55-7.54 (1H, s), 7.43-7.10 (37H, m), 5.85 (2H, s), 5.17-5.00 (12H, m), 4.90-4.88 (3H, m), 4.16-4.01 (6H, m), 3.72 (4H, bs), 3.65 (2H, s), 3.52 (1H, bs), 3.33 (2H, s), 3.27 (4H, bs), 2.38 (3H, s), 1.33-1.16 (4H, m).

A portion of **21** (8.6 mg, 5.1 μmol) was dissolved in 2 mL of 1:1 1,4-dioxane/EtOH, and 9.0 mg Pd/C (10% wt, Sigma-Aldrich) was added after the flask was purged by N_2. The reaction was stirred under H_2 (1 atm) at rt for 3 h, and the Pd/C was removed by centrifugation (13,000 rpm, 10 min). The clear solution was concentrated and redissolved in 4:2:1 1,4-dioxane/H_2O/MeOH and purified by semi-preparative HPLC (10-70% B over 20 min, 4 mL/min). The product eluted at 19.5 min and the combined fractions were lyophilized to give **22** as white solid (1.2 mg, 20%). The HPLC trace of purified **22** was reported in main text. HRMS (ESI): $[M+H]^+$ *m/z* calcd., 1158.3228; found, 1158.3193.

7-(4-((1-Chloroethoxy)carbonyl)piperazin-1-yl)-1-cyclopropyl-6-fluoro-4-oxo-1,4-dihydroquinoline-3-carboxylic acid (23). Ciprofloxacin (993 mg, 3.00 mmol) and TMSCl (800 μL, 6.27 mmol) were combined in 50 mL of dry CH_2Cl_2. After stirring at rt for 10 min, DIPEA (5.1 mL, 29 mmol) was added to afford a clear light yellow solution. Chloroethyl chloroformate (400 μL, 3.70 mmol) was subsequently added slowly to afford a dark orange solution with a little smoke forming. The reaction was stirred overnight at rt. MeOH (10 mL) was added, and the mixture was stirred vigorously for another 0.5 h. The crude reaction solution was concentrated, redissoved in 80 mL of CH_2Cl_2, and washed with 0.1 M HCl (3 x 30 mL) and H_2O (2 x 50 mL). After drying over Na_2SO_4, the organic phase was concentrated to give **23** as an orange solid (746 mg, 57%). TLC R_f = 0.75 (10% MeOH/CH_2Cl_2). ^{1}H NMR ($CDCl_3$, 300 MHz) δ 14.9 (1H, s), 8.75 (1H, s), 8.02 (1H, d, J = 12.6 Hz), 7.37 (1H, d, J =7.2 Hz), 6.62 (1H, q, J = 4.4 Hz), 3.83 (2H, bs), 3.75-3.71 (2H, m), 3.57-3.52 (1H, m), 3.33-3.32 (4H, m), 1.85 (3H, d, J = 6.0 Hz), 1.44-1.37 (2H, m), 1.24-1.19 (2H, m). HRMS (ESI): $[M+H]^+$ *m/z* calcd., 438.1232; found, 438.1221.

1-Cyclopropyl-6-fluoro-7-(4-((1-(2-(methylamino)acetoxy)ethoxy)carbonyl)pipera-zin-1-yl)-4-oxo-1,4-dihydroquinoline-3-carboxylic acid (24). TMSCl (100 μL, 0.785 mmol), DIPEA (236 μL,

1.34 mmol) and **23** (118 mg, 0.269 mmol) were combined in 3 mL of dry DMF and stirred for 5 min at rt to give a light yellow solution. *N*-Trityl-methylglycine (223 mg, 0.675 mmol) and DIPEA (236 μL, 1.34 mmol) were combined in 2 mL of dry DMF to give a colorless solution. The two solutions were mixed together and stirred overnight at 65 °C. MeOH (2 mL) was added to the reaction, and the mixture was stirred for another 15 min. A brown precipitate formed. The crude reaction was concentrated and redissolved in 50 mL of EtOAc. The organic phase was washed with brine (3 x 20 mL) and dried over Na_2SO_4. The crude reaction product was purified by flash chromatography on silica gel (40% EtOAc/CH_2Cl_2 and 10% MeOH/CH_2Cl_2) to afford **24** as a yellow solid (56 mg, 28%). It was found that **24** decomposes on silica gel. TLC R_f = 0.5 (10% MeOH/CH_2Cl_2). ^{1}H NMR ($CDCl_3$, 300 MHz) δ 8.72 (1H, s), 8.01 (1H, d, J = 12.6 Hz), 7.53-7.12 (16H, m), 6.94 (1H, q, J = 4.0 Hz), 3.82-3.67 (4H, m), 3.38-3.32 (5H, m), 3.08-2.98 (2H, m), 2.13 (3H, s), 1.54 (3H, d, J = 5.5 Hz), 1.31-1.24 (4H, m). This product was used in the next step without further purification.

The trityl group was removed from **24** (56 mg) as described for **18** to give **26** as orange solid (31 mg, 81%). TLC R_f = 0.1 (10% MeOH/CH_2Cl_2). ^{1}H NMR ($CDCl_3$, 300 MHz) δ 8.64 (1H, s), 7.84 (1H, d, J = 12.9 Hz), 7.32 (1H, d, J = 6.9 Hz), 6.79 (1H, q, J = 5.4 Hz), 3.80-3.53 (11H, m), 2.68 (3H, s), 1.48 (3H, d, J = 5.4 Hz), 1.34-1.32 (2H, m), 1.1 (2H, bs). HRMS (ESI): $[M+H]^+$ *m/z* calcd., 491.1942; found, 491.1927.

1-Cyclopropyl-6-fluoro-7-(4-((1-((3-methyl-2-(methylamino)butanoyl)oxy)ethoxy)carbonyl)-piperazin-1-yl)-4-oxo-1,4-dihydroquinoline-3-carboxylic acid (27). Compound **25** was synthesized as described for **24** except that *N*-Boc-methylvaline (156 mg, 0.675 mmol) was used. Compound **25** was obtained as orange solid (93 mg, 53%). TLC R_f= 0.7 (10% MeOH/CH_2Cl_2). ^{1}H NMR ($CDCl_3$, 300 MHz) δ 8.68 (1H, s), 7.92 (1H, d, J = 12.6 Hz), 7.37 (1H, bs), 6.88-6.85 (1H, m), 4.42-4.04 (1H, m, due to rotamers), 3.70 (5H, m), 3.30 (4H, bs), 2.86-2.78 (3H, m, due to rotamers), 2.19-2.16 (1H, m), 1.53-1.40 (14H, m), 1.19 (2H, bs), 0.99-0.96 (3H, m), 0.87 (3H, d, J = 6.6 Hz).

A portion of **25** (93 mg, 0.15 mmol) was dissolved in 10 mL of 40% TFA/CH_2Cl_2 and the green-brown solution was stirred at rt for 2.5 h. The crude reaction material was then concentrated to ~1 mL, and the product was precipitated by addition of 17 mL of diethyl ether. After filtration and washing with ether, **27** was obtained as orange solid (73.7 mg, 94%). TLC R_f = 0.5 (10% MeOH/CH_2Cl_2). ^{1}H NMR (CD_3OD, 300 MHz) δ 8.64 (1H, s), 7.68 (1H, d, J = 12.6 Hz), 7.53 (1H, bs), 6.99-6.96 (1H, m), 3.98 (1H, bs), 3.76 (5H, m), 3.39 (4H, bs), 2.78-2.75 (3H, m, due to rotamers), 2.34 (1H, bs), 1.63 (3H, d, J = 5.1 Hz), 1.42 (2H, bs), 1.22-1.06 (8H, m). HRMS (ESI): $[M+H]^+$ *m/z* calcd., 533.2416; found, 533.2414.

1-Cyclopropyl-6-fluoro-7-(4-(((hept-6-enoyloxy)methoxy)carbonyl)piperazin-1-yl)-4-oxo-1,4-dihydroquinoline-3-carboxylic acid (28). As described for **18** except that hept-6-enoic acid (92 mg, 0.71 mmol) was used instead of *N*-trityl-methylglycine and the crude reaction organic phase was purified by passing through a silica plug in 10% MeOH/CH_2Cl_2. Compound **28** was obtained as yellow solid (77 mg, 57%). TLC R_f = 0.6 (10% MeOH/CH_2Cl_2). ^{1}H NMR ($CDCl_3$, 300 MHz) δ 14.9 (1H, bs), 8.78 (1H, s), 8.05 (1H, d, J = 12.9 Hz), 7.36 (1H, d, J = 6.9 Hz), 5.83-5.72 (3H, m), 5.04-4.94 (1H, m), 3.76 (4H, bs), 3.57-3.49 (1H, m), 3.32 (4H, bs), 2.39 (2H, t, J = 7.5 Hz), 2.07 (2H, dt, J = 7.1, 7.1 Hz), 1.72-1.62 (2H, m), 1.48-1.18 (6H, m). HRMS (ESI): $[M+H]^+$ *m/z* calcd., 516.2146; found, 516.2157.

7-(4-((1-(((S)-2-Benzamidopropanoyl)oxy)ethoxy)carbonyl)piperazin-1-yl)-1-cyclopropyl-6-fluoro-4-oxo-1,4-dihydroquinoline-3-carboxylic acid (29). Compound **29** was synthesized similarly as **24** using 0.054 mmol of **23** and *N*-benzoyl alanine was used instead of *N*-trityl-methylglycine. Preparative TLC (7% MeOH/CH_2Cl_2) purification afforded **29** as yellow solid (14 mg, 44%). TLC R_f = 0.7 (10% MeOH/CH_2Cl_2). ^{1}H NMR ($CDCl_3$, 300 MHz) δ 14.9 (1H, bs), 8.73 (1H, s), 7.98 (1H, d, J = 12.0 Hz), 7.78-7.42 (6H, m), 6.94-6.89 (1H, m), 6.77 (1H, bs), 4.80-4.78 (1H, m), 3.74-3.32 (9H, m), 1.58-1.20 (10H, m). HRMS (ESI): $[M+H]^+$ *m/z* calcd., 595.2204; found, 595.2202.

7-(4-((1-(((S)-2-Benzamido-3-methylbutanoyl)oxy)ethoxy)carbonyl)piperazin-1-yl)-1-cyclopropyl-6-fluoro-4-oxo-1,4-dihydroquinoline-3-carboxylic acid (30). Compound **30** was synthesized as **29** except that *N*-benzoyl valine was used instead of *N*-benzoyl alanine and obtained as a yellow solid (16 mg, 48%). TLC R_f = 0.5 (10% MeOH/CH_2Cl_2). ^{1}H NMR ($CDCl_3$, 300 MHz) δ 14.9 (1H, bs), 8.73 (1H, s), 7.98 (1H, d, J = 12.0 Hz), 7.80-7.38 (6H, m), 6.94 (1H, q, J = 5.6 Hz), 6.63 (1H, d, J = 9 Hz), 4.82-4.75 (1H, m), 3.72-3.31 (9H, m), 2.31 (1H, bs), 1.57 (3H, d, J = 5.1 Hz), 1.38-0.98 (10H, m). HRMS (ESI): $[M+Na]^+$ *m/z* calcd., 645.2337; found, 645.2306.

7-(4-((1-(((S)-2-(Benzyl(methyl)amino)-3-methylbutanoyl)oxy)ethoxy)carbonyl)piperazin-1-yl)-1-cyclopropyl-6-fluoro-4-oxo-1,4-dihydroquinoline-3-carboxylic acid (31). A portion of **27** (9.5 mg, 18 μmol) and benzaldehyde (1.8 μL, 18 μmol) were dissolved in DMSO (0.2 mL). $NaBH_3CN$ (2.3 mg, 36 μmol) was added to the solution and the reaction was stirred at rt overnight. The crude reaction was partitioned with 0.8 mL of CH_2Cl_2 and 0.8 mL of H_2O. The organic phase was washed by brine (2 x 1 mL) and dried over Na_2SO_4. The product was purified by preparative TLC (10% MeOH/CH_2Cl_2) to give an orange solid (4.5 mg, 40%). HRMS (ESI): $[M+H]^+$ *m/z* calcd., 623.2881; found, 623.2879.

7-(4-((1-(((S)-2-Aminopropanoyl)oxy)ethoxy)carbonyl)piperazin-1-yl)-1-cyclopropyl-6-fluoro-4-oxo-1,4-dihydroquinoline-3-carboxylic acid (32). Compound **32** was synthesized as **27** except *N*-Boc-alanine (127.6 mg, 0.675 mmol) was used instead of *N*-Boc-methyl-valine. The final product was obtained as orange solid (72 mg, overall 44% yield from **23**). TLC R_f = 0.4 (10% MeOH/CH_2Cl_2). ^{1}H NMR ($CDCl_3$, 300 MHz) δ 8.52-8.51 (1H, m, due to diastereomers), 7.71-7.64 (1H, m, due to diastereomers), 7.26 (1H, bs), 6.71-6.66 (1H, m, due to diastereomers), 4.45 (1H, bs), 3.86 (1H, m), 3.53 (5H, bs), 3.17-3.14 (4H, m), 1.40-1.02 (10H, m). HRMS (ESI): $[M+H]^+$ *m/z* calcd., 491.1942; found, 491.1919.

7-(4-((1-(((S)-2-Amino-3-methylbutanoyl)oxy)ethoxy)carbonyl)piperazin-1-yl)-1-cyclopropyl-6-fluoro-4-oxo-1,4-dihydroquinoline-3-carboxylic acid (33). Compound **33** was synthesized as **27** except *N*-Boc-valine (146.6 mg, 0.675 mmol) was used instead of *N*-Boc-methyl-valine. The final product was obtained as orange solid (39 mg, overall yield 27% from **23**). TLC R_f = 0.5 (10% MeOH/CH_2Cl_2). ^{1}H NMR (CD_3OD, 300 MHz) δ 8.62 (1H, s), 7.67-7.51 (2H, m), 6.98-6.93 (1H, m, due to diastereomers), 3.98 (1H, bs), 3.75-3.35 (9H, m), 2.32 (1H, bs), 1.62-1.60 (3H, m), 1.42 (2H, bs), 1.22 (2H, bs), 1.12-1.08 (6H, m, due to diastereomers). HRMS (ESI): $[M+H]^+$ *m/z* calcd., 519.2255; found, 519.2247.

7-(4-((1-(((S)-2-(3-(((3S,7S,11S)-7,11-Bis(2,3-dihydroxybenzamido)-2,6,10-trioxo-1,5,9-trioxacyclododecan-3-yl)carbamoyl)-4,5-dihydroxybenzamido)propanoyl)oxy)ethoxy)carbonyl)-piperazin-1-yl)-1-cyclopropyl-6-fluoro-4-oxo-1,4-dihydroquinoline-3-carboxylic acid (37). In a mixture of 0.5 mL of DMSO and 1 mL of CH_2Cl_2, **34** (29 mg, 23.2 μmol) and **32** (28.0 mg, 46.4 μmol) were combined, and PyAOP (17.5 mg, 33.6 μmol) and DIPEA (40.4 μL, 0.232 mmol) were added. The reaction was stirred at rt overnight and partitioned in CH_2Cl_2 (5 mL) and brine (5 mL). The organic phase was washed twice with 5 mL of H_2O, dried over Na_2SO_4 and concentrated. Compound **35** was purified by preparative TLC (8% MeOH/CH_2Cl_2) and obtained as a white-yellow solid (9.6 mg, 22%). TLC R_f = 0.6 (10% MeOH/CH_2Cl_2). ^{1}H NMR ($CDCl_3$, 300 MHz) δ 14.9 (1H, bs), 8.76-8.71 (1H, m), 8.50-8.47 (3H, m), 8.06-7.97 (2H, m), 7.79-7.76 (1H, m), 7.65-7.60 (2H, m), 7.40-7.10 (49H, m), 6.90-6.86 (2H, m), 5.22-5.01 (12H, m), 4.89 (3H, m), 4.77-4.70 (1H, m), 4.14-4.01 (6H, m), 3.75-3.30 (9H, m), 1.58-1.50 (6H, m), 1.38-1.14 (4H, m).. HRMS (ESI): $[M+H]^+$ *m/z* calcd., 1726.5994; found, 1726.5964.

A portion of **35** (9.6 mg, 5.6 μmol) was dissolved in 2 mL of 1:1 1,4-dioxane/EtOH, and 10.0 mg Pd/C (10% wt) was added after the flask was purged with N_2. The reaction was stirred under H_2 (1 atm) at rt for 5 h, and the Pd/C was removed by centrifugation (13,000 rpm, 10 min). The clear reaction solution was concentrated and redissolved in 4:2:1 1,4-dioxane/H_2O/MeOH and purified by semi-preparative HPLC (20-70% B over 15 min, 4 mL/min). The product eluted at 17.2 and 17.5 min (diastereomers) and

lyophilized to give **37** as white solid (2.0 mg, 30%). The HPLC trace of the purified product is reported in Appendix 2. HRMS (ESI): $[M+H]^+$ *m/z* calcd., 1186.3177; found, 1186.3145.

7-(4-((1-(((S)-2-(3-(((3S,7S,11S)-7,11-Bis(2,3-dihydroxybenzamido)-2,6,10-trioxo-1,5,9-trioxacyclododecan-3-yl)carbamoyl)-4,5-dihydroxybenzamido)-3-methylbutanoyl)oxy)ethoxy)carbonyl)piperazin-1-yl)-1-cyclopropyl-6-fluoro-4-oxo-1,4-dihydroquinoline-3-carboxylic acid (38). Compound **36** was synthesized as described for **35** except that the reaction scale was adjusted to using 50 mg (39.9 μmol) of **34** and compound **33** (21.3 mg, 34.4 μmol) was used instead of **32**. After purification, **36** was obtained as white solid (46.6 mg, 74%). TLC R_f = 0.5 (5% MeOH/CH_2Cl_2). ^1H NMR ($CDCl_3$, 300 MHz) δ 14.9 (1H, bs), 8.2 (1H, bs), 8.51-8.47 (3H, m), 8.00-7.97 (2H, m), 7.79-7.77 (1H, m), 7.64-7.62 (2H, m), 7.40-7.10 (49H, m), 6.94-6.79 (2H, m), 5.22-5.01 (12H, m), 4.89 (3H, bs), 4.78-4.70 (1H, m), 4.14-4.00 (6H, m), 3.75-3.13 (9H, m), 1.83-1.79 (1H, m), 1.58-1.55 (3H, m), 1.37-1.18 (4H, m), 1.04-0.99 (6H, m). HRMS (ESI): $[M+H]^+$ *m/z* calcd., 1754.6307; found, 1754.6267.

Compound **38** was obtained from **36** following the same procedure as described for **37**. A mixture of two diastereomers was obtained as a white-yellow solid (7.1 mg, 22%). The HPLC trace of the purified product (diastereomeric mixture) is reported in Appendix 2. HRMS (ESI): $[M+H]^+$ *m/z* calcd., 1236.3309; found, 1236.3321.

Antimicrobial Activity Assays. *E. coli* K12 was obtained from Christopher T. Walsh (Harvard Medical School). Frozen cell stocks of *E. coli* K12 were stored in M9 minimal media, which is necessary for the strain to maintain its ability to grow in minimal media. *E. coli* NR698 was kindly provided by Professor Daniel Kahne (Department of Chemistry and Chemical Biology, Harvard University). *E. coli* H1876 (*fepA-, cir-, fiu-*) was a gift from Professor Klaus Hantke (Department of Membrane Physiology, University of Tübingen). *Staphylococcus aureus* ATCC 25923, *E. coli* ent- (ATCC 33475) and *E. coli* CFT073 (ATCC 700928) were purchased from American Type Culture Collection (ATCC) and revived and stored in LB medium.

For antimicrobial assays, bacterial strains were grown in LB media at 37 °C for 16 h and diluted in a 1:100 ratio with fresh LB with or without 200 μM 2,2'-dipyridyl (DP) and incubated at 150 rpm at 37 °C until the optical density at 600 nm (OD_{600}) reached ~0.6. The cultures were subsequently diluted with poor-broth (PB) nutrient medium (1% Bacto Tryptone, 5% NaCl, w/v) with or without 200 μM DP to OD_{600} = 0.001 (except for *E. coli* ent- where 50% MHB medium was used because PB cannot support its growth in the presence of DP). The concentration of each Ent-ciprofloxacin conjugate was determined by using the extinction coefficient of **39** at 279 nm (ε_{279nm} = 12600 $M^{-1}cm^{-1}$), which was determined based on accurate sample mass recorded by a 5-digit balance (Professor Klibanov's lab). Working dilutions of

the conjugates were prepared in filter-sterilized milli-Q H_2O except for the iron-loaded samples where filter-sterilized 75 mM HEPES buffer at pH 7.5 was used. A 90-μL aliquot of the diluted culture was mixed with a 10-μL aliquot of the conjugate solution at various concentrations in 96-well plates and incubated at 30 °C for 19 h. Bacterial growth was assayed by measuring OD_{600} using a BioTek Synergy HT plate reader. The growth recovery assay was conducted in the same manner.

Stability Studies of the Ciprofloxacin Conjugates. All compounds tested were stored as DMSO stock solutions and diluted with 75 mM HEPES buffer at pH 7.5 to a final concentration of 40 μM. The samples, with a total volume of 600 μL, were placed into the HPLC auto-sampler thermostated at 30 °C. At 1-h intervals, 50-μL of the sample was injected into the analytical column and analyzed using a gradient of 10% B for 5 min and then 10-70% B over 7 min at 1 mL/min. The HPLC traces obtained by monitoring absorbance at 280 nm were used to evaluate conjugate stability. The signal at 316 nm was used to monitor hydrolysis of native Ent. The peak area of the tested compound was manually integrated and plotted over time to obtain a degradation curve. The degradation curves were fitted by Prism to first order reactions. Three repetitions were performed for each compound, and the averaged half-lives of the three trials are reported in Table 4.1. Example fits for each compound are shown at the end of the chapter in Figure 4.11.

MceD Hydrolysis Assay with Ent-ciprofloxacin Conjugates. MceD (provided by Professor Elizabeth Nolan, with a His_6 tag on the C-terminus, 103 μM) was diluted 10-fold by 75 mM HEPES buffer at pH 7.5. The reaction solution (500 μL) was prepared in 75 mM HEPES buffer at pH 7.5, containing 32 μM substrate and 20 nM MceD. At t = 0, 2, 5, 8, 25 min, 100 μL of the reaction was taken and quenched by addition of 20 μL of 3% TFA/H_2O. The quenched reactions were stored on ice, centrifuged (13,000 rpm, 10 min) and analyzed by HPLC using the same method for the stability assays.

Results and Discussion

Design of Ent-Antibiotic Conjugates with Acyloxymethyl Ester Linker via Olefin Metathesis. To incorporate the acyloxymethyl ester linker, we first designed a synthetic route involving an olefin metathesis reaction. This route was chosen because the metathesis reaction is highly chemoselective, therefore no additional protection/deprotection steps are needed for the antibiotics or the Ent scaffold during the syntheses. If successful, this approach could be easily applied to a variety of molecules featuring different functional groups for Ent conjugation. We placed the metathesis reaction towards the end of the syntheses such that the enterobactin and antibiotic portions could be synthesized in parallel as a convergent synthetic route. We therefore aimed to (i) couple the acyloxymethyl ester with a

terminal olefin group to the antibiotics (Scheme 4.1), and (ii) use olefin metathesis to connect the antibiotic to Ent (Scheme 4.2). The *cis*- and *trans*-alkene isomers generated from the metathesis will be reduced when removing the benzyl groups from the catechol hydroxyls, which will afford the final enterobactin-antibiotic conjugates.

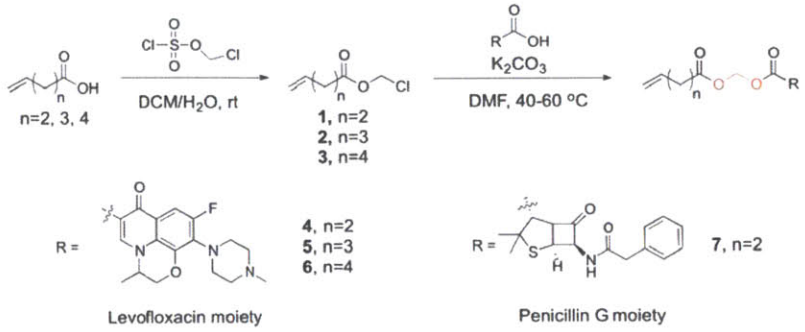

Scheme 4.1. Syntheses of antibiotic-alkenes with acyloxymethyl ester (labeled red) linkages.

Synthesis of Modified Antibiotics with Acyloxymethyl Ester Linked Olefin Groups. Acyloxymethyl esters are usually formed between two carboxylic acids,[10] and have also been inserted between one carboxylic acid and one amino group.[13] We chose levofloxacin, ciprofloxacin and penicillin as targeted antibiotics for this study, all of which have a free carboxylic acid group. The secondary amine on ciprofloxacin was protected with *tert*-butyloxycarbonyl (Boc) to avoid side reactions. The acyloxymethyl esters were first synthesized by reacting each antibiotic with chloromethyl chlorosulfate to yield chloromethyl esters. We intended to couple each chloromethyl ester to a carboxylic acid with a terminal alkene moiety to give the antibiotic-alkenes containing an acyloxymethyl ester linker. Unfortunately, following the reported procedure,[10] no significant new species could be found judging by analytical TLC. We changed the reaction order (Scheme 4.1), and the alkene-acids were first reacted with chloromethyl chlorosulfate, which gave yields of 50% to 70%, and the antibiotics were coupled to chloromethyl ester **1-3** under basic conditions to give the corresponding antibiotics **4-7** modified with acyloxymethyl ester and olefin groups.

It should be noted that compounds **1-3** are very volatile and using the rotavap to remove the reaction solvent (CH_2Cl_2) resulted in significant product loss. These three compounds were purified by passing the crude reactions through a silica plug followed by distillation under atmospheric pressure. During the purification of **4-7**, it was also found that these molecules are unstable on silica gel. 2-D analytical TLC showed product decomposition. The reason might be that the antibiotic moieties are good leaving groups and the silica gel is slightly acidic, the latter of which catalyzes decomposition.

Olefin Cross Metathesis Screening for the Synthesis of Ent-antibiotic Conjugates. With the antibiotic-alkyne **4-7** in hand, we proceeded to connect them with the mono-alkene functionalized Ent precursor **8** through olefin metathesis (Scheme 4.2). Compound **8** can be synthesized as described for the compound **9** in Chapter 2 by using the terminal olefin modified benzyl-protected 2,3-dihyroxylbenzoic acid (**21**, Chapter 2) instead of the substituted olefin derivative (**22**, Chapter 2). Many metal-based catalysts for olefin metathesis have been developed. We chose four widely used ruthenium catalysts, shown in Figure 4.2, for our initial screening. These catalysts are relatively stable when exposed to air and water, and can tolerate many functional groups including alcohols, carboxylic acids and amides.[14]

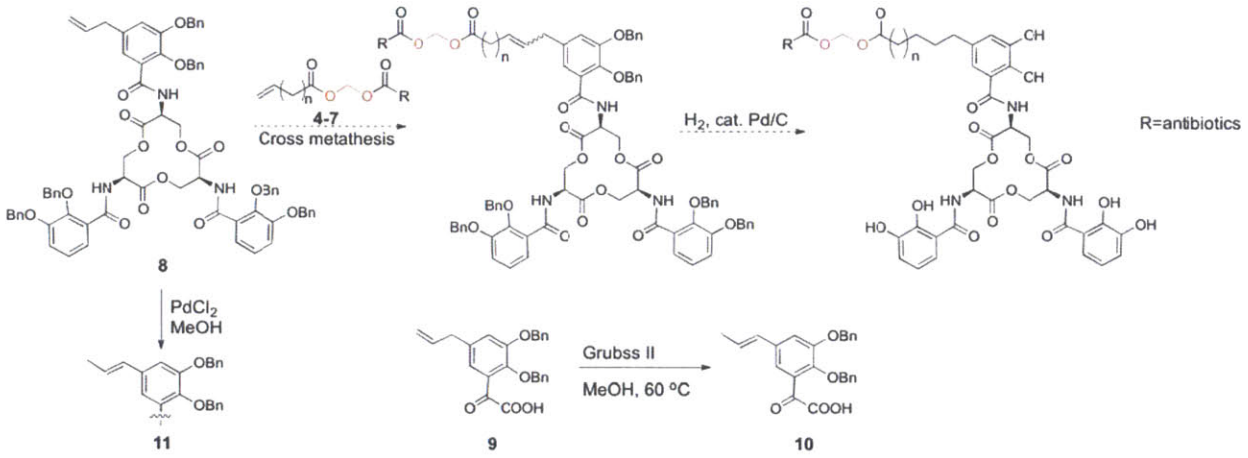

Scheme 4.2 Proposed syntheses of Ent-antibiotics conjugates through olefin cross metathesis and olefin isomerization on **9** observed under catalysis conditions. The labile linker is labeled red.

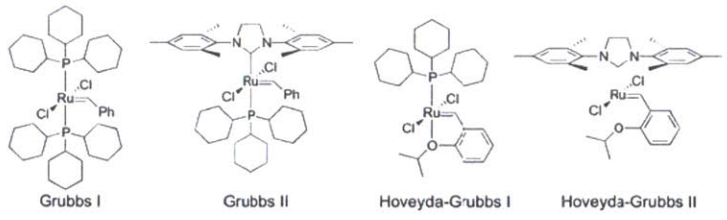

Figure 4.2. Ruthenium-based olefin metathesis catalysts used for screening.

Various metathesis reaction conditions were screened on a 1 μmol (1.5 mg) scale of **8**, and 2 or 4 equiv. of **4** / **5** in the presence of 30% catalyst in mol. The reagents were weighed in 10 to 20 mg quantities, dissolved in solvent and aliquoted to provide the required amounts. Two solvents, CH_2Cl_2 and toluene, were used in the screening, and the reactions were carried at 35 °C (CH_2Cl_2) or 40 °C (toluene)

overnight. Analytical TLC of these reactions revealed many new species without a major product. Data obtained from MALDI-TOF mass spectroscopy of the crude reactions showed that cross-metathesis occurred when Grubbs first/second generation or Grubbs-Hoveyda second generation catalyst and a 4:1 ratio of compounds **4** and **8** were employed. However, a peak with -14 Da relative to the *m/z* of the desired product was always present in the mass spectra. In the reaction of **8** with **5**, another peak with -28 Da was also observed. In all of the conditions where the desired products were identified, the homo-dimer of **4** or **5** was also present, again accompanied by a -14 Da peak. For reactions employing compound **5**, species with +14, +28 and -28 Da relative to the homo-dimmer of **5** were also observed. One likely origin for these unexpected peaks is migration of the C-C double bond during the reaction; cross metathesis of the isomerized starting materials gives the mass of losing methylene groups (14 Da). Similar side reactions have been reported.[15] This hypothesis was further confirmed by treating **9** with Grubbs second generation catalyst in MeOH at 60 °C for 3 h, which afforded 50% conversion of **9** to **10** (Scheme 4.2) based on crude NMR analysis.

These metathesis results suggest isomerization of the starting materials during the reaction. To overcome this problem, **8** was isomerized to **11** using $PdCl_2$ as a catalyst (Scheme 4.2). It was expected that, by using **11**, the cross metathesis step would be improved. However, when treating compound **11** and **5** under the previously described conditions (Hoveyda-Grubbs II, CH_2Cl_2, 35 °C, overnight), no cross-metathesis product was observed in the crude reaction by mass spectrometry. Homodimers of **5** were found as well as peaks corresponding to -14 and +14 Da compared to the homodimer of compound **5** (*m/z* $[M+H]^+$ cald. 919.3684; found 919.3161, 905.2579, 933.3160). This result indicated that the reactivity of substituted olefin **11** was much lower than the terminal olefin **8**. Therefore, the conversion from terminal olefin **8** to substituted olefin **11** was not a good approach to solve the isomerization problem.

Olefin isomerization/migration is a common side reaction in olefin metathesis.[15] It was reported that 1,4-benzoquinone could inhibit the isomerization of certain long-chain aliphatic alkenes by reacting with the metal hydrides formed by the decomposition of the catalysts.[16] The cross metathesis between **5** and **8** was thus performed again using the same catalyst (Hoveyda-Grubbs II) and 0.2 equiv of 1,4-benzoquinone. Unfortunately, analysis of the crude reaction by mass spectrometry showed that a byproduct with a mass of 14 Da less than the desired product resulting from isomerization was still present ($[M+Na]^+$ *m/z* cald. 1718.6153; found 1718.6162 and 1704.6027). Significant amounts of starting materials were also observed. Effort was made to isolate the product by preparative TLC (10% $MeOH/CH_2Cl_2$), and hydrogenation of the putative product fraction was performed. However, it afforded a mixture of multiple species analyzed by HPLC without significant amount of the desired product as analyzed by mass spectrometry.

In conclusion, the attempts of using olefin cross metathesis to connect the antibiotics with Ent were not successful under the conditions explored above. It was possible that the complex structure of levofloxacin affected the cross metathesis reaction. To test this hypothesis, a simple olefin substrate hept-6-enoic acid was reacted with **8** using Hoveyda-Grubbs II as the catalyst and 0.2 eq 1,4-benzoquinone (Scheme 4.3). The desired product **12** was formed without any -14 Da peak observed ($[M+H]^+$ *m/z* cald. 1350.5175; found 1350.5531). Then, compound **12** was coupled to acetyl chloride activated ciprofloxacin **13**, which should afford the benzyl protected Ent-ciprofloxacin conjugate housing the acyloxymethyl ester linker. After evaluating several conditions, these coupling did not proceed well and no desired product was identified by mass spectrometry. Moreover, the TLC of the crude reaction revealed many byproducts. We decided to no longer pursue a metathesis route for Ent conjugate synthesis.

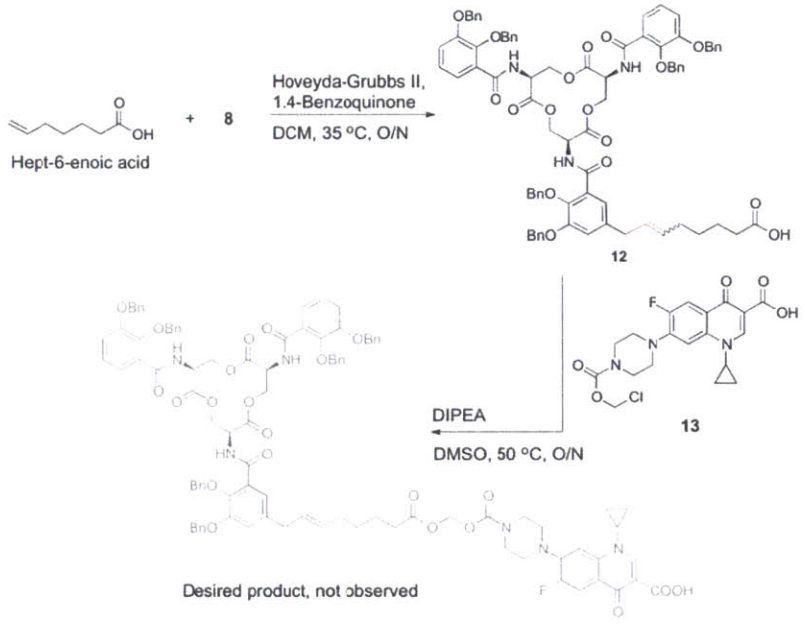

Scheme 4.3. Proposed synthesis of Ent-ciprofloxacin conjugate through cross metathesis.

Design and Synthesis of Ent-Antibiotic Conjugates with Acyloxymethyl Ester Linker via Aldehyde-Amine Reductive Amination. Because the olefin metathesis was unsuccessful, we pursued another route for conjugate assembly. As described in Chapter 2, the olefin group on **11** can be oxidized to an aldehyde, which affords several possible means to couple Ent to antibiotics. One route is through aldehyde-amine reductive amination. First, an antibiotic harboring a carboxylic acid moiety can be modified to a chloromethyl ester (**13**, Scheme 4.4), which can be coupled to an amino acid to yield an antibiotic-acyloxymethyl ester with free amine group (**14**, Scheme 4.4). Reaction of this amine group with

the aldehyde on the Ent scaffold will afford the final conjugates (Scheme 4.5). The reductive amination step was designed to be the last step before the deprotection of benzyl group on Ent to reduce the reaction steps and allow more flexibility.

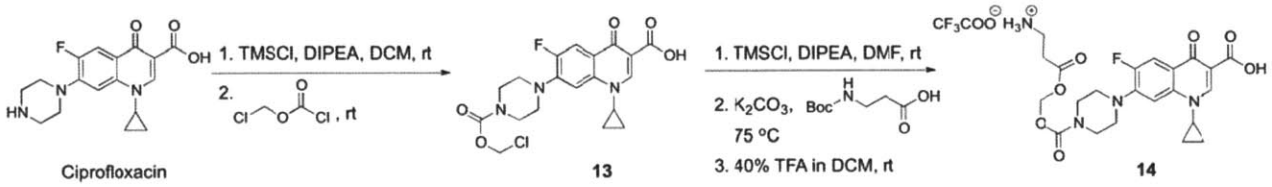

Scheme 4.4. Synthesis of amine-modified ciprofloxacin with acyloxymethyl ester linkage.

The synthesis of the amine-modified antibiotic with acyloxymethyl ester linkage was similar to previously described synthesis of **4-7**. Ciprofloxacin was used in this study and the reactions were carried out according to reported procedures.[13] The poor solubility of ciprofloxacin in organic solvents was significantly improved by *in situ* protection of the carboxylic acid using trimethylsilyl (TMS) group prior to the addition of chloromethyl chloroformate. Compound **13** was isolated following on an aqueous work up (Scheme 4.4). Compound **14** was obtained by the coupling of Boc-β-alanine with **13** with *in situ* protection of TMS, and subsequent TFA treatment afforded **14** as the final amine-modified antibiotic. This synthetic route can be applied to any antibiotic with an amine group, and the resulting conjugates are ready to be coupled to the aldehyde-modified Ent precursor **20** (Scheme 4.5).

The next step was to attach modified ciprofloxacin **14** to aldehyde-modified Ent precursor **20** through reductive amination (Scheme 4.5). We performed this reaction before the deprotection of phenol groups on the Ent precursor because the deprotection conditions (catalytic hydrogenation with Pd/C) will also reduce the aldehyde. Compound **14** was shown to be stable under these conditions.

For reductive amination, commonly used reagents include the hydride reducing agents $NaBH_4$, $NaBH_3CN$ and $NaBH(OAc)_3$.[17] Catalytic hydrogenation is also routinely employed.[18] Initial screening revealed that, in MeOH, ciprofloxacin decomposed in the presence of $NaBH_4$, but remained intact with $NaBH_3CN$ and $NaBH(OAc)_3$. We therefore performed small-scale screenings to optimize the reaction conditions with **14** and **15** (benzylaldehyde analog of **20)** using $NaBH_3CN$, $NaBH(OAc)_3$ and Pd/C catalyzed hydrogenation. Different solvents (THF, CH_2Cl_2/MeOH, and DMSO) were also screened. The optimal results came from the reaction using 1 equiv. of **15**, 1 equiv. of **14** and 12 equiv. of $NaBH_3CN$ in DMSO, where the desired product **16** was observed by mass spectrometry ($[M+H]^+$ *m/z* cald. 837.3147, found 837.3099). However, compound **17** was also detected ($[M+H]^+$ *m/z* cald. 1197.4430, found 1197.4446), which is a tertiary amine formed by two equiv. of **15** reacting with **14**. Varying the ratio of

the amine and aldehyde did not reduce the formation of **17** as revealed by MS analysis (Scheme 4.5A). This result was reasonable since the product of a single reductive amination was a secondary amine, which is more nucleophilic and thus may be prone to additional reductive amination. This problem can be avoided by putting a secondary amine on the terminus of compound **14**. A test reaction was performed by substituting **14** with N-methylglycine in the reaction. As expected, only one-to-one adduction was observed in mass spectrometry.

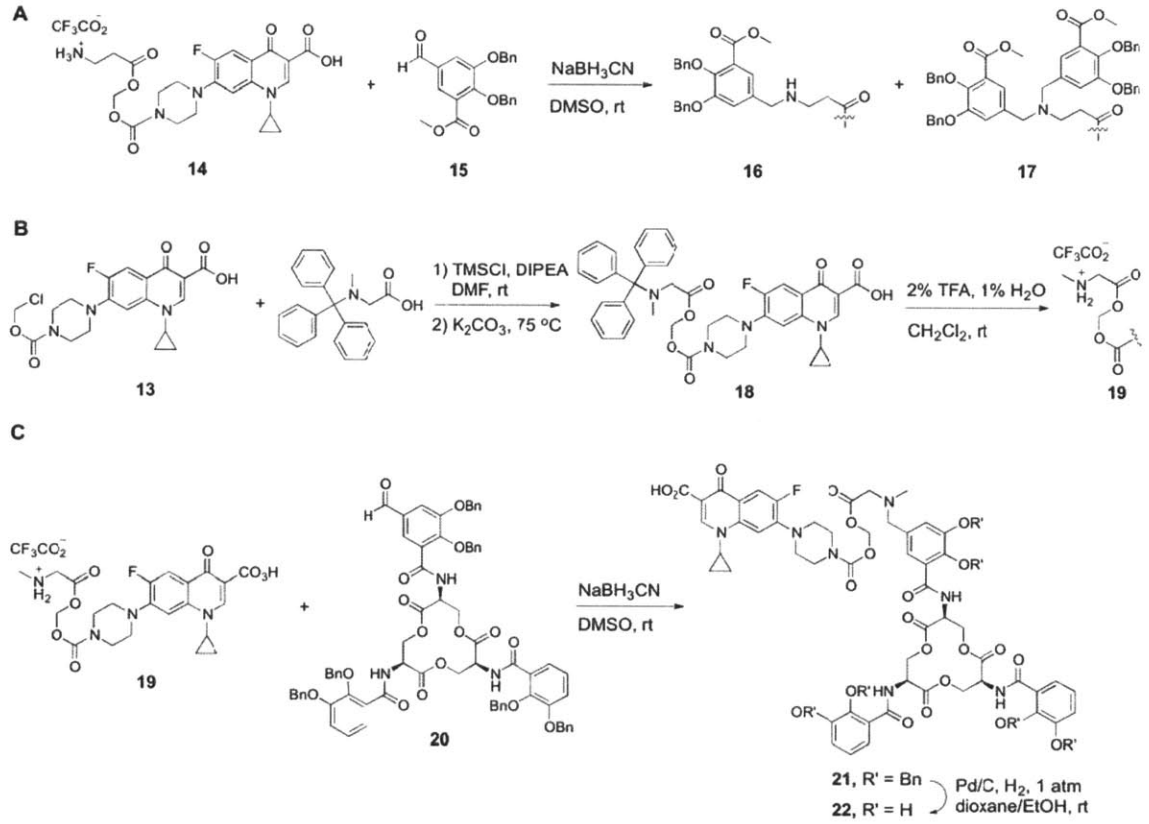

Scheme 4.5 Synthesis of Ent-ciprofloxacin conjugates via reductive amination.

Based on these results, a new ciprofloxacin-linker moiety **19** containing a secondary amine was synthesized (Scheme 4.5B). Compound **19** was reacted with **20** using $NaBH_3CN$ in DMSO, which gave the expected product **21** in moderate yield (51%). Catalytic hydrogenation in 1,4-dioxane/ethanol afforded the final Ent-ciprofloxacin conjugate **22** in 20% yield after HPLC purification (Scheme 4.5C). HPLC analysis indicated that conjugate **22** was not very stable (Figure 4.3). Re-injection of freshly collected pure fractions gave impurity peaks with quite different retention times (from 18 to 23 min,

Figure 4.3). Given the fact that acyloxymethyl ester linkers are known to be labile and the HPLC solvents are acidic (with 0.1% TFA), it was not surprising that some degradation was observed.

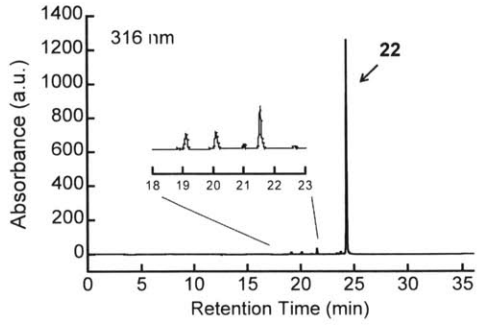

Figure 4.3. HPLC trace of purified Ent-Ciprofloxacin conjugate **22**. (0-100% MeCN over 30 min, 1 mL/min)

Antimicrobial Activity of Ent-ciprofloxacin Conjugate 22. Preliminary antimicrobial activity assays with compound **22** were performed by using a broth dilution method as described in Chapter 3. In these assays, three *E. coli* strains were tested under iron sufficient or deficient (by including 200-μM 2,2'-dipyridyl (DP) in the growth medium) conditions. *E. coli* K12 was used as a wild-type strain, *E. coli ent-* (ATCC 33475) is deficient in Ent biosynthesis, and *E. coli* H1876 lacks the receptors (FepA, Fiu and Cir) for Ent and its degradation fragments.[19] The growth of bacteria was represented by OD_{600} values normalized by dividing the apparent OD_{600} values with the value of the untreated *E. coli* K12 culture under iron sufficient conditions. It was observed that the minimal inhibitory concentration (MIC) values of **22** were the same (1 μM) for all strains tested and independent of whether the media contained DP (Figure 4.4A). It should be noted that *E. coli* H1876 cannot grow in PB containing 200 μM DP, therefore this strain was not tested in the presence of DP. Ciprofloxacin was tested as a positive control, and gave MIC values of ~100 nM against *E. coli* K12 and H1876 and ~10 nM against the ent⁻ strain. The activity decrease of **22** relative to ciprofloxacin may result from the extra hydrolysis step required for drug release. However, it was a surprise to see the same activity of **22** towards *E. coli* H1876, which lacks the Ent receptor, as the other strains. If the activity observed was from the uptake of **22**, this strain should not be sensitive. This result, together with the HPLC data, indicated that ciprofloxacin may be released from **22** before it is transported into the bacterial cell. The linker incorporated here may be too unstable within the timeframe of the assay (16 h at 30 °C). In earlier work by Hennard *et al.*,[20] pyoverdin-fluoroquinolone conjugates employing the same linker were found to exhibit activity against pyoverdin receptor deficient

strain as well, although with a four-fold increased MIC than against wild type strain. Noel *et al.* observed slightly enhanced activity of pyochelin analog-fluoroquinolone conjugates with the same linker against a TonB deficient strain compared to the wild type strain.[21] These results agree with our observations and support the notion of linker instability, although no linker stability study was reported in these examples. Further investigation of the linker stability was therefore conducted.

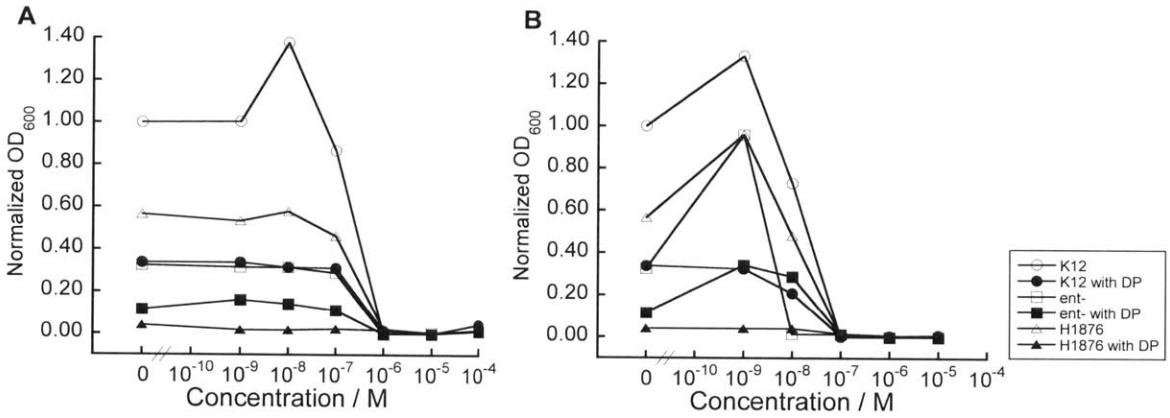

Figure 4.4. Antimicrobial activity of compound **22** (**A**) and ciprofloxacin (**B**) against *E. coli* K12, H1876, and *ent-*. Bacteria were grown in PB medium with or without 200 μM DP at 30 °C for 16 h. Normalized growth was calculated by dividing the OD_{600} value in each condition by the OD_{600} value of the *E. coli* K12 grown in PB with no compound added. The experiment was performed only once.

Stability Study of the Acyloxymethyl Ester Linker and Linker Modification. The unexpected activity of the Ent-ciprofloxacin conjugate **22** against the Ent receptor-deficient strain *E. coli* H1876 raised the question of whether ciprofloxacin remained attached to Ent before entering the bacterial cell. If the cargo is released from Ent in the extracellular environment, then Ent-mediated delivery cannot be achieved. Therefore, we evaluated the stability of the compound **22** as well as the cipro-linker moiety **19** using HPLC.

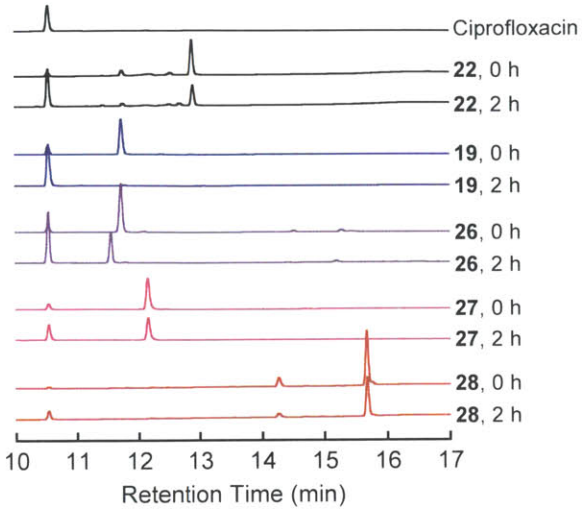

Figure 4.5 HPLC traces (280 nm) of the ciprofloxacin conjugates with acyloxymethyl/ethyl linkers. Conditions: 40-μM compound in 75-mM HEPES pH 7.5, 30 °C; 50-μL injections. HPLC gradient: 10% B for 5 min, 10-70% B over 8 min and 100%B for 5 min. The traces of 0 h and 2 h incubation for each compound were plotted.

HPLC analysis of compounds **19** (ciprofloxacin with the ester linker) and **22** (Ent-ciprofloxacin conjugate connected with the ester linker) incubated in HEPES buffer (75 mM, pH 7.5) at 30 °C confirmed that these compounds decompose readily. By plotting the changes in peak area of these compounds over time, the degradation reaction was best fitted to a first order reaction and the half-lives ($t_{1/2}$) of these compounds were determined. Compound **19** has a $t_{1/2}$ value of 0.35 h under these conditions (this value may be inaccurate because the first data point taken was at 1 h), and ciprofloxacin was observed in the degradation products (Figure 4.5 and Table 4.1). The Ent-ciprofloxacin conjugate **22** exhibited a longer $t_{1/2}$ of ~2.4 h, probably because it doesn't contain a secondary amine as in compound **19** (Figure 4.5 and Table 4.1). LC-MS analysis identified free ciprofloxacin (*m/z* calcd, 332.14104; found, 332.14162) and Ent-*N*-mentylglycine (*m/z* calcd, 771.19972; found, 771.19907) as the decomposition products of **22**. A proposed decomposition mechanism is shown in Figure 4.6, although other degradation mechanisms like OH^- attacking the carbonyl group at the carbamate site will also result in formation of free ciprofloxacin.

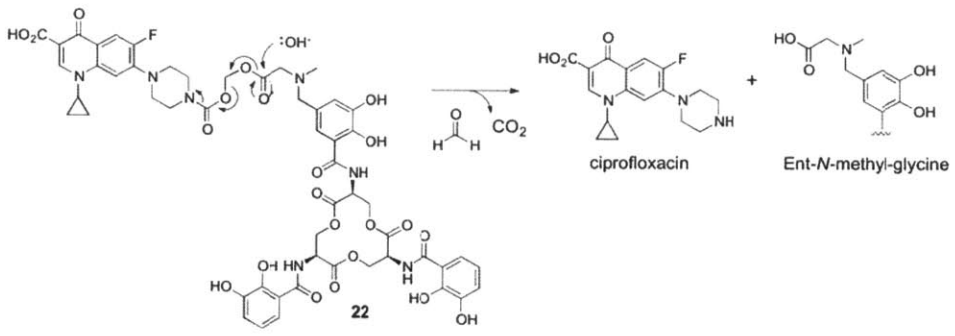

Figure 4.6. Proposed degradation mechanism of **22.**

Table 4.1. Half-lives of the ciprofloxacin derivatives.[a]

Compound	Structure	$t_{1/2}$ / h	Compound	Structure	$t_{1/2}$ / h
19	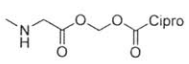	0.35±0.02	**29**	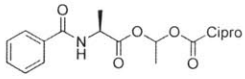	>60[b]
22	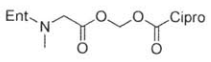	2.38±0.73	**30**	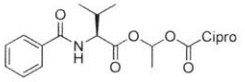	>130[b]
26	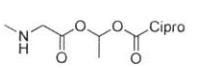	1.57±0.02	**31**	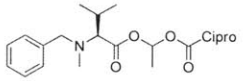	16.2±2.20
27	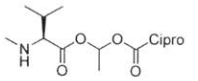	2.36±0.42	**37**	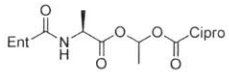	8.12±1.43
28	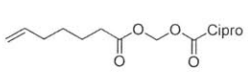	8.94±0.10	**38**	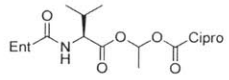	9.95±1.13
Ent	see Fig. **1A**	3.75±0.62	**39**	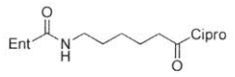	8.73±0.77

[a] The stability assay was performed as described in Figure 4.5, and the $t_{1/2}$ values were determined by assuming the decay is a first order reaction. Three repetitions were performed for each compound and the average $t_{1/2}$ values with the standard error of the mean were reported unless noted otherwise. Example fitting curves for $t_{1/2}$ determination are shown at the end of the chapter in Figure 4.11. [b] The compound decay was slow and more error was observed from the peak area measurement which results in relatively big variations of the calculated $t_{1/2}$ values. The shortest value among the repetitions was reported.

The data indicate that a more stable linker is needed for the conjugate design. In the development of tranexamic acid drugs for better absorption, more steric hindrance at either ester carbonyl group enhanced the stability.[22] We therefore synthesized compounds **26** and **27,** in which additional methyl or isopropyl groups are incorporated to either side of the carbonyl group (Scheme 4.6). Judged by HPLC analysis, both **26** and **27** were more stable than **19** with $t_{1/2}$ values of ~1.6 h and ~2.4 h, respectively (Figure 4.5 and Table 4.1). To further investigate whether the secondary amine from the N-methylglycine

moiety contributed to the fast decomposition of **19**, a similar synthetic route used to synthesize **19** was used to obtain **28** (Scheme 4.6). Compound **28** has a terminal olefin group instead of an amine, and it decomposed much more slowly ($t_{1/2}$ = 8.9 h) (Figure 4.5 and Table 4.1), indicating that the amine group may facilitate decomposition.

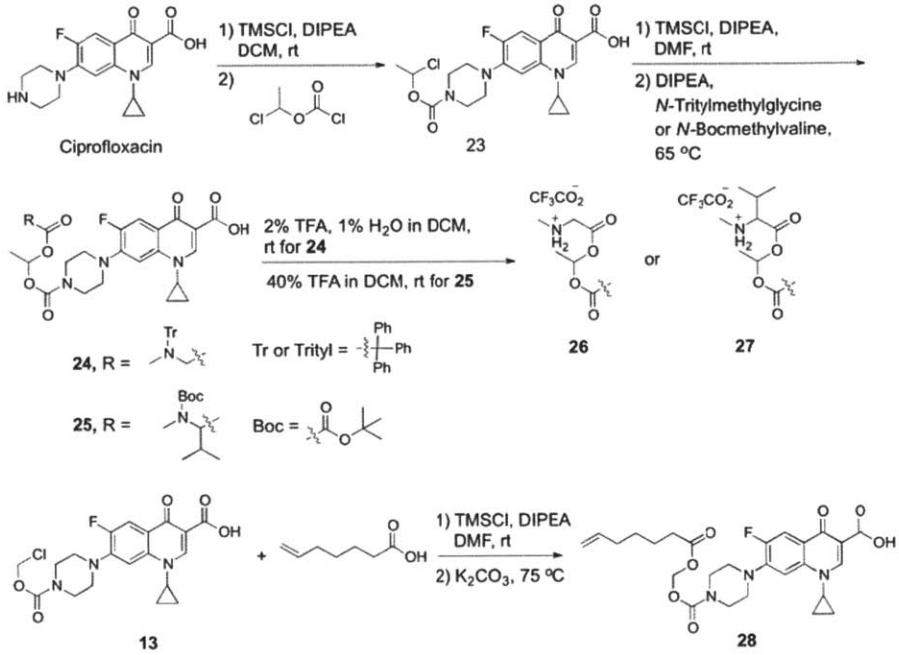

Scheme 4.6. Syntheses of ciprofloxacin-acyloxyethyl linker.

Stability Study of Ciprofloxacin-acyloxyethyl-benzoic Acid Conjugate with Amide Linkage. The stability study of compounds **19, 22, 26, 27** and **28** revealed that two aspects can be improved to achieve better stability for this linker: (i) to increase steric hindrance in the vicinity of the ester as seen in **26** and **27**; (ii) to avoid the amine group as evidenced by the enhanced stability of **28**. One possibility to avoid the amine in the final conjugate is to form an amide bond through acid-amine coupling. Two ciprofloxacin-benzoic acid conjugates **29** and **30** were therefore synthesized using **23** and commercially available *N*-benzoyl alanine and *N*-benzoyl valine under similar conditions as in the synthesis of **24** and **25**. As a comparison, compound **27** was reacted with benzylaldehyde through reductive amination to give compound **31** presenting an amine-based linkage (Scheme 4.7).

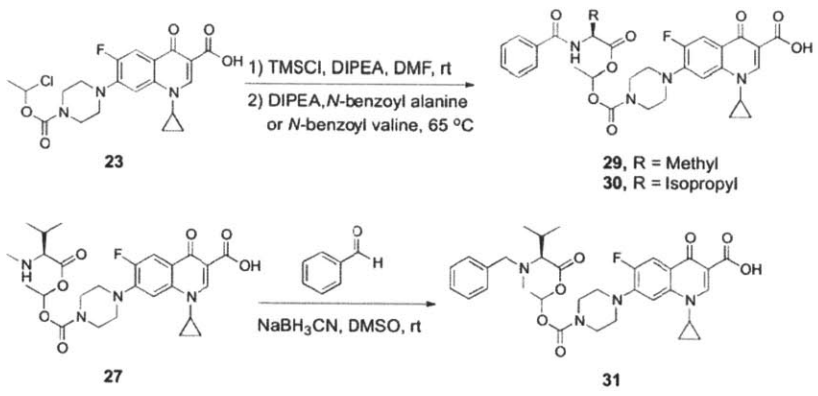

Scheme 4.7. Syntheses of ciprofloxacin-acyloxyethyl-benzoic acids.

The stability of these three compounds was also evaluated at pH 7.5 (75 mM HEPES) and 30 °C. After 21 h incubation, only ~20% of **29** and ~10% of **30** decomposed, demonstrating increased stability relative to **26, 27** and **28**. The slow decomposition rate results in more error when monitoring the peak-area change of these two compounds, and more error in the $t_{1/2}$ values was observed (ranging from ~60 h to ~920 h). The shortest half-lifes among repetition was reported in Table 4.1, which are 60 h and 130 h, respectively. As expected, the $t_{1/2}$ value of compound **31** was determined to be ~16.2 h, less stable than the amide containing analog **30**. The HPLC traces for these compounds after 0 and 9 h incubation are shown in Figure 4.7. One observation to note is that for compound **31**, two peaks with identical *m/z* value for the desired product were found in the HPLC trace, which may come from the two diastereomers of this compound. Moreover, not much ciprofloxacin was detected in the degradation products of **31**, although the peak area of **31** decreased in a time-dependent manner. When incubated in PB medium at 30 °C for 10 h, ~33% of **29** and ~3% of **30** decomposed. Antimicrobial activity assays showed that both **29** and **30** had MIC values of 1 μM towards *E coli* K12 and *E coli* NR698 (data not shown). The NR698 strain has a compromised outer membrane and is more permeable for antibiotics. Ciprofloxacin exhibited a MIC of 0.1 μM with these two strains. The similar MIC value obtained for K12 and the NR698 strain indicates that **29** and **30** enters both strains with similar efficiency, and their decreased activity compared to ciprofloxacin is not due to decreased cellular entry. We cannot rule out the possibility that the observed activity was still from extracellular release of ciprofloxacin as a result of degradation, although for compound **30**, within the timeframe of the experiment (19 h) the release of ciprofloxacin should be less than 10% unless the bacteria interfere with the progress. Nevertheless, it is evident that amide linker is more stable than a tertiary amine.

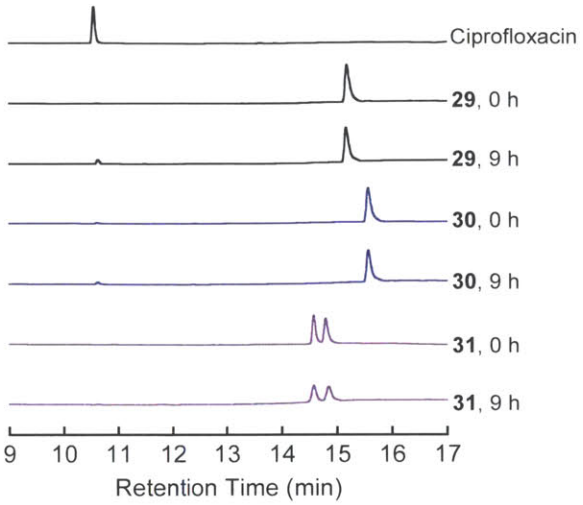

Figure 4.7. HPLC traces (280 nm) of the ciprofloxacin-acyloxyethyl linker conjugates with amide or amine connection for stability study. Conditions: 40-μM compound incubated in 75 mM HEPES, pH 7.5, 30 °C; 50-μL injection. HPLC gradient: 10% B for 5 min, 10-70% B over 8 min and 100%B for 5 min.

Synthesis and Stability of Ent-Ciprofloxacin Conjugates with Acyloxyethyl Linker via Acid-amine Coupling. Given that the amide linkage is more stable, we modified the synthetic route towards Ent-ciprofloxacin conjugate. The new approach applied the carboxylic acid-modified Ent precursor **34** reported in Chapter 2 and a ciprofloxacin-acyloxyethyl linker with a primary amine terminus. The acid-amine coupling is designed to be performed before the removal of benzyl protection on the phenols to avoid side reactions and likely simplify the purification.

To assemble the ciprofloxacin-acyloxyethyl intermediates with primary amine terminus, *N*-Boc-alanine and *N*-Boc-valine were reacted with **23** in basic condition and the Boc group was removed by 40% TFA/CH_2Cl_2 to give compounds **32** and **33** in 44% and 27% yield, respectively (Scheme 4.8A). Then, **32** and **33** were reacted with **34** in CH_2Cl_2 using PyAOP as the coupling reagent. Catalytic hydrogenation of the resulting benzyl-protected conjugates afforded the final products **37** and **38** after HPLC purification in 7.1% and 16% yield respectively (Scheme 4.8A). During the coupling step of **32**/**33** with **34**, it was found that if the TMSCl was quenched with MeOH, byproducts with a mass of 14 Da larger than the desired products formed, and these byproducts were hard to separate from the desired products. In each reaction, the byproduct likely formed from methylation of the carboxylic acid of ciprofloxacin when quenched with MeOH under basic conditions. When MeOH was substituted by water, the byproduct was not observed. Because the chloro-ethyl-chloro ester used was a racemic mixture, compounds **37** and **38** were formed as diastereomers as seen for compound **31**. In the case of **37**, the two diastereomers were separable on HPLC

and hence collected separately, but the relative stereochemistry was not determined. Two diastereomers of **38** were collected as a mixture due to poor separation on HPLC.

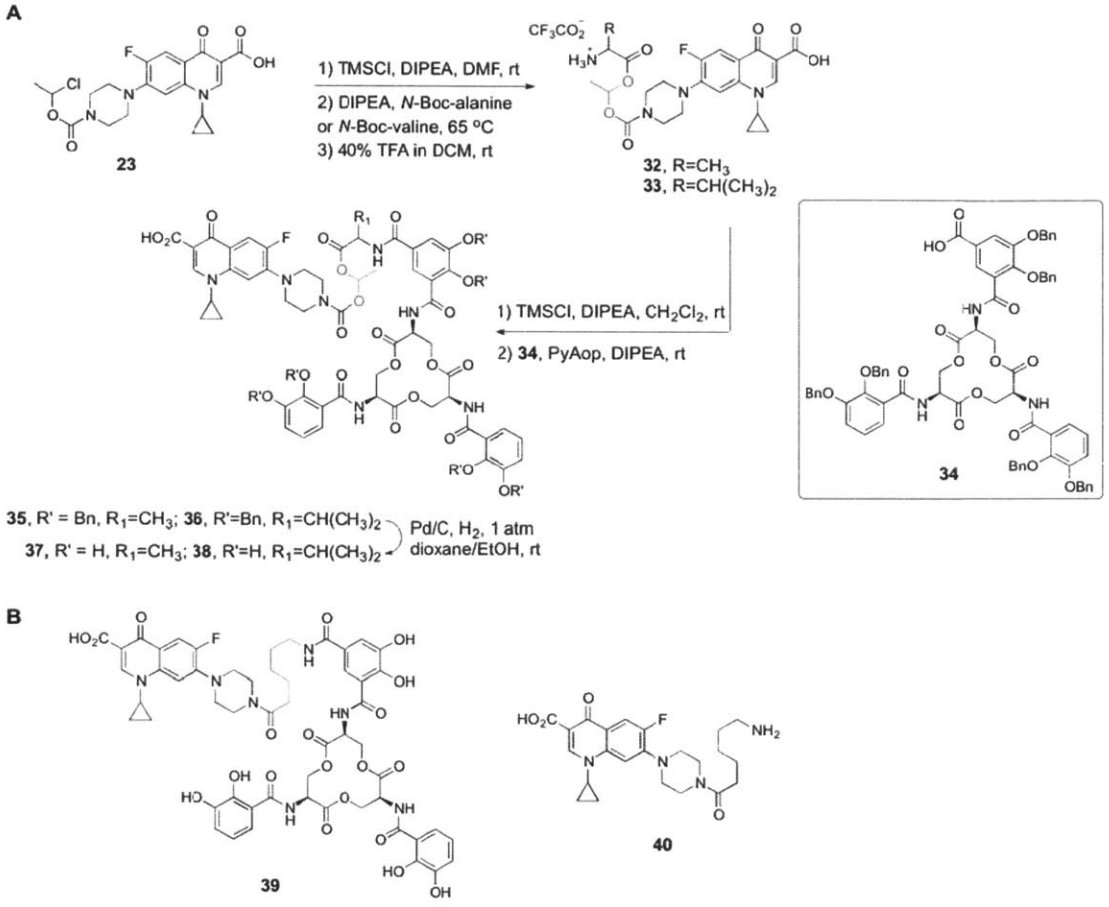

Scheme 4.8. Syntheses of Ent-ciprofloxacin conjugates with acyloxyethyl linker via acid-amine coupling. The linkers are labeled in red.

An analog of **37**/**38** with non-hydrolyzable linker was also employed in this study (**39**, Scheme 4.8B), in which the linker was an alkyl chain with the same length as in **37**/**38**. Compound **39** will be used to probe the linker stability properties in antimicrobial activity studies. The synthesis of **39** is described in Chapter 2.

The stabilities of ciprofloxacin-Ent conjugates **37**, **38** and **39** were evaluated as for the other ciprofloxacin-conjugates (Figure 4.8). Compared to the model compounds **29** and **30**, these molecules exhibited shorter half-lives (**37,** ~8.1 h; **38**, ~9.9 h; **39**, ~8.7 h), but compared to **22** the stability was greatly increased (Table 4.1). The same test was also performed on Ent and the result indicated that degradation of the Ent moiety contributed to the overall degradation of the conjugates as well (Figure 4.8

and Table 4.1). During the degradation of **37** and **38**, the new peak at 10.7 min was identified to be ciprofloxacin by HPLC retention time and mass spectrometry. This peak was not observed for compound **39**, which indicates that no free ciprofloxacin was released in this conjugate with the stable alkyl linker, as expected. The stability of these conjugates was also tested once, subsequent to pre-incubation of 0.9 equiv. of Fe(III), to determine whether Fe(III)-bound forms will have enhanced stability. The results showed that the conjugates became less stable ($t_{1/2}$ of **37-Fe** ~3 h; **39-Fe** ~4.4 h; Ent-Fe ~1.6 h), which suggests in growth media, following iron coordination, the conjugates may decompose even faster.

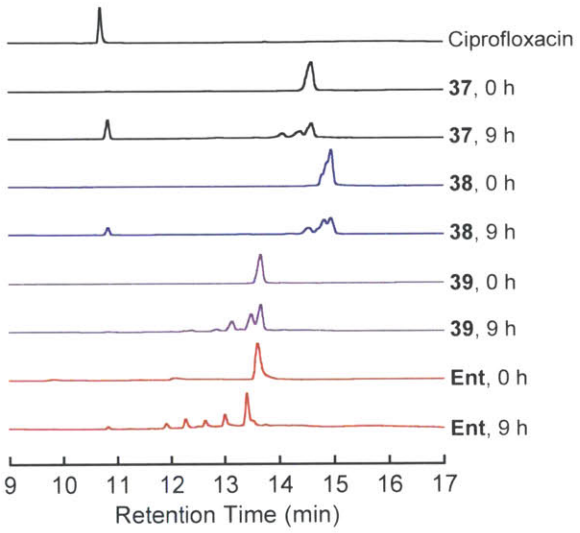

Figure 4.8. HPLC traces (280 nm) of the Ent-ciprofloxacin conjugates. Conditions: 40-μM compound, 75-mM HEPES pH 7.5, 30 °C; 50-μL injection. HPLC gradient: 10% B for 5 min, 10-70% B over 8 min and 100%B for 5 min.

Antimicrobial Activity of Ciprofloxacin-Ent Conjugates with Acyloxyethyl Linker. Antimicrobial assays were performed for **37**, **38**, and **39** against several *E. coli* strains including K12, ent- and H1876. The MIC values obtained in the absence and presence of DP are summarized in Table 4.2.

The conjugates **37** and **38** were 10- to 100-fold less active than ciprofloxacin, and no increase of activity was observed when using the Ent biosynthesis deficient strain (ent-) or under iron deficient conditions. Moreover, compounds **37** and **38** remained active towards the H1876 strain lacking Ent receptors, although they were less active than **22** which had a less stable linker. Taken together, the data indicate that the observed activity does not correlate with Ent-mediated delivery. The activity may still result from conjugate degradation before cellular uptake, which is reasonable because the stability study revealed that in the time frame of the activity assay (19 h), enough free ciprofloxacin may accumulate

(e.g., for the 10-μM conditions, 1% degradation would afford 0.1 μM ciprofloxacin, which is the MIC of the free antibiotic) and cause bacterial death.

Compounds **39** and the ciprofloxacin-alkyl linker conjugate **40** (Scheme 4.8C) both exhibit weak activity (MIC of 100 μM). The growth inhibition observed for **40** may come from the DNA gyrase inhibition by the ciprofloxacin moiety. The 1000-fold activity decrease may due to lower binding affinity to its target because of the linker modification or less efficient cellular uptake because of increased molecular weight and the hydrophobic alkyl chain. An *in vitro* DNA gyrase assay will be helpful to evaluate this hypothesis. When ciprofloxacin and Ent were added together to the bacterial culture in a 1:1 ratio, the activity of ciprofloxacin remained the same (Table 4.2), which supports the hypothesis that the conjugation between ciprofloxacin and Ent as seen in compound **39** resulted in the activity decrease. Similar to compound **40**, the Ent modification may affect the antibiotic-target interaction, but it is also possible that the observed activity is due to poor internalization of the iron-bound conjugate by the tested bacteria strains and chelation of Fe(III) of the media.

Table 4.2. MIC values of ciprofloxacin-Ent conjugate against *E. coli*.[a]

	Compound												
Strain	**37**	**38**	**38** +DP[b]	**39**	**39** +DP	**40**	**40** +DP	**40** +Ent[c]	**40** +Ent +DP	Cipro +Ent	Cipro +Ent +DP	Cipro	Cipro +DP
K12	1	1	1	100	100	100	100	100	100	0.1	0.1	0.1	0.1
ent[e]	10	1	>100	100	>100	100	100	100	100	0.1	0.1	0.1	0.1
H1876	10	10	N/A[d]	>100	N/A	>100	N/A	100	N/A	0.1	N/A	0.1	N/A

[a] All MIC values are presented in μM, and each experiment had been repeated at least twice. [b] 200 μM DP was added to the tested culture. [c] Compound and Ent were mixed in 1:1 ratio. [d] H1876 strain did not grow in the presence of DP, therefore these experiments were not performed. [e] ent⁻ strain did not grow well in the presence of DP, and the MIC values in such conditions are inaccurate.

As discussed above, one key question to fully understand the antimicrobial activity observed for these conjugates is whether they are still able to be transported by the Ent uptake system. The growth recovery assay described in Chapter 2 suggests that the delivery efficiency of Ent-ciprofloxacin conjugates in *E. coli* may be low. A direct monitor of the conjugate internalization can be achieved by using ^{55}Fe(III) loaded conjugates and monitoring the radioactivity retained by the bacteria over time. An alternative method to probe whether the conjugates are internalized is to pre-incubate the conjugates with Fe(III) and test their antimicrobial activity. If the conjugates enter the cell, the same activity as the apo form should be observed; if they cannot enter the cell and the growth inhibition observed is due to iron starvation, the pre-loaded conjugates should have no activity because they cannot chelate iron from the medium. To avoid the interference from endogenous Ent, the *E. coli* ent⁻ strain was used in this study.

And, to simply the analysis, only **39** was studied since no free ciprofloxacin will be released. The results showed that after pre-incubating with 0.3 equiv. of Fe(III), compound **39** lost its activity (Figure 4.9), which was evidence that **39** could not be internalized efficiently. It was a surprise to see only 0.3 equiv. Fe(III) was enough to eliminate all activity and when 0.5 equiv. and 0.9 equiv. Fe(III) were loaded, the growth was promoted. One possible reason was the actual concentration of **39** was lower than calculated, and the extra free iron facilitated bacterial growth. As a putative positive control, D-Ent (D-serine instead of L-serine composed the trilactone backbone) was tested under the same conditions. It is known that D-Ent has the same binding affinity towards iron but cannot be used by the bacteria to uptake iron, because it is not a substrate of Fes (esterase in cytosol for Ent degradation and iron release).[23] We hypothesized that the growth inhibition observed for D-Ent was solely from chelation effect and pre-incubation with iron should abolish its activity. The result agreed with our expectation (Figure 4.9). We also tested whether **39** was a substrate to MceD, an analog of Fes available in our lab, to see whether the chelation effect was from failure of iron release.[24] It was found that **39** was hydrolyzed when incubated with MceD (Figure 4.10). At this point, all data indicate that **39** might not be able to enter the bacteria. Therefore, besides the requirement for the releasing step, the low uptake efficiency makes ciprofloxacin not a good cargo candidate for Ent-mediated delivery into the tested *E. coli* strains. However, from the data in Chapter 2, *P. aeruginosa* PAO1 exhibit similar level of growth recovery when treated with **39** and Ent, which suggests that ciprofloxacin was tolerated by the Ent transport machinery in this organism. Moreover, in Chapter 3, *E. coli* CFT073 exhibited growth recovery when treated with Ent-Hy-Amp/Amx while *E. coli* K12 was slightly inhibited by the conjugates, indicating different *E. coli* strains may have different tolerance to the cargos being delivered by Ent. Therefore, with proper linker design, it is promising that Ent-mediated delivery of ciprofloxacin will result in enhanced antimicrobial activity towards certain bacteria species.

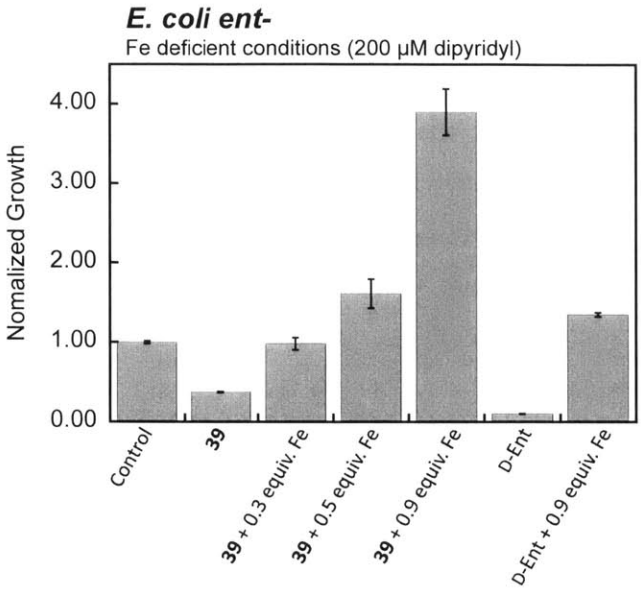

Figure 4.9. *E. coli ent-* growth in the presence of Fe-preloaded **39** (100 μM) and D-Ent (100 μM). DP (200 μM) was added to the growth medium. Normalized growth was calculated by dividing the OD_{600} value of each condition by the OD_{600} value of the untreated control. Error bars are standard deviation of the mean (n = 3).

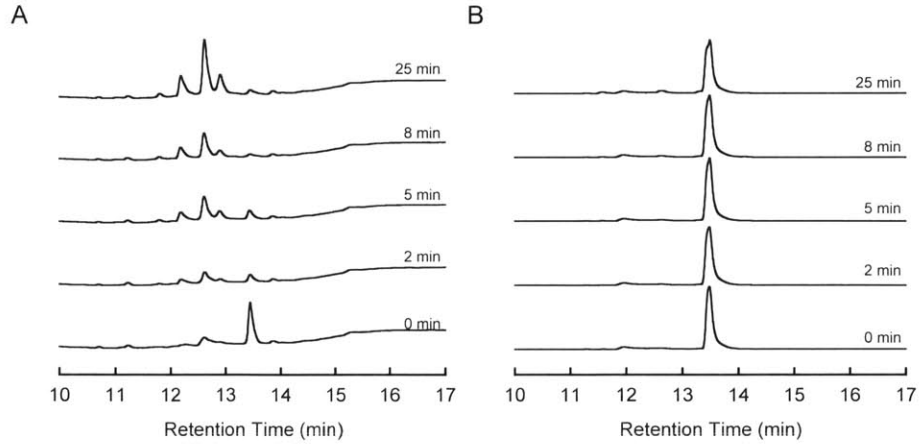

Figure 4.10. HPLC traces (316 nm) of compound **39** treated with (A) or without (B) MceD.

Summary and Perspectives

In this chapter, continued efforts to develop the Ent-mediated cargo delivery strategy were described. In particular, this chapter focused on the incorporation of labile linkers into the conjugate

scaffold for cargos requiring release after cytosolic delivery. We chose an ester linker that has been reported in the siderophore-fluoroquinilone conjugate literature and explored several synthetic routes to achieve Ent-ciprofloxacin conjugates. Stabilities of ciprofloxacin derivatives connected to the labile acyloxymethyl ester linker were evaluated together with the Ent-ciprofloxacin conjugates harboring these linkers or a stable alkyl linker. The labile linkers were found to be unstable at neutral pH and promote sufficient premature ciprofloxacin release to fully account for the observed antimicrobial activity. We also indirectly demonstrated that ciprofloxacin was not efficiently delivered into the *E. coli ent-* cytosol when conjugated to Ent with a stable alkyl linker, which is in agreement with our hypothesis in Chapter 2.

In the synthetic siderophore-conjugate field, there are few examples of applying antibiotics with specific cytoplasmic targets except for the siderophore-fluoroquinolone conjugates. The requirement of a labile linker has been reported by several groups;[6-8,21] although to date a successful design has not been reported. We conclude that the examples applying the acyloxymethyl linkers all suffered from premature release and the 'trimethyl-lock' based linkers reported by the Miller group recently have limitations.[5] Albomycins, naturally occurring siderophore-antibiotic conjugates, contain linkers that are cleaved by specific intracellular enzymes,[25] and can therefore provide inspiration for an alternative linker choice. This linker may be more challenging to incorporate into the conjugates synthetically, and the application may be limited as a result of the distribution of the specific enzymes among different bacterial species. Disulfide based linkages have been used in antibody-drug conjugates as anti-tumor reagents, and the reduction of the disulfide bond during endocytosis was proposed to result in release of the free drug.[26] The reducing environment in bacteria cytosol with a redox potential estimated to be -260 mV to -280 mV may also afford cleavage of disulfide bond (e.g., the redox potential for oxidized glutathione is -220 mV),[27] and the linker should remain oxidized in the periplasm because of the oxidizing environment (estimated to be -165 mV).[28] In conclusion, further optimization of the linker design is needed for delivering cargos with specific cellular target by the siderophore mediated uptake systems. Future work addressing whether the efflux pumps will extrude the cargos after cytosol delivery and release step is needed as well.

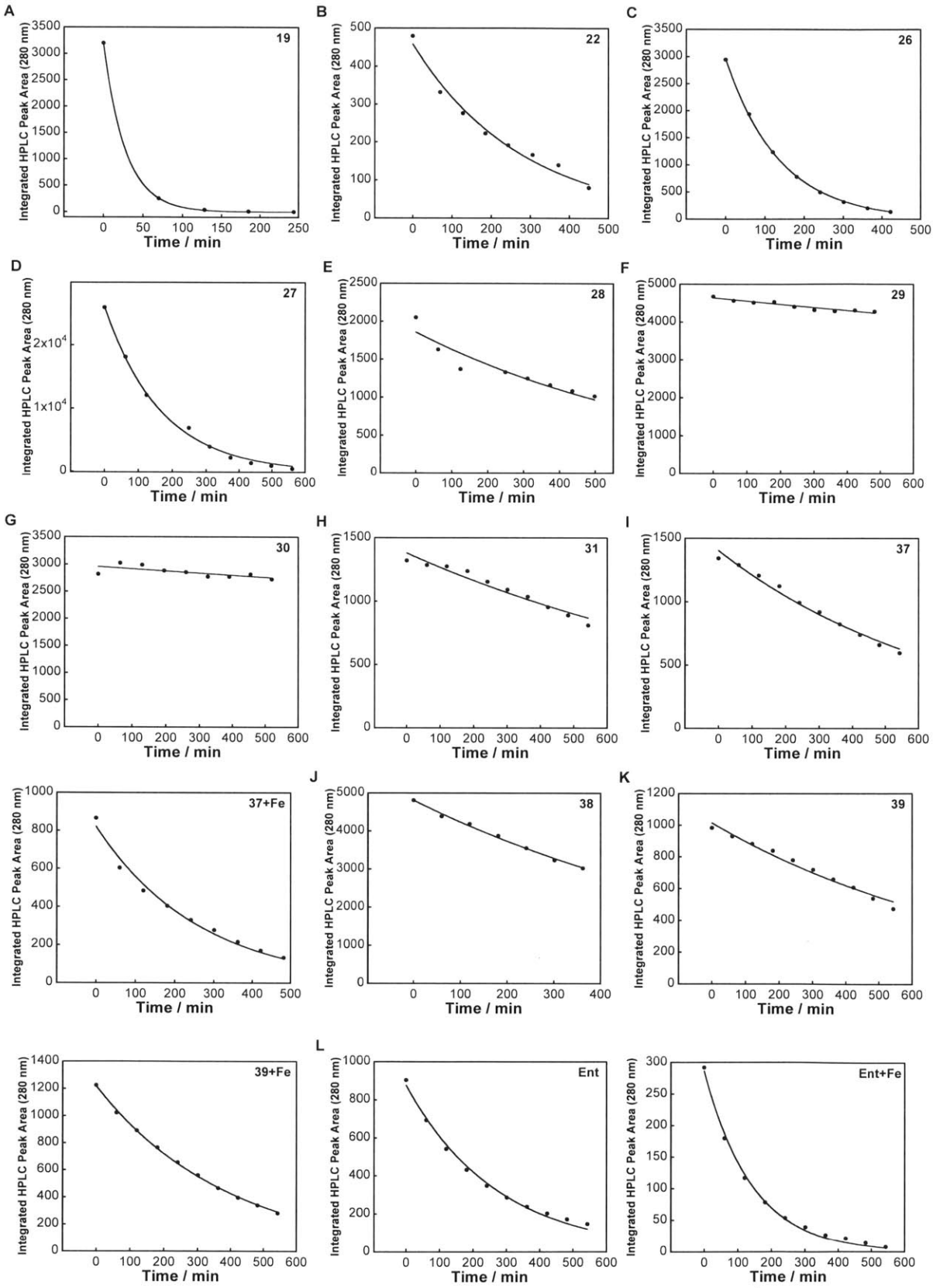

Figure 4.11. Representative fitted degradation curves of ciprofloxacin conjugates listed in Table 4.1.

Acknowledgement

I thank Professor Elizabeth Nolan for providing the MceD enzyme.

References

1. Hooper, D. C., Mode of action of fluoroquinolones. *Drugs* **1999,** *58, Suppl 2*, 6-10.
2. Levine, C.; Hiasa, H.; Marians, K. J., DNA gyrase and topoisomerase IV: biochemical activities, physiological roles during chromosome replication, and drug sensitivities. *Biochim. Biophys. Acta.* **1998,** *1400* (1-3), 29-43.
3. Mitscher, L. A., Bacterial topoisomerase inhibitors: quinolone and pyridone antibacterial agents. *Chem. Rev.* **2005,** *105* (2), 559-592.
4. Aldred, K. J.; Kerns, R. J.; Osheroff, N., Mechanism of quinolone action and resistance. *Biochemistry* **2014,** *53* (10), 1565-1574.
5. Ji, C.; Miller, M. J., Chemical syntheses and in vitro antibacterial activity of two desferrioxamine B-ciprofloxacin conjugates with potential esterase and phosphatase triggered drug release linkers. *Bioorg. Med. Chem.* **2012,** *20* (12), 3828-3836.
6. Hennard, C.; Truong, Q. C.; Desnottes, J. F.; Paris, J. M.; Moreau, N. J.; Abdallah, M. A., Synthesis and activities of pyoverdin-quinolone adducts: a prospective approach to a specific Therapy against Pseudomonas aeruginosa. *J. Med. Chem.* **2001,** *44* (13), 2139-2151.
7. Rivault, F.; Liebert, C.; Burger, A.; Hoegy, F.; Abdallah, M. A.; Schalk, I. J.; Mislin, G. L., Synthesis of pyochelin-norfloxacin conjugates. *Bioorg. Med. Chem. Lett.* **2007,** *17* (3), 640-644.
8. Milner, S. J.; Seve, A.; Snelling, A. M.; Thomas, G. H.; Kerr, K. G.; Routledge, A.; Duhme-Klair, A. K., Staphyloferrin A as siderophore-component in fluoroquinolone-based Trojan horse antibiotics. *Org. Biomol. Chem.* **2013,** *11* (21), 3461-3468.
9. Gupta, D.; Gupta, S. V.; Lee, K. D.; Amidon, G. L., Chemical and enzymatic stability of amino acid prodrugs containing methoxy, ethoxy and propylene glycol linkers. *Mol. Pharm.* **2009,** *6* (5), 1604-1611.
10. Burks, S. R.; Ni, J. H.; Muralidharan, S.; Coop, A.; Kao, J. P. Y.; Rosen, G. M., Optimization of Labile Esters for Esterase-Assisted Accumulation of Nitroxides into Cells: A Model for In Vivo EPR Imaging. *Bioconjugate Chem.* **2008,** *19* (10), 2068-2071.
11. Barlos, K.; Papaioannou, D.; Theodoropoulos, D., Efficient "one-pot" synthesis of N-tritylamino acids. *J. Org. Chem.* **1982,** *47* (7), 1324-1326.
12. Applegate, H. E.; Cimarusti, C. M.; Dolfini, J. E.; Funke, P. T.; Koster, W. H.; Puar, M. S.; Slusarchyk, W. A.; Young, M. G., Synthesis of 2-Methylthio-Substituted,4-Methylthio-Substituted, and 7-Methylthio-Substituted Cephalosporins. *J. Org. Chem.* **1979,** *44* (5), 811-818.
13. Rivault, F.; Liébert, C.; Burger, A.; Hoegy, F.; Abdallah, M. A.; Schalk, I. J.; Mislin, G. L. A., Synthesis of pyochelin-norfloxacin conjugates. *Bioorg. Med. Chem. Lett.* **2007,** *17* (3), 640-644.
14. Binder, J. B.; Raines, R. T., Olefin metathesis for chemical biology. *Curr. Opin. Chem. Biol.* **2008,** *12* (6), 767-773.
15. Hanessian, S.; Giroux, S.; Larsson, A., Efficient allyl to propenyl isomerization in functionally diverse compounds with a thermally modified Grubbs second-generation catalyst. *Org. Lett.* **2006,** *8* (24), 5481-5484.
16. Hong, S. H.; Sanders, D. P.; Lee, C. W.; Grubbs, R. H., Prevention of undesirable isomerization during olefin metathesis. *J. Am. Chem. Soc.* **2005,** *127* (49), 17160-17161.
17. Cheng, M. F.; Yu, H. M.; Ko, B. W.; Chang, Y.; Chen, M. Y.; Ho, T. I.; Tsai, Y. M.; Fang, J. M., Practical synthesis of potential endothelin receptor antagonists of 1,4-benzodiazepine-2,5-dione derivatives bearing substituents at the C3-, N1- and N4-positions. *Org. Biomol. Chem.* **2006,** *4* (3), 510-518.

18. Abdel-Magid, A. F.; Carson, K. G.; Harris, B. D.; Maryanoff, C. A.; Shah, R. D., Reductive Amination of Aldehydes and Ketones with Sodium Triacetoxyborohydride. Studies on Direct and Indirect Reductive Amination Procedures(1). *J. Org. Chem.* **1996,** *61* (11), 3849-3862.
19. Rabsch, W.; Winkelmann, G., The specificity of bacterial siderophore receptors probed by bioassays. *BioMetals* **1991,** *4* (4), 244-250.
20. Hennard, C.; Truong, Q. C.; Desnottes, J. F.; Paris, J. M.; Moreau, N. J.; Abdallah, M. A., Synthesis and activities of pyoverdin-quinolone adducts: a prospective approach to a specific Therapy against Pseudomonas aeruginosa. *J. Med. Chem.* **2001,** *44* (13), 2139-2151.
21. Noel, S.; Gasser, V.; Pesset, B.; Hoegy, F.; Rognan, D.; Schalk, I. J.; Mislin, G. L. A., Synthesis and biological properties of conjugates between fluoroquinolones and a N3 "-functionalized pyochelin. *Org. Biomol. Chem.* **2011,** *9* (24), 8288-8300.
22. Svahn, C. M.; Merenyi, F.; Karlson, L.; Widlund, L.; Gralls, M., Tranexamic Acid-Derivatives with Enhanced Absorption. *J. Med. Chem.* **1986,** *29* (4), 445-448.
23. Abergel, R. J.; Zawadzka, A. M.; Hoette, T. M.; Raymond, K. N., Enzymatic Hydrolysis of Trilactone Siderophores: Where Chiral Recognition Occurs in Enterobactin and Bacillibactin Iron Transport. *J. Am. Chem. Soc.* **2009,** *131* (35), 12682-12692.
24. Nolan, E. M.; Fischbach, M. A.; Koglin, A.; Walsh, C. T., Biosynthetic tailoring of microcin e492m: Post-translational modification affords an antibacterial siderophore-peptide conjugate. *J. Am. Chem. Soc.* **2007,** *129* (46), 14336-14347.
25. Braun, V.; Gunthner, K.; Hantke, K.; Zimmermann, L., Intracellular activation of albomycin in Escherichia coli and Salmonella typhimurium. *J. Bacteriol.* **1983,** *156* (1), 308-315.
26. Austin, C. D.; Wen, X. H.; Gazzard, L.; Nelson, C.; Scheller, R. H.; Scales, S. J., Oxidizing potential of endosomes and lysosomes limits intracellular cleavage of disulfide-based antibody-drug conjugates. *Proc. Natl. Acad. Sci. U. S. A.* **2005,** *102* (50), 17987-17992.
27. Jocelyn, P. C., The standard redox potential of cysteine-cystine from the thiol-disulphide exchange reaction with glutathione and lipoic acid. *Eur. J. Biochem.* **1967,** *2* (3), 327-331.
28. Depuydt, M.; Messens, J.; Collet, J. F., How Proteins Form Disulfide Bonds. *Antioxid. Redox. Sign.* **2011,** *15* (1), 49-66.

Appendix 1

Chemoenzymatic Syntheses of Enterobactin-antibiotic Conjugates and Studies of Antimicrobial Activity

Introduction

The "Trojan horse" strategy of conjugating antimicrobial agents to siderophores has been utilized by Nature. Naturally occurring antibiotics covalently linked to siderophores have been discovered and termed "sideromycins."[1] One example of these siderophore-antibiotic conjugates is Microcin E492m (MccE492m), which was discovered in cultures of *Klebsiella pneumoniae* RYC492 (Figure A1.1B).[2] MccE492m has MIC values in the nM to μM range for several *E. coli* and other Gram-negative strains.[2] This conjugate is comprised of an 84-residue peptide and a monoglycosylated enterobactin moiety (linearized MGE, Figure A1.1B). The 84-residue peptide has possible membrane-disrupting activity. The unmodified peptide in MccE492m exhibits lower activity compared to the enterobactin-modified conjugate. Furthermore, if the enterobactin (Ent) receptor protein FepA is mutated, the conjugate loses its activity.[2] These results suggest that if synthetic small molecules or peptides with antimicrobial activity are attached to enterobactin, they may be co-transported through the iron-uptake pathways and compromise bacterial growth. It is also reported that the Ent receptor FepA is able to transport colicins and bacteriophages into the periplasm.[3] This promiscuity suggests that a variety of cargo, including antimicrobial peptides, may be recognized and transported by the Ent uptake system.

The Ent scaffold is perfect for chelating iron, but it is relatively difficult to chemically modify its structure for attachment without affecting the iron-binding affinity. The synthetic routes described in Chapters 2 and 3 successfully tackled this challenge. As an alternative route, the biosynthetic pathway for MccE492m was characterized recently and this work revealed the enzymes responsible for the ligation of the peptide moiety to Ent.[4] In this work, the biosynthetic enzymes MceCDIJ for MccE492m maturation were isolated with *in vitro* activity. Milligram quantities of products can be isolated applying the *in vitro* assay, and the native 84-amino acid peptide substrate can be substituted with a 10-mer peptide.[5] These results make the attachment of antimicrobial agents and other types of cargos to Ent through a chemoenzymatic approach practical and appealing.

In this Appendix, conjugates of Ent and several antimicrobial peptides, small molecule antibiotics, and one fluorophore were synthesized chemoenzymatically by using the enzymes from the MccE492 gene cluster. Although we did not pursue this route further due to lack of improvement of antimicrobial activity from the conjugates, the utility of the enzymes for cargo attachment to Ent is demonstrated.

Experimental Section

General Materials and Methods. Chemicals and resins for solid-phase peptide synthesis were purchased from Novabiochem. MSI-C_{10}E492, PGI-C_{10}E492, ATCUN-G_x-C_{10}E492 (x=2, 4, 6) and FL-C_{10}E492 were ordered from Chi Scientific and used as received. Other chemicals were purchased from Sigma-Aldrich, TCI or Alfa Aesar and used without further purification. The pET-20b-sp-H10-TEV

plasmid was a kind gift from Dr. Susan Buchanan at NIH. Mass spectrometry was performed by using a Bruker Omniflex MALDI-TOF instrument located in the Department of Chemistry Instrumentation Facility and using α-cyano-4-hydroxycinnamic acid as the matrix. In some instances, high-resolution mass spectrometry was performed by staff at the MIT Department of Chemistry Instrumentation Facility, which houses a Bruker Daltonics APEXIV 4.7 Tesla Fourier Transform Ion Cyclotron Resonance Mass Spectrometer (FT-ICR-MS) with a direct analysis in real time (DART) ionization source. Semi-preparative and analytical high-performance liquid chromatography (HPLC) were performed by using an Agilent 1200 series HPLC system outfitted with an Agilent Zorbax reverse-phase C18 column (5-μm pore size, 9.4 x 250 mm) at a flow rate of 4 mL/min or a Clipeus reverse-phase C18 column (5-μm pore size, 4.6 x 250 mm) from Higgins Analytical, Inc. at a flow rate of 1 mL/min, respectively. Solvents used in all HPLC experiments are: solvent A, 0.2%TFA/H_2O; solvent B, 0.2%TFA/MeCN. Absorption at 220 and 316 nm was monitored. Product purity was verified by analytical HPLC (0-80% B over 40 min) and the traces are reported in the main text or in Appendix 4. NMR spectra were collected by using a Varian 300 MHz spectrometer operating at ambient probe temperature (283 K) in the Department of Chemistry Instrumentation Facility. Chemical shifts are referenced to internal solvent peaks. ^{1}H NMR spectra are provided in Appendix 4.

General Spectroscopic Methods. Millipore water (18.2 MΩ.cm) from Professor JoAnne Stubbe's lab was used for all aqueous solutions. Minimum 99.5% (titration) 4-(2-hydroxyethyl)-1-piperazineethanesulfonic acid (HEPES) from Sigma-Aldrich was used as received. A Mettler ToleDo Inlab Routine Pro glass electrode, calibrated prior to each use, was used to adjust solution pH. Optical absorption spectra and optical density measurement were obtained by using an Agilent 8453 UV-visible diode array spectrophotometer. An Agilent ultra-micro quartz cuvette (50 μL) or VWR semi-micro two sided disposable plastic cuvettes (1 mL) with 1-cm path lengths were employed for UV-visible measurements. Fluorescence spectra were collected on a SPECTRAmax™ GEMINI XS Dual-Scanning Microplate Spectrofluorometer housed in the MIT Biophysical Instrumentation Facility and samples were placed in 96-well plates (Corstar, Black plate, clear bottom with lid).

Antimicrobial Activity Assays. *E. coli* BL21 (DE3) were purchased from Stratagene. *E. coli* K12 and *Pseudomonas patho virus putida* were obtained from Professor Christopher T. Walsh (Harvard Medical School). Frozen cell stocks of *E. coli* K12 were stored in M9 minimal media, which is necessary for the strain to maintain its ability to grow in minimal media. *E. coli* NR698 was kindly provided by Professor Daniel Kahne (Department of Chemistry and Chemical Biology, Harvard University). *E. coli* H1876 and *E. coli* KB4 were gifts from Professor Klaus Hantke (Department of Membrane Physiology,

University of Tübingen). *E. coli* K12RW193 and *E. coli* B were purchased from ATCC. The minimal inhibitory concentrations (MIC) were determined following a reported procedure.[6] Overnight culture of the bacteria strains were grown in fresh LB media with 1:500 dilution at 37 °C with shaking at 150 rpm until the optical density at 600 nm (OD_{600}) reached 0.6. The cultures were subsequently diluted with poor-broth (PB) nutrient medium (1% Bacto Tryptone, 5% NaCl, w/v) with or without 200 μM 2,2'-dipyridyl to OD_{600} = 0.001. A 90-μL aliquot of the diluted culture was mixed with a 10-μL aliquot of the conjugate solution at various concentrations in 96-well plates and incubated at 30 °C for 16 h. Bacterial growth was assayed by measuring OD_{600}. The growth recovery assay was conducted in the same manner. Stock solutions of the conjugates were prepared in filter-sterilized milli-Q H_2O and the resulting concentrations were verified by measuring absorbance at 316 nm and using the calculated extinction coefficient of enterobactin in MeOH (ε_{316} = 9500 $cm^{-1}M^{-1}$).[7]

Preparation of MGE (1). MceC, the C-glucosyltransferase expressed by *Klebsiella pneumoniae* RYC492, was over-expressed as a His_6-fusion protein in *E. coli* BL21 (DE3) and purified as previously described.[4] C-Glucosylation of enterobactin was carried out by a modified literature protocol.[4] A-10 mL solution containing 200 μM enterobactin, 800 μM uridine diphosphoglucose (UDP-glucose), 5 mM $MgCl_2$, and 0.4 μM MceC was prepared in 75 mM Tris-HCl buffer at pH 8.0 and divided into ten 1000-μL aliquots. The 1000-μL reactions were incubated at room temperature, monitored by analytical HPLC, and quenched by addition of 200 μL of 3% TFA (aq). The quenched reactions were centrifuged (13,000 rpm, 10 min) and **1** was purified from the supernatant by using semi-preparative HPLC (0-40% B over 8 min, 4 mL/min). The purity and identity of the isolated product was verified by analytical HPLC and mass spectrometry. HPLC retention time, 7.6 min; MS (MALDI-TOF): $[M+H^+]$ *m/z* calcd, 832.21; found 832.39.

General Method for MceIJ-catalyzed Conjugate Assembly. MceIJ, the protein complex that links MGE to the C-terminus of C_{10}E492 (Figure A1.1C), was over-expressed and purified as reported elsewhere.[4] MceIJ-catalyzed reactions were conducted as previously described.[5] In brief, 500 μM modified C_{10}E492 peptide (SATSSSGSGS), 5 mM $MgCl_2$, 2.5 mM TCEP, 500 μM ATP, 100 μM MGE, and 2 μM MceIJ were combined in 75 mM Tris-HCl buffer at pH 8. The 1000-μL reactions were incubated at room temperature for 8 h and quenched by addition of 200 μL 3% TFA aq. The quenched reactions were centrifuged at 13,000 rpm for 10 min, and the conjugates were purified from the supernatant by using semi-preparative HPLC (10-40% B over 10 min, 4 mL/min).

Synthesis of MSI-C_{10}E492-MGE (2). The MceIJ catalyzed reaction was performed as described above using 8 μmol peptide. Product **2** eluted at 9.7 min and was obtained as a white powder after lyophilization (1.7 mg). MS (MALDI-TOF): $[M+H^+]$ *m/z* calcd, 4101.28; found, 4101.62.

Synthesis of PGI-C_{10}E492-MGE (3). As described for **2** except that before using in the MceIJ assay, the PGI-C_{10}E492 peptide was oxidized by stirring in 75 mM Tris-HCl buffer (pH 8.0) at room temperature for 3 h with the solution open to air. The oxidation process was monitored by analytical HPLC (10-40% B over 10 min, 1 mL/min) until the peak at 6.9 min, corresponding to the reduced peptide, completely converted to a 7.5 min peak corresponding to the oxidized peptide. The oxidized peptide was used in MceIJ assay without further purification. Conjugate **3** eluted at 8.4 min, and was obtained as a white powder after lyophilization (0.5 mg). The MS was not determined (the product did not ionize well under the standard MS condition and cannot be detected using MALDI-TOF).

Synthesis of ATCUN-G_x-C_{10}E492-MGE (x=2, 4; x=4, 5; x=6, 6). As described for **2** except that **4, 5** and **6** eluted at 10.2 min, 11.0 min and 10.2 min, respectively, and were obtained as white powders after lyophilization (**4,** 0.3 mg; **5,** 0.8 mg; **6,** 0.2 mg). MS (MALDI-TOF): $[M+H^+]$ *m/z* calcd, 2093.68, 2207.72, 2321.76; found, 2094.00, 2208.07, 2322.11 for **4, 5** and **6,** respectively.

Synthesis of FL-C_{10}E492-MGE (7). As described for **2** except that **7** eluted at 8.5 min and was obtained as an orange powder (1.5 mg). The isolated product contained multiple peaks in analytical HPLC analysis which may result from isomers of fluorescein. MS (MALDI-TOF): $[M+H^+]$ *m/z* calcd, 1998.56; found, 1998.95.

Synthesis of Penicillin-C_{10}E492 (8). The C_{10}E492 peptide was synthesized on a 0.066 mmol scale by using 2-chlorotrityl chloride resin and standard Fmoc solid-phase peptide synthesis methodology. The synthesis was performed manually in a 10-mL peptide synthesis vessel (Chemglass). For each coupling reaction, 2.5 equiv. amino acid, 2.5 equiv. benzotriazol-1-yl-oxytripyrrolidinophosphonium hexafluorophosphate (PyBOP) and 5 equiv. *N,N*-diisopropylethylamine (DIPEA) were dissolved in dry DMF (1 mL), and incubated with the resin for 2 h at rt with vigorous shaking. The reaction solution was drained and the resin was washed with DMF (3 x 5 mL). Subsequently, the Fmoc protecting group was removed by incubating the resin with 25% piperidine in DMF for 0.5 h at rt, and then the resin was washed by DMF (3 x 5 mL), and subjected to the next coupling reaction. After the Fmoc group of the N-terminal serine of C_{10}E492 was removed, 6.5 equiv. succinic acid, 2.5 equiv. PyBOP and 17.5 equiv. DIPEA were dissolved in 1 mL of dry DMF, and incubated with the resin for 2 h to attach a succinic acid

moiety to the C_{10}E492 N-terminus. The resin was washed by DMF (3 x 5 mL) and 0.5 mL of dry DMF containing 1 equiv. PyBOP, 2.5 equiv. DIPEA was added, the reaction was vigorously shaken for 20 min at rt, the solution was drained, and the resin was washed with DMF (1 x 5 mL). A solution containing 2.5 equiv. 6-aminopenicllic acid, 5 equiv. DIPEA, 2 mL DMF and 200 μL H_2O was added to the resin and the reaction was shaken vigorously at rt overnight. Following cleavage from the resin (95% TFA, 2.5% H_2O and 2.5% *p*-cresol), the product was purified by using HPLC with a gradient of 0-7.5% B over 10 min. A white powder was obtained (1.6 mg). The calculated *m/z* for desired product [M+H$^+$] is 1125.39. A *m/z* of 1143.39 was found, which corresponds to addition of water to the desired product. Hydrolytic ring-opening of the β-lactam ring was confirmed by tandem MS-MS spectrometry (data not shown).

Synthesis of Boc-ciprofloxacin (9). Ciprofloxacin (1.66 g, 5.00 mmol) and $NaHCO_3$ (0.84 g, 10 mmol) were combined in 100 mL of H_2O with stirring. A 10 M NaOH aqueous solution was added drop-wise until all of the solids dissolved. Di-*tert*-butyl dicarbonate (2.29 g, 10.5 mmol) was added and the reaction was stirred overnight at rt. The product precipitated as a white solid. The precipitate was filtered and washed with an aqueous NaOH solution of pH 9-10 (10 mL) and then with H_2O (2 x 10 mL), which afforded **9** as a white solid (2.0 g, 94%). TLC R_f = 0.6 (silica, 9:1 dichloromethane/MeOH). ^{1}H NMR ($CDCl_3$, 300 MHz) δ (ppm) 1.20 (2H, m), 1.39 (2H, m), 1.49 (9H, s), 3.29 (4H, t), 3.55 (1H, m), 3.66 (4H, t), 7.35 (1H, d), 7.95 (1H, d), 8.70 (1H, s), 14.94 (1H, s). HRMS (DART): [M+H]$^+$ *m/z* calcd., 432.1929; found, 432.1926.

Synthesis of Boc-ciprofloxacin-C_{10}E492 (10). The C_{10}E492 peptide was synthesized as described for penicillin-C_{10}E492 on a 0.03 mmol scale except that pre-loaded Fmoc-Ser-Wang resin was employed. Some peptides were synthesized by using a peptide synthesizer in Professor Tania A. Baker's lab in the Department of Biology. One additional L-serine building block with an unprotected side chain hydroxyl group was added at the N-terminus of the C_{10}E492 sequence. Before removing the Fmoc group on this additional serine, 4 equiv. Boc-ciprofloxacin, 10 equiv. 1-ethyl-3-(3-dimethylaminopropyl)carbodiimide hydrochloride (EDC-HCl) and 8 equiv. 4-dimethylaminopyridine (DMAP) were dissolved in 4 mL of dry CH_2Cl_2 and combined with the resin. The mixture was incubated overnight at rt with shaking. The crude peptide was cleaved from the resin, deprotected and purified as described for **8**, which yielded a white powder (4.7 mg). MS (MALDI-TOF): [M+H$^+$] *m/z* calcd, 1227.49; found, 1227.82.

Synthesis of Ciprofloxacin-C_{10}E492-MGE (11). As described for **2** except that 2.5 μM ciprofloxacin-C_{10}E492 was used and the HPLC gradient for purification was adjusted to 0 to 55% B over

20 min, which afforded **11** as a white powder (0.4 mg). MS (MALDI-TOF): [M+H$^+$] *m/z* calcd, 2040.6789; found 2040.6803.

Synthesis of Levofloxacin-C_{10}E492-MGE (12). Levofloxacin-C_{10}E492-MGE was synthesized and purified as described for **11**. The product was obtained as a white powder (0.6 mg). MS (MALDI): [M+H$^+$] *m/z* calcd, 2070.6875; found, 2070.6972.

Fluorescence Study of FL-C_{10}E492-MGE (7). A 50 μM Fe(III) solution was prepared by dissolving 16.2 mg of $FeCl_3$ in a minimal amount of 12 M HCl, then bringing the volume up to 10 mL by addition of milli-Q H_2O, followed by an 1:1000 dilution by using 75 mM HEPES buffer, pH 7.5 and used immediately. Stock solutions of FL-C10E492-MGE and FL-C_{10}E492 were prepared in 1:5 DMSO/H_2O, and the concentrations were determined by absorbance at 493 nm (ε = 76900 $M^{-1}cm^{-1}$ for fluorescein).[8] For each experiment, the peptide stock solutions were diluted to 10 μM with 75 mM HEPES buffer, pH 7.5. MceD enzyme was over-expressed and purified as reported[4] and diluted to 200 nM with 75 mM HEPES buffer, pH 7.5. In a 96-well fluorescence plate, 1 μM FL-C_{10}E492-MGE or FL-C_{10}E492 was mixed with varying concentrations of aqueous $FeCl_3$ with or without MceD and incubated for 0.5 h at rt. The total volume of each well was 100 μL. The emission spectra were measured by using SPECTRAmax™ GEMINI XS Dual-Scanning Microplate Spectrofluorometer (excitation wavelength, 494 nm; scan, 250 nm to 850 nm; cut off, 495 nm).

FepA Cloning, Overexpression and Purification. The *fepA* gene was amplified from *E. coli* CFT073 genomic DNA using the forward primer 5'-ggaattcggatccgaacaagaagattcatcc-3' (*Bam*HI restriction site underlined) and reverse primer 5'-gatcctcgagtcagaagtgagtattaatgctc-3' (*Xho*I restriction site underlined). Pfu Turbo DNA polymerase (Stratagene) was employed for polymerase chain reactions, and the amplified genes were digested with *BamH*I and *Xho*I (New England Biolabs), ligated into the *Bam*HI and *Xho*I-digested pET20b-sp-H10-TEV using T4 DNA ligase (New England Biolabs) and transformed into chemically-competent *E. coli* TOP 10 cells. The identity of the resulting construct was confirmed by DNA sequencing. The over-expression and purification of His_{10}-FepA followed a previously reported procedure.[9] *E. coli* BL21 (DE3) cells were transformed with pET20b-sp-H10-TEV-FepA. A single colony was picked and grown in LB media containing 50 μg/mL ampcillin at 37 °C until OD_{600} reached 0.5-0.6 (not over 0.6). Glycerol cell stocks were prepared by mixing 100 μL of the culture with an equal volume of sterile-filtered 50% glycerol/LB. The resulting cell solution was flash frozen in liquid nitrogen and stored at -80 °C.

For trial over-expression of His_{10}-TEV-FepA, a 200-μL aliquot of the glycerol cell stock was thawed on ice and added to 20 mL of terrific broth (TB). The culture was grown at 37 °C until the OD_{600} reached 0.5-0.6 (not over 0.6). This starter culture was diluted with TB (1:1000, 750 mL final volume) and incubated at 20 °C for 3 days with shaking at 150 rpm. The final OD_{600} of the culture was around 10, and the cells were pelleted by centrifugation, flash frozen in liquid nitrogen, and stored at -80 °C.

For protein purification, all buffers were prepared according to reported procedures.[9] Approximately 10 g (wet weight, from one 750-mL culture) of cells were suspended in 40 mL of lysis buffer (50 mM Tris-HCl at pH 8.0, 200 mM NaCl, 10 mM $MgCl_2$), and disrupted by sonication (1s on followed by 4s off, with a total sonication time of three minutes) on ice. The crude lysate was clarified by centrifugation (10,000 rpm, 10 min). The resulting supernatant was centrifuged at 160,000×g for 1 h at 4 °C to pellet the membranes. The membrane pellet was transferred to a glass homogenizer and homogenized in 20 mL of solubilizaion buffer (50 mM potassium phosphate buffer at pH 7.5, 200 mM NaCl, 30 mM imidzole, 5% Elugent). The mixture was stirred at 4 °C overnight, and centrifuged at 200,000×g for 1h. The supernatant containing solubilized proteins was passed through 1 mL pre-washed Ni-NTA resin slurry (Qiagen) and eluted by using an imidazole gradient (100 mM to 250 mM). Fractions rich in FepA, determined by SDS-PAGE, were combined and dialyzed in dialysis buffer (50mM Tris-HCl buffer at pH 7.5, 2 mM DTT, 1 mM EDTA) at 4 °C overnight. The protein solution was concentrated to 600 μL by using a 30-kDa cut-off centrifuge tube and applied to 12% SDS-PAGE gel (Tris-HCl) with or without 100 °C heating after mixing with the loading dye.

Results and Discussion

General Strategy for the Design of Enterobactin-antibacterial Conjugates. With the aim of directing antibiotics to Gram-negative bacteria, a "Trojan horse" strategy was conceived to overcome the outer membrane permeability barrier. In this work, antimicrobials, including membrane-disrupting peptides, DNA-damaging agents and small-molecule antibiotics, were connected to enterobactin via a 10-amino acid peptide linker and a glucose molecule (Figure A1.1A). This linkage design was based on the known biosynthetic pathway of MccE492m. The MceIJ protein complex, which catalyzes ester bond formation between the C-terminal serine residue of the microcin peptide and the glucose moiety of MGE, can accept a 10-mer peptide (C_{10}E492) comprised of the ten C-terminal amino acids (SATSSSGSGS) of the 84-residue peptide as a substrate.[5] It also accepts C_{10}E492 derivitized at the N-terminus and links these substrates to MGE.[5] Based on these data, we picked several antimicrobial agents and chemoenzymatically attached them to Ent, which yielded the final Ent-antimicrobial agents conjugates (Figure A1.1C). Because *E. coli* has a dedicated Ent uptake and transport machinery, we expected that

these conjugates would be transported into the bacterial cytosol via this pathway, thus bypassing the outer membrane permeability barrier of Gram-negative bacteria.

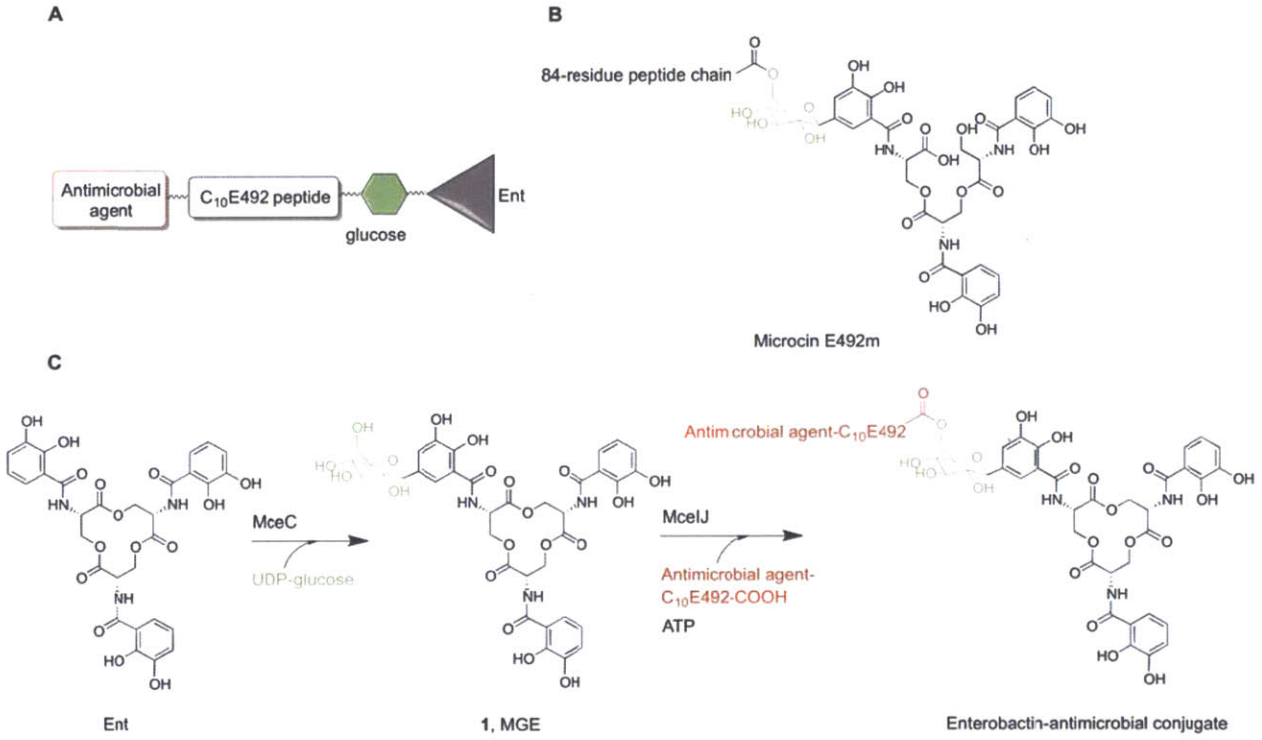

Figure A1.1 General design of the Ent-antimicrobial conjugates. (A) Scheme of the conjugate components. (B) Structure of Microcin E492m. (C) General synthetic route for the conjugates.

Synthesis and Activity Study of Enterobactin-antimicrobial Peptides Conjugates. Many organisms biosynthesize short, ribosomal-derived antibacterial peptides that exhibit broad spectrum antimicrobial activity. Examples include melittin,[10] LL-37,[11] protegrin,[12] and members of the defensin family.[13] These peptides can be attached easily to C_{10}E492 by solid-phase peptide synthesis, and thus provided a good starting point to test the Trojan-horse strategy. We selected two antimicrobial peptides, Magainin-I (MSI) and Protegrin-I (PGI), for preliminary work. Their sequences are listed in Table A1.1. MSI and PGI are short peptides (about 20 residues) and have broad spectrum antimicrobial activity via membrane disrupting effects.[14] The peptides exhibit α-helical and β-sheet secondary structures, respectively.

It is well-established that the inner membrane of Gram-negative bacteria is more permeable than the outer membrane. We therefore expected that MSI- and PGI-C_{10}E492-MGE (**2** and **3**, Table A.1.1) may have higher activity compared to the MSI and PGI peptides alone resulting from FepA-mediated

transport across the outer membrane. The chimeric peptides containing the MSI/PGI and C_{10}E492 components were purchased from Chi Scientific and used in the MceIJ catalyzed reaction with MGE to afford the final conjugates following HPLC purification. Unfortunately, the observed antimicrobial activity of MSI-Ent and PGI-Ent did not agree with our expectation. The MIC values against several *E. coli* and one *Pseudomonas* strain are listed in Table A1.2. MSI and PGI peptides and their Ent conjugates yielded similar MIC values. To test whether these results were due to lack of FepA expression, identical assays were performed in the presence of 2,2'-dipyridyl (DP, 200 μM). This small molecule is routinely employed to chelate iron present in the growth medium and thus induce the iron-uptake pathway related gene expression level, including FepA.[15] No enhancement of bactericidal activity was observed under these iron-limiting conditions (Table A1.3). MSI and PGI are membrane-penetrating peptides, and it is possible that interaction between MSI/PGI peptides and the outer membrane interfered with the FepA-mediated uptake of the conjugate.

Synthesis and Activity Study of Enterobactin-Amino Terminal Cu and Ni Binging Motif (ATCUN) Conjugates. Besides membrane disrupting peptides, the amino terminal Cu and Ni binding motif (ATCUN), a peptide comprised of three amino acids (e.g., AspSerHis) with potential DNA damage activity, was also selected in this study. The ATCUN motif is a binding site found in the N-terminus of many naturally occurring proteins. Upon Cu(II) binding in the presence of a reducing reagent such as ascorbate, the motif catalyzes the reducing reaction of O_2 and generates hydroxyl radical, which has been indicated to cause DNA damage *in vitro*.[16] To avoid interference from the C_{10}E492 sequence, four glycine residues were inserted between the ATCUN motif and the C_{10}E492 peptide (**5**, ATCUN-G_4-C_{10}E492-MGE); conjugates with two or six glycine spacers were also synthesized (**4**, ATCUN-G_2-C_{10}E492-MGE and **6,** ATCUN-G_6-C_{10}E492-MGE, Table A1.1).

The synthesis of these conjugates followed the same routes as the antimicrobial peptide derived conjugates, and we questioned whether these ATCUN conjugates would deliver the ATCUN motif into the cytoplasm and generate hydroxyl radicals to cause DNA damage and cell death. The conjugates did not exhibit any activity within the tested concentration range (up to mM, Table A1.2). Supplement the assay media with copper provided the same results.

Synthesis and Activity Study of Enterobactin-small Molecule Antibiotic Conjugates. In addition to short peptides, small-molecule antibiotics are another class of candidates for this strategy. 6-Aminopenicillanic acid (6-APA), ciprofloxacin, and levofloxacin were considered in this study. Penicillin is a well-known antibiotic that inhibits formation of peptidoglycan cross-links in the bacterial cell wall. Ciprofloxacin and levofloxacin are both fluoroquinoline drugs that target DNA gyrase in bacteria,

inhibiting DNA replication.[17] These small molecules are all commercially available and contain functional groups amenable to synthetic modification, and were therefore attached to the N-terminus of C_{10}E492 by solid-phase peptide synthesis.

Table A1.1 Characterizations of the Ent-antimicrobial conjugates synthesized in this chapter.

Compound	Peptide sequence	HPLC retention time	*m/z* cald.[a]	*m/z* obs.
MSI-C_{10}E492-MGE (**2**)	GIGKFLKKAKKFGKAFVKILKK-SATSSSGSGS	9.7 min[b]	4101.28	4101.62
PGI-C_{10}E492-MGE (**3**)	RGGRLCYCRRRFCVCVGR-SATSSSGSGS	8.4 min[b]	3780.57	N.A.
ATCUN-G2-C_{10}E492-MGE (**4**)	DSHGGSATSSSGSGS	10.2 min[b]	2093.68	2094.00
ATCUN-G4-C_{10}E492-MGE (**5**)	DSHGGGGSATSSSGSGS	11.0 min[b]	2207.72	2208.07
ATCUN-G6-C_{10}E492-MGE (**6**)	DSHGGGGGGSATSSSGSGS	10.2 min[b]	2321.76	2322.11
Fluoroscein-C10E492-MGE (**7**)	FL-SATSSSGSGS	8.5 min[b]	1998.56	1998.95
Ciprofloxacin-C10E492-MGE (**11**)	Cipro-SSATSSSGSGS	12.6 min[c]	2040.6789	2040.6803
Levofloxacin-C10E492-MGE (**12**)	Levo-SSATSSSGSGS	14.2 min[c]	2070.6875	2070.6972

[a] The values are calculated for $[M+H]^+$. [b] The retention time was obtained with a HPLC gradient of 10-40% B over 10 min. [c] The retention time was obtained with a HPLC gradient of 0-55% B over 20 min.

Scheme A1.1 illustrates the attempted synthesis of 6-APA-C_{10}E492 (**8**). Because many penicillanic acid derivatives, including those used in the clinic, are prepared by N-acetylation of the 6-APA amino group and the 6-APA carboxylic acid moiety is required for antibacterial action, we chose to connect 6-APA to C_{10}E492 off the primary amine group via a succinic acid linker. The succinic acid was coupled to the N-terminus of C_{10}E492 first to afford **8a,** and then the free carboxylic acid was coupled to the amino group on 6-APA. The coupling of the amino group of 6-APA to the carboxylic group of **8a** did not follow the normal solid-phase synthesis procedure because the 6-APA is an unprotected amino acid, therefore the homo coupling of 6-APA must be prevented. This selectivity was achieved by incubating **8a** with PyBOP and DIPEA first to activate the carboxylic acid group on the peptide, followed by a wash step to remove the activation reagents, and then 6-APA was added to the reaction. This strategy was proved to be successful judged by the relatively clean HPLC trace of the crude reaction. Unfortunately, a *m/z* of 1143.39 was found for the purified product whereas the calculated *m/z* for penicillin-C_{10}E492 $[M+H^+]$ is 1125.39. Tandem MS-MS spectrometry data indicated that the C_{10}E492 moiety in the purified product was intact. We reasoned that the increase of 18.00 Da results from the hydrolysis of the β-lactam ring. The TFA cleavage step in the penicillin-C_{10}E492 synthesis probably caused the opening of β-lactam

ring (see Figure A1.2A). This hypothesis was confirmed by incubating 6-APA in the TFA cleavage mixture used in the synthesis, which also resulted in decomposition of 6-APA as seen by analytical HPLC (data not shown). The penicillanic acid conjugate was not pursued further.

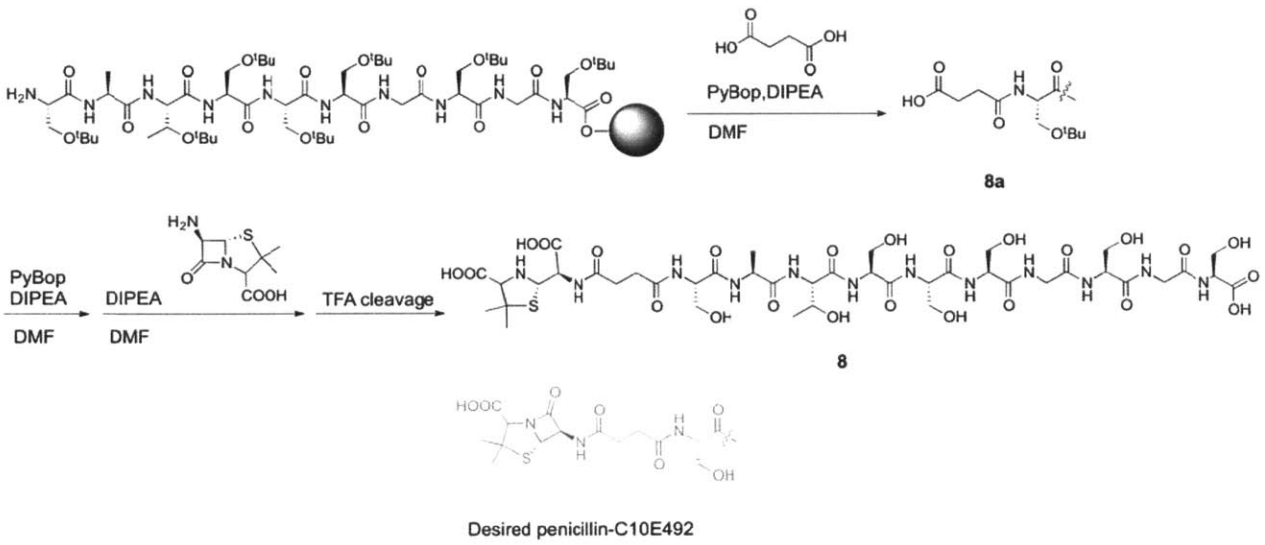

Scheme A1.1. Synthesis of penicillin-C_{10}E492 (**8**).

Ciprofloxacin contains both an amino and a carboxylic acid group. Like 6-APA (Scheme A1.2), the acid moiety is also required for its activity. However, the target for its antimicrobial action is an enzyme localized in cytosol (DNA gyrase). In this case, a stable amide bond linkage between ciprofloxacin and C_{10}E492-MGE may be problematic because the appended peptide and MGE structure may interfere with the binding of ciprofloxacin to its target. This agrees with our previous observations in Chapter 2 and 4. Other siderophore-fluoroquinolone conjugates with stable linkers have been shown to be inactive as well.[18] From these considerations, we decided to install a labile ester linker in the target compound ciprofloxacin-C_{10}E492-MGE (**11**) to allow release of the antibiotic after the conjugate is transported into the cell. Levofloxacin has a similar structure and the same antimicrobial mechanism as ciprofloxacin, so the same strategy was used to synthesize levofloxacin-C_{10}E492-MGE (**12**). As shown in Scheme A1.2 and Table A1.1, one additional serine was added between cipro/levofloxacin and C_{10}E492 and its hydroxyl side chain was used to form an ester bond with the carboxylic acid moiety of cipro/levofloxacin. Due to the low solubility of ciprofloxacin in organic solvents, the secondary amine of this molecule was protected by using *tert*-butyl carbamate (Boc) and Boc-ciprofloxacin (**9**) was obtained in 94% yield. The C_{10}E492 peptide was coupled with **9** and the Boc group on ciprofloxacin was removed during the TFA cleavage step (Scheme A1.2). Levofloxacin was soluble in organic solvent and was used

in the coupling without any modification. The ciprofloxacin-C_{10}E492 and levofloxacin-C_{10}E492 were purified by semi-preparative HPLC and subjected to the MceIJ catalyzed reaction with MGE. Figure A1.2 illustrate the analytical HPLC traces obtained for compound **11** and **12**.

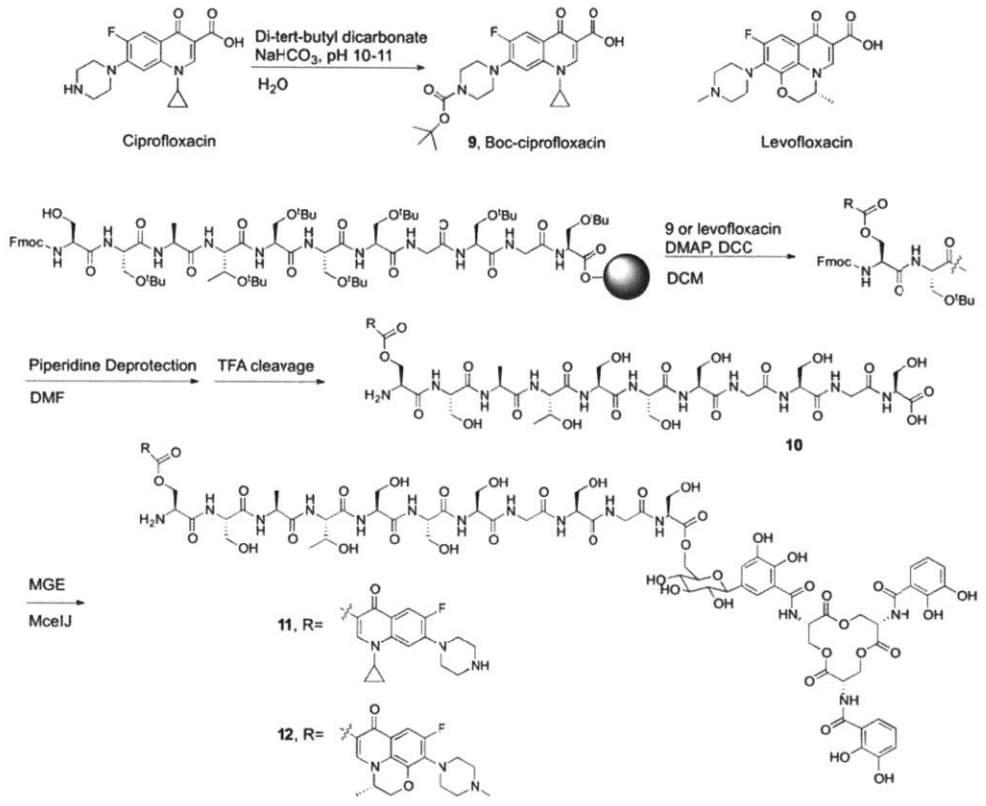

Scheme A1.2. Synthetic route for cipro/levofloxacin-C_{10}E492-MGE **11** and **12**.

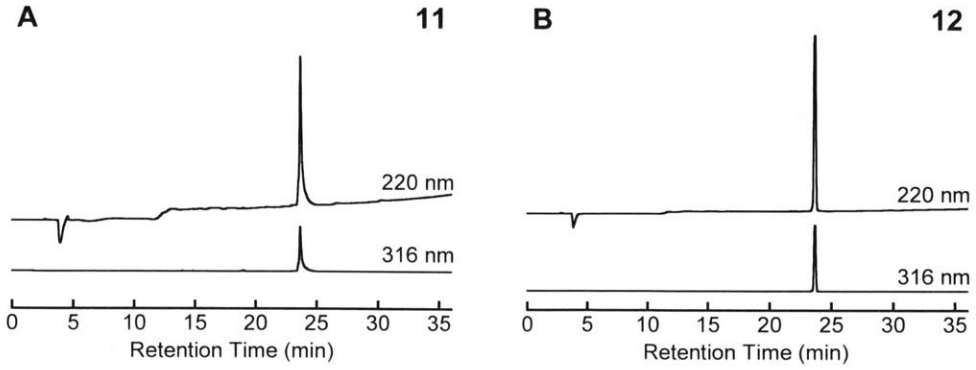

Figure A1.2. Analytical HPLC traces for ciprofloxacin-C_{10}E492-MGE (**11**, A) and levofloxacin-C_{10}E492-MGE (**12**, B).

Results from antimicrobial activity studies for ciprofloxacin, levofloxacin, **10**, **11**, and **12** are summarized in Table A1.2. We expected enhanced activities of **10** and **11** relative to the free antibiotics because the active transport machinery of enterobactin should deliver more antibiotics into the cell compared to diffusion. In contrast, the results showed that the conjugates did not exhibit improved activity. The MIC values of the conjugates increased at least ten-fold compared to the corresponding small molecules. In case of cipro-C_{10}E492, the MIC value increased over 300-fold. Adding 2,2'-dipyridyl did not decrease the MIC values (Table A1.3). Possible explanations for these results are (i) the conjugates did not enter the cell or (ii) the conjugates were not able to release the small molecule after crossing the outer membrane.

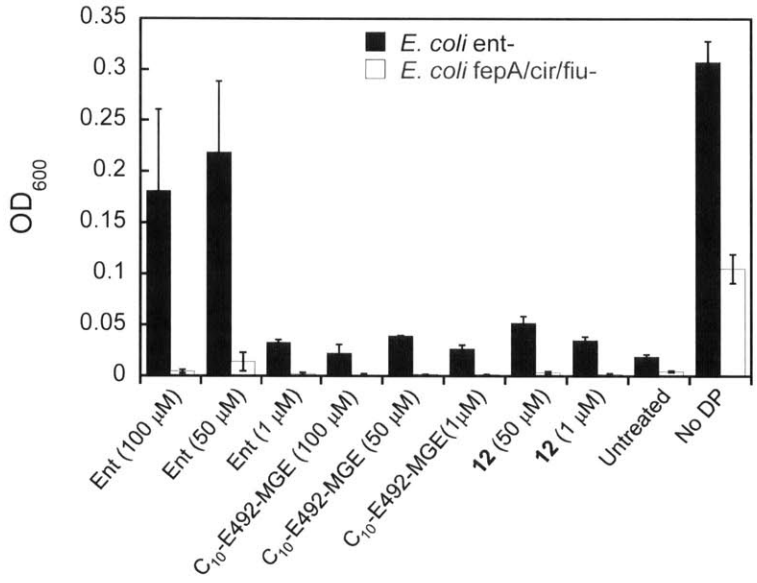

Figure A1.3. Recovery assay for Ent and relative conjugates. All conditions has 200 μM 2,2'-dipyridyl except the noted one. The error bars represent the standard error for three independent repetitions.

To test whether the conjugates were transported into the cell, *E. coli* K12RW193, which is deficient in enterobactin synthesis, was used in a recovery assay. The bacteria was grown in PB media supplemented with 2,2'-dipyridyl (200 μM), and in the presence of varying concentrations of enterobactin, C_{10}E492-MGE or **12** (Figure A1.3). As a negative control, the *E. coli* H1876 strain, which lacks all enterobactin receptor proteins (FepA, Fiu and Cir), was also evaluated. The data in Figure 5 show that, by adding enterobactin, the growth of *E. coli* K12RW193 recovered (at 50 μM, 71% recovery based on OD_{600}). As expected, there was no recovery for E. *coli* H1876 lacking enterobactin receptors. When C_{10}E492-MGE or levo-C_{10}E492-MGE **12** was added to the medium, some recovery (at 50 μM of levo-C_{10}E492-MGE, 17% recovery based on OD_{600}), but not as much as with the same concentration of Ent,

was observed. There was no obvious difference between C_{10}E492-MGE and levo-C_{10}E492-MGE in the recovery assay, which agrees with the previous MIC results where no activity was detected for levo-C_{10}E492-MGE. These results indicate that the conjugates entered the cell and at least some of that conjugate-bound iron was utilized. Nevertheless, the conjugates may not transport iron as well as unmodified enterobactin, which may result from less efficient uptake by outer membrane receptors. Alternatively, the conjugates may not reach the cytosol to be hydrolyzed by Fes, a cytoplasmic esterase that cleaves the enterobactin trilactone ring to allow iron release, or they are not good substrate for Fes.

Table A1.2 Minimal inhibitory concentrations (MIC) of the Ent-antimicrobial conjugates determined without DP.[a]

Compound	Strain							
	E. *coli* BL21 (DE3)	E. *coli* K12	E. *coli* B	E. *coli* H1876 (*fepA*$^-$,*cir*$^-$, *fiu*$^-$)	E. *coli* KB4 (*ompF*$^-$)	E. *coli* K12RW193 (*entA*$^-$, ATCC 33475)	E. *coli* NR698	*Pseudomonas Pathovirus putida*
MSI-C_{10}E492	3.5±1.5	3.5±1.5		3.5±1.5				
MSI-C_{10}E492-MGE	3.5±1.5	5±0		5±0				
PGI-C_{10}E492	5±0	5±0		5±0				
PGI-C_{10}E492-MGE	50	5±0		50				
Ciprofloxacin		0.07±0.03		0.1±0	0.1±0	0.1±0		
Ciprofloxacin-C_{10}E492		>25	>25	>25	>25	>25	>25	>25
Ciprofloxacin-C_{10}E492-MGE		>1		>1	>1	>1		
Levofloxacin		0.09±0.01	0.08±0.02	0.1±0.2	0.1±0	0.1±0	0.08±0.2	1
Levofloxacin-C_{10}E492-MGE		>1		>1	>1	>1		
C_{10}E492-MGE		>100	>100	50	>100	>100	>100	>100
MccE492m	0.5±0	0.08±0	0.09±0.01	>10		0.08±0	0.08±0	>0.3
MccE492	>20	15±5		>20				
ATCUN-G4-C_{10}E492		>200		>200				
ATCUN-G4-C_{10}E492+Cu(II)		>200		>200				
ATCUN-G4-C_{10}E492-MGE		200		10				
ATCUN-G4-C_{10}E492-MGE+Cu(II)		>200		10				

[a] The values listed are in μM. Values in the table with standard errors are the average of two or three experiments and the standard deviation of the mean was shown. Other values are from a single experiment.

Table A1.3. The MIC of the Ent-antimicrobial conjugates determined in the presence of 200 μM of 2,2'-dipyridyl.[a]

Compound	Strain			
	E. *coli* K12	E. *coli* H1876 (*fepA-,cir-, fiu-*)	E. *coli* KB4 (*ompF-*)	E. *coli* K12RW193 (*entA-*, ATCC 33475)
MSI-C10E492	2			
MSI-C10E492-MGE	2			
PGI-C10E492	2			
PGI-C10E492-MGE	5			
Ciprofloxacin	0.1		0.1	
Ciprofloxacin-C10E492-MGE	>1	>1	>1	>1
Levofloxacin	0.1		0.1	
Levofloxacin-C10E492-MGE	>1	>1	>1	>1
MccE492m	0.5			
MccE492	10			
ATCUN-G4-C10E492	>200			
ATCUN-G4-C10E492+Cu(II)	>200			
ATCUN-G4-C10E492-MGE	>100			
ATCUN-G4-C10E492-MGE+Cu(II)	>100			

[a] The values listed are in μM from a single experiment.

Fluorescence Study of FL-C_{10}E492-MGE (7). In addition to antimicrobial delivery, we are also interested in having conjugate with a fluorescence tags so that by tracking the fluorescence signal we will be able to probe the uptake efficiency of the conjugate.

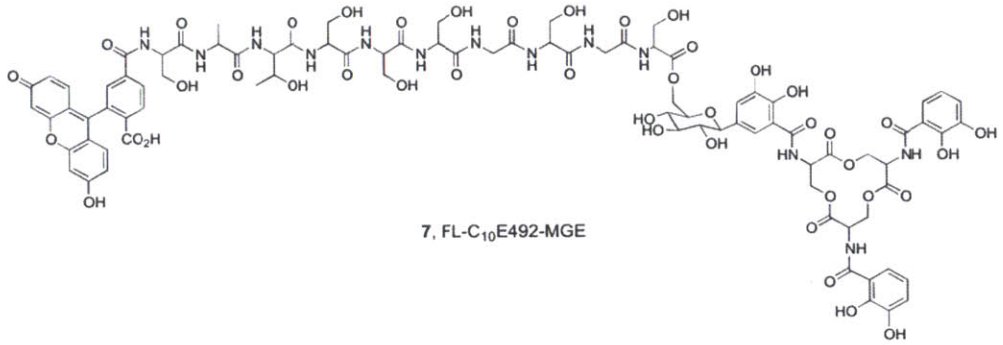

7, FL-C_{10}E492-MGE

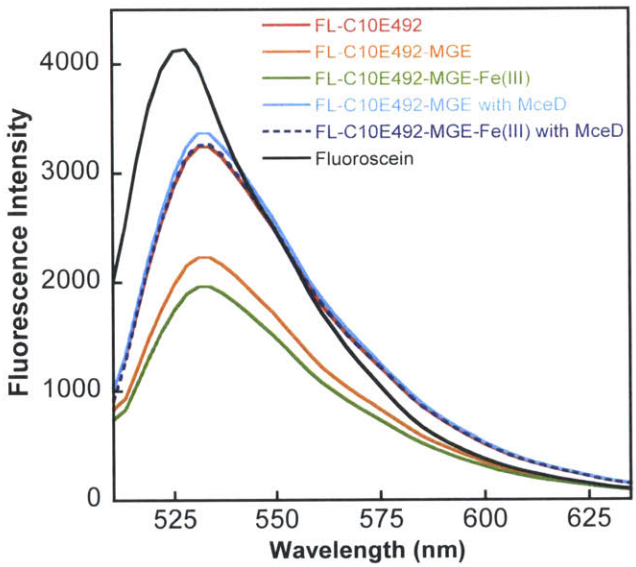

Figure A1.4. Structure and fluorescent spectra of FL-C_{10}E492-MGE (**7**) in the absence or present of Fe(III) compared to FL-C_{10}E492 and fluorescein. MceD treatment result in recovery of fluorescent signal with or without ferric ion.

Fluorescein (FL)-C_{10}E492-MGE (**7**) was synthesized via chemoenzymatic reactions as conjugates **2-6** from fluorescein-C_{10}E492 (Chi Scientific) and MGE. Before using it to track conjugate uptake, it was necessary to determine the effect of Fe(III) binding on the fluorescence signal. Because of its $3d^5$ electronic configuration, Fe(III) has the propensity to quench fluorophore emission. In this experiment, the emission spectra of FL-C_{10}E492 and **7** were compared to evaluate the effect of MGE on fluorescence quenching. FL-C_{10}E492-MGE (1 μM) was also mixed with $FeCl_3$ with different molar ratios in HEPES

buffer (pH 7.5) with or without MceD, the enzyme in the MccE492m biosynthesis pathway that hydrolyzes the Ent backbone, and the emission fluorescence spectra were recorded (Figure A1.4). A comparison of the emission spectra of FL-C_{10}E492 and **7** reveals that Ent quenches the fluorescence signal of FL-C_{10}E492 by ~45% independent of Fe(III) binding. MceD-catalyzed hydrolysis of the Ent macrolactone results in signal recovery. Although the conjugates are not as emissive as fluorescein alone, we expect that FL-C_{10}E492-MGE is sufficiently bright for use in intracellular tracking studies.

Over-expression and Purification of FepA. For *in vitro* binding studies between the synthesized conjugates and FepA, the *fepA* gene from E. *coli* CFT073 genomic DNA was cloned. Originally, the *fepA* gene was cloned into the *Nde*I and *Xho*I restriction site of the pET28b vector, which affords a His_6-FepA fusion protein.

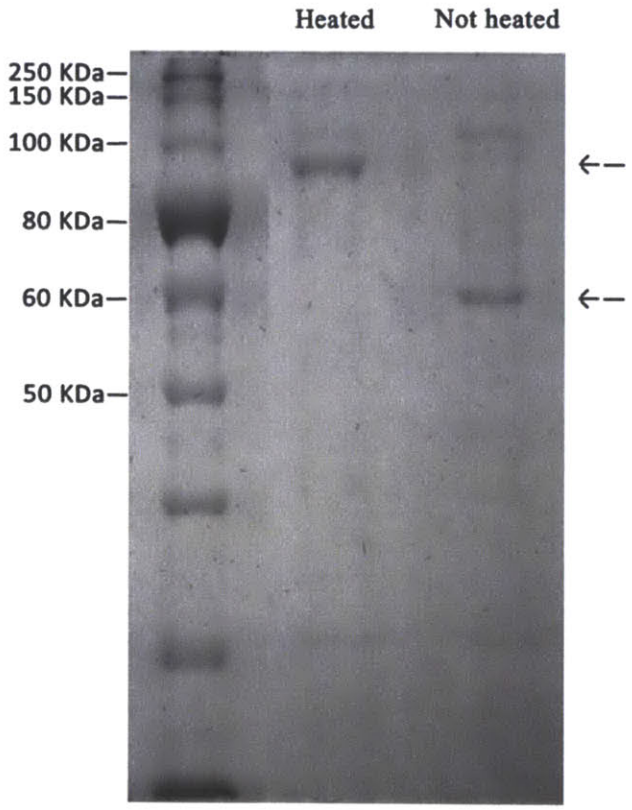

Figure A1.5. SDS-Page of purified FepA (12% Tris-HCl gel) illustrating the shift on the FepA band upon heating.

Preliminary attempts at overexpression and purification of His_6-FepA in E. *coli* BL21(DE3) indicated that the expression level was high (observed by SDS-PAGE), but most of the protein was insoluble. Several different detergents were used to solubilize the protein, but the protein remained insoluble. As a result, a new vector was used for the cloning. This vector (pET20b-sp-H10-TEV) includes a membrane-targeting signal sequence (*pelB*) so that after expression the FepA protein is transported to the outer membrane.[9] The N-terminus PelB sequence of the recombined protein is cleaved off after the protein is transported to the outer membrane, which affords His_{10}-TEV-FepA. The over-expression strain was grown at 20 °C in terrific broth (TB) until OD_{600} reached 10 without induction. The purification was performed as previously described.[9] A SDS-PAGE gel shift was observed upon heating at 100 °C (Figure A1.5), which indicated that the purified FepA is properly folded.[19] FepA will be further purified and used in *in vitro* binding studies in the future. The yield of this purification was low (~300 μL of FepA solutions was obtained from a 10-g pellet and the gel in Figure A1.6 was run with only 1.25 times dilution from this sample). IN the purification, a significant portion of the protein remained in the insoluble portion. Further improvement of this purification is needed in the future.

Summary and Perspective

This Appendix details the synthesis of some Ent-cargo conjugates containing several antimicrobial peptides and small-molecule antibiotics. A chemoenzymatic approach was developed and utilized to successfully prepare eight conjugates comprised of Ent, a peptide linker, and a cargo moiety. This synthetic route provides an alternative way to attach cargo to the Ent platform. A series of antimicrobial assays revealed that the Ent-antibiotic conjugates did not provide improved activity as compared to the antibiotic alone. Nevertheless, growth recovery assays employing C_{10}E492-MGE suggested that this conjugate is indeed transported by FepA, but with decreased efficiency compared to Ent. In related work, an Ent-fluorophore conjugate was synthesized and it affords significant fluorescence decrease with iron binding, which indicates that it may be useful for labeling studies.

There are many possible reasons for the lack of antimicrobial activity observed for these conjugates. For example, the interaction of the membrane-disrupting peptides PGI and MSI with the *E. coli* outer membrane might be strong and thus interfere with the binding of Ent to FepA or impede FepA-mediated transport. The ATCUN motif presents a relatively complicated mechanism. It requires copper binding, the presence of reducing reagents, and must be in close proximity to DNA to cause DNA damage. These conditions may not be all sufficient at the same time when treating the target with an ATCUN conjugate. Another concern is that even if some DNA (or cellular) damage occurs, it might not be significant to kill the cell due to DNA repair mechanisms. For the small molecule conjugates described above employing fluoroquinolones, the release of the drug after entering the periplasm or cytosol is quite

important, especially for the molecules chosen in this study, because the acid moiety used for the ester linkage is required for activity. In the cases of cipro-C_{10}E492-MGE and levo-C_{10}E492-MGE, it is highly possible that release did not occur based on the MIC and recovery assay results.

Our innate immune system employs defense mechanisms that target bacterial iron uptake pathways by releasing iron-chelating proteins or ferric-siderophore binding proteins at sites of infection, and by increasing peptide hormone levels, which effectively blocks iron uptake by the gut and iron release from storage when infection is detected.[20] Inspired by the innate immune response, siderophore mimics, molecules that would chelate iron but cannot be utilized by bacteria, could be another way to combat bacterial infection. The results in Figure A1.4 illustrated that C_{10}E492-MGE and levo-C_{10}E492-MGE could not recover the growth as well as Ent when the extracellular iron level was low. This observation indicates that these conjugates are not used as effectively as the siderophore alone, which could be a starting point to develop modified siderophores that compete with normal siderophores and inhibit bacteria growth by causing iron starvation.

Acknowledgement

I thank Professor Elizabeth Nolan for preparing the MceC, MceD and MceIJ enzymes. I thank Professor Tania Baker at the Biology Department MIT for helping us with solid phase peptide synthesis. I thank Professor Susan Buchanan at NIH for providing us the FepA plasmid and helpful discussions for purifying the protein. I thank Professor Barbara Imperiali for sharing the ultracentrifuge instrument.

Reference

1. Braun, V.; Pramanik, A.; Gwinner, T.; Koberle, M.; Bohn, E., Sideromycins: tools and antibiotics. *BioMetals* **2009**, *22* (1), 3-13.
2. Thomas, X.; Destoumieux-Garzon, D.; Peduzzi, J.; Afonso, C.; Blond, A.; Birlirakis, N.; Goulard, C.; Dubost, L.; Thai, R.; Tabet, J. C.; Rebuffat, S., Siderophore peptide, a new type of post-translationally modified antibacterial peptide with potent activity. *J. Biol. Chem.* **2004**, *279* (27), 28233-28242.
3. (a) Wayne, R.; Neilands, J. B., Evidence for common binding sites for ferrichrome compounds and bacteriophage phi 80 in the cell envelope of Escherichia coli. *J. Bacteriol.* **1975**, *121* (2), 497-503; (b) Wayne, R.; Frick, K.; Neilands, J. B., Siderophore protection against colicins M, B, V, and Ia in Escherichia coli. *J. Bacteriol.* **1976**, *126* (1), 7-12.
4. Nolan, E. M.; Fischbach, M. A.; Koglin, A.; Walsh, C. T., Biosynthetic tailoring of microcin e492m: Post-translational modification affords an antibacterial siderophore-peptide conjugate. *J. Am. Chem. Soc.* **2007**, *129* (46), 14336-14347.
5. Nolan, E. M.; Walsh, C. T., Investigations of the MceIJ-catalyzed posttranslational modification of the microcin E492 C-terminus: Linkage of ribosomal and nonribosomal peptides to form "Trojan Horse" antibiotics. *Biochemistry* **2008**, *47* (35), 9289-9299.
6. Destoumieux-Garzon, D.; Thomas, X.; Santamaria, M.; Goulard, C.; Barthelemy, M.; Boscher, B.; Bessin, Y.; Molle, G.; Pons, A. M.; Letellier, L.; Peduzzi, J.; Rebuffat, S., Microcin E492 antibacterial

activity: evidence for a TonB-dependent inner membrane permeabilization on Escherichia coli. *Mol. Microbiol.* **2003**, *49* (4), 1031-1041.
7. Scarrow, R. C.; Ecker, D. J.; Ng, C.; Liu, S.; Raymond, K. N., Iron(iii) Coordination Chemistry of Linear Dihydroxyserine Compounds Derived from Enterobactin. *Inorg. Chem.* **1991**, *30* (5), 900-906.
8. Robert Sjöback, J. N., Mikael Kubista, Absorption and fluorescence properties of fluorescein. *Spectrochim. Acta, Part A* **1995**, *51* (6), L7-L21.
9. Buchanan, S. K.; Lukacik, P.; Grizot, S.; Ghirlando, R.; Ali, M. M.; Barnard, T. J.; Jakes, K. S.; Kienker, P. K.; Esser, L., Structure of colicin I receptor bound to the R-domain of colicin Ia: implications for protein import. *EMBO J.* **2007**, *26* (10), 2594-2604.
10. Storm, D. R.; Rosenthal, K. S.; Swanson, P. E., Polymyxin and Related Peptide Antibiotics. *Annu. Rev. Biochem.* **1977**, *46*, 723-763.
11. Nold, M. F.; Nold-Petry, C. A.; Zepp, J. A.; Palmer, B. E.; Bufler, P.; Dinarello, C. A., IL-37 is a fundamental inhibitor of innate immunity. *Nat. Immunol.* **2010**, *11* (11), 1014-1064.
12. Steinberg, D. A.; Hurst, M. A.; Fujii, C. A.; Kung, A. H. C.; Ho, J. F.; Cheng, F. C.; Loury, D. J.; Fiddes, J. C., Protegrin-1: A broad-spectrum, rapidly microbicidal peptide with in vivo activity. *Antimicrob. Agents Chemother.* **1997**, *41* (8), 1738-1742.
13. Ganz, T., Defensins: Antimicrobial peptides of innate immunity. *Nat. Rev. Immunol.* **2003**, *3* (9), 710-720.
14. Lam, K. L.; Ishitsuka, Y.; Cheng, Y.; Chien, K.; Waring, A. J.; Lehrer, R. I.; Lee, K. Y., Mechanism of supported membrane disruption by antimicrobial peptide protegrin-1. *J. Phys. Chem. B* **2006**, *110* (42), 21282-21286.
15. Fernandez-Beros, M. E.; Gonzalez, C.; McIntosh, M. A.; Cabello, F. C., Immune response to the iron-deprivation-induced proteins of Salmonella typhi in typhoid fever. *Infect. Immun.* **1989**, *57* (4), 1271-1275.
16. Sankararamakrishnan, R.; Verma, S.; Kumar, S., ATCUN-like metal-binding motifs in proteins: Identification and characterization by crystal structure and sequence analysis. *Proteins* **2005**, *58* (1), 211-221.
17. Drlica, K.; Zhao, X., DNA gyrase, topoisomerase IV, and the 4-quinolones. *Microbiol. Mol. Biol. Rev.* **1997**, *61* (3), 377-392.
18. Rivault, F.; Liebert, C.; Burger, A.; Hoegy, F.; Abdallah, M. A.; Schalk, I. J.; Mislin, G. L., Synthesis of pyochelin-norfloxacin conjugates. *Bioorg. Med. Chem. Lett.* **2007**, *17* (3), 640-644.
19. Jalal, M. A.; van der Helm, D., Purification and crystallization of ferric enterobactin receptor protein, FepA, from the outer membranes of Escherichia coli UT5600/pBB2. *FEBS Lett.* **1989**, *243* (2), 366-370.
20. Chu, B. C.; Garcia-Herrero, A.; Johanson, T. H.; Krewulak, K. D.; Lau, C. K.; Peacock, R. S.; Slavinskaya, Z.; Vogel, H. J., Siderophore uptake in bacteria and the battle for iron with the host; a bird's eye view. *BioMetals* **2010**, *23* (4), 601-611

Appendix 4

NMR Spectra, HPLC Traces and UV-Vis Characterizations of Reported Compounds

Chapter 2
NMR Spectra

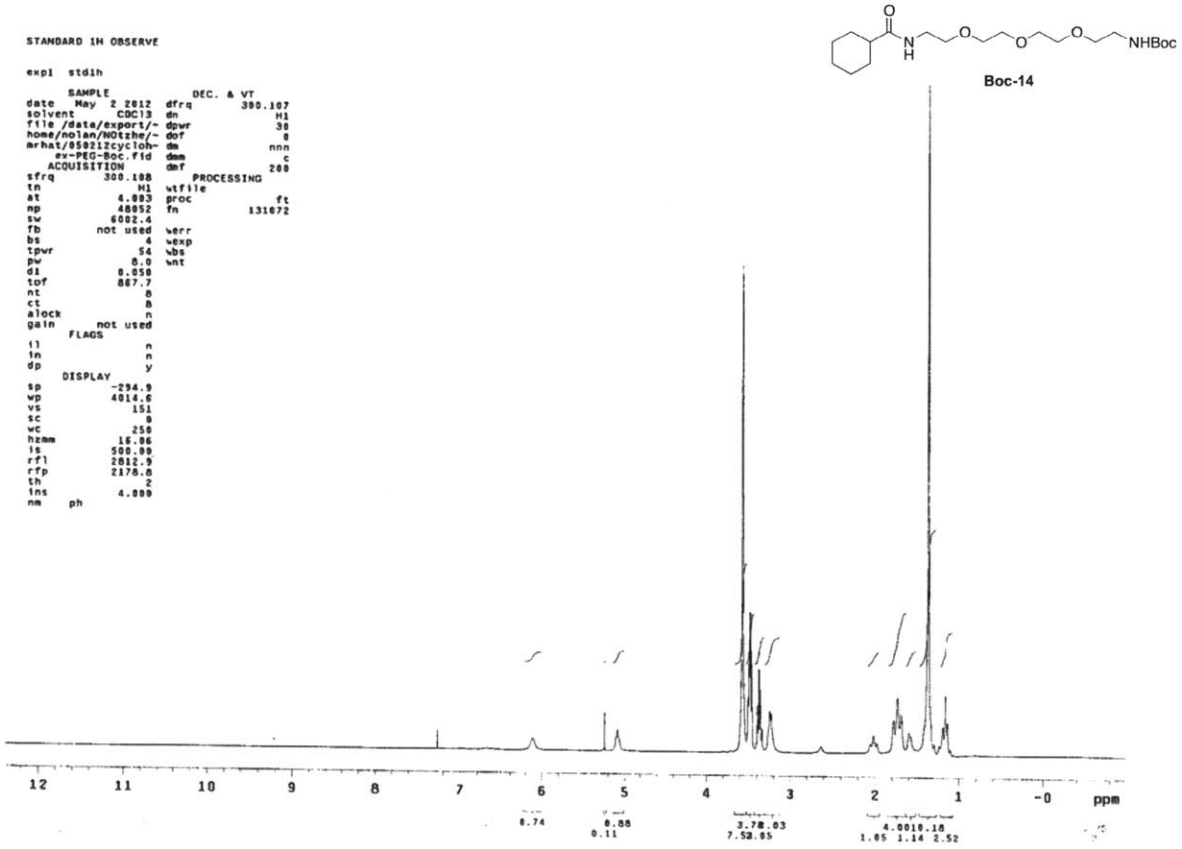
STANDARD 1H OBSERVE
expl stdih
SAMPLE
date May 2 2012
solvent CDCl3
file /data/export/~
home/nolan/NOtzhe/~
mrhat/050212cycloh~
ex-PEG-Boc.fid
ACQUISITION
sfrq 300.188
tn H1
at 4.083
np 48052
sw 6002.4
fb not used
bs 4
tpwr 54
pw 8.0
dl 8.050
tof 867.7
nt 8
ct 8
alock n
gain not used
FLAGS
il n
in n
dp y
DISPLAY
sp -294.9
wp 4014.6
vs 151
sc 0
wc 250
hzmm 16.86
is 500.00
rfl 2812.9
rfp 2178.8
th 2
ins 4.000
nm ph
DEC. & VT
dfrq 300.107
dn H1
dpwr 38
dof 0
dm nnn
dmm c
dmf 200
PROCESSING
wtfile
proc ft
fn 131072
werr
wexp
wbs
wnt
NHBoc
Boc-14
12
11
10
9
8
7
6
5
4
3
2
1
-0
ppm
0.74
0.88
0.11
3.78.03
7.52.05
4.0010.18
1.05 1.14 2.52

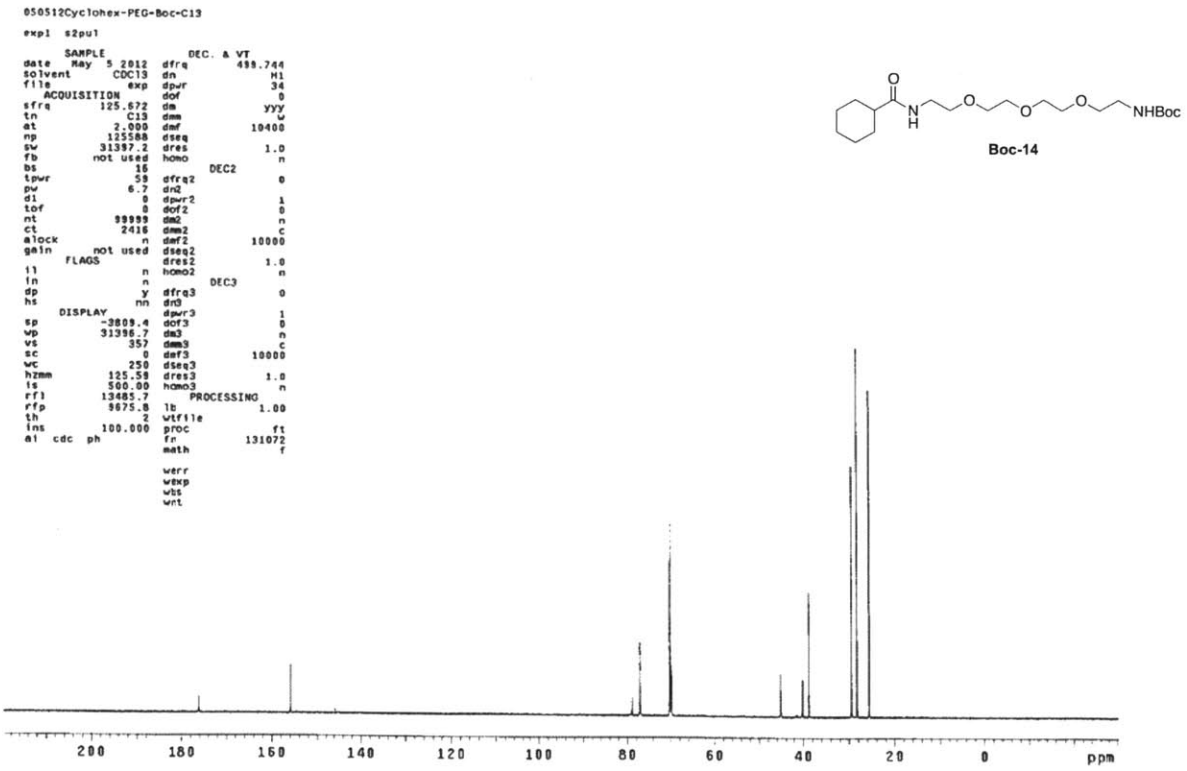
050512Cyclohex-PEG-Boc-C13
expl s2pul
SAMPLE
date May 5 2012
solvent CDCl3
file exp
ACQUISITION
sfrq 125.672
tn C13
at 2.000
np 125588
sw 31397.2
fb not used
bs 16
tpwr 59
pw 6.7
dl 0
tof 0
nt 99999
ct 2416
alock n
gain not used
FLAGS
il n
in n
dp y
hs nn
DISPLAY
sp -3809.4
wp 31396.7
vs 357
sc 0
wc 250
hzmm 125.58
is 500.00
rfl 13485.7
rfp 9675.8
th 2
ins 100.000
al cdc ph
DEC. & VT
dfrq 499.744
dn H1
dpwr 34
dof 0
dm yyy
dmm w
dmf 10400
dseq
dres 1.0
homo n
DEC2
dfrq2 0
dn2
dpwr2 1
dof2 0
dm2 n
dmm2 c
dmf2 10000
dseq2
dres2 1.0
homo2 n
DEC3
dfrq3 0
dn3
dpwr3 1
dof3 0
dm3 n
dmm3 c
dmf3 10000
dseq3
dres3 1.0
homo3 n
PROCESSING
lb 1.00
wtfile
proc ft
fn 131072
math f
werr
wexp
wbs
wnt
NHBoc
Boc-14
200
180
160
140
120
100
80
60
40
20
0
ppm

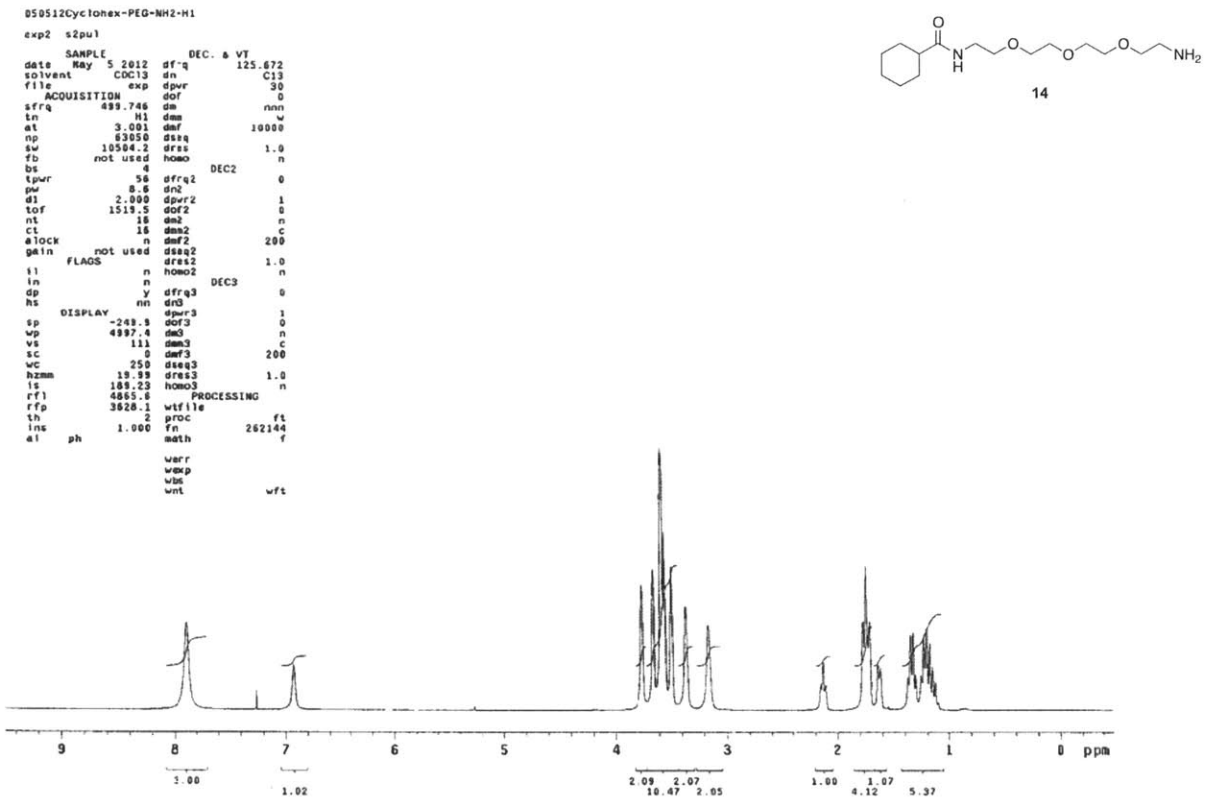
050512Cyclohex-PEG-NH2-H1
exp2 s2pul
SAMPLE
date May 5 2012
solvent CDCl3
file exp
ACQUISITION
sfrq 499.746
tn H1
at 3.001
np 63050
sw 10504.2
fb not used
bs 4
tpwr 56
pw 8.6
d1 2.000
tof 1519.5
nt 16
ct 16
alock n
gain not used
FLAGS
DISPLAY
DEC. & VT
PROCESSING
O
N
H
O
O
O
NH2
14
9
8
7
6
5
4
3
2
1
0 ppm
3.00
1.02
2.09
2.07
10.47
2.05
1.00
1.07
4.12
5.37

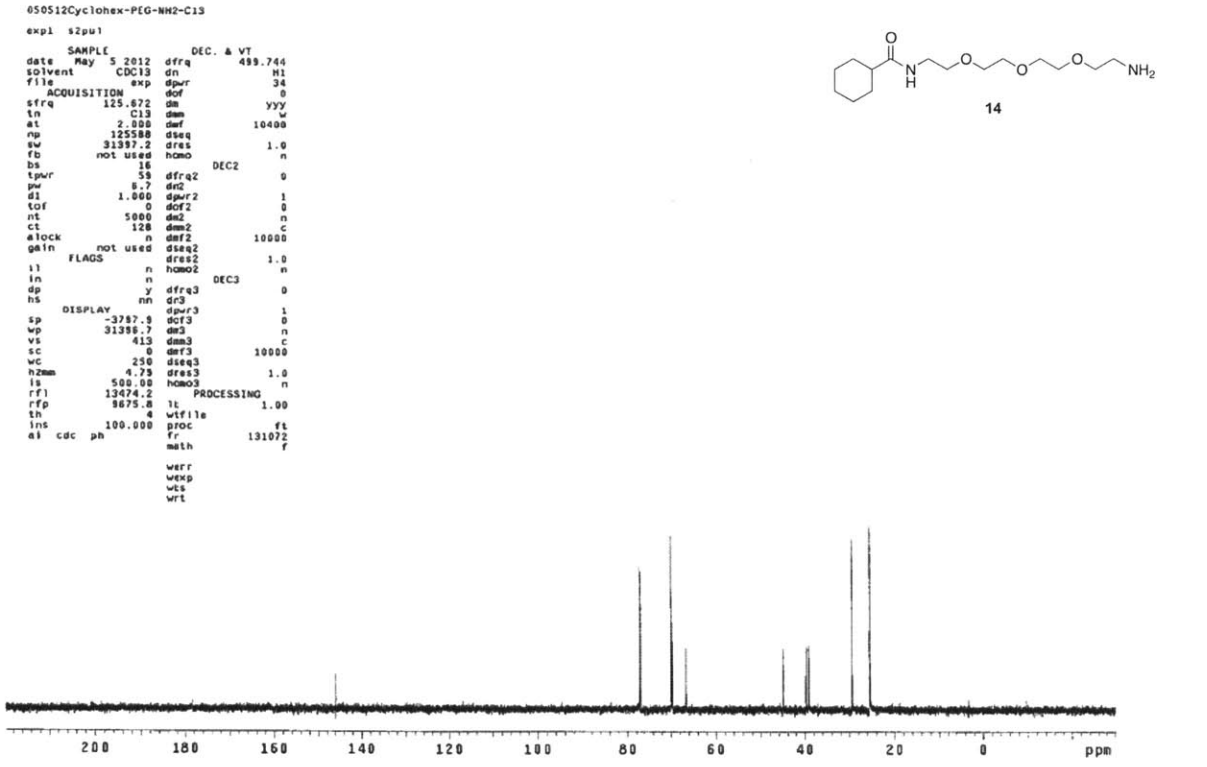
050512Cyclohex-PEG-NH2-C13
exp1 s2pul
SAMPLE
date May 5 2012
solvent CDCl3
file exp
ACQUISITION
sfrq 125.672
tn C13
at 2.808
np 125588
sw 31397.2
fb not used
bs 16
tpwr 59
pw 8.7
d1 1.000
tof 0
nt 5000
ct 128
alock n
gain not used
FLAGS
DISPLAY
DEC. & VT
PROCESSING
O
N
H
O
O
O
NH2
14
200
180
160
140
120
100
80
60
40
20
0 ppm

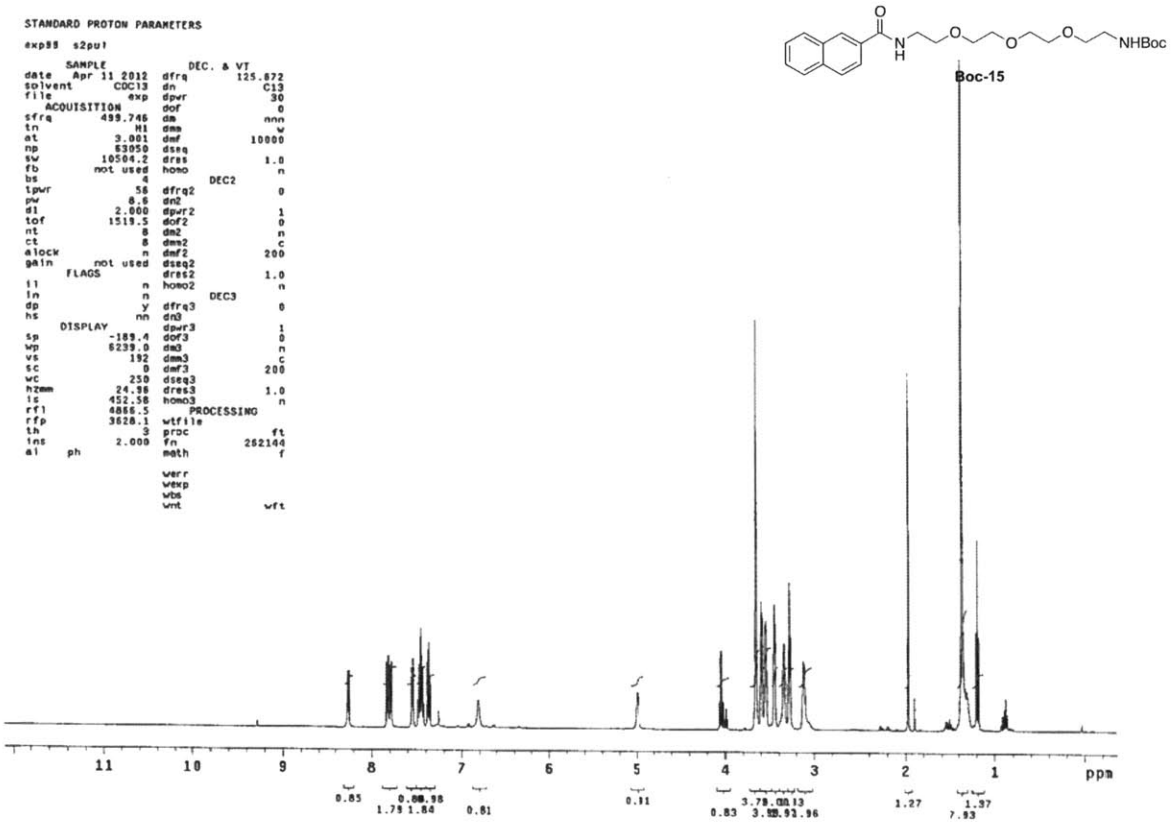
STANDARD PROTON PARAMETERS
exp98 s2pul
SAMPLE
date Apr 11 2012
solvent CDCl3
file exp
ACQUISITION
sfrq 499.746
tn H1
at 3.001
np 53050
sw 10504.2
fb not used
bs 4
tpwr 56
pw 8.6
d1 2.000
tof 1519.5
nt 8
ct 8
alock n
gain not used
FLAGS
il n
in n
dp y
hs nn
DISPLAY
sp -189.4
wp 6239.0
vs 192
sc 0
wc 250
hzmm 24.98
is 452.58
rfl 4886.5
rfp 3628.1
th 3
ins 2.000
ph
DEC. & VT
dfrq 125.872
dn C13
dpwr 30
dof 0
dm nnn
dmm w
dmf 10000
dseq
dres 1.0
homo n
DEC2
dfrq2 0
dn2
dpwr2 1
dof2 0
dm2 n
dmm2 c
dmf2 200
dseq2
dres2 1.0
homo2 n
DEC3
dfrq3 0
dn3
dpwr3 1
dof3 0
dm3 n
dmm3 c
dmf3 200
dseq3
dres3 1.0
homo3 n
PROCESSING
wtfile
proc ft
fn 262144
math f
werr
wexp
wbs
wnt wft
NHBoc
Boc-15
11
10
9
8
7
6
5
4
3
2
1
ppm
0.85
1.79
1.84
0.81
0.91
0.83
1.27
7.93

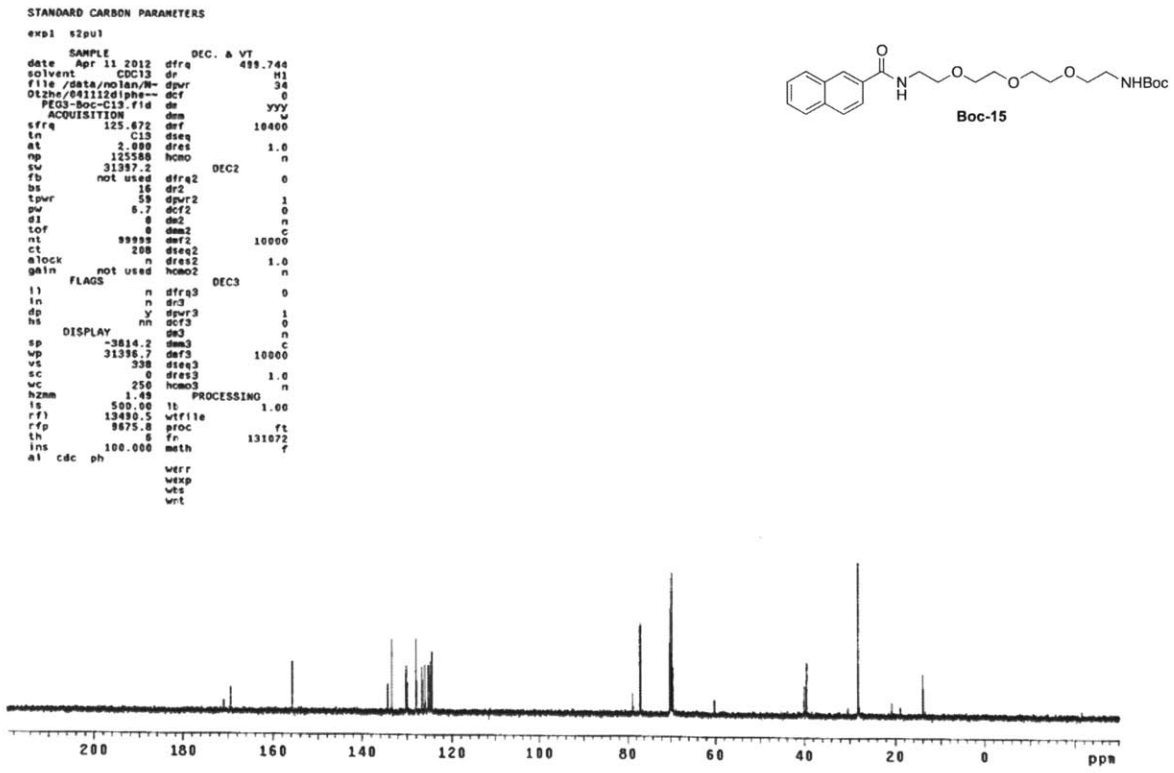
STANDARD CARBON PARAMETERS
exp1 s2pul
SAMPLE
date Apr 11 2012
solvent CDCl3
file /data/nolan/R~
Olzhe/041112dlphe~~
PEG3-Boc-C13.fid
ACQUISITION
sfrq 125.672
tn C13
at 2.000
np 125588
sw 31397.2
fb not used
bs 16
tpwr 59
pw 8.7
d1 0
tof 0
nt 99999
ct 208
alock n
gain not used
FLAGS
il n
in n
dp y
hs nn
DISPLAY
sp -3814.2
wp 31396.7
vs 338
sc 0
wc 250
hzmm 1.49
is 500.00
rfl 13490.5
rfp 9875.8
th 6
ins 100.000
ph cdc
DEC. & VT
dfrq 499.744
dn H1
dpwr 34
dof 0
dm yyy
dmm w
dmf 10400
dseq
dres 1.0
homo n
DEC2
dfrq2 0
dn2
dpwr2 1
dof2 0
dm2 n
dmm2 c
dmf2 10000
dseq2
dres2 1.0
homo2 n
DEC3
dfrq3 0
dn3
dpwr3 1
dof3 0
dm3 n
dmm3 c
dmf3 10000
dseq3
dres3 1.0
homo3 n
PROCESSING
lb 1.00
wtfile
proc ft
fn 131072
math f
werr
wexp
wbs
wnt
NHBoc
Boc-15
200
180
160
140
120
100
80
60
40
20
0
ppm

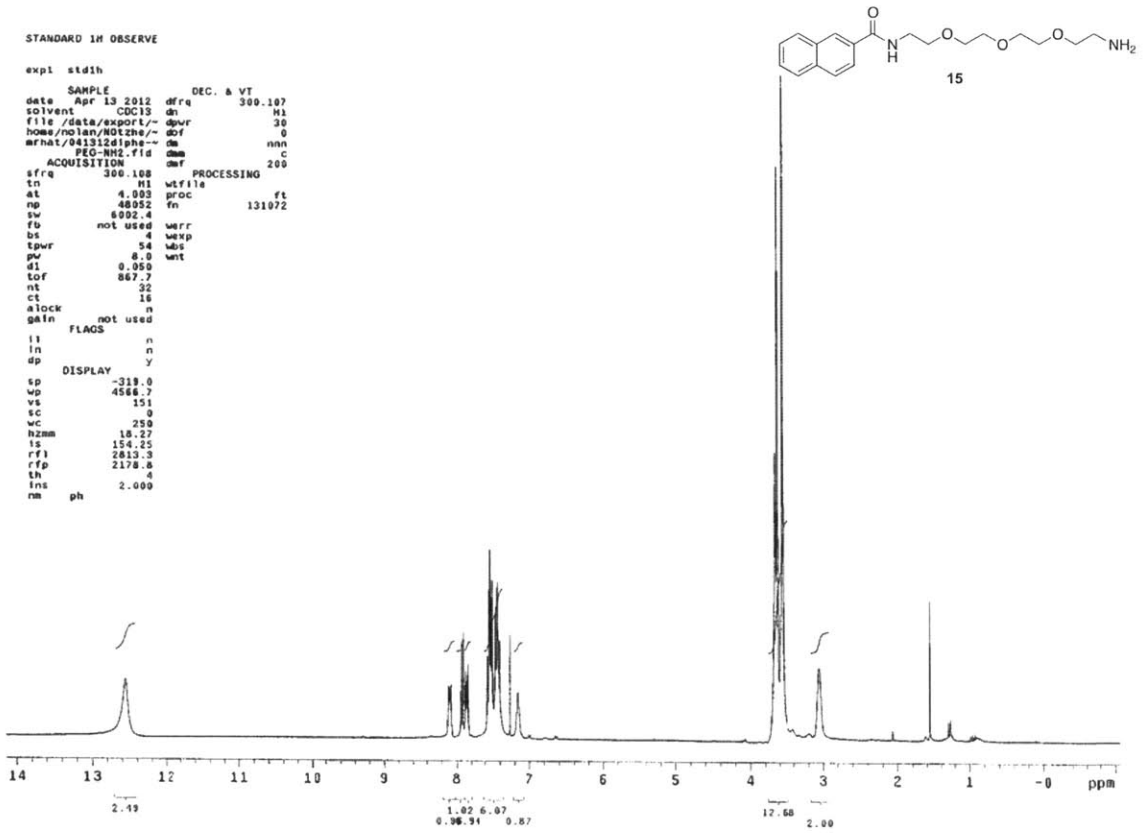
STANDARD 1H OBSERVE
expl std1h
SAMPLE
date Apr 13 2012
solvent CDCl3
file /data/export/~
home/nolan/MOIzhe/~
mrhat/041312diphe~~
PEG-NH2.fid
ACQUISITION
sfrq 300.108
tn H1
at 4.003
np 48052
sw 6002.4
fb not used
bs 4
tpwr 54
pw 8.0
d1 0.050
tof 867.7
nt 32
ct 16
alock n
gain not used
FLAGS
il n
in n
dp y
DISPLAY
sp -319.0
wp 4566.7
vs 151
sc 0
wc 250
hzmm 18.27
is 154.25
rfl 2813.3
rfp 2178.8
th 4
ins 2.000
nm ph
DEC. & VT
dfrq 300.107
dn H1
dpwr 30
dof 0
dm nnn
dmm c
dmf 200
PROCESSING
wtfile
proc ft
fn 131072
werr
wexp
wbs
wnt
15
14 13 12 11 10 9 8 7 6 5 4 3 2 1 -0 ppm
2.19
1.02 6.07
0.96 0.87
12.58
2.00

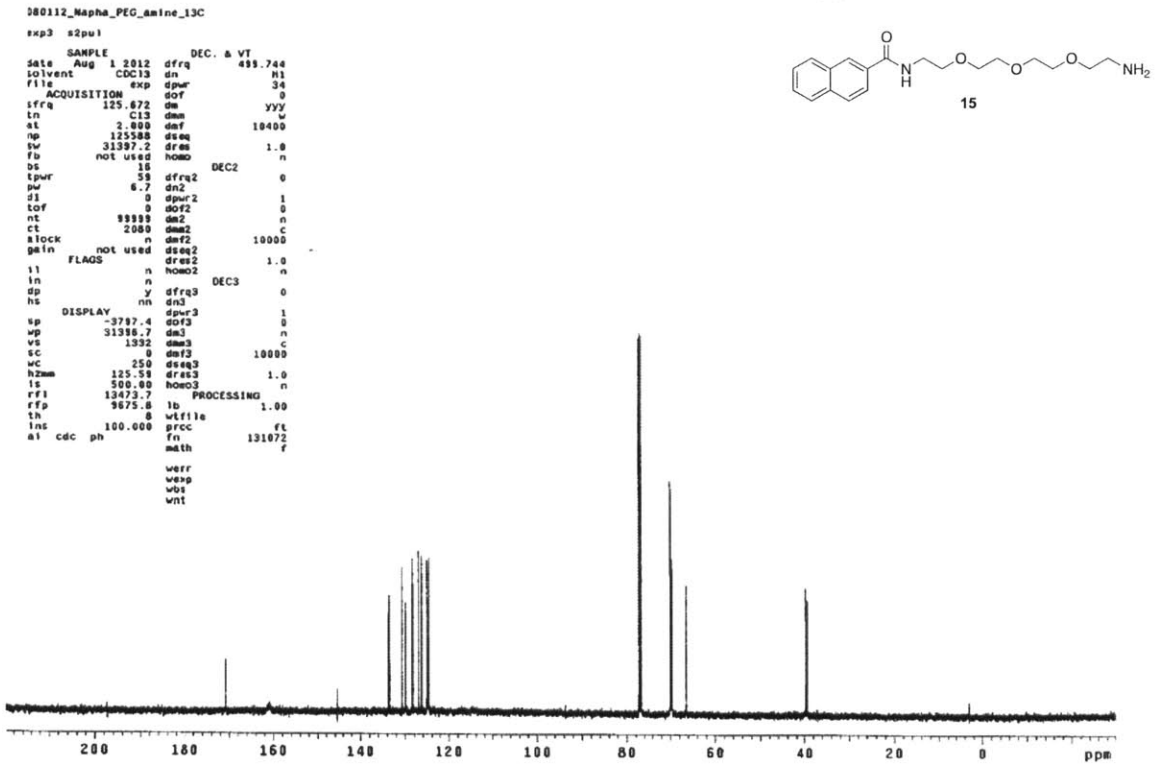
080112_Napha_PEG_amine_13C
exp3 s2pul
SAMPLE
date Aug 1 2012
solvent CDCl3
file exp
ACQUISITION
sfrq 125.672
tn C13
at 2.000
np 125588
sw 31397.2
fb not used
bs 16
tpwr 59
pw 6.7
d1 0
tof 0
nt 99999
ct 2080
alock n
gain not used
FLAGS
il n
in n
dp y
hs nn
DISPLAY
sp -3797.4
wp 31386.7
vs 1332
sc 0
wc 250
hzmm 125.59
is 500.00
rfl 13473.7
rfp 9675.8
th 8
ins 100.000
ai cdc ph
DEC. & VT
dfrq 499.744
dn H1
dpwr 34
dof 0
dm yyy
dmm w
dmf 10400
seq
dres 1.0
homo n
DEC2
dfrq2 0
dn2
dpwr2 1
dof2 0
dm2 n
dmm2 c
dmf2 10000
seq2
dres2 1.0
homo2 n
DEC3
dfrq3 0
dn3
dpwr3 1
dof3 0
dm3 n
dmm3 c
dmf3 10000
seq3
dres3 1.0
homo3 n
PROCESSING
lb 1.00
wtfile
proc ft
fn 131072
math f
werr
wexp
wbs
wnt
15
200 180 160 140 120 100 80 60 40 20 0 ppm

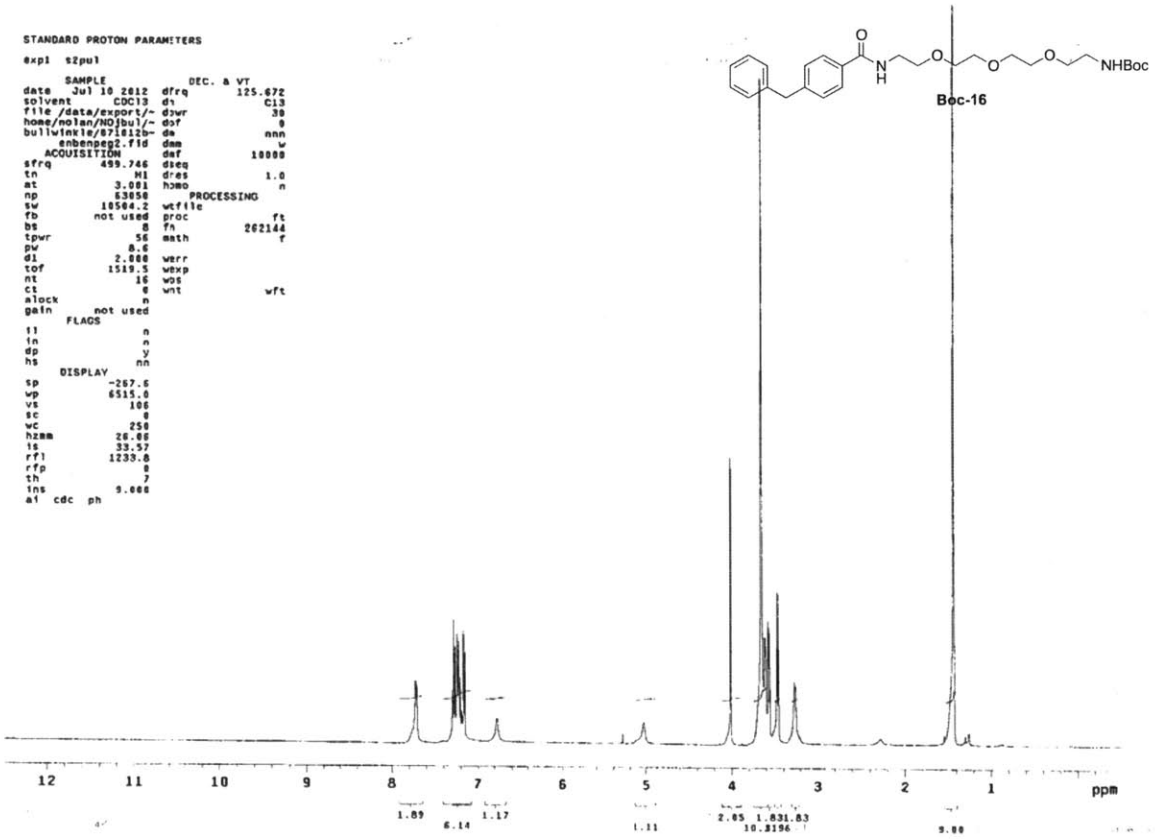
STANDARD PROTON PARAMETERS
expl s2pul
SAMPLE
date Jul 10 2012
solvent CDCl3
file /data/export/~
home/nolan/NOjbul/~
bullwinkle/071812b~
enbenpegZ.fid
ACQUISITION
sfrq 499.746
tn H1
at 3.081
np 63050
sw 10504.2
fb not used
bs 8
tpwr 56
pw 8.6
dl 2.000
tof 1519.5
nt 16
ct 0
alock n
gain not used
FLAGS
il n
in n
dp y
hs nn
DISPLAY
sp -267.6
wp 6515.8
vs 106
sc 0
wc 250
hzmm 26.66
is 33.57
rfl 1233.8
rfp 0
th 7
ins 9.000
ai cdc ph
DEC. & VT
dfrq 125.672
dn C13
dpwr 38
dof 0
dm nnn
dmm w
daf 18088
dseq
dres 1.0
homo n
PROCESSING
wtfile
proc ft
fn 262144
math f
werr
wexp
wbs
wnt wft
NHBoc
Boc-16
12
11
10
9
8
7
6
5
4
3
2
1
ppm
1.89
6.14
1.17
1.11
2.65
1.83
1.83
10.3196
9.00

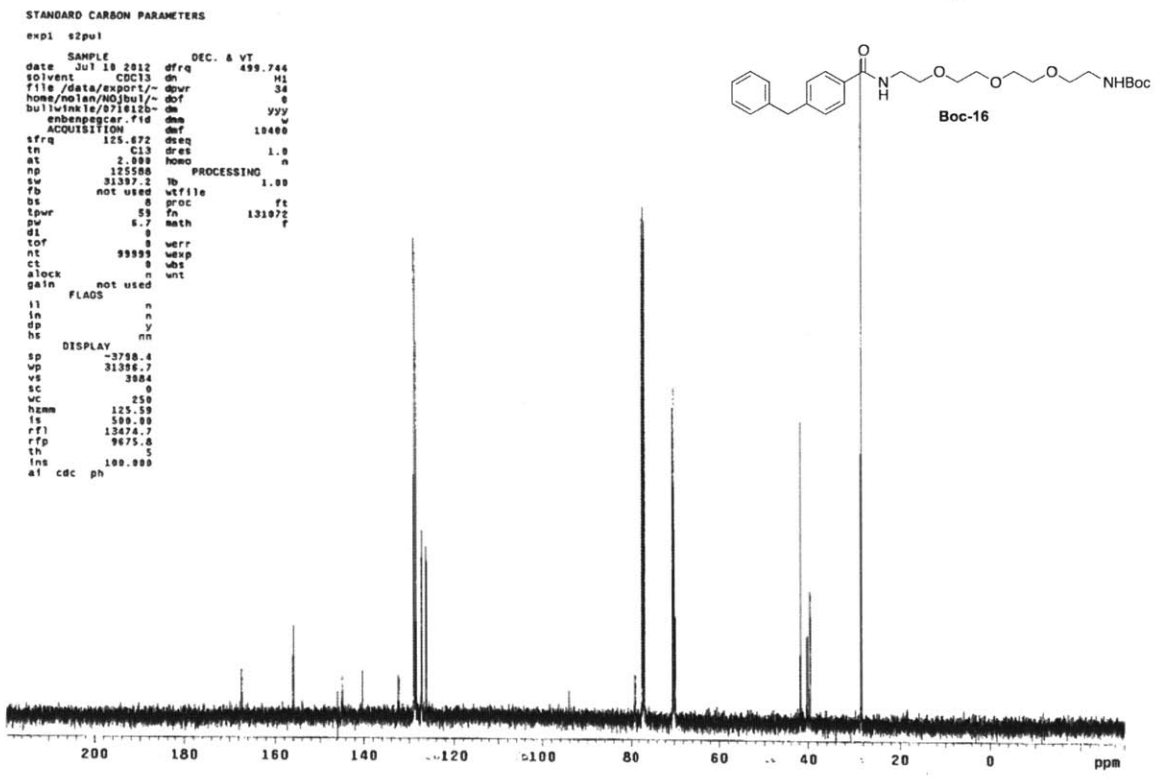
STANDARD CARBON PARAMETERS
expl s2pul
SAMPLE
date Jul 18 2012
solvent CDCl3
file /data/export/~
home/nolan/NOjbul/~
bullwinkle/071812b~
enbenpegcar.fid
ACQUISITION
sfrq 125.672
tn C13
at 2.998
np 125588
sw 31397.2
fb not used
bs 8
tpwr 59
pw 6.7
dl 0
tof 0
nt 99999
ct 0
alock n
gain not used
FLAGS
il n
in n
dp y
hs nn
DISPLAY
sp -3798.4
wp 31396.7
vs 3984
sc 0
wc 250
hzmm 125.59
is 500.00
rfl 13474.7
rfp 9675.6
th 5
ins 100.000
ai cdc ph
DEC. & VT
dfrq 499.744
dn H1
dpwr 34
dof 0
dm yyy
dmm w
daf 19488
dseq
dres 1.0
homo n
PROCESSING
lb 1.00
wtfile
proc ft
fn 131072
math f
werr
wexp
wbs
wnt
NHBoc
Boc-16
200
180
160
140
120
100
80
60
40
20
0
ppm

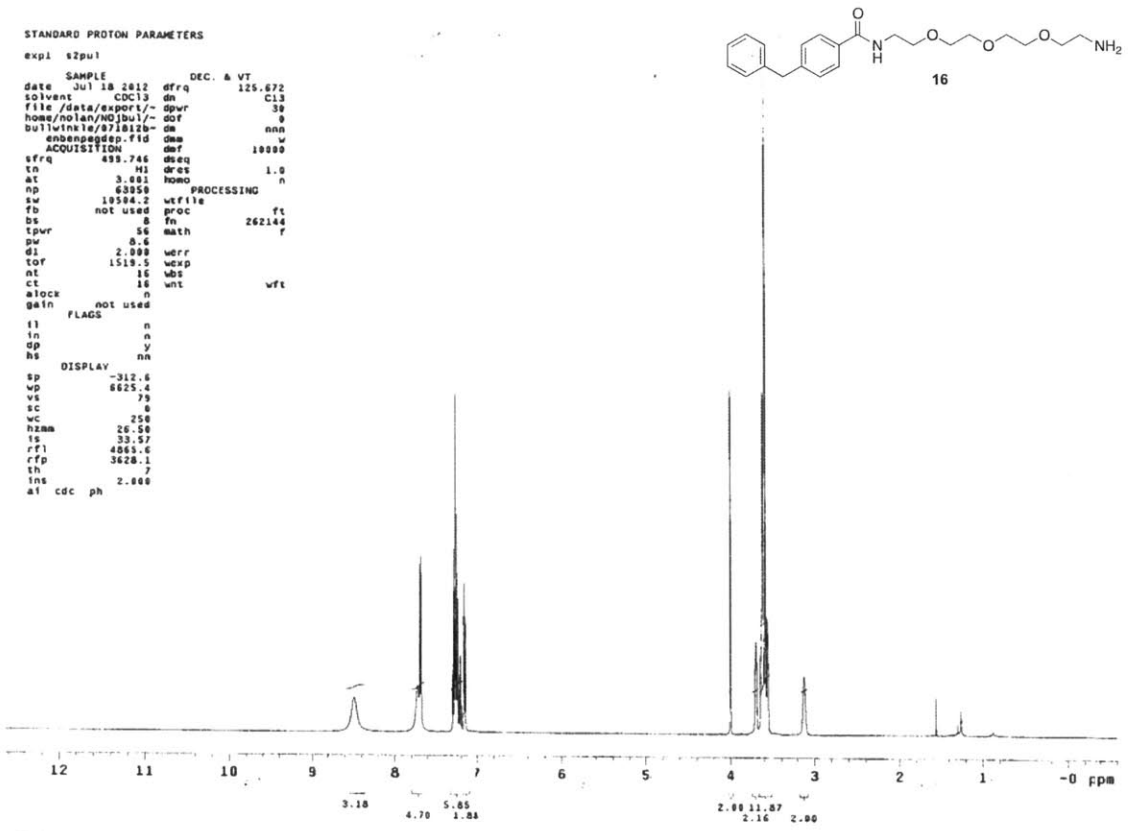
STANDARD PROTON PARAMETERS
expl s2pul
SAMPLE
date Jul 18 2012
solvent CDCl3
file /data/export/~
home/nolan/NOjbul/~
bullwinkle/071812b~
enbenpegdep.fid
ACQUISITION
sfrq 499.746
tn H1
at 3.881
np 63050
sw 10504.2
fb not used
bs 8
tpwr 56
pw 8.6
d1 2.000
tof 1519.5
nt 16
ct 16
alock n
gain not used
FLAGS
il n
in n
dp y
hs nn
DISPLAY
sp -312.6
wp 6625.4
vs 79
sc 0
wc 250
hzmm 26.50
is 33.57
rfl 4865.6
rfp 3628.1
th 7
ins 2.000
at cdc ph
DEC. & VT
dfrq 125.672
dn C13
dpwr 39
dof 0
dm nnn
dmm w
dmf 10000
dseq
dres 1.0
homo n
PROCESSING
wtfile
proc ft
fn 262144
math f
werr
wexp
wbs
wnt wft
O
N
H
O
O
O
NH2
16
12
11
10
9
8
7
6
5
4
3
2
1
-0 ppm
3.18
4.70
5.85
1.88
2.00
11.87
2.16
2.00

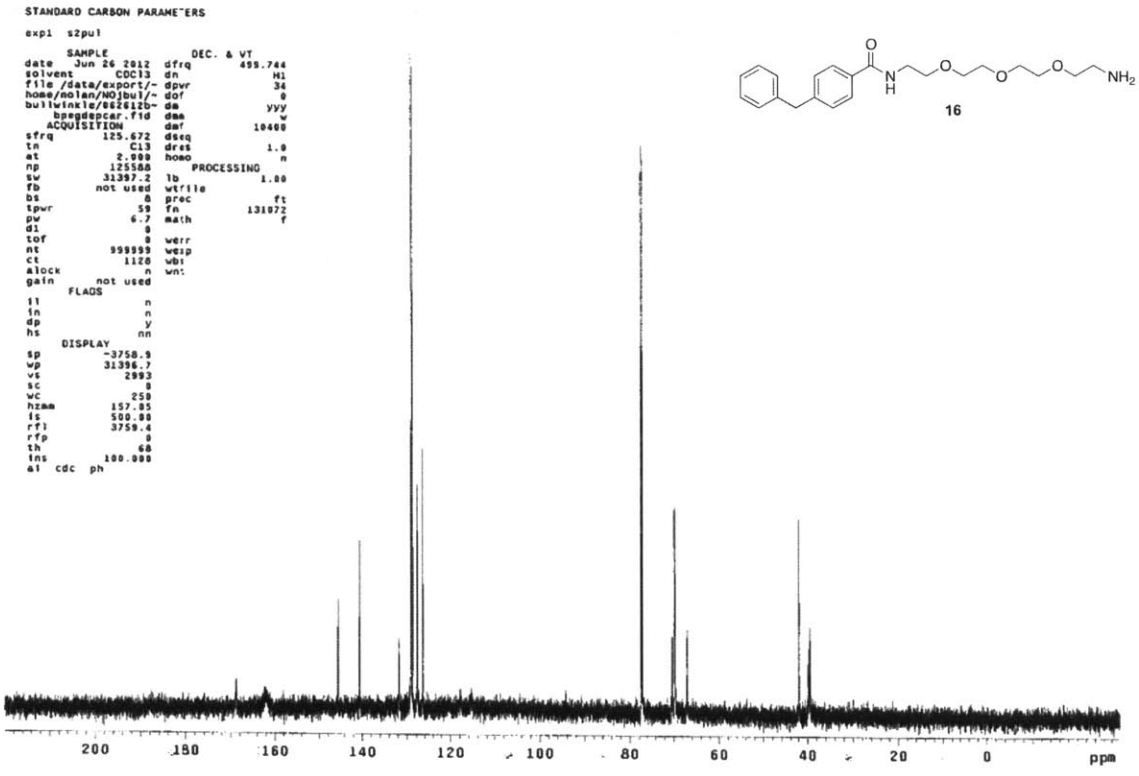
STANDARD CARBON PARAMETERS
expl s2pul
SAMPLE
date Jun 26 2012
solvent CDCl3
file /data/export/~
home/nolan/NOjbul/~
bullwinkle/062612b~
bpegdepcar.fid
ACQUISITION
sfrq 125.672
tn C13
at 2.000
np 125588
sw 31397.2
fb not used
bs 8
tpwr 59
pw 6.7
d1 0
tof 0
nt 999999
ct 1128
alock n
gain not used
FLAGS
il n
in n
dp y
hs nn
DISPLAY
sp -3758.9
wp 31396.7
vs 2993
sc 0
wc 250
hzmm 157.85
is 500.88
rfl 3759.4
rfp 0
th 68
ins 100.000
at cdc ph
DEC. & VT
dfrq 499.744
dn H1
dpwr 34
dof 0
dm yyy
dmm w
dmf 10460
dseq
dres 1.0
homo n
PROCESSING
lb 1.00
wtfile
proc ft
fn 131072
math f
werr
wexp
wbs
wnt
O
N
H
O
O
O
NH2
16
200
180
160
140
120
100
80
60
40
20
0
ppm

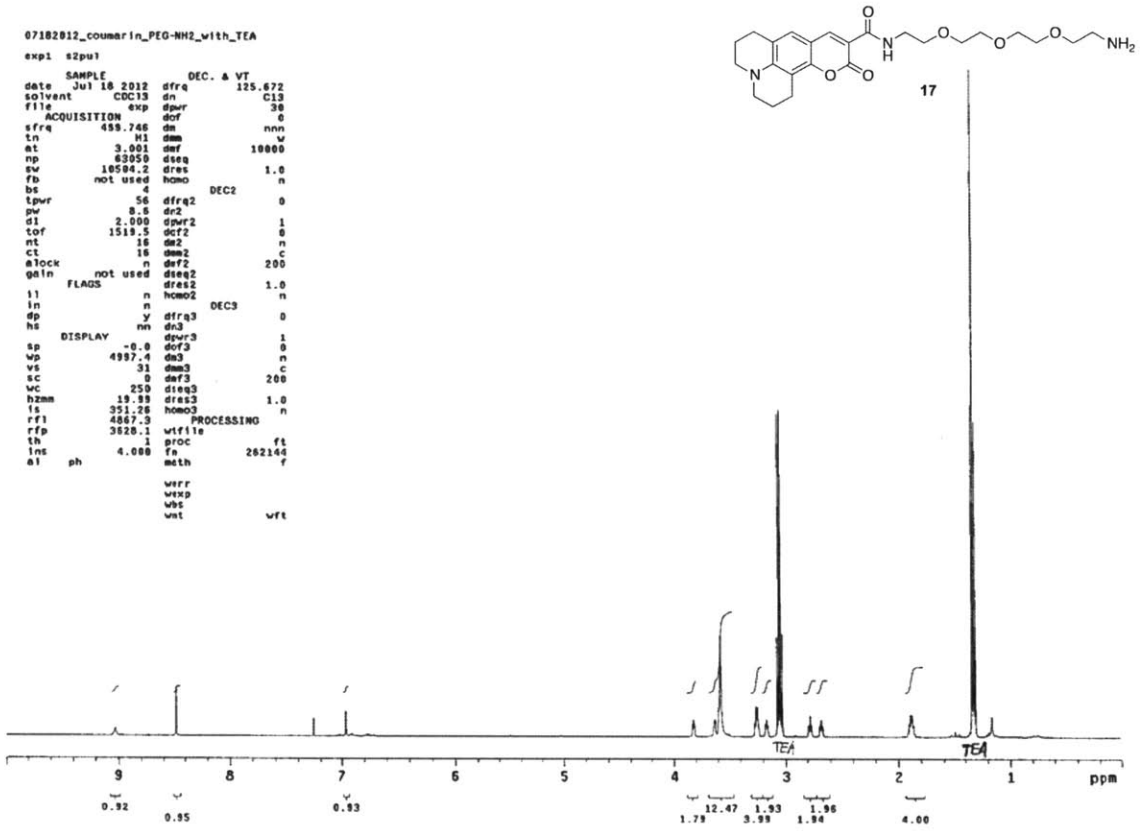
07182012_coumarin_PEG-NH2_with_TEA
exp1 s2pul
SAMPLE
date Jul 18 2012
solvent CDCl3
file exp
ACQUISITION
sfrq 499.746
tn H1
at 3.001
np 63950
sw 10594.2
fb not used
bs 4
tpwr 56
pw 8.6
d1 2.000
tof 1519.5
nt 16
ct 16
alock n
gain not used
FLAGS
ll n
in n
dp y
hs nn
DISPLAY
sp -0.8
wp 4997.4
vs 31
sc 0
wc 250
hzmm 19.99
is 351.26
rfl 4867.3
rfp 3628.1
th 1
ins 4.000
ai ph
DEC. & VT
dfrq 125.672
dn C13
dpwr 38
dof 0
dm nnn
dmm w
dmf 10000
dseq
dres 1.0
homo n
DEC2
dfrq2 0
dn2
dpwr2 1
dof2 0
dm2 n
dmm2 c
dmf2 200
dseq2
dres2 1.0
homo2 n
DEC3
dfrq3 0
dn3
dpwr3 1
dof3 0
dm3 n
dmm3 c
dmf3 200
dseq3
dres3 1.0
homo3 n
PROCESSING
wtfile
proc ft
fn 262144
mth f
wrr
wexp
wbs
wnt wft
17
TEA
TEA
9
8
7
6
5
4
3
2
1
ppm
0.92
0.95
0.93
1.79
12.47
3.99
1.93
1.94
1.96
4.00

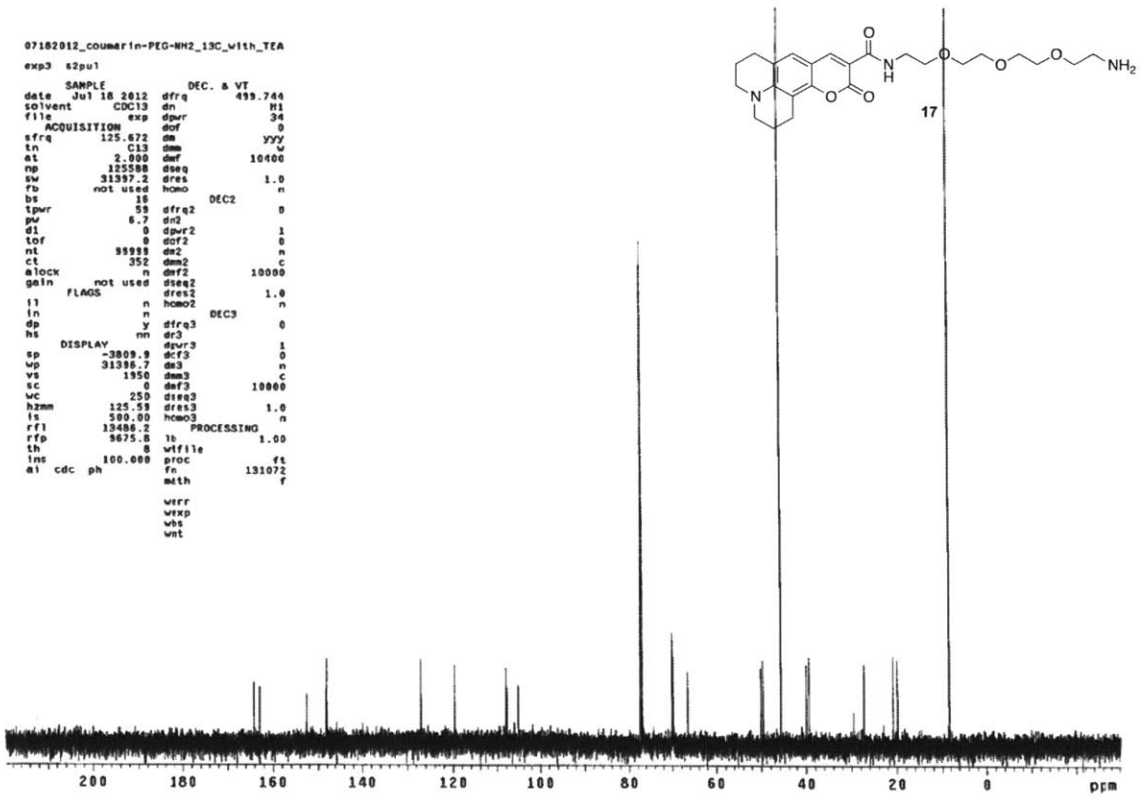
07182012_coumarin-PEG-NH2_13C_with_TEA
exp3 s2pul
SAMPLE
date Jul 18 2012
solvent CDCl3
file exp
ACQUISITION
sfrq 125.672
tn C13
at 2.000
np 125588
sw 31397.2
fb not used
bs 16
tpwr 59
pw 6.7
d1 0
tof 0
nt 99999
ct 352
alock n
gain not used
FLAGS
ll n
in n
dp y
hs nn
DISPLAY
sp -3809.9
wp 31398.7
vs 1950
sc 0
wc 250
hzmm 125.59
is 500.00
rfl 13486.2
rfp 9675.8
th 8
ins 100.000
ai cdc ph
DEC. & VT
dfrq 499.744
dn H1
dpwr 34
dof 0
dm yyy
dmm w
dmf 10400
dseq
dres 1.0
homo n
DEC2
dfrq2 0
dn2
dpwr2 1
dof2 0
dm2 n
dmm2 c
dmf2 10000
dseq2
dres2 1.0
homo2 n
DEC3
dfrq3 0
dn3
dpwr3 1
dof3 0
dm3 n
dmm3 c
dmf3 10000
dseq3
dres3 1.0
homo3 n
PROCESSING
lb 1.00
wtfile
proc ft
fn 131072
mth f
wrr
wexp
wbs
wnt
17
200
180
160
140
120
100
80
60
40
20
0
ppm

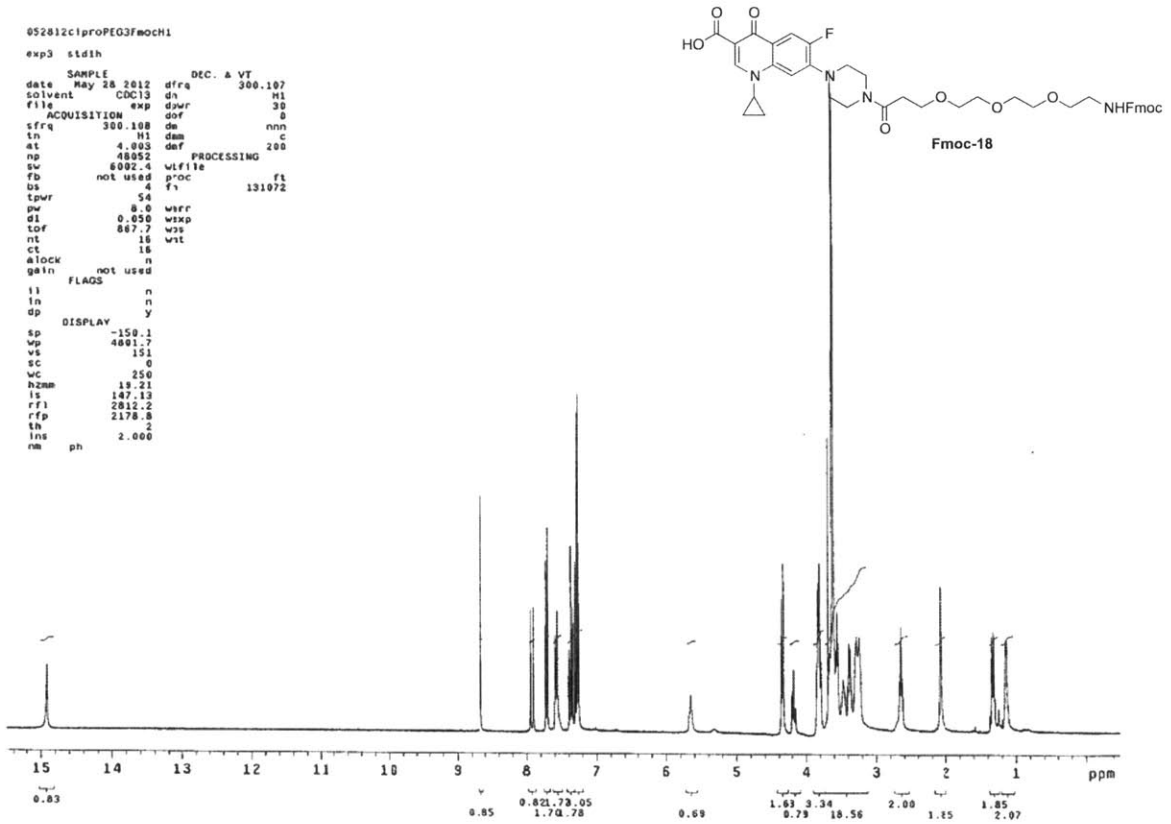
052812ciproPEG3FmocH1
exp3 stdlh
SAMPLE
date May 28 2012
solvent CDCl3
file exp
ACQUISITION
sfrq 300.108
tn H1
at 4.003
np 48052
sw 6002.4
fb not used
bs 4
tpwr 54
pw 8.0
dl 0.050
tof 867.7
nt 16
ct 16
alock n
gain not used
FLAGS
il n
in n
dp y
DISPLAY
sp -150.1
wp 4801.7
vs 151
sc 0
wc 250
hzmm 19.21
is 147.13
rfl 2812.2
rfp 2178.8
th 2
ins 2.000
nm ph
DEC. & VT
dfrq 300.107
dn H1
dpwr 39
dof 0
dm nnn
dmm c
def 200
PROCESSING
wtfile
proc ft
fn 131072
wtmf
wtxp
wbs
wnt
HO
F
NHFmoc
Fmoc-18
15 14 13 12 11 10 9 8 7 6 5 4 3 2 1 ppm
0.83
0.85
0.82 1.73 3.05
1.70 0.78
0.69
1.63 3.34
0.79 18.56
2.00
1.85
1.85
2.07

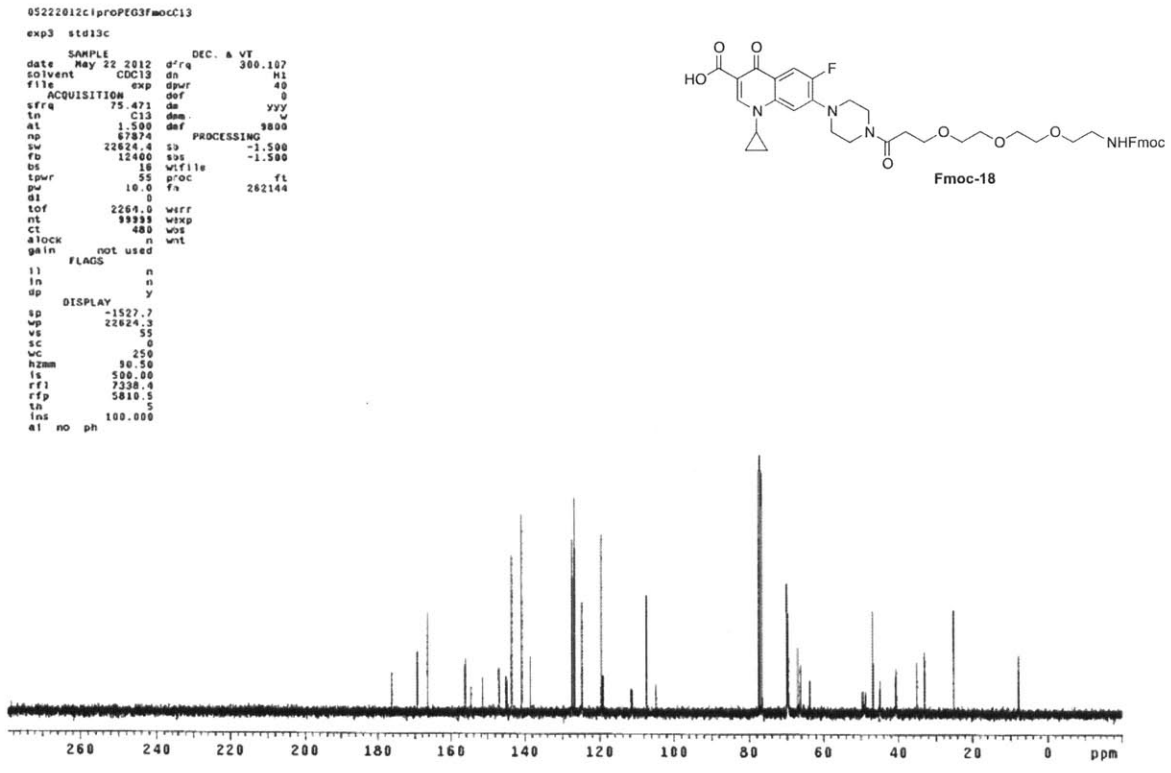
05222012ciproPEG3FmocC13
exp3 stdl3c
SAMPLE
date May 22 2012
solvent CDCl3
file exp
ACQUISITION
sfrq 75.471
tn C13
at 1.500
np 67874
sw 22624.4
fb 12400
bs 16
tpwr 55
pw 10.0
dl 0
tof 2264.0
nt 99999
ct 480
alock n
gain not used
FLAGS
il n
in n
dp y
DISPLAY
sp -1527.7
wp 22624.3
vs 55
sc 0
wc 250
hzmm 80.50
is 500.00
rfl 7338.4
rfp 5810.5
th 5
ins 100.000
al no ph
DEC. & VT
dfrq 300.107
dn H1
dpwr 40
dof 0
dm yyy
dmm w
def 9800
PROCESSING
sb -1.500
sbs -1.500
wtfile
proc ft
fn 262144
wtmf
wtxp
wbs
wnt
HO
F
NHFmoc
Fmoc-18
260 240 220 200 180 160 140 120 100 80 60 40 20 0 ppm

052812ciproPEG3FmocF1)

exp3 s2pul

SAMPLE		DEC. & VT	
date	May 28 2012	dfrq	300.107
solvent	CDCl3	dn	H1
file	exp	dpwr	38
ACQUISITION		dof	0
sfrq	282.382	dn	nnn
tn	F19	dnm	c
at	0.300	dmf	200
np	59906	PROCESSING	
sw	100000.0	lb	0.30
fb	55000	wtfile	
bs	16	proc	ft
tpwr	56	fn	262144
pw	11.0		
d1	4.000	werr	
tof	29837.2	wexp	
nt	64	wbs	
ct	64	wnt	
alock	n		
gain	not used		
FLAGS			
il	n		
in	n		
dp	y		
DISPLAY			
sp	-49681.9		
wp	99999.2		
vs	22		
sc	0		
wc	250		
hzmm	50.46		
is	500.00		
rfl	49682.6		
rfp	0		
th	12		
ins	100.000		
nm	ph		

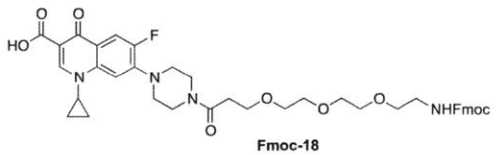

Fmoc-18

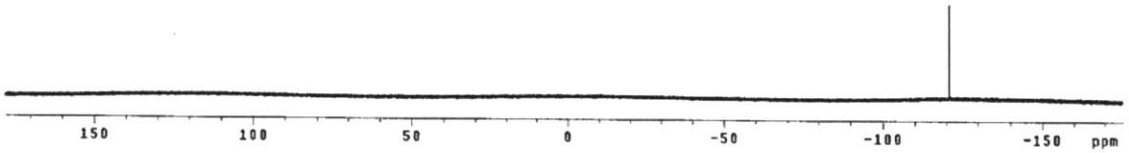

STANDARD PROTON PARAMETERS

expl s2pul

SAMPLE		DEC. & VT	
date	Jul 12 2012	dfrq	125.672
solvent	CDCl3	dn	C13
file /data/export/~		dpwr	38
home/nolan/NOtzhe/~		dof	0
bullwinkle/071212C~		dm	nnn
tpro-PEG-NH2.fid		dmm	w
ACQUISITION		dmf	10000
sfrq	499.746	dseq	
tn	H1	dres	1.0
at	3.081	homo	n
np	63650	PROCESSING	
sw	10504.2	wtfile	
fb	not used	proc	ft
bs	8	fn	262144
tpwr	56	math	f
pw	8.6		
d1	2.000	werr	
tof	1519.5	wexp	
nt	1	wbs	
ct	1	wnt	wft
alock	n		
gain	not used		
FLAGS			
il	n		
in	n		
dp	y		
hs	nn		
DISPLAY			
sp	-354.9		
wp	6777.3		
vs	171		
sc	0		
wc	250		
hzmm	27.11		
is	219.52		
rfl	4866.5		
rfp	3628.1		
th	5		
ins	1.000		
at	ph		

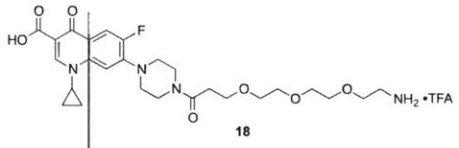

18

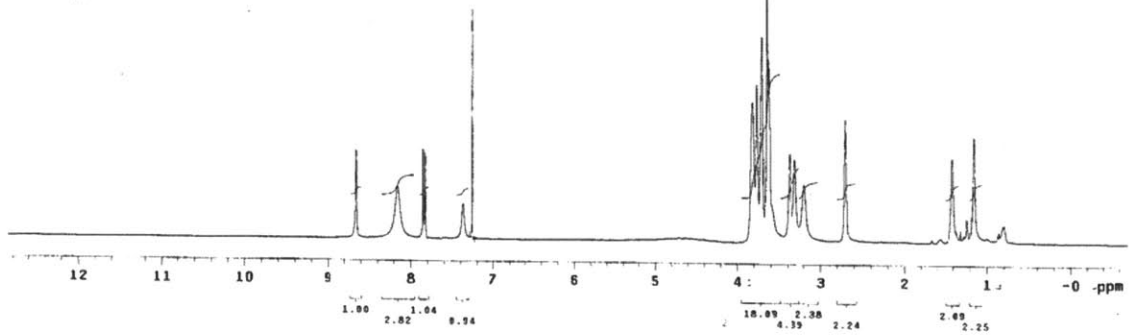

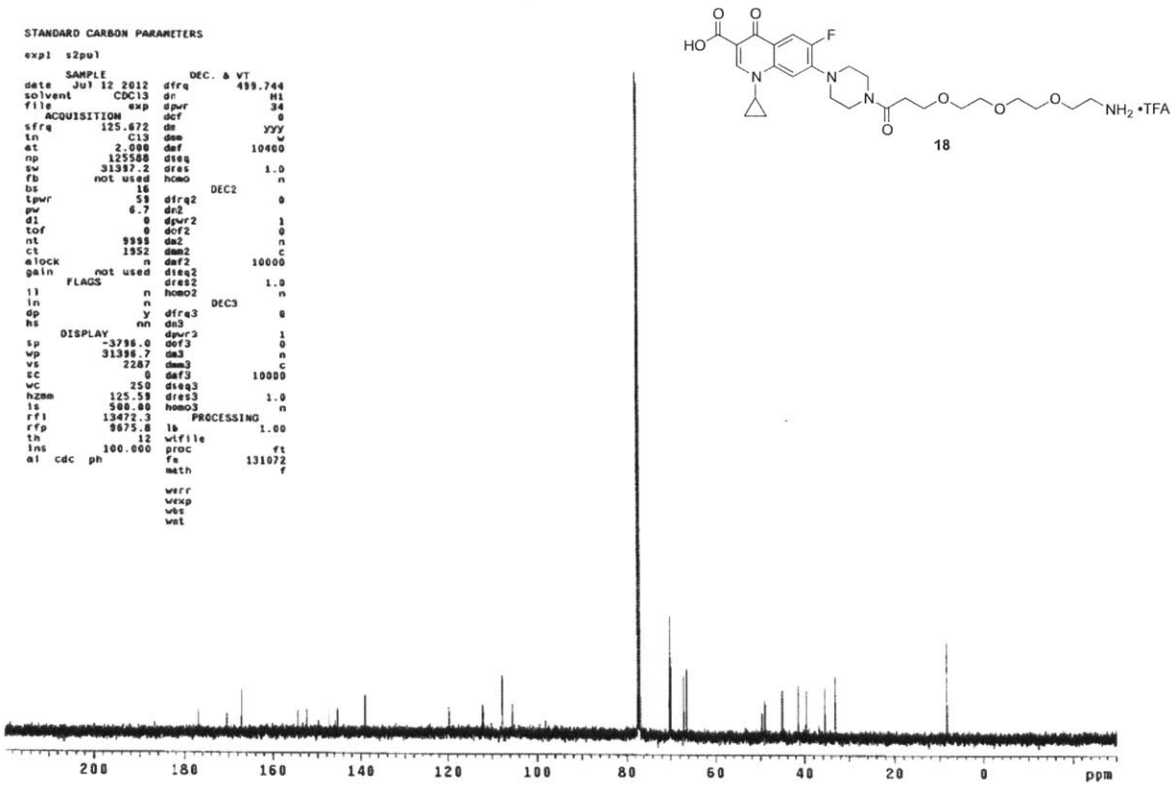
STANDARD CARBON PARAMETERS
expl s2pul
SAMPLE
date Jul 12 2012
solvent CDCl3
file exp
ACQUISITION
sfrq 125.672
tn C13
at 2.000
np 125588
sw 31397.2
fb not used
bs 16
tpwr 59
pw 6.7
d1 0
tof 0
nt 9999
ct 1952
alock n
gain not used
FLAGS
il n
in n
dp y
hs nn
DISPLAY
sp -3796.0
wp 31396.7
vs 2287
sc 0
wc 250
hzmm 125.59
is 500.00
rfl 13472.3
rfp 9675.8
th 12
ins 100.000
al cdc ph
DEC. & VT
dfrq 499.744
dn H1
dpwr 34
dof 0
dm yyy
dmm w
dmf 10400
dseq
dres 1.0
homo n
DEC2
dfrq2 0
dn2
dpwr2 1
dof2 0
dm2 n
dmm2 c
dmf2 10000
dseq2
dres2 1.0
homo2 n
DEC3
dfrq3 0
dn3
dpwr3 1
dof3 0
dm3 n
dmm3 c
dmf3 10000
dseq3
dres3 1.0
homo3 n
PROCESSING
lb 1.00
wtfile
proc ft
fn 131072
math f
werr
wexp
wbs
wnt
18
200
180
160
140
120
100
80
60
40
20
0
ppm

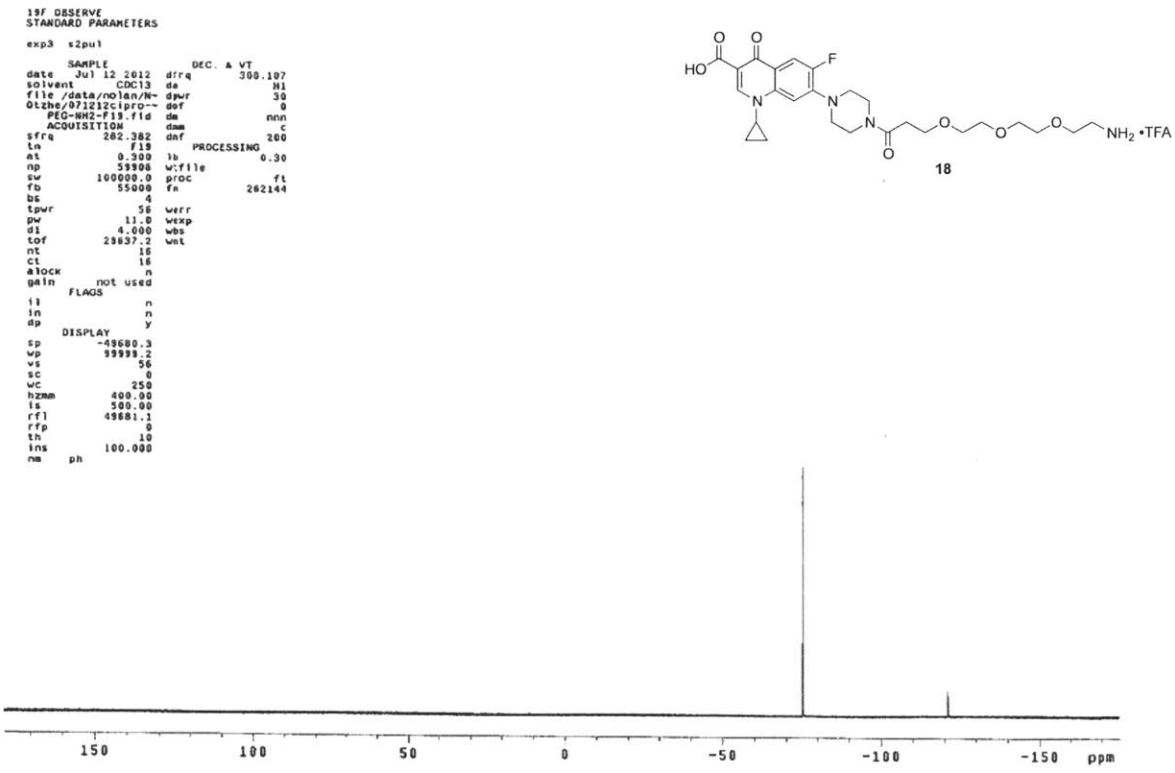
19F OBSERVE
STANDARD PARAMETERS
exp3 s2pul
SAMPLE
date Jul 12 2012
solvent CDCl3
file /data/nolan/N-Otzhe/071212cipro-~PEG-NH2-F19.fid
ACQUISITION
sfrq 282.382
tn F19
at 0.300
np 59908
sw 100000.0
fb 55000
bs 4
tpwr 56
pw 11.0
d1 4.000
tof 28637.2
nt 16
ct 16
alock n
gain not used
FLAGS
il n
in n
dp y
DISPLAY
sp -49680.3
wp 99999.2
vs 56
sc 0
wc 250
hzmm 400.00
is 500.00
rfl 49681.1
rfp 0
th 10
ins 100.000
nm ph
DEC. & VT
dfrq 300.107
dn H1
dpwr 30
dof 0
dm nnn
dmm c
dmf 200
PROCESSING
lb 0.30
wtfile
proc ft
fn 262144
werr
wexp
wbs
wnt
18
150
100
50
0
-50
-100
-150
ppm

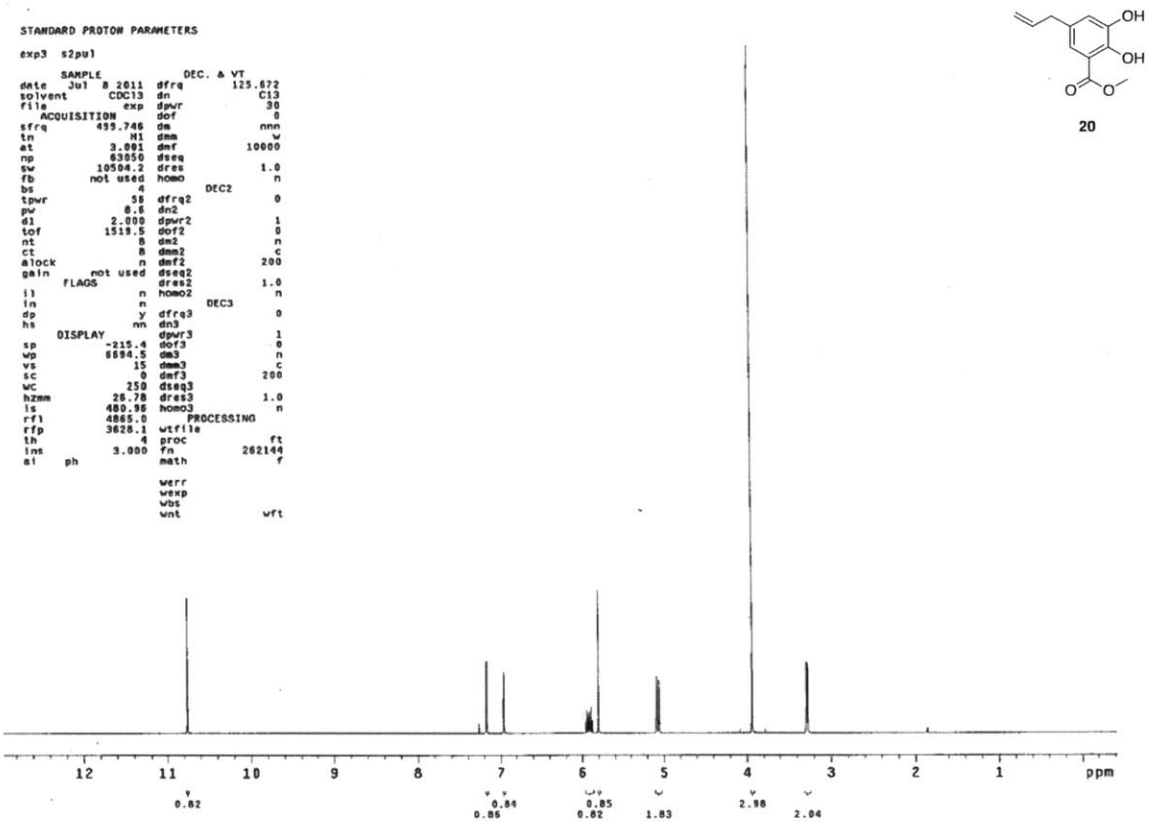
STANDARD PROTON PARAMETERS
exp3 s2pul
SAMPLE
date Jul 8 2011
solvent CDCl3
file exp
ACQUISITION
sfrq 499.746
tn H1
at 3.001
np 63050
sw 10504.2
fb not used
bs 4
tpwr 58
pw 8.6
d1 2.000
tof 1519.5
nt 8
ct 8
alock n
gain not used
FLAGS
il n
in n
dp y
hs nn
DISPLAY
sp -215.4
wp 8694.5
vs 15
sc 0
wc 250
hzmm 26.78
is 480.96
rfl 4865.0
rfp 3628.1
th 4
ins 3.000
ai ph
DEC. & VT
dfrq 125.672
dn C13
dpwr 30
dof 0
dm nnn
dmm w
dmf 10000
dseq
dres 1.0
homo n
DEC2
dfrq2 0
dn2
dpwr2 1
dof2 0
dm2 n
dmm2 c
dmf2 200
dseq2
dres2 1.0
homo2 n
DEC3
dfrq3 0
dn3
dpwr3 1
dof3 0
dm3 n
dmm3 c
dmf3 200
dseq3
dres3 1.0
homo3 n
PROCESSING
wtfile
proc ft
fn 262144
math f
werr
wexp
wbs
wnt wft
OH
OH
O
O
20
12
11
10
9
8
7
6
5
4
3
2
1
ppm
0.82
0.84
0.86
0.85
0.82
1.83
2.98
2.04

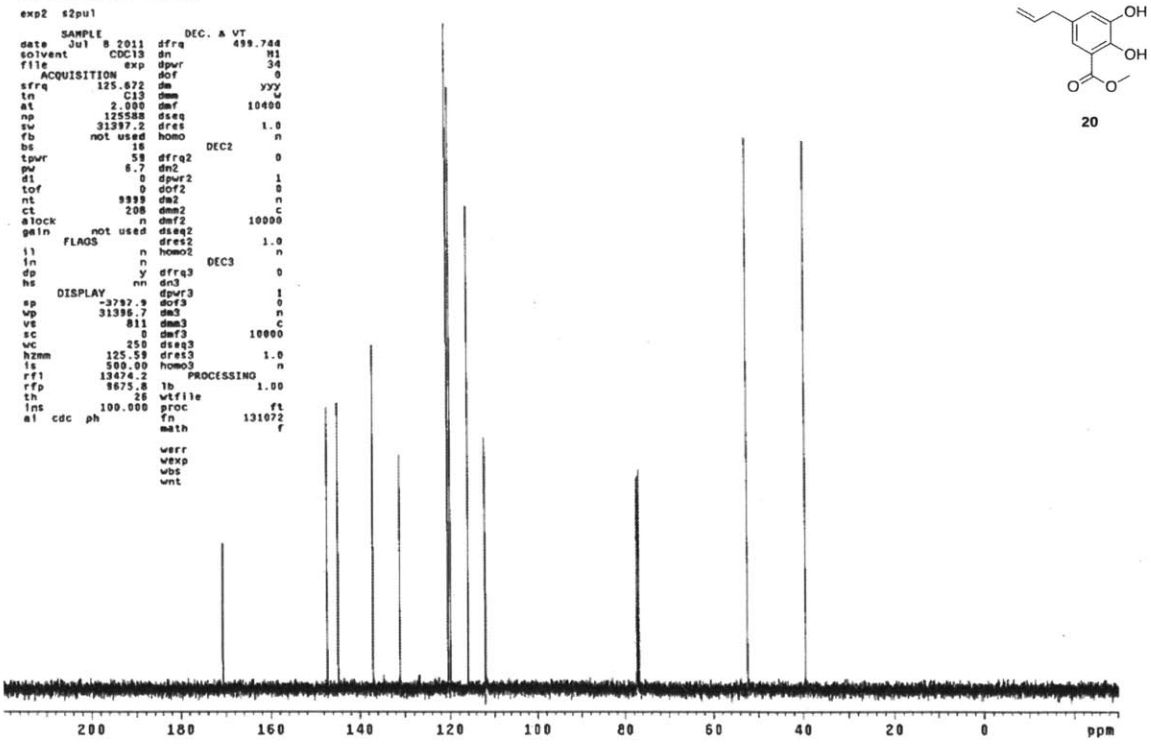
STANDARD CARBON PARAMETERS
exp2 s2pul
SAMPLE
date Jul 8 2011
solvent CDCl3
file exp
ACQUISITION
sfrq 125.672
tn C13
at 2.000
np 125588
sw 31397.2
fb not used
bs 16
tpwr 58
pw 8.7
d1 0
tof 0
nt 9999
ct 208
alock n
gain not used
FLAGS
il n
in n
dp y
hs nn
DISPLAY
sp -3797.9
wp 31398.7
vs 811
sc 0
wc 250
hzmm 125.59
is 500.00
rfl 13474.2
rfp 9675.8
th 28
ins 100.000
ai cdc ph
DEC. & VT
dfrq 499.744
dn H1
dpwr 34
dof 0
dm yyy
dmm w
dmf 10400
dseq
dres 1.0
homo n
DEC2
dfrq2 0
dn2
dpwr2 1
dof2 0
dm2 n
dmm2 c
dmf2 10000
dseq2
dres2 1.0
homo2 n
DEC3
dfrq3 0
dn3
dpwr3 1
dof3 0
dm3 n
dmm3 c
dmf3 10000
dseq3
dres3 1.0
homo3 n
PROCESSING
lb 1.00
wtfile
proc ft
fn 131072
math f
werr
wexp
wbs
wnt
OH
OH
O
O
20
200
180
160
140
120
100
80
60
40
20
0
ppm

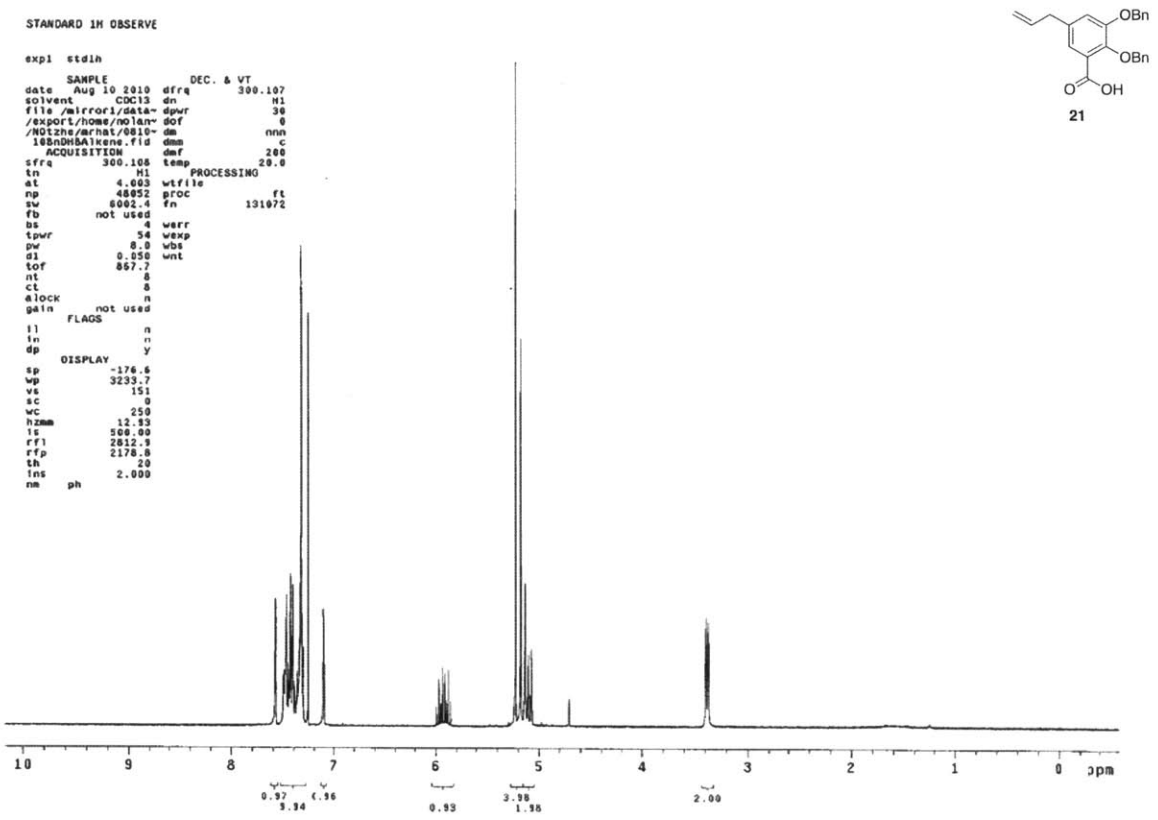
STANDARD 1H OBSERVE
expl stdih
SAMPLE
date Aug 10 2010
solvent CDCl3
file /mirror1/data~
/export/home/nolan~
/NOtzhe/mrhat/0810~
10BnDHBAlkene.fid
ACQUISITION
sfrq 300.108
tn H1
at 4.003
np 48052
sw 6002.4
fb not used
bs 4
tpwr 54
pw 8.8
d1 0.050
tof 867.7
nt 8
ct 8
alock n
gain not used
FLAGS
il n
in n
dp y
DISPLAY
sp -176.6
wp 3233.7
vs 151
sc 0
wc 250
hzmm 12.83
is 500.00
rfl 2612.9
rfp 2178.8
th 20
ins 2.000
nm ph
DEC. & VT
dfrq 300.107
dn H1
dpwr 36
dof 0
dm nnn
dmm c
dmf 200
temp 20.0
PROCESSING
wtfile
proc ft
fn 131072
werr
wexp
wbs
wnt
OBn
OBn
OH
21
10
9
8
7
6
5
4
3
2
1
0
ppm
0.97
1.96
3.94
0.93
3.98
1.98
2.00

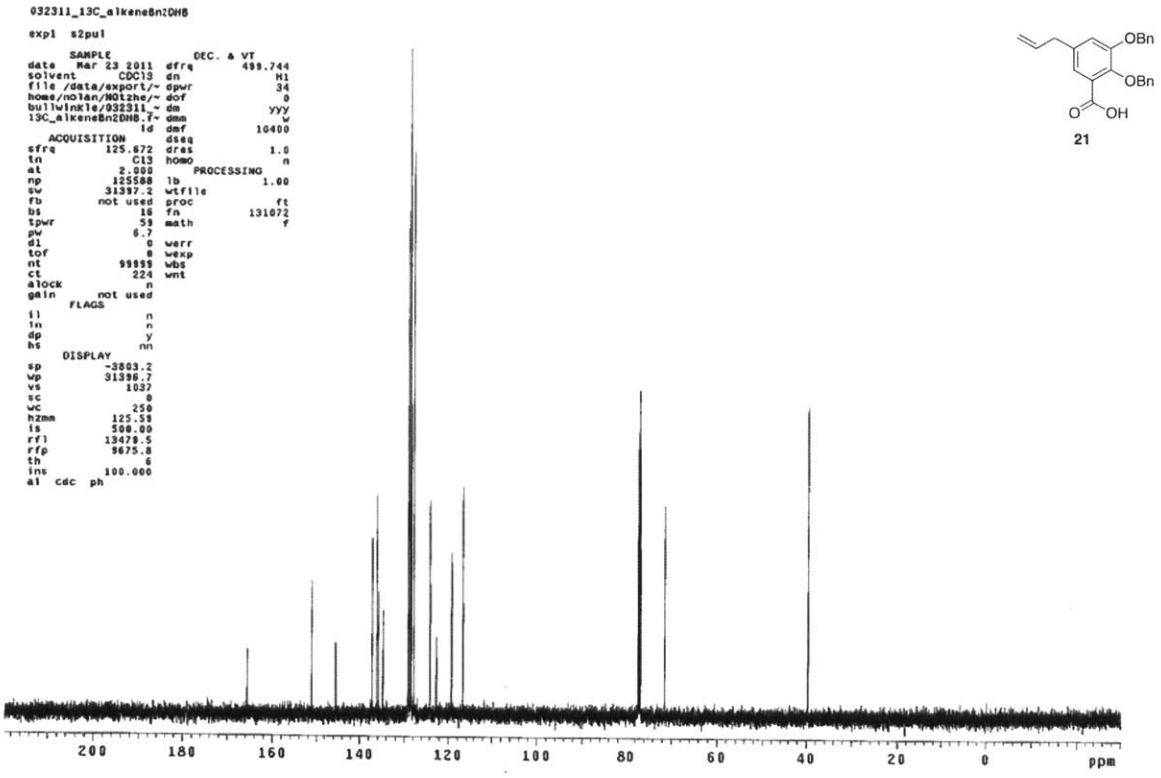
032311_13C_alkeneBn2OH8
expl s2pul
SAMPLE
date Mar 23 2011
solvent CDCl3
file /data/export/~
home/nolan/NOtzhe/~
bullwinkle/032311_~
13C_alkeneBn2OH8.7~
id
ACQUISITION
sfrq 125.672
tn C13
at 2.000
np 125588
sw 31397.2
fb not used
bs 16
tpwr 59
pw 6.7
d1 0
tof 0
nt 99999
ct 224
alock n
gain not used
FLAGS
il n
in n
dp y
hs nn
DISPLAY
sp -3803.2
wp 31396.7
vs 1037
sc 0
wc 250
hzmm 125.59
is 500.00
rfl 13479.5
rfp 9675.8
th 6
ins 100.000
al cdc ph
DEC. & VT
dfrq 499.744
dn H1
dpwr 34
dof 0
dm yyy
dmm w
dmf 10400
dseq
drss 1.0
homo n
PROCESSING
lb 1.00
wtfile
proc ft
fn 131072
math f
werr
wexp
wbs
wnt
OBn
OBn
OH
21
200
180
160
140
120
100
80
60
40
20
0
ppm

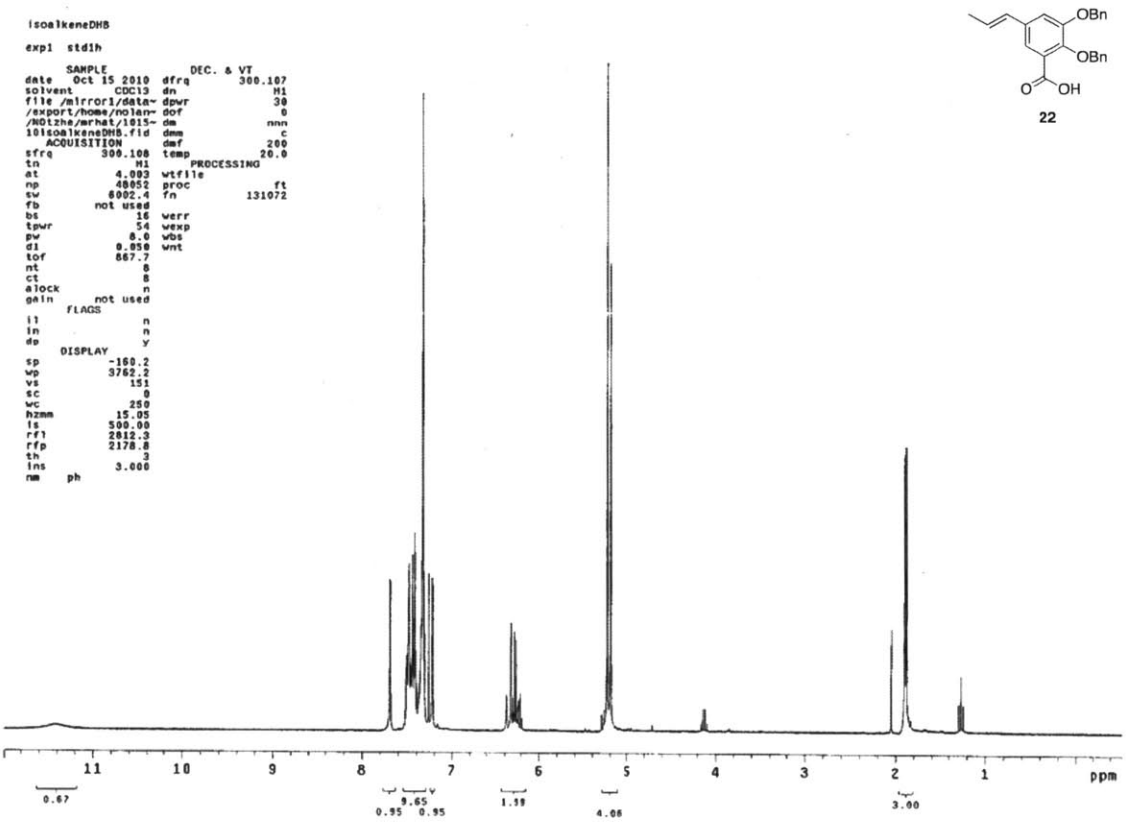
isoalkeneDHB
expl stdlh
SAMPLE
date Oct 15 2010
solvent CDCl3
file /mirror1/data~
/export/home/nolan~
/NOtzhe/mrhet/1015~
10isoalkeneDHB.fid
ACQUISITION
sfrq 300.108
tn H1
at 4.093
np 48052
sw 6002.4
fb not used
bs 16
tpwr 54
pw 8.6
dl 0.050
tof 867.7
nt 8
ct 8
alock n
gain not used
FLAGS
il n
in n
dp y
DISPLAY
sp -160.2
wp 3762.2
vs 151
sc 0
wc 250
hzmm 15.05
is 500.00
rfl 2812.3
rfp 2178.8
th 3
ins 3.000
nm ph
DEC. & VT
dfrq 300.107
dn H1
dpwr 30
dof 0
dm nnn
dmm c
dmf 200
temp 20.0
PROCESSING
wtfile
proc ft
fn 131072
werr
wexp
wnt
OBn
OBn
OH
22
11
10
9
8
7
6
5
4
3
2
1
ppm
0.67
9.65
0.95
0.95
1.19
4.08
3.00

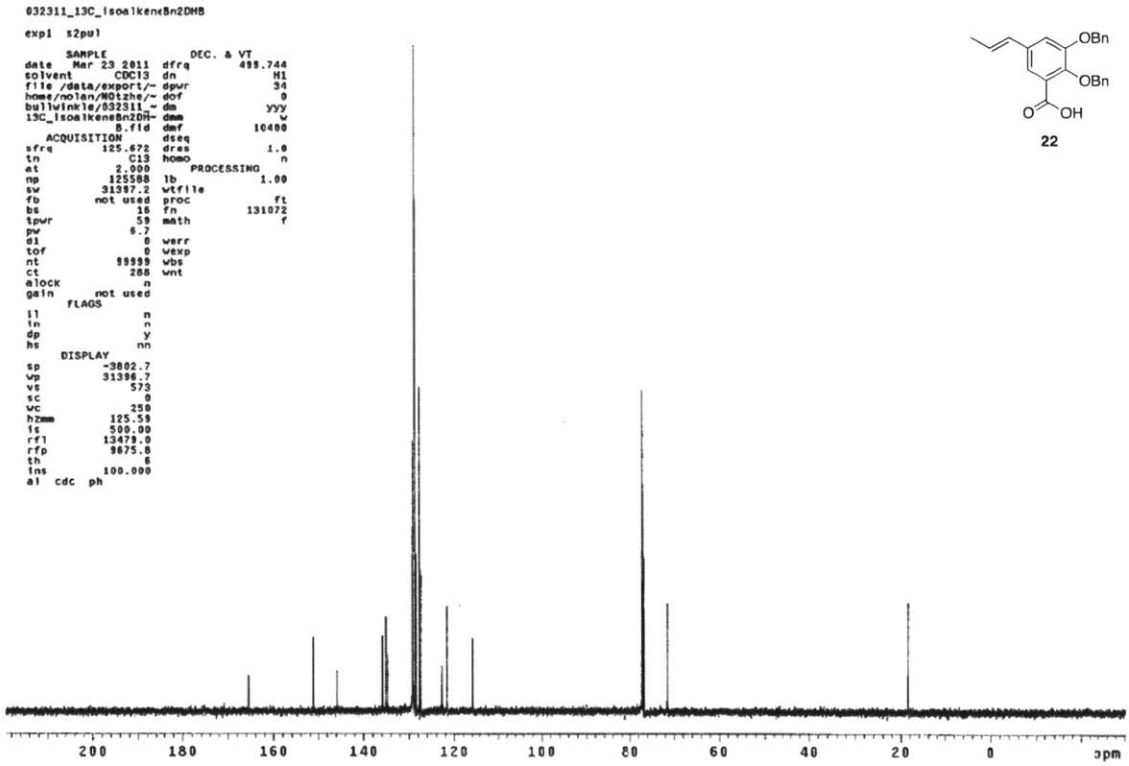
032311_13C_isoalkeneBn2DHB
expl s2pul
SAMPLE
date Mar 23 2011
solvent CDCl3
file /data/export/~
home/nolan/NOtzhe/~
bullwinkle/032311_~
13C_isoalkeneBn2DH~
8.fid
ACQUISITION
sfrq 125.672
tn C13
at 2.000
np 125588
sw 31397.2
fb not used
bs 16
tpwr 59
pw 6.7
dl 0
tof 0
nt 99999
ct 288
alock n
gain not used
FLAGS
il n
in n
dp y
hs nn
DISPLAY
sp -3802.7
wp 31396.7
vs 573
sc 0
wc 250
hzmm 125.59
is 500.00
rfl 13479.0
rfp 9875.8
th 6
ins 100.000
al cdc ph
DEC. & VT
dfrq 499.744
dn H1
dpwr 34
dof 0
dm yyy
dmm w
dmf 10480
dseq
dres 1.0
homo n
PROCESSING
lb 1.00
wtfile
proc ft
fn 131072
math f
werr
wexp
wbs
wnt
OBn
OBn
OH
22
200
180
160
140
120
100
80
60
40
20
0
ppm

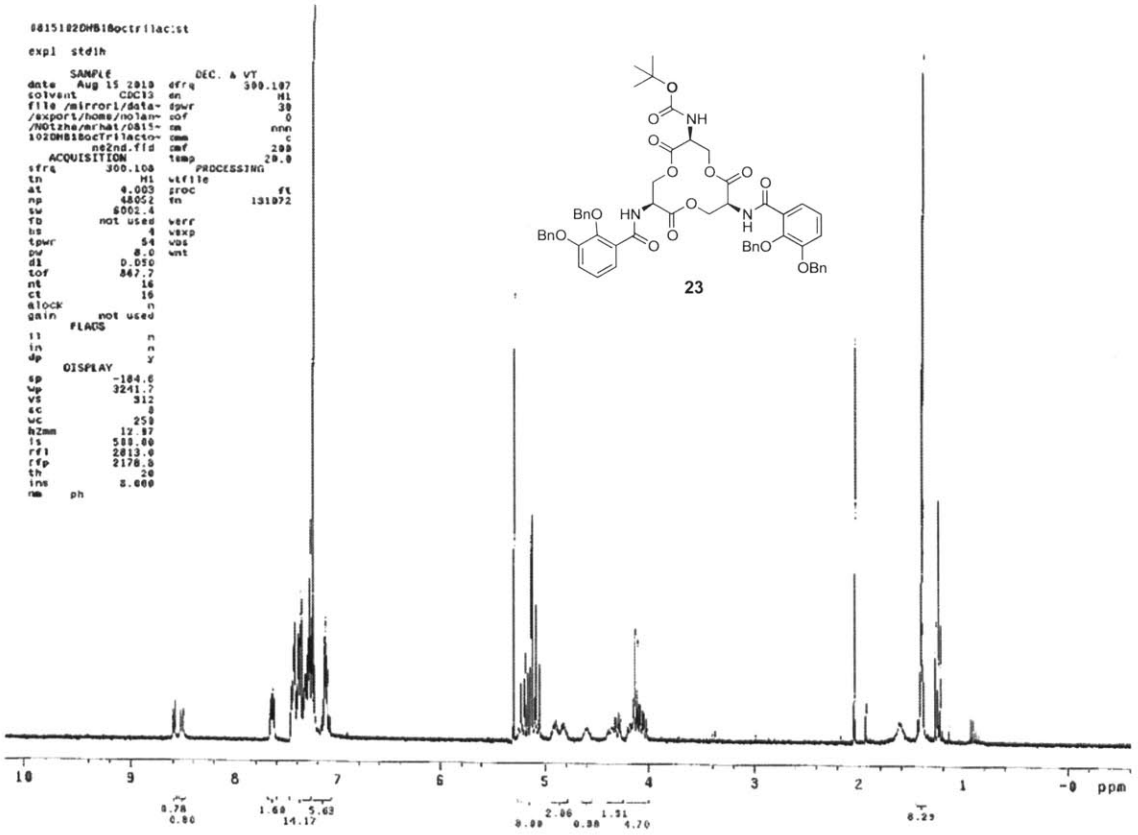
8815182DMB18octrilactst
expl stdih
SAMPLE
date Aug 15 2018
solvent CDCl3
file /mirror1/data~
/export/home/nolan~
/NOtzhe/mrhat/0815~
102DMB18octrilacto~
ne2nd.fid
ACQUISITION
sfrq 300.108
tn H1
at 4.003
np 48052
sw 8002.4
fb not used
bs 4
tpwr 54
pw 8.0
dl D.050
tof 867.7
nt 16
ct 16
alock n
gain not used
FLAGS
ii n
in n
dp y
DISPLAY
sp -184.6
wp 3241.7
vs 312
sc 8
wc 250
hzmm 12.97
is 588.00
rfl 2813.6
rfp 2178.8
th 20
ins 8.000
nm ph
DEC. & VT
dfrq 300.107
dn H1
dpwr 30
dof 0
dm nnn
dmm c
dmf 200
temp 20.0
PROCESSING
wtfile
proc ft
fn 131072
werr
wexp
wbs
wnt
23
10
9
8
7
6
5
4
3
2
1
-0
ppm
0.78
0.86
1.60
14.17
5.63
2.06
0.88
1.51
4.70
8.29

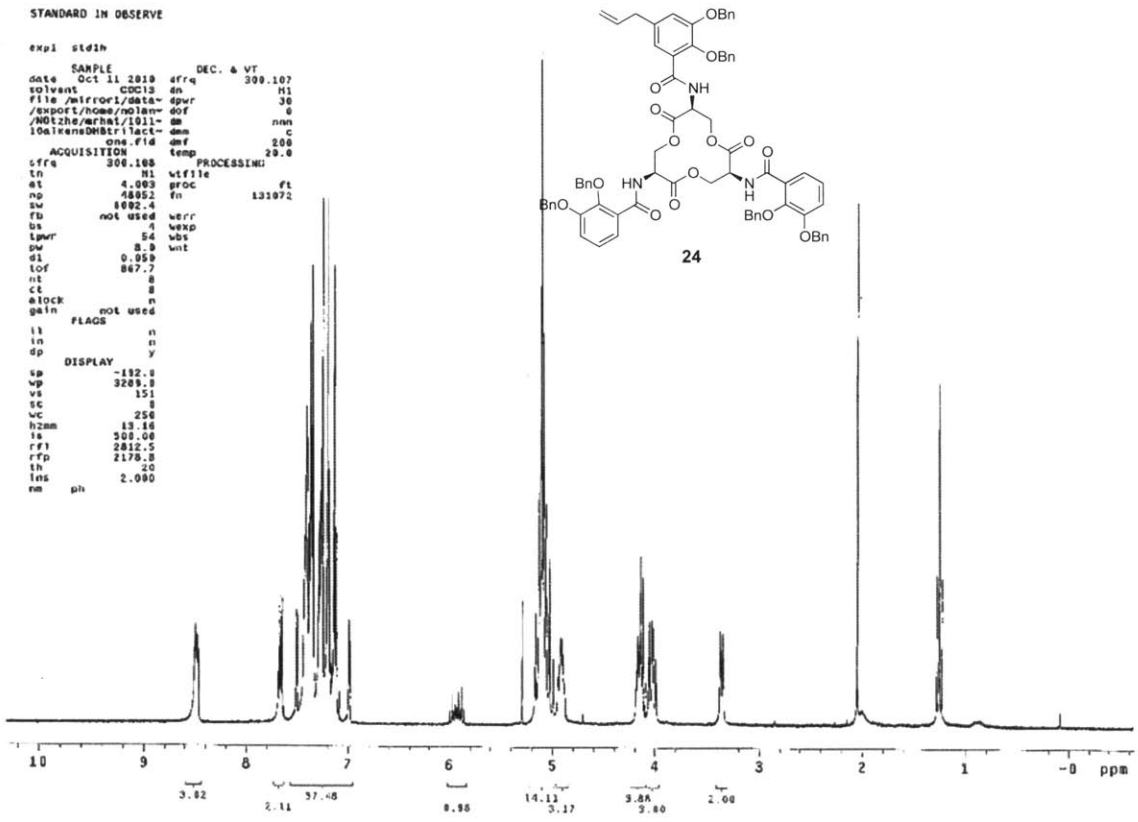
STANDARD IN OBSERVE
expl stdih
SAMPLE
date Oct 11 2018
solvent CDCl3
file /mirror1/data~
/export/home/nolan~
/NOtzhe/mrhat/1011~
10alkensDMBtrilact~
one.fid
ACQUISITION
sfrq 300.108
tn H1
at 4.003
np 48052
sw 8002.4
fb not used
bs 4
tpwr 54
pw 8.0
dl 0.050
tof 867.7
nt 8
ct 8
alock n
gain not used
FLAGS
ii n
in n
dp y
DISPLAY
sp -182.8
wp 3289.8
vs 151
sc 8
wc 250
hzmm 13.16
is 588.00
rfl 2812.5
rfp 2178.8
th 20
ins 2.000
nm ph
DEC. & VT
dfrq 300.107
dn H1
dpwr 30
dof 0
dm nnn
dmm c
dmf 200
temp 20.0
PROCESSING
wtfile
proc ft
fn 131072
werr
wexp
wbs
wnt
24
10
9
8
7
6
5
4
3
2
1
-0
ppm
3.82
2.11
37.48
8.98
14.11
3.17
3.84
3.80
2.08

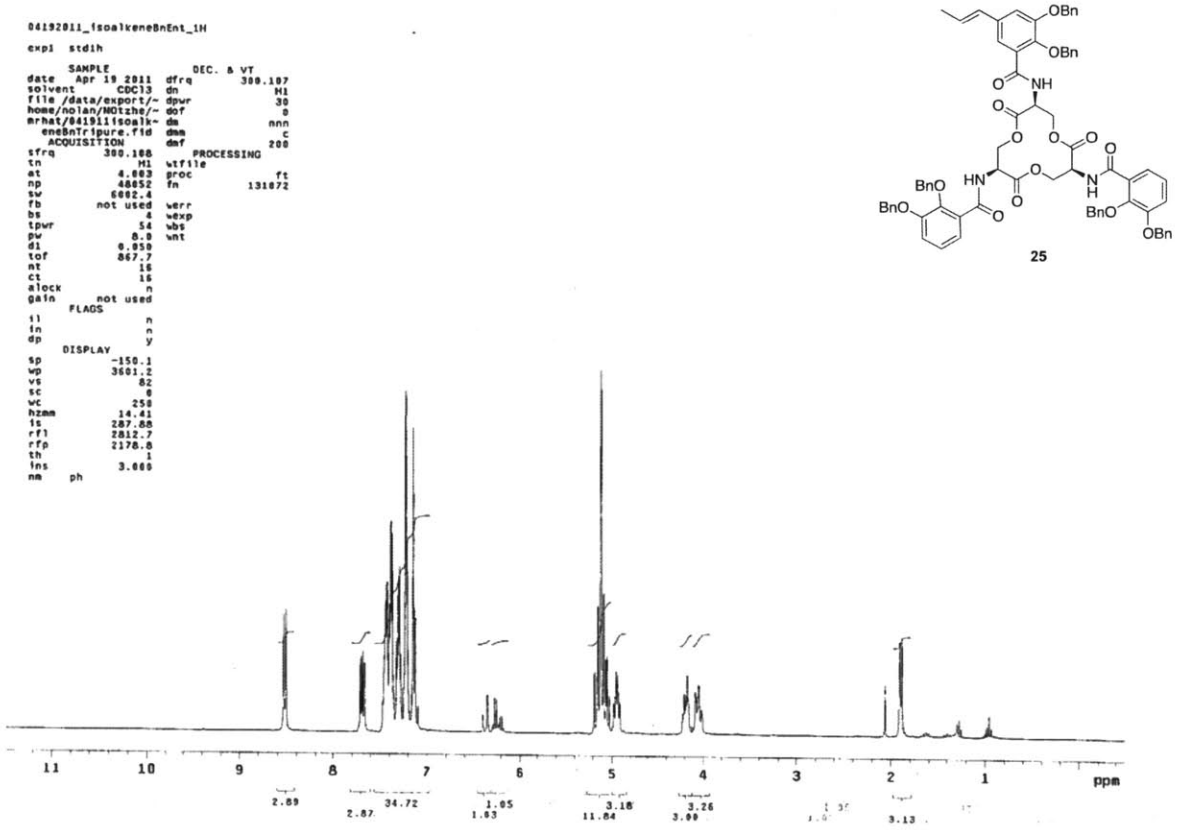
04192011_fsoalkeneBnEnt_1H
expl stdih
SAMPLE
date Apr 19 2011
solvent CDCl3
file /data/export/~
home/nolan/NOtzhe/~
mrhat/0419lilsoalk~
ene8nTripure.fid
ACQUISITION
sfrq 300.108
tn H1
at 4.083
np 48852
sw 6002.4
fb not used
bs 4
tpwr 54
pw 8.8
dl 0.959
tof 867.7
nt 16
ct 16
alock n
gain not used
FLAGS
il n
in n
dp y
DISPLAY
sp -150.1
wp 3601.2
vs 82
sc 0
wc 258
hzmm 14.41
is 287.88
rfl 2812.7
rfp 2178.8
th 1
ins 3.000
nm ph
DEC. & VT
dfrq 300.107
dn H1
dpwr 30
dof 0
dm nnn
dmm c
dmf 200
PROCESSING
wtfile
proc ft
fn 131072
werr
wexp
wbs
wnt
OBn
OBn
NH
HN
BnO
BnO
BnO
OBn
25
11
10
9
8
7
6
5
4
3
2
1
ppm
2.89
34.72
1.05
3.18
3.26
3.13

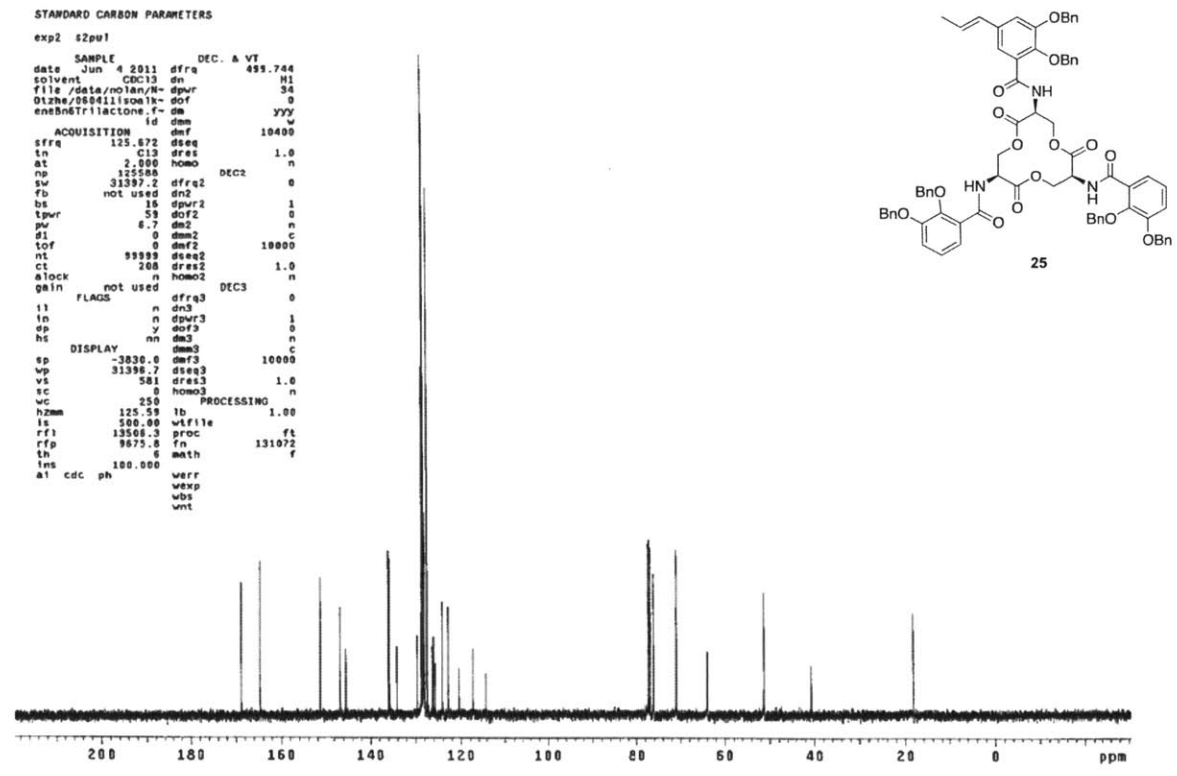
STANDARD CARBON PARAMETERS
exp2 s2pul
SAMPLE
date Jun 4 2011
solvent CDCl3
file /data/nolan/N~
Otzhe/0604lilsoalk~
ene8nNTrilactone.f~
id
ACQUISITION
sfrq 125.672
tn C13
at 2.000
np 125588
sw 31397.2
fb not used
bs 16
tpwr 59
pw 8.7
dl 0
tof 0
nt 99999
ct 208
alock n
gain not used
FLAGS
il n
in n
dp y
hs nn
DISPLAY
sp -3830.0
wp 31398.7
vs 581
sc 0
wc 250
hzmm 125.59
is 500.00
rfl 13568.3
rfp 9675.8
th 6
ins 100.000
ai cdc ph
DEC. & VT
dfrq 499.744
dn H1
dpwr 34
dof 0
dm yyy
dmm w
dmf 10400
dseq
dres 1.0
homo n
DEC2
dfrq2 0
dn2
dpwr2 1
dof2 0
dm2 n
dmm2 c
dmf2 10000
dseq2
dres2 1.0
homo2 n
DEC3
dfrq3 0
dn3
dpwr3 1
dof3 0
dm3 n
dmm3 c
dmf3 10000
dseq3
dres3 1.0
homo3 n
PROCESSING
lb 1.00
wtfile
proc ft
fn 131072
math f
werr
wexp
wbs
wnt
OBn
OBn
NH
HN
BnO
BnO
BnO
OBn
25
200
180
160
140
120
100
80
60
40
20
0
ppm

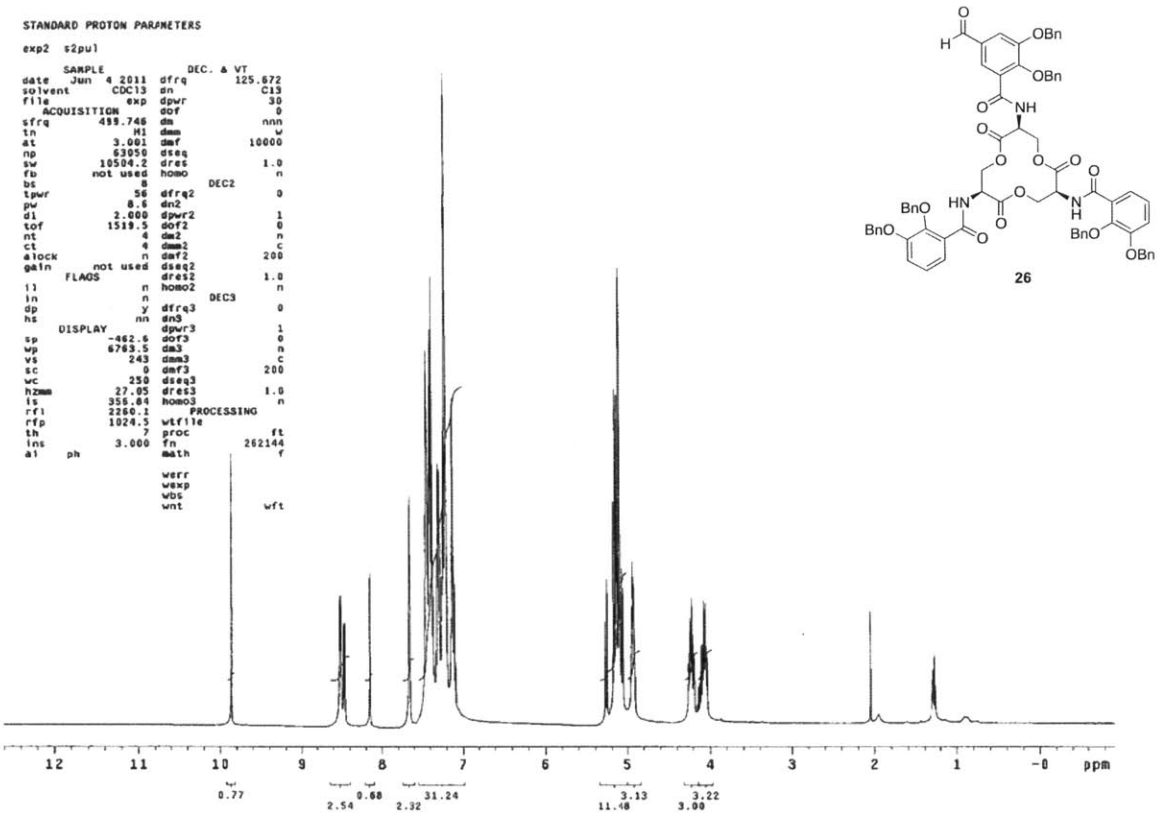
STANDARD PROTON PARAMETERS
exp2 s2pul
SAMPLE
date Jun 4 2011
solvent CDCl3
file exp
ACQUISITION
sfrq 499.746
tn H1
at 3.001
np 63050
sw 10504.2
fb not used
bs 8
tpwr 56
pw 8.6
d1 2.000
tof 1519.5
nt 4
ct 4
alock n
gain not used
FLAGS
il n
in n
dp y
hs nn
DISPLAY
sp -462.6
wp 6763.5
vs 243
sc 0
wc 250
hzmm 27.05
is 356.84
rfl 2260.1
rfp 1024.5
th 7
ins 3.000
ai ph
DEC. & VT
dfrq 125.672
dn C13
dpwr 30
dof 0
dm nnn
dmm w
dmf 10000
dseq
dres 1.0
homo n
DEC2
dfrq2 0
dn2
dpwr2 1
dof2 0
dm2 n
dmm2 c
dmf2 200
dseq2
dres2 1.0
homo2 n
DEC3
dfrq3 0
dn3
dpwr3 1
dof3 0
dm3 n
dmm3 c
dmf3 200
dseq3
dres3 1.0
homo3 n
PROCESSING
wtfile
proc ft
fn 262144
math f
werr
wexp
wbs
wnt wft
26
12
11
10
9
8
7
6
5
4
3
2
1
-0
ppm
0.77
2.54
0.68
2.32
31.24
3.13
11.48
3.22
3.00

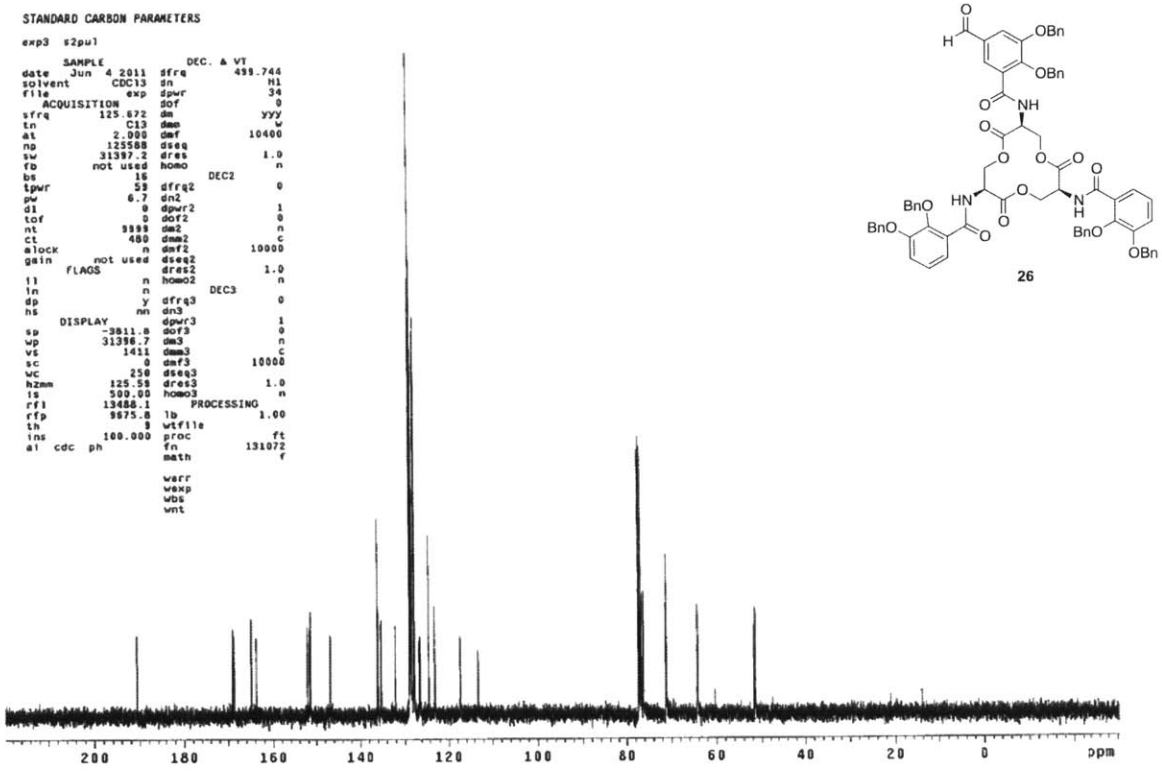
STANDARD CARBON PARAMETERS
exp3 s2pul
SAMPLE
date Jun 4 2011
solvent CDCl3
file exp
ACQUISITION
sfrq 125.672
tn C13
at 2.000
np 125588
sw 31397.2
fb not used
bs 16
tpwr 59
pw 6.7
d1 0
tof 0
nt 9388
ct 480
alock n
gain not used
FLAGS
il n
in n
dp y
hs nn
DISPLAY
sp -3811.8
wp 31396.7
vs 1411
sc 0
wc 250
hzmm 125.59
is 500.00
rfl 13488.1
rfp 9675.8
th 9
ins 100.000
ai cdc ph
DEC. & VT
dfrq 499.744
dn H1
dpwr 34
dof 0
dm yyy
dmm w
dmf 10400
dseq
dres 1.0
homo n
DEC2
dfrq2 0
dn2
dpwr2 1
dof2 0
dm2 n
dmm2 c
dmf2 10000
dseq2
dres2 1.0
homo2 n
DEC3
dfrq3 0
dn3
dpwr3 1
dof3 0
dm3 n
dmm3 c
dmf3 10000
dseq3
dres3 1.0
homo3 n
PROCESSING
lb 1.00
wtfile
proc ft
fn 131072
math f
werr
wexp
wbs
wnt
26
200
180
160
140
120
100
80
60
40
20
0
ppm

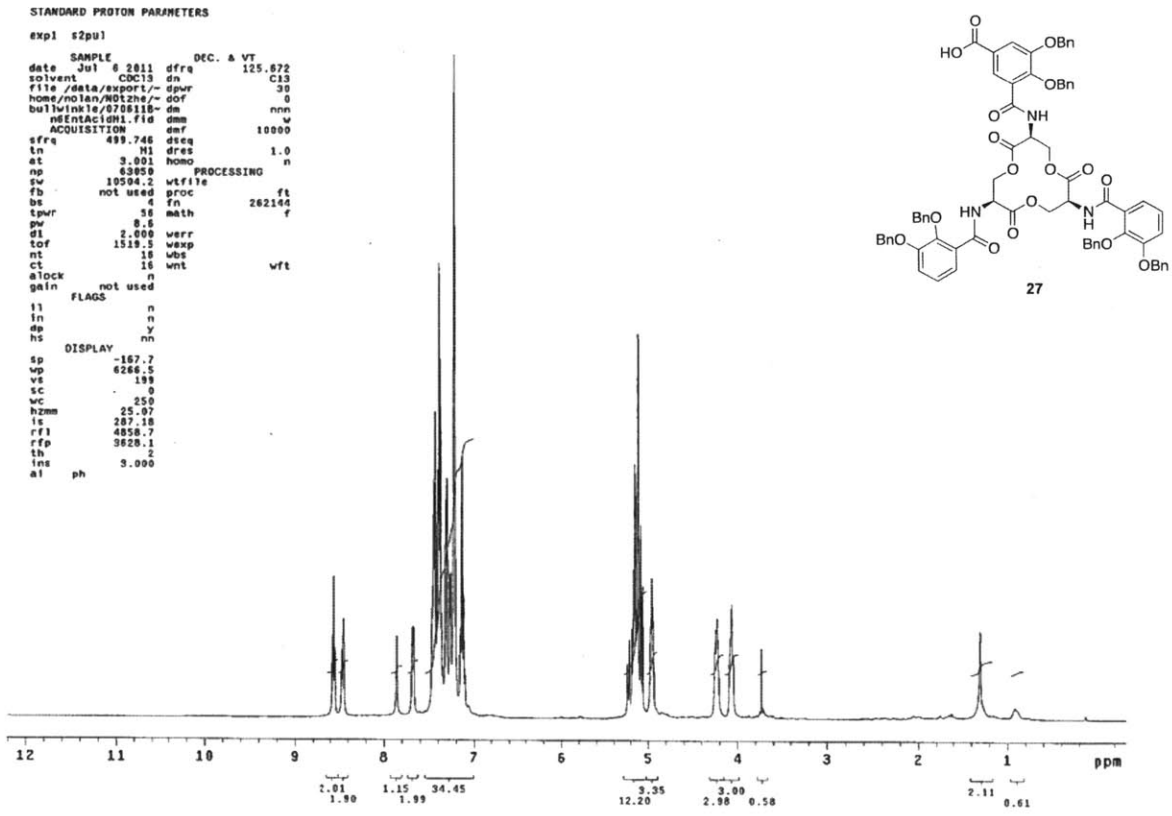
STANDARD PROTON PARAMETERS
expl s2pul
SAMPLE
date Jul 6 2011
solvent CDCl3
file /data/export/~
home/nolan/NOtzhe/~
bullwinkle/0706115~
mEEntAcidH1.fid
ACQUISITION
sfrq 499.746
tn H1
at 3.001
np 63050
sw 10504.2
fb not used
bs 4
tpwr 56
pw 8.6
d1 2.000
tof 1519.5
nt 16
ct 16
alock n
gain not used
FLAGS
il n
in n
dp y
hs nn
DISPLAY
sp -167.7
wp 6266.5
vs 199
sc 0
wc 250
hzmm 25.07
is 287.18
rfl 4858.7
rfp 3628.1
th 2
ins 3.000
ai ph
DEC. & VT
dfrq 125.672
dn C13
dpwr 30
dof 0
dm nnn
dmm w
dmf 10000
dseq
dres 1.0
homo n
PROCESSING
wtfile
proc ft
fn 262144
math f
werr
wexp
wbs
wnt wft
27
12
11
10
9
8
7
6
5
4
3
2
1
ppm
2.01
1.90
1.15
1.99
34.45
3.35
12.20
3.09
2.98
0.58
2.11
0.61

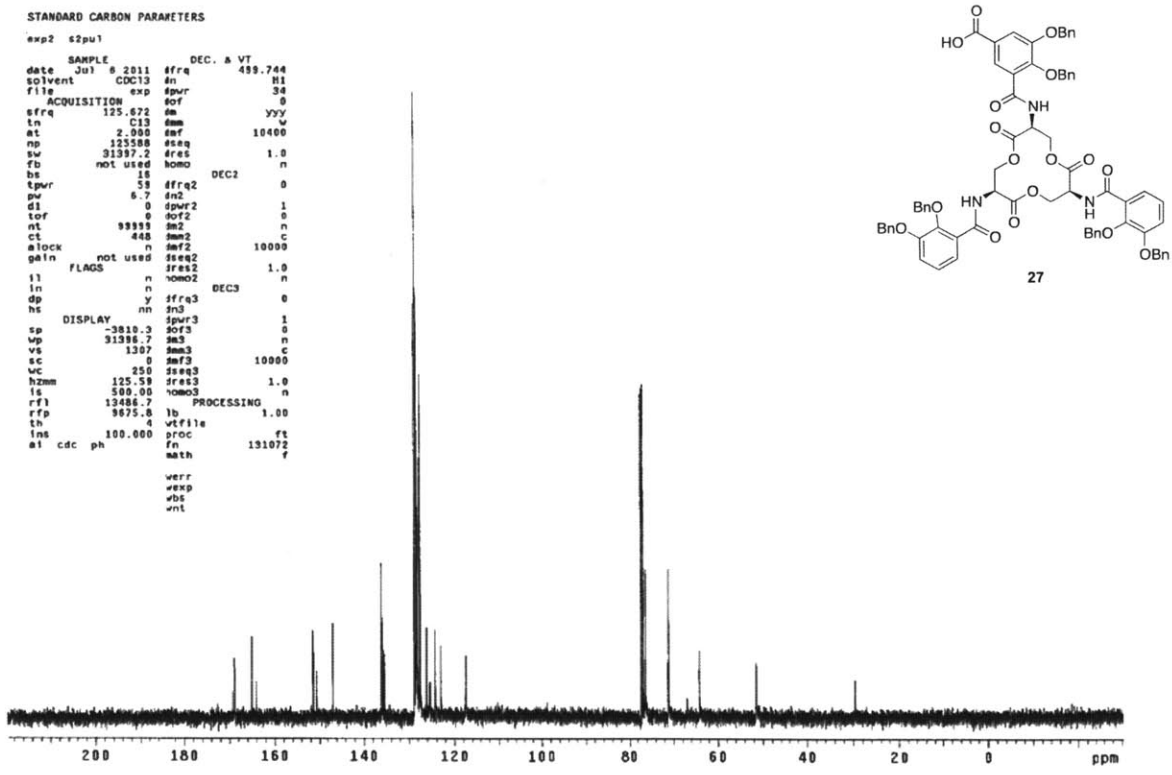
STANDARD CARBON PARAMETERS
exp2 s2pul
SAMPLE
date Jul 6 2011
solvent CDCl3
file exp
ACQUISITION
sfrq 125.672
tn C13
at 2.000
np 125588
sw 31397.2
fb not used
bs 16
tpwr 59
pw 6.7
d1 0
tof 0
nt 99999
ct 448
alock n
gain not used
FLAGS
il n
in n
dp y
hs nn
DISPLAY
sp -3810.3
wp 31396.7
vs 1307
sc 0
wc 250
hzmm 125.59
is 500.00
rfl 13486.7
rfp 9675.8
th 4
ins 100.000
ai cdc ph
DEC. & VT
dfrq 499.744
dn H1
dpwr 34
dof 0
dm yyy
dmm w
dmf 10400
dseq
dres 1.0
homo n
DEC2
dfrq2 0
dn2
dpwr2 1
dof2 0
dm2 n
dmm2 c
dmf2 10000
dseq2
dres2 1.0
homo2 n
DEC3
dfrq3 0
dn3
dpwr3 1
dof3 0
dm3 n
dmm3 c
dmf3 10000
dseq3
dres3 1.0
homo3 n
PROCESSING
lb 1.00
wtfile
proc ft
fn 131072
math f
werr
wexp
wbs
wnt
27
200
180
160
140
120
100
80
60
40
20
0
ppm

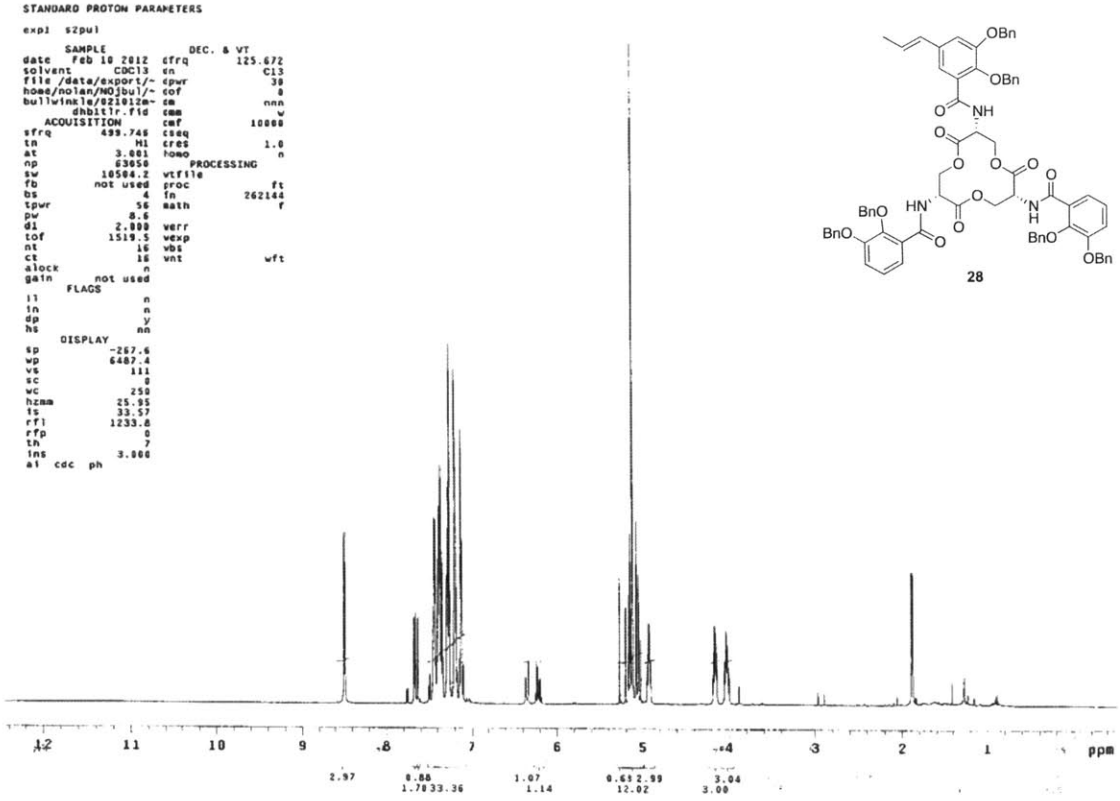
STANDARD PROTON PARAMETERS
expl szpul
SAMPLE
date Feb 10 2012
solvent CDCl3
file /data/export/~
home/nolan/NOJbul/~
bullwinkle/821012m~
dhbitlr.fid
ACQUISITION
sfrq 499.748
tn H1
at 3.001
np 63050
sw 10504.2
fb not used
bs 4
tpwr 56
pw 8.6
dl 2.000
tof 1519.5
nt 16
ct 16
alock n
gain not used
FLAGS
il n
in n
dp y
hs nn
DISPLAY
sp -267.6
wp 6487.4
vs 111
sc 0
wc 250
hzmm 25.95
is 33.57
rfl 1233.8
rfp 0
th 7
ins 3.000
al cdc ph
DEC. & VT
cfrq 125.672
cn C13
cpwr 38
cof 0
cm nnn
cmm w
cmf 10000
cseq
cres 1.0
homo n
PROCESSING
vtfile
proc ft
fn 262144
math f
verr
vexp
vbs
vnt wft
OBn
OBn
NH
HN
BnO
BnO
BnO
OBn
28
12
11
10
9
8
7
6
5
4
3
2
1
ppm
2.97
0.86
1.70
33.36
1.07
1.14
0.63
2.99
12.02
3.04
3.00

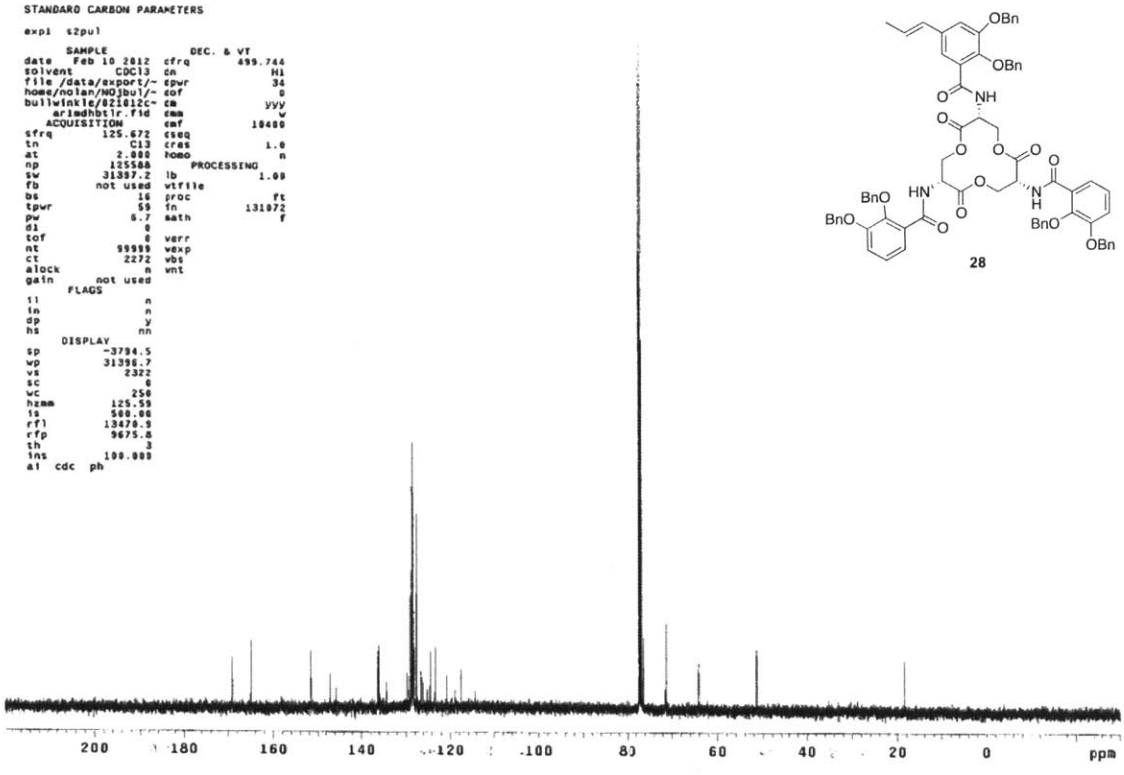
STANDARD CARBON PARAMETERS
expl szpul
SAMPLE
date Feb 10 2012
solvent CDCl3
file /data/export/~
home/nolan/NOJbul/~
bullwinkle/821012c~
arlmdhbtlr.fid
ACQUISITION
sfrq 125.672
tn C13
at 2.000
np 125588
sw 31397.2
fb not used
bs 16
tpwr 58
pw 8.7
dl 0
tof 0
nt 99999
ct 2272
alock n
gain not used
FLAGS
il n
in n
dp y
hs nn
DISPLAY
sp -3794.5
wp 31398.7
vs 2322
sc 0
wc 250
hzmm 125.59
is 500.00
rfl 13470.9
rfp 9675.8
th 3
ins 100.000
al cdc ph
DEC. & VT
cfrq 499.744
cn H1
cpwr 34
cof 0
cm yyy
cmm w
cmf 10400
cseq
cres 1.0
homo n
PROCESSING
lb 1.00
vtfile
proc ft
fn 131072
math f
verr
vexp
vbs
vnt
OBn
OBn
NH
HN
BnO
BnO
BnO
OBn
28
200
180
160
140
120
100
80
60
40
20
0
ppm


Bn_Ent_Aldehyde_1_1H
exp2 s2pul
SAMPLE
date Aug 1 2012
solvent CDCl3
file exp
ACQUISITION
sfrq 500.176
tn H1
at 2.048
np 32768
sw 8000.8
fb 4000
bs 4
ss 2
tpwr 58
pw 5.0
d1 0
tof 0
nt 32
ct 32
alock n
gain not used
FLAGS
il n
in n
dp y
hs nn
DISPLAY
sp -250.1
wp 6002.0
vs 38
sc 0
wc 250
hzmm 24.01
is 88.64
rfl 5139.8
rfp 3631.3
th 2
ins 3.000
nm ph
DEC. & VT
dfrq 500.176
dn H1
dpwr 32
dof 0
dm nnn
dmm c
dmf 8770
dseq
dres 1.0
homo n
temp 23.0
PROCESSING
lb 0.50
wtfile
proc ft
fn not used
math f
werr
wexp
wbs
wnt wft
11
10
9
8
7
6
5
4
3
2
1
ppm
0.75
3.19
0.75
2.61
12.26
17.46
13.83
3.00
3.57
3.54
OBn
OBn
NH
HN
BnO
BnO
BnO
OBn
29

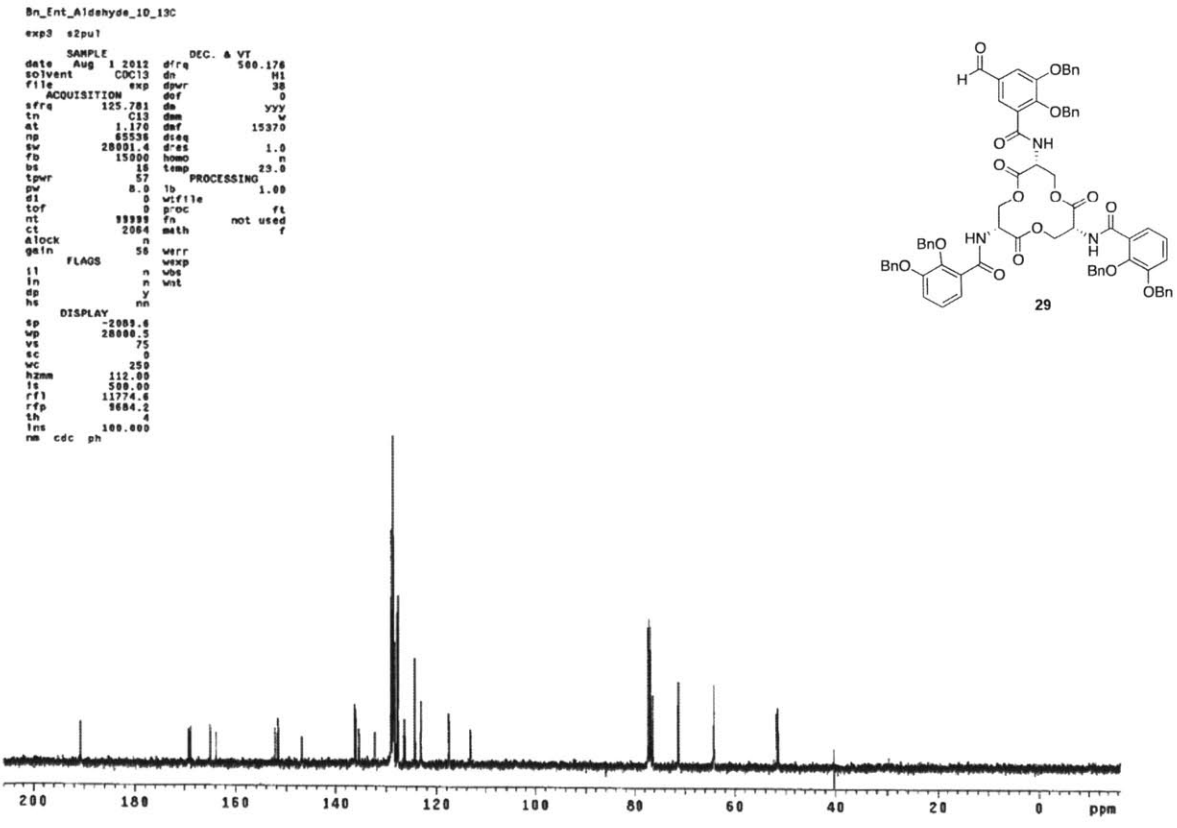
Bn_Ent_Aldehyde_1D_13C
exp3 s2pul
SAMPLE
date Aug 1 2012
solvent CDCl3
file exp
ACQUISITION
sfrq 125.781
tn C13
at 1.170
np 65536
sw 28031.4
fb 15000
bs 16
tpwr 57
pw 8.0
d1 0
tof 0
nt 99999
ct 2064
alock n
gain 58
FLAGS
il n
in n
dp y
hs nn
DISPLAY
sp -2083.6
wp 28000.5
vs 75
sc 0
wc 259
hzmm 112.00
is 500.00
rfl 11774.6
rfp 9684.2
th 4
ins 100.000
nm cdc ph
DEC. & VT
dfrq 500.176
dn H1
dpwr 38
dof 0
dm yyy
dmm w
dmf 15370
dseq
dres 1.0
homo n
temp 23.0
PROCESSING
lb 1.00
wtfile
proc ft
fn not used
math f
werr
wexp
wbs
wnt
200
180
160
140
120
100
80
60
40
20
0
ppm
OBn
OBn
NH
HN
BnO
BnO
BnO
OBn
29

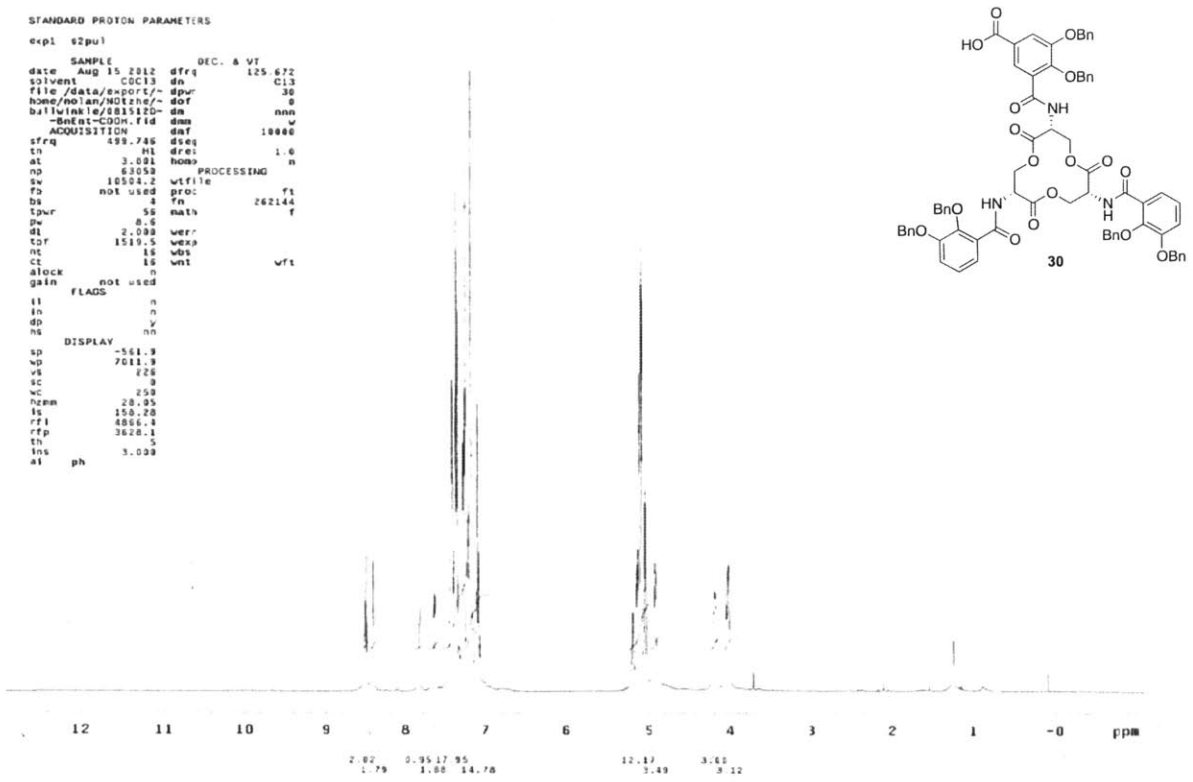
STANDARD PROTON PARAMETERS
expl s2pul
SAMPLE
date Aug 15 2012
solvent CDCl3
file /data/export/~
home/nolan/NOtzhe/~
bullwinkle/081512D~
-BnEnt-COOH.fid
ACQUISITION
sfrq 499.746
tn H1
at 3.081
np 63058
sw 10504.2
fb not used
bs 4
tpwr 56
pw 8.6
d1 2.000
tof 1519.5
nt 16
ct 16
alock n
gain not used
FLAGS
il n
in n
dp y
hs nn
DISPLAY
sp -561.9
wp 7011.9
vs 226
sc 0
wc 250
hzcm 28.05
hs 150.28
rfl 4866.4
rfp 3628.1
th 5
ins 3.000
ai ph
DEC. & VT
dfrq 125.672
dn C13
dpwr 36
dof 0
dm nnn
dmm w
daf 10000
dseq
dres 1.6
homo n
PROCESSING
wtfile
proc ft
fn 262144
math f
werr
wexp
wbs
wnt wft
HO
OBn
OBn
NH
BnO
HN
BnO
BnO
OBn
30
12
11
10
9
8
7
6
5
4
3
2
1
-0
ppm
2.02
1.79
0.95
1.88
17.95
14.78
12.17
3.49
3.00
3.12

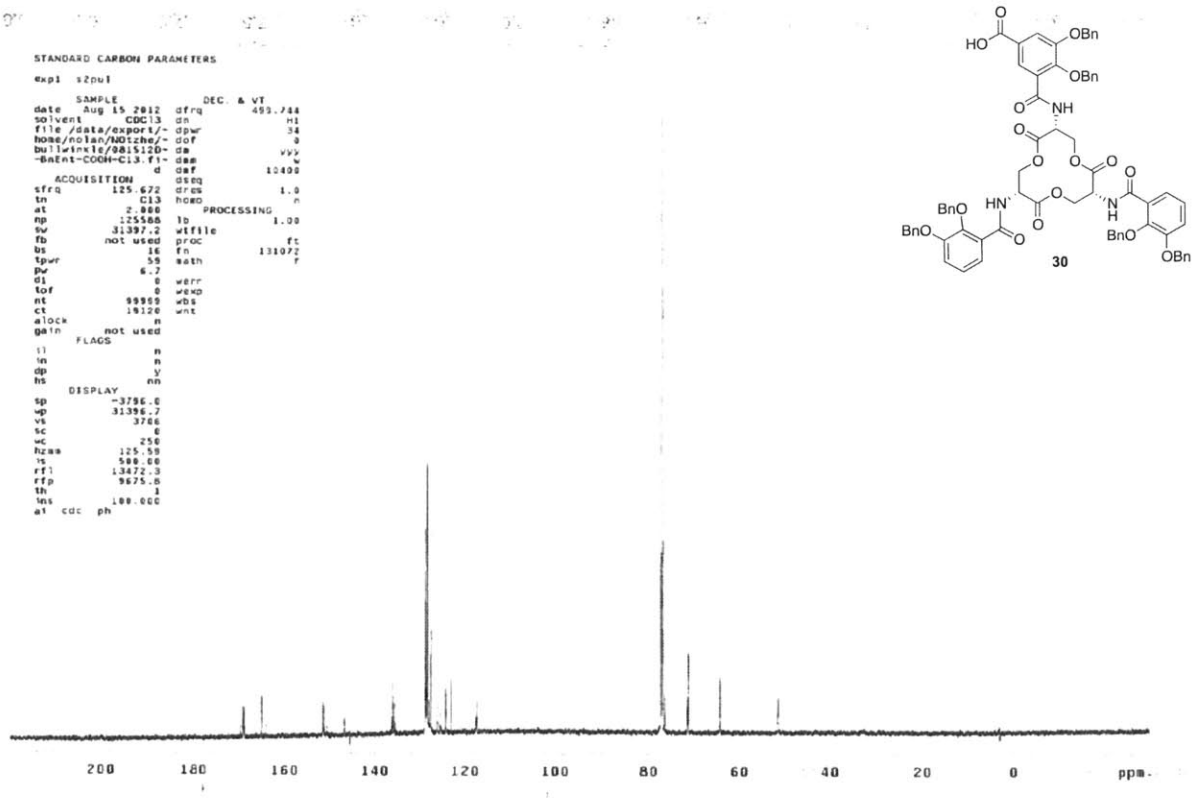
STANDARD CARBON PARAMETERS
expl s2pul
SAMPLE
date Aug 15 2012
solvent CDCl3
file /data/export/~
home/nolan/NOtzhe/~
bullwinkle/081512D~
-BnEnt-COOH-C13.fi~
d
ACQUISITION
sfrq 125.672
tn C13
at 2.888
np 125588
sw 31397.2
fb not used
bs 16
tpwr 55
pw 6.7
d1 0
tof 0
nt 99959
ct 19120
alock n
gain not used
FLAGS
il n
in n
dp y
hs nn
DISPLAY
sp -3796.8
wp 31396.7
vs 3786
sc 0
wc 256
hzpp 125.59
hs 500.00
rfl 13472.3
rfp 9675.8
th 1
ins 100.000
ai cdc ph
DEC. & VT
dfrq 499.744
dn H1
dpwr 34
dof 0
dm yyy
dmm w
daf 10400
dseq
dres 1.0
homo n
PROCESSING
lb 1.00
wtfile
proc ft
fn 131072
math f
werr
wexp
wbs
wnt
HO
OBn
OBn
NH
BnO
HN
BnO
BnO
OBn
30
200
180
160
140
120
100
80
60
40
20
0
ppm

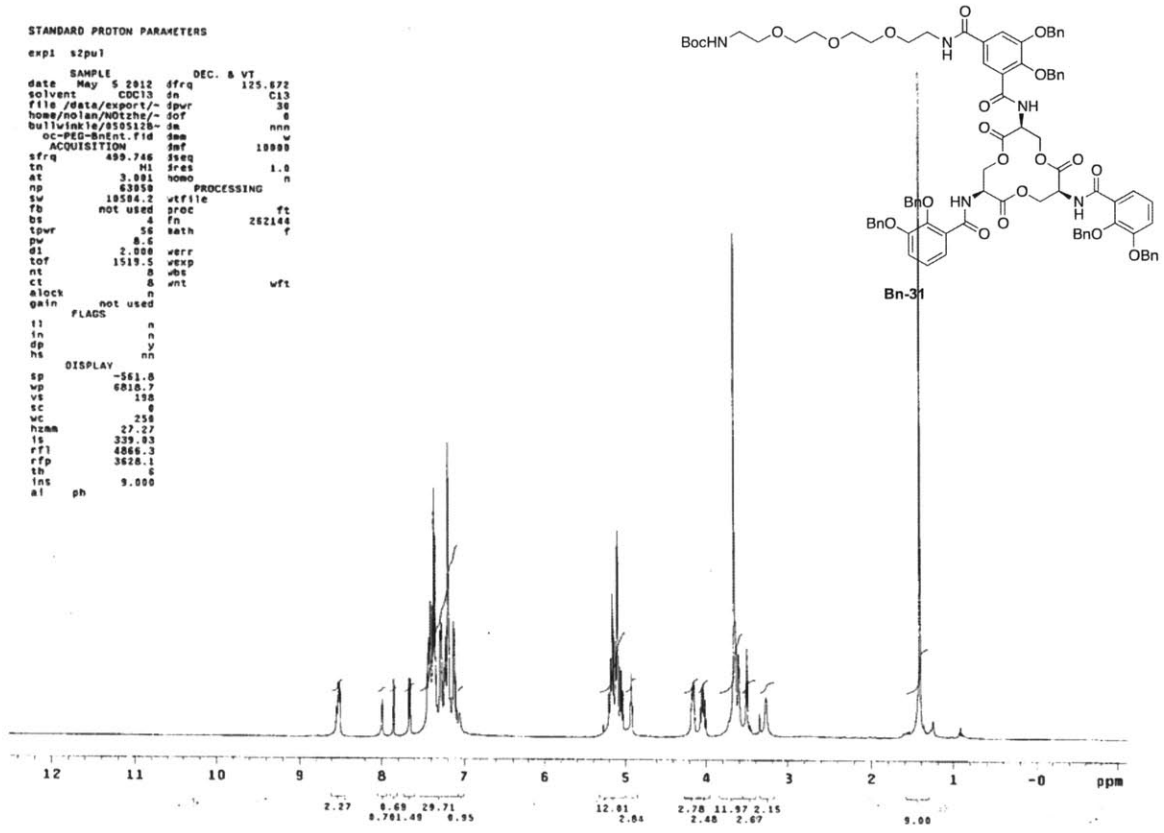
STANDARD PROTON PARAMETERS
expl s2pul
SAMPLE
date May 5 2012
solvent CDCl3
file /data/export/~
home/nolan/NOtzhe/~
bullwinkle/050512B~
oc-PEG-BnEnt.fid
ACQUISITION
sfrq 499.746
tn H1
at 3.881
np 63959
sw 10504.2
fb not used
bs 4
tpwr 56
pw 8.6
d1 2.000
tof 1519.5
nt 8
ct 8
alock n
gain not used
FLAGS
ll n
in n
dp y
hs nn
DISPLAY
sp -561.8
wp 6818.7
vs 198
sc 0
wc 250
hzmm 27.27
is 339.83
rfl 4866.3
rfp 3628.1
th 6
ins 9.000
al ph
DEC. & VT
dfrq 125.672
dn C13
dpwr 38
dof 0
dm nnn
dmm w
dmf 18998
dseq
dres 1.8
homo n
PROCESSING
wtfile
proc ft
fn 262144
math f
werr
wexp
wbs
wnt wft
BocHN
OBn
OBn
NH
BnO
HN
BnO
BnO
OBn
Bn-31
12
11
10
9
8
7
6
5
4
3
2
1
-0
ppm
2.27
0.69
29.71
8.78
1.48
0.95
12.01
2.04
2.78
2.48
11.97
2.67
2.15
9.00

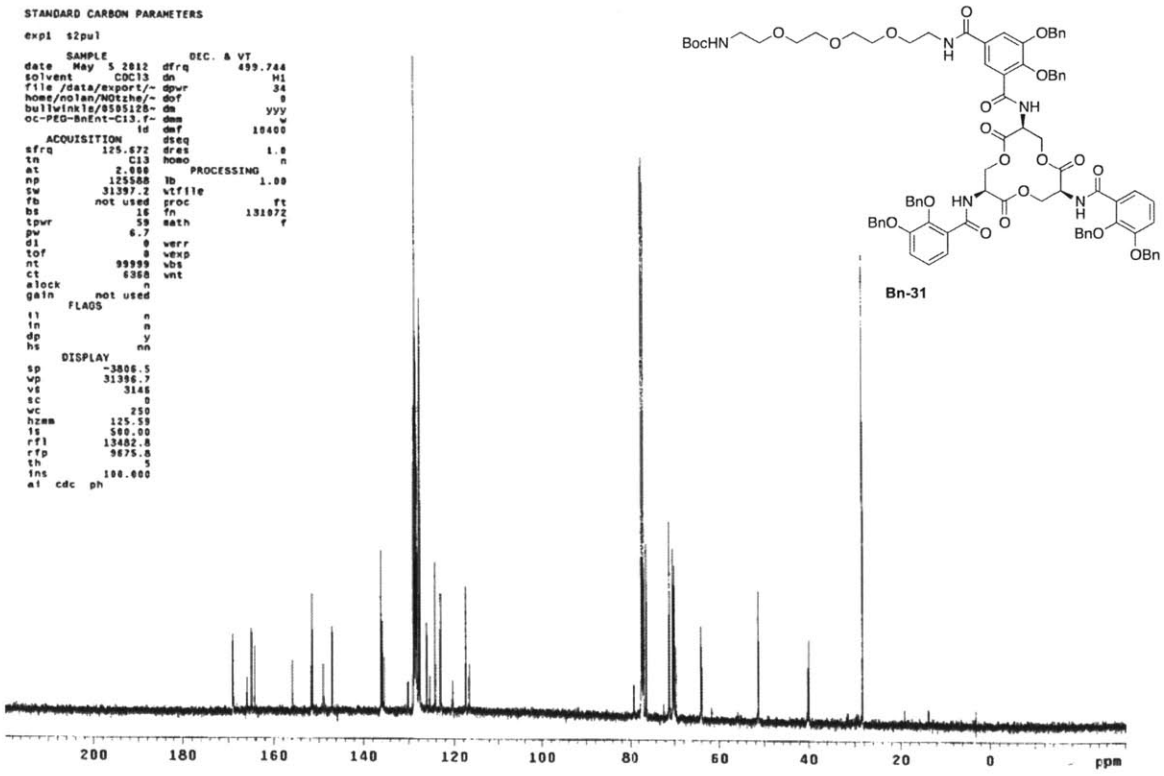
STANDARD CARBON PARAMETERS
expl s2pul
SAMPLE
date May 5 2012
solvent CDCl3
file /data/export/~
home/nolan/NOtzhe/~
bullwinkle/050512B~
oc-PEG-BnEnt-C13.fid
ACQUISITION
sfrq 125.672
tn C13
at 2.088
np 125588
sw 31397.2
fb not used
bs 16
tpwr 59
pw 6.7
d1 0
tof 0
nt 99999
ct 6368
alock n
gain not used
FLAGS
ll n
in n
dp y
hs nn
DISPLAY
sp -3806.5
wp 31396.7
vs 3148
sc 0
wc 250
hzmm 125.59
is 500.00
rfl 13402.8
rfp 9675.8
th 5
ins 100.000
al cdc ph
DEC. & VT
dfrq 499.744
dn H1
dpwr 34
dof 0
dm yyy
dmm w
dmf 18400
dseq
dres 1.8
homo n
PROCESSING
lb 1.00
wtfile
proc ft
fn 131072
math f
BocHN
OBn
OBn
NH
BnO
HN
BnO
BnO
OBn
Bn-31
200
180
160
140
120
100
80
60
40
20
0
ppm

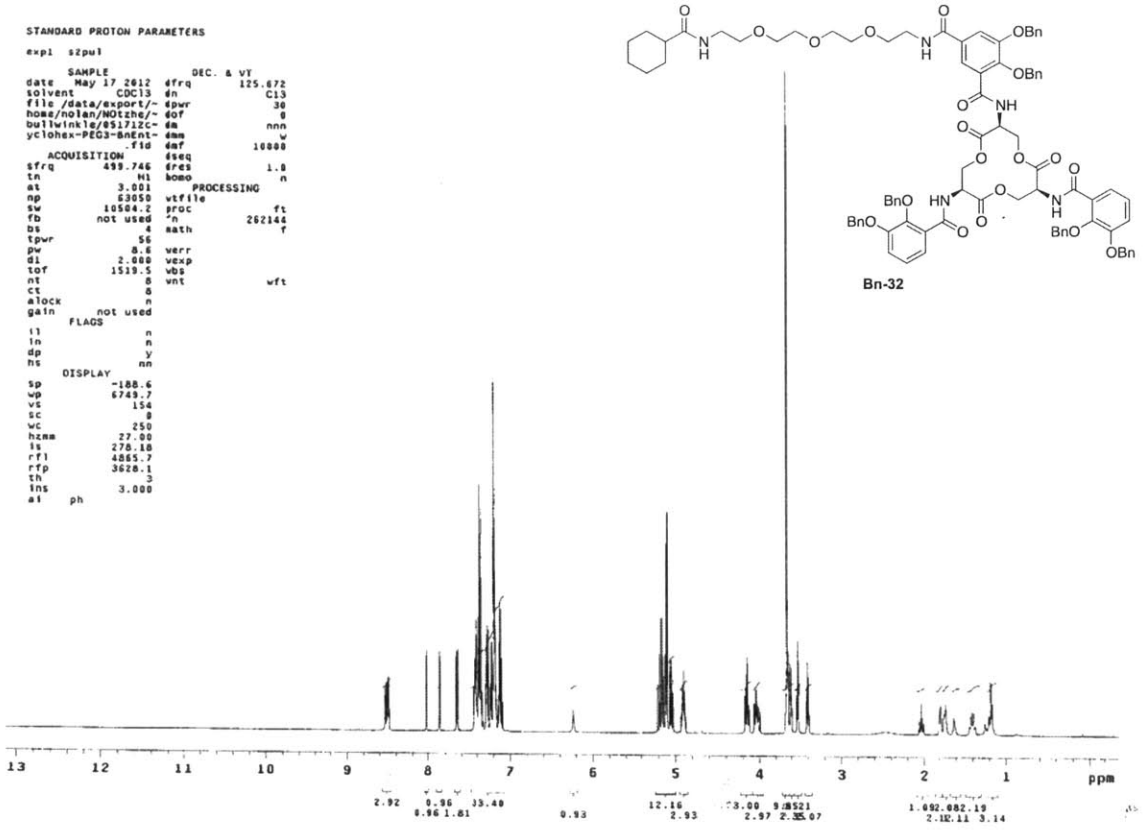
STANDARD PROTON PARAMETERS
expl szpul
SAMPLE
date May 17 2012
solvent CDCl3
file /data/export/~
home/nolan/NOtizhe/~
bullwinkle/05171Zc~
yclohex-PEG3-BnEnt~
.fid
ACQUISITION
sfrq 499.746
tn H1
at 3.001
np 63050
sw 10504.2
fb not used
bs 4
tpwr 56
pw 8.6
dl 2.000
tof 1519.5
nt 8
ct 8
alock n
gain not used
FLAGS
il n
in n
dp y
hs nn
DISPLAY
sp -188.6
wp 6749.7
vs 154
sc 0
wc 250
hzmm 27.00
is 278.18
rfl 4865.7
rfp 3628.1
th 3
ins 3.000
ai ph
DEC. & VT
dfrq 125.672
dn C13
dpwr 30
dof 0
dm nnn
dmm w
dmf 10000
dseq
dres 1.8
homo n
PROCESSING
vtfile
proc ft
fn 262144
math f
werr
wexp
wbs
wnt wft
OBn
NH
BnO
HN
Bn-32
13
12
11
10
9
8
7
6
5
4
3
2
1
ppm
2.92
0.96
33.40
0.96 1.81
0.93
12.16
2.93
3.00
2.97
2.35.07
1.092.082.19
2.12.11
3.14

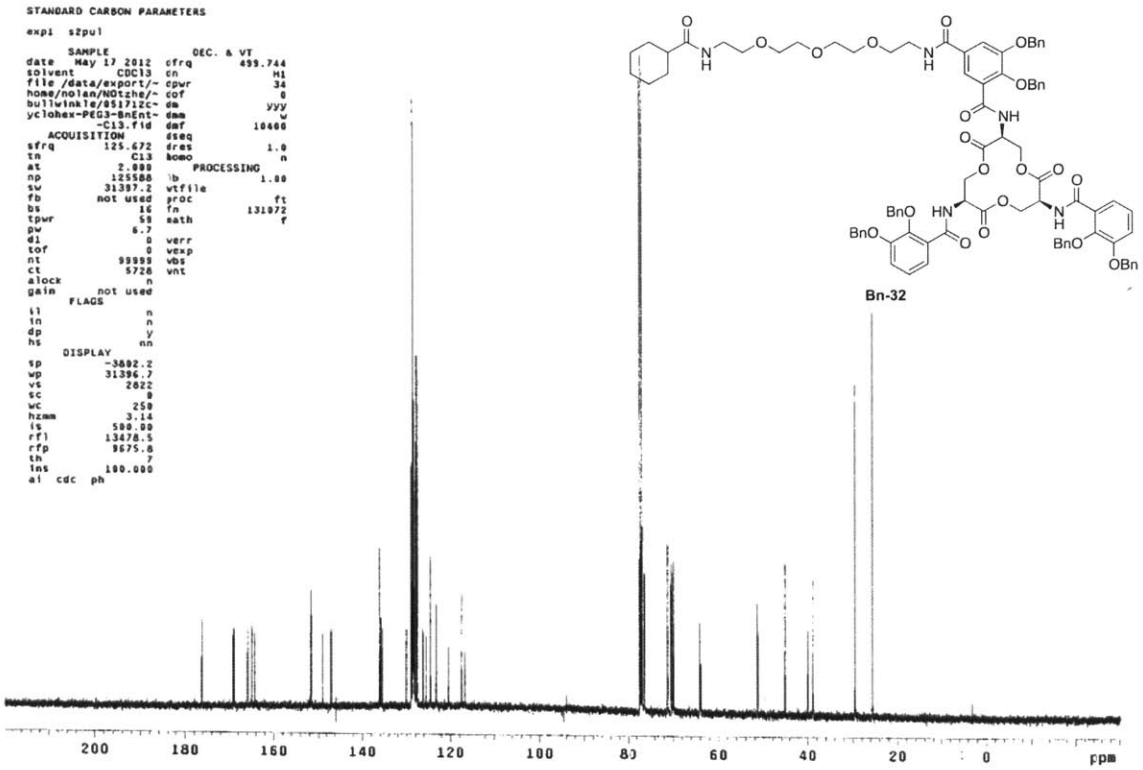
STANDARD CARBON PARAMETERS
expl szpul
SAMPLE
date May 17 2012
solvent CDCl3
file /data/export/~
home/nolan/NOtizhe/~
bullwinkle/05171Zc~
yclohex-PEG3-BnEnt~
-C13.fid
ACQUISITION
sfrq 125.672
tn C13
at 2.088
np 125588
sw 31397.2
fb not used
bs 16
tpwr 59
pw 6.7
dl 0
tof 0
nt 99999
ct 5728
alock n
gain not used
FLAGS
il n
in n
dp y
hs nn
DISPLAY
sp -3892.2
wp 31396.7
vs 2822
sc 0
wc 250
hzmm 3.14
is 500.00
rfl 13478.5
rfp 9675.8
th 7
ins 100.000
ai cdc ph
DEC. & VT
dfrq 499.744
dn H1
dpwr 34
dof 0
dm yyy
dmm w
dmf 10400
dseq
dres 1.0
homo n
PROCESSING
lb 1.00
vtfile
proc ft
fn 131072
math f
werr
wexp
wbs
wnt
OBn
NH
BnO
HN
Bn-32
200
180
160
140
120
100
80
60
40
20
0
ppm

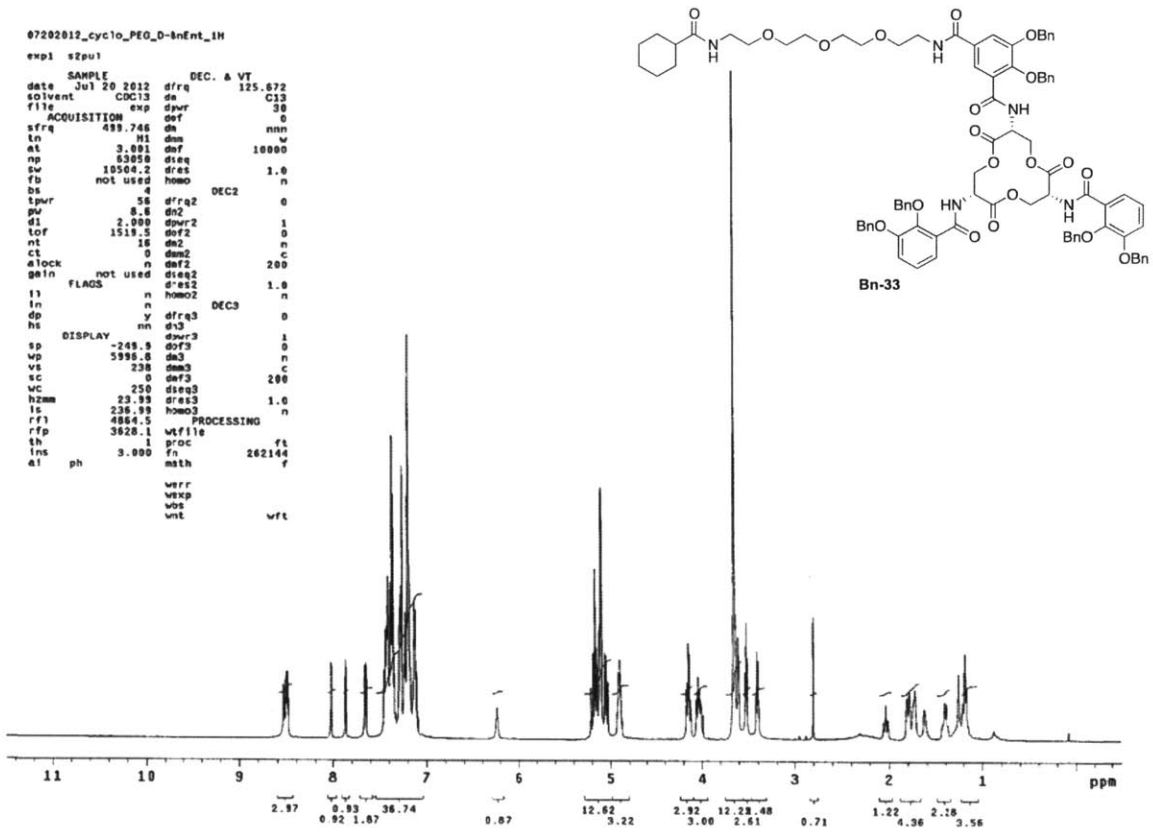
07202012_cyclo_PEG_D-BnEnt_1H
Bn-33
ppm

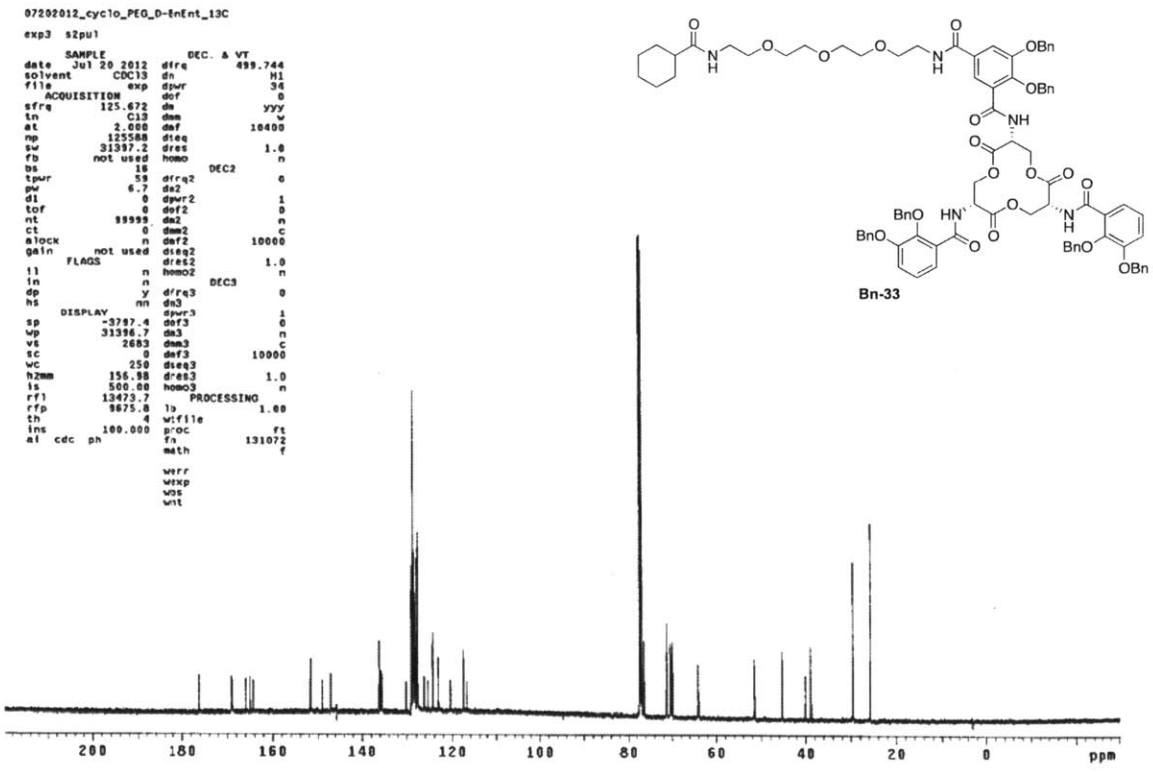
07202012_cyclo_PEG_D-BnEnt_13C
Bn-33
ppm

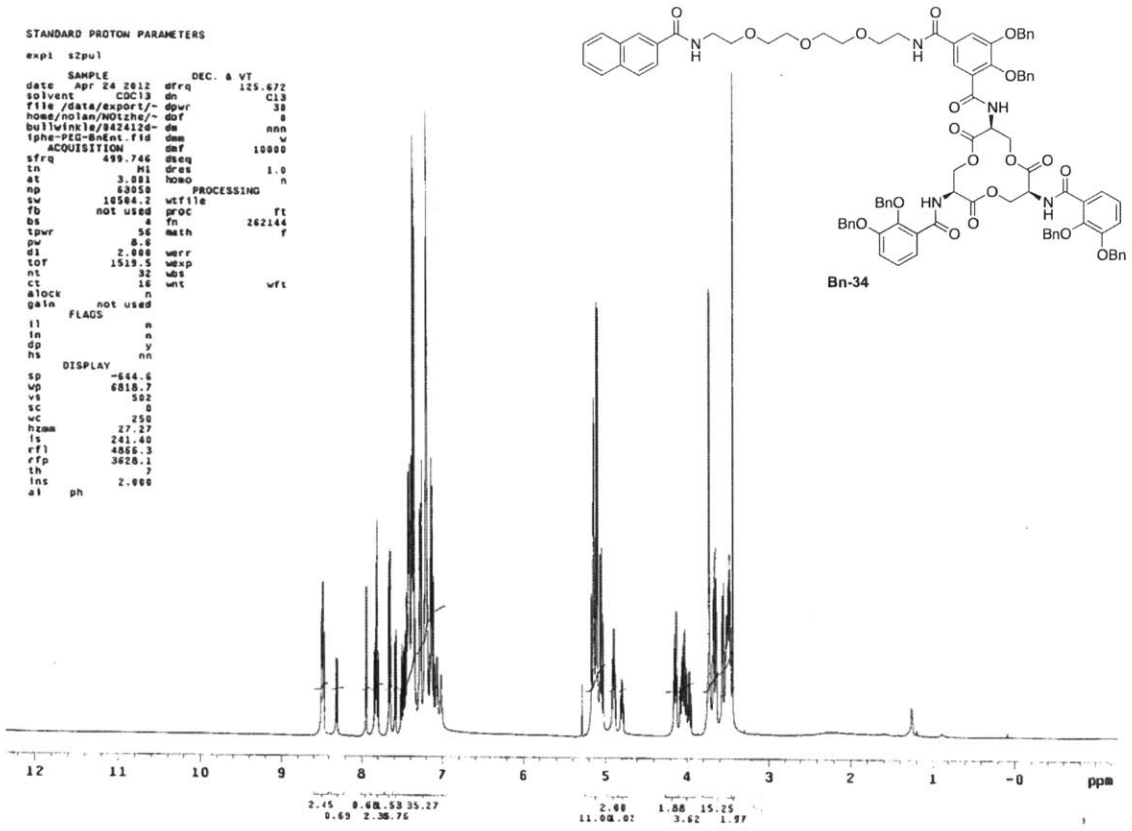
STANDARD PROTON PARAMETERS
expl s2pul
SAMPLE
date Apr 24 2012
solvent CDCl3
file /data/export/~
home/nolan/NOtzhe/~
bullwinkle/042412d~
iphe-PEG-BnEnt.fid
ACQUISITION
sfrq 499.746
tn H1
at 3.001
np 63058
sw 10504.2
fb not used
bs 4
tpwr 56
pw 8.6
d1 2.000
tof 1519.5
nt 32
ct 16
alock n
gain not used
FLAGS
il n
in n
dp y
hs nn
DISPLAY
sp -644.6
wp 6818.7
vs 502
sc 0
wc 250
hzmm 27.27
is 241.40
rfl 4866.3
rfp 3628.1
th 7
ins 2.000
al ph
DEC. & VT
dfrq 125.672
dn C13
dpwr 38
dof 0
dm nnn
dmm w
dmf 10000
dseq
dres 1.0
homo n
PROCESSING
wtfile
proc ft
fn 262144
math f
werr
wexp
wbs
wnt wft
Bn-34
12
11
10
9
8
7
6
5
4
3
2
1
-0
ppm
2.45
0.69
2.38.76
2.00
11.00
1.88
3.62
15.25
1.97

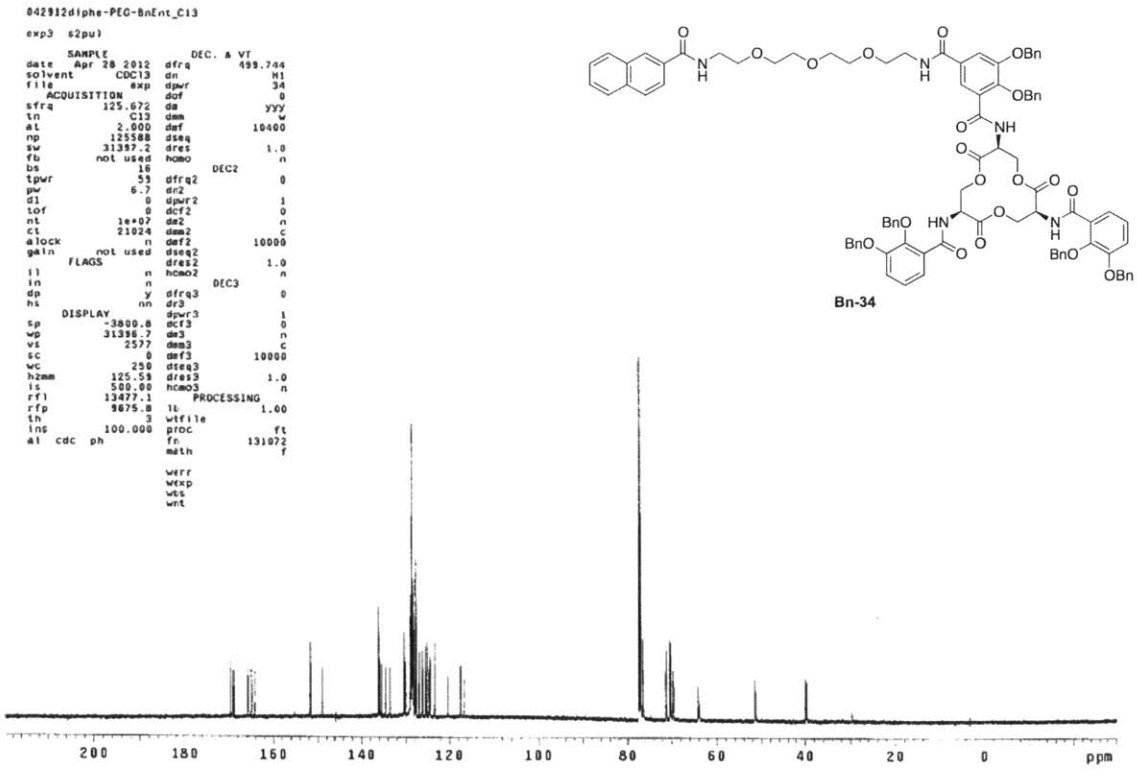
042912diphe-PEG-BnEnt_C13
exp3 s2pul
SAMPLE
date Apr 28 2012
solvent CDCl3
file exp
ACQUISITION
sfrq 125.672
tn C13
at 2.000
np 125588
sw 31397.2
fb not used
bs 16
tpwr 53
pw 6.7
d1 0
tof 0
nt 1e+07
ct 21024
alock n
gain not used
FLAGS
il n
in n
dp y
hs nn
DISPLAY
sp -3800.8
wp 31396.7
vs 2577
sc 0
wc 250
hzmm 125.55
is 500.00
rfl 13477.1
rfp 9875.8
th 3
ins 100.000
al cdc ph
DEC. & VT
dfrq 499.744
dn H1
dpwr 34
dof 0
dm yyy
dmm w
dmf 10400
dseq
dres 1.0
homo n
DEC2
dfrq2 0
dn2
dpwr2 1
dcf2 0
dm2 n
dmm2 c
dmf2 10000
dseq2
dres2 1.0
homo2 n
DEC3
dfrq3 0
dn3
dpwr3 1
dcf3 0
dm3 n
dmm3 c
dmf3 10000
dseq3
dres3 1.0
homo3 n
PROCESSING
lb 1.00
wtfile
proc ft
fn 131072
math f
werr
wexp
wbs
wnt
Bn-34
200
180
160
140
120
100
80
60
40
20
0
ppm

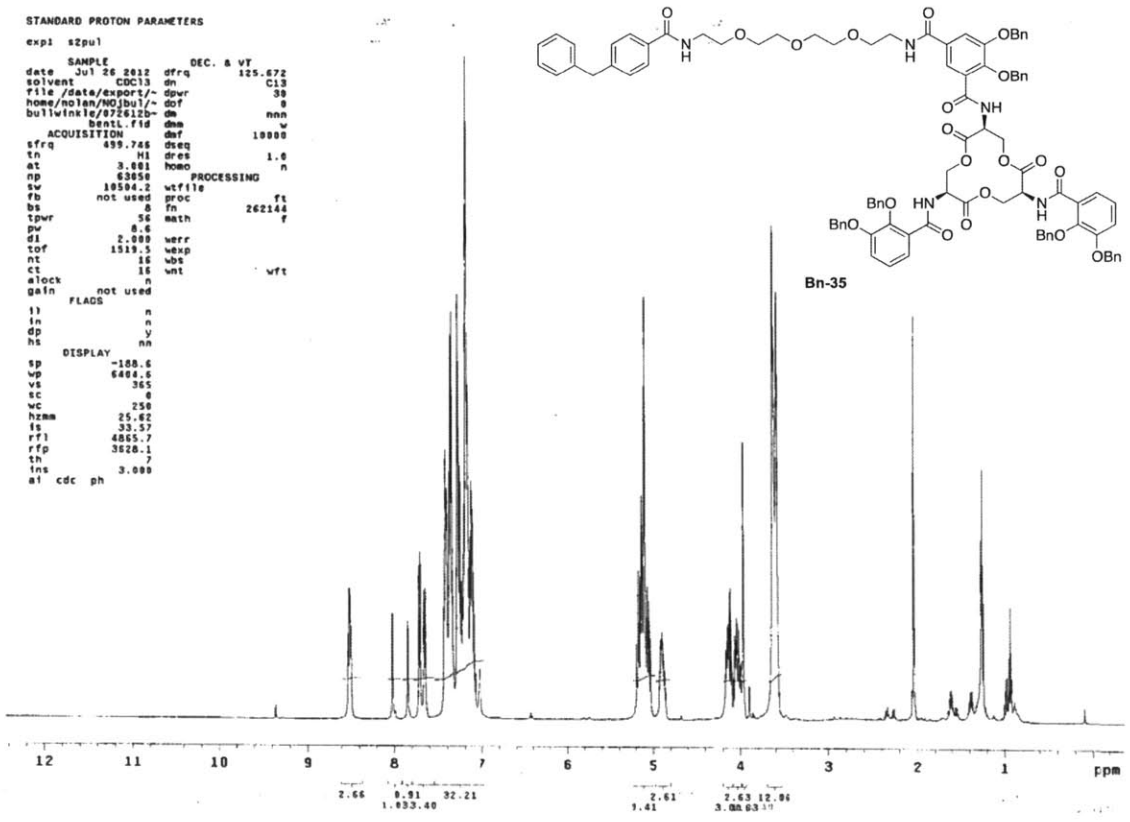
STANDARD PROTON PARAMETERS
exp1 szpul
SAMPLE
date Jul 26 2012
solvent CDCl3
file /data/export/~
home/nolan/NOjbul/~
bullwinkle/0726125-
bentL.fid
ACQUISITION
sfrq 499.746
tn H1
at 3.481
np 63050
sw 10504.2
fb not used
bs 8
tpwr 56
pw 6.6
dl 2.000
tof 1519.5
nt 16
ct 16
alock n
gain not used
FLAGS
il n
in n
dp y
hs nn
DISPLAY
sp -188.6
wp 6404.6
vs 365
sc 0
wc 250
hzmm 25.62
is 33.57
rfl 4865.7
rfp 3828.1
th 7
ins 3.000
ai cdc ph
DEC. & VT
dfrq 125.672
dn C13
dpwr 38
dof 0
dm nnn
dmm w
dmf 10000
dseq
dres 1.6
homo n
PROCESSING
wtfile
proc ft
fn 262144
math f
werr
wexp
wbs
wnt wft
OBn
OBn
NH
BnO
HN
BnO
BnO
OBn
Bn-35
12
11
10
9
8
7
6
5
4
3
2
1
ppm
2.66
0.91
1.033.40
32.21
2.61
9.41
2.63
12.86

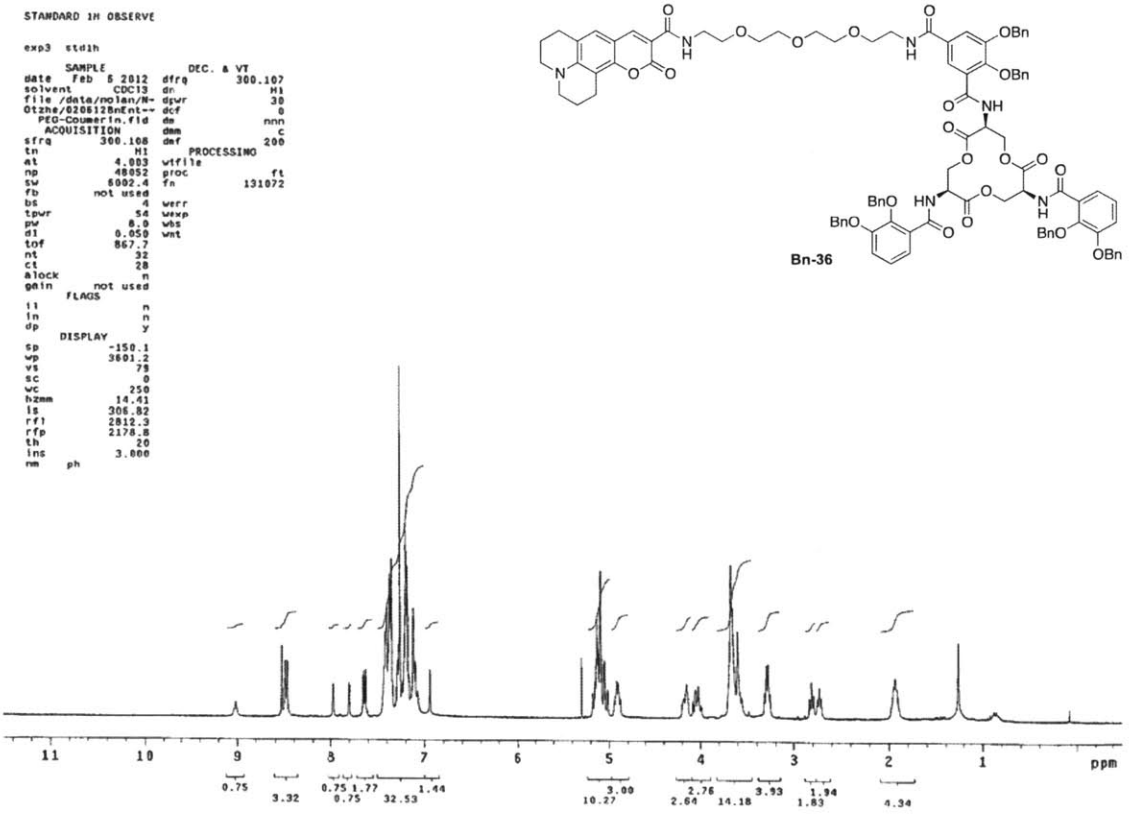
STANDARD 1H OBSERVE
exp3 std1h
SAMPLE
date Feb 6 2012
solvent CDCl3
file /data/nolan/N-
Otzhe/0206128nEnt-~
PEG-Coumerin.fid
ACQUISITION
sfrq 300.108
tn H1
at 4.083
np 48052
sw 5902.4
fb not used
bs 4
tpwr 56
pw 8.0
dl 0.050
tof 867.7
nt 32
ct 28
alock n
gain not used
FLAGS
il n
in n
dp y
DISPLAY
sp -150.1
wp 3601.2
vs 79
sc 0
wc 250
hzmm 14.41
is 306.82
rfl 2812.3
rfp 2178.8
th 20
ins 3.000
nm ph
DEC. & VT
dfrq 300.107
dn H1
dpwr 30
dof 0
dm nnn
dmm c
dmf 200
PROCESSING
wtfile
proc ft
fn 131072
werr
wexp
wbs
wnt
OBn
OBn
NH
BnO
HN
BnO
BnO
OBn
Bn-36
11
10
9
8
7
6
5
4
3
2
1
ppm
0.75
3.32
0.75
1.77
32.53
1.44
3.00
10.27
2.76
2.64
14.18
3.93
1.94
1.83
4.34

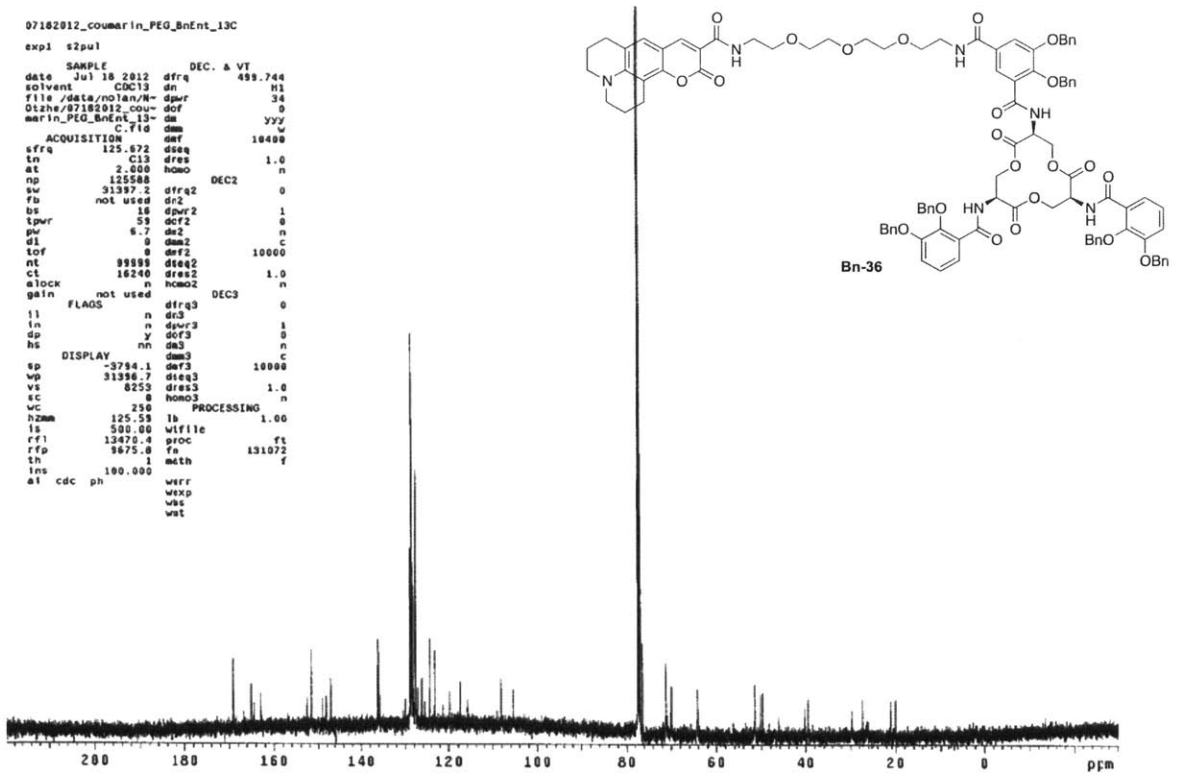
07162012_coumarin_PEG_BnEnt_13C
expl s2pul
SAMPLE
date Jul 18 2012
solvent CDCl3
file /data/nolan/N~
Otzhe/07162012_cou~
marin_PEG_BnEnt_13~
C.fid
ACQUISITION
sfrq 125.672
tn C13
at 2.000
np 125588
sw 31397.2
fb not used
bs 16
tpwr 59
pw 6.7
d1 0
tof 0
nt 99999
ct 16240
alock n
gain not used
FLAGS
il n
in n
dp y
hs nn
DISPLAY
sp -3794.1
wp 31396.7
vs 8259
sc 0
wc 250
hzmm 125.55
is 500.00
rfl 13470.4
rfp 9675.8
th 1
ins 100.000
al cdc ph
DEC. & VT
dfrq 499.744
dn H1
dpwr 34
dof 0
dm yyy
dmm w
dmf 10400
dseq
dres 1.0
homo n
DEC2
dfrq2 0
dn2
dpwr2 1
dof2 0
dm2 n
dmm2 c
dmf2 10000
dseq2
dres2 1.0
homo2 n
DEC3
dfrq3 0
dn3
dpwr3 1
dof3 0
dm3 n
dmm3 c
dmf3 10000
dseq3
dres3 1.0
homo3 n
PROCESSING
lb 1.00
wtfile
proc ft
fa 131072
math f
werr
wexp
wbs
wnt
Bn-36
200
180
160
140
120
100
80
60
40
20
0
ppm

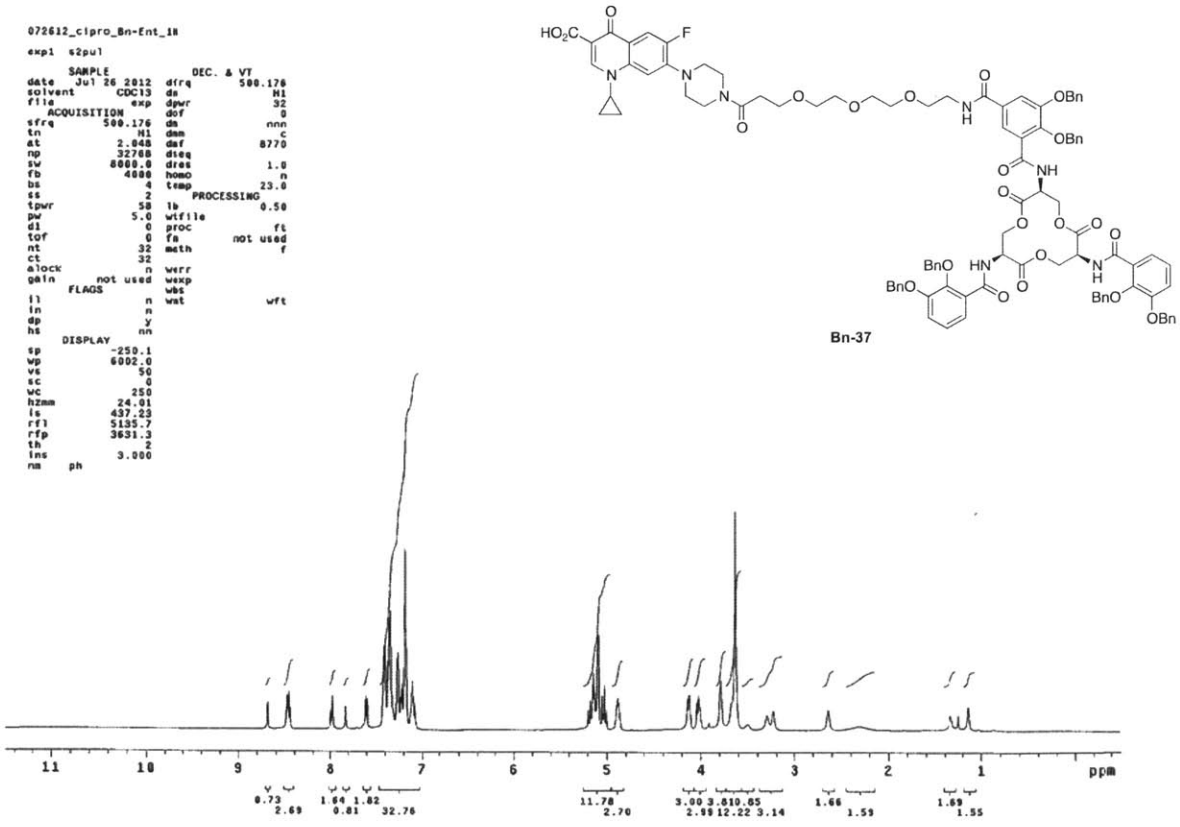
072612_cipro_Bn-Ent_1H
expl s2pul
SAMPLE
date Jul 26 2012
solvent CDCl3
file exp
ACQUISITION
sfrq 500.176
tn H1
at 2.048
np 32768
sw 8000.0
fb 4000
bs 4
ss 2
tpwr 58
pw 5.0
d1 0
tof 0
nt 32
ct 32
alock n
gain not used
FLAGS
il n
in n
dp y
hs nn
DISPLAY
sp -250.1
wp 6002.0
vs 50
sc 0
wc 250
hzmm 24.01
is 437.23
rfl 5135.7
rfp 3631.3
th 2
ins 3.000
nm ph
DEC. & VT
dfrq 500.176
dn H1
dpwr 32
dof 0
dm nnn
dmm c
dmf 8770
dseq
dres 1.0
homo n
temp 23.0
PROCESSING
lb 0.50
wtfile
proc ft
fa not used
math f
werr
wexp
wbs
wnt wft
Bn-37
11
10
9
8
7
6
5
4
3
2
1
ppm
0.73
2.69
1.64
0.81
1.82
32.76
11.78
2.70
3.00
2.99
3.81
12.22
0.65
3.14
1.66
1.59
1.69
1.55

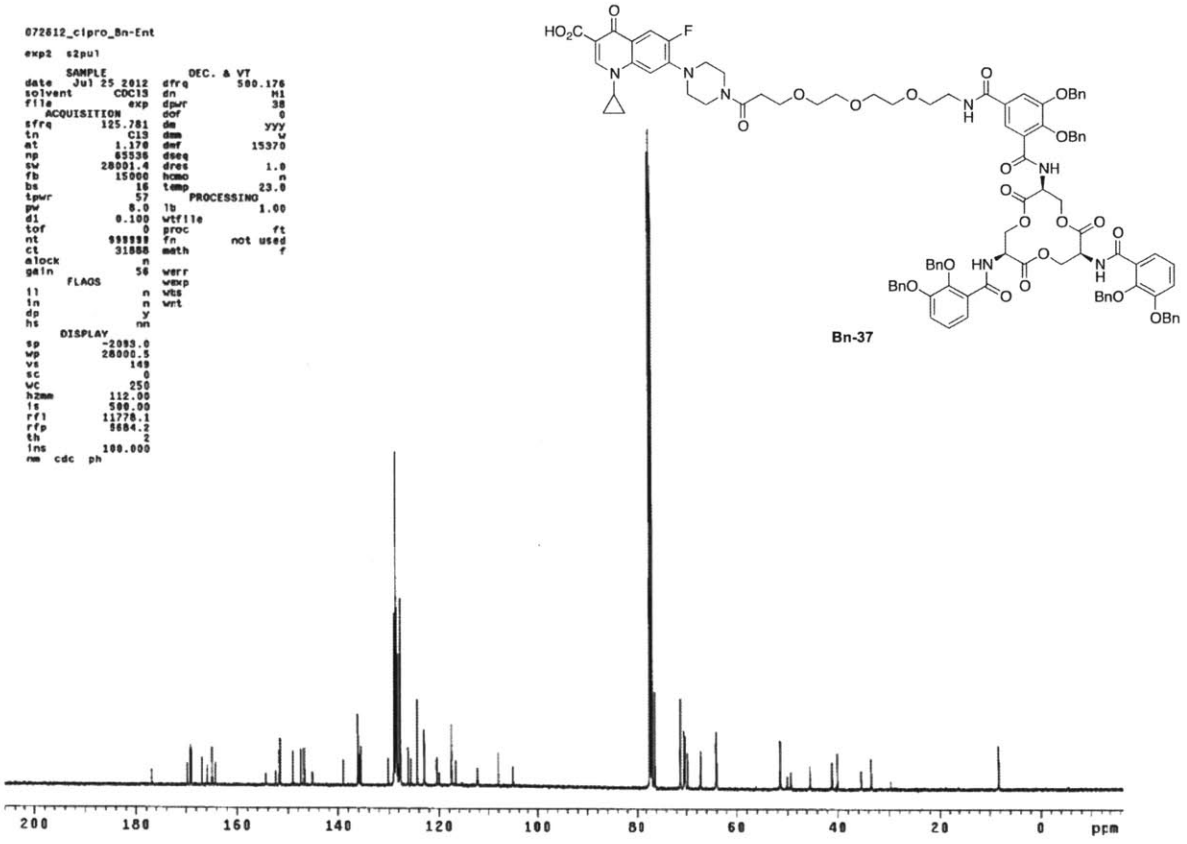
072812_cipro_Bn-Ent
exp2 s2pul
SAMPLE
date Jul 25 2012
solvent CDCl3
file exp
ACQUISITION
sfrq 125.781
tn C13
at 1.170
np 65536
sw 28001.4
fb 15000
bs 16
tpwr 57
pw 8.0
d1 0.100
tof 0
nt 999999
ct 31888
alock n
gain 58
FLAGS
DISPLAY
sp -2089.0
wp 28000.5
vs 149
sc 0
wc 250
hzmm 112.00
is 500.00
rf1 11778.1
rfp 9684.2
th 2
ins 100.000
nm cdc ph
DEC. & VT
dfrq 500.176
dn H1
dpwr 38
dof 0
dm yyy
dmm w
dmf 15370
dseq
dres 1.0
homo n
temp 23.0
PROCESSING
lb 1.00
wtfile
proc ft
fn not used
math f
werr
wexp
wbs
wnt
Bn-37
200
180
160
140
120
100
80
60
40
20
0
ppm

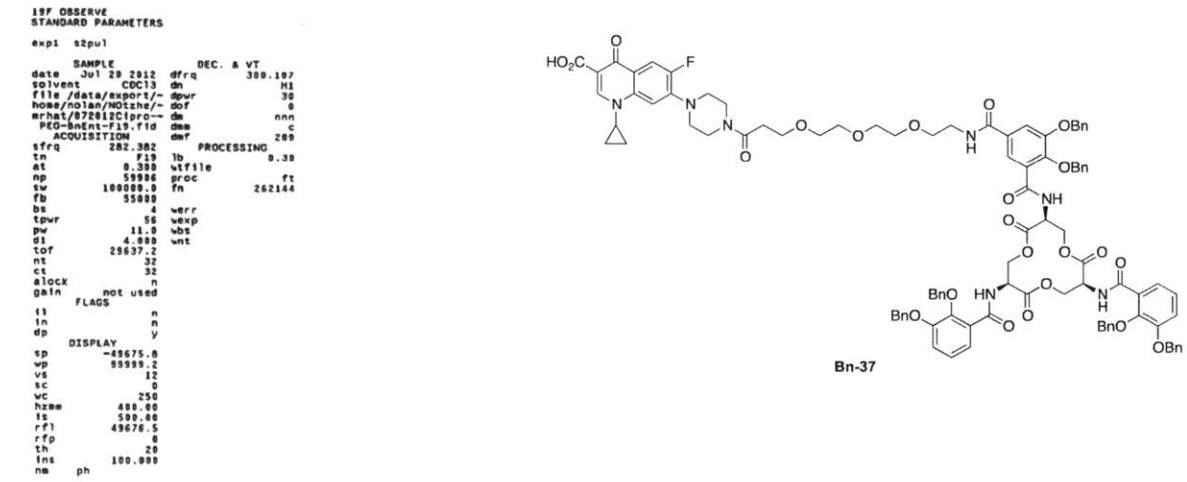
19F OBSERVE
STANDARD PARAMETERS
exp1 s2pul
SAMPLE
date Jul 29 2012
solvent CDCl3
file /data/export/~
home/nolan/NOtizhe/~
mrhat/072812Cipro~n
PEG-BnEnt-F19.fid
ACQUISITION
sfrq 282.382
tn F19
at 0.380
np 59986
sw 108089.0
fb 55000
bs 4
tpwr 56
pw 11.0
d1 4.000
tof 29637.2
nt 32
ct 32
alock n
gain not used
FLAGS
DISPLAY
sp -49675.8
wp 99999.2
vs 12
sc 0
wc 250
hzmm 488.60
is 500.00
rf1 49676.5
rfp 0
th 20
ins 100.000
nm ph
DEC. & VT
dfrq 300.187
dn H1
dpwr 38
dof 0
dm nnn
dmm c
dmf 209
PROCESSING
lb 0.30
wtfile
proc ft
fn 262144
Bn-37
150
100
50
0
-50
-100
-150
ppm

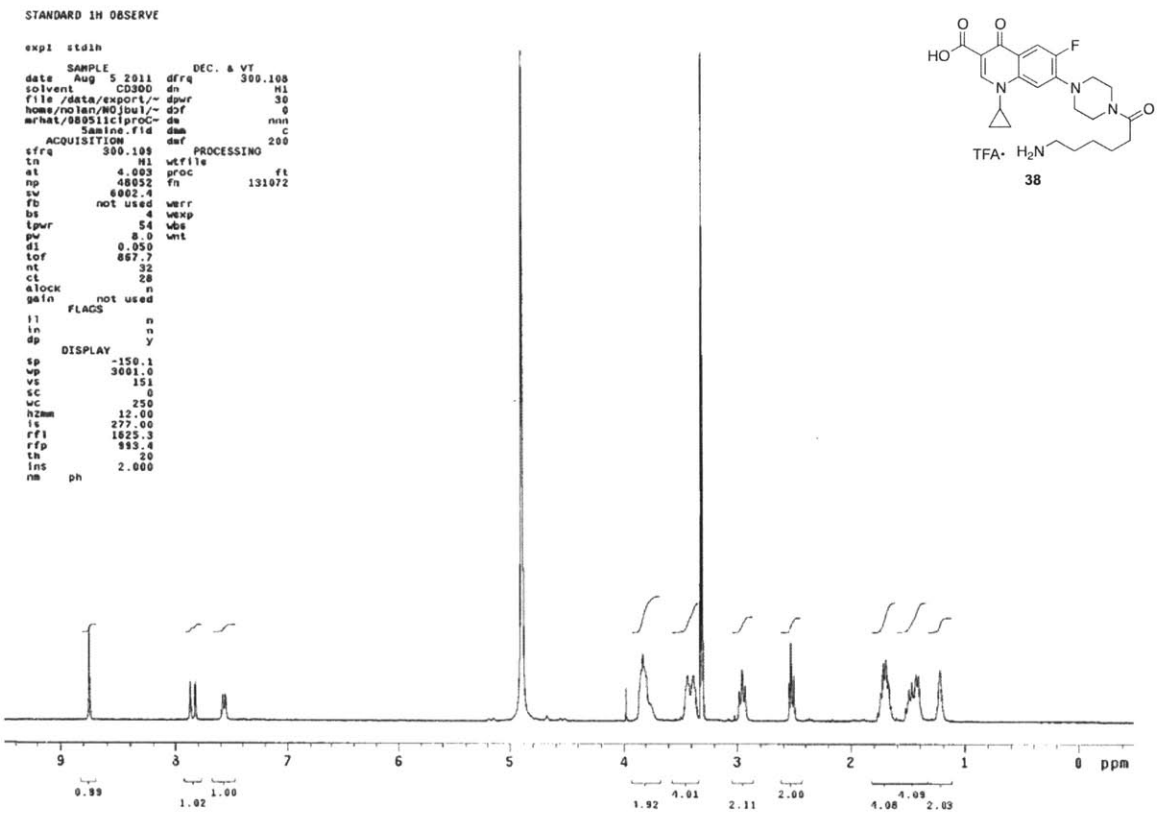
STANDARD 1H OBSERVE
expl stdih
SAMPLE
date Aug 5 2011
solvent CD3OD
file /data/export/~
home/nolan/NOjbul/~
mrhat/080511ciproC~
5amine.fid
ACQUISITION
sfrq 300.109
tn H1
at 4.003
np 48052
sw 6002.4
fb not used
bs 4
tpwr 54
pw 8.0
d1 0.050
tof 867.7
nt 32
ct 28
alock n
gain not used
FLAGS
il n
in n
dp y
DISPLAY
sp -150.1
wp 3001.0
vs 151
sc 0
wc 250
hzmm 12.00
is 277.00
rfl 1625.3
rfp 993.4
th 20
ins 2.000
nm ph
DEC. & VT
dfrq 300.108
dn H1
dpwr 30
dof 0
dm nnn
dmm c
dmf 200
PROCESSING
wtfile
proc ft
fn 131072
werr
wexp
wbs
wnt
HO
O
O
F
N
N
N
O
TFA· H2N
38
9
8
7
6
5
4
3
2
1
0 ppm
0.99
1.02
1.00
1.92
4.01
2.11
2.00
4.08
4.09
2.03

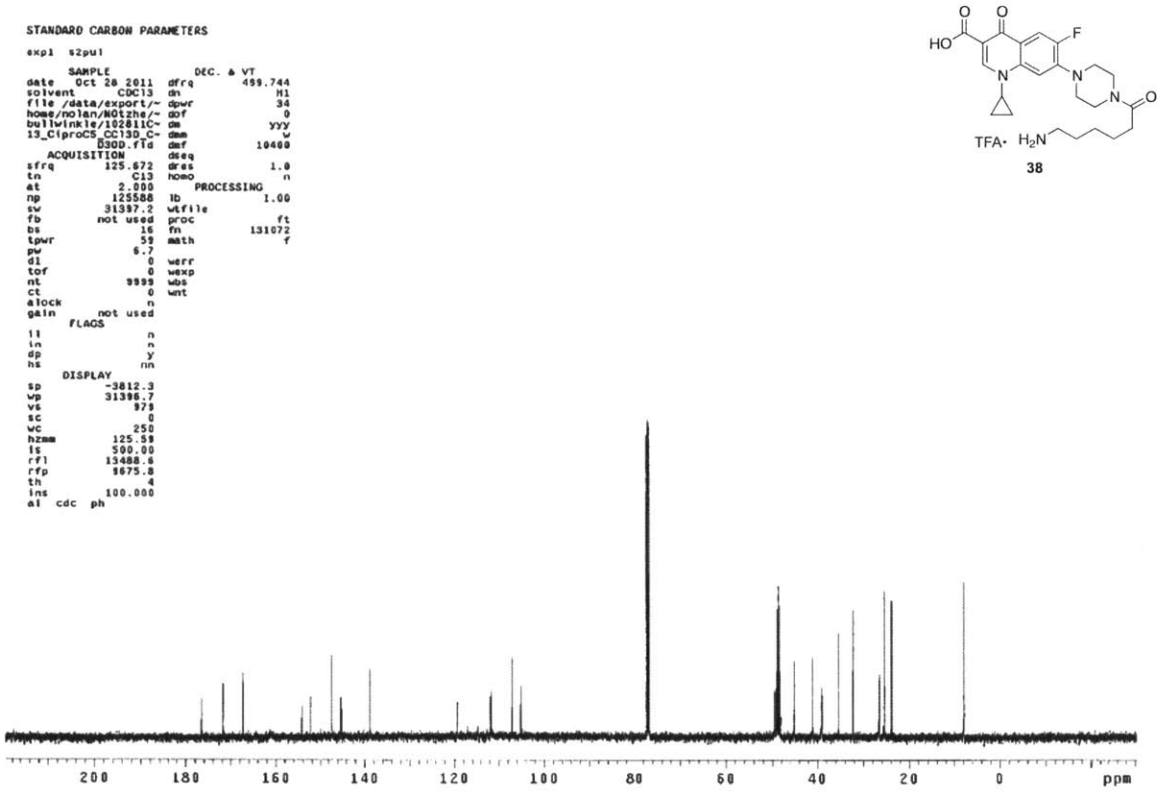
STANDARD CARBON PARAMETERS
expl s2pul
SAMPLE
date Oct 28 2011
solvent CDCl3
file /data/export/~
home/nolan/NOtzhe/~
bullwinkle/102811C~
13_CiproCS_CC13D_C~
D30D.fid
ACQUISITION
sfrq 125.672
tn C13
at 2.000
np 125588
sw 31397.2
fb not used
bs 16
tpwr 59
pw 6.7
d1 0
tof 0
nt 9999
ct 0
alock n
gain not used
FLAGS
il n
in n
dp y
hs nn
DISPLAY
sp -3812.3
wp 31396.7
vs 979
sc 0
wc 250
hzmm 125.59
is 500.00
rfl 13488.6
rfp 9675.8
th 4
ins 100.000
ai cdc ph
DEC. & VT
dfrq 499.744
dn H1
dpwr 34
dof 0
dm yyy
dmm w
dmf 10480
dseq
dres 1.0
homo n
PROCESSING
lb 1.00
wtfile
proc ft
fn 131072
math f
werr
wexp
wbs
wnt
HO
O
O
F
N
N
N
O
TFA· H2N
38
200
180
160
140
120
100
80
60
40
20
0
ppm

19F OBSERVE
STANDARD PARAMETERS

expl s2pul

SAMPLE		DEC. & VT	
date	Oct 28 2011	dfrq	300.107
solvent	CDCl3	dn	H1
file	/data/export/~	dpwr	39
home/nolan/NOlzhe/~		dof	0
mrhat/102811F19Cip~		dm	nnn
	roC5.fid	dmm	c
ACQUISITION		dmf	200
sfrq	282.382	PROCESSING	
tn	F19	lb	0.30
at	0.300	wtfile	
np	59904	proc	ft
sw	100000.0	fn	262144
fb	55000		
bs	4	werr	
tpwr	56	wexp	
pw	11.0	wbs	
d1	4.000	wnt	
tof	29637.2		
nt	64		
ct	64		
alock	n		
gain	not used		
FLAGS			
ll	n		
in	n		
dp	y		
DISPLAY			
sp	-48635.3		
wp	99999.2		
vs	101		
sc	0		
wc	250		
hzmm	400.00		
is	2.5e+08		
rfl	49636.1		
rfp	0		
th	6		
ins	1.000		
nm	ph		

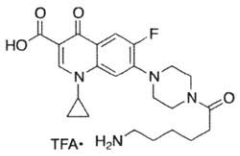

38

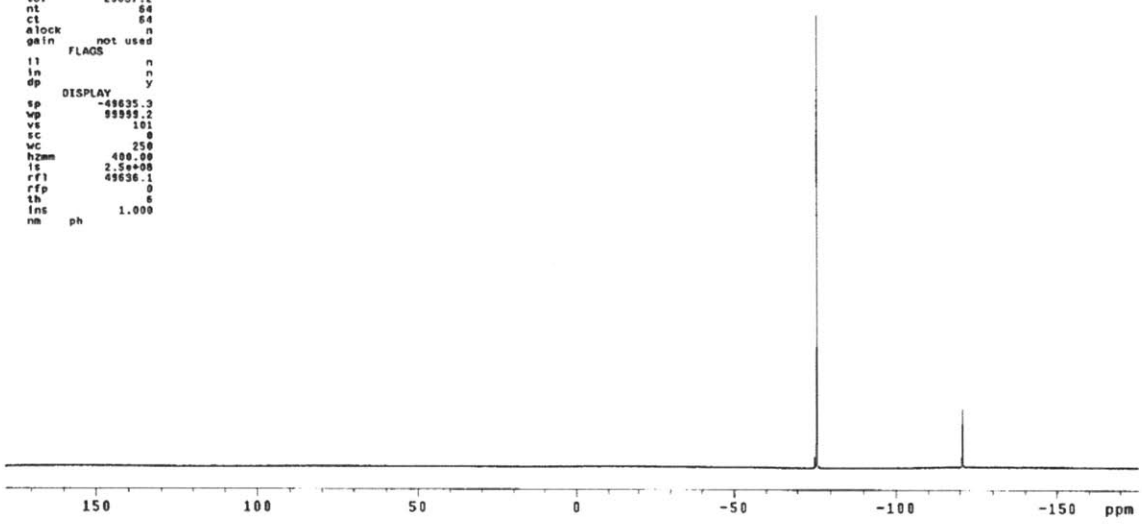

STANDARD 1H OBSERVE

expl stdih

SAMPLE		DEC. & VT	
date	Aug 1 2011	dfrq	300.107
solvent	CDCl3	dn	H1
file	/data/export/~	dpwr	39
home/nolan/NOlzhe/~		dof	0
mrhat/080111cipro~~		dm	nnn
	stable-Boc.fid	dmm	c
ACQUISITION		dmf	200
sfrq	300.108	PROCESSING	
tn	H1	wtfile	
at	4.083	proc	ft
np	48052	fn	131072
sw	6002.4		
fb	not used	werr	
bs	4	wexp	
tpwr	54	wbs	
pw	8.0	wnt	
d1	0.050		
tof	867.7		
nt	16		
ct	16		
alock	n		
gain	not used		
FLAGS			
ll	n		
in	n		
dp	y		
DISPLAY			
sp	-150.1		
wp	4801.7		
vs	151		
sc	0		
wc	250		
hzmm	19.21		
is	181.52		
rfl	2812.5		
rfp	2178.8		
th	20		
ins	2.000		
nm	ph		

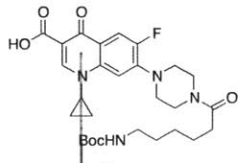

40

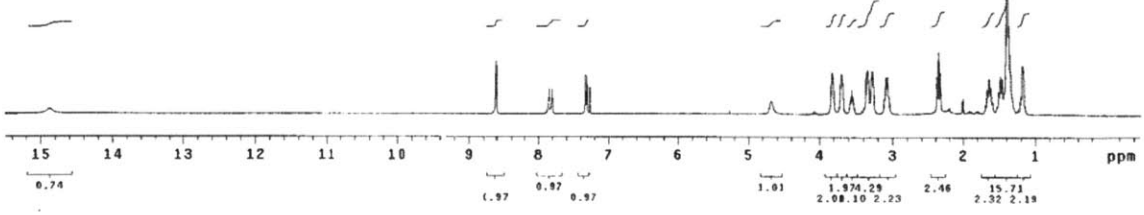

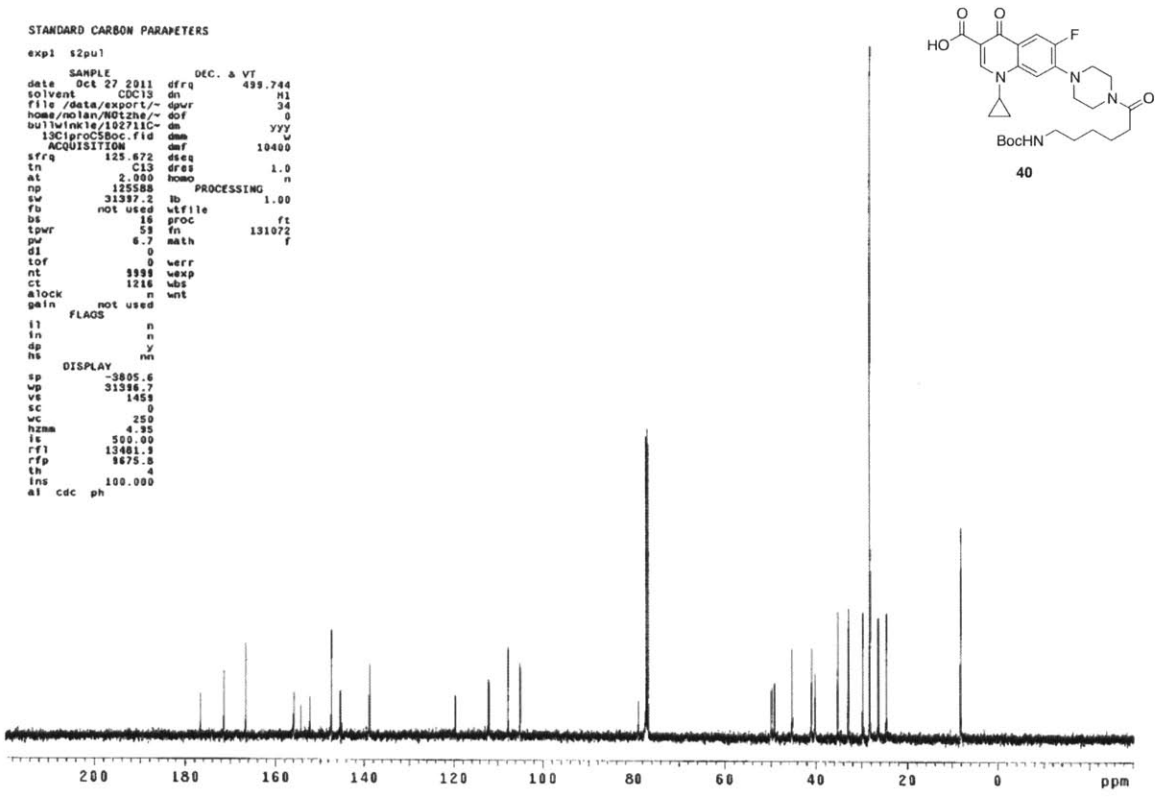
STANDARD CARBON PARAMETERS
expl s2pul
SAMPLE
date Oct 27 2011
solvent CDCl3
file /data/export/~
home/nolan/NOtzhe/~
bullwinkle/102711C~
13CiproC5Boc.fid
ACQUISITION
sfrq 125.672
tn C13
at 2.000
np 125588
sw 31397.2
fb not used
bs 16
tpwr 53
pw 6.7
d1 0
tof 0
nt 9999
ct 1216
alock n
gain not used
FLAGS
il n
in n
dp y
hs nn
DISPLAY
sp -3805.6
wp 31396.7
vs 1453
sc 0
wc 250
hzmm 4.95
is 500.00
rfl 13481.9
rfp 9675.8
th 4
ins 100.000
al cdc ph
DEC. & VT
dfrq 499.744
dn H1
dpwr 34
dof 0
dm yyy
dmm w
dmf 10400
dseq
dres 1.0
homo n
PROCESSING
lb 1.00
wtfile
proc ft
fn 131072
math f
werr
wexp
wbs
wnt
HO
F
BocHN
40
200
180
160
140
120
100
80
60
40
20
0
ppm

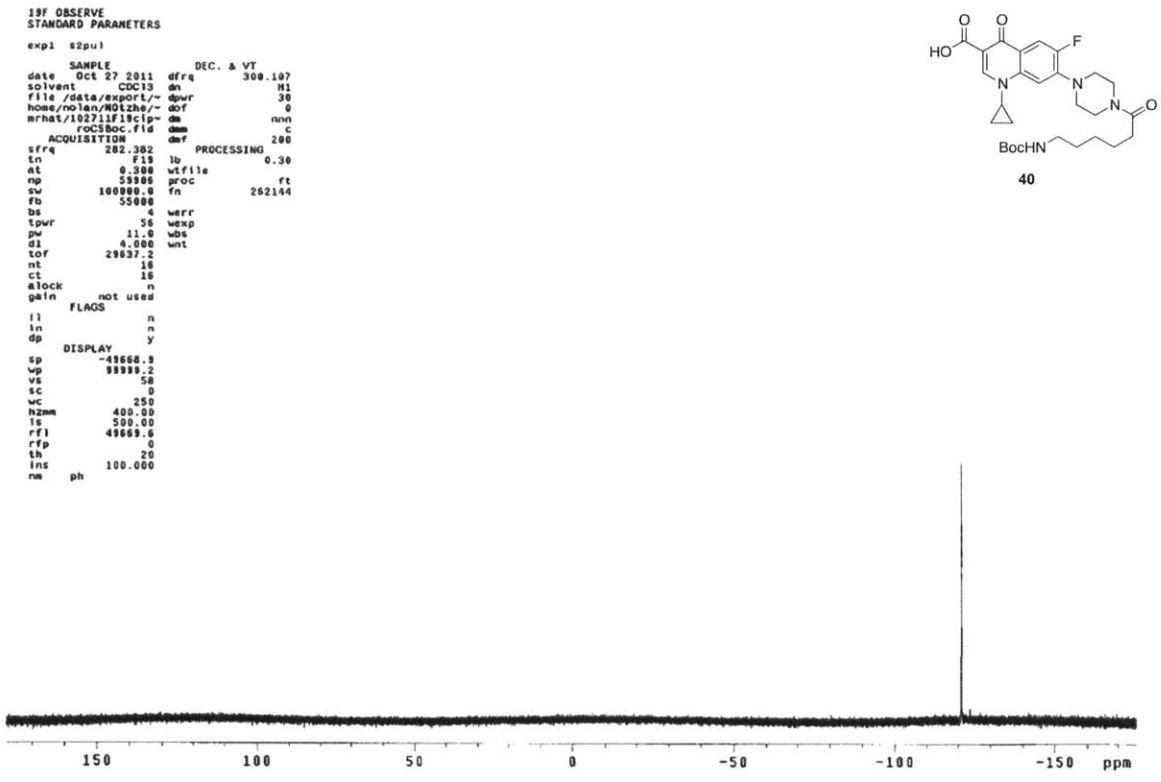
19F OBSERVE
STANDARD PARAMETERS
expl s2pul
SAMPLE
date Oct 27 2011
solvent CDCl3
file /data/export/~
home/nolan/NOtzhe/~
mrhat/102711f19cip~
roC5Boc.fid
ACQUISITION
sfrq 282.382
tn F19
at 0.300
np 59306
sw 100000.0
fb 55000
bs 4
tpwr 56
pw 11.0
d1 4.000
tof 29637.2
nt 16
ct 16
alock n
gain not used
FLAGS
il n
in n
dp y
DISPLAY
sp -49668.8
wp 99999.2
vs 58
sc 0
wc 250
hzmm 400.00
is 500.00
rfl 49669.6
rfp 0
th 20
ins 100.000
nm ph
DEC. & VT
dfrq 300.107
dn H1
dpwr 30
dof 0
dm nnn
dmm c
dmf 200
PROCESSING
lb 0.30
wtfile
proc ft
fn 262144
werr
wexp
wbs
wnt
HO
F
BocHN
40
150
100
50
0
-50
-100
-150
ppm

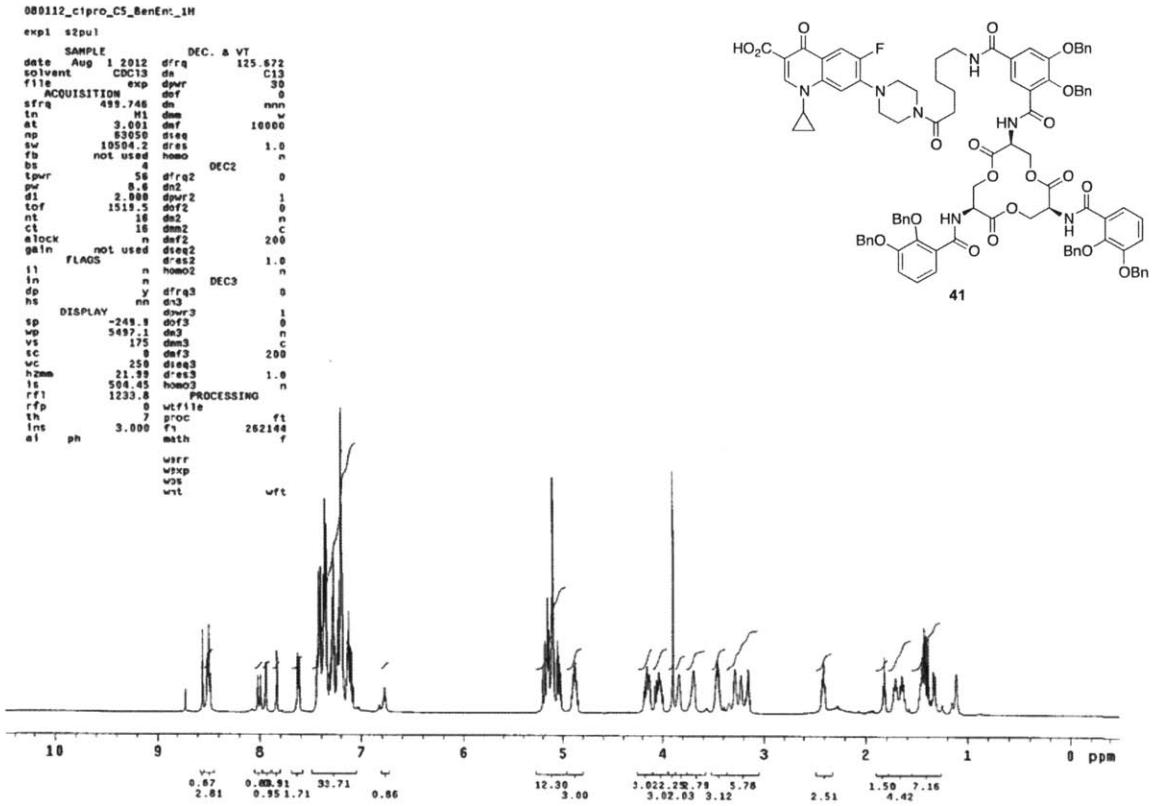
080112_cipro_C5_BenEnt_1H
exp1 s2pul
SAMPLE
date Aug 1 2012
solvent CDCl3
file exp
ACQUISITION
sfrq 499.746
tn H1
at 3.001
np 63050
sw 10504.2
fb not used
bs 4
tpwr 56
pw 8.6
d1 2.000
tof 1519.5
nt 16
ct 16
alock n
gain not used
FLAGS
il n
in n
dp y
hs nn
DISPLAY
sp -249.1
wp 5497.1
vs 175
sc 0
wc 250
hzmm 21.99
is 504.45
rfl 1233.8
rfp 0
th 7
ins 3.000
ai ph
DEC. & VT
dfrq 125.672
dn C13
dpwr 30
dof 0
dm nnn
dmm w
dmf 10000
dseq
dres 1.0
homo n
DEC2
dfrq2 0
dn2
dpwr2 1
dof2 0
dm2 n
dmm2 c
dmf2 200
dseq2
dres2 1.0
homo2 n
DEC3
dfrq3 0
dn3
dpwr3 1
dof3 0
dm3 n
dmm3 c
dmf3 200
dseq3
dres3 1.0
homo3 n
PROCESSING
wtfile
proc ft
fn 262144
math f
wrr
wexp
wbs
wnt wft
HO2C
F
OBn
BnO
HN
41
10
9
8
7
6
5
4
3
2
1
0 ppm
0.87
2.81
0.91
0.95
1.71
33.71
0.86
12.30
3.00
3.02
3.02
3.12
5.78
2.51
1.50
4.42
7.16

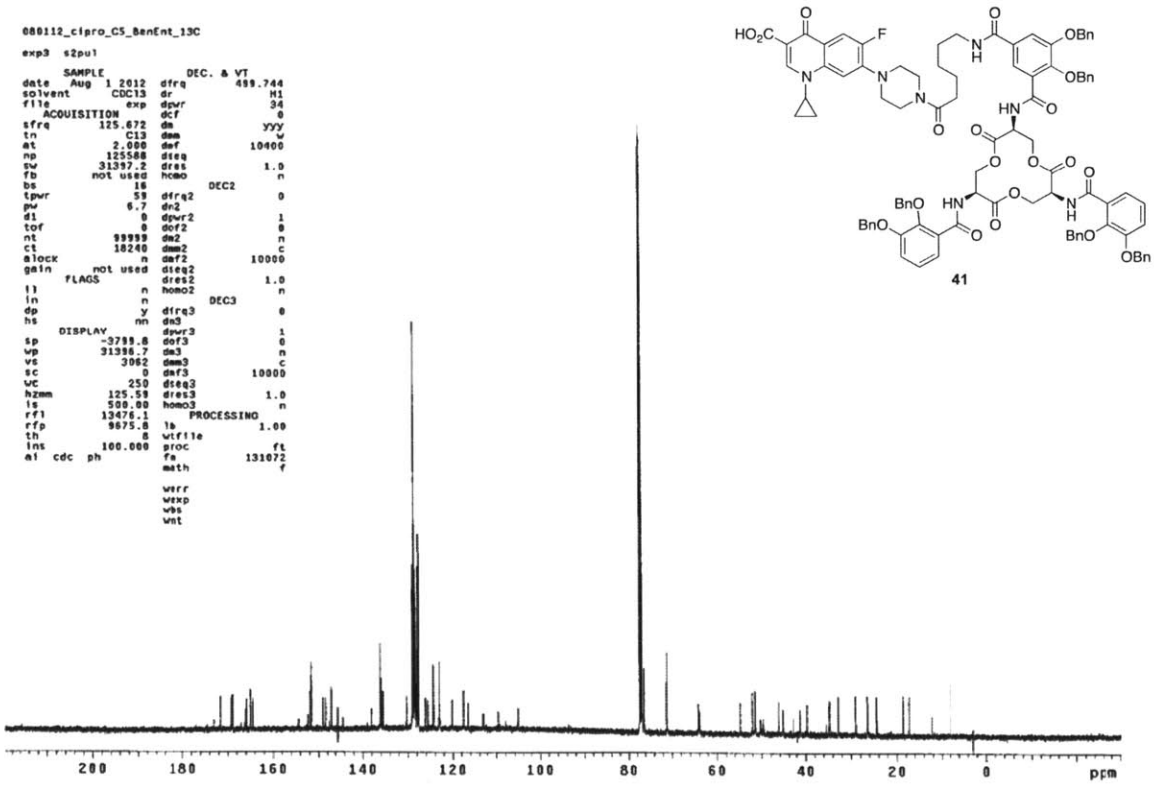
080112_cipro_C5_BenEnt_13C
exp3 s2pul
SAMPLE
date Aug 1 2012
solvent CDCl3
file exp
ACQUISITION
sfrq 125.672
tn C13
at 2.000
np 125588
sw 31397.2
fb not used
bs 16
tpwr 59
pw 6.7
d1 0
tof 0
nt 99999
ct 18240
alock n
gain not used
FLAGS
il n
in n
dp y
hs nn
DISPLAY
sp -3799.8
wp 31396.7
vs 3062
sc 0
wc 250
hzmm 125.59
is 500.00
rfl 13476.1
rfp 9675.8
th 8
ins 100.000
ai cdc ph
DEC. & VT
dfrq 499.744
dn H1
dpwr 34
dof 0
dm yyy
dmm w
dmf 10400
dseq
dres 1.0
homo n
DEC2
dfrq2 0
dn2
dpwr2 1
dof2 0
dm2 n
dmm2 c
dmf2 10000
dseq2
dres2 1.0
homo2 n
DEC3
dfrq3 0
dn3
dpwr3 1
dof3 0
dm3 n
dmm3 c
dmf3 10000
dseq3
dres3 1.0
homo3 n
PROCESSING
lb 1.00
wtfile
proc ft
fn 131072
math f
wrr
wexp
wbs
wnt
HO2C
F
OBn
BnO
HN
41
200
180
160
140
120
100
80
60
40
20
0
ppm

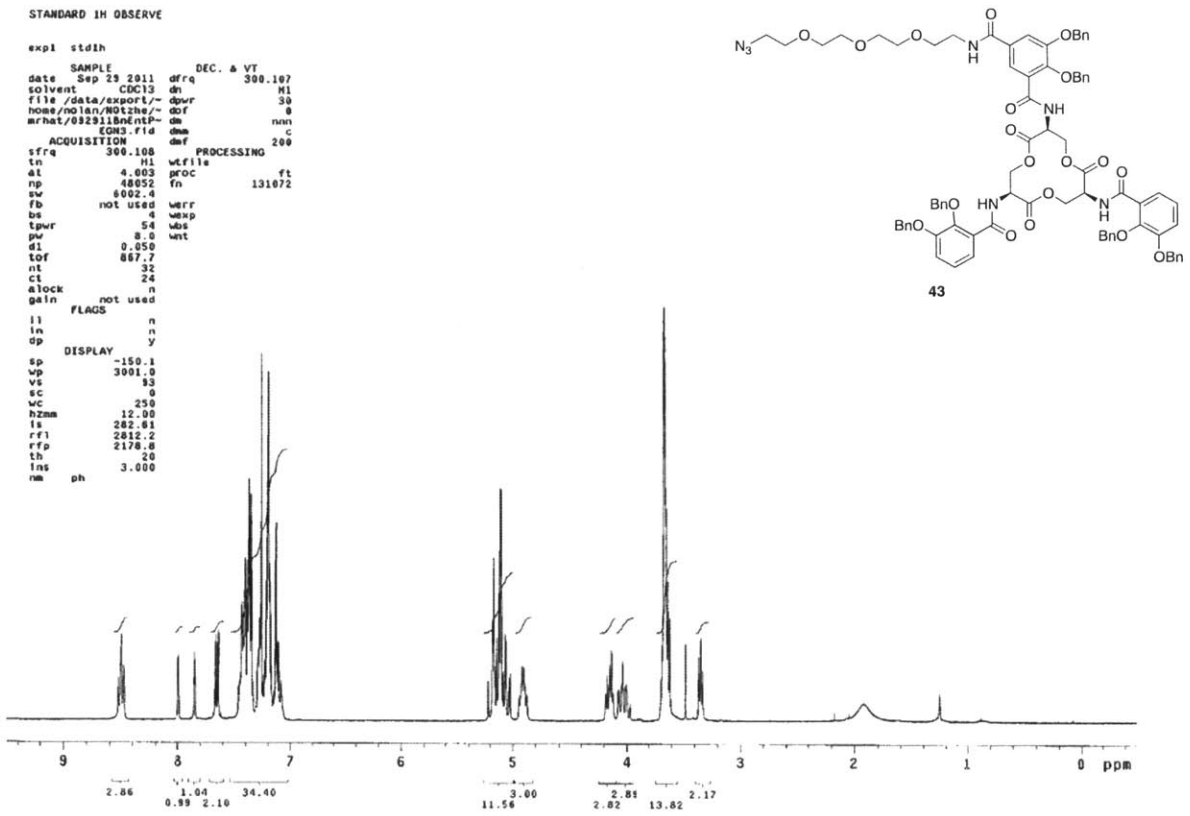
STANDARD 1H OBSERVE
expl stdih
SAMPLE
date Sep 23 2011
solvent CDCl3
file /data/export/~
home/nolan/NOtzhe/~
mrhat/032911bnEntP~
EGN3.fid
ACQUISITION
sfrq 300.108
tn H1
at 4.003
np 48052
sw 6002.4
fb not used
bs 4
tpwr 54
pw 8.0
d1 0.050
tof 867.7
nt 32
ct 24
alock n
gain not used
FLAGS
il n
in n
dp y
DISPLAY
sp -150.1
wp 3001.0
vs 83
sc 0
wc 250
hzmm 12.00
is 282.61
rfl 2812.2
rfp 2178.8
th 20
ins 3.000
nm ph
DEC. & VT
dfrq 300.107
dn H1
dpwr 30
dof 0
dm nnn
dmm c
dmf 200
PROCESSING
wtfile
proc ft
fn 131072
werr
wexp
wbs
wnt
43
9
8
7
6
5
4
3
2
1
0 ppm
2.86
1.04
0.99 2.10
34.40
3.00
11.56
2.85
2.82
13.82
2.17

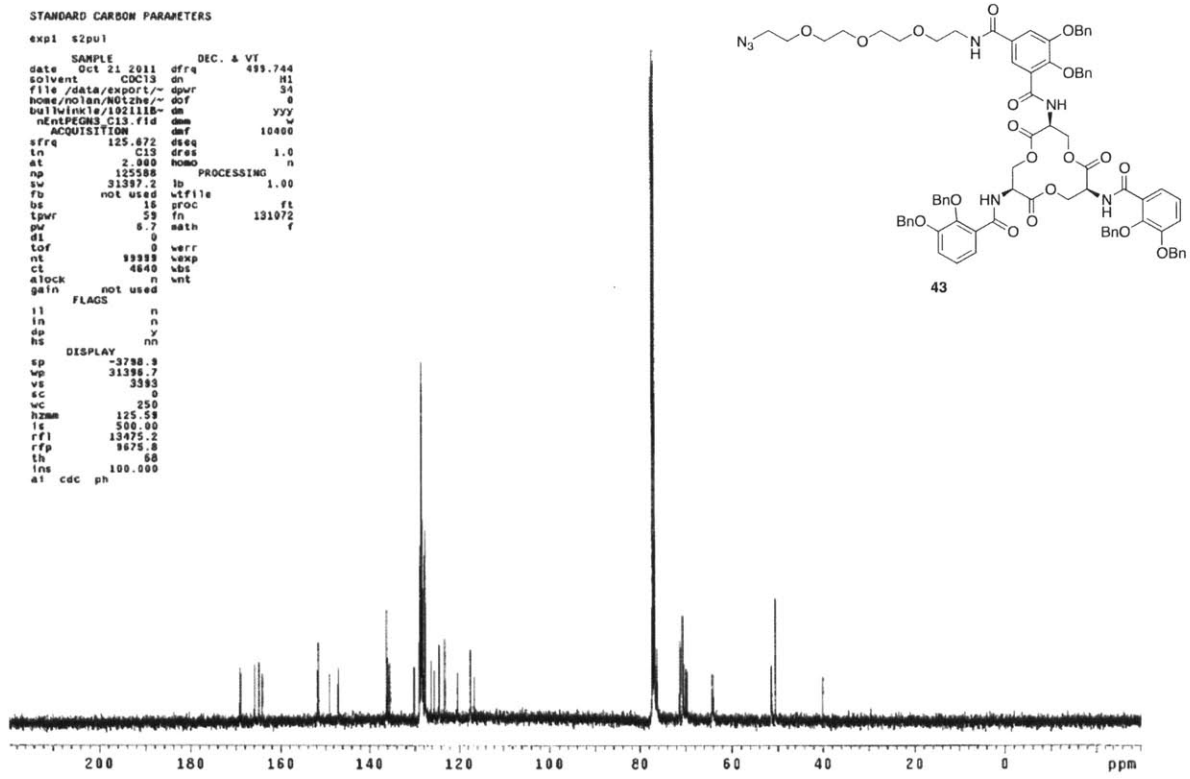
STANDARD CARBON PARAMETERS
expl s2pul
SAMPLE
date Oct 21 2011
solvent CDCl3
file /data/export/~
home/nolan/NOtzhe/~
bullwinkle/102111B~
nEntPEGN3_C13.fid
ACQUISITION
sfrq 125.672
tn C13
at 2.080
np 125588
sw 31397.2
fb not used
bs 16
tpwr 59
pw 6.7
d1 0
tof 0
nt 99999
ct 4640
alock n
gain not used
FLAGS
il n
in n
dp y
hs nn
DISPLAY
sp -3798.9
wp 31396.7
vs 3393
sc 0
wc 250
hzmm 125.59
is 500.00
rfl 13475.2
rfp 9675.8
th 68
ins 100.000
ai cdc ph
DEC. & VT
dfrq 499.744
dn H1
dpwr 34
dof 0
dm yyy
dmm w
dmf 10400
dseq
dres 1.0
homo n
PROCESSING
lb 1.00
wtfile
proc ft
fn 131072
math f
werr
wexp
wbs
wnt
43
200
180
160
140
120
100
80
60
40
20
0 ppm

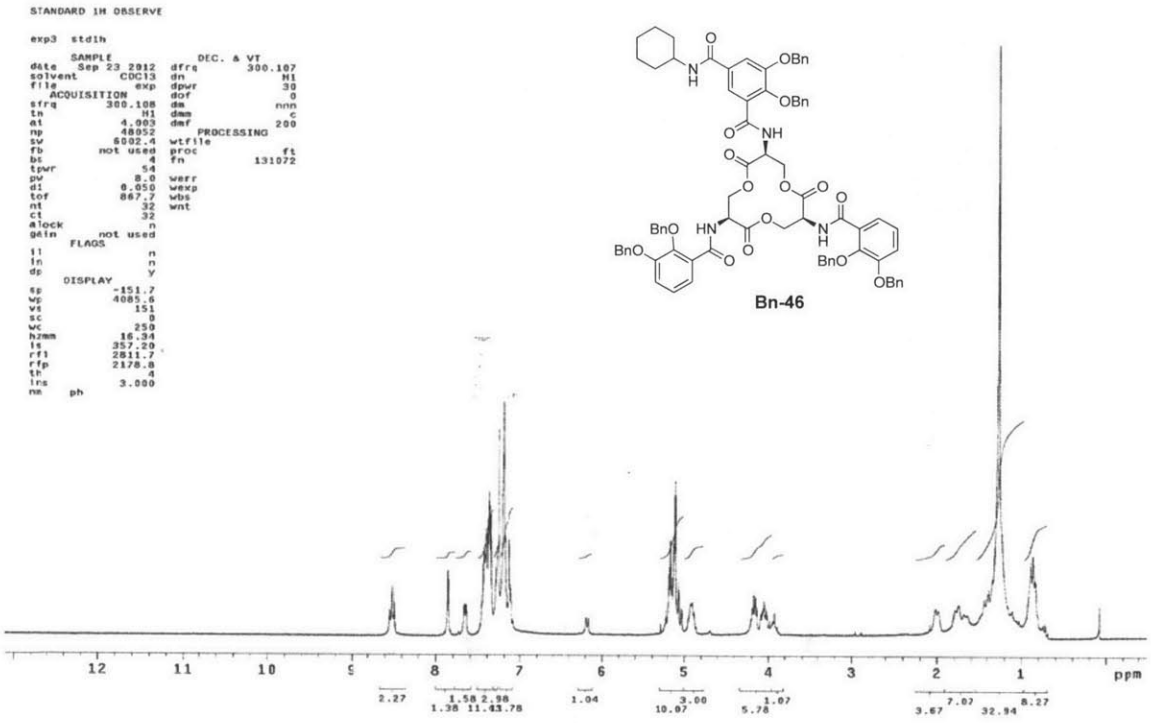
STANDARD 1H OBSERVE
exp3 std1h
SAMPLE
date Sep 23 2012
solvent CDCl3
file exp
ACQUISITION
sfrq 300.108
tn H1
at 4.003
np 48052
sw 6002.4
fb not used
bs 4
tpwr 54
pw 8.0
d1 0.050
tof 867.7
nt 32
ct 32
alock n
gain not used
FLAGS
il n
in n
dp y
DISPLAY
sp -151.7
wp 4085.6
vs 151
sc 0
wc 250
hzmm 16.34
is 357.20
rf1 2811.7
rfp 2178.8
th 4
lrs 3.000
ne ph
DEC. & VT
dfrq 300.107
dn H1
dpwr 39
dof 0
da nnn
dmm c
dmf 200
PROCESSING
wtfile
proc ft
fn 131072
werr
wexp
wbs
wnt
Bn-46
12
11
10
9
8
7
6
5
4
3
2
1
ppm
2.27
1.58 2.98
1.38 11.43.78
1.04
3.00
10.07
1.07
5.78
7.07
3.67
32.94
8.27

Chapter 2
Analytical HPLC Traces

31

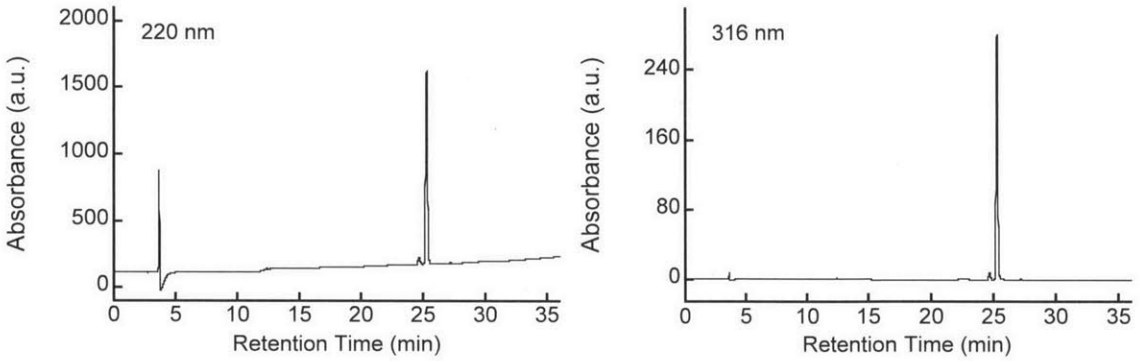
220 nm
Absorbance (a.u.)
2000
1500
1000
500
0
0 5 10 15 20 25 30 35
Retention Time (min)
316 nm
Absorbance (a.u.)
240
160
80
0
0 5 10 15 20 25 30 35
Retention Time (min)

32

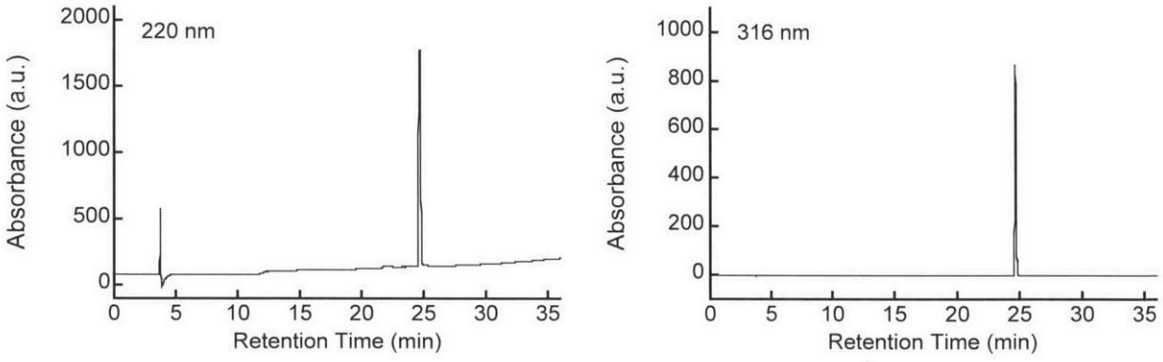
220 nm
Absorbance (a.u.)
2000
1500
1000
500
0
0 5 10 15 20 25 30 35
Retention Time (min)
316 nm
Absorbance (a.u.)
1000
800
600
400
200
0
0 5 10 15 20 25 30 35
Retention Time (min)

33

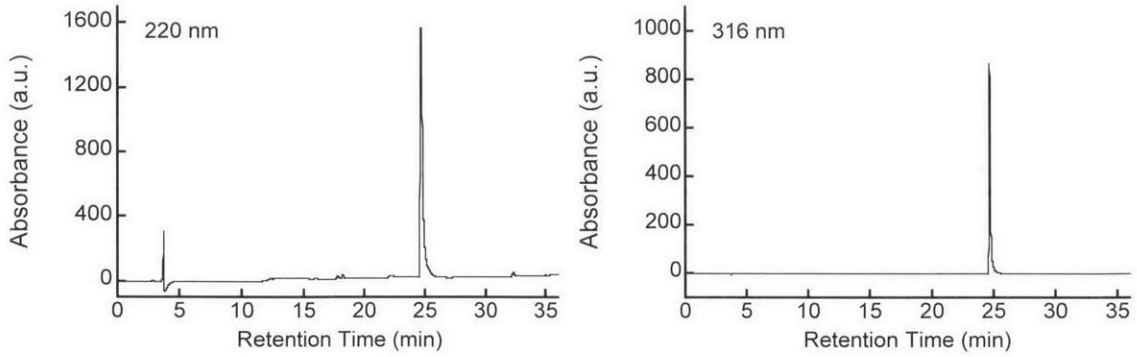
220 nm
Absorbance (a.u.)
1600
1200
800
400
0
0 5 10 15 20 25 30 35
Retention Time (min)
316 nm
Absorbance (a.u.)
1000
800
600
400
200
0
0 5 10 15 20 25 30 35
Retention Time (min)

34

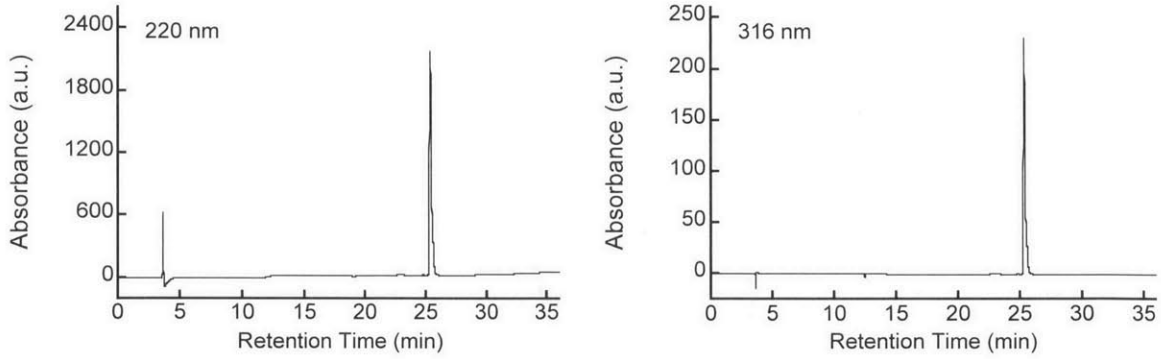
220 nm
Absorbance (a.u.)
2400
1800
1200
600
0
0 5 10 15 20 25 30 35
Retention Time (min)
316 nm
Absorbance (a.u.)
250
200
150
100
50
0
0 5 10 15 20 25 30 35
Retention Time (min)

35

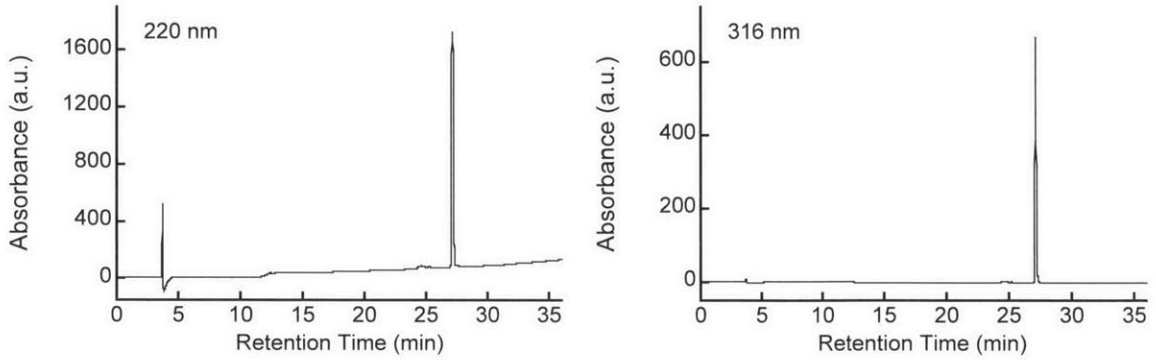
220 nm
Absorbance (a.u.)
1600
1200
800
400
0
0 5 10 15 20 25 30 35
Retention Time (min)
316 nm
Absorbance (a.u.)
600
400
200
0
0 5 10 15 20 25 30 35
Retention Time (min)

36

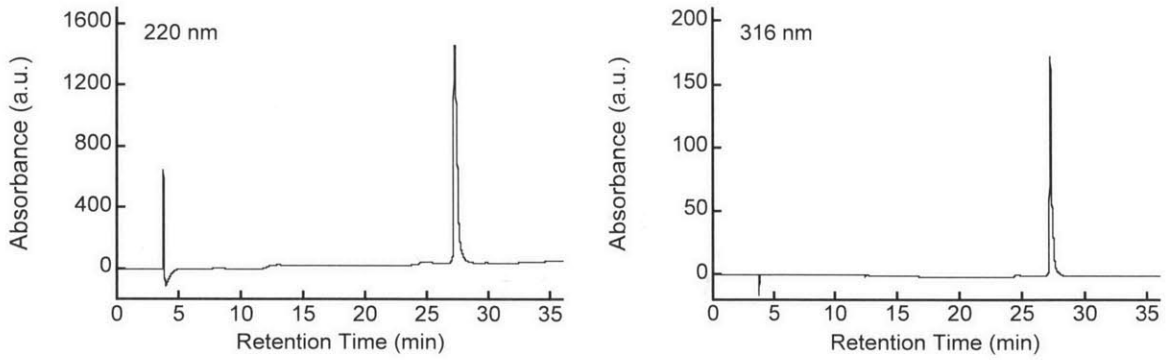
220 nm
Absorbance (a.u.)
1600
1200
800
400
0
0 5 10 15 20 25 30 35
Retention Time (min)
316 nm
Absorbance (a.u.)
200
150
100
50
0
0 5 10 15 20 25 30 35
Retention Time (min)

37

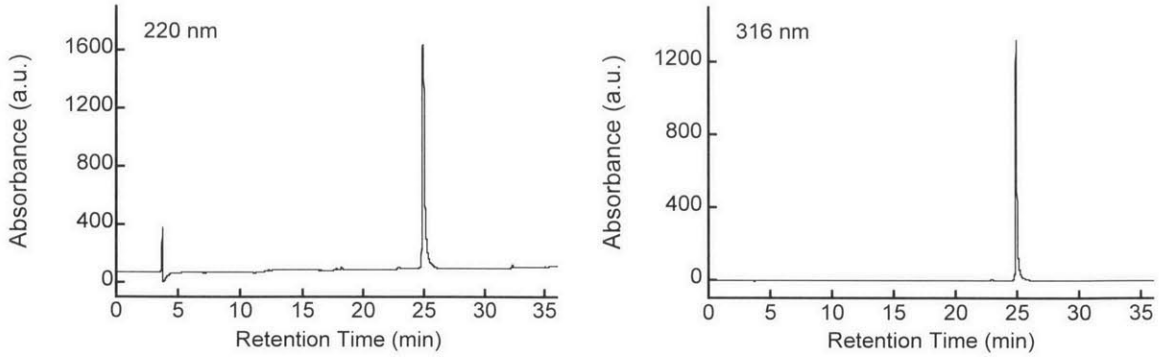
220 nm
Absorbance (a.u.)
1600
1200
800
400
0
0 5 10 15 20 25 30 35
Retention Time (min)
316 nm
Absorbance (a.u.)
1200
800
400
0
0 5 10 15 20 25 30 35
Retention Time (min)

42

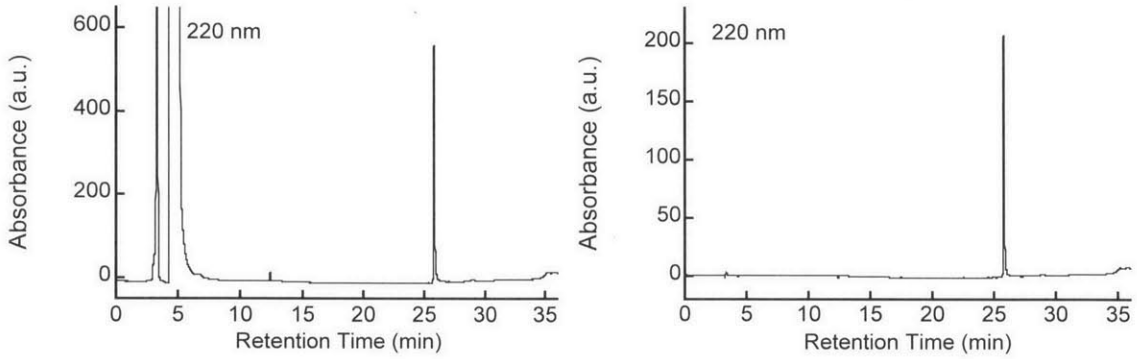
220 nm
Absorbance (a.u.)
600
400
200
0
0 5 10 15 20 25 30 35
Retention Time (min)
220 nm
Absorbance (a.u.)
200
150
100
50
0
0 5 10 15 20 25 30 35
Retention Time (min)

44

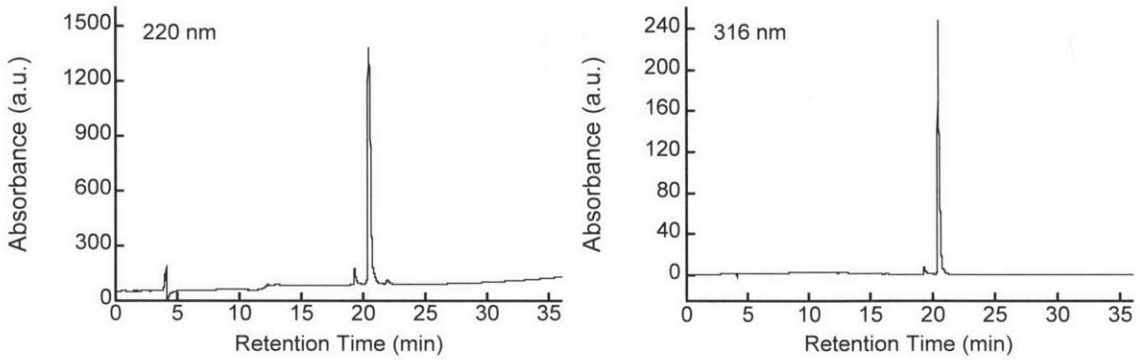
220 nm
Absorbance (a.u.)
Retention Time (min)
316 nm
Absorbance (a.u.)
Retention Time (min)

45

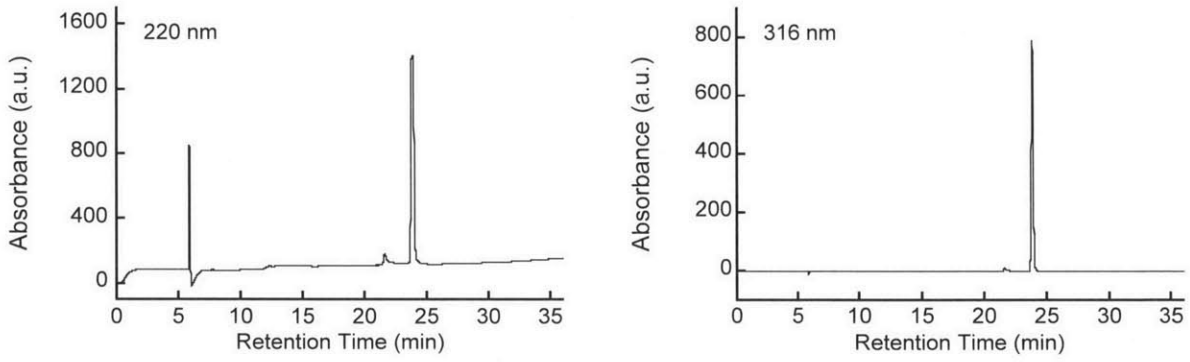
220 nm
Absorbance (a.u.)
Retention Time (min)
316 nm
Absorbance (a.u.)
Retention Time (min)

46

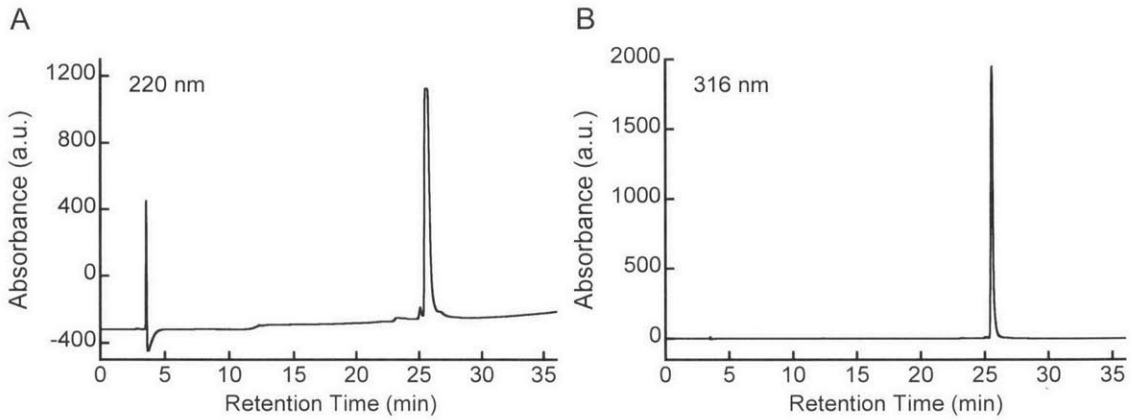
A
220 nm
Absorbance (a.u.)
1200
800
400
0
-400
0
5
10
15
20
25
30
35
Retention Time (min)
B
316 nm
Absorbance (a.u.)
2000
1500
1000
500
0
0
5
10
15
20
25
30
35
Retention Time (min)

Chapter 2
UV-Vis Spectra

L-Ent **1**

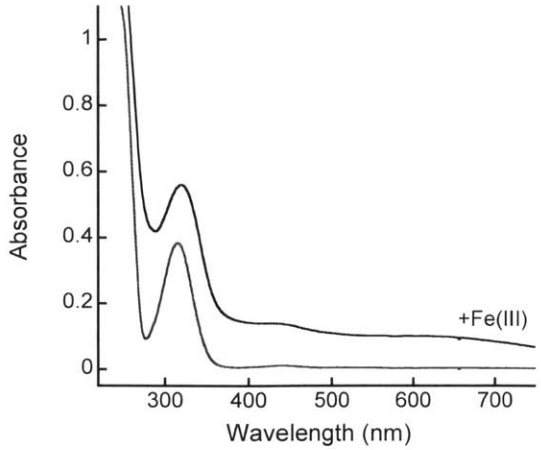

Conjugate **31**

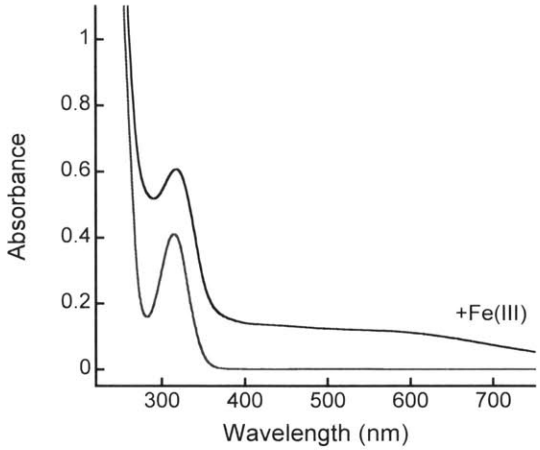

Conjugate **32**

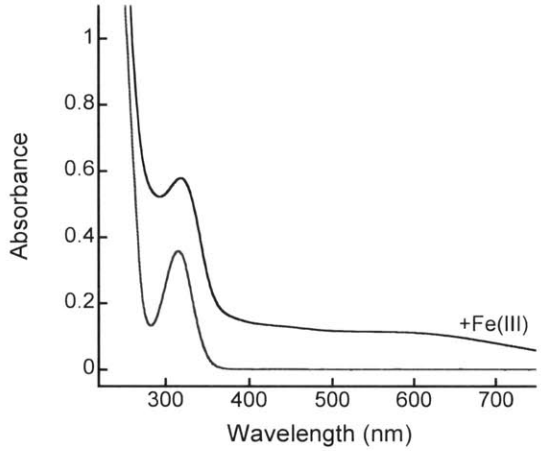

Conjugate **33**

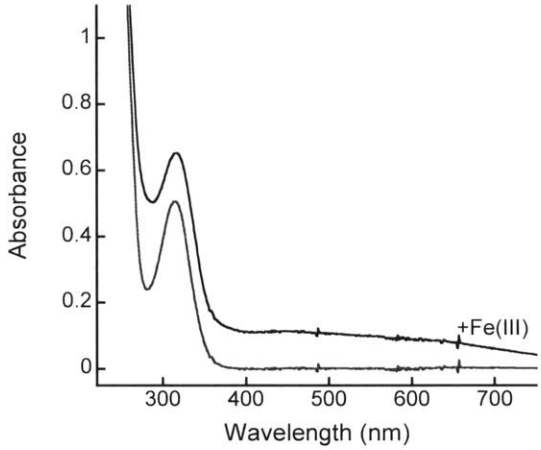

Conjugate **34**

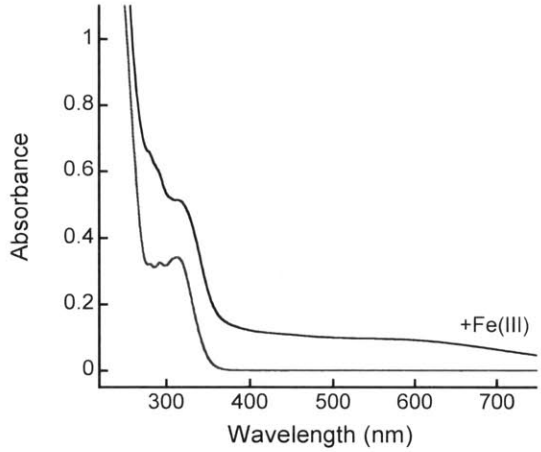

Conjugate **35**

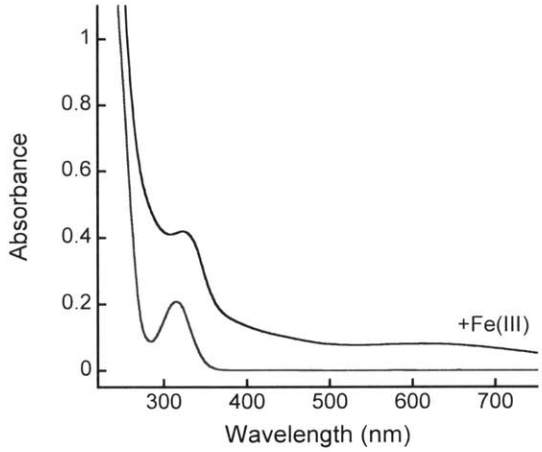

Conjugate **36**

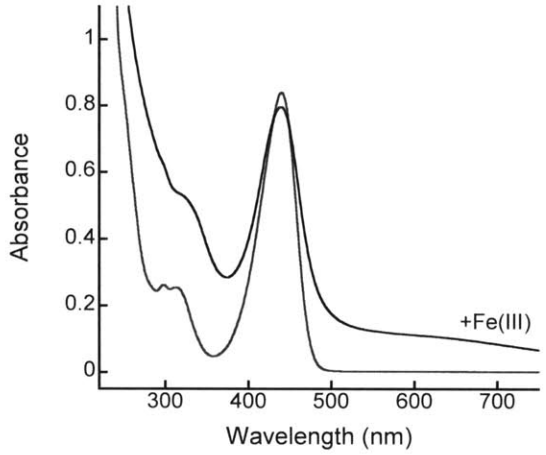

Conjugate **37**

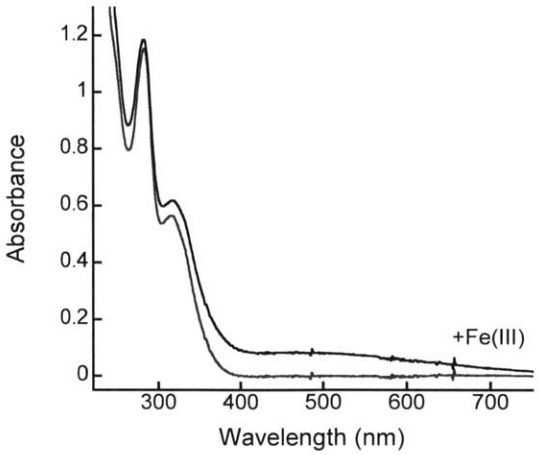

Conjugate **42**

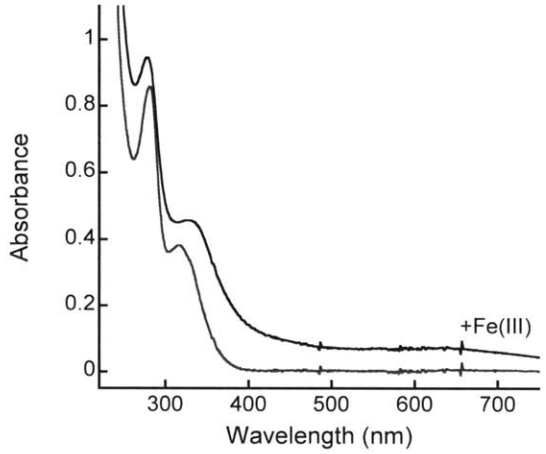

Conjugate **44**

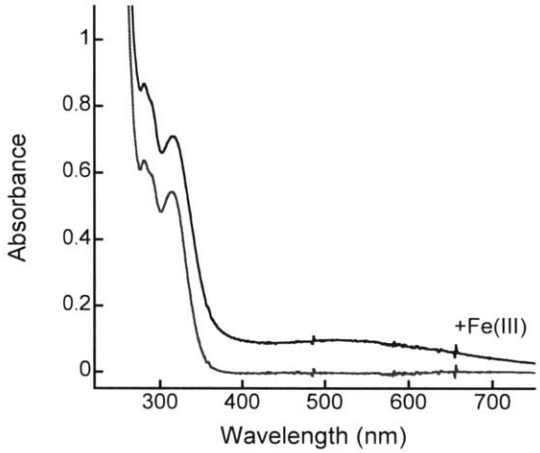

Conjugate **45**

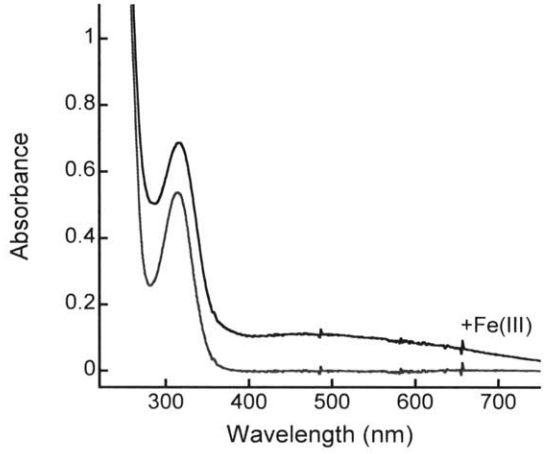

Chapter 3
NMR Spectra

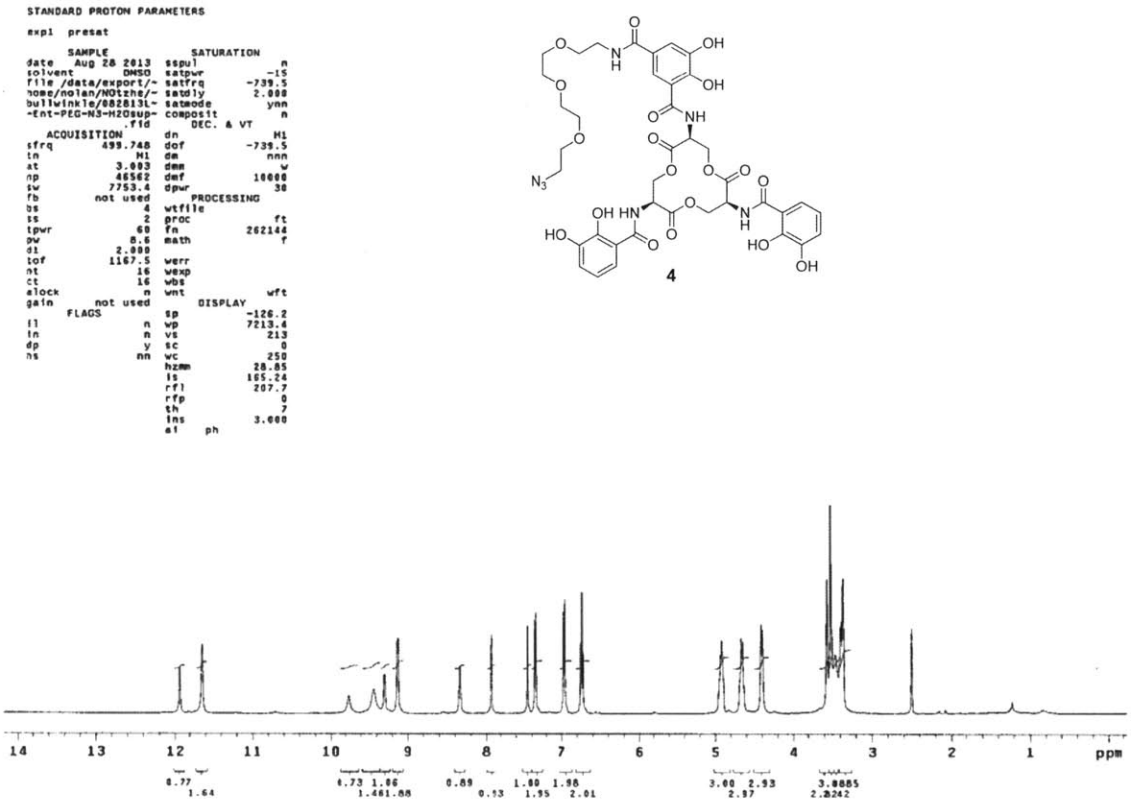
STANDARD PROTON PARAMETERS
exp1 presat
SAMPLE
date Aug 28 2013
solvent DMSO
file /data/export/~
home/nolan/NOtzhe/~
bullwinkle/082813L~
-Ent-PEG-N3-H2Osup-
.fid
ACQUISITION
sfrq 499.748
tn H1
at 3.003
np 46562
sw 7753.4
fb not used
bs 4
ss 2
tpwr 60
pw 8.6
d1 2.000
tof 1167.5
nt 16
ct 16
alock n
gain not used
FLAGS
il n
in n
dp y
hs nn
SATURATION
sspul n
satpwr -15
satfrq -739.5
satdly 2.000
satmode ynn
compsit n
DEC. & VT
dn H1
dof -739.5
dm nnn
dmm w
dmf 10000
dpwr 38
PROCESSING
wtfile
proc ft
fn 262144
math f
werr
wexp
wbs
wnt wft
DISPLAY
sp -126.2
wp 7213.4
vs 213
sc 0
wc 250
hzmm 28.85
is 185.24
rfl 207.7
rfp 0
th 7
ins 3.000
ai ph
4
14
13
12
11
10
9
8
7
6
5
4
3
2
1
ppm
0.77
1.64
6.73 1.86
1.46 1.88
0.89
0.53
1.88 1.98
1.95 2.01
3.00 2.93
2.97
3.9885
2.8242

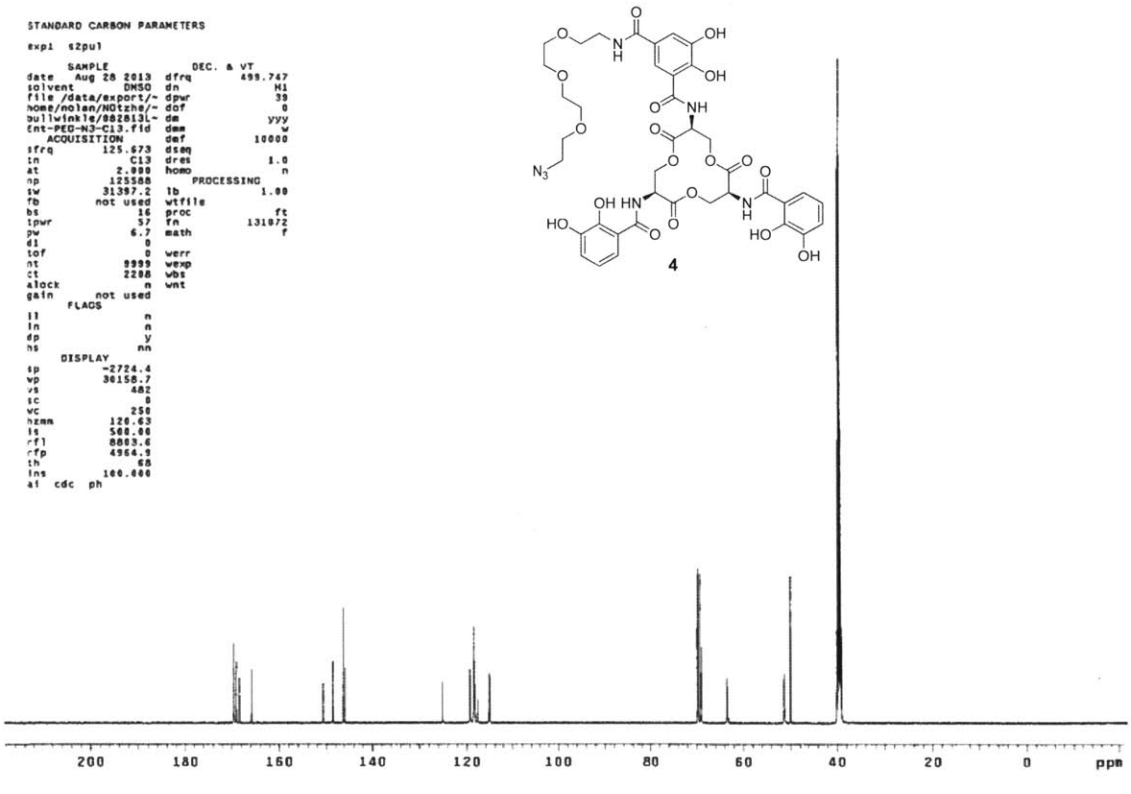
STANDARD CARBON PARAMETERS
exp1 s2pul
SAMPLE
date Aug 28 2013
solvent DMSO
file /data/export/~
home/nolan/NOtzhe/~
bullwinkle/082813L~
ent-PEG-N3-C13.fid
ACQUISITION
sfrq 125.673
tn C13
at 2.998
np 125588
sw 31397.2
fb not used
bs 16
tpwr 57
pw 6.7
d1 0
tof 0
nt 9999
ct 2208
alock n
gain not used
FLAGS
il n
in n
dp y
hs nn
DISPLAY
sp -2724.4
wp 30158.7
vs 482
sc 0
wc 250
hzmm 126.63
is 508.86
rfl 8803.6
rfp 4964.9
th 68
ins 100.000
ai cdc ph
DEC. & VT
dfrq 499.747
dn H1
dpwr 39
dof 0
dm yyy
dmm w
dmf 10000
dseq
dres 1.0
homo n
PROCESSING
lb 1.00
wtfile
proc ft
fn 131072
math f
werr
wexp
wbs
wnt
4
200
180
160
140
120
100
80
60
40
20
0
ppm

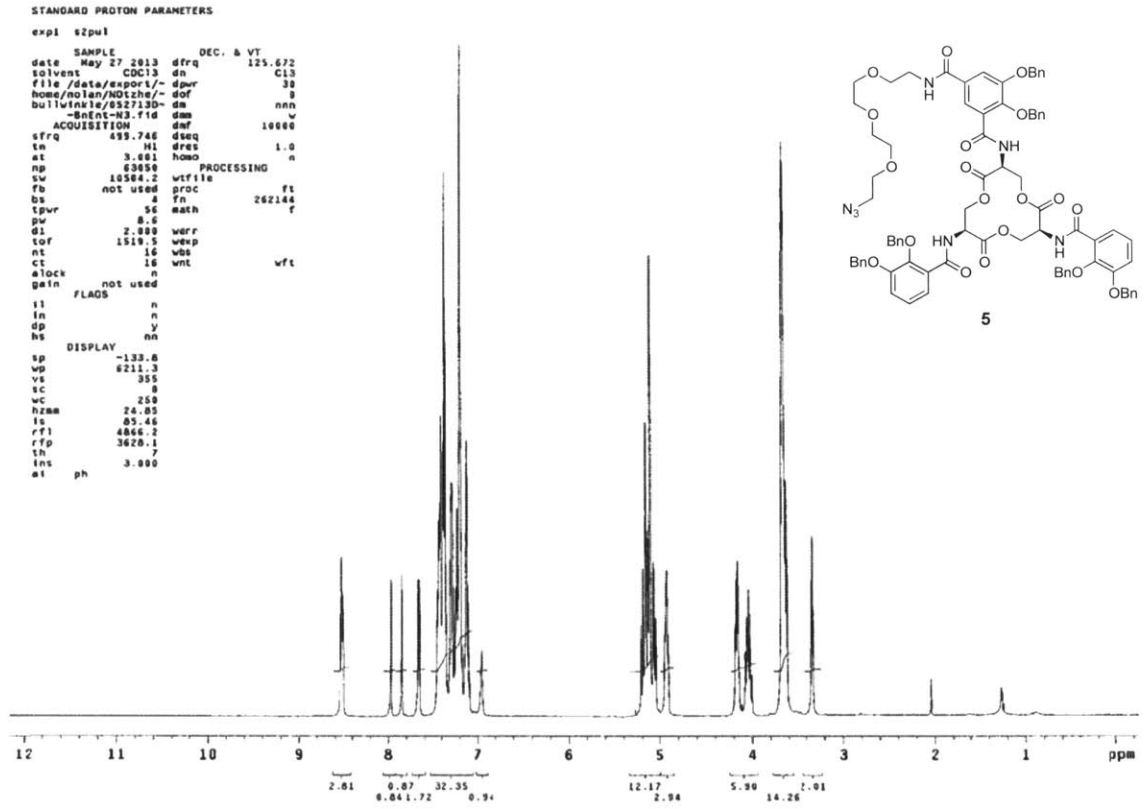
STANDARD PROTON PARAMETERS
expl s2pul
SAMPLE
date May 27 2013
solvent CDCl3
file /data/export/~
home/nolan/NOtzhe/~
bullwinkle/052713D~
~BnEnt-N3.fid
ACQUISITION
sfrq 499.746
tn H1
at 3.881
np 63850
sw 10504.2
fb not used
bs 4
tpwr 56
pw 8.6
d1 2.000
tof 1519.5
nt 16
ct 16
alock n
gain not used
FLAGS
il n
in n
dp y
hs nn
DISPLAY
sp -133.8
wp 6211.3
vs 355
sc 0
wc 250
hzmm 24.85
is 85.46
rf1 4866.2
rfp 3628.1
th 7
ins 3.000
ai ph
DEC. & VT
dfrq 125.672
dn C13
dpwr 38
dof 0
dm nnn
dmm w
dmf 10000
dseq
dres 1.0
homo n
PROCESSING
wtfile
proc ft
fn 262144
math f
werr
wexp
wbs
wnt wft
OBn
BnO
HN
NH
N3
5
12
11
10
9
8
7
6
5
4
3
2
1
ppm
2.81
0.87
0.84
1.72
32.35
0.94
12.17
2.94
5.90
14.26
2.01

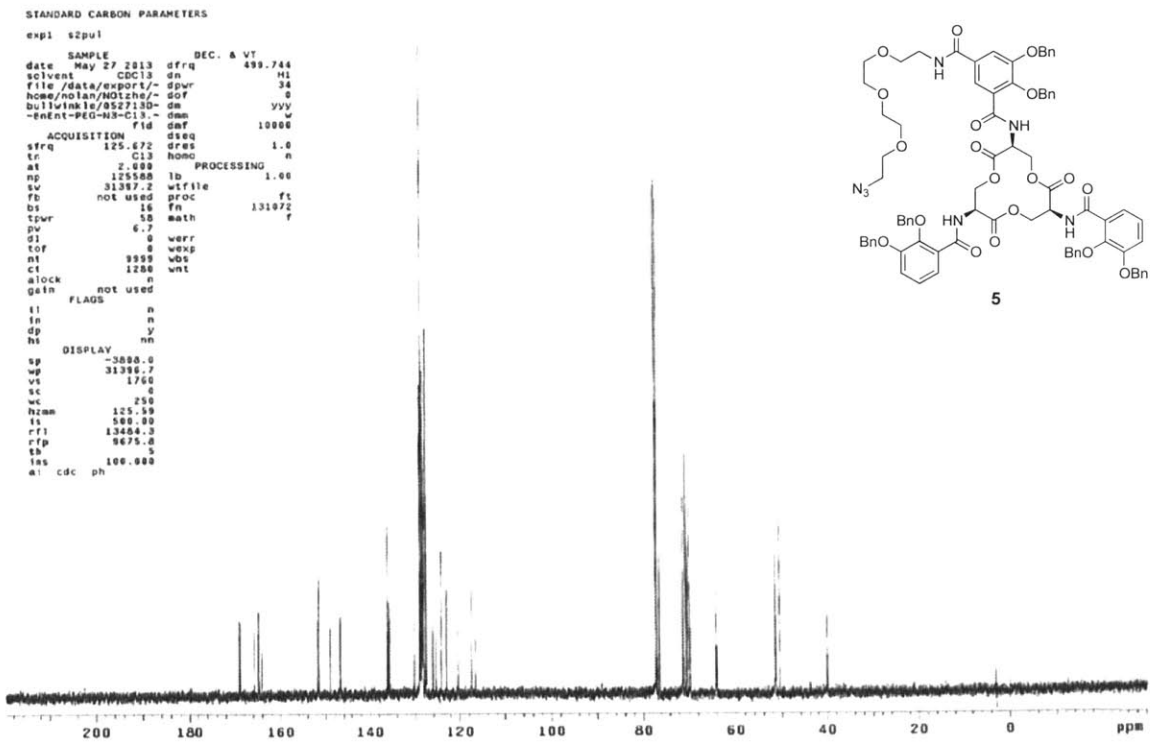
STANDARD CARBON PARAMETERS
expl s2pul
SAMPLE
date May 27 2013
solvent CDCl3
file /data/export/~
home/nolan/NOtzhe/~
bullwinkle/052713D~
~BnEnt-PEG-N3-C13.~
fid
ACQUISITION
sfrq 125.672
tn C13
at 2.089
np 125588
sw 31387.2
fb not used
bs 16
tpwr 58
pw 6.7
d1 0
tof 0
nt 9999
ct 1280
alock n
gain not used
FLAGS
il n
in n
dp y
hs nn
DISPLAY
sp -3888.0
wp 31396.7
vs 1760
sc 0
wc 250
hzmm 125.59
is 500.80
rf1 13464.3
rfp 9675.8
th 5
ins 100.000
ai cdc ph
DEC. & VT
dfrq 499.744
dn H1
dpwr 34
dof 0
dm yyy
dmm w
dmf 10000
dseq
dres 1.0
homo n
PROCESSING
lb 1.00
wtfile
proc ft
fn 131072
math f
werr
wexp
wbs
wnt
OBn
BnO
HN
NH
N3
5
200
180
160
140
120
100
80
60
40
20
0
ppm

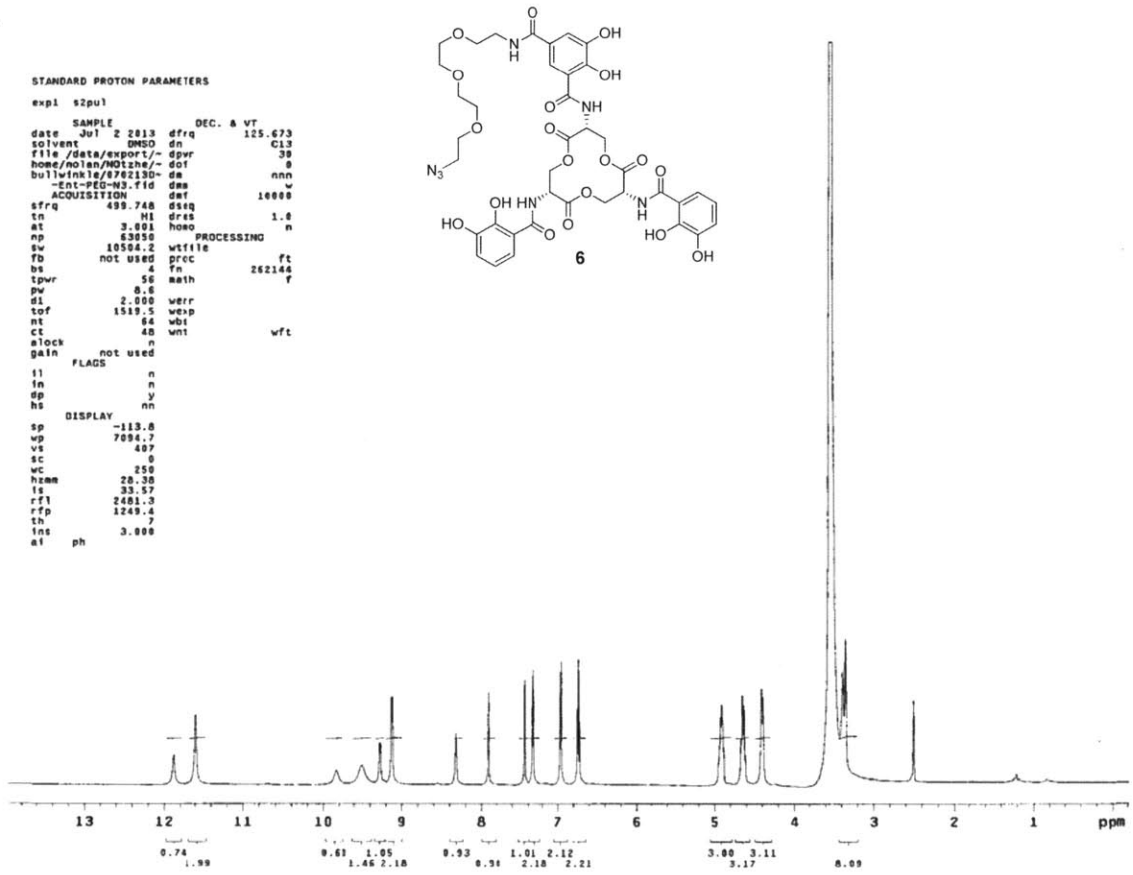
STANDARD PROTON PARAMETERS
expl s2pul
SAMPLE
date Jul 2 2013
solvent DMSO
file /data/export/~
home/nolan/NOtzhe/~
bullwinkle/8702130~
~Ent-PEG-N3.fid
ACQUISITION
sfrq 499.748
tn H1
at 3.001
np 63050
sw 10504.2
fb not used
bs 4
tpwr 56
pw 8.6
d1 2.000
tof 1519.5
nt 64
ct 48
alock n
gain not used
FLAGS
il n
in n
dp y
hs nn
DISPLAY
sp -113.8
wp 7094.7
vs 407
sc 0
wc 250
hzmm 28.38
is 33.57
rfl 2481.3
rfp 1249.4
th 7
ins 3.000
ai ph
DEC. & VT
dfrq 125.673
dn C13
dpwr 38
dof 0
dm nnn
dmm w
dmf 10000
dseq
dres 1.0
homo n
PROCESSING
wtfile
prec ft
fn 262144
math f
werr
wexp
wbt
wnt wft
6
13 12 11 10 9 8 7 6 5 4 3 2 1 ppm
0.74 1.99
0.61 1.85 1.46 2.18
0.93 0.98
1.01 2.12 2.18 2.21
3.00 3.11 3.17
8.09

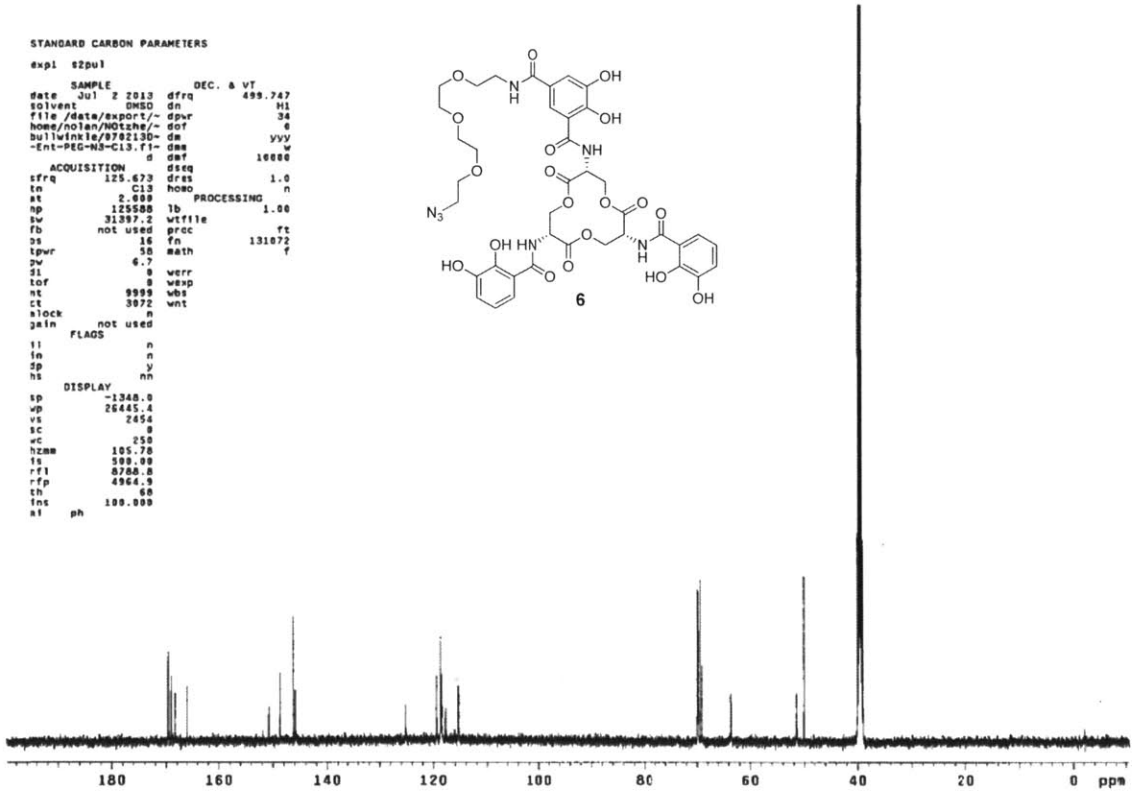
STANDARD CARBON PARAMETERS
expl s2pul
SAMPLE
date Jul 2 2013
solvent DMSO
file /data/export/~
home/nolan/NOtzhe/~
bullwinkle/8702130~
~Ent-PEG-N3-C13.fi~
d
ACQUISITION
sfrq 125.673
tn C13
at 2.089
np 125588
sw 31397.2
fb not used
bs 16
tpwr 58
pw 6.7
d1 0
tof 0
nt 9999
ct 3072
alock n
gain not used
FLAGS
il n
in n
dp y
hs nn
DISPLAY
sp -1348.0
wp 26445.4
vs 2654
sc 0
wc 250
hzmm 105.78
is 598.09
rfl 8788.8
rfp 4964.9
th 68
ins 100.000
ai ph
DEC. & VT
dfrq 499.747
dn H1
dpwr 34
dof 0
dm yyy
dmm w
dmf 10000
dseq
dres 1.0
homo n
PROCESSING
lb 1.00
wtfile
prec ft
fn 131072
math f
werr
wexp
wbs
wnt
6
180 160 140 120 100 80 60 40 20 0 ppm

STANDARD PROTON PARAMETERS

```
expl  szpul

      SAMPLE                    DEC. & VT
date    Jun 24 2013  dfrq          125.672
solvent       CDCl3  dn                C13
file /data/export/~  dpwr               38
home/nolan/NOtzhe/~  dof                 0
bullwinkle/062413A~  dm                nnn
mp-alkyne-HPLC.fid   dmm                 w
   ACQUISITION       dmf             10000
sfrq        499.746  dseq
tn               H1  dres               1.0
at            3.681  homo                 n
np           63056       PROCESSING
sw         10504.2  wtfile
fb       not used   proc                ft
bs              4   fn              262144
tpwr           56   math                 f
pw            8.6
d1          2.000   werr
tof         1519.5   wexp
nt              32   wbs
ct              28   wnt               wft
alock            n
gain      not used
     FLAGS
il               n
in               n
dp               y
hs              nn
    DISPLAY
sp         -222.1
wp         5720.2
vs            258
sc              0
wc            250
hzmm        22.91
is         330.14
rfl        4853.2
rfp        1249.4
th              7
ins          3.000
ai   ph
```

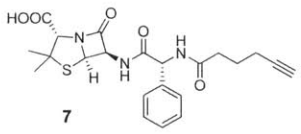

7

STANDARD CARBON PARAMETERS

```
expl  szpul

      SAMPLE                    DEC. & VT
date    Jun 24 2013  dfrq          499.747
solvent       DMSO   dn                H1
file /data/export/~  dpwr               34
home/nolan/NOtzhe/~  dof                 0
bullwinkle/062413A~  dm                yyy
mp-alkyneHPLC-C13.~  dmm                 w
              fid    dmf             10000
   ACQUISITION       dseq
sfrq        125.673  dres               1.0
tn              C13  homo                 n
at            2.000       PROCESSING
np           125588  lb                1.00
sw         31397.2  wtfile
fb       not used   proc                ft
bs             16   fn              131072
tpwr           58   math                 f
pw            6.7
d1              0   werr
tof             0   wexp
nt           9999   wbs
ct            912   wnt
alock            n
gain      not used
     FLAGS
il               n
in               n
dp               y
hs              nn
    DISPLAY
sp         -3841.5
wp         31396.7
vs            1224
sc               0
wc             250
hzmm        125.59
is          500.00
rfl        8805.5
rfp        4963.6
th               68
ins         100.000
ai   cdc  ph
```

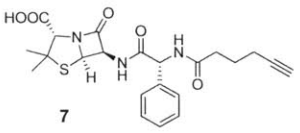

7

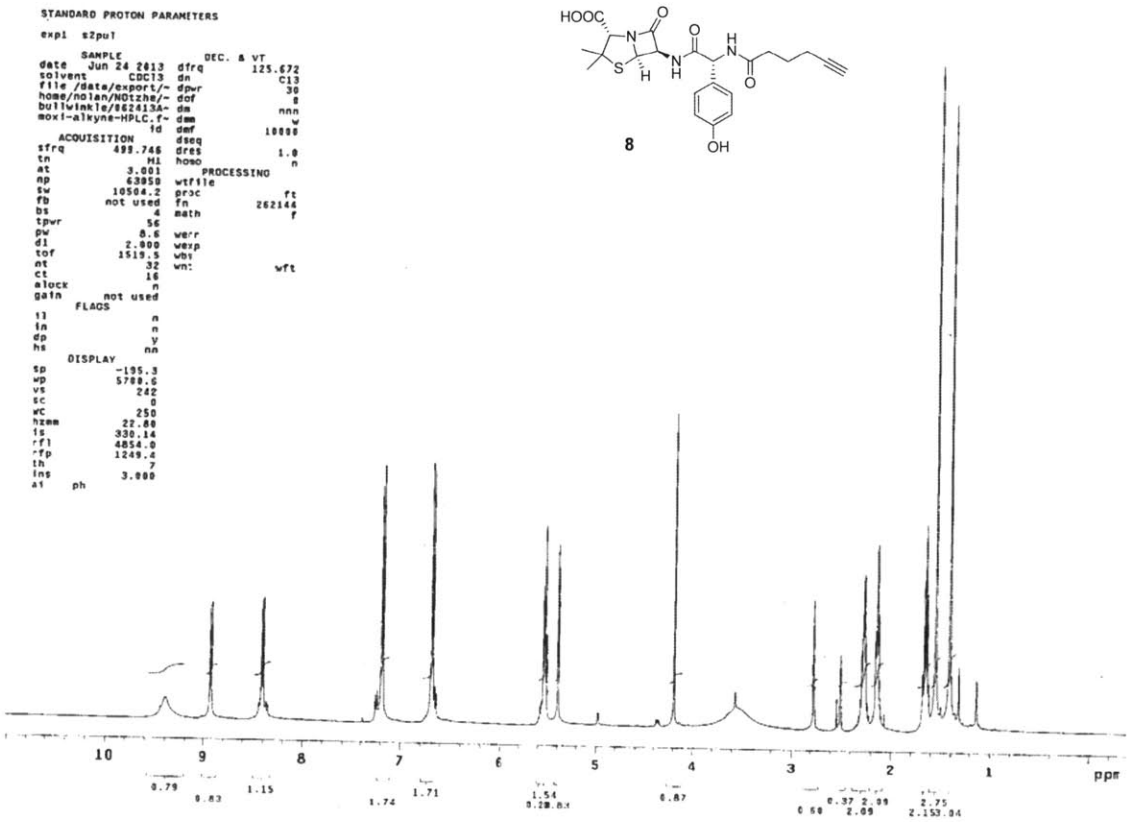
STANDARD PROTON PARAMETERS
expl szpul
SAMPLE
date Jun 24 2013
solvent CDCl3
file /data/export/~
home/nolan/NOtzhe/~
bullwinkle/062413A~
moxi-alkyne-HPLC.f~
id
ACQUISITION
sfrq 499.746
tn H1
at 3.001
np 63950
sw 10504.2
fb not used
bs 4
tpwr 56
pw 8.6
dl 2.000
tof 1519.5
nt 32
ct 16
alock n
gain not used
FLAGS
il n
in n
dp y
hs nn
DISPLAY
sp -195.3
wp 5788.6
vs 242
sc 0
wc 250
hzmm 22.88
is 330.14
rfl 4854.0
rfp 1249.4
th 7
ins 3.888
ai ph
DEC. & VT
dfrq 125.672
dn C13
dpwr 30
dof 0
dm nnn
dmm w
dmf 10888
dseq
dres 1.0
homo n
PROCESSING
wtfile
proc ft
fn 262144
math f
werr
wexp
wbs
wnt wft
HOOC
O
N
S
H
O
H
N
O
H
N
O
OH
8
10
9
8
7
6
5
4
3
2
1
ppm
0.79
0.83
1.15
1.74
1.71
1.54
0.87
0.37
2.09
2.69
2.75
2.153.04

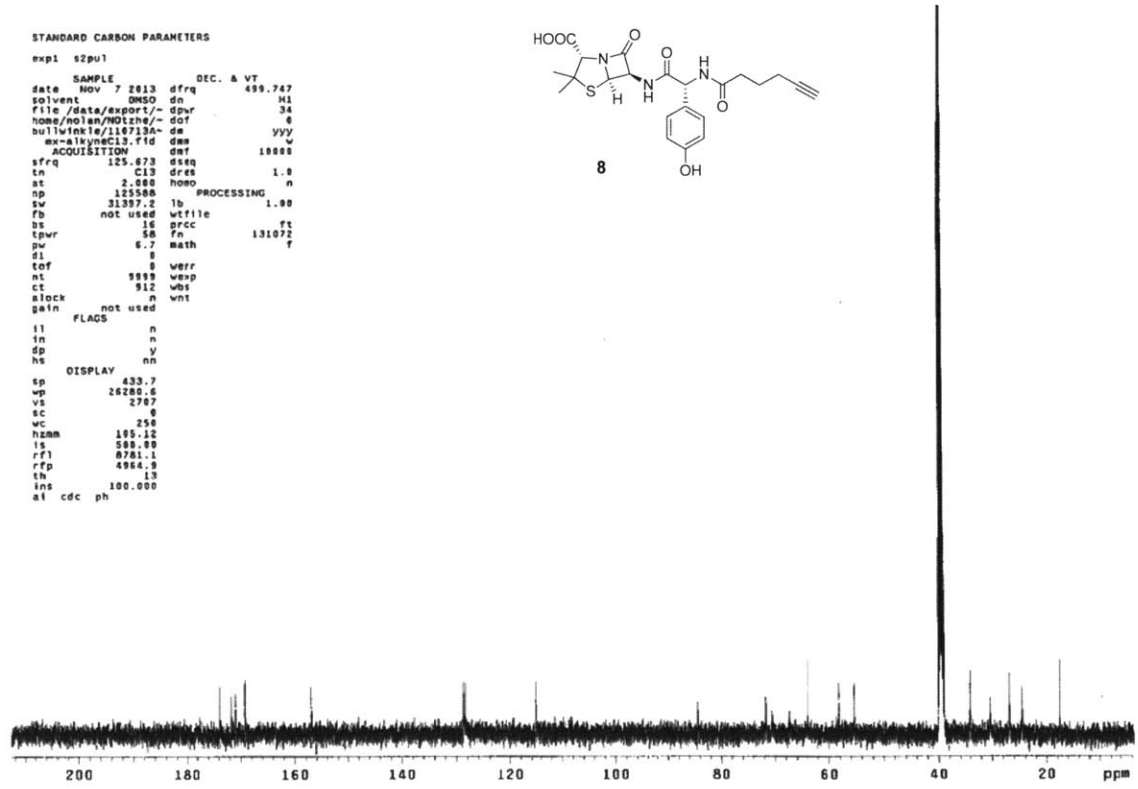
STANDARD CARBON PARAMETERS
expl szpul
SAMPLE
date Nov 7 2013
solvent DMSO
file /data/export/~
home/nolan/NOtzhe/~
bullwinkle/110713A~
mx-alkyneC13.fid
ACQUISITION
sfrq 125.673
tn C13
at 2.060
np 125508
sw 31397.2
fb not used
bs 16
tpwr 58
pw 6.7
dl 0
tof 0
nt 9999
ct 912
alock n
gain not used
FLAGS
il n
in n
dp y
hs nn
DISPLAY
sp 433.7
wp 26280.6
vs 2707
sc 0
wc 250
hzmm 185.12
is 500.00
rfl 8781.1
rfp 4964.9
th 13
ins 100.000
ai cdc ph
DEC. & VT
dfrq 499.747
dn H1
dpwr 34
dof 0
dm yyy
dmm w
dmf 10888
dseq
dres 1.0
homo n
PROCESSING
lb 1.00
wtfile
proc ft
fn 131072
math f
werr
wexp
wbs
wnt
HOOC
O
N
S
H
O
H
N
O
H
N
O
OH
8
200
180
160
140
120
100
80
60
40
20
ppm

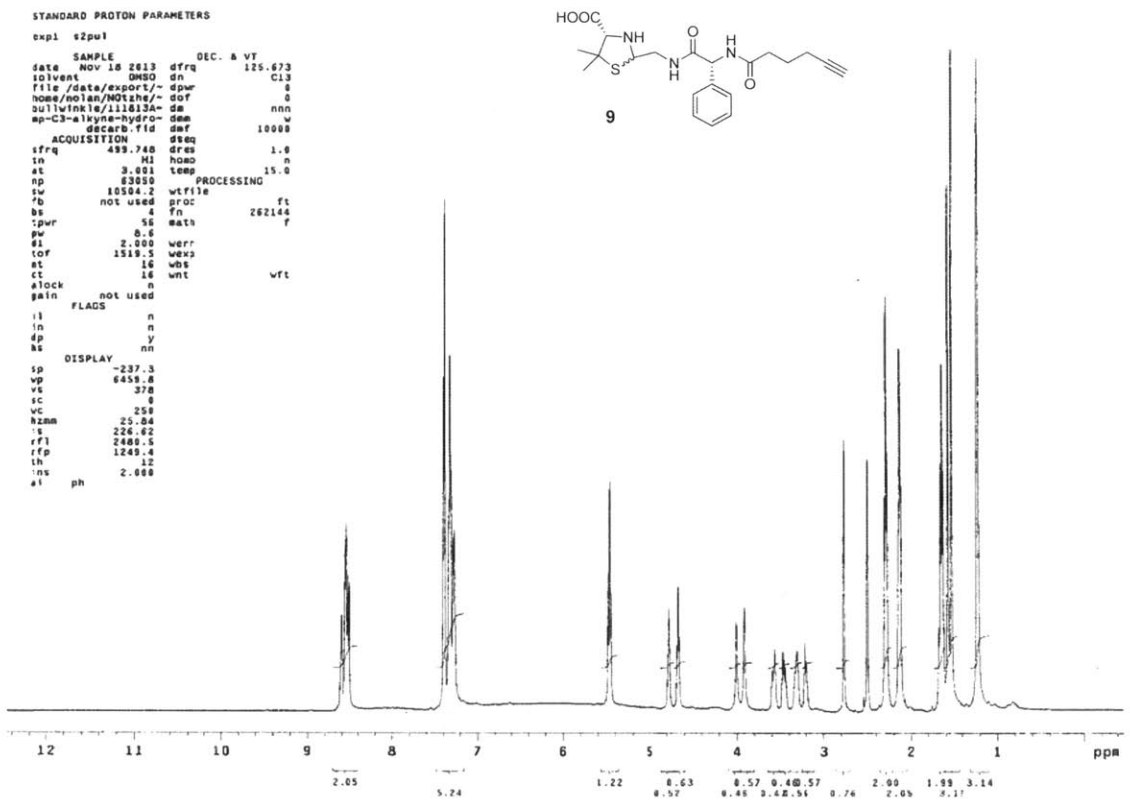
STANDARD PROTON PARAMETERS
expl s2pul
SAMPLE
date Nov 18 2013
solvent DMSO
file /data/export/~
home/nolan/NOtzhe/~
bullwinkle/111813A~
mp-C3-alkyne-hydro~
dscarb.fid
ACQUISITION
sfrq 499.748
tn H1
at 3.001
np 83050
sw 18504.2
fb not used
bs 4
tpwr 56
pw 8.6
dl 2.000
tof 1519.5
nt 16
ct 16
alock n
gain not used
FLAGS
il n
in n
dp y
hs nn
DISPLAY
sp -237.3
wp 6459.8
vs 378
sc 0
wc 250
hzmm 25.84
is 226.62
rfl 2480.5
rfp 1249.4
th 12
ins 2.000
ai ph
DEC. & VT
dfrq 125.673
dn C13
dpwr 8
dof 0
dm nnn
dmm w
dmf 10000
dseq
dres 1.0
homo n
temp 15.0
PROCESSING
wtfile
proc ft
fn 262144
math f
werr
wexp
wbs
wnt wft
HOOC
NH
S
N
H
O
H
N
O
9
12
11
10
9
8
7
6
5
4
3
2
1
ppm
2.05
5.24
1.22
0.63
0.57
0.57
2.00
1.99
3.14

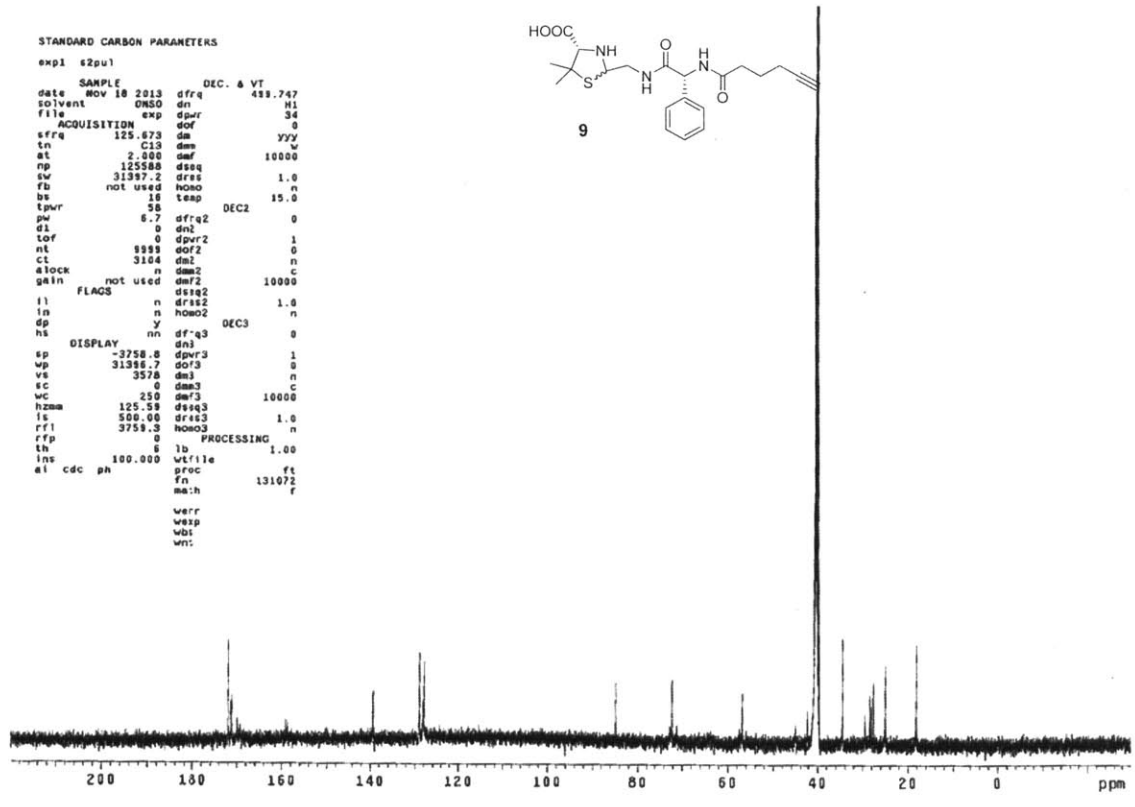
STANDARD CARBON PARAMETERS
expl s2pul
SAMPLE
date Nov 18 2013
solvent DMSO
file exp
ACQUISITION
sfrq 125.673
tn C13
at 2.000
np 125588
sw 31397.2
fb not used
bs 16
tpwr 58
pw 6.7
dl 0
tof 0
nt 9999
ct 3104
alock n
gain not used
FLAGS
il n
in n
dp y
hs nn
DISPLAY
sp -3758.8
wp 31386.7
vs 3578
sc 0
wc 250
hzmm 125.59
is 500.00
rfl 3759.3
rfp 0
th 6
ins 100.000
ai cdc ph
DEC. & VT
dfrq 499.747
dn H1
dpwr 34
dof 0
dm yyy
dmm w
dmf 10000
dseq
dres 1.0
homo n
temp 15.0
DEC2
dfrq2 0
dn2
dpwr2 1
dof2 0
dm2 n
dmm2 c
dmf2 10000
dseq2
dres2 1.0
homo2 n
DEC3
df:q3 0
dn3
dpwr3 1
dof3 0
dm3 n
dmm3 c
dmf3 10000
dseq3
dres3 1.0
homo3 n
PROCESSING
lb 1.00
wtfile
proc ft
fn 131072
ma:h f
werr
wexp
wbs
wnt
HOOC
NH
S
N
H
O
H
N
O
9
200
180
160
140
120
100
80
60
40
20
0
ppm

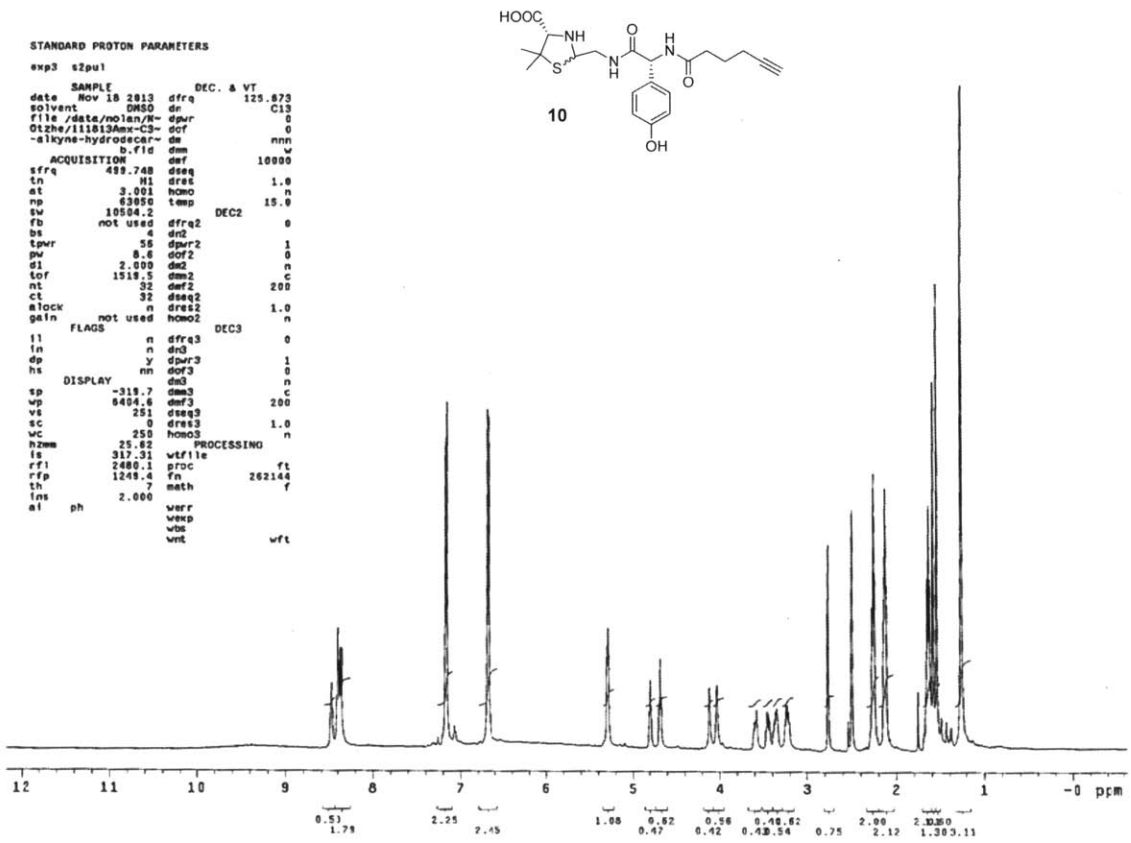
STANDARD PROTON PARAMETERS
exp3 szpul
SAMPLE
date Nov 18 2013
solvent DMSO
file /data/nolan/N~
0tzhe/111813Amx-CS~
-alkyne-hydrodecar~
b.fid
ACQUISITION
sfrq 499.748
tn H1
at 3.001
np 63856
sw 10584.2
fb not used
bs 4
tpwr 56
pw 8.6
d1 2.000
tof 1518.5
nt 32
ct 32
alock n
gain not used
FLAGS
il n
in n
dp y
hs nn
DISPLAY
sp -319.7
wp 6404.6
vs 251
sc 0
wc 250
hzmm 25.62
is 317.31
rfl 2480.1
rfp 1248.4
th 7
ins 2.000
ai ph
DEC. & VT
dfrq 125.873
dn C13
dpwr 0
dof 0
dm nnn
dmm w
dmf 10000
dseq
drst 1.0
homo n
temp 15.0
DEC2
dfrq2 0
dn2
dpwr2 1
dof2 0
dm2 n
dmm2 c
dmf2 200
dseq2
drst2 1.0
homo2 n
DEC3
dfrq3 0
dn3
dpwr3 1
dof3 0
dm3 n
dmm3 c
dmf3 200
dseq3
drst3 1.0
homo3 n
PROCESSING
wtfile
proc ft
fn 262144
math f
werr
wexp
wbs
wnt wft
HOOC
NH
S
N
H
O
O
OH
10
12
11
10
9
8
7
6
5
4
3
2
1
-0 ppm
0.53
1.79
2.25
2.45
1.08
0.62
0.47
0.56
0.42
0.46
0.54
0.75
2.00
2.12
1.30
3.11

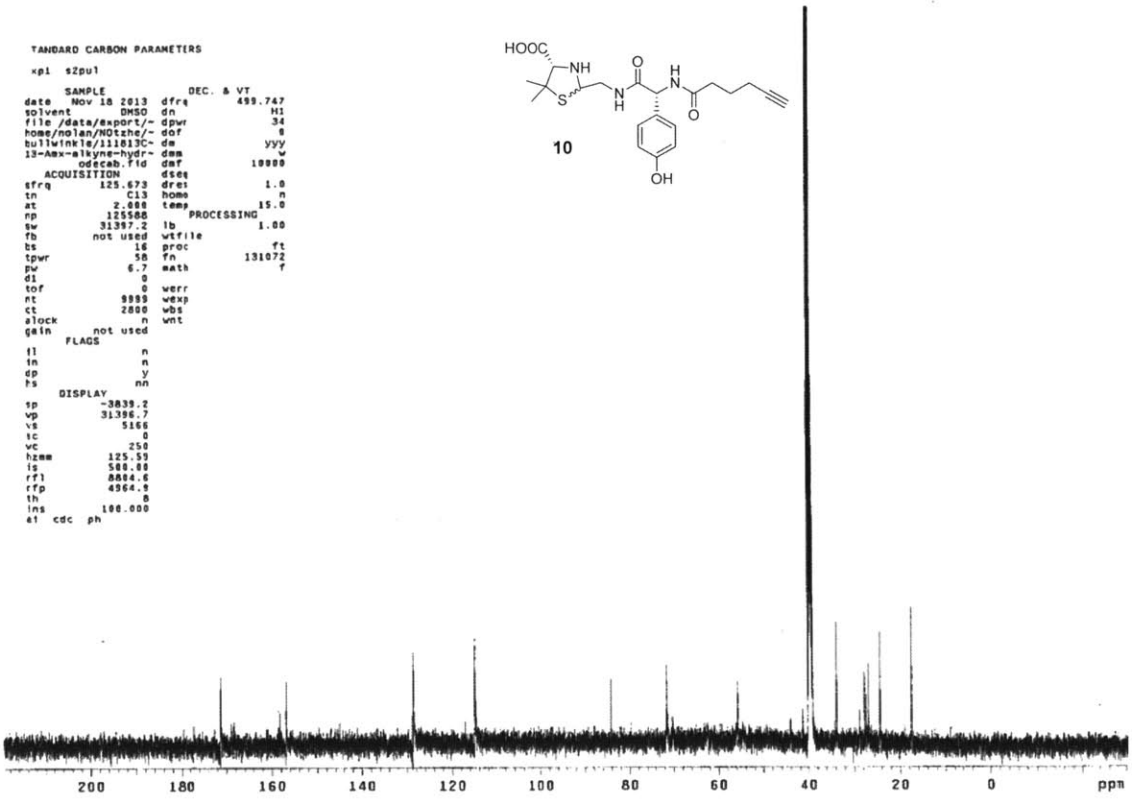
TANDARD CARBON PARAMETERS
xp1 szpul
SAMPLE
date Nov 18 2013
solvent DMSO
file /data/Export/~
home/nolan/NOtzhe/~
bullwinkle/111813C~
13-Amx-alkyne-hydr~
odecab.fid
ACQUISITION
sfrq 125.673
tn C13
at 2.888
np 125588
sw 31397.2
fb not used
bs 16
tpwr 58
pw 6.7
d1 0
tof 0
nt 9889
ct 2800
alock n
gain not used
FLAGS
il n
in n
dp y
hs nn
DISPLAY
sp -3835.2
wp 31386.7
vs 5166
sc 0
wc 250
hzmm 125.59
is 500.00
rfl 8884.6
rfp 4564.9
th 8
ins 100.000
ai cdc ph
DEC. & VT
dfrq 499.747
dn H1
dpwr 34
dof 0
dm yyy
dmm w
dmf 10000
dseq
drst 1.0
homo n
temp 15.0
PROCESSING
lb 1.00
wtfile
proc ft
fn 131072
math f
werr
wexp
wbs
wnt
HOOC
NH
S
N
H
O
O
OH
10
200
180
160
140
120
100
80
60
40
20
0
ppm

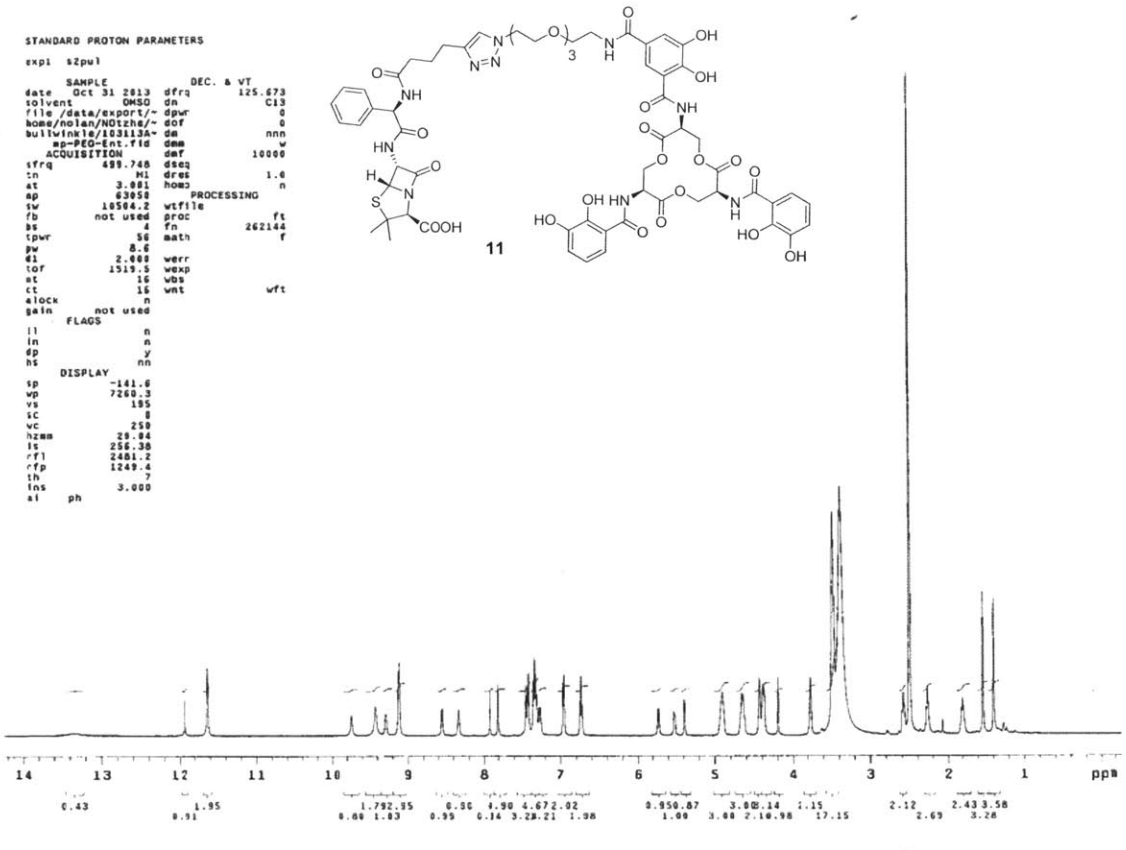
STANDARD PROTON PARAMETERS
expl szpul
SAMPLE
date Oct 31 2013
solvent DMSO
file /data/export/~
home/nolan/NOtzhe/~
bullwinkle/103113A~
mp-PEG-Ent.fid
ACQUISITION
sfrq 499.748
tn H1
at 3.081
np 63058
sw 10504.2
fb not used
bs 4
tpwr 56
pw 8.6
d1 2.000
tof 1519.5
nt 16
ct 16
alock n
gain not used
FLAGS
il n
in n
dp y
hs nn
DISPLAY
sp -141.6
wp 7260.3
vs 195
sc 8
wc 250
hzcm 29.84
hs 256.38
fl 2481.2
fp 1249.4
th 7
ins 3.000
ai ph
DEC. & VT
dfrq 125.673
dn C13
dpwr 0
dof 0
dm nnn
dmm w
dmf 10000
dseq
dres 1.6
homo n
PROCESSING
wtfile
proc ft
fn 262144
math f
werr
wexp
wbs
wnt wft
11
14 13 12 11 10 9 8 7 6 5 4 3 2 1 ppm

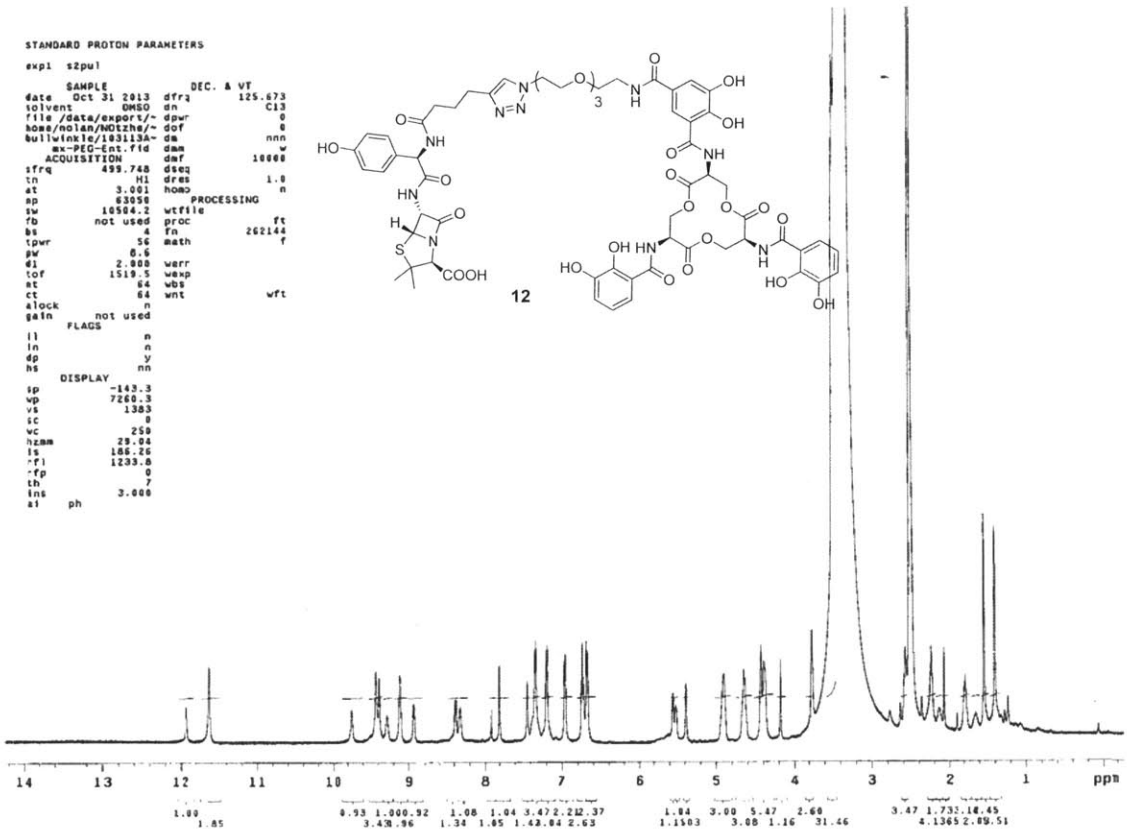
STANDARD PROTON PARAMETERS
expl szpul
SAMPLE
date Oct 31 2013
solvent DMSO
file /data/export/~
home/nolan/NOtzhe/~
bullwinkle/103113A~
mx-PEG-Ent.fid
ACQUISITION
sfrq 499.748
tn H1
at 3.081
np 63058
sw 10504.2
fb not used
bs 4
tpwr 56
pw 8.6
d1 2.000
tof 1519.5
nt 64
ct 64
alock n
gain not used
FLAGS
il n
in n
dp y
hs nn
DISPLAY
sp -143.3
wp 7260.3
vs 1383
sc 8
wc 250
hzcm 29.84
hs 186.26
fl 1233.8
fp 0
th 7
ins 3.000
ai ph
DEC. & VT
dfrq 125.673
dn C13
dpwr 0
dof 0
dm nnn
dmm w
dmf 10000
dseq
dres 1.8
homo n
PROCESSING
wtfile
proc ft
fn 262144
math f
werr
wexp
wbs
wnt wft
12
14 13 12 11 10 9 8 7 6 5 4 3 2 1 ppm

Chapter 3
Analytical HPLC Traces

4

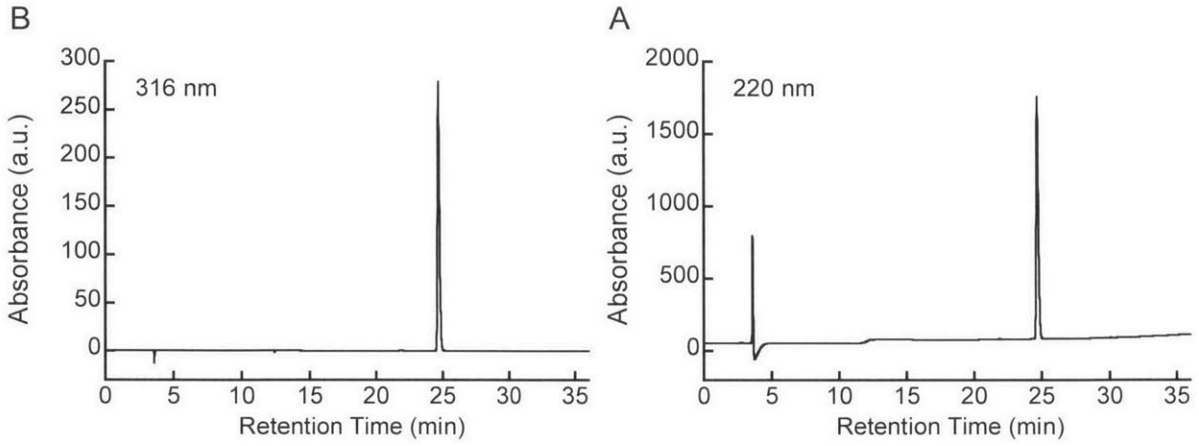
B
316 nm
Absorbance (a.u.)
300
250
200
150
100
50
0
0 5 10 15 20 25 30 35
Retention Time (min)
A
220 nm
Absorbance (a.u.)
2000
1500
1000
500
0
0 5 10 15 20 25 30 35
Retention Time (min)

6

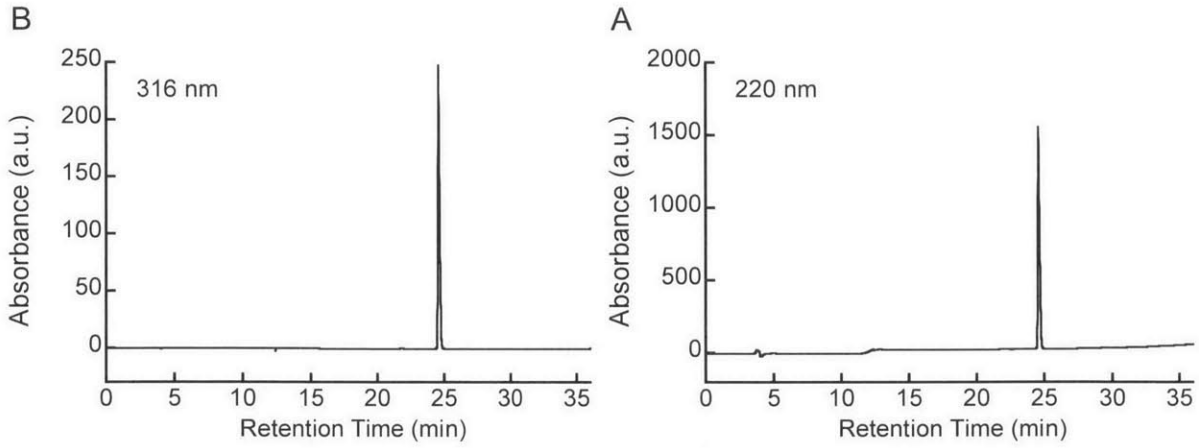
B
316 nm
Absorbance (a.u.)
250
200
150
100
50
0
0 5 10 15 20 25 30 35
Retention Time (min)
A
220 nm
Absorbance (a.u.)
2000
1500
1000
500
0
0 5 10 15 20 25 30 35
Retention Time (min)

11

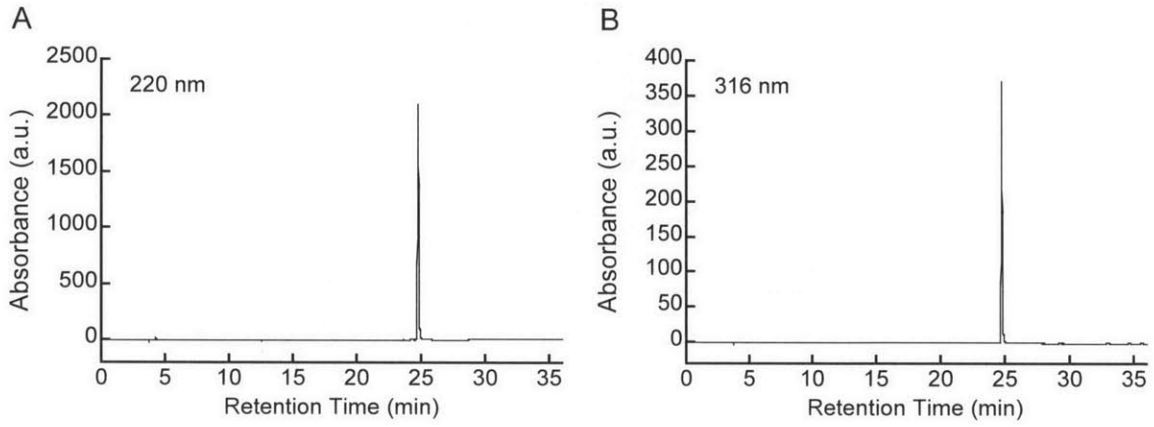
A
220 nm
Absorbance (a.u.)
2500
2000
1500
1000
500
0
0 5 10 15 20 25 30 35
Retention Time (min)
B
316 nm
Absorbance (a.u.)
400
350
300
250
200
150
100
50
0
0 5 10 15 20 25 30 35
Retention Time (min)

12

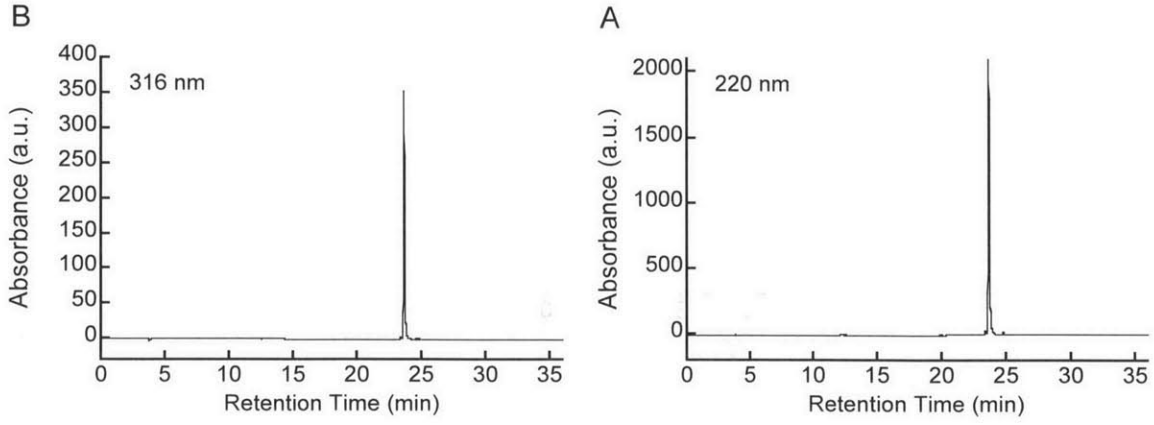
B
316 nm
Absorbance (a.u.)
400
350
300
250
200
150
100
50
0
0 5 10 15 20 25 30 35
Retention Time (min)
A
220 nm
Absorbance (a.u.)
2000
1500
1000
500
0
0 5 10 15 20 25 30 35
Retention Time (min)

13

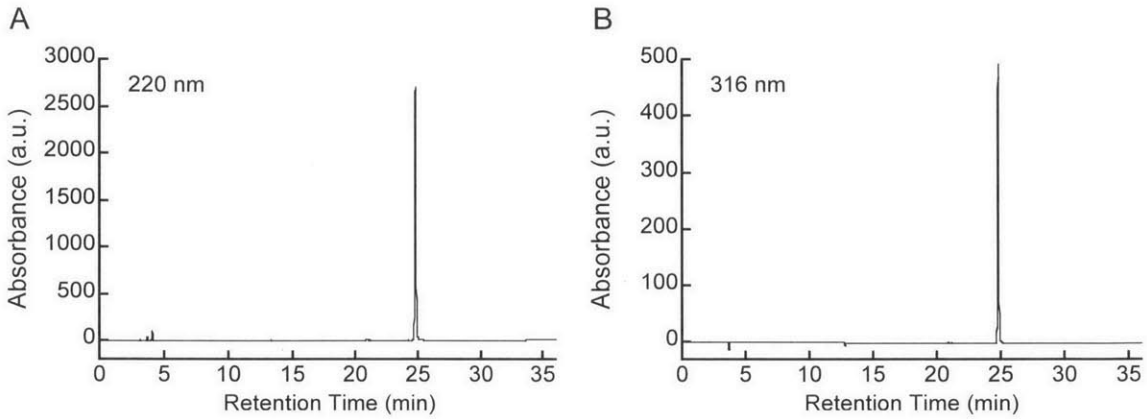
A
220 nm
Absorbance (a.u.)
3000
2500
2000
1500
1000
500
0
0 5 10 15 20 25 30 35
Retention Time (min)
B
316 nm
Absorbance (a.u.)
500
400
300
200
100
0
0 5 10 15 20 25 30 35
Retention Time (min)

14

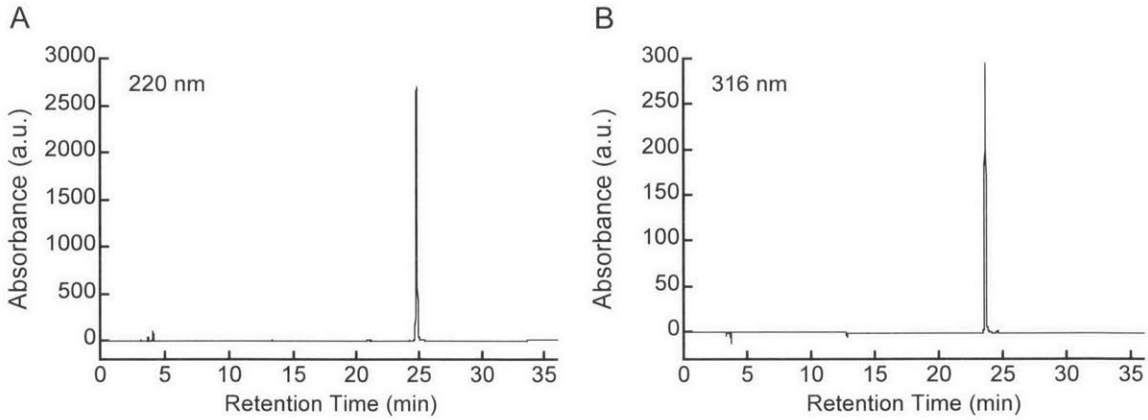
A
220 nm
Absorbance (a.u.)
3000
2500
2000
1500
1000
500
0
0 5 10 15 20 25 30 35
Retention Time (min)
B
316 nm
Absorbance (a.u.)
300
250
200
150
100
50
0
0 5 10 15 20 25 30 35
Retention Time (min)

15

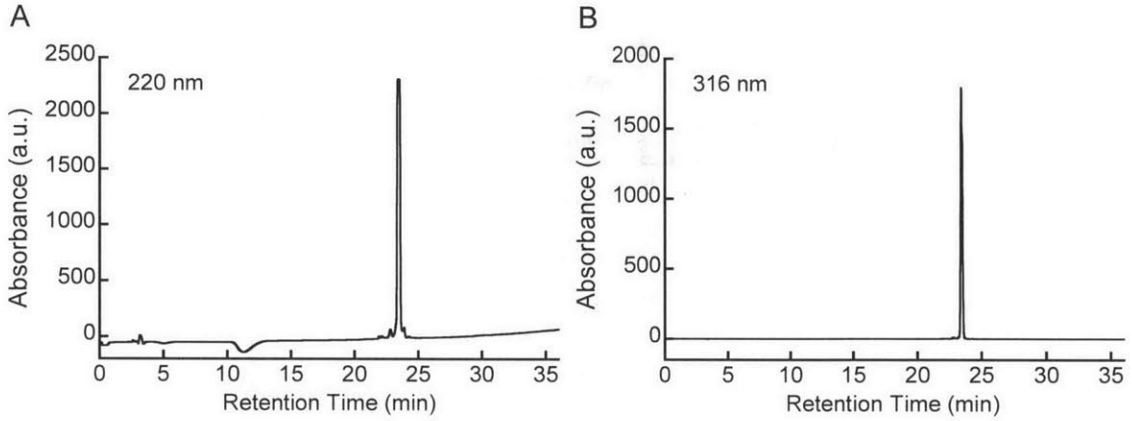
A
220 nm
Absorbance (a.u.)
2500
2000
1500
1000
500
0
0 5 10 15 20 25 30 35
Retention Time (min)
B
316 nm
Absorbance (a.u.)
2000
1500
1000
500
0
0 5 10 15 20 25 30 35
Retention Time (min)

16

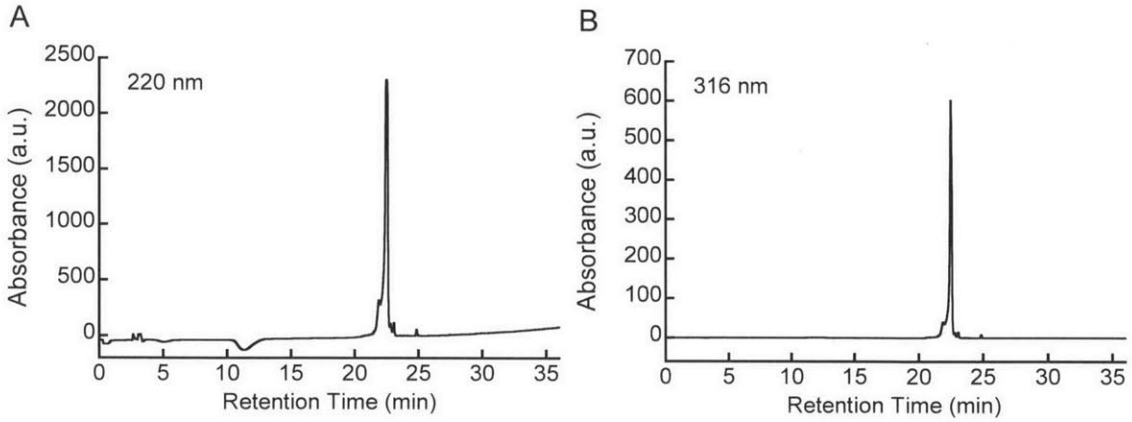
A
220 nm
Absorbance (a.u.)
2500
2000
1500
1000
500
0
0 5 10 15 20 25 30 35
Retention Time (min)
B
316 nm
Absorbance (a.u.)
700
600
500
400
300
200
100
0
0 5 10 15 20 25 30 35
Retention Time (min)

Chapter 3
UV-Vis Spectra

11

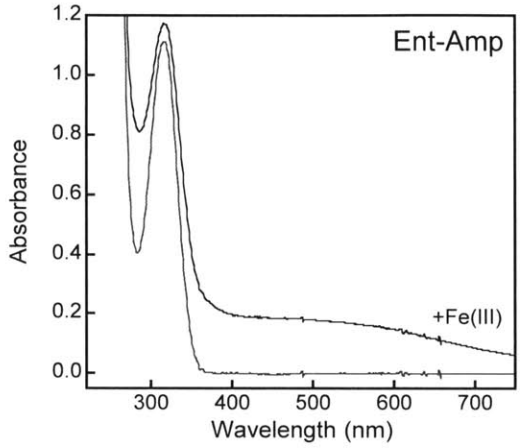

12

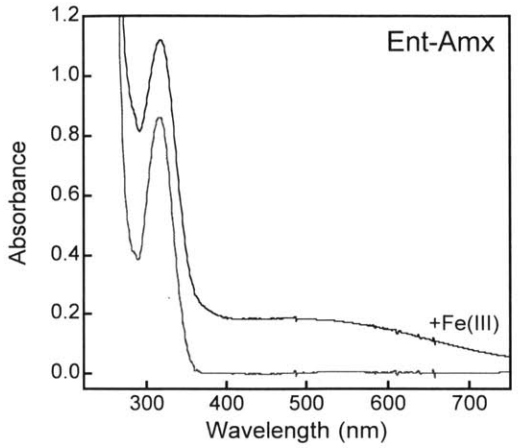

13

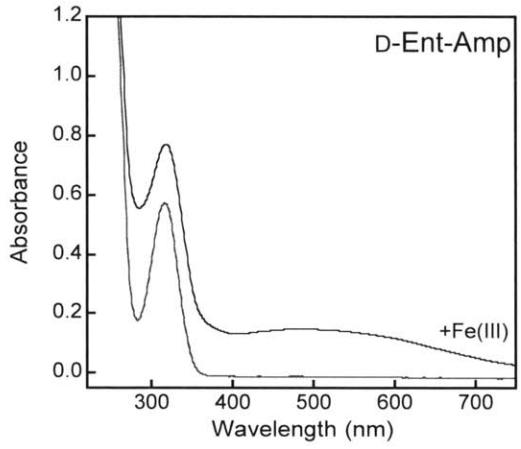

14

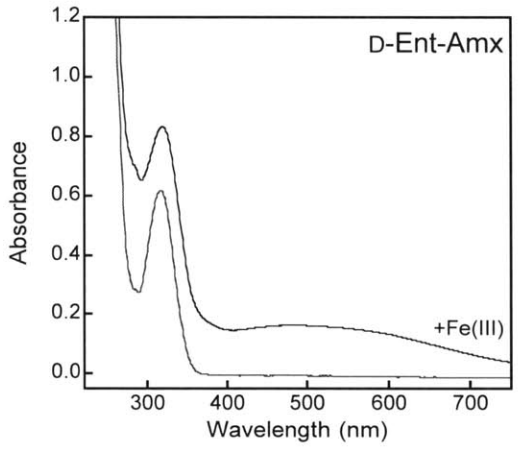

15

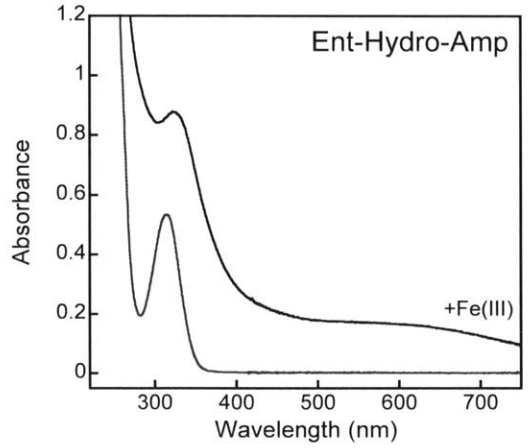

16

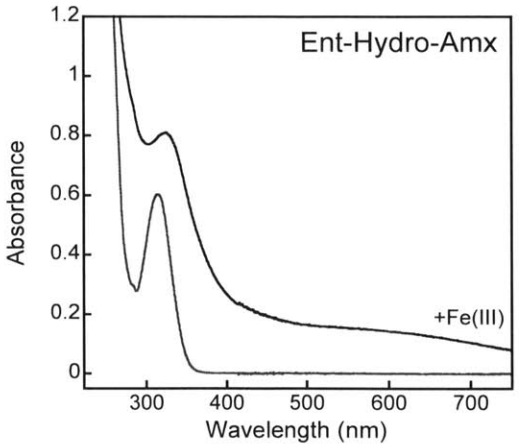

Chapter 4
NMR Spectra

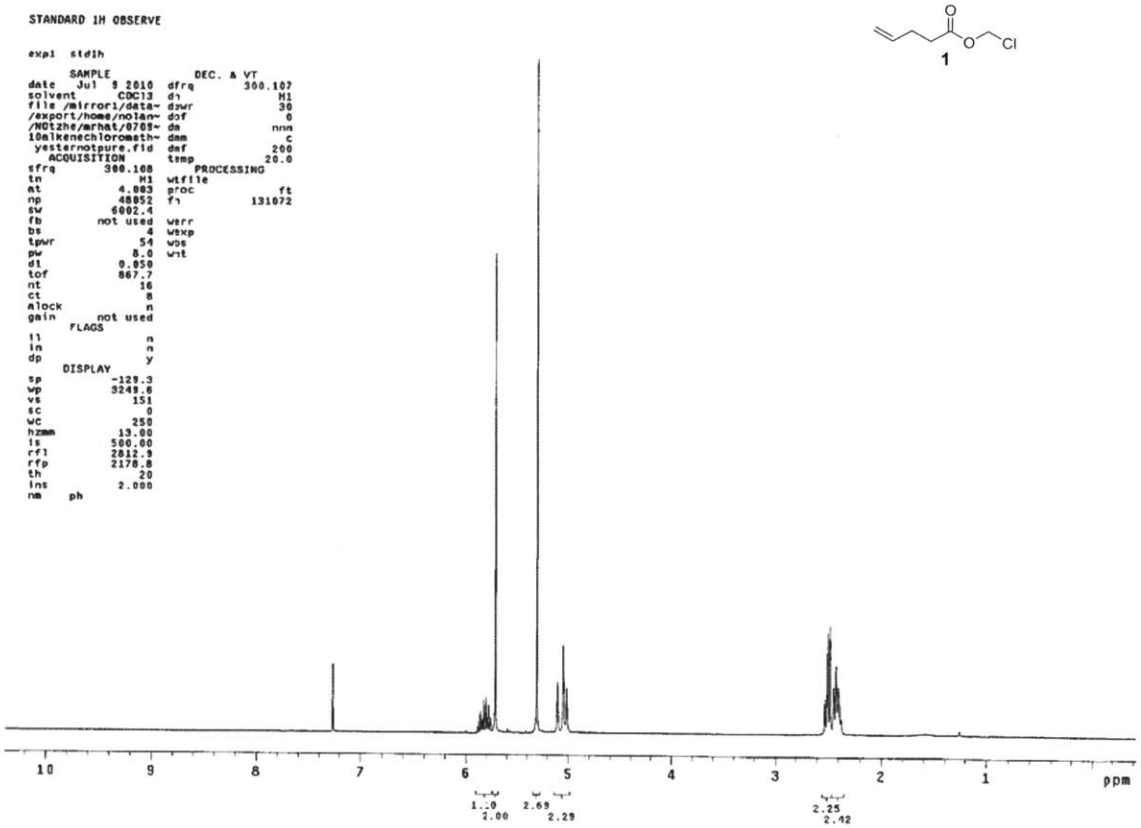
STANDARD 1H OBSERVE
expl stdih
SAMPLE
date Jul 8 2010
solvent CDCl3
file /mirror1/data~
/export/home/nolan~
/NOtzhe/mrhat/0708~
10alkenechloromath~
yesternotpure.fid
ACQUISITION
sfrq 300.108
tn H1
at 4.883
np 48052
sw 6002.4
fb not used
bs 4
tpwr 54
pw 8.0
d1 0.050
tof 867.7
nt 16
ct 8
alock n
gain not used
FLAGS
il n
in n
dp y
DISPLAY
sp -129.3
wp 3249.6
vs 151
sc 0
wc 250
hzmm 13.00
is 500.00
rfl 2812.9
rfp 2178.8
th 20
ins 2.000
nm ph
DEC. & VT
dfrq 300.107
dn H1
dpwr 30
dof 0
dm nnn
dmm c
dmf 200
temp 20.0
PROCESSING
wtfile
proc ft
fn 131072
werr
wexp
wbs
wnt
1
10
9
8
7
6
5
4
3
2
1
ppm
1.0
2.00
2.69
2.29
2.25
2.42

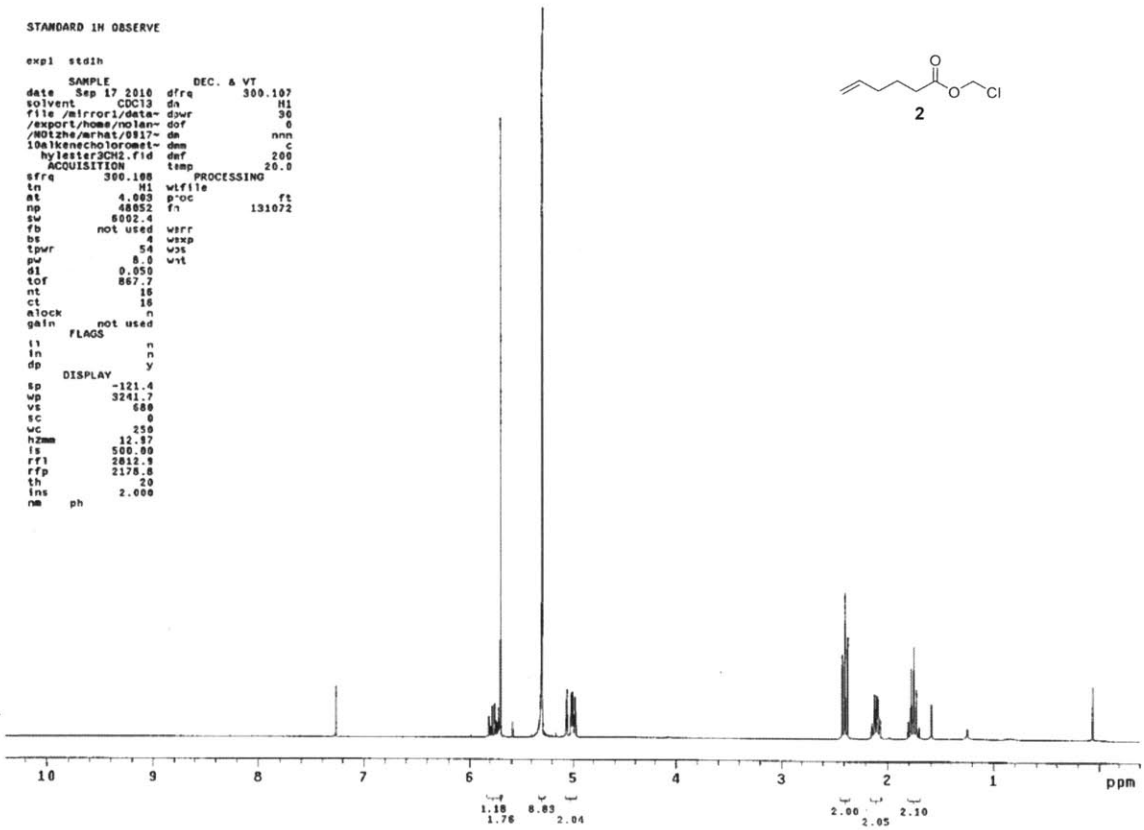
STANDARD 1H OBSERVE
expl stdih
SAMPLE
date Sep 17 2010
solvent CDCl3
file /mirror1/data~
/export/home/nolan~
/NOtzhe/mrhat/0917~
10alkenecholoromet~
hylester3CH2.fid
ACQUISITION
sfrq 300.108
tn H1
at 4.883
np 48052
sw 6002.4
fb not used
bs 4
tpwr 54
pw 8.0
d1 0.050
tof 867.7
nt 16
ct 16
alock n
gain not used
FLAGS
il n
in n
dp y
DISPLAY
sp -121.4
wp 3241.7
vs 680
sc 0
wc 250
hzmm 12.97
is 500.00
rfl 2812.9
rfp 2178.8
th 20
ins 2.000
nm ph
DEC. & VT
dfrq 300.107
dn H1
dpwr 30
dof 0
dm nnn
dmm c
dmf 200
temp 20.0
PROCESSING
wtfile
proc ft
fn 131072
werr
wexp
wbs
wnt
2
10
9
8
7
6
5
4
3
2
1
ppm
1.18
1.76
8.83
2.04
2.00
2.05
2.10

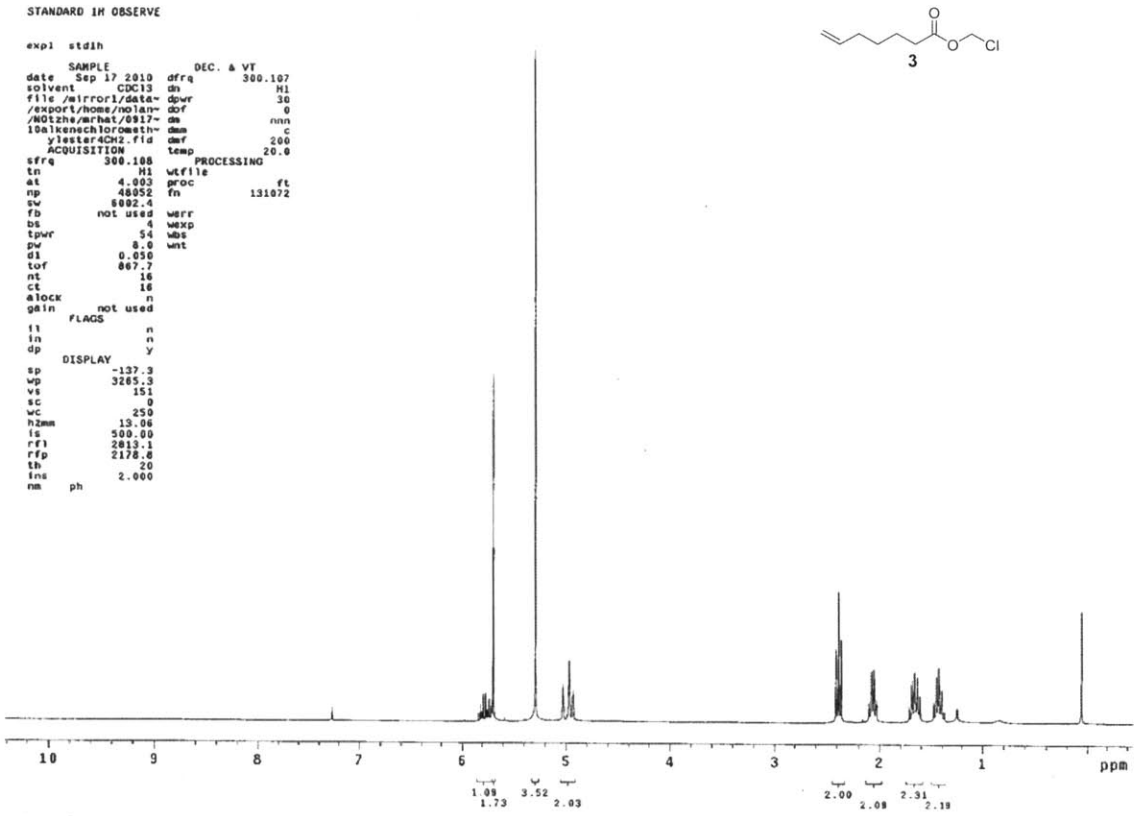
STANDARD 1H OBSERVE
expl stdih
SAMPLE
date Sep 17 2010
solvent CDCl3
file /mirror1/data~
/export/home/nolan~
/NOlzhe/marbat/0917~
10alkenechloromeeth~
ylester4CH2.fid
ACQUISITION
sfrq 300.108
tn H1
at 4.003
np 48052
sw 6002.4
fb not used
bs 4
tpwr 54
pw 8.0
d1 0.050
tof 867.7
nt 16
ct 16
alock n
gain not used
FLAGS
il n
in n
dp y
DISPLAY
sp -137.3
wp 3285.3
vs 151
sc 0
wc 250
hzmm 13.06
is 500.00
rfl 2813.1
rfp 2178.8
th 20
ins 2.000
nm ph
DEC. & VT
dfrq 300.107
dn H1
dpwr 30
dof 0
dm nnn
dmm c
dmf 200
temp 20.0
PROCESSING
wtfile
proc ft
fn 131072
werr
wexp
wbs
wnt
3
10
9
8
7
6
5
4
3
2
1
ppm
1.09
1.73
3.52
2.03
2.00
2.08
2.31
2.19

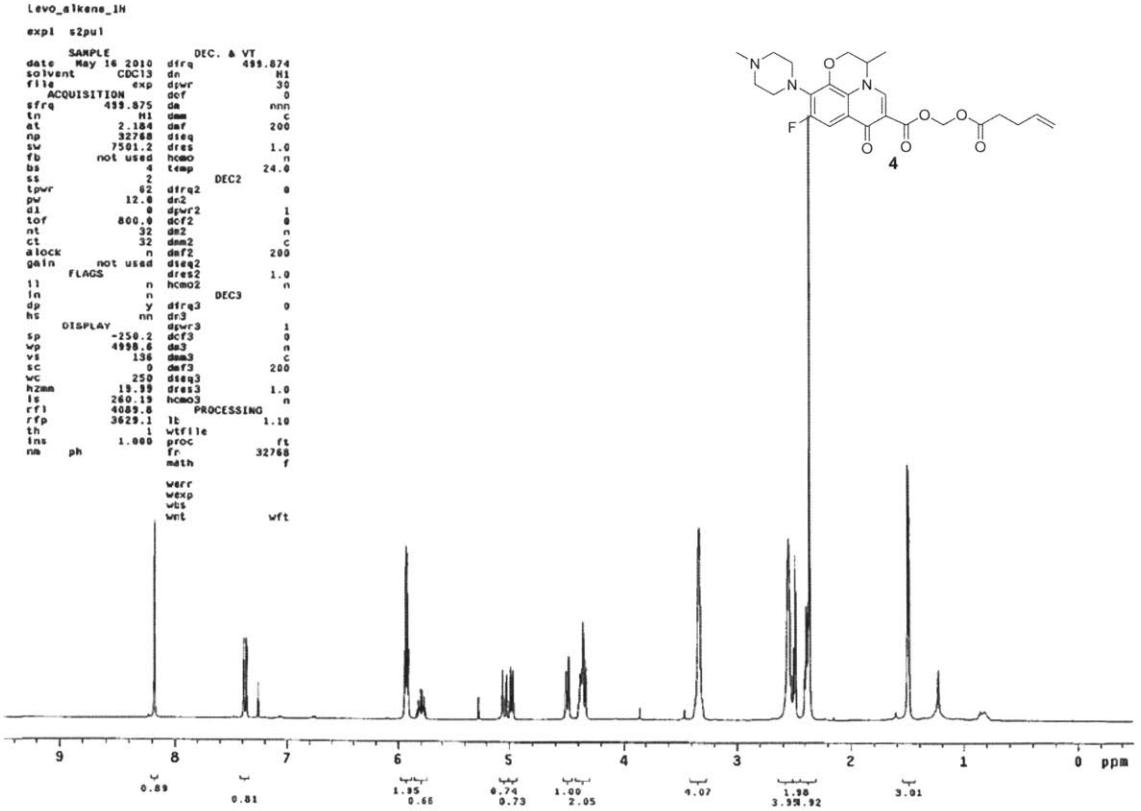
Levo_alkene_1H
expl s2pul
SAMPLE
date May 16 2010
solvent CDCl3
file exp
ACQUISITION
sfrq 499.875
tn H1
at 2.184
np 32768
sw 7501.2
fb not used
bs 4
ss 2
tpwr 62
pw 12.0
d1 0
tof 800.0
nt 32
ct 32
alock n
gain not used
FLAGS
il n
in n
dp y
hs nn
DISPLAY
sp -250.2
wp 4998.6
vs 136
sc 0
wc 250
hzmm 18.99
is 260.19
rfl 4089.8
rfp 3629.1
th 1
ins 1.000
nm ph
DEC. & VT
dfrq 499.874
dn H1
dpwr 30
dof 0
dm nnn
dmm c
dmf 200
dseq
dres 1.0
hcmo n
temp 24.0
DEC2
dfrq2 0
dn2
dpwr2 1
dof2 0
dm2 n
dmm2 c
dmf2 200
dseq2
dres2 1.0
hcmo2 n
DEC3
dfrq3 0
dn3
dpwr3 1
dof3 0
dm3 n
dmm3 c
dmf3 200
dseq3
dres3 1.0
hcmo3 n
PROCESSING
lb 1.10
wtfile
proc ft
fn 32768
math f
werr
wexp
wbs
wnt wft
4
9
8
7
6
5
4
3
2
1
0 ppm
0.89
0.81
1.95
0.66
0.79
0.73
1.00
2.05
4.07
1.98
3.99
2.92
3.01

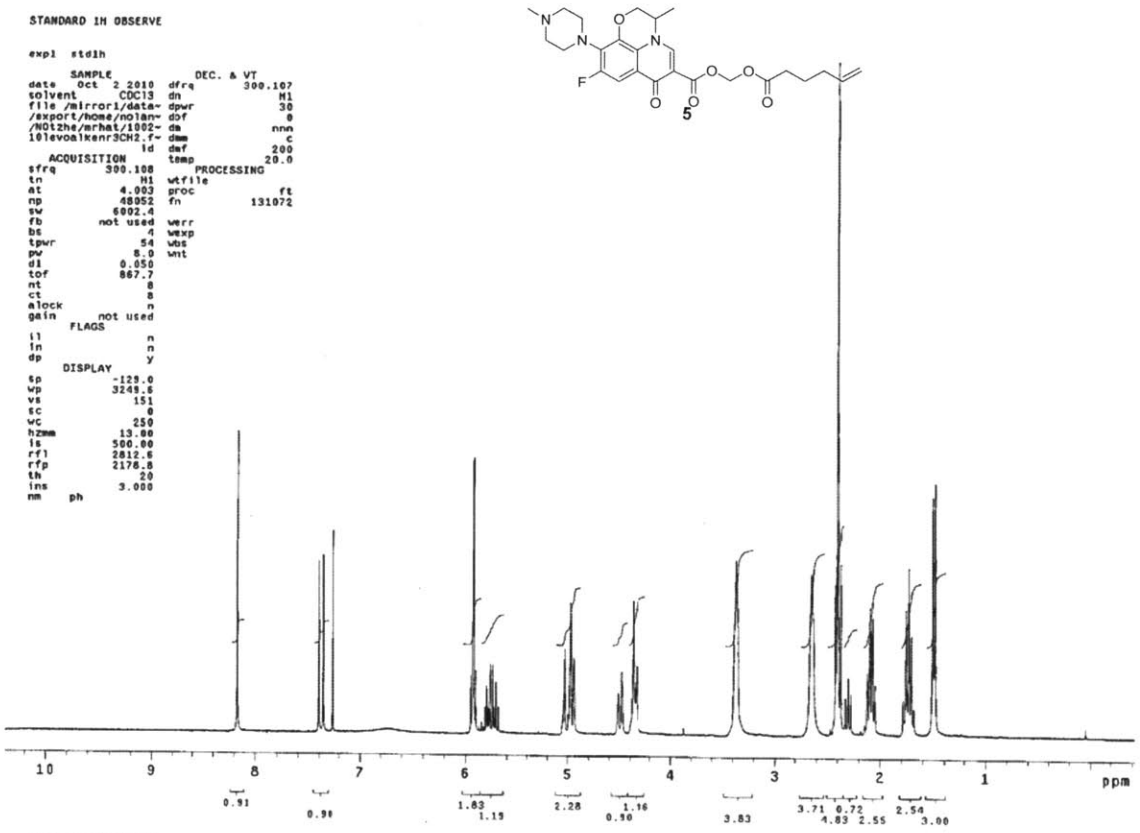
STANDARD 1H OBSERVE
expl stdlh
SAMPLE
date Oct 2 2010
solvent CDCl3
file /mirror1/data~
/export/home/nolan~
/NOtzhe/mrhat/1002~
101evoalkenr3CH2.f~
id
ACQUISITION
sfrq 300.108
tn H1
at 4.003
np 48052
sw 6002.4
fb not used
bs 4
tpwr 54
pw 8.0
d1 0.050
tof 867.7
nt 8
ct 8
alock n
gain not used
FLAGS
il n
in n
dp y
DISPLAY
sp -123.0
wp 3249.6
vs 151
sc 0
wc 250
hzmm 13.00
is 500.00
rfl 2812.6
rfp 2178.8
th 20
ins 3.000
nm ph
DEC. & VT
dfrq 300.107
dn H1
dpwr 30
dof 0
dm nnn
dmm c
dmf 200
temp 20.0
PROCESSING
wtfile
proc ft
fn 131072
werr
wexp
wbs
wnt
5
10 9 8 7 6 5 4 3 2 1 ppm
0.91 0.98 1.83 1.19 2.28 1.16 0.90 3.83 3.71 0.72 4.83 2.55 2.54 3.00

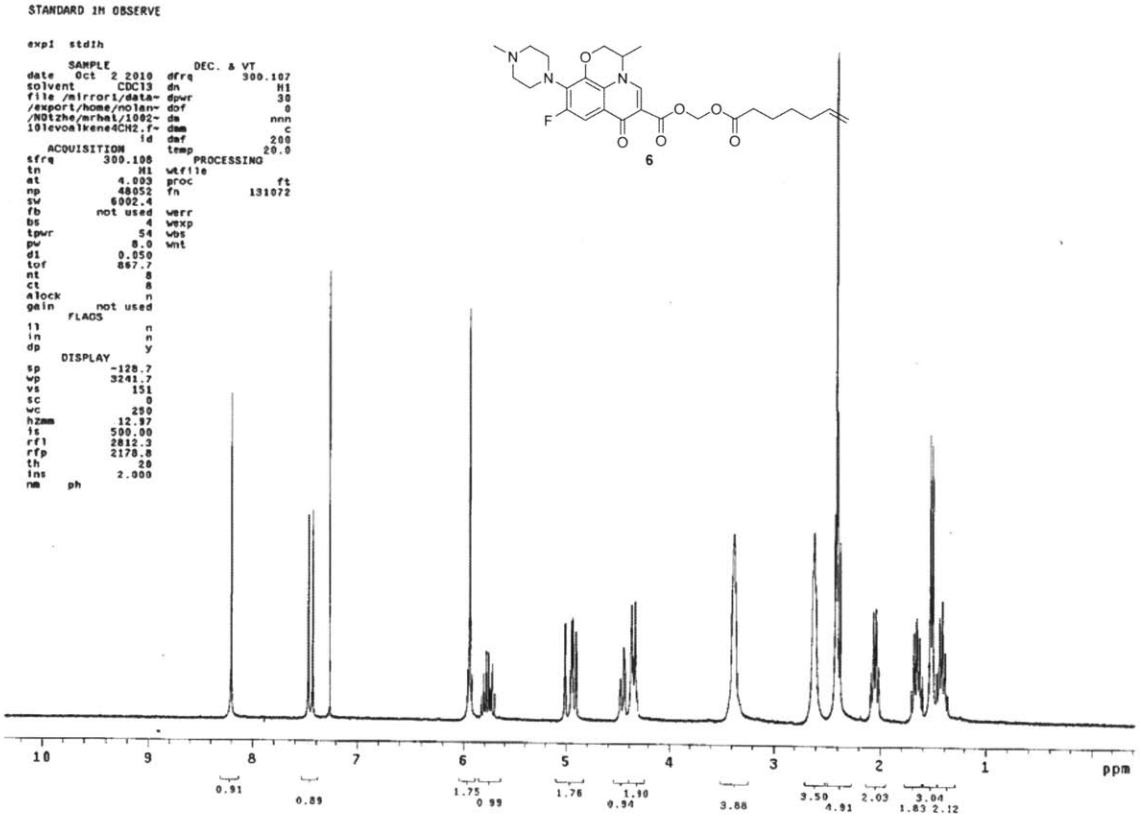
STANDARD 1H OBSERVE
expl stdlh
SAMPLE
date Oct 2 2010
solvent CDCl3
file /mirror1/data~
/export/home/nolan~
/NOtzhe/mrhat/1002~
101evoalkene4CH2.f~
id
ACQUISITION
sfrq 300.108
tn H1
at 4.003
np 48052
sw 6002.4
fb not used
bs 4
tpwr 54
pw 8.0
d1 0.050
tof 867.7
nt 8
ct 8
alock n
gain not used
FLAGS
il n
in n
dp y
DISPLAY
sp -128.7
wp 3241.7
vs 151
sc 0
wc 250
hzmm 12.97
is 500.00
rfl 2812.3
rfp 2178.8
th 20
ins 2.000
nm ph
DEC. & VT
dfrq 300.107
dn H1
dpwr 30
dof 0
dm nnn
dmm c
dmf 200
temp 20.0
PROCESSING
wtfile
proc ft
fn 131072
werr
wexp
wbs
wnt
6
10 9 8 7 6 5 4 3 2 1 ppm
0.91 0.89 1.75 0.99 1.76 1.10 0.94 3.88 3.59 4.91 2.03 3.04 1.83 2.12

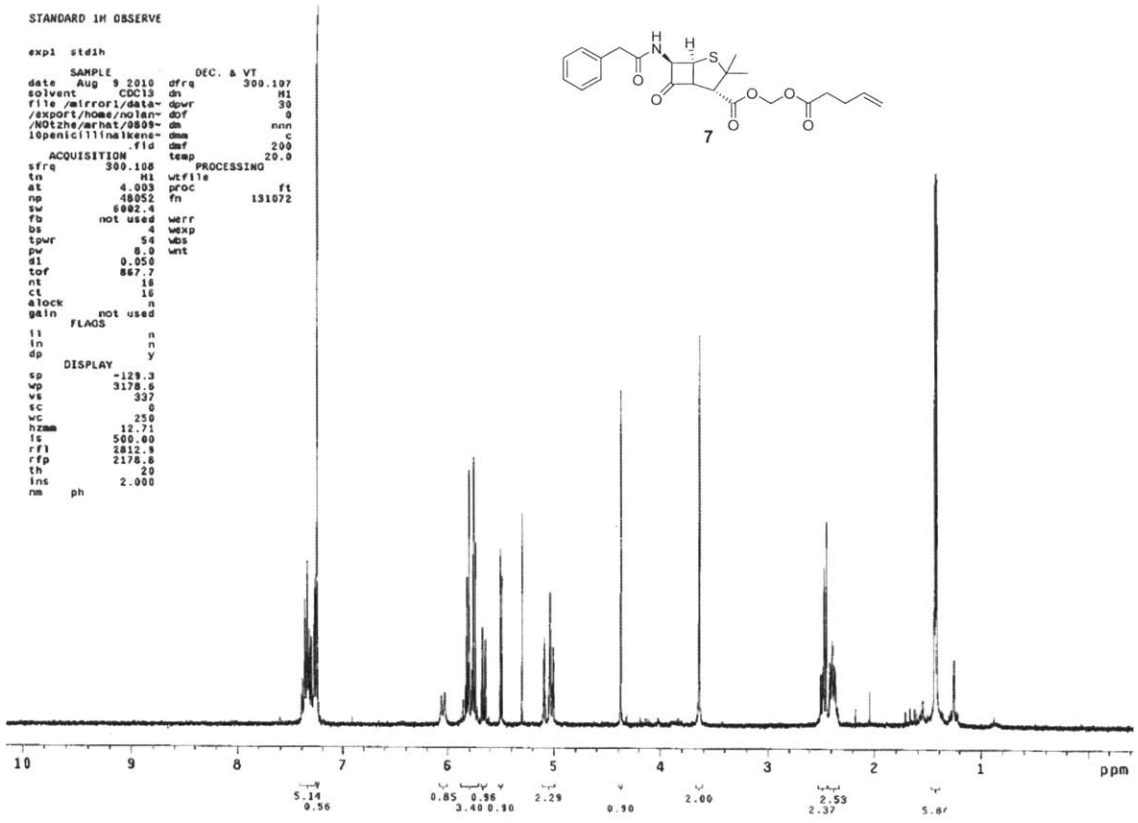
STANDARD 1H OBSERVE
expl stdlh
SAMPLE
date Aug 9 2010
solvent CDCl3
file /mirror1/data~
/export/home/nolan~
/NOtzhe/mrhat/0809~
10penicillinalkene~
.fid
ACQUISITION
sfrq 300.108
tn H1
at 4.003
np 48052
sw 6002.4
fb not used
bs 4
tpwr 54
pw 8.0
d1 0.050
tof 867.7
nt 16
ct 16
alock n
gain not used
FLAGS
il n
in n
dp y
DISPLAY
sp -129.3
wp 3178.6
vs 337
sc 0
wc 250
hzmm 12.71
is 500.00
rfl 2812.9
rfp 2178.8
th 20
ins 2.000
nm ph
DEC. & VT
dfrq 300.107
dn H1
dpwr 30
dof 0
dm nnn
dmm c
dmf 200
temp 20.0
PROCESSING
wtfile
proc ft
fn 131072
werr
wexp
wbs
wnt
7
10
9
8
7
6
5
4
3
2
1
ppm
5.14
0.56
0.85
0.96
3.40
0.90
2.29
0.90
2.00
2.53
2.37

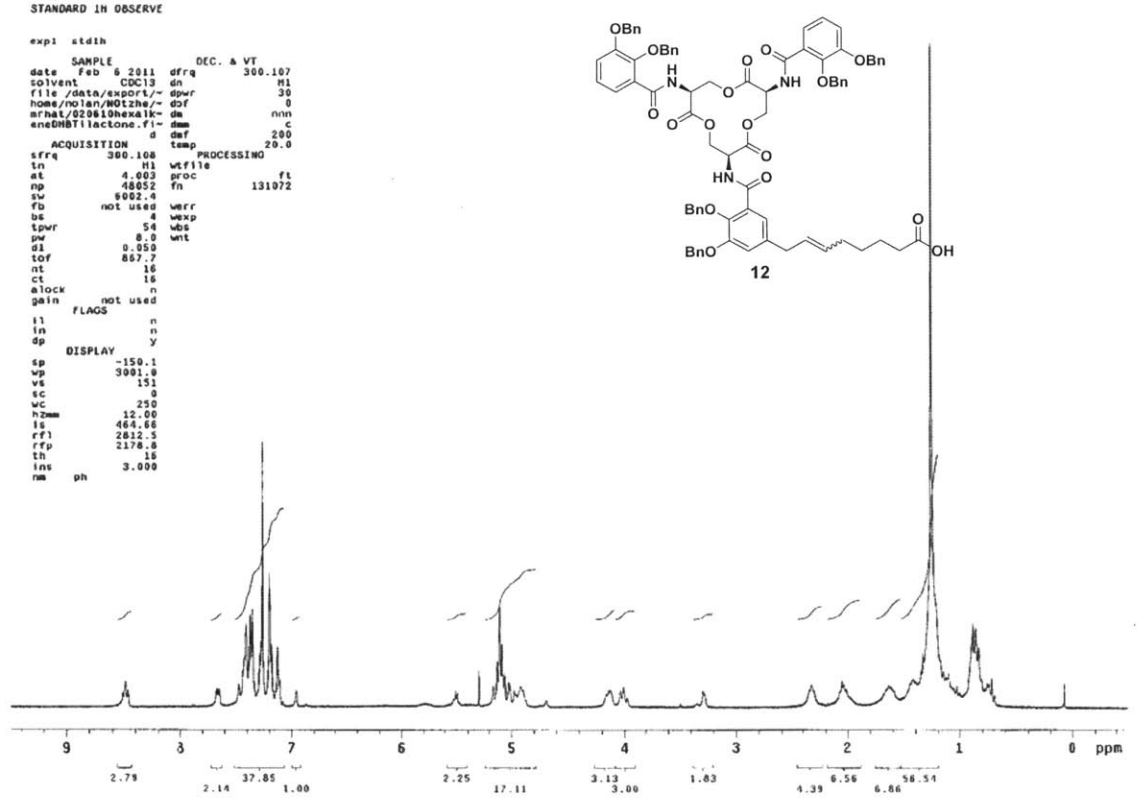
STANDARD 1H OBSERVE
expl stdlh
SAMPLE
date Feb 6 2011
solvent CDCl3
file /data/export/~
home/nolan/NOtzhe/~
mrhat/020610hexalk~
eneDMBTilactone.fi~
d
ACQUISITION
sfrq 300.108
tn H1
at 4.003
np 48052
sw 6002.4
fb not used
bs 4
tpwr 54
pw 8.0
d1 0.050
tof 867.7
nt 16
ct 16
alock n
gain not used
FLAGS
il n
in n
dp y
DISPLAY
sp -150.1
wp 3001.8
vs 151
sc 0
wc 250
hzmm 12.00
is 464.66
rfl 2812.5
rfp 2178.8
th 18
ins 3.000
nm ph
DEC. & VT
dfrq 300.107
dn H1
dpwr 30
dof 0
dm nnn
dmm c
dmf 200
temp 20.0
PROCESSING
wtfile
proc ft
fn 131072
werr
wexp
wbs
wnt
OBn
OBn
OBn
OBn
NH
HN
BnO
BnO
OH
12
9
8
7
6
5
4
3
2
1
0
ppm
2.79
2.14
37.85
1.00
2.25
17.11
3.13
3.00
1.83
4.39
6.56
6.86
58.54

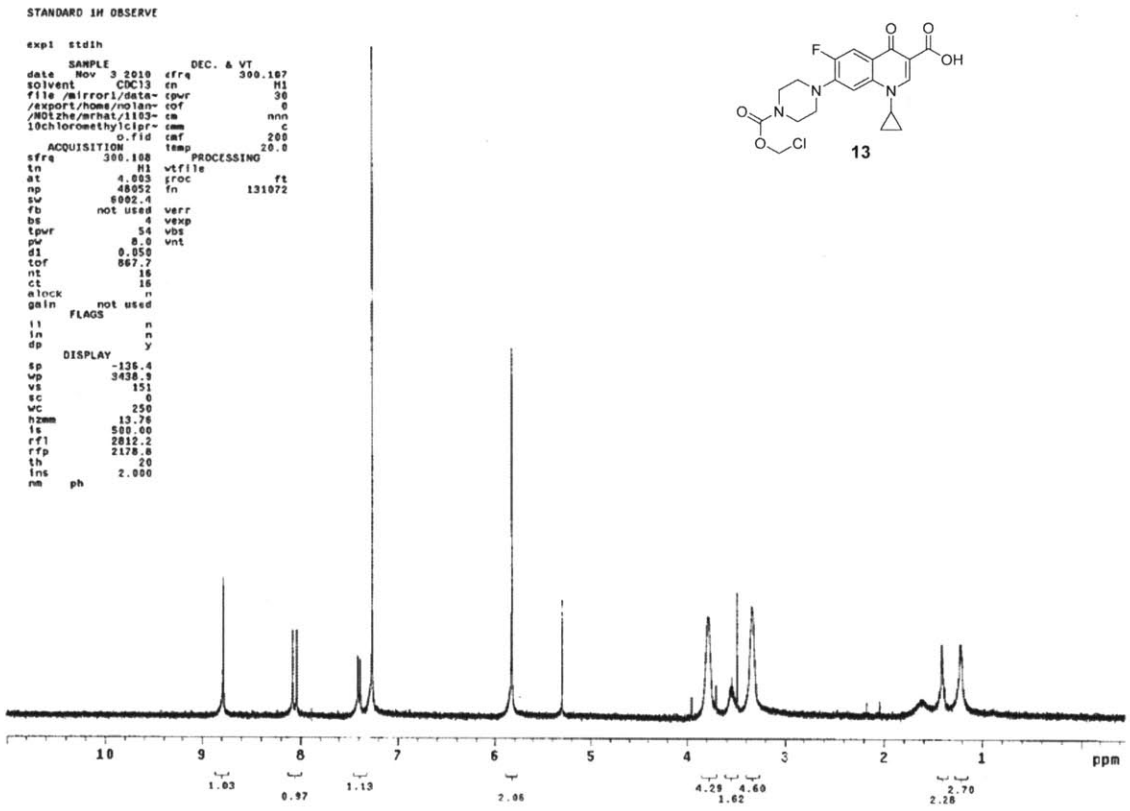
STANDARD 1H OBSERVE
expl stdih
SAMPLE
date Nov 3 2010
solvent CDCl3
file /mirror1/data-
/export/home/nolan-
/NOtzhe/mrhat/1103-
10chloromethylcipr-
o.fid
ACQUISITION
sfrq 300.108
tn H1
at 4.003
np 48052
sw 6002.4
fb not used
bs 4
tpwr 54
pw 8.0
d1 0.050
tof 867.7
nt 16
ct 16
alock n
gain not used
FLAGS
il n
in n
dp y
DISPLAY
sp -136.4
wp 3438.9
vs 151
sc 0
wc 250
hzmm 13.76
is 500.00
rfl 2812.2
rfp 2178.8
th 20
ins 2.000
nm ph
DEC. & VT
dfrq 300.107
dn H1
dpwr 30
dof 0
dm nnn
dmm c
dmf 200
temp 20.0
PROCESSING
wtfile
proc ft
fn 131072
werr
wexp
wbs
wnt
13
10
9
8
7
6
5
4
3
2
1
ppm
1.03
0.97
1.13
2.06
4.29
4.60
1.62
2.70
2.28

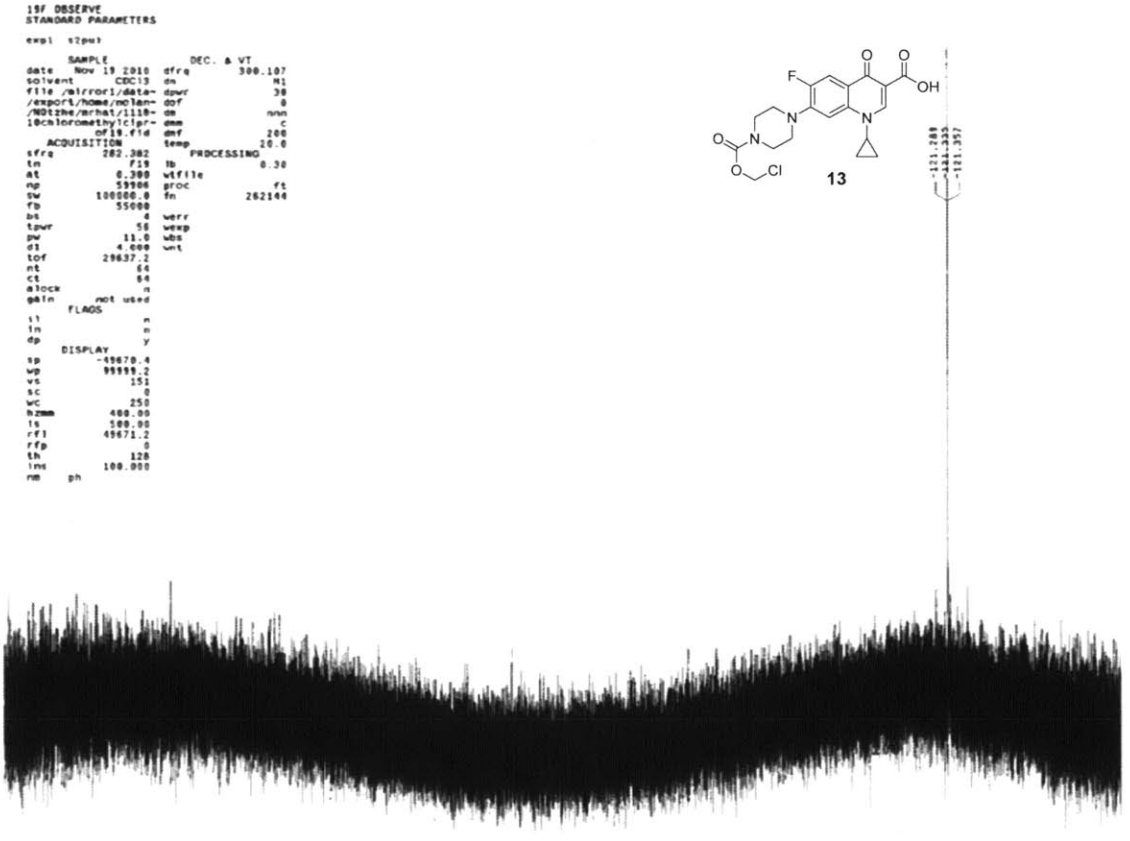
19F OBSERVE
STANDARD PARAMETERS
expl stpwh
SAMPLE
date Nov 19 2010
solvent CDCl3
file /mirror1/data-
/export/home/nolan-
/NOtzhe/mrhat/1110-
10chloromethylcipr-
of19.fid
ACQUISITION
sfrq 282.382
tn F19
at 0.300
np 59906
sw 100000.0
fb 55000
bs 4
tpwr 58
pw 11.0
d1 4.000
tof 29637.2
nt 64
ct 64
alock n
gain not used
FLAGS
il n
in n
dp y
DISPLAY
sp -49679.4
wp 99999.2
vs 151
sc 0
wc 250
hzmm 400.00
is 500.00
rfl 49671.2
rfp 0
th 128
ins 100.000
nm ph
DEC. & VT
dfrq 300.107
dn H1
dpwr 30
dof 0
dm nnn
dmm c
dmf 200
temp 20.0
PROCESSING
lb 0.30
wtfile
proc ft
fn 262144
13
-121.268
-121.353
-121.357

STANDARD 1H OBSERVE

```
expl  stdlh

      SAMPLE                  DEC. & VT
date    Dec 20 2010   dfrq          300.107
solvent       CDCl3   dn                H1
file /mirror1/data-   dpwr              30
/export/home/nolan-   dof                0
/NOlzhe/mrhat/1220-   dm               nnn
10bocbalaninecipro-   dmm                c
              .fid    dmf              200
   ACQUISITION        temp            20.0
sfrq        300.108             PROCESSING
tn               H1   wtfile
at            4.003   proc              ft
np            48052   fn            131072
sw           6002.4
fb         not used   werr
bs                4   wexp
tpwr             54   wbs
pw              8.0   wnt
d1            0.050
tof           867.7
nt               16
ct               16
alock             n
gain       not used
      FLAGS
il                n
in                n
dp                y
     DISPLAY
sp           -633.9
wp           6002.3
vs              151
sc                0
wc              250
hzmm          24.01
is           500.00
rfl          2812.7
rfp          2178.8
th                1
ins           2.000
nm    ph
```

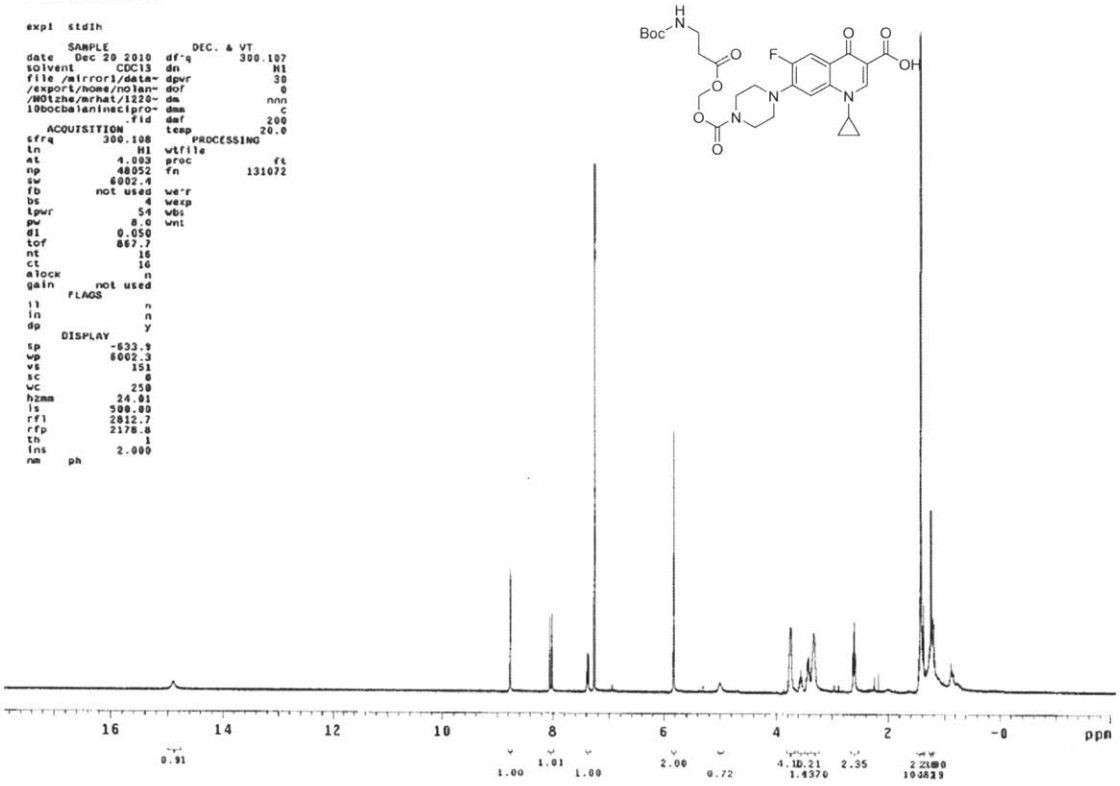

19F OBSERVE
STANDARD PARAMETERS

```
expl  s2pul

      SAMPLE                  DEC. & VT
date    Nov 16 2010   dfrq          282.382
solvent       CDCl3   dn                F19
file /mirror1/data-   dpwr              30
/export/home/nolan-   dof                0
/NOlzhe/mrhat/1115-   dm               nnn
10balaninecipro f19-  dmm                c
              .fid    dmf              200
   ACQUISITION        temp            20.0
sfrq        282.382             PROCESSING
tn               F19  lb              0.30
at             0.300  wtfile
np             59906  proc              ft
sw         100000.0   fn            262144
fb             55000
bs                4   werr
tpwr             56   wexp
pw             11.0   wbs
d1            4.000   wnt
tof         25637.2
nt               16
ct               16
alock             n
gain       not used
      FLAGS
il                n
in                n
dp                y
     DISPLAY
sp         -45681.9
wp         99999.2
vs              114
sc                0
wc              250
hzmm          400.00
is            500.00
rfl         43882.6
rfp               0
th               77
ins          100.000
nm    ph
```

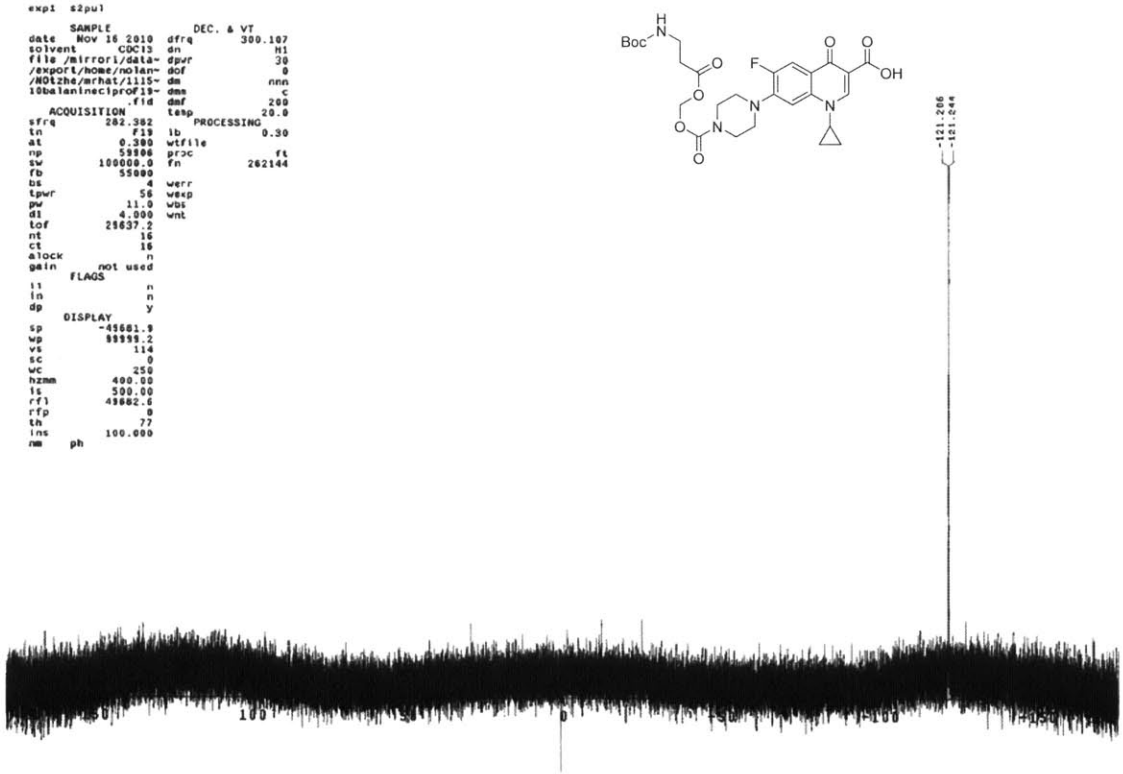

STANDARD 1H OBSERVE

expl std1h

SAMPLE		DEC. & VT	
date	Dec 1 2010	dfrq	300.108
solvent	DMSO	dn	H1
file	/mirror1/data~	dpwr	30
	/export/home/nolan~	dof	0
	/NOtizhe/mrhat/1201~	dm	nnn
	10balaninecipro.fi~	dmm	c
	d	dmf	200
ACQUISITION		temp	20.0
sfrq	300.109	PROCESSING	
tn	H1	wtfile	
at	4.003	proc	ft
np	48052	fn	131072
sw	6002.4		
fb	not used	werr	
bs	4	wexp	
tpwr	54	wbs	
pw	8.0	wnt	
dl	0.050		
tof	867.7		
nt	64		
ct	64		
alock	n		
gain	not used		
FLAGS			
il	n		
in	n		
dp	y		
DISPLAY			
sp	-124.3		
wp	3738.6		
vs	151		
sc	0		
wc	250		
hzmm	14.95		
is	500.00		
rfl	1379.4		
rfp	750.3		
th	20		
ins	2.000		
nm	ph		

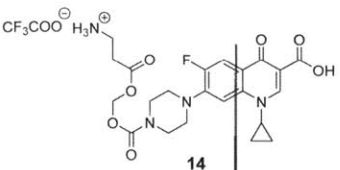

14

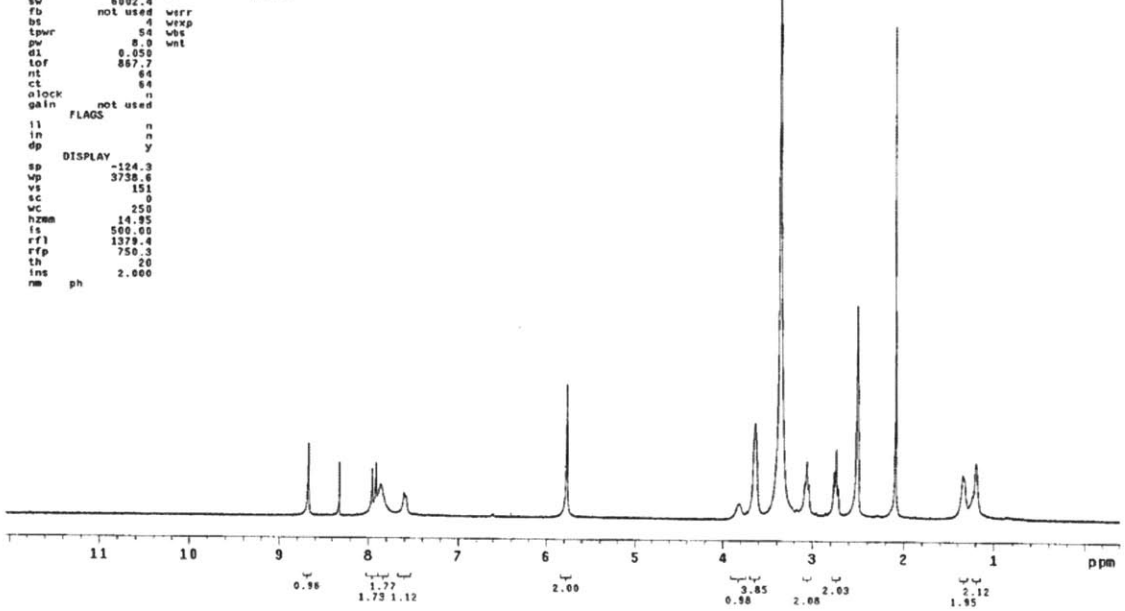

19F OBSERVE
STANDARD PARAMETERS

expl s2pul

SAMPLE		DEC. & VT	
date	Dec 1 2010	dfrq	300.108
solvent	DMSO	dn	H1
file	/mirror1/data~	dpwr	30
	/export/home/nolan~	dof	0
	/NOtizhe/mrhat/1201~	dm	nnn
	10F19balaninecipro~	dmm	c
	.fid	dmf	200
ACQUISITION		temp	20.0
sfrq	282.383	PROCESSING	
tn	F19	lb	0.30
at	0.300	wtfile	
np	58986	proc	ft
sw	100000.0	fn	262144
fb	55000		
bs	4	werr	
tpwr	56	wexp	
pw	11.0	wbs	
dl	4.000	wnt	
tof	29637.2		
nt	32		
ct	0		
alock	n		
gain	not used		
FLAGS			
il	n		
in	n		
dp	y		
DISPLAY			
sp	-49525.5		
wp	99999.2		
vs	151		
sc	0		
wc	250		
hzmm	400.00		
is	500.00		
rfl	49526.2		
rfp	0		
th	8		
ins	3.000		
nm	ph		

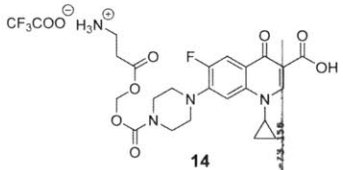

14

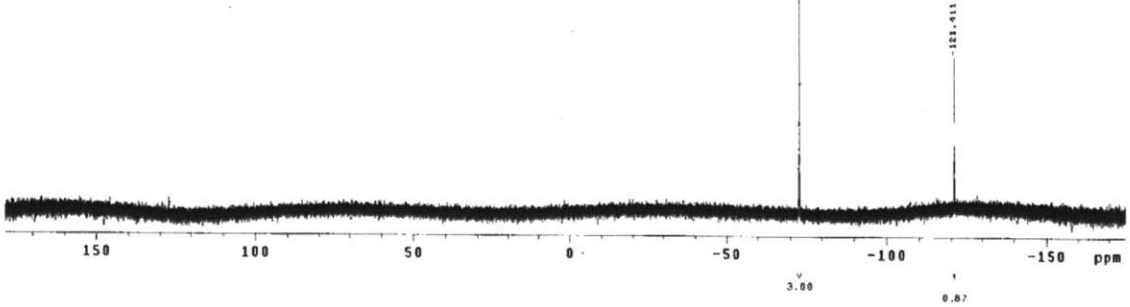

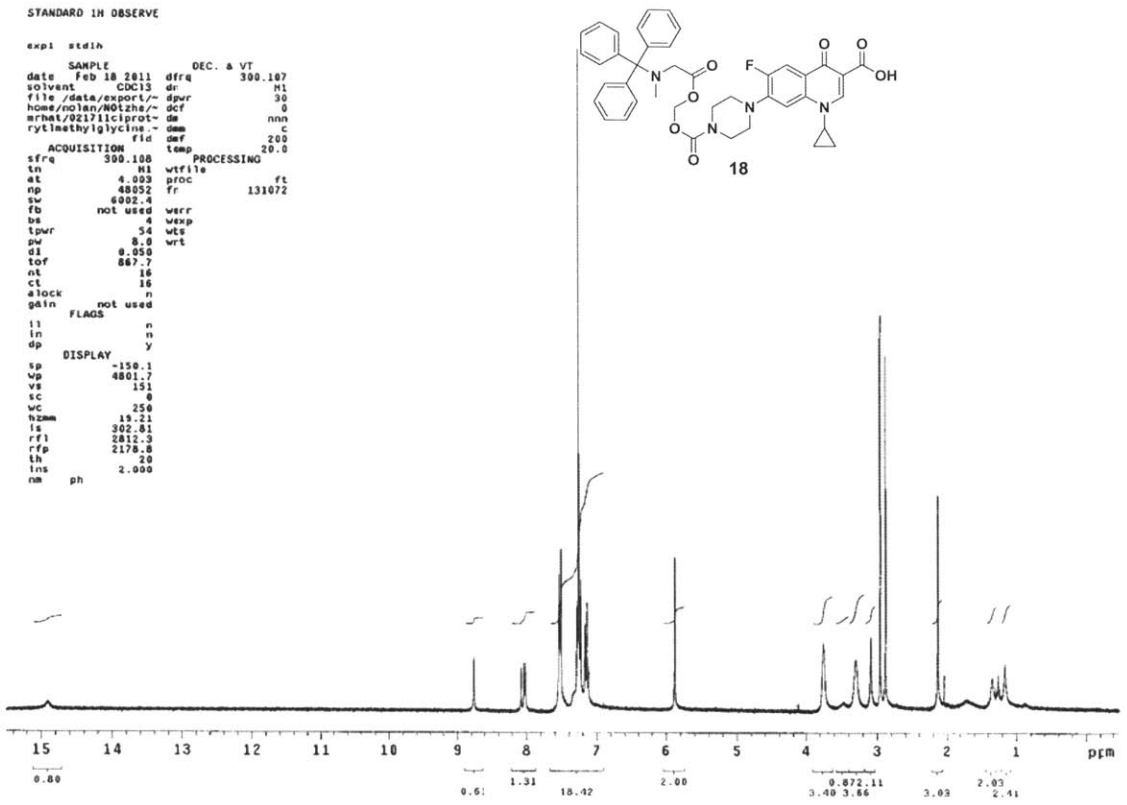
STANDARD 1H OBSERVE
expl stdih
SAMPLE
date Feb 18 2011
solvent CDCl3
file /data/export/~
home/nolan/NOtzhe/~
mrhat/021711ciprot~
rytlmethylglycine.~
fid
ACQUISITION
sfrq 300.108
tn H1
at 4.003
np 48052
sw 6002.4
fb not used
bs 4
tpwr 54
pw 8.0
d1 0.050
tof 867.7
nt 16
ct 16
alock n
gain not used
FLAGS
il n
in n
dp y
DISPLAY
sp -150.1
wp 4801.7
vs 151
sc 0
wc 250
hzmm 19.21
is 302.81
rfl 2812.3
rfp 2178.8
th 20
ins 2.000
nm ph
DEC. & VT
dfrq 300.107
dn H1
dpwr 30
dcf 0
de nnn
dmm c
dmf 200
temp 20.0
PROCESSING
wtfile
proc ft
fn 131072
wexp
wbs
wnt
18
15 14 13 12 11 10 9 8 7 6 5 4 3 2 1 ppm
0.80
0.61 1.31 18.42 2.00 0.872.11 3.40 3.86 3.03 2.03 2.41

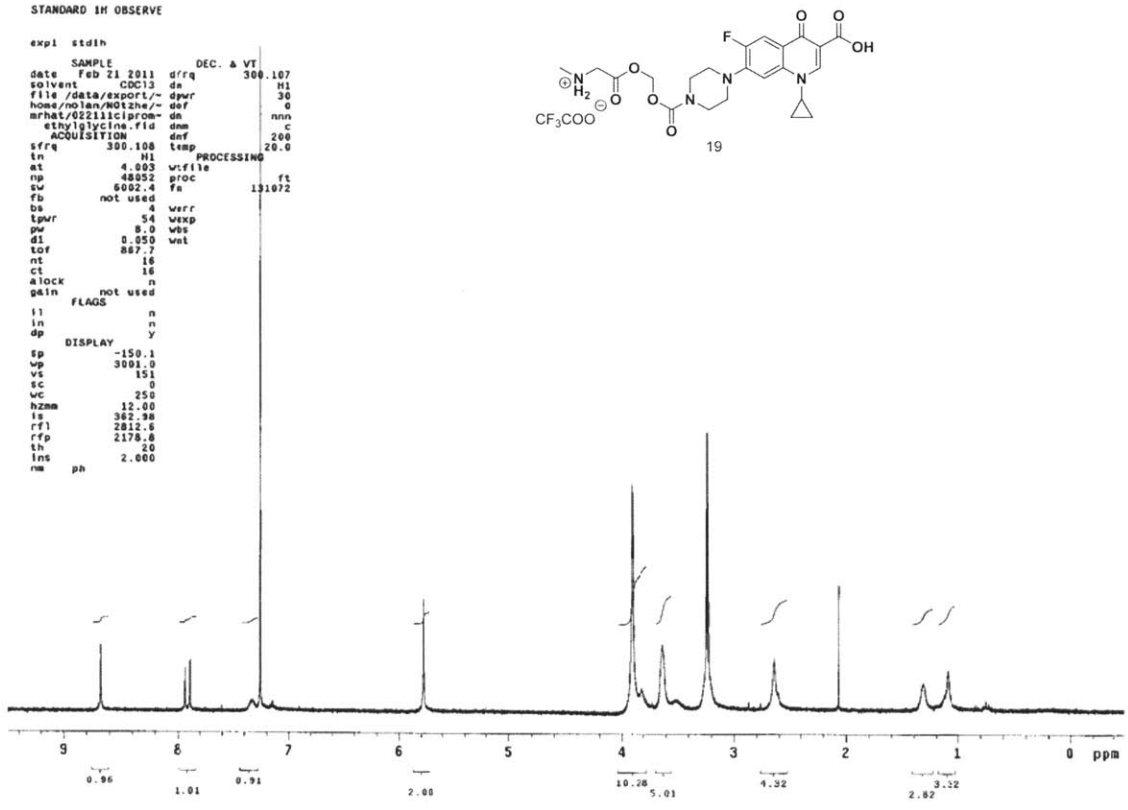
STANDARD 1H OBSERVE
expl stdih
SAMPLE
date Feb 21 2011
solvent CDCl3
file /data/export/~
home/nolan/NOtzhe/~
mrhat/022111ciprom~
ethylglycine.fid
ACQUISITION
sfrq 300.108
tn H1
at 4.003
np 48052
sw 6002.4
fb not used
bs 4
tpwr 54
pw 8.0
d1 0.050
tof 867.7
nt 16
ct 16
alock n
gain not used
FLAGS
il n
in n
dp y
DISPLAY
sp -150.1
wp 3001.0
vs 151
sc 0
wc 250
hzmm 12.00
is 302.98
rfl 2812.6
rfp 2178.8
th 20
ins 2.000
nm ph
DEC. & VT
dfrq 300.107
dn H1
dpwr 30
dcf 0
de nnn
dmm c
dmf 200
temp 20.0
PROCESSING
wtfile
proc ft
fn 131072
wexp
wbs
wnt
19
9 8 7 6 5 4 3 2 1 0 ppm
0.96 1.01 0.91 2.00 10.28 5.01 4.32 3.32 2.82

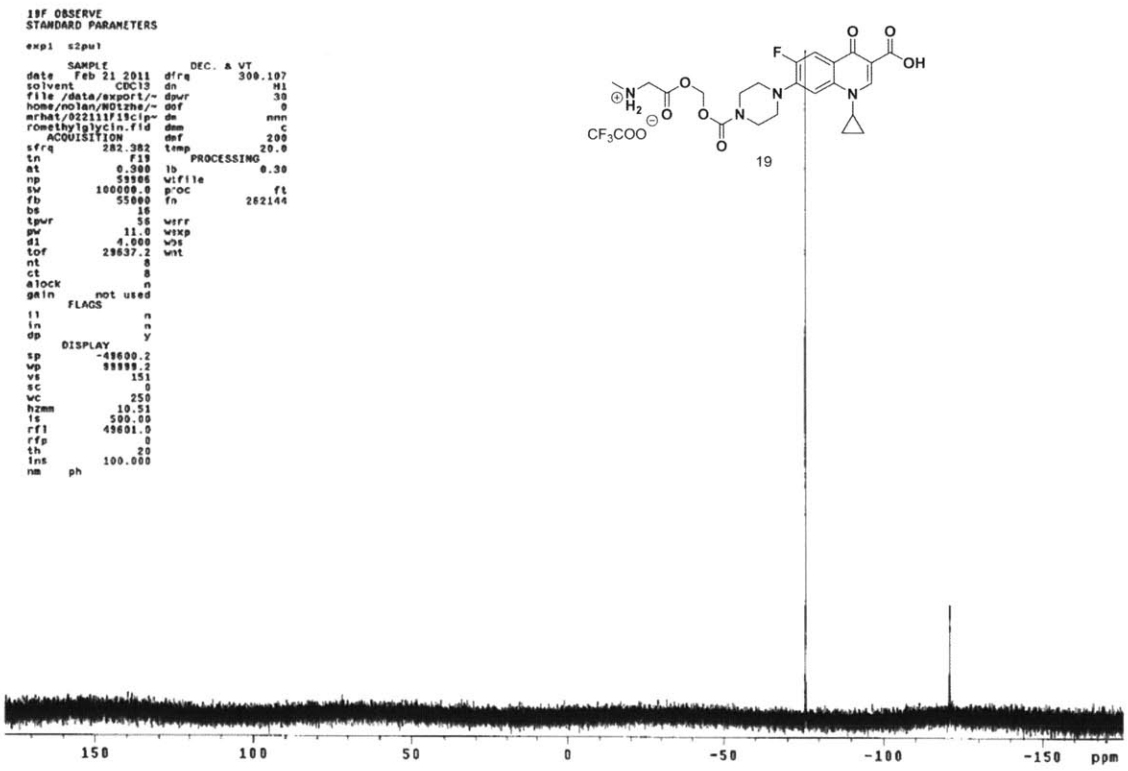
19F OBSERVE
STANDARD PARAMETERS
expl s2pul
SAMPLE
date Feb 21 2011
solvent CDCl3
file /data/export/~
home/nolan/NOlzhe/~
mrhat/022111F19clp~
romethylglycln.fid
ACQUISITION
sfrq 282.382
tn F19
at 0.300
np 59986
sw 100000.0
fb 55000
bs 16
tpwr 56
pw 11.0
d1 4.000
tof 29637.2
nt 8
ct 8
alock n
gain not used
FLAGS
il n
in n
dp y
DISPLAY
sp -45600.2
wp 99999.2
vs 151
sc 0
wc 250
hzmm 10.51
is 500.00
rfl 49601.0
rfp 0
th 20
ins 100.000
nm ph
DEC. & VT
dfrq 300.107
dn H1
dpwr 30
dof 0
dm nnn
dmm c
def 200
temp 20.0
PROCESSING
lb 0.30
wtfile
proc ft
fn 262144
wrr
wxp
wbs
wnt
F
OH
19
150
100
50
0
-50
-100
-150
ppm

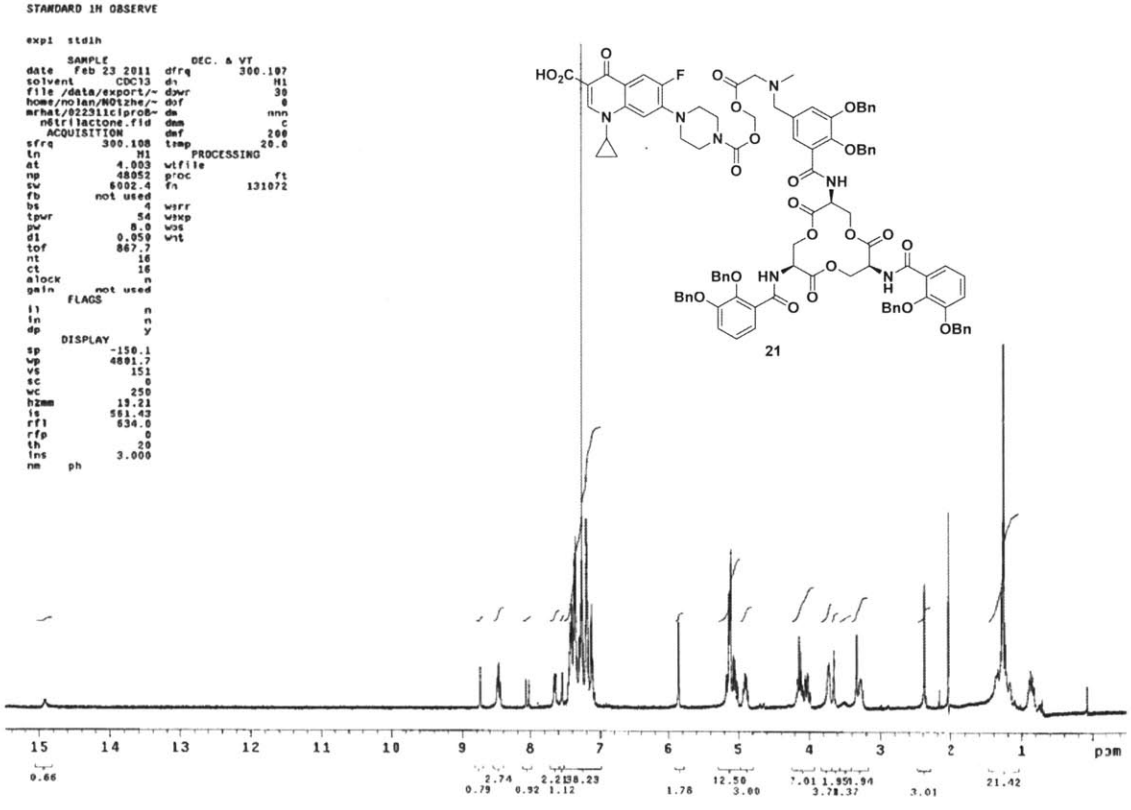
STANDARD 1H OBSERVE
expl stdlh
SAMPLE
date Feb 23 2011
solvent CDCl3
file /data/export/~
home/nolan/NOlzhe/~
mrhat/022311clproB~
n6trilactone.fid
ACQUISITION
sfrq 300.108
tn H1
at 4.003
np 48052
sw 6002.4
fb not used
bs 4
tpwr 54
pw 8.0
d1 0.950
tof 867.7
nt 16
ct 16
alock n
gain not used
FLAGS
il n
in n
dp y
DISPLAY
sp -150.1
wp 4801.7
vs 151
sc 0
wc 250
hzmm 15.21
is 581.42
rfl 634.0
rfp 0
th 20
ins 3.000
nm ph
DEC. & VT
dfrq 300.107
dn H1
dpwr 30
dof 0
dm nnn
dmm c
def 200
temp 20.0
PROCESSING
wtfile
proc ft
fn 131072
wrr
wxp
wbs
wnt
HO2C
F
OBn
NH
BnO
HN
21
15
14
13
12
11
10
9
8
7
6
5
4
3
2
1
ppm
0.66
2.74
0.79
0.92
1.12
2.23
8.23
1.78
12.50
3.00
7.01
1.95
1.94
3.78
3.37
3.01
21.42

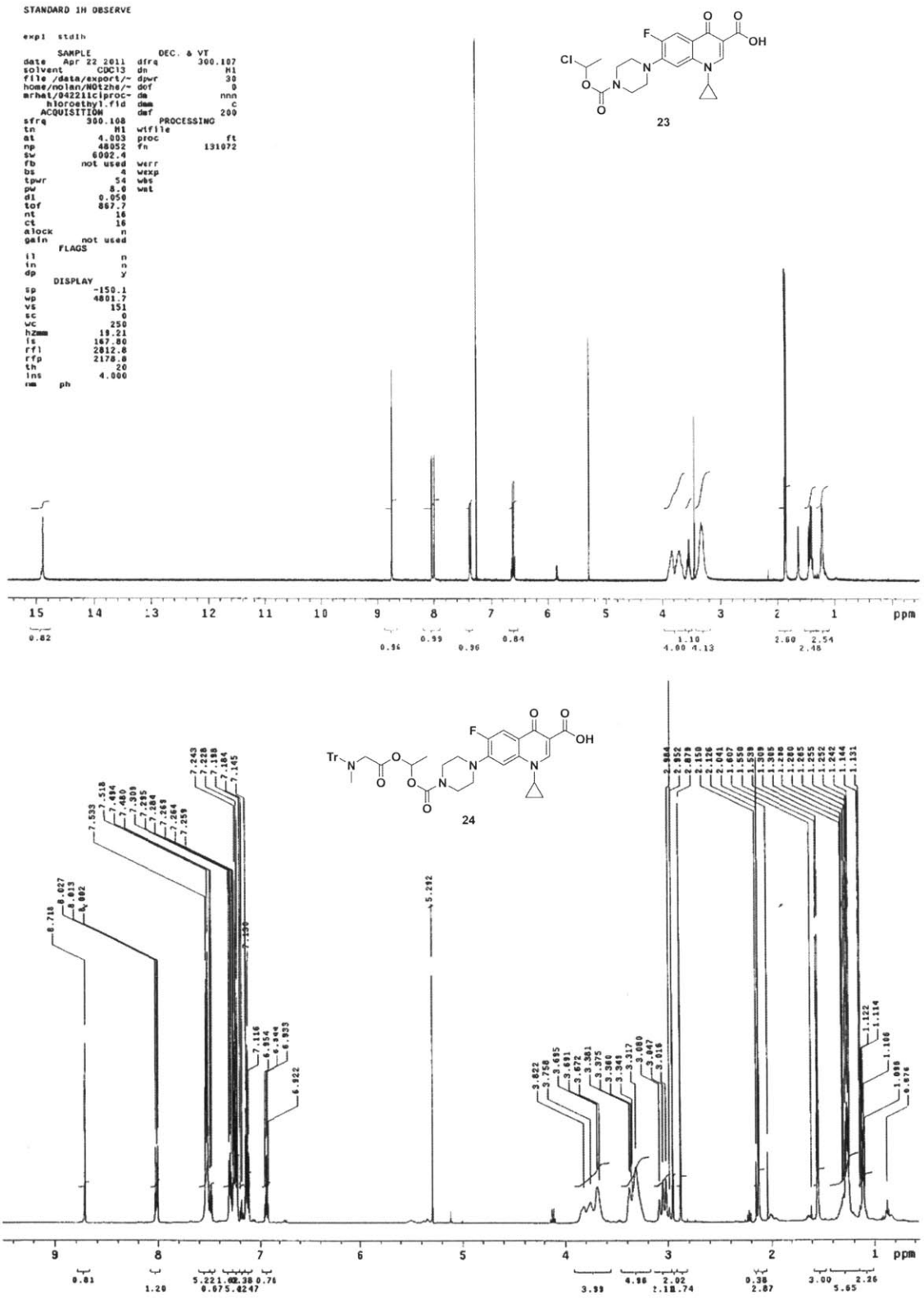
STANDARD 1H OBSERVE
expl stdih
SAMPLE
date Apr 22 2011
solvent CDCl3
file /data/export/~
home/nolan/NOtzhe/~
mrhat/04221iciproc-
hloroethyl.fid
ACQUISITION
sfrq 300.108
tn H1
at 4.003
np 48052
sw 6002.4
fb not used
bs 4
tdwr 54
pw 8.0
d1 0.050
tof 867.7
nt 16
ct 16
alock n
gain not used
FLAGS
il n
in n
dp y
DISPLAY
sp -150.1
wp 4801.7
vs 151
sc 0
wc 250
hzmm 19.21
is 167.80
rfl 2812.8
rfp 2178.8
th 20
ins 4.000
ph
DEC. & VT
dfrq 300.107
dn H1
dpwr 30
dof 0
dm nnn
dmm c
daf 200
PROCESSING
wtfile
proc ft
fn 131072
werr
wexp
wbs
wnt
23
24
ppm

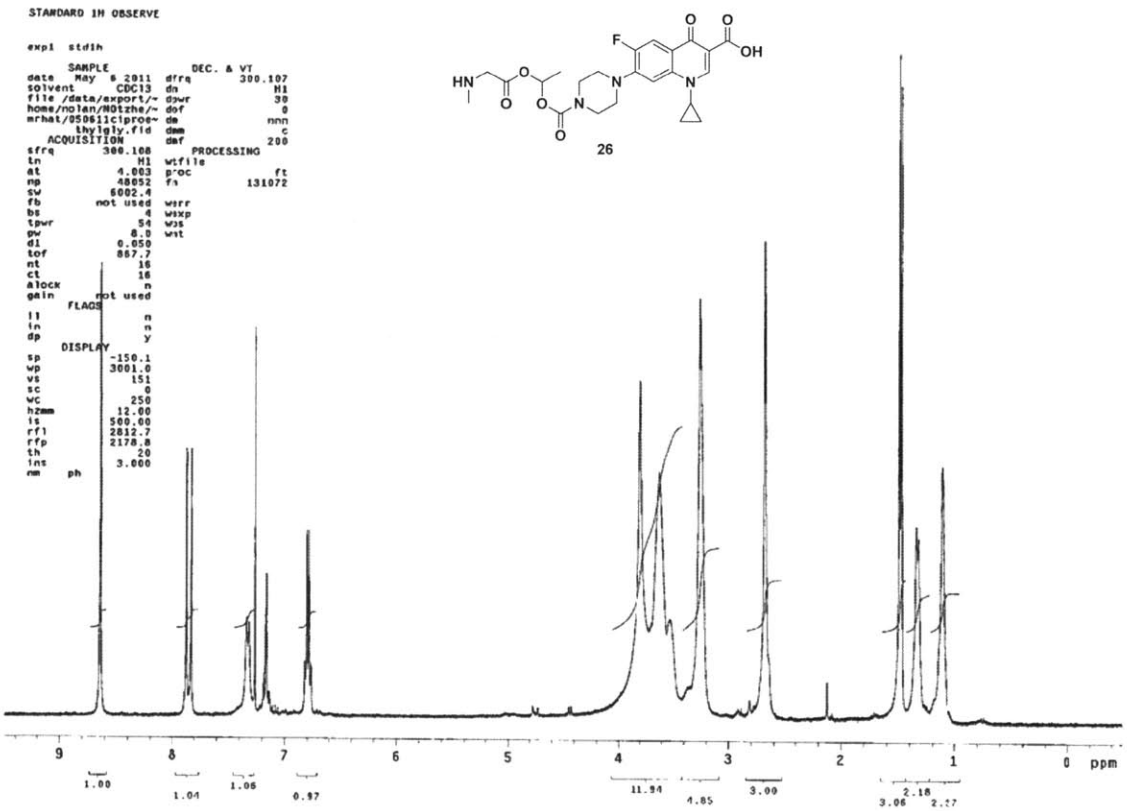
STANDARD 1H OBSERVE
expl stdih
SAMPLE
date May 6 2011
solvent CDCl3
file /data/export/~
home/nolan/NOtzhe/~
mrhat/050611ciproc~
thylglly.fid
ACQUISITION
sfrq 300.108
tn H1
at 4.003
np 48052
sw 6002.4
fb not used
bs 4
tpwr 54
pw 8.8
d1 0.050
tof 867.7
nt 16
ct 16
alock n
gain not used
FLAGS
il n
in n
dp y
DISPLAY
sp -150.1
wp 3001.0
vs 151
sc 0
wc 250
hzmm 12.00
is 500.00
rf1 2812.7
rfp 2178.8
th 20
ins 3.000
nm ph
DEC. & VT
dfrq 300.107
dn H1
dpwr 30
dof 0
da nnn
dmm c
dmf 200
PROCESSING
wtfile
proc ft
fn 131072
wtmr
wtxp
wts
wnt
F
O
OH
HN
O
O
O
O
N
N
N
O
26
9
8
7
6
5
4
3
2
1
0 ppm
1.00
1.04
1.06
0.97
11.94
4.85
3.00
2.18
3.06
2.27

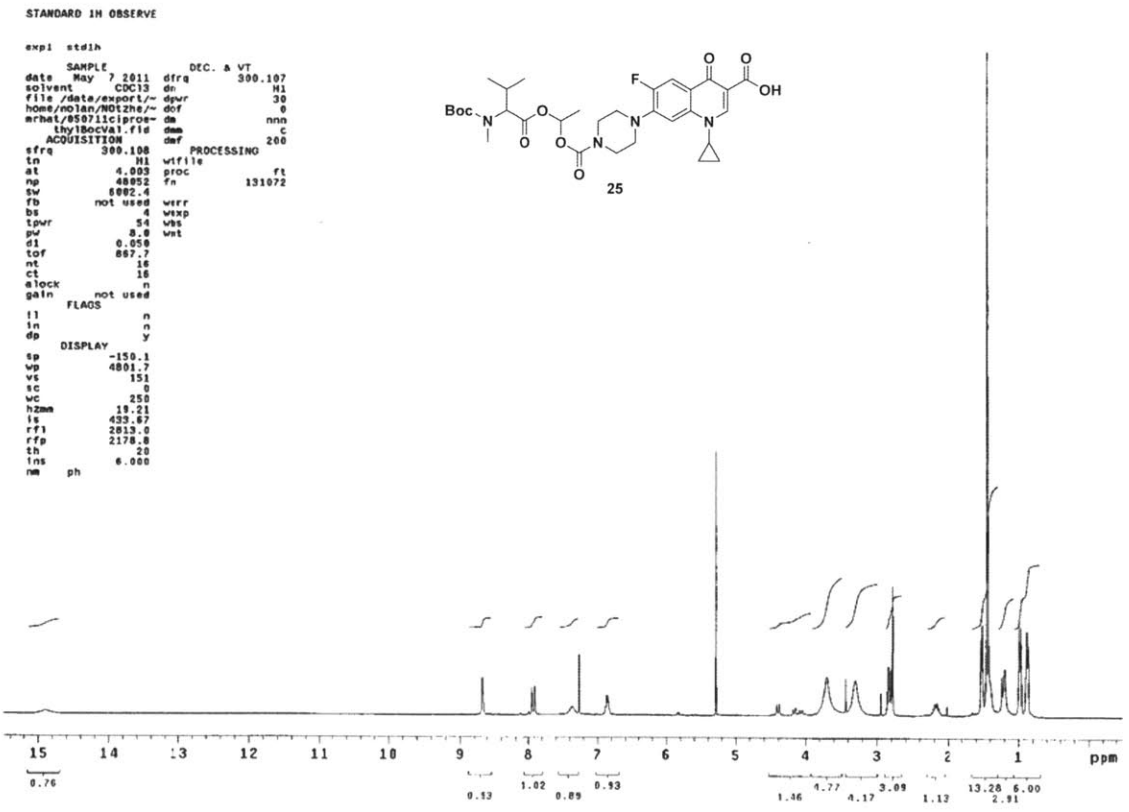
STANDARD 1H OBSERVE
expl stdih
SAMPLE
date May 7 2011
solvent CDCl3
file /data/export/~
home/nolan/NOtzhe/~
mrhat/050711ciproc~
thylBocVal.fid
ACQUISITION
sfrq 300.108
tn H1
at 4.003
np 48052
sw 6002.4
fb not used
bs 4
tpwr 54
pw 8.8
d1 0.050
tof 867.7
nt 16
ct 16
alock n
gain not used
FLAGS
il n
in n
dp y
DISPLAY
sp -150.1
wp 4801.7
vs 151
sc 0
wc 250
hzmm 19.21
is 433.67
rf1 2813.0
rfp 2178.8
th 20
ins 6.000
nm ph
DEC. & VT
dfrq 300.107
dn H1
dpwr 30
dof 0
da nnn
dmm c
dmf 200
PROCESSING
wtfile
proc ft
fn 131072
wtmr
wtxp
wts
wnt
Boc
N
O
O
O
O
N
N
F
O
OH
25
15
14
13
12
11
10
9
8
7
6
5
4
3
2
1
ppm
0.76
0.53
1.02
0.89
0.93
1.46
1.77
4.17
3.09
1.13
13.26
6.00
2.91

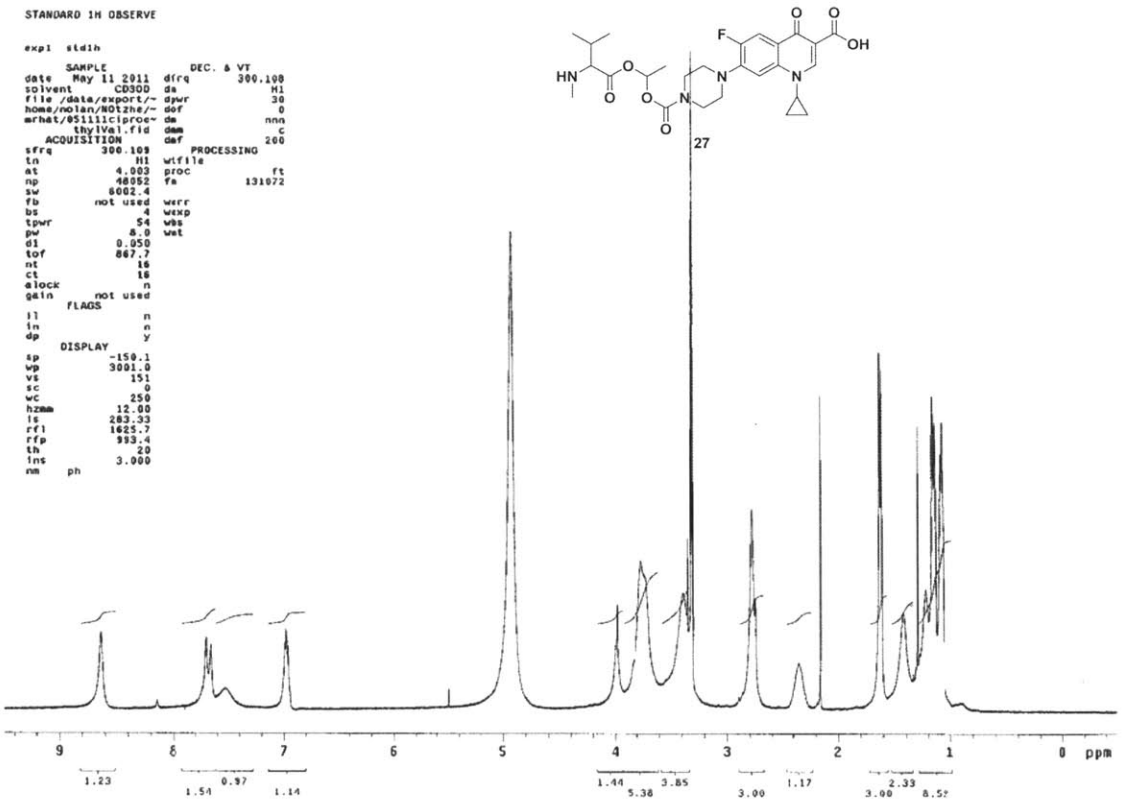
STANDARD 1H OBSERVE
expl stdih
SAMPLE
date May 11 2011
solvent CD3OD
file /data/export/~
home/nolan/NOlzhe/~
mrhat/051111ciproc~
thylVal.fid
ACQUISITION
sfrq 300.109
tn H1
at 4.003
np 48052
sw 6002.4
fb not used
bs 4
tpwr 54
pw 8.0
d1 0.050
tof 867.7
nt 16
ct 16
alock n
gain not used
FLAGS
il n
in n
dp y
DISPLAY
sp -150.1
wp 3001.0
vs 151
sc 0
wc 250
hzmm 12.00
is 283.33
rfl 1625.7
rfp 993.4
th 20
ins 3.000
nm ph
DEC. & VT
dfrq 300.108
dn H1
dpwr 30
dof 0
dm nnn
dmm c
dmf 200
PROCESSING
wtfile
proc ft
fn 131072
werr
wexp
wbs
wnt
27
9
8
7
6
5
4
3
2
1
0 ppm
1.23
0.97
1.54
1.14
1.44
3.85
5.38
3.00
1.17
2.33
3.00
8.57

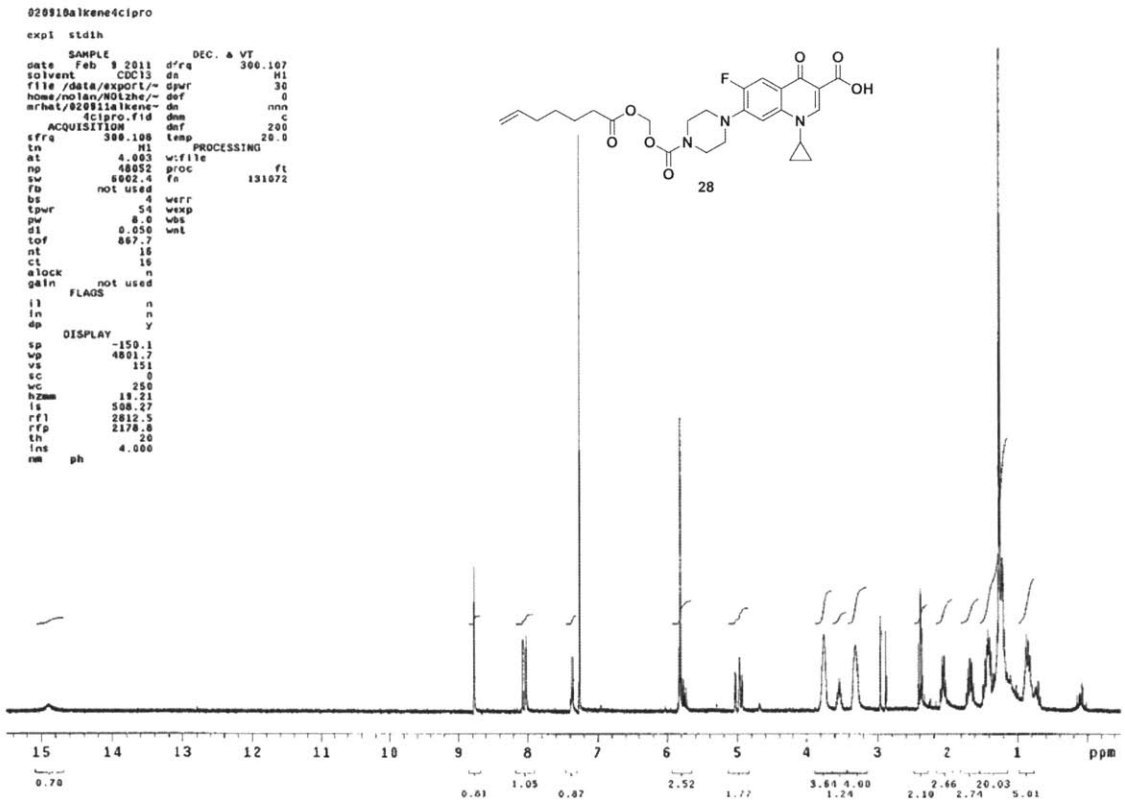
020918alkene4cipro
expl stdih
SAMPLE
date Feb 9 2011
solvent CDCl3
file /data/export/~
home/nolan/NOlzhe/~
mrhat/020911alkene~
4cipro.fid
ACQUISITION
sfrq 300.108
tn H1
at 4.003
np 48052
sw 6002.4
fb not used
bs 4
tpwr 54
pw 8.0
d1 0.050
tof 867.7
nt 16
ct 16
alock n
gain not used
FLAGS
il n
in n
dp y
DISPLAY
sp -150.1
wp 4801.7
vs 151
sc 0
wc 250
hzmm 19.21
is 508.27
rfl 2812.5
rfp 2178.8
th 20
ins 4.000
nm ph
DEC. & VT
dfrq 300.107
dn H1
dpwr 30
dof 0
dm nnn
dmm c
dmf 200
temp 20.0
PROCESSING
wtfile
proc ft
fn 131072
werr
wexp
wbs
wnt
28
15
14
13
12
11
10
9
8
7
6
5
4
3
2
1
ppm
0.78
0.61
1.05
0.87
2.52
1.77
3.61
4.00
1.24
2.66
20.03
2.10
2.74
5.01

STANDARD 1H OBSERVE

```
exp1  std1h

      SAMPLE                  DEC. & VT
date   Jul 12 2011  dfrq          300.107
solvent       CDCl3  dn                H1
file /data/export/~  dpwr              30
home/nolan/NOtzhe/~  dof                0
mrhat/071211cipro#~  dm               nnn
     thyl8zAla.fid   dmm                c
   ACQUISITION       dmf              200
sfrq         300.108  PROCESSING
tn                H1  wtfile
at             4.003  proc              ft
np             48052  fn            131072
sw            6002.4
fb         not used   wtrr
bs                4   wtxp
tpwr             54   wbs
pw              8.0   wnt
d1            0.050
tof           867.7
nt               32
ct               32
alock             n
gain       not used
      FLAGS
il                n
in                n
dp                y
    DISPLAY
sp            150.0
wp           4801.7
vs              151
sc                0
wc              250
hzmm          19.21
is           500.00
rfl          2810.1
rfp          2178.8
th               20
ins           1.000
nm    ph
```

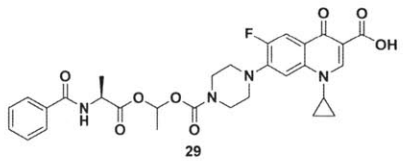

29

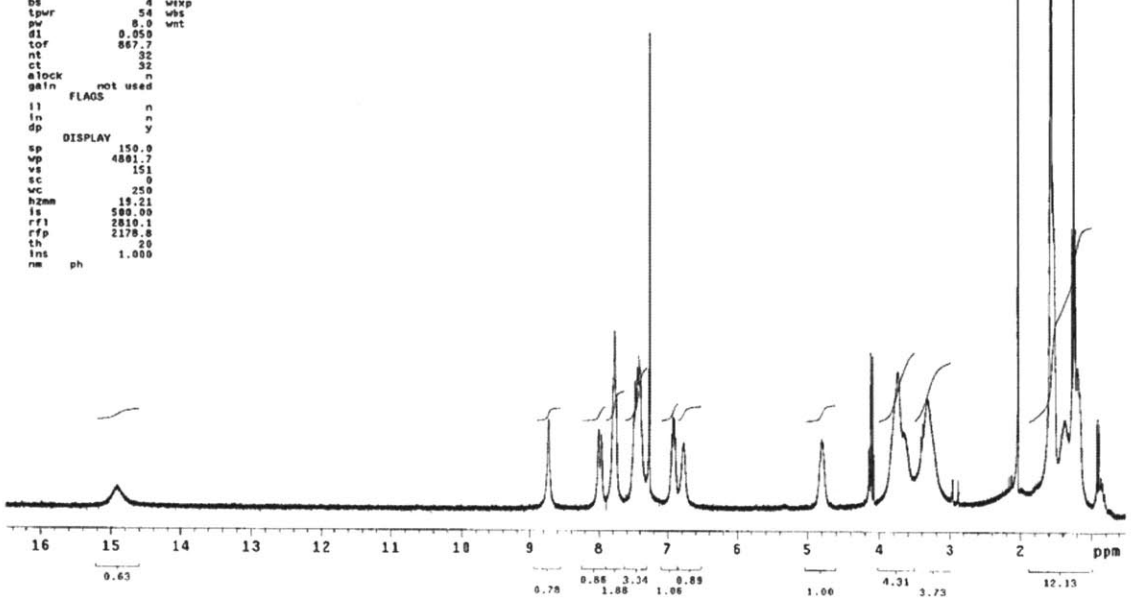

STANDARD 1H OBSERVE

```
exp1  std1h

      SAMPLE                  DEC. & VT
date   Jul 12 2011  dfrq          300.107
solvent       CDCl3  dn                H1
file /data/export/~  dpwr              30
home/nolan/NOtzhe/~  dof                0
mrhat/071211cipro#~  dm               nnn
     thyl8zVal.fid   dmm                c
   ACQUISITION       dmf              200
sfrq         300.108  PROCESSING
tn                H1  wtfile
at             4.003  proc              ft
np             48052  fn            131072
sw            6002.4
fb         not used   wtrr
bs                4   wtxp
tpwr             54   wbs
pw              8.0   wnt
d1            0.050
tof           867.7
nt               32
ct               32
alock             n
gain       not used
      FLAGS
il                n
in                n
dp                y
    DISPLAY
sp           -150.1
wp           4801.7
vs              151
sc                0
wc              250
hzmm          19.21
is           684.23
rfl          2811.5
rfp          2178.8
th               20
ins           1.000
nm    ph
```

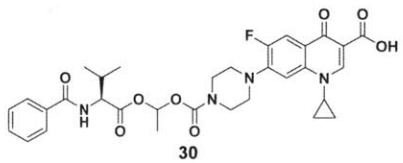

30

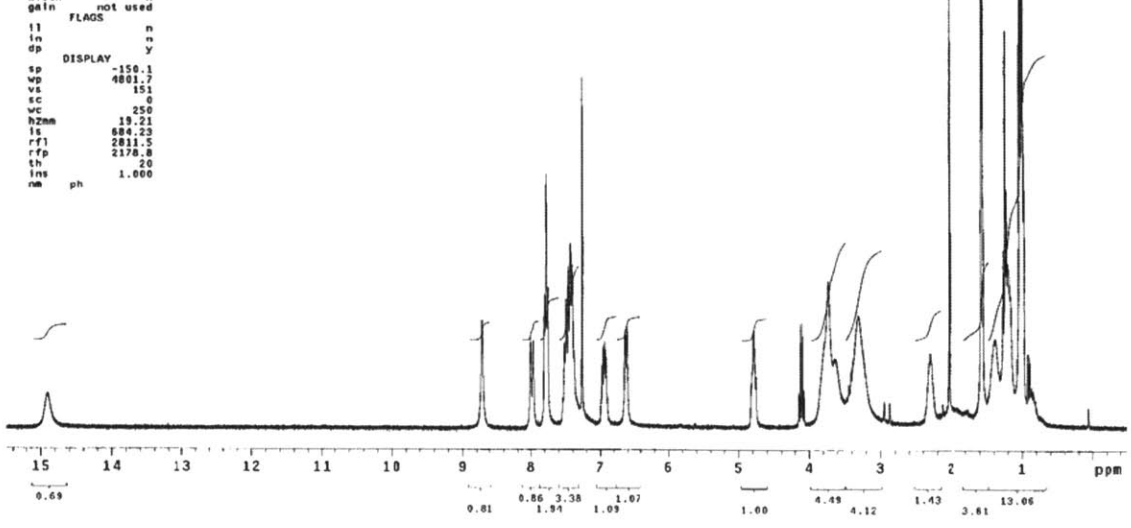

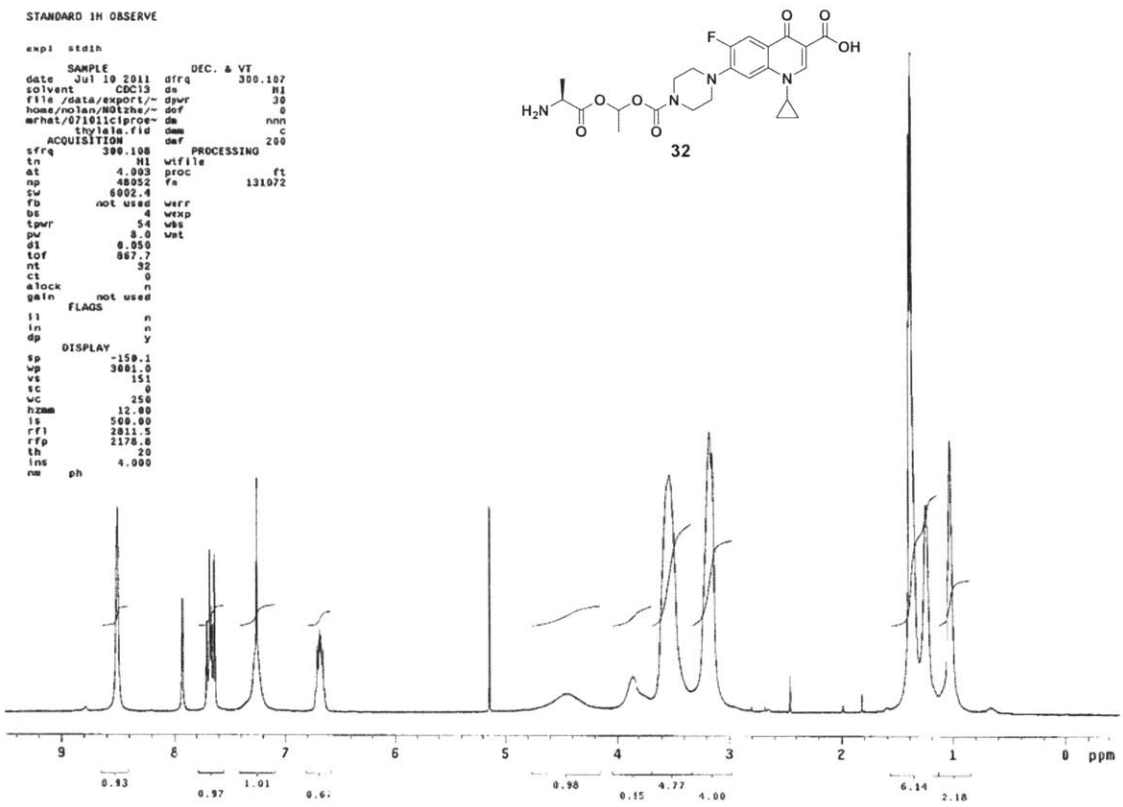
STANDARD 1H OBSERVE
expl stdih
SAMPLE
date Jul 10 2011
solvent CDCl3
file /data/export/~
home/nolan/NOtizhe/~
mrhat/071011ciproe~
thylala.fid
ACQUISITION
sfrq 300.108
tn H1
at 4.003
np 48052
sw 6002.4
fb not used
bs 4
tpwr 54
pw 8.0
dl 0.050
tof 867.7
nt 32
ct 0
alock n
gain not used
FLAGS
il n
in n
dp y
DISPLAY
sp -159.1
wp 3001.0
vs 151
sc 0
wc 250
hzmm 12.00
is 508.00
rfl 2811.5
rfp 2178.8
th 20
ins 4.000
nm ph
DEC. & VT
dfrq 300.107
dn H1
dpwr 30
dof 0
dm nnn
dmm c
dmf 200
PROCESSING
wtfile
proc ft
fn 131072
werr
wexp
wbs
wnt
32
9
8
7
6
5
4
3
2
1
0 ppm
0.93
0.97
1.01
0.98
0.15
4.77
4.00
6.14
2.18

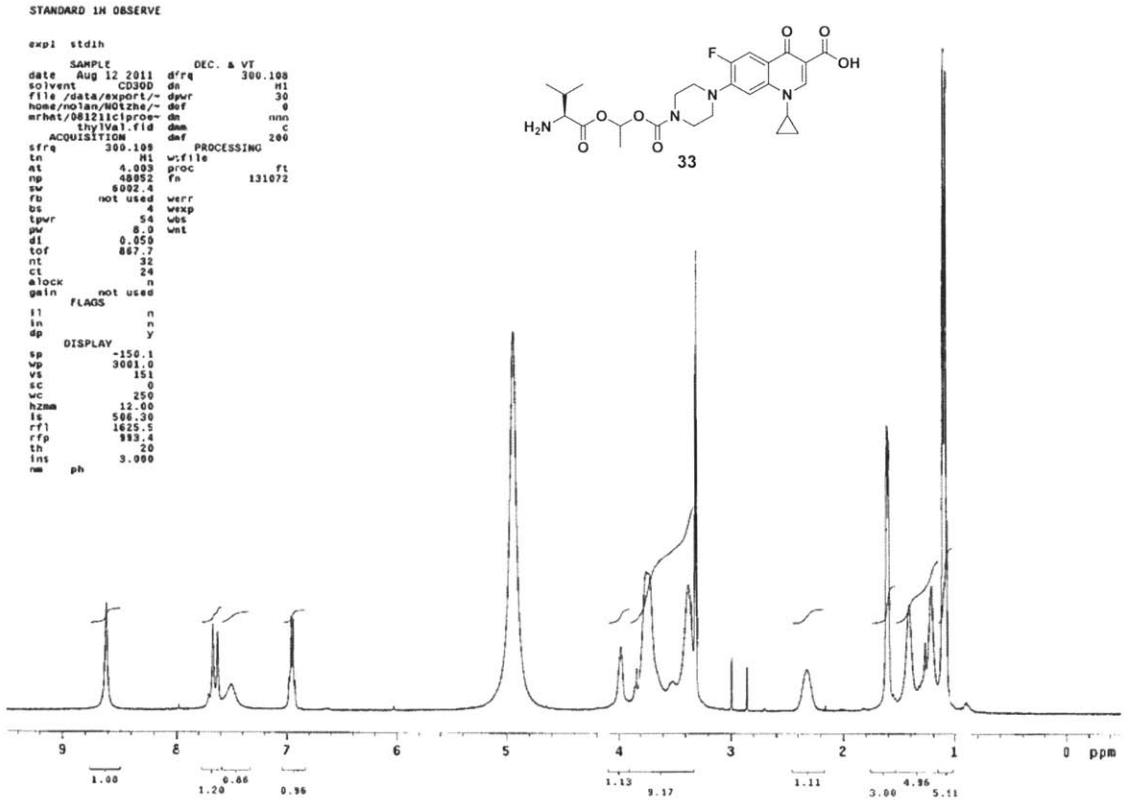
STANDARD 1H OBSERVE
expl stdih
SAMPLE
date Aug 12 2011
solvent CD3OD
file /data/export/~
home/nolan/NOtizhe/~
mrhat/081211ciproe~
thylVal.fid
ACQUISITION
sfrq 300.108
tn H1
at 4.003
np 48052
sw 6002.4
fb not used
bs 4
tpwr 54
pw 8.0
dl 0.050
tof 867.7
nt 32
ct 24
alock n
gain not used
FLAGS
il n
in n
dp y
DISPLAY
sp -150.1
wp 3001.0
vs 151
sc 0
wc 250
hzmm 12.00
is 506.30
rfl 1625.5
rfp 983.4
th 20
ins 3.000
nm ph
DEC. & VT
dfrq 300.108
dn H1
dpwr 30
dof 0
dm nnn
dmm c
dmf 200
PROCESSING
wtfile
proc ft
fn 131072
werr
wexp
wbs
wnt
33
9
8
7
6
5
4
3
2
1
0 ppm
1.00
0.86
1.20
0.96
1.13
9.17
1.11
3.00
4.96
5.11

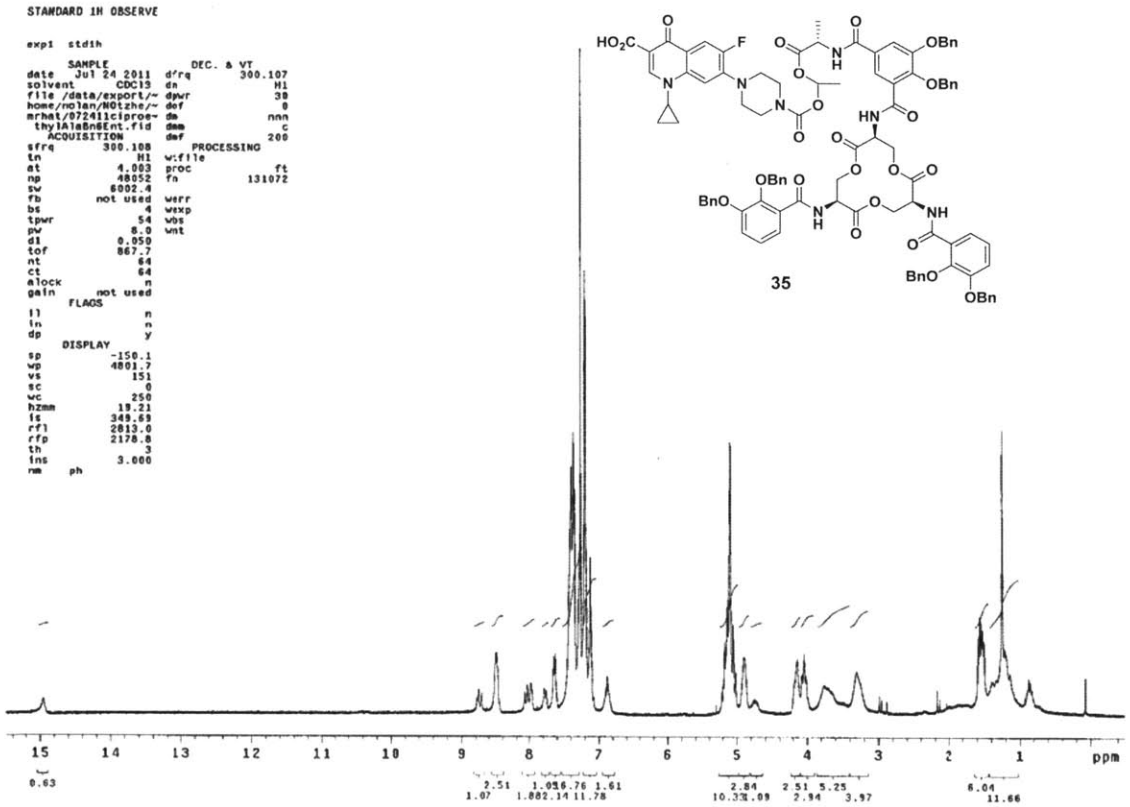
STANDARD 1H OBSERVE
exp1 stdih
SAMPLE
date Jul 24 2011
solvent CDCl3
file /data/export/~
home/nolan/NOlzhe/~
mrhat/072411ciproe-
thylAlaBn6Ent.fid
ACQUISITION
sfrq 300.108
tn H1
at 4.003
np 48052
sw 6002.4
fb not used
bs 4
tpwr 54
pw 8.0
d1 0.050
tof 867.7
nt 64
ct 64
alock n
gain not used
FLAGS
il n
in n
dp y
DISPLAY
sp -150.1
wp 4801.7
vs 151
sc 0
wc 250
hzmm 19.21
is 349.69
rfl 2813.0
rfp 2178.8
th 3
ins 3.000
nm ph
DEC. & VT
dfrq 300.107
dn H1
dpwr 38
def 0
dm nnn
dmm c
dmf 200
PROCESSING
wtfile
proc ft
fn 131072
werr
wexp
wnt
35
ppm

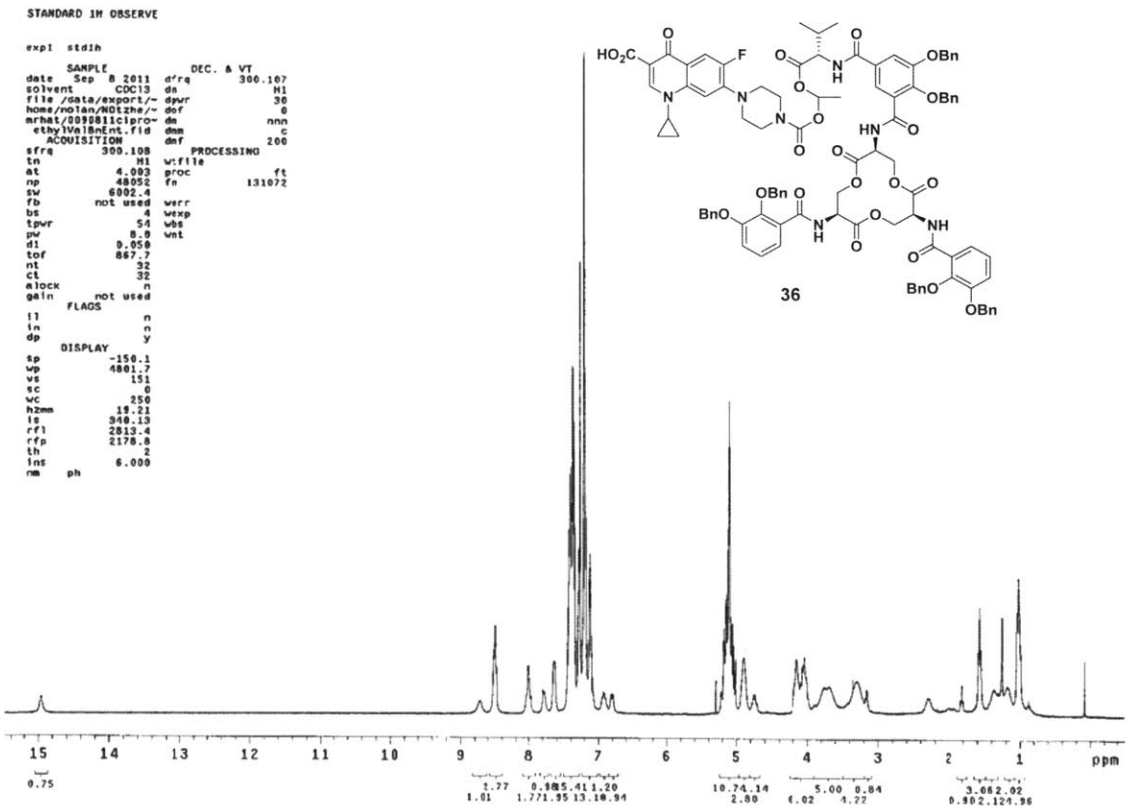
STANDARD 1H OBSERVE
exp1 stdih
SAMPLE
date Sep 8 2011
solvent CDCl3
file /data/export/~
home/nolan/NOlzhe/~
mrhat/0090811ciproe-
ethylValBnEnt.fid
ACQUISITION
sfrq 300.108
tn H1
at 4.003
np 48052
sw 6002.4
fb not used
bs 4
tpwr 54
pw 8.0
d1 0.050
tof 867.7
nt 32
ct 32
alock n
gain not used
FLAGS
il n
in n
dp y
DISPLAY
sp -150.1
wp 4801.7
vs 151
sc 0
wc 250
hzmm 19.21
is 340.13
rfl 2813.4
rfp 2178.8
th 2
ins 6.000
nm ph
DEC. & VT
dfrq 300.107
dn H1
dpwr 38
def 0
dm nnn
dmm c
dmf 200
PROCESSING
wtfile
proc ft
fn 131072
werr
wexp
wnt
36
ppm

Chapter 4
Analytical HPLC Traces

37

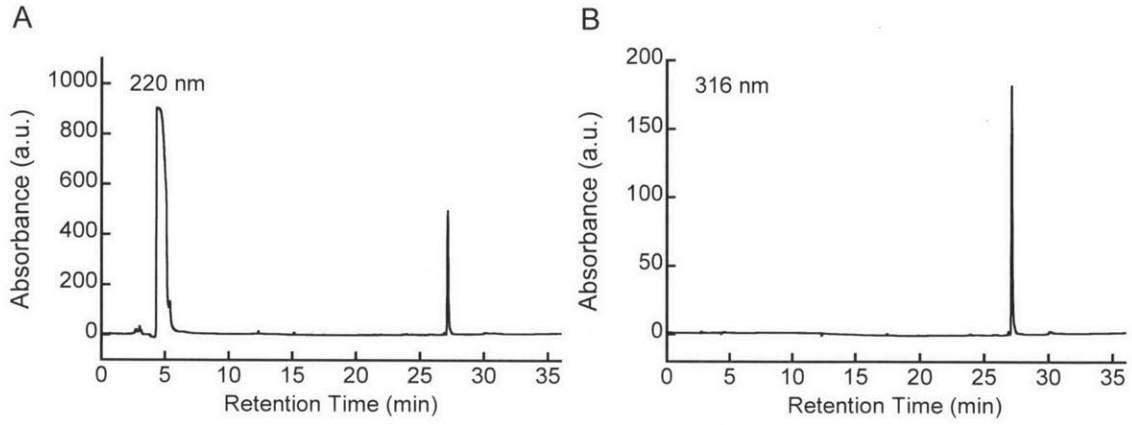
A
220 nm
Absorbance (a.u.)
Retention Time (min)
B
316 nm
Absorbance (a.u.)
Retention Time (min)

38

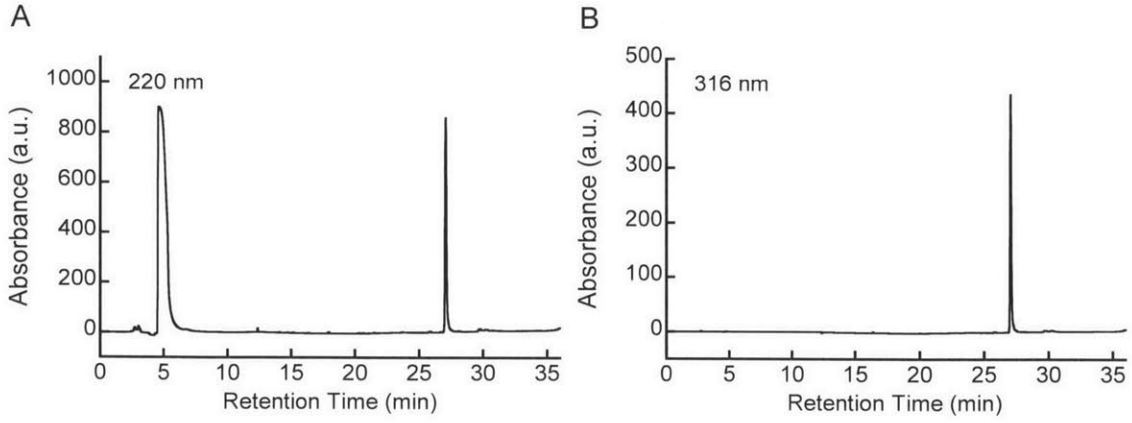
A
220 nm
Absorbance (a.u.)
Retention Time (min)
B
316 nm
Absorbance (a.u.)
Retention Time (min)

Appendix 1
NMR Spectra

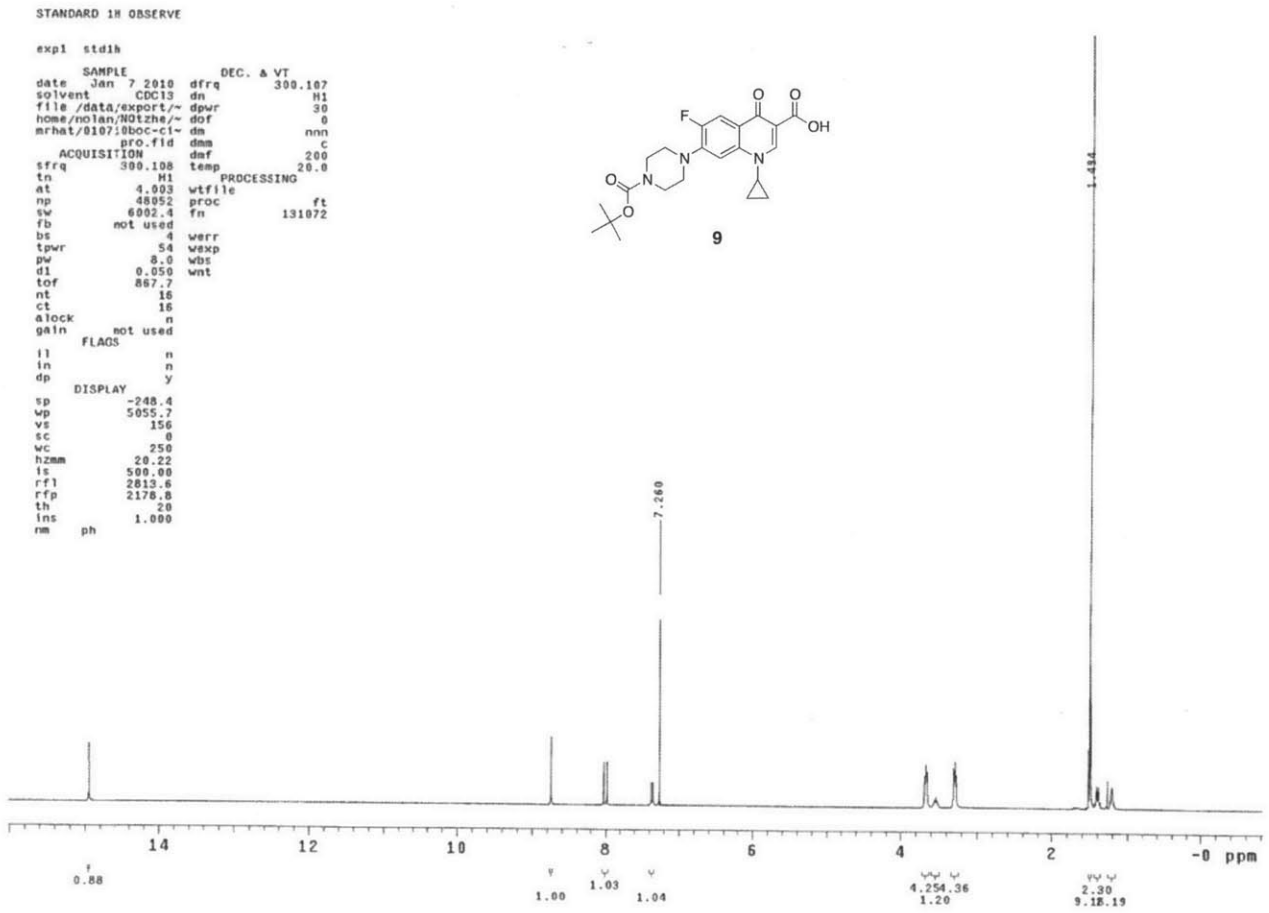
STANDARD 1H OBSERVE
expl stdlh
SAMPLE
date Jan 7 2010
solvent CDCl3
file /data/export/~
home/nolan/NOtzhe/~
mrhat/0107;0boc-ci~
pro.fld
ACQUISITION
sfrq 300.108
tn H1
at 4.003
np 48052
sw 6002.4
fb not used
bs 4
tpwr 54
pw 8.0
d1 0.050
tof 867.7
nt 16
ct 16
alock n
gain not used
FLAGS
il n
in n
dp y
DISPLAY
sp -248.4
wp 5055.7
vs 156
sc 0
wc 250
hzmm 20.22
is 500.00
rfl 2813.6
rfp 2178.8
th 20
ins 1.000
nm ph
DEC. & VT
dfrq 300.107
dn H1
dpwr 30
dof 0
dm nnn
dmm c
dmf 200
temp 20.0
PROCESSING
wtfile
proc ft
fn 131072
werr
wexp
wbs
wnt
F
O
O
OH
N
N
N
O
O
9
7.260
1.484
14
12
10
8
6
4
2
-0 ppm
0.88
1.00
1.03
1.04
4.254.36
1.20
2.30
9.18.19

Appendix 1
Analytical HPLC Traces

4

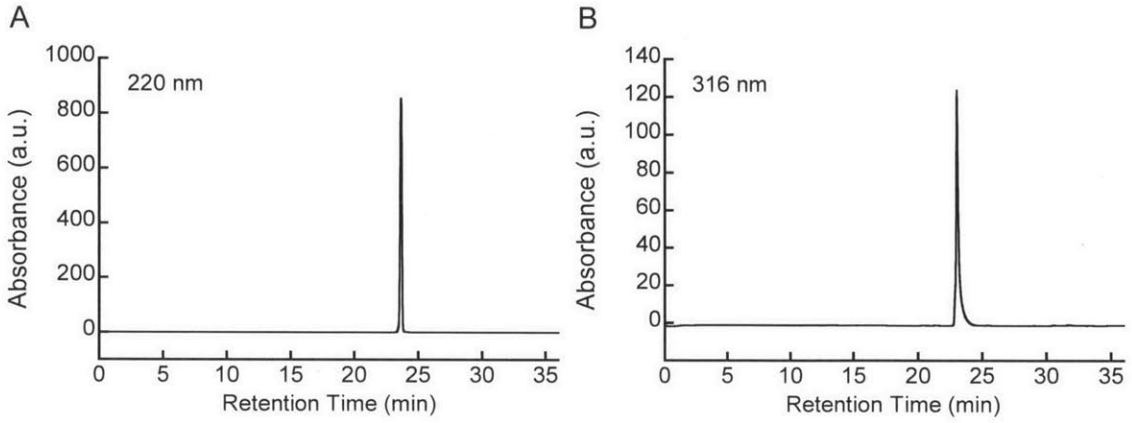
A
220 nm
Absorbance (a.u.)
1000
800
600
400
200
0
0 5 10 15 20 25 30 35
Retention Time (min)
B
316 nm
Absorbance (a.u.)
140
120
100
80
60
40
20
0
0 5 10 15 20 25 30 35
Retention Time (min)

5

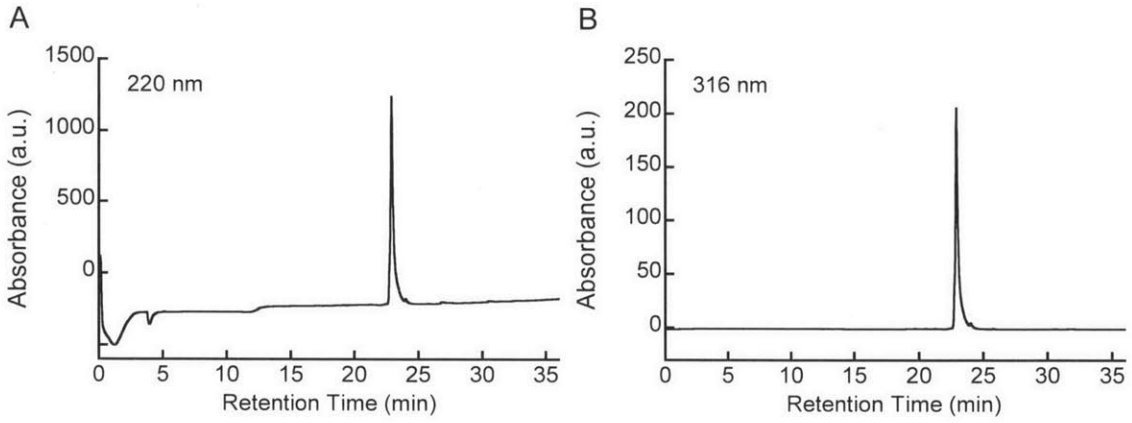
A
220 nm
Absorbance (a.u.)
1500
1000
500
0
0 5 10 15 20 25 30 35
Retention Time (min)
B
316 nm
Absorbance (a.u.)
250
200
150
100
50
0
0 5 10 15 20 25 30 35
Retention Time (min)

6

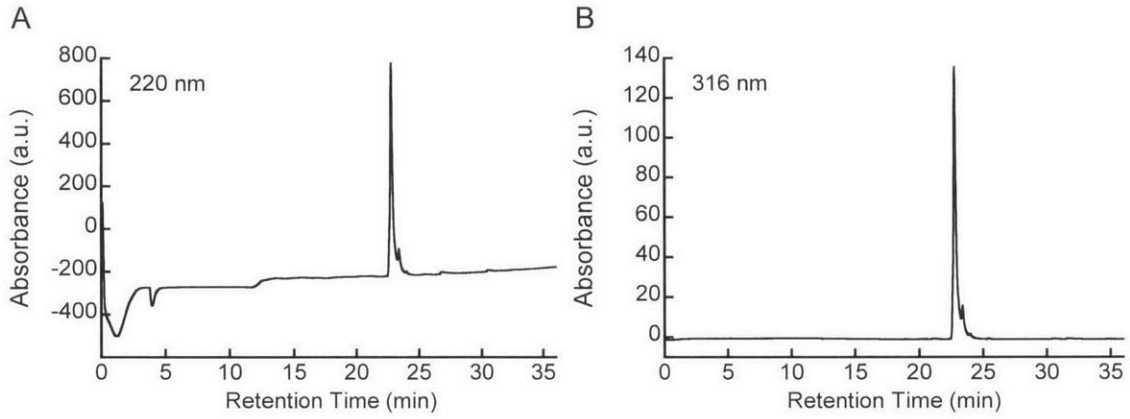
A
220 nm
Absorbance (a.u.)
800
600
400
200
0
-200
-400
0 5 10 15 20 25 30 35
Retention Time (min)
B
316 nm
Absorbance (a.u.)
140
120
100
80
60
40
20
0
0 5 10 15 20 25 30 35
Retention Time (min)

7

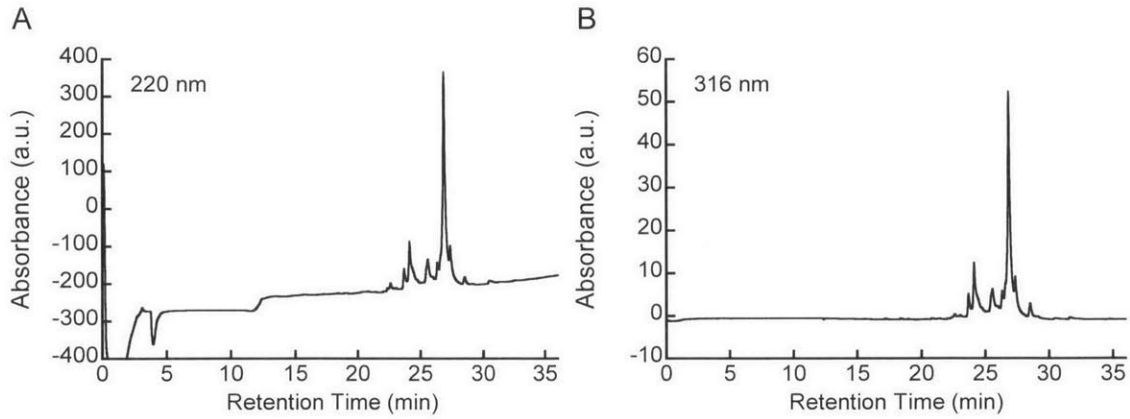
A
220 nm
Absorbance (a.u.)
400
300
200
100
0
-100
-200
-300
-400
0 5 10 15 20 25 30 35
Retention Time (min)
B
316 nm
Absorbance (a.u.)
60
50
40
30
20
10
0
-10
0 5 10 15 20 25 30 35
Retention Time (min)

8

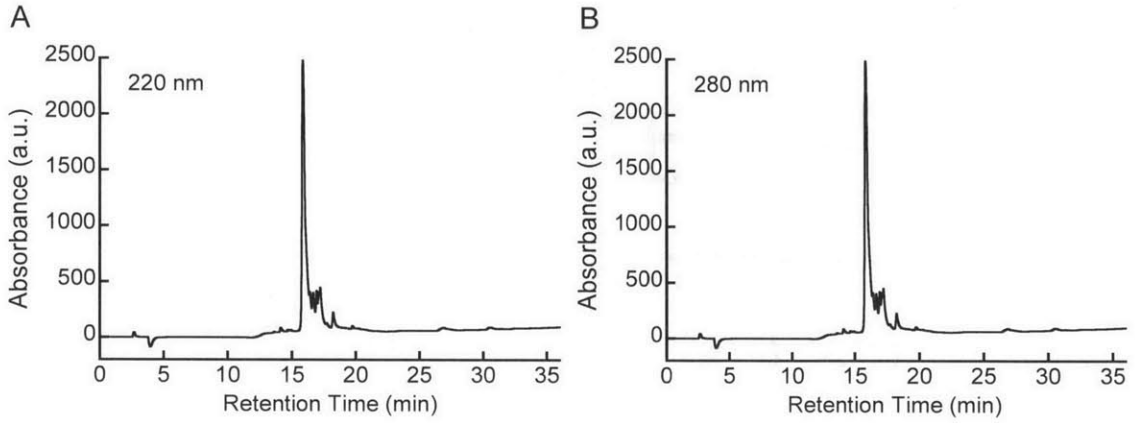
A
220 nm
Absorbance (a.u.)
2500
2000
1500
1000
500
0
0 5 10 15 20 25 30 35
Retention Time (min)
B
280 nm
Absorbance (a.u.)
2500
2000
1500
1000
500
0
0 5 10 15 20 25 30 35
Retention Time (min)

10

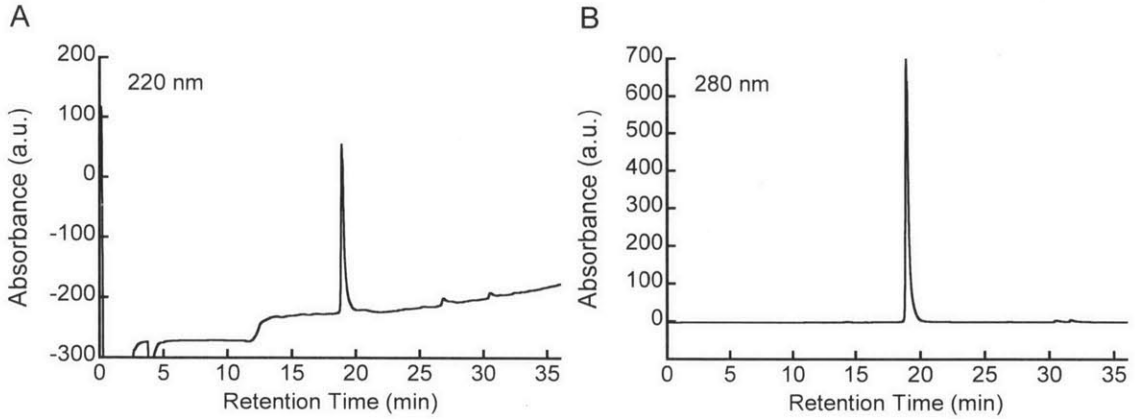
A
220 nm
Absorbance (a.u.)
200
100
0
-100
-200
-300
0 5 10 15 20 25 30 35
Retention Time (min)
B
280 nm
Absorbance (a.u.)
700
600
500
400
300
200
100
0
0 5 10 15 20 25 30 35
Retention Time (min)